

**REINFORCED CONCRETE FLAT PLATES UNDER LATERAL LOADING:
AN EXPERIMENTAL STUDY INCLUDING BIAXIAL EFFECTS**

by

Austin P. Pan

Jack P. Moehle

Report to the National Science Foundation

Report No. UCB/EERC-88/16
Earthquake Engineering Research Center
University of California at Berkeley

October 1988

ABSTRACT

Slab-column subassemblages, modelled after a reinforced concrete flat plate building, are tested under combined gravity and lateral loads. The tests include different levels of gravity loads and compare biaxial lateral loading with uniaxial loading. To study the behavior of a repaired connection, one test is repeated after the slab-column specimen is repaired with epoxy and grout. The post-failure behavior of slab-column connections is investigated and the adequacy of bottom slab reinforcement detailing to prevent progressive collapse is assessed. Existing strength and lateral stiffness models are compared with the experimental results. Data from past research are collected to investigate the ductility and drift capacity of slab-column connections. Studies are conducted on the seismic response of reinforced concrete buildings with flat slab construction. Nonlinear dynamic analyses are performed on five typical building systems. A simple seismic design recommendation is proposed for slab-column connections that limits the level of gravity shear to ensure minimal drift capacity.

ACKNOWLEDGEMENTS

The authors gratefully acknowledge the support of the National Science Foundation for providing funds for this research.

Except for editorial changes, this report is the same as the doctoral dissertation of Austin P. Pan submitted in October 1988 to the Graduate Division of the University of California at Berkeley. The dissertation committee consisted of Professors Jack P. Moehle (Chairman) and Stephen A. Mahin of the Department of Civil Engineering and Professor Jean-Pierre Protzen of the Department of Architecture. The authors are grateful to Professors Mahin and Protzen for reviewing the manuscript and suggesting improvements.

The staffs of the following organizations are thanked for their services during the conduct of the experimental program: Structural Engineering Laboratory of the Department of Civil Engineering, Material Testing Laboratory, Office of Research Services, and the Earthquake Engineering Research Center. The work of Michael Pitrola, chief technician in charge of the program, is particularly appreciated, together with the assistance of the engineering aids: Michael Fotch, Gus Bergsma, and Tien-Kwang Liu.

TABLE OF CONTENTS

ABSTRACT	i
ACKNOWLEDGEMENTS	ii
TABLE OF CONTENTS	iii
LIST OF TABLES	viii
LIST OF FIGURES	ix
LIST OF NOTATIONS	xvii
1. INTRODUCTION	1
1.1 Statement of the Problem	1
1.2 Objectives and Scope	2
1.3 Previous Research	3
1.3.1 Stiffness	3
1.3.2 Strength	4
1.3.3 Seismic Response	5
1.3.4 Progressive Collapse	6
2. PROTOTYPE STRUCTURE	7
2.1 Description	7
2.2 Design of the Prototype Structure	7
2.2.1 Slab	8
2.2.2 Column	9
2.3 Alternative Prototype Structures	9

3. TEST SPECIMENS	10
3.1 Introduction	10
3.2 Modelling	10
3.3 Description	11
3.4 Reinforcement	12
3.4.1 Slab	12
3.4.2 Column	13
3.5 Construction	13
3.6 Material Properties	14
3.6.1 Concrete	14
3.6.2 Reinforcement	14
3.6.3 Grout	14
3.7 Repaired Specimen	15
4. TESTING	16
4.1 Objectives	16
4.2 Test Setup	17
4.2.1 Transducer Struts	17
4.2.2 Torsional Restraining Frame	18
4.3 Instrumentation and Data Recording	19
4.4 Testing Procedures	21
4.4.1 Loading	22
5. EXPERIMENTAL RESULTS	25
5.1 Introduction	25
5.2 Sign Convention	25

5.3 Lateral Load versus Drift	25
5.3.1 Post-Failure Behavior	26
5.4 Connection Shear	27
5.5 Slab Connection Rotation	27
5.6 Column Rotation	28
5.7 Slab Displacement, Rotation, and Twist Profiles	28
5.8 Reinforcement Strains	29
5.9 In-Plane Torsion	29
5.10 Crack Patterns	30
6. DISCUSSION OF EXPERIMENTAL RESULTS	31
6.1 Introduction	31
6.2 Effects of Gravity Loads	31
6.3 Effects of Biaxial Loading	32
6.4 Repeated Load Cycles	33
6.5 Post-Failure Behavior	34
6.6 Repaired Specimen Behavior	35
6.7 Slab Moments due to Gravity Loads	36
6.8 Lateral Stiffness	37
6.8.1 Effective Beam Width Model	38
6.8.2 Equivalent Frame Model	39
6.9 Ultimate Strength	41
6.9.1 Linear Stress Variation Model	41
6.9.2 Beam Analogy by Hawkins	42
6.9.3 Park and Islam Model	44

7. DUCTILITY AND DRIFT CAPACITY	46
7.1 Introduction	46
7.2 Review of Experimental Observations	46
7.2.1 Tests Description	47
7.2.2 Lateral Load-Displacement Relation	47
7.3 The Effect of Gravity Load on Lateral Displacement Ductility	49
7.4 The Effect of Biaxial Loading on Lateral Displacement Ductility	50
7.5 Effects of other Parameters on Drift Capacity	51
7.6 Ductility, Drift, and Seismic Performance	51
8. STUDIES OF THE SEISMIC RESPONSE OF REINFORCED CONCRETE BUILDINGS WITH FLAT SLAB CONSTRUCTION	53
8.1 Introduction	53
8.2 Description of Buildings	53
8.2.1 Buildings in UBC Zone No. 2	53
8.2.2 Buildings in UBC Zone No. 4	54
8.3 Design	54
8.4 Dynamic Analysis	55
8.4.1 Modelling	56
8.4.2 Mass and Damping	57
8.4.3 Ground Motions	57
8.5 Discussion of Analysis Results	57
8.6 Design of Flat Slab Connections under Seismic Conditions	59
9. SUMMARY AND CONCLUSIONS	61
9.1 Summary	61

9.2 Conclusions	63
REFERENCES	65
TABLES	69
FIGURES	78
APPENDIX A: INSTRUMENTATION CHANNEL NUMBERS	250

LIST OF TABLES

3.1 - Concrete Mix Design	69
3.2 - Concrete Properties	69
3.3 - Slab Reinforcement Properties	69
4.1 - Test Program	70
6.1 - Summary of Test Results	70
7.1 - Data of Experimental Specimens	71
7.2 - Summary of Analysis Results	72
8.1 (a) - Properties of Frame System in UBC Zone No. 2	73
8.1 (b) - Properties of Shear Wall System in UBC Zone No. 2	74
8.1 (c) - Properties of Flat Plate System in UBC Zone No. 2	75
8.1 (d) - Properties of Frame System in UBC Zone No. 4	76
8.1 (e) - Properties of Shear Wall System in UBC Zone No. 4	77

LIST OF FIGURES

2.1 Plan and Elevation of Prototype	78
2.2 Alternative Prototype Structures	79
3.1 Relation of Test Specimen to Prototype	80
3.2 Test Specimen	81
3.3 Top Slab Reinforcement	82
3.4 Slab Reinforcement Detail	83
3.5 Bottom Slab Reinforcement	84
3.6 Column Reinforcement	85
3.7 Photo of Test Specimens	86
3.8 Honeycombs in Column of Specimen 3	86
3.9 Measured Concrete Stress-Strain for Specimens 3 and 4 (Cylinder B)	87
3.10 Measured Stress-Strain of Slab Reinforcement - No. 3, Grade 60 (Sample c)	88
4.1 (a) Test Setup - Plan	89
4.1 (b) Test Setup - Elevation	90
4.2 Detail of Column Base	91
4.3 Detail of Column Top	92
4.4 Transducer Strut	93
4.5 (a) Instrumentation - Plan	94
4.5 (b) Instrumentation - Elevation	95
4.6 Slab-Column Instrumentation	96
4.7 Top Strain Gauge Locations - Uniaxial Tests	97

4.8 Bottom Strain Gauge Locations - Uniaxial Tests	98
4.9 Top Strain Gauge Locations - Biaxial Tests	99
4.10 Bottom Strain Gauge Locations - Biaxial Tests	100
4.11 Lateral Displacement History and Loading Patterns	101
4.12 Biaxial Loading	102
5.1 Schematic Drawing of Test	103
5.2 EW Lateral Load vs Displacement - Test 1	104
5.3 (a) EW Lateral Load vs Displacement - Test 2	105
5.3 (b) NS Lateral Load vs Displacement - Test 2	106
5.4 EW Lateral Load vs Displacement - Test 3	107
5.5 (a) EW Lateral Load vs Displacement - Test 4	108
5.5 (b) NS Lateral Load vs Displacement - Test 4	109
5.6 (a) EW Lateral Load vs Displacement - Test 5	110
5.6 (b) NS Lateral Load vs Displacement - Test 5	111
5.7 (a) Post-Failure Lateral Load vs Displacement (EW - Test 2)	112
5.7 (b) Post-Failure Lateral Load vs Displacement (NS - Test 2)	113
5.8 Connection Shear History - Test 1	114
5.9 Connection Shear History - Test 2	115
5.10 Connection Shear History - Test 3	116
5.11 Connection Shear History - Test 4	117
5.12 Connection Shear History - Test 5	118
5.13 (a) Slab Moment vs Rotation (East Side) - Test 1	119
5.13 (b) Slab Moment vs Rotation (West Side) - Test 1	120
5.14 (a) Slab Moment vs Rotation (East Side) - Test 2	121

5.14 (b) Slab Moment vs Rotation (West Side) - Test 2	122
5.14 (c) Slab Moment vs Rotation (North Side) - Test 2	123
5.14 (d) Slab Moment vs Rotation (South Side) - Test 2	124
5.15 (a) Slab Moment vs Rotation (East Side) - Test 3	125
5.15 (b) Slab Moment vs Rotation (West Side) - Test 3	126
5.16 (a) Slab Moment vs Rotation (East Side) - Test 4	127
5.16 (b) Slab Moment vs Rotation (West Side) - Test 4	128
5.16 (c) Slab Moment vs Rotation (North Side) - Test 4	129
5.16 (d) Slab Moment vs Rotation (South Side) - Test 4	130
5.17 (a) Slab Moment vs Rotation (East Side) - Test 5	131
5.17 (b) Slab Moment vs Rotation (West Side) - Test 5	132
5.17 (c) Slab Moment vs Rotation (North Side) - Test 5	133
5.17 (d) Slab Moment vs Rotation (South Side) - Test 5	134
5.18 Column Moment vs Rotation (Test 3)	135
5.19 (a) Slab Displacement Profiles (West Side) - Test 1	136
5.19 (b) Slab Rotation Profiles (West Side) - Test 1	137
5.19 (c) Slab Twist Profiles (South Side) - Test 1	138
5.20 (a) Slab Displacement Profiles (West Side) - Test 2	139
5.20 (b) Slab Rotation Profiles (West Side) - Test 2	140
5.20 (c) Slab Twist Profiles (West Side) - Test 2	141
5.20 (d) Slab Displacement Profiles (South Side) - Test 2	142
5.20 (e) Slab Rotation Profiles (South Side) - Test 2	143
5.20 (f) Slab Twist Profiles (South Side) - Test 2	144
5.21 (a) Slab Displacement Profiles (West Side) - Test 3	145

5.21 (b) Slab Rotation Profiles (West Side) - Test 3	146
5.21 (c) Slab Twist Profiles (South Side) - Test 3	147
5.22 (a) Slab Displacement Profiles (West Side) - Test 4	148
5.22 (b) Slab Rotation Profiles (West Side) - Test 4	149
5.22 (c) Slab Twist Profiles (West Side) - Test 4	150
5.22 (d) Slab Displacement Profiles (South Side) - Test 4	151
5.22 (e) Slab Rotation Profiles (South Side) - Test 4	152
5.22 (f) Slab Twist Profiles (South Side) - Test 4	153
5.23 (a) Slab Displacement Profile History (West Side - Test 3)	154
5.23 (b) Slab Twist Profile History (South Side - Test 3)	155
5.24 (a) Slab Displacement Profile History (West Side - Test 4)	156
5.24 (b) Slab Twist Profile History (South Side - Test 4)	157
5.25 (a) Top Reinforcement Strain Profiles (East Side) - Test 1	158
5.25 (b) Top Reinforcement Strain Profiles (West Side) - Test 1	159
5.25 (c) Bottom Reinforcement Strain Profiles (East Side) - Test 1	160
5.25 (d) Bottom Reinforcement Strain Profiles (West Side) - Test 1	161
5.26 (a) Top Reinforcement Strain Profiles (West Side) - Test 2	162
5.26 (b) Top Reinforcement Strain Profiles (South Side) - Test 2	163
5.26 (c) Bottom Reinforcement Strain Profiles (North Side) - Test 2	164
5.26 (d) Bottom Reinforcement Strain Profiles (East Side) - Test 2	165
5.27 (a) Top Reinforcement Strain Profiles (East Side) - Test 3	166
5.27 (b) Top Reinforcement Strain Profiles (West Side) - Test 3	167
5.27 (c) Bottom Reinforcement Strain Profiles (East Side) - Test 3	168
5.27 (d) Bottom Reinforcement Strain Profiles (West Side) - Test 3	169

5.28 (a) Top Reinforcement Strain Profiles (West Side) - Test 4	170
5.28 (b) Top Reinforcement Strain Profiles (South Side) - Test 4	171
5.28 (c) Bottom Reinforcement Strain Profiles (North Side) - Test 4	172
5.28 (d) Bottom Reinforcement Strain Profiles (East Side) - Test 4	173
5.29 Reinforcement Strain Profile History (Top West Side - Test 3)	174
5.30 Reinforcement Strain Profile History (Bottom North Side - Test 4)	175
5.31 In-Plane Torsion History (Test 2)	176
5.32 Crack Patterns - Test 1	177
5.33 Crack Patterns - Test 2	178
5.34 Crack Patterns - Test 3	179
5.35 Crack Patterns - Test 4	180
5.36 Crack Patterns - Test 5	181
5.37 (a) Initial Failure - Test 2	182
5.37 (b) Connection After Experiment - Test 3	182
5.37 (c) Initial Failure of Repaired Specimen - Test 5	183
6.1 (a) Effect of Gravity Loads - Uniaxial Tests	184
6.1 (b) Effect of Gravity Loads - Biaxial Tests	185
6.2 (a) Effect of Gravity Loads on Stiffness - Uniaxial Tests	186
6.2 (b) Effect of Gravity Loads on Stiffness - Biaxial Tests	187
6.3 (a) Effect of Biaxial Loading - Tests with High Gravity Loads	188
6.3 (b) Effect of Biaxial Loading - Tests with Low Gravity Loads	189
6.4 (a) Effect of Biaxial Loading on Stiffness - Tests with High Gravity Loads	190
6.4 (b) Effect of Biaxial Loading on Stiffness - Tests with Low Gravity Loads	191
6.5 (a) Comparison of Absolute Load-Displacement Envelopes (High Gravity Loads)	192

6.5 (b) Comparison of Absolute Load-Displacement Envelopes (Low Gravity Loads)	193
6.6 (a) Repeated Load Cycles (0.8 % Drift Cycle - Test 3)	194
6.6 (b) Repeated Load Cycles (0.8 % Drift Cycle - Test 4 (EW))	195
6.7 Stiffness Degradation	196
6.8 Load-Displacement Envelopes of Repaired and Original Specimens	197
6.9 Comparison of Stiffness Between Repaired and Original Specimens	198
6.10 Measured Top Reinforcement Strain Profile Due to Gravity Loads (East Side - Test 1)	199
6.11 Moment-Strain Relationship of Slab Section (3 in. Top Reinforcement Spacing)	200
6.12 (a) Gravity Moment Profiles - Low Gravity Load Tests	201
6.12 (b) Gravity Moment Profiles - High Gravity Load Tests	202
6.12 (c) Comparison of Gravity Moment Profiles (Test 1)	203
6.13 Lateral Stiffness Models	204
6.14 (a) Comparison Between Effective Beam Width Model and Experimental Envelopes	205
6.14 (b) Comparison Between Effective Beam Width Model and Experimental Envelopes	206
6.15 (a) Comparison Between Equivalent Frame Model and Experimental Envelopes	207
6.15 (b) Comparison Between Equivalent Frame Model and Experimental Envelopes	208
6.16 Linear Stress Variation Model	209
6.17 Maximum Shear Stress by the Linear Stress Variation Model	210
6.18 Test Results on Shear-Moment Interaction Diagram	211
6.19 Beam Analogy Model	212
6.20 (a) Comparison Between Beam Analogy Model and Experimental Envelopes	213
6.20 (b) Comparison Between Beam Analogy Model and Experimental Envelopes	214
6.21 (a) Comparison Between Park and Islam Model and Experimental Envelopes	215
6.21 (b) Comparison Between Park and Islam Model and Experimental Envelopes	216

7.1 Lateral Load Simulation	217
7.2 Classification of Specimen Response	218
7.3 Definition of Displacement Ductility	219
7.4 Effect of Gravity Load on Ductility	220
7.5 Effect of Gravity Load on Drift	221
7.6 Forces on Connection under Uniaxial Loading	222
7.7 (a) Effect of Top Reinforcement Ratio on Drift	223
7.7 (b) Effect of Column Size to Span Length Ratio on Drift	224
7.7 (c) Effect of Slab Thickness to Span Length Ratio on Drift	225
7.8 Comparison of Ductility Requirements at 1.5 Percent Drift	226
8.1 A Multistory Building With Flat-Slab Construction	227
8.2 (a) Generic Buildings in UBC Zone No. 2	228
8.2 (b) Generic Buildings in UBC Zone No. 4	229
8.2 (c) Comparison Between 1985 and 1988 UBC Seismic Provisions	230
8.3 Computer Model of Shear Wall Building	231
8.4 (a) Simplified Takeda Model with Degrading Stiffness	232
8.4 (b) Total Slab Connection Moment vs Interstory Drift - El Centro	233
8.5 Records of Ground Motion	234
8.6 (a) Elastic Response Spectra (UBC Zone No. 2)	235
8.6 (b) Elastic Response Spectra (UBC Zone No. 4)	236
8.7 (a) Response of Shear Wall Building (UBC Zone No. 2) - Mexico City Record	237
8.7 (b) Response of Shear Wall Building (UBC Zone No. 2) - 0.2g El Centro Record	238
8.7 (c) Response of Shear Wall Building (UBC Zone No. 2) - 0.2g Taft Record	239
8.7 (d) Response of Frame Building (UBC Zone No. 2) - 0.2g El Centro Record	240

8.7 (e) Response of Flat-Plate Building (UBC Zone No. 2) - 0.2g El Centro Record	241
8.7 (f) Response of Frame Building (UBC Zone No. 4) - 0.4g El Centro Record	242
8.7 (g) Response of Shear Wall Building (UBC Zone No. 4) - 0.4g El Centro Record	243
8.8 (a) Summary of Maximum Drifts - UBC Zone No. 2 Buildings	244
8.8 (b) Summary of Maximum Drifts - UBC Zone No. 4 Buildings	245
8.8 (c) Comparison of Computed Drifts to Design Drifts - UBC Zone No. 2 Buildings	246
8.8 (d) Comparison of Computed Drifts to Design Drifts - UBC Zone No. 4 Buildings	247
8.9 Holiday Inn Building (Orion Avenue)	248
8.10 Detailing of Flat Plate Connections to Prevent Progressive Collapse	249

LIST OF NOTATIONS

A_{bm}	minimum continuous bottom slab reinforcement over column
A_c	cross sectional area of slab critical section
A_s	area of tension reinforcement
b	width of compression face of member
b_o	perimeter of critical section for slab
C	base shear constant
C_t	torsional constant
c	dimension of square column
c_c	distance from the centroid of the slab-column critical perimeter to the critical section
c_1	column dimension in direction of loading
c_2	column dimension transverse to direction of loading
D_h	horizontal displacement at top of column
D_u	ultimate displacement at failure
D_v	difference of the vertical displacement at opposite ends of the slab
D_y	yield displacement
d	distance from extreme compression fiber to centroid of tension reinforcement
d_{avg}	average d
EW	East-West
E_c	modulus of elasticity of concrete
E_{cs}	modulus of elasticity of slab concrete
E_s	modulus of elasticity of steel
Et	tangent modulus of elasticity of concrete

- E_{45} secant modulus of elasticity of concrete at 45% of ultimate strength
- EPA effective peak acceleration
- F_t portion of base shear applied at top of structure
- f'_c concrete compression strength
- f_t tensile strength of concrete
- f_y steel yield strength
- h overall thickness of slab
- h_c column height
- I occupancy importance factor
- I_{eb} moment of inertia of effective beam
- I_{eff} effective moment of inertia of slab
- J property of the slab-column critical section analogous to the polar moment of inertia
- K numerical coefficient dependent on the framing type
- K_c column stiffness
- K_{ec} equivalent column stiffness
- K_t torsional stiffness of torsional member
- l span length of square panel
- l_1 span length in direction of lateral load
- l_2 span length transverse to direction of lateral load
- M_{gc} average gravity moment at face of slab-column critical section based on finite element analysis
- M'_{gc} average gravity moment at face of slab-column critical section based on experimental results
- M_t transfer moment
- M'_t transfer moment in the n-s direction
- M_u ultimate moment

- m_u ultimate flexural capacity per unit length, top compression
- m'_u ultimate flexural capacity per unit length, bottom compression
- NS North-South
- P_{abs} absolute lateral force applied at top of column
- P_{ew} east-west lateral force applied at top of column
- P_{ns} north-south lateral force applied at top of column
- R_w resistance factor of framing system
- S numerical coefficient for site-structure resonance
- T fundamental period of the building
- V service level design base shear
- V_g shear due to gravity loads including self weight
- V_{all} allowable shear stress
- V_{gc} average gravity shear at face of slab-column critical section based on finite element analysis
- V'_{gc} average gravity shear at face of slab-column critical section based on experimental results
- V_o theoretical punching shear strength
- v_g gravity shear stress at critical section
- v_c shear stress at slab-column critical section
- v_{max} maximum shear stress at slab-column critical section
- W total dead load of the building
- w_u factored ultimate uniform load
- Z numerical coefficient dependent on the seismic zone
- β stiffness reduction factor
- Δ_{abs} absolute horizontal displacement at top of column
- Δ_{ew} east-west horizontal displacement at top of column

- Δ_{ns} north-south horizontal displacement at top of column
- γ_v fraction of transfer moment that is considered transferred by eccentric shear
- μ displacement ductility
- ϕ strength reduction factor
- ρ ratio of tension reinforcement = A_s/bd

1. INTRODUCTION

1.1 Statement of the Problem

The reinforced concrete flat plate is a simple structural system that consists of a flat slab supported directly by columns. This system is favored by many designers for its functional form and construction economy. It is widely used for both low and highrise buildings. Under vertical loads, the structural performance and design of reinforced concrete flat plates are well established. Testing and analytical research since the early 1900's have resulted in standard methods of analysis and design that are embodied in many building codes. However, under lateral loads, uncertainty in the behavior of flat plates persists. Proper methods of lateral design are currently unsettled particularly with regards to the slab-column connection. A resolution of these issues is critical in view of the fact that punching shear is the common mode of failure for flat plates. By initiating a progressive collapse, the failure of one slab-column connection has the potential of catastrophic consequences for the whole building.

It is generally recognized that in seismic zones the high flexibility and low energy dissipation capacity of flat plates make it necessary to combine them with another lateral load resistant system such as shear walls or moment resistant frames. From past experience, the seismic performance of even these dual systems remains questionable. After the 1985 Mexico City earthquake, a number of failures of flat-slab structures were reported, some in dual systems. During the 1964 Alaska earthquake, the J. C. Penney building which comprised flat plates and shear walls suffered a partial collapse. Although the Holiday Inn buildings of the 1971 San Fernando earthquake did not collapse, extensive nonstructural damage occurred. A better understanding of the lateral behavior of flat plates is needed together with more specific design criteria for slab-column connections in seismic regions.

To ensure the safety of building occupants, it is vital that flat slabs are prevented from collapsing after punching failure occurs. Additional experimental data are needed in this area to supplement past research. There is evidence that the detailing of continuous bottom slab bars directly over columns prevents the slab from collapsing.

It is often economical to repair structures that have been damaged by earthquakes. The adequacy of

repaired structures and their connections under subsequent strong ground motions is an area of active research. There is a scarcity of data on the behavior of repaired slab-column connections.

Despite the problems mentioned above, the trend towards more architecturally versatile buildings with economical construction will motivate the increased use of reinforced concrete flat plates as the primary vertical load carrying system, even in areas of high seismicity. The present study will address the issues mentioned above and other topics related to reinforced concrete flat plates under lateral loading.

1.2 Objectives and Scope

Specific objectives of the study reported herein are:

- (1) To study the behavior of a typical slab-column subassemblage under realistic lateral loading.
- (2) To study the effects of vertical loads on slab-column lateral load behavior.
- (3) To investigate the post-failure behavior of slab-column connections.
- (4) To investigate the performance of a repaired connection.
- (5) To assess various analytical techniques for estimating the strength and stiffness of reinforced concrete flat plates.
- (6) To investigate the lateral displacement ductility and drift capacity of slab-column connections.
- (7) To study the seismic performance of typical buildings with flat-slab construction.

To achieve these objectives, the present research includes five tests of interior slab-column subassemblages. Four identical specimens were constructed at sixty percent of full scale. Slab plan dimensions (scaled) are 13 ft (3.96 m) by 13 ft (3.96 m) with a thickness of 4.8 in. (122 mm). The column has dimensions of 10.8 in. (274 mm) by 10.8 in. (274 mm) in cross section and extends 3 ft (0.91 m) above and below the slab. Concrete compression strength is specified at 4,000 psi (28 MPa). All slab reinforcement are No. 3, Grade 60 (9.5 mm, nominal 414 MPa). The specimen is supported at the column base and slab edges. Two hydraulic load actuators are connected to the top of the column for lateral load simulation. The specimens are instrumented to measure deflections, slab rotations and profiles, reinforcement strains, and secondary displacements.

To investigate the influence of gravity load on connection behavior, "high" gravity load ($1.40\sqrt{f'_c}$ connection shear) is imposed on Test Specimens 1 and 2, and "low" gravity load ($0.88\sqrt{f'_c}$) is imposed on Test Specimens 3 and 4. Gravity load is simulated and maintained at a constant value by lead blocks on the slab and a vertical jack located beneath the base of the column.

Since realistic lateral loads such as wind and earthquakes act in multiple directions, some of the specimens are tested under bidirectional loading. A biaxial "clover leaf" loading pattern is used in Tests 2 and 4. In Tests 1 and 3, uniaxial cyclic loading is applied. Test Specimen 4 was later repaired with epoxy and grout and a fifth test, Test 5, was conducted to observe the effectiveness of a repaired connection.

The prototype structure after which the test specimens are modelled is discussed in Chapter 2. Chapter 3 describes the test specimens in detail. The test setup and method of testing are described in Chapter 4. The results of the slab-column tests are presented in Chapter 5. Chapter 6 discusses these results and compares them with various analytical models. The ductility and drift capacity of slab-column connections are investigated in Chapter 7. Chapter 8 presents a study of the seismic response of typical flat-plate buildings and a simple seismic design recommendation is proposed for slab-column connections. A summary and conclusions are in Chapter 9.

1.3 Previous Research

The performance of reinforced concrete flat plate structures under vertical and lateral loads has been the subject of numerous experiments and analytical studies. However, a review of the literature reveals that no experiments on flat plates have considered biaxial lateral loading. The following discusses briefly some of the past research.

1.3.1 Stiffness

A number of researchers such as Allen and Darvall [6], Pecknold [27], Mehraïn and Aalami [20], and Elias [9], have investigated the lateral load stiffness of flat slabs using isotropic elastic plate-bending theory. Results of these analyses differ significantly depending on whether the region of the slab within the column is treated as rigid or flexible. The effective beam width model for use in estimating stiffness was derived from these elastic solutions and is discussed extensively by Vanderbilt and Corley [33]. They and

others conclude that the validity of elastic analysis is limited for reinforced concrete plates because of cracking effects. Mulcahy and Rotter [23], based on tests of six slab-column connections, also concluded that the application of elastic theoretical models leads to overestimation of stiffness. Zee and Moehle [35] suggested that when a stiffness reduction factor is applied to the effective beam width model, a reasonably good estimate of working load stiffness may be obtained.

By adding a similar stiffness reduction factor to account for cracking, the equivalent frame method (originally developed for gravity load analysis) was extended by Vanderbilt and Corley for the lateral analysis of flat plates. A stiffness reduction factor of one-third was recommended unless a more detailed analysis of cracking is made. Others [21,35] have also recommended a similar reduction value based on test results. These studies emphasize that the magnitude of the reduction factor depends a great deal on the chosen lateral drift criterion.

Hawkins [3] proposes a general beam analogy model to predict the full nonlinear response of slab-column systems. The model was calibrated from an extensive series of tests on interior, edge, and corner slab-column connections. It idealizes the connection as a system of short flexural elements and torsional elements that have trilinear moment-rotation properties. Strength and stiffness of the connection are computed incrementally and various assumptions are made for failure, bond slip, and stress redistribution. The beam analogy model gives a reasonably good estimate of the response of Hawkins' slab-columns, but the procedure is relatively complex. A simplified version of the model is proposed by Akiyama and Hawkins [3].

Morrison and Sozen [22] and Sheu and Hawkins [28] have proposed grid models capable of estimating stiffness through the entire range of loading. Because of the relative complexity of these models, they are not widely implemented.

1.3.2 Strength

An ACI Special Publication [12] summarizes several procedures for estimating the strength of slab-column connections. For combined shear and moment transfer, the publication recommends the linear stress variation model as proposed by Hanson and Hanson [11]. This model assumes that stresses induced

by shear and moment transfer vary linearly across the critical section of the connection. Failure is predicted when the nominal shear stress reaches a critical value of $4\sqrt{f'_c}$ (for square columns). Compared with test results, the model gives generally conservative estimates of strength for interior and exterior connections [1]. Sufficient reinforcement must be placed to carry the moments carried by eccentric shear stresses. According to ACI 318-83 [7], the proportion of moment that can be carried by the reinforcement is limited. Tests by Hawkins and Ghali et al. [10] have demonstrated that strength and stiffness of slab-column connections can be increased by increasing the slab reinforcement or by concentrating the reinforcement in the connection region. The increase is effective only up to a reinforcement ratio of 0.8 to 1 percent.

The beam analogy model discussed in Section 1.3.1 has been shown by Hawkins and others [16,35] to give good estimates of strength for slab-column connections. Based on simplified concepts of the model, Park and Islam [16] proposed a single equation to predict the moment transfer strength of slab-column connections. They also showed that yield line theory provides an upper bound solution on strength.

1.3.3 Seismic Response

It is generally recognized that flat plates are not well suited to resist severe seismic loads unless special detailing is used. Hawkins concluded that gravity loads have a large influence on the stiffness and the capacity of flat plates to absorb lateral loads [3]. Slab-column connections exhibit a high degree of stiffness degradation under repeated cyclic loading. For seismic zones, Hawkins recommends the use of shear reinforcement in the slab to increase ductility and strength. Islam and Park reached the same conclusions on shear reinforcement [16].

Morrison and Sozen [22] tested slab-column connections under static and dynamic loading. They concluded that under low levels of gravity loads, the effect of gravity loads on lateral behavior is not significant. Under dynamic loads, their specimens had observed strengths of 20 to 30 percent over those of the statically tested specimens. Effective viscous damping ranged from four to eight percent. Ghali et al. [10] tested specimens under monotonic static and dynamic lateral loads. They concluded that the energy absorption capacity and rotation capacity are higher under dynamic loading. An increase of 15 to 28 percent in strength was observed.

Moehle and Diebold [21] reported the only shaking table test of a flat-plate structure. A two-story three-bay building was built at three-tenths of full scale and subjected to eleven earthquake simulations of varying intensities. The tests demonstrated that reliably tough slab-column connections can be achieved given the proper design proportions (relatively low gravity loads) and details. The structure experienced a maximum peak horizontal acceleration of 0.83g and vertical acceleration of 0.2g. Maximum lateral drifts reached 5.2 percent of the total height and the maximum base shear was equal to 84 percent of the weight of the structure. During the tests, the measured damping of the structure varied from two to seven percent of critical damping. Aspects of present design procedures were identified as having contributed to the over-strength of the structure. They concluded that response may have been less favorable under bidirectional horizontal base motions and further research on this topic was recommended.

1.3.4 Progressive Collapse

Hawkins and Mitchell examined factors influencing the initiation and propagation of progressive collapse in flat plate structures. They concluded that the failure of an interior column is the most likely mechanism to trigger such collapse. The progressive collapse spreads because the capacities in combined moment and shear of the surrounding slab to column connections are inadequate to carry the additional forces placed on them. Designing the slab for higher live loads is a fundamentally unsatisfactory procedure for guarding against progressive collapse. Integral beam stirrup reinforcement in the slab may be used to prevent catastrophic shear failure but is considered impractical by many engineers. Hawkins and Mitchell recommend that a tensile membrane be provided having a capacity at least equal to the maximum loading expected during the lifetime of the structure. Only bottom reinforcement continuous through a column or properly anchored in a wall or beam should be considered effective as tensile membrane reinforcement.

To verify the effectiveness of continuous bottom reinforcement in guarding against collapse, Hawkins et al. [13] conducted residual shear capacity tests on slab-column connections after punching failure. These tests were conducted with vertical loads only. Research has not been conducted on the residual capacity of connections under combined vertical and lateral loads.

2. PROTOTYPE STRUCTURE

2.1 Description

The prototype structure after which the experimental specimens are modelled is based on the prototype structure used by Moehle and Diebold [21] in their shaking table tests and by Zee and Moehle [35] in the follow up connection tests. The only change to this original prototype structure was a minor reduction in reinforcement detailing as described in Section 2.2.1. This prototype structure is described fully by Moehle and Diebold in chapter 2 of their report [21].

The prototype structure adopted by Moehle and Diebold is a simple two story flat-plate building with edge beams (Fig. 2.1). Each story is 10 ft (3.0 m) tall measured from top of slab to top of slab. Three bays span one direction of the building, and multiple bays span the other direction. Each bay measures 20 ft (6.1 m) in both directions. A slab depth of 8 in. (203 mm) is used on both floors. An edge beam that is 18 in. (457 mm) wide by 14 in. (355 mm) deep frames into the exterior columns. All columns on both floors have a square cross section with dimension of 18 in. (457 mm). Columns are assumed to be supported on footings in stiff soil. No column capitals, drop panels, shear caps, shearheads, or slab shear reinforcement are used.

2.2 Design of the Prototype Structure

A detailed explanation of the design of the prototype structure can be found in reference [21]. The prototype structure was designed to satisfy overall requirements for serviceability and strength as specified by the "Building Code Requirements for Reinforced Concrete" of the American Concrete Institute (ACI 318-83) [7]. The structure is assumed to be in a region classified as Zone No. 2 of the 1985 Uniform Building Code (UBC [32]) which is a region of moderate seismic intensity that may be expected to experience a design seismic event corresponding to Intensity VII on the Modified Mercalli Scale [4]. Wind loads for this low-rise building are not a significant factor in the design.

Service gravity loads comprise 100 psf (4790 Pa) slab self weight and 60 psf (2870 Pa) live load. Normal weight concrete with a specified compressive strength of 4000 psi (28 MPa) is assumed. The reinforcement has a specified yield strength of 60,000 psi (414 MPa).

Major aspects of slab, edge beam, and column design are outlined in the following subsections.

2.2.1 Slab

The slab thickness of 8 in. (203 mm) is established based on the minimum thickness requirements of ACI 318-83 section 9.5.3 [7]. This minimum thickness is found to be adequate for all strength requirements of ACI 318-83 for both gravity and combined gravity and seismic loads.

The maximum design moments and required proportions of the slab are controlled by the factored gravity dead and live load effects as determined using the Direct Design Method of ACI 318-83 section 13.6. Because of the relatively low height of the structure, the seismic design loads have no influence on the total slab design moments.

Seismic loads have a more significant influence on connection unbalanced moments, that is, the moment that must be transferred from the slab to the column. The design of the slab connection for unbalanced moment was checked for dead, live, and seismic load combinations including those specified by ACI 318-83 section A.9, which addresses requirements for frames in regions of moderate seismic risk. The highest shear and unbalanced moments are due to the load combination specified by section A.9.3 of ACI 318-83 in which twice the seismic load effect is combined with gravity loads. Details of the requirements are in reference [21].

Slab reinforcement is arranged as required by ACI 318-83 section 13.4, and section A.9.6 for beamless slabs in regions of moderate seismic risk. Briefly, the specified details require that reinforcement be banded near the columns and that minimum top and bottom bar continuity be provided.

The original prototype structure used by Moehle and Diebold [21] provides a slab reinforcement detail which is in addition to the requirements of ACI 318-83. Four short bars of 18 in. (457 mm) in length are placed at the bottom of the slab directly over the interior columns for both directions. Zee and Moehle [35] also kept this detail in their interior connection specimen. The results of experimental tests by these researchers show no significant behavioral influences due to the presence of these extra bottom bars. Because such detail is not commonly used in construction practice and adds to congestion at the connection, it was not included in the present study. This action had no effect on the other design aspects of the

prototype structure.

2.2.2 Column

Columns are designed to ensure that their strengths would exceed the unbalanced moment capacity of the slabs at all connections in accordance to the weak-beam strong-column seismic design philosophy. Details follow recommendations of ACI 318-83 for frames in regions of moderate seismicity.

2.3 Alternative Prototype Structures

In designing this study it was necessary to select a specific prototype structure after which the experimental specimens are modelled. To take advantage of the data and experience of previous research it was decided to use the prototype structure chosen by Moehle and Diebold [21]. This does not mean that the results of this study are valid only for this particular prototype structure. It is possible to generalize and assume a large range of alternative prototype structures for which the modelling of the experimental specimens of this study would remain valid.

Fig. 2.2 shows some of these alternative prototype structures. For the experimental specimens to remain valid, it is necessary that the material properties and basic geometry of the prototype structure remain the same. It is assumed that the structures in Fig. 2.2 are located in seismic Zone No. 4 of the UBC code [32] and lateral seismic forces are resisted mainly by the shear walls or ductile moment resistant frames. Given this latter assumption, the slabs are designed mainly to carry vertical loads, and design assumptions are the same as those required for the prototype shown in Fig. 2.1. The assumption that the slabs can be designed solely for gravity loads is common in west coast design practise. The validity of this assumption will be evaluated in this study.

3. TEST SPECIMENS

3.1 Introduction

This chapter describes the test specimens of the present study. The test specimens are reduced scale models of interior slab-column subassemblages of the prototype structure described in Chapter 2. Four nominally identical test specimens were constructed and are designated as Specimens 1, 2, 3, and 4. A fifth specimen was tested by repairing Specimen 4. It is designated as Specimen R and is described in Section 3.7.

3.2 Modelling

The purpose of the experimental program is to study the behavior of typical interior slab-column connections subjected to lateral loading. To carry out the experimental program economically, a scaled model of the interior slab-column subassemblage is used. The relation of the test specimen to the prototype is shown in Fig. 3.1.

The test specimen designed for this study is 60 percent of full scale. At this scale, the 20-ft (6.1-m) bay length of the full scale prototype structure is scaled down to 12 ft (3.66 m), the 10-ft (3.05-m) story height is scaled down to 6 ft (1.83 m), and the 8-in. (203-mm) slab thickness is scaled down to 4.8 in. (122 mm). No. 5 (16 mm) bars that are used throughout the full scale prototype slab scale down to No. 3 (10 mm) bars in the test slab. One advantage of the scale chosen for the test specimen is that it permits concrete mixes with regular aggregate sizes that are typically used in construction practise. The use of pea gravel concrete as in past research [21,35] was not necessary.

Fig. 3.1 depicts the idealization of the interior slab-column subassemblage. Under lateral loading, a simple portal frame analysis model for an elastic structure has points of inflection at column mid-heights and at slab mid-spans. This assumption is verified very closely in the analysis of the prototype structure [21] using a direct stiffness structural analysis program. Therefore, by taking cuts at these inflection points, an interior slab-column subassemblage can be obtained that behaves similarly under lateral loading to its corresponding interior connection in the full structure (Fig. 3.1). The column of the subassemblage extends above and below the slab to story mid-height. The bottom of the column is pinned and lateral load

in the form of a concentrated load is applied at the top of the column. The slab edges have roller supports located at the corners and mid-points.

There is a good deal of past experience and analytical research to validate this method of modelling for interior slab-column connections. Allen [5] shows analytically that the replacement of the lines of symmetry by free edges made only small differences to the moment rotation stiffness of elastic plates (approximately 2 percent). Mulcahy and Rotter [23], using elastic finite element analyses on slabs, indicate that the replacement of lines of symmetry and antisymmetry by point supports would change the moment-rotation stiffness by only 3 percent. Cracking around the column will make this stiffness even less sensitive to the experimental boundary conditions. Aalami [2] shows that extrapolating the behavior of a single slab-column subassemblage to the behavior of the complete slab system is a realistic procedure.

3.3 Description

A drawing of the test specimen is shown in Fig. 3.2. The thickness of the slab is 4.8 in. (122 mm). To accommodate the installation of the slab edge support assemblies, an additional 6-in. (152-mm) slab overhang is added. Thus the overall plan dimension of the slab is 13 ft (3.96 m) by 13 ft (3.96 m). The eight edge support assemblies (Chapter 4) are fitted through 1-in. (25.4 mm) diameter steel tubes embedded along the sides of the slab.

The column of the test specimen is located at the center of the slab and has a cross section of 10.8 in. (274 mm) by 10.8 in. (274 mm). It extends 3 ft (0.914 m) above and below the slab (Fig. 3.2). To attach both ends of the column to the test apparatus, four 1-in. (25.4-mm) diameter A325 bolts are embedded 13 in. (330 mm) into the concrete at each end of the column. The bottom of the column is fitted with a 1-3/8-in. (35-mm) thick steel plate, and the top of the column has a 1-in. (25.4-mm) thick steel plate.

The materials specified for the test specimen are typical of those used in construction practice. The concrete specified for the slab and column is 4000-psi (28 MPa) normal weight concrete with 1-in. (25.4-mm) maximum aggregate size. The reinforcement has a specified yield strength of 60,000 psi (414 MPa). The actual measured properties of the materials are given in Section 3.6.

The total volume of the test specimen is approximately 73 cubic ft (2.07 cubic m). The total weight

of the test specimen is estimated at approximately 11,000 lbs (4990 kg).

3.4 Reinforcement

3.4.1 Slab

All slab reinforcement is No. 3 (10 mm) Grade 60 (414 MPa) deformed rebar. The top slab reinforcement layout is shown in Fig. 3.3 and is symmetric about both centerline axes. Top reinforcement is concentrated at the slab-column connection region where the spacing is 3 in. (76 mm) between bars. Further away from the connection region the bar spacing increases to 4.5 in. (114 mm) and 9 in. (229 mm). The top reinforcement percentage varies from a maximum of 0.76% at the center of the slab to a minimum of 0.25%. There are 35 top bars in each direction of which 12 are cut off at a distance of 4 ft (1.22 m) from the center of the column. The cut off point is determined based on moment and development length requirements. All continuous top bars running to the edge of the slab are provided with 180 degree hooks for anchorage (Fig. 3.4). To ensure the integrity of the supporting edges, an additional continuous bar is placed parallel to each slab edge.

Figure 3.5 shows the bottom slab reinforcement layout which is symmetric about both center line axes. The bottom bars are spaced at 9 in. (229 mm) throughout the slab except at the edges. 27 bars span each direction with 8 of them stopping at a distance of 5 ft (1.52 m) from the slab ends. All bottom bars are provided with 180 degree hooks for anchorage at the slab edge and additional bottom bars are placed parallel to the edges. Note that two continuous bottom bars are placed directly over the column. This detail is recommended [14] to prevent progressive collapse of the slab.

A cross section of the slab reinforcement detail is shown in Fig. 3.4. The nominal clear cover for the slab reinforcement is 0.45 in. (11 mm). Since the N-S top bars and E-W bottom bars are placed in the inner layers, they have a larger nominal clear cover of 0.825 in. (21 mm).

3.4.2 Column

The column reinforcement detail is depicted in Fig. 3.6. Twelve No. 7 (22 mm) Grade 60 bars run continuously from top to bottom in the column, providing a reinforcement percentage of 7.1%. The 22

column stirrups are fabricated from No. 2 (6.4 mm) plain bars. The first stirrup is spaced at 1.5 in. (38 mm) from the face of the slab, then the spacing is uniform at 3.5 in. (89 mm). A closer spacing of 2.5 in. (64 mm) is used at the column ends to provide better confinement for the embedded bolts. The nominal clear cover for the column reinforcement is 0.6 in. (15 mm).

The column reinforcement in the test specimen does not follow the design of the two story flat-plate prototype structure described in Chapter 2 [21]. A higher reinforcement percentage is provided to minimize the effect of column deformations during testing and to ensure adequate strength when the test specimen is lifted to the test site.

3.5 Construction

Test specimens were constructed and cast in pairs so that the same material properties would exist when comparing the effects of uniaxial versus biaxial lateral loading. Specimens 1 and 2 were first constructed simultaneously, followed by Specimens 3 and 4. For both sets of specimens, the same forms and construction procedure were used with only minor modifications. The forms were basically platforms made of 3/4-in. (11-mm) thick plywood supported on timber frames. The column forms were also made of plywood and were bolted together.

After the forms were set up and oiled, the column reinforcement cages were constructed and installed. This was followed by the placement and tying of the slab reinforcement. Reinforcement chairs supported the top bars and short pieces of steel bars provided the cover for the bottom bars. Concrete was delivered in a ready-mix truck and placed using a bucket supported by a crane in the testing lab. The concrete was vibrated by hand and by vibrators clamped to the column forms. The slab surfaces were finished by the lab technicians. A wet cure was achieved by covering the specimens with wet burlap and plastic for 14 days. Column forms and the slab edge forms were stripped at the end of the wet cures.

A photograph of two test specimens is shown in Fig. 3.7. Steel cables are used for lifting the specimens before and after testing. For Specimens 3 and 4, some honeycombs appeared in the columns due to inadequate vibration (Fig. 3.8). Grout was applied to patch up the columns and this did not have a significant effect on the behavior of the specimens during testing.

3.6 Material Properties

3.6.1 Concrete

The concrete mix was designed by Carl R. Sundquist P.E., Manager of Quality Control, Kaiser Sand & Gravel Company of Walnut Creek, California. The mix design is shown in Table 3.1 and was specified at 4000 psi (27.6 MPa) in 28 days, 1-in. (25.4-mm) maximum aggregate size, and 4-in. (102-mm) slump. Zeecon R40 was added to improve workability.

A number of standard 6-in. by 12-in. (150 mm by 305 mm) test cylinders were cast with the specimens, and concrete strengths were monitored at 7, 14, 21, 28 days, and at the time of testing. Compression tests and splitting tension tests were performed following ASTM C39-72 and C496-71 specifications. The final material properties of the concrete at the time of testing are tabulated in Table 3.2. Specimens 1 and 2 had a mean compressive strength of 4825 psi (33.3 MPa), and a mean tension strength of 570 psi (3.93 MPa). Specimens 3 and 4 had a mean compressive strength of 4550 psi (31.4 MPa), and a mean tension strength of 540 psi (3.72 MPa). The tangent modulus and 45% secant modulus of the concrete are also tabulated in Table 3.2. A typical measured stress-strain curve of the concrete is shown in Fig. 3.9.

3.6.2 Reinforcement

Tensile tests of the reinforcement (not machined) were performed according to ASTM A615-85, except a gage length of 2 in. was used. A typical measured stress-strain curve is shown in Fig. 3.10. The material properties of the reinforcement are tabulated in Table 3.3. The steel has a mean yield stress of 68,440 psi (472 MPa) and a mean tensile strength of 106,430 psi (734 MPa).

3.6.3 Grout

Damp Pack is the product name of the grout supplied by the Burke Company of Oakland, California. It is a blend of special Portland cements, precisely graded silica sands, and proprietary components. It features non-shrink performance and high early strength. According to laboratory test data supplied by the Burke Company, Damp Pack has a 25% flow at 5 drops, a final set time of 80 minutes, and a 28-day compressive strength of 13759 psi.

3.7 Repaired Specimen

To observe the behavior of a repaired slab-column connection under lateral loading, a fifth specimen, Specimen R, was tested. Specimen R was constructed by repairing Specimen 4.

A simple repair method commonly used in construction practice was adopted after Specimen 4 was tested to failure. The Burke Company of Oakland, California, was consulted to provide the materials and procedure for the repair of Specimen R. All damaged concrete in the connection region of the slab was removed by a technician using a cold chisel and hammer. A void was created at the slab-column connection. The surfaces of the broken concrete and the exposed reinforcement were cleaned with a high-pressure air hose and then a coat of epoxy was applied. High-strength grout was packed in the connection void to replace the damaged concrete. The epoxy coating provided a strong bond between the original concrete and high-strength grout. After the surface of the grout was finished, the repaired region of the slab was wet cured for three days. Five 3-in. by 6-in. (75-mm by 150-mm) cylinders were also cast to monitor the strength of the grout. At the time of testing, the compressive strength of the grout reached a mean value of 7345 psi (50.6 MPa).

4. TESTING

4.1 Objectives

The four main objectives of the testing program are:

- (1) To compare the behavior of interior slab-column connections under biaxial lateral loading versus uniaxial lateral loading.
- (2) To investigate the effect of gravity loads on the lateral load behavior of interior slab-column connections.
- (3) To study the post-failure behavior of slab-column connections and to assess the adequacy of reinforcement detailing to prevent collapse.
- (4) To investigate the behavior of a repaired slab-column connection.

In order to achieve these objectives, five tests were conducted in the Structural Testing Laboratory of the Department of Civil Engineering, University of California at Berkeley. These tests are tabulated in Table 4.1.

Tests 1 and 3 are nominally identical uniaxial lateral tests, but with different levels of gravity load applied. Test 1 has a gravity load that produces an average shear stress of approximately $1.4\sqrt{f'c}$ psi on the critical section of the slab-column connection. Test 3 has a lower gravity load that produces a stress of $0.88\sqrt{f'c}$ psi on the critical section. The critical section is defined according to ACI section 11.11.1.2 [7] at a distance $d/2$ from the perimeter of the column.

Test 2 is similar to Test 1 in all respects except that lateral load is applied biaxially. Both the level of gravity load and material properties of the specimens for Test 2 and Test 1 are nominally identical. Likewise, Test 4 is the biaxial companion of Test 3. The methods used in the tests to apply uniaxial and biaxial lateral loads are described in Section 4.4.1.

Test 5 is a test of a repaired specimen. After the completion of Test 4, Specimen 4 was repaired as described in Section 3.7 and retested. Test 5 is a biaxial test with the same level of gravity load as Test 3 and Test 4.

4.2 Test Setup

Figure 4.1 is a drawing of the overall test setup. Details of Fig. 4.1 are shown in Figs. 4.2 to 4.4. The test setup is designed so that a slab-column specimen can be tested under uniaxial or biaxial lateral loading while a constant level of gravity load is maintained.

The test specimen is supported at the base of the column and at the slab edges (Fig. 4.1). A universal bearing is used at the base of the column to allow rotation in all direction (Fig. 4.2). Between this bearing and the test floor is a vertical hydraulic jack with a capacity of 100 kips (445 KN). The vertical jack is used to simulate gravity loads (Section 4.4.1). The horizontal reaction of the column base is resisted by steel struts located on the east and south side of the column (Fig. 4.2). These steel struts transfer the reaction forces to steel beams anchored to the floor and are pinned on both ends to allow for vertical movement of the base as the column is jacked up. The edges of the slab are supported by eight transducer struts that are described in the Section 4.2.1. The transducer struts provide an effective roller support for the slab edges.

Lateral loading is applied at the top of the column by two hydraulic actuators with capacities of 100 kips (445 KN). The east-west actuator is supported by a steel frame anchored to the test floor on the east side of the specimen (Fig. 4.1). The north-south actuator is supported on a steel column fixed to the side of a concrete reaction block located on the north side of the specimen. The two actuators are fitted with load cells and are connected to the top of the column through a universal bearing that enables the bi-directional application of lateral loading (Fig. 4.3).

A torsional restraining frame, described in Section 4.2.2, stabilizes the test specimen. Section 4.3 describes the T-shape instrumentation frame installed above the slab.

4.2.1 Transducer Struts

The edges of the test specimen are supported by eight transducer struts located at the corners and mid-way points of the slab edges (Fig. 4.1). Not only do they model the roller supports for the slab boundary conditions, they are also instrumented to measure the level of vertical load and serve as a check for the magnitude of lateral loading.

A transducer strut consists of universal bearings and a steel tube with strain gauges glued to the surface (Fig. 4.4). The outside diameter of the steel tube is 1-3/4 in. (44.5 mm) and the wall thickness is 3/8 in. (9.5 mm). Four electrical resistance strain gauges (CEA-06-125UN-120) with a gauge length of 1/8 in. (3.18 mm) and a maximum strain capacity of 0.05 are glued at the mid-length of the steel tube. They are wired to form a 4-Active Arm Wheatstone Bridge. This type of transducer measures pure axial loads and compensates for the effects of temperature, torsion, bending, and Poisson's ratio. The strain gauges are covered with sheet metal for protection. Prior to installation, a transducer strut is calibrated under tension and compression in a universal testing machine.

The ends of a transducer strut are fitted with spherical rod-end bearings that permit bi-directional movement of the slab (Fig. 4.4). The top rod-end bearing is bolted to a clevis and threaded-rod assembly that is connected through steel tubes embedded in the slab. A transducer strut is anchored to a steel floor beam below by the same clevis and threaded-rod assembly.

Under lateral loading, sources of error are introduced in the transducer strut as it sways about its base. As the transducer strut inclines, vertical displacements are introduced and a horizontal reaction component is created at the ends. Another source of error is the axial deformations of the strut when it is loaded. Zee and Moehle [35] show that all these sources of error are negligible for the levels of lateral displacement the test specimen experiences and therefore can be ignored.

4.2.2 Torsional Restraining Frame

The use of universal bearings for the column supports and transducer struts results in a test specimen that is unstable in the in-plane torsional direction. To counteract this rigid-body twisting of the test specimen when lateral loads are applied, a torsional restraining frame is attached to the west side of the slab (Fig. 4.1).

The torsional restraining frame is a space truss structure combined with steel struts. Its overall dimensions are 12 ft (3.65 m) in length, 2 ft (0.61 m) in width, and 3 ft (0.91 m) in height. The truss is made of 2-1/4 in. x 2-1/4 in. x 3/8-in (57-mm x 57-mm x 9.5-mm) steel angle sections. The steel struts are identical to the transducer struts described in Section 4.3.1 fitted with spherical rod-end bearings. Steel

struts are also used to connect the torsional restraining frame to the north-west and south-west corners of the slab. The torsional restraining frame is designed to allow unrestrained bi-directional translation of the slab, but to restrain twist.

4.3 Instrumentation and Data Recording

The test specimen is instrumented as shown Fig. 4.5 to obtain data on lateral and vertical forces, slab displacements, slab rotations, reinforcement strains, and secondary displacements. Instrumentation is categorized as follows:

(a) Lateral Loads

Lateral loads applied to the top of the column are measured by load cells attached to the actuators (Fig. 4.5). Prior to testing, these load cells were calibrated in a universal testing machine.

(b) Column Displacements and Deformations

X-Y lateral displacements at the top of the column are measured by positional transducers located on the west and south side of the specimen (Fig. 4.5). Each positional transducer has a range of ± 8 in. (± 190 mm) and is connected by stainless-steel wire between the top of the column and a "fixed" reference point in the laboratory. Displacements at the base of the column relative to the laboratory floor are monitored by three linear potentiometers. One vertical and two lateral components of displacement are measured by these potentiometers as shown in Fig. 4.5.

At the bottom of the top column, three linear voltage displacement transducers (LVDTs) are attached to monitor the biaxial deformations of the column. The LVDTs are clamped to an aluminum collar mounted on the column concrete and are targeted to aluminum blocks epoxied to the top surface of the slab. Details are in Fig. 4.6.

(c) Gravity Loads

Gravity (vertical) loads are measured by eight transducer struts supporting the slab edges. Refer to Section 4.2.1 and Section 4.4.1 for details.

(d) Slab Connection Rotations

On each side of the slab-column connection, LVDTs are attached to the top and bottom surface of the slab to measure rotations of the slab connection (Fig. 4.6). These LVDTs are mounted on aluminum stands glued to the slab surface at a distance equal to the slab thickness, h (4.8 in. (122 mm)), from the face of the column. Targets for the LVDTs are mounted on aluminum collars attached to the column. Rotations of the slab relative to the column are deduced using readings from these instruments.

(e) Slab Displacement and Twist Profiles

An instrumentation frame is mounted above the slab in order to measure vertical displacements and rotations along the west and south sides of the slab (Fig. 4.1). It is supported on spherical bearings and braced so that it remains undeformed and horizontal, but translates with the slab during testing. Installed on the instrumentation frame are four LVDTs and eight clip gauges. Vertical displacements at the slab centerline are calculated by taking the average displacements of two opposite LVDTs or clip gauges. Slab twists at the centerline are calculated by dividing the absolute sum of these two displacements by the horizontal distance between them. This horizontal distance was set at $c+d$, which is equal to 14.8 in. (376 mm).

(f) Rigid-Body Torsion

To check the effectiveness of the torsional restraining frame (Section 4.2.2), three linear potentiometers are located on the north side and north-east corner of the slab to measure the amount of in-plane rigid-body torsion of the slab (Fig. 4.5).

(g) Reinforcement Strains

Figures 4.7 and 4.8 show the locations of strain gauges glued to the reinforcement for the uniaxial tests (Test 1 and 3). Figures 4.9 and 4.10 show the locations for the biaxial tests (Test 2 and Test 4). All strain gauges are electrical resistance type gauges (CEA-06-125UN-120) with a gauge length of 1/8 in. (3.18 mm) and a maximum strain capacity of 0.05. The strain gauges were water-proofed with an epoxy resin.

All experimental data were recorded on a Data General Nova computer through a high speed data acquisition system. Throughout each test, selected instruments were monitored on a Tektronix terminal. X-Y plotters were used to monitor lateral loads and deflections at the top of the column.

4.4 Testing Procedures

This section outlines the testing procedures. The procedures were identical in all five tests except for minor modifications.

(1) *Specimen Lifted to Test Site*

After a test specimen is cast and cured, it is lifted from the formwork to the test site by an overhead crane using a cable attached to the top of the column. Before the top of the column is hooked to the crane and lifted, four 1/2-in. (12.7-mm) diameter steel cables are installed from the corners of the slab to the top of the column and hand-tightened. These cables help to support the slab self-weight and reduce stresses in the slab during the lifting operation. At the test site, the base of the column is first placed on the universal bearing located above the vertical jack, and then the slab edges are attached to the eight transducer strut supports (Fig. 4.1). The slab is temporarily clamped to the two reaction frames that support the actuators and the bottom universal bearing is blocked to stabilize the specimen during the test setup operations.

(2) *Set Up Specimen for Testing*

The transducer strut supports are balanced to level the slab, then the torsional restraining frame is attached to the west side of the slab (Fig. 4.1). To facilitate monitoring of cracking during testing, the entire specimen is white-washed with diluted latex paint and grid lines spaced at 6-in. (152-mm) intervals are drawn on the top and bottom surfaces of the slab. After the instrumentation frame (Section 4.3) is installed above the slab, the horizontal actuators are attached to the top of the column. The horizontal actuators and vertical jack are connected to manually controlled hydraulic pumps.

(3) *Install Instrumentation*

Instrumentation (Section 4.3) that measures the response of the specimen are wired, calibrated, checked, and installed onto the test specimen. The data acquisition system, plotters, and other instrumentation monitors are set up.

(4) *Testing*

The temporary clamps and blocks are removed to begin testing. All instrumentation and data acquisition

is rechecked and zeroed. The first stage of testing is the simulation of gravity load that is performed by jacking up the vertical hydraulic jack under the column. For Tests 1 and 2, lead blocks are also placed on the slab prior to testing to simulate part of the gravity loading. During the vertical jacking operation, the level of gravity load is monitored on the data acquisition terminal screen. After the target gravity load is achieved, the second stage of testing begins with the pumping of the horizontal actuators to apply lateral loads at the top of the column. Section 4.4.1 describes in more detail the application of gravity and lateral loading. During testing, data are collected at appropriate intervals, the level of gravity load is monitored and held constant, cracks on the slab surfaces are marked and recorded, and any vertical movement of the instrumentation frame is checked with a surveyor's theodolite.

(5) *Post-Failure Investigation*

When the first punching shear failure occurs in the slab-column connection, testing is stopped, the specimen is inspected, and photos are taken. To investigate the post-failure behavior of slab-column connections, lateral loading is continued for a few more cycles. To assess the effectiveness of detailing and the residual capacity of connections, additional vertical loads are applied gradually through the vertical jack below the column. The specimens were not tested to collapse to avoid damaging the transducer struts.

(6) *End of Test*

After the instrumentation is removed, the specimen is disconnected from the test setup and lifted out. The test site and setup are prepared for the next test.

4.4.1 Loading

Two types of loading are applied to the specimen during testing - gravity and lateral. This section describes in detail the application of these loads.

(a) Gravity Loading

In addition to the self weight of the specimen, additional gravity load is induced by jacking up the vertical hydraulic jack located below the column (Fig. 4.2). For Tests 1 and 2, lead blocks are also added on the slab to simulate additional gravity loading.

The simulated gravity shear force in the slab-column connection can be calculated by simple statics as the sum of the forces in the transducer struts, the slab self-weight, and any additional lead blocks. For Tests 1 and 2, the total gravity shear force applied is approximately 23 kips which is equivalent to a condition in the prototype structure with the full dead and design live loads. For Tests 3, 4 and 5, the total gravity shear force is approximately 14 kips which is equivalent to the full dead load only. When lateral load is applied to the specimen, the slab-column connection cracks and deteriorates, resulting in the redistribution and decrease of the simulated gravity shear. Therefore, to maintain a constant level of gravity shear, the transducer struts are monitored continuously during testing and additional gravity load is added as needed by the vertical jack.

For Tests 1 and 2, 48 lead blocks, each weighing an average of 98 lb (436 N), are placed symmetrically on the slab as shown in Fig. 4.1. Elastic finite element analyses of the slab determined the locations of the lead blocks in order that the ratio of the moment to shear at the slab critical section are modelled approximately. The two layers of lead blocks are placed on rubber pads so that the stiffness and crack propagation of the concrete slab would not be affected. Due to the boundary conditions of the specimens it is only possible to obtain an approximate modelling of gravity moments. Chapter 6 further discusses the modelling of gravity loads.

(b) Lateral Loading

Lateral load is applied at the top of the column by manually controlled hydraulic actuators (Fig. 4.1). Displacement is controlled by manually operating pump pressure. Horizontal displacements at the top of the column are monitored during testing by the two positional transducers described in Section 4.3. These positional transducers are also connected to calibrated voltmeters to obtain continuous digital readouts of column displacements. With the north-south actuator locked, uniaxial lateral loading was applied to Tests 1 and 3 by the east-west actuator. Both actuators were used to apply biaxial lateral loading in Tests 2, 4, and 5.

Uniaxial Lateral Loading

The lateral displacement history adopted for the uniaxial tests is shown in Fig. 4.11. The aim of the displacement history is to subject the test specimen to a broad range of lateral loading, simulating

conditions that the prototype structure can be expected to experience. These include low-level wind loading to severe seismic excitation. The displacement history is divided into five cycle sets with target displacements of 0.16 in. (4.06 mm), 0.31 in. (7.87 mm), 0.62 in. (15.7 mm), 1.25 in. (31.8 mm), and 2.50 in. (63.5 mm). These cycle sets are denoted by their equivalent drifts: 0.2%, 0.4%, 0.8%, 1.6%, and 3.2%.

Figure 4.11 also traces out one cycle of the uniaxial lateral load pattern on a typical load-displacement curve. From the initial undeformed state, the top of the column is pulled eastward until the target displacement of the cycle set is reached (steps 1 and 2 in Fig. 4.11). Then the direction of the load is reversed and the column is pushed westward to the reverse target displacement (2-3). Then the column is pulled backed to its initial undeformed state (3-4). The cycle is then repeated to complete a cycle set. For the 0.8%, 1.6%, and 3.2% cycle sets, one extra cycle of the previous cycle set is added. The purpose of this is to study degradation of the specimen after larger cycles.

Biaxial Lateral Loading

For biaxial loading, a lateral displacement history analogous to the uniaxial case was adopted so that an equivalent comparison can be made between biaxial and uniaxial tests (Table 1). The same five cycle sets and target displacements of the uniaxial case are used, but applied in a bi-directional pattern which consists of increasing and decreasing lateral loading combinations (Fig. 4.11). Because of its resemblance, this biaxial load pattern with its four quadrant loops (1-14) is often referred to as a "clover leaf" pattern.

Figure 4.12 separates the biaxial load pattern into its east-west and north-south components. These are used during testing to coordinate the movements of each actuator. When constant displacement is required, the actuator pump is turned to neutral and locked. Figure 4.12 also traces out for each direction the biaxial load path on typical load-displacement curves. One cycle set is equivalent to one completed biaxial load pattern (1-14). For the 0.8%, 1.6%, and 3.2% cycle sets, an extra biaxial load pattern of the previous cycle is added. Note that when the displacement in one direction is held constant as displacement in the orthogonal direction is activated, the peak load decreases (i.e. Fig. 4.12, E-W Load vs. Displacement, step 2-3). This is typical for biaxial behavior since loading in one direction interacts with the orthogonal direction that results in a decrease of stiffness and strength.

5. EXPERIMENTAL RESULTS

5.1 Introduction

This chapter presents the experimental results of the five tests described in Chapter 4. Figure 5.1 shows a schematic drawing of the selected experimental results which include: lateral load vs. drift, connection shear, slab connection rotation, column rotation, and slab displacement, rotation, and twist profiles. Also presented in this chapter are slab reinforcement strains, in-plane slab torsion, post-failure behavior, and crack patterns. The experimental data presented serve as a basis for analysis and interpretation in subsequent chapters.

All experimental data from the five tests are stored on magnetic tapes. Appendix A lists and describes each recorded channel number.

5.2 Sign Convention

The orientation of the test specimen is indicated in Fig. 4.1 (a). East-west lateral load and drift are positive when directed towards the east. North-south lateral load and drift are positive when directed towards the north. Slab displacements are positive in the upward vertical direction. Slab rotations along the west and south centerlines are clockwise positive when viewed from the south and west, respectively. Thus, positively increasing slab rotation is normally associated with positively increasing vertical displacements or lateral loads. Slab twist is clockwise positive when viewed from the center of the column. Thus, positive drift and twist usually occur simultaneously. Positive slab moments correspond to tension on the top surface of the slab and produce positive slab connection rotations. Tension in the reinforcement corresponds to positive strain.

5.3 Lateral Load versus Drift

Figures 5.2 to 5.6 present the lateral load versus drift data of Tests 1 through 5 (See Table 4.1 for information on the specimen number, the number of lateral load directions, and the level of vertical load). Tests 1 and 3 (Figs. 5.2 and 5.4) are uniaxial tests and no north-south lateral load versus drift data are presented. The bottom horizontal axis of Figs. 5.2 to 5.6 is the drift displacement which is defined as the

relative horizontal displacement between the top and base of the column (Fig. 5.1). The top horizontal axis is the drift percentage which is equal to the drift displacement divided by the height between the top and base of the column (Fig. 5.1). The vertical axis is the lateral force in kips applied at the top of the column measured by load cells attached to the horizontal actuators (Fig. 4.5).

All tests experienced a sudden punching shear failure in the slab-column connection region. Tests with the higher vertical load applied (Figs. 5.2 and 5.3) failed at lower levels of lateral load and drift than their companion tests with less vertical load (Figs. 5.4 and 5.5). Specimens with low connection shear (Figs. 5.4 and 5.5) exhibit pinching in their hysteresis curves and display a high degree of yielding. Specimens with high connection shear (Figs. 5.2 and 5.3) show less of this pinching phenomenon and yielding behavior. All tests show an increasing level of stiffness degradation at higher drift levels as can be seen by comparing the second loop with the first of each drift cycle.

Compared with their companion uniaxial tests, the biaxial tests show decreased strength and stiffness. The biaxial tests (Figs. 5.3, 5.5, and 5.6) also exhibit drops in the applied lateral force at their displacement peaks. This behavior is due to biaxial loading which reduces the peak lateral resistance in one direction when lateral load in the orthogonal direction is applied (Section 4.4.1 (b)).

Figure 5.6 shows the results of the repaired specimen (Section 3.7). The curves display a significant decrease in strength and stiffness as compared with the original specimen (Fig. 5.5). However, it should be noted that the repaired specimen does sustain the original maximum drift capacity.

5.3.1 Post-Failure Behavior

After shear failure occurred in each test, the test specimen was loaded laterally for a few more cycles to investigate its post-failure behavior. A typical example is shown in Fig. 5.7 which depicts the post-failure behavior of Test 2. It is important to note that although "failure" had occurred, the specimen still has some lateral resistance. More importantly, the slab-column did not collapse and was still capable of sustaining gravity loads.

In order to test the effectiveness of the continuous bottom reinforcement detailing in preventing progressive collapse (Section 3.4.1), additional vertical load was added after punching failure. This additional

load was applied by the vertical jack below the column base and was monitored by the transducer struts. As Fig. 5.8 shows, the slab-column connection of Test 1 was capable of carrying higher vertical loads even after punching failure.

5.4 Connection Shear

Figures 5.8 to 5.12 plots the slab-column connection shear history for the five tests. The connection shear is calculated by summing the reactions of the transducer struts (Section 4.2.1), the self-weight of the concrete slab, and any loads from the lead blocks (Section 4.4.1 (a)). The goal during each test was to maintain a constant level of connection shear in order to achieve an accurate simulation of the conditions in the prototype structure. This was effectively accomplished as Figs. 5.8 to 5.12 show.

Figures 5.10 and 5.11 show a greater variability in the level of connection shear than Figs. 5.8, 5.9, and 5.12. This can be explained by the fact that variability in connection shear is mainly due to the level of imposed lateral loads. Tests 3 and 4 experienced significantly higher lateral loads than Tests 1, 2, and 5. The greater lateral load made maintaining a constant level of shear more difficult during testing. Lateral loads decrease the stiffness of the slab-column connection, thereby transferring shear to the slab edge supports.

The time of shear failure can be identified in each test by a sharp drop in connection shear. To investigate the collapse capacity of the slab specimen, Tests 1, 2, and 3 were reloaded after shear failure as shown in Figs. 5.8 to 5.10. As noted in the previous section, the slab specimen is capable of sustaining gravity loads in excess of the original loads.

5.5 Slab Connection Rotation

Figures 5.13 through 5.17 present plots of the total slab moment against the slab connection rotation relative to the column (Fig. 5.1). The slab connection rotation is measured at a distance d away from the column face and is obtained from LVDT measurements attached to the top and bottom slab surfaces (Section 4.3 (d)). The total slab moment is the moment across the entire slab section taken at the column face. It is calculated by summing moments of the three transducer struts on the side where the section is taken and adding moments due to the self-weight of the slab and lead blocks. For the biaxial tests (Figs. 5.14,

5.16, and 5.17), slab connection rotations of all four sides of the connection are presented. For the uniaxial tests (Figs. 5.13 and 5.15), only the east and west sides, where significant slab connection behavior occurred, are presented.

The biaxial tests (Figs. 5.14 and 5.16) have lower slab rotation capacities than their companion uniaxial tests (Figs. 5.13 and 5.15). This can be explained by the more significant interaction of torsion at the slab connection due to biaxial loading. Particularly evident in Figs. 5.13 and 5.14, yielding of the connections results in the tendency for slab rotation residuals to develop at higher displacement cycles. The repaired specimen exhibits very low slab connection stiffness (Fig. 5.17).

5.6 Column Rotation

In all tests, the column generally behaved elastically as shown in Fig. 5.18 for Test 3. Column rotation is measured for a height equal to the column width, c , above the top slab surface (Fig. 5.1). The column moment in Fig. 5.18 is the average moment in the column rotation region.

5.7 Slab Displacement, Rotation, and Twist Profiles

Figures 5.19 through 5.22 present for Tests 1 to 4 the following profiles along the slab's west and south centerlines: (a) displacement, (b) slab rotation, and (c) slab twist (Fig. 5.1). These experimental data are derived from measurements made from the instrumentation frame described in Section 4.3 (e). For the uniaxial tests (Figs. 5.19 and 5.21), twist along the west centerline, together with displacement and rotation along the south centerline are not presented since they do not experience significant changes. The instrumentation frame was not installed in Test 5.

Zero displacement, rotation, and twist correspond to the condition of the slab prior to testing. Only peak profiles of each drift cycle set (Fig. 4.11) are plotted in Figs. 5.19 to 5.22. The slab displacements at the center of the column are calculated from measurements taken at the base of the column (Fig. 4.5 (b)). Note that the increase in displacement at the column center is due to the column being jacked up periodically during testing to maintain a constant connection shear force (Section 4.4.1 (a)). Slab rotations are derived from the slab displacement profile using the center difference method. With the exception of the first point from the column center, slab twist represent measurements taken $c+d$ apart, across the slab

centerline. The first slab twist (plotted at 5.4 in. (137 mm) from the column center) only approximates the twist at the column and slab interface. It is derived from the drift displacement measurements.

Figures 5.23 and 5.24 show typical displacement and twist profile histories for one complete drift cycle set. With Fig. 5.23 representing a uniaxial test and Fig. 5.24 a biaxial test, the profile lines are numbered according to the load pattern numbering system depicted in Fig. 4.11. As expected, near symmetry is evident from load reversals.

5.8 Reinforcement Strains

Peak strain profiles for Tests 1 to 4 are shown in Figs. 5.25 to 5.28. The exact locations of the strain measurements from which these profiles are derived are shown in Figs. 4.7 to 4.10.

Strains are typically concentrated near the column. The yield strain for the No. 3 slab reinforcement is approximately 0.002 ($f_y=69$ ksi, $E_s=29,000$ ksi). All the top and bottom strain profiles of Tests 3 and 4 (Figs. 5.27 and 5.28) eventually reached yield at higher drifts. In Tests 1 and 2 (Figs. 5.25 and 5.26), only the top strain profiles reached yield. The high gravity moments in those tests induce large compressive stresses at the bottom of the slab that result in low tensile strains in the bottom reinforcement. Broken strain gauges caused a number of profiles lines to be incomplete.

Figure 5.29 follows the strain profiles of a uniaxial test for one complete drift cycle set. Similarly, Fig. 5.30 shows strain profiles for a typical biaxial test. The profiles are numbered according to the numbering of the load pattern depicted in Fig. 4.11. These Figures show that when the top of the slab is in tension, relatively large reinforcement strains result because the concrete is cracked and all tension is carried by the steel. On reversal of the load, relatively low compressive strains occur because cracks close and strains are taken up by the concrete.

5.9 In-Plane Torsion

During testing, the torsional restraining frame (Section 4.2.2) successfully limited the level of in-plane torsional movement of the slab as shown typically in Fig. 5.31. The maximum value in Fig. 5.31 is 0.0013 rad. which is equivalent to a horizontal slab displacement of only 0.09 in. (2.3 mm) Compared with the maximum drift displacement of 1.25 in. (31.8 mm), in-plane torsion had a minimal effect on these tests.

5.10 Crack Patterns

The visible crack patterns on the slab surface are reproduced in Figs. 5.32 to 5.36 for each test. Cracking is more extensive for the tests with higher gravity loads (Figs. 5.32 and 5.33). Biaxial loading tends to spread the cracks more throughout the slab (Figs. 5.33 and 5.35). The bottom slab surface and column showed very little visible cracking. Shear failure of the slab-column connection is characterized by a deep top surface crack located approximately h away from the column face. The angle of the crack is relatively shallow (approximately 10 to 30 degrees) and, in many instances, the crack exposed the top slab reinforcement. Photographs of failure are reproduced in Fig. 5.37.

6. DISCUSSION OF EXPERIMENTAL RESULTS

6.1 Introduction

This chapter discusses the experimental results presented in Chapter 5. The effects of gravity load and biaxial loading on specimen behavior are first presented followed by discussions on the results of repeated load cycles, the post-failure behavior, and the behavior of the repaired specimen (Test 5). A study of the slab moments due to gravity loads is also presented. Analytical models that are used to estimate the lateral stiffness of the test specimen include the effective beam width model and the equivalent frame model [33]. Ultimate strength models include the linear stress variation method [11], the beam analogy model by Hawkins [3], and the method proposed by Park and Islam [25]. The various analytical models are discussed and compared.

6.2 Effects of Gravity Loads

Test results of the present study show that the level of gravity load on the flat slab is one of the most important factors determining the lateral behavior of reinforced concrete flat-plate connections. Previous research [3,19] has also shown evidence of this conclusion. Most failures in reinforced concrete flat-plate connections can be attributed to excessive vertical shear stresses that are induced from the applied gravity loads and unbalanced moments. Therefore, with higher gravity loads, the available shear capacity left over to resist unbalanced moments due to lateral loads is reduced.

Table 6.1 summarizes the test results of the present study. Comparing the low-gravity uniaxial Test 3 with the high-gravity Test 1, the maximum lateral force decreases from 10.02 kips to 6.62 kips, and the maximum drift decreases from 4.76% to 1.54%. Likewise, the biaxial tests (Tests 2 and 4) show a significant decrease in lateral force and drift capacity under the higher gravity load condition.

Figure 6.1 further illustrates the effect of gravity loads by comparing the lateral load versus drift envelopes. The envelopes of Fig. 6.1 are derived from the measured load-drift relations shown in Fig. 5.2 to 5.5. From Fig. 6.1, it can be observed that strength, stiffness, ductility, and drift capacity are all significantly reduced in the higher gravity load tests (Tests 1 and 2). The following figure (Fig. 6.2) compares the secant stiffness envelopes. The reduction in stiffness due to higher gravity loads is more

significant for the biaxial tests (Fig. 6.2 (b)) than for the uniaxial tests (Fig. 6.2 (a)). The effect of gravity loads on ductility and drift capacity is further discussed in Chapter 7. A related design recommendation is made in Chapter 8.

6.3 Effects of Biaxial Loading

The results of the present experimental study show that biaxial loading is another important factor influencing the lateral behavior of reinforced concrete flat-plate connections. Test results tabulated in Table 6.1 show that the maximum lateral force and drift measured from uniaxial tests are significantly reduced if biaxial loading is applied. This is evident by comparing the results of Test 2 with its uniaxial companion, Test 1, or by comparing Test 4 with Test 3.

In the east-west direction, Test 2 experiences a 21% reduction in maximum lateral strength as compared with Test 1. In the north-south direction, the reduction is even greater at 36%. Maximum drifts in the east-west direction are about the same for Tests 2 and 1 (1.51% and 1.54%), but in the north-south direction Test 2 reaches a lower drift of 1.04%. Although drifts in the east-west direction were similar for Tests 1 and 2, the biaxial Test 2 failed after a half cycle whereas Test 1 did not fail until one and a half cycles (Figs. 5.2 and 5.3)

With lower gravity loading (Tests 3 and 4) the effect of biaxial loading remains significant. In the east-west direction, the maximum lateral force for Test 4 is reduced by 4% as compared with its uniaxial companion, Test 3. In the north-south direction the reduction is 21%. Test 3 exhibits very ductile behavior and reaches a maximum drift of 4.76%. The drift capacities of Test 4 under biaxial loading are much lower: 3.22% in the east-west direction and 1.54% in the north-south direction. The number of cycles in the biaxial test is correspondingly less than in the uniaxial test.

Lateral load versus drift envelopes illustrating the effects of biaxial loading are shown in Fig. 6.3. The effect of biaxial loading is less significant when drifts are low. Figure 6.3 shows that the difference between biaxial and uniaxial behavior is small when drifts are less than approximately 0.5%.

Lateral secant stiffness envelopes are compared in Fig. 6.4. Stiffness is less affected by biaxial loading when the gravity load is low (Fig. 6.4 (b) versus Fig. 6.4 (a)). Comparing Test 2 with Test 1, the reduc-

tion in the secant stiffness due to biaxial loading range from 20% to 30%. Comparing Test 4 with Test 3, the reduction is between 2% to 10%.

The difference in the level of damage between biaxial and uniaxial loading can be observed from the crack patterns shown in Figs. 5.32 through 5.35. For the biaxial tests, cracking is more extensive in the slab-column connection region. Under biaxial loading, the combined actions of shear, moment, and torsion result in a higher rate of deterioration.

It must be pointed out that the effects of biaxial loading are also dependent on the type of biaxial load pattern the test specimen experiences. The present study is based entirely on the chosen "clover-leaf" load pattern depicted in Fig. 4.11. However, within the limitation of the present test data, it is clear that biaxial loading causes a reduction in strength, stiffness, ductility, and drift capacity.

As a matter of interest, the absolute lateral force versus drift of the biaxial tests (Tests 2 and 4) are compared with their companion uniaxial tests (Tests 1 and 3) in Fig 6.5. The absolute lateral force, P_{abs} , and absolute drift displacement, Δ_{abs} , are defined as

$$P_{abs} = \sqrt{P_{ew}^2 + P_{ns}^2} \quad (6.1)$$

$$\Delta_{abs} = \sqrt{\Delta_{ew}^2 + \Delta_{ns}^2} \quad (6.2)$$

where the subscripts "ew" and "ns" denote the east-west and north-south directions.

A close comparison exists between the absolute biaxial envelopes and their uniaxial companions when the lateral force is less than approximately 80% of the maximum value (Fig. 6.5). Since the slab reinforcement layout of the test specimens is nominally identical in both direction, Fig. 6.5 provides evidence that the behavior of reinforced concrete flat slabs is not highly dependent on direction or orientation when the applied load is low.

6.4 Repeated Load Cycles

The lateral load history adopted in the tests follows a general pattern of load cycles at one deformation level, followed by cycles at double the deformation level, then followed by repeated cycles at the original deformation level (Section 4.4.1 (b) and Fig. 4.11). The repeated cycles provide information on low-amplitude responses following high amplitudes.

The original and repeated 0.8% drift cycles of Test 3 are compared in Fig. 6.6 (a). The same information is shown in Fig. 6.6 (b) for Test 4, a biaxial test. Prior to repeating the 0.8% drift cycles, the test specimens underwent drift cycles of 1.6% (Fig. 4.11) which are not shown in Fig. 6.6. Both figures display evidence that reinforced concrete flat-plate connections experience a significant degree of stiffness degradation after large displacement cycles. The repeated 0.8% cycles possesses approximately half the stiffness of the original cycles. Ratios of original to repeated cycle secant stiffnesses (secant to peak of first cycle) are plotted for Tests 1 to 4 in Fig. 6.7.

The high degree of stiffness degradation has importance consequences for the performance of flat plates under seismic loading, particularly if the ground acceleration record includes strong shaking followed by less intense shaking. During an intense seismic event, reinforced concrete buildings can be expected to experience maximum drifts as large as 1.5% [29]. After experiencing drifts of this magnitude, Figs. 6.6 and 6.7 demonstrate that a sharp decrease in lateral stiffness would occur, adversely affecting the flat plate's performance under additional seismic excitation. Similar degradation of stiffness has been observed for other forms of reinforced concrete construction [26].

Figure 6.6 (b) also shows the effect of biaxial loading on the hysteretic behavior of slab-column connections. Lateral loads applied from one direction reduces the stiffness and strength of the orthogonal direction. Sharp drops in strength occur in the east-west direction when lateral load is applied from the north-south direction. For the original 0.8% drift cycles, the drop in peak strength range from 25% to 30%. A higher rate of deterioration due to biaxial loading is also evident by comparing the biaxial cycles shown in Fig. 6.6 (b) with its uniaxial companion (Fig. 6.6 (a)).

6.5 Post-Failure Behavior

After punching failure of the slab-column connections, lateral and vertical loading were continued to assess post-failure behavior. Although the lateral strength and stiffness capacity left over in the connection were very low, additional vertical loads could still be applied. It is concluded that bottom continuous reinforcement placed over the column (Section 3.4.1) was effective in holding up the slab. The top slab reinforcement probably also contributed to the residual load capacity of the slab-column connection. However, based on observations of the level of damage on the slab top surface and the high degree of bond

deterioration, top reinforcement should not be relied on to carry vertical loads.

Figure 5.8 shows that the slab-column connection was capable of sustaining vertical loads exceeding the factored design dead and live loads even after punching shear failure. This is particularly important for seismic design where the magnitudes of lateral loads may be high and unpredictable. In order to prevent progressive collapse, continuous bottom reinforcement should be placed over the columns for all reinforced concrete flat plate buildings.

6.6 Repaired Specimen Behavior

The ability of a repaired flat-plate structure to perform adequately under gravity and lateral loads is of great concern in terms of structural safety and the economic feasibility of repair. The present study includes Test 5 which is a test of the repaired specimen of Test 4. Section 3.7 describes how the repair was carried out.

The effectiveness of the repair can be evaluated by comparing Test 5 with the original Test 4 (Figs. 6.8 and 6.9). These figures and the maximum lateral forces tabulated in Table 6.1 show that the repaired specimen exhibits a drastic reduction in strength and stiffness. The level of lateral load and stiffness of the repaired specimen is reduced by more than one half compared with the original specimen. However, the maximum deformation capacity of the repaired specimen is approximately the same as the original specimen (Table 6.1).

The ability of the repaired specimen to retain its original drift capacity is a favorable characteristic of flat plate structures. The results of Test 5 suggest that a repaired flat-plate connection would be able to sustain without premature failure the levels of drifts that could occur under intense seismic loading. However, to make up for the loss of the original stiffness and strength, it would be necessary to stiffen and strengthen the flat-plate structure by adding shear walls or bracings.

Figure 6.8 also shows that the repaired specimen possesses different strengths in each direction. This may be due to the unequal levels of damage and yielding that occurred in the original slab specimen or due to inconsistent quality of workmanship during repair. The different strengths underscore the uncertainty involved in the behavior of a repaired connection and the necessity of providing bracings or shear walls to

strengthen the damaged structure. Further study of repair and retrofit is recommended to substantiate these conclusions.

6.7 Slab Moments due to Gravity Loads

Gravity moments greatly influence the moment transfer capacity of flat-plate connections [3]. Thus it is important to accurately determine the magnitude of gravity moments around the slab-column connection. The present study adopts a method that estimates the gravity moment distribution across the slab width based on the reinforcement strain profile. This method is similar to one used in past research [3] and is illustrated in Figs. 6.10 to 6.12 for Test 1. The measured top reinforcement strain profile under gravity load is shown in Fig. 6.10. Using the moment-strain relations of various slab sections across the test specimen (i.e. Fig. 6.11), this reinforcement strain profile is converted to a slab moment profile (Fig. 6.12 (a)). The moment-strain relation shown in Fig. 6.11 is derived analytically using a moment-curvature program that also accounts for the nonlinear material properties of steel and concrete [17]. A number of moment strain curves are derived to include all the different reinforcement arrangements across the slab (i.e. top reinforcement spacings of 3 in., 4.5 in., and 9 in.). By taking strain readings across the reinforcement strain profile (Fig. 6.10) and then reading off the slab moment from the appropriate moment-strain curve (i.e. Fig. 6.11), a point on the slab moment profile is obtained (Fig. 6.12 (a)). A check of the total gravity moment is performed by computing the area under the slab moment profile and comparing it with the gravity moment obtained by statics (summing the moments due to the self weight of the slab, lead blocks, and transducer strut reaction (Section 4.2.1)). The statical moments are 5.6% to 18.7% greater than the computed moments.

Figure 6.12 also compares the experimentally derived slab moment profiles with the results of elastic finite element analysis using 4-node shell elements (SAP80 [34]). The discrepancy that exists between these two profiles is attributed to the inelastic behavior of the slab specimen and, in particular, the effect of reinforcement that the elastic finite element solution does not take into consideration. The experimental results of Fig. 6.12 show that gravity moment is concentrated over the central region of the slab where the top reinforcement is more closely spaced (Fig. 3.3). A sharp drop in slab moment occurs at approximately 18 in. from the center of the column, the point where the top reinforcement spacing increases to 9 in. A 9-in.

spacing is equivalent to a very low reinforcement ratio, less than $200/\rho$, and as a result, slab moments near the edge of the slab are redistributed towards the center where higher flexural capacity and stiffness properties exist.

The difference between the elastic and experimental results (Fig. 6.12) indicates that the gravity load finite element simulation significantly underestimates slab moments at the slab-column connection region. For Tests 1 and 2, the actual gravity moments on the critical section are on average 37% greater than those predicted by finite element analysis (Fig. 6.12 (a)). For low gravity tests, Tests 3 and 4, the difference is less, averaging 14% greater than the elastic solution (Fig. 6.12 (b)).

Gravity moment profiles of the prototype and Test 1 are compared in Fig. 6.12 (c). Near the critical section, a close comparison exists between the scaled prototype and specimen moments that are both based on finite element analyses. Although the gravity moments derived experimentally are significantly larger than the prototype moments, this does not indicate an error in the gravity load simulation. As discussed previously, the larger experimental moment is attributed to concentration of reinforcement near the column. Similar moment concentration would be expected for the prototype.

Average gravity moment to shear ratios (M_{gc}/V_{gc}) are computed at the face of the slab-column critical section. Based on the elastic finite element analyses: $M_{gc}/V_{gc} = 10.8$ in. for the scaled prototype structure; $M_{gc}/V_{gc} = 9.5$ in. for Tests 1 and 2; and $M_{gc}/V_{gc} = 10.4$ in. for Tests 3 and 4. Using the experimental gravity moments (Fig. 6.12) and measured shears: $M'_{gc}/V'_{gc} = 13.2$ in. for Test 1, 13.4 in. for Test 2; and $M'_{gc}/V'_{gc} = 11.8$ in. for Test 3, 11.7 in. for Test 4.

6.8 Lateral Stiffness

In the design of flat plate buildings, not only is adequate strength required, but sufficient lateral stiffness must be provided to produce a serviceable structure. An estimation of initial stiffness is typically required under working load conditions such as wind loads. Two elastic methods, the effective beam width model and the equivalent frame model, are presented and their results are compared with the experimental tests. The present study offers a unique opportunity for comparing these analytical methods against a more realistic basis that includes biaxial effects and extreme conditions of gravity loading.

Other stiffness models such as the beam analogy model have been proposed to take into consideration the full nonlinear behavior of slab-column connection [3]. Although these methods can provide excellent predictions of strength-stiffness behavior, they usually involve using complex iterative techniques that are not suitable for design applications. The beam analogy model proposed by Hawkins [3] is discussed in Section 6.9.2.

6.8.1 Effective Beam Width Model

In the effective or equivalent beam width model, slabs are replaced by beams spanning in the direction of lateral loading [33]. The depth of the beam is equal to the slab thickness, h , and the width of the beam is equal to the product of an effective beam coefficient and the transverse slab dimension, l_2 (Fig. 6.13 (a)). The moment of inertia of the effective beam, I_{eb} , is thus defined as

$$I_{eb} = \frac{l_2 h^3}{12} \times \text{Effective Width Coefficient} \quad (6.3)$$

Using the column gross moment of inertia, an elastic direct stiffness program (SAP80 [34]) is used to analyze the effective beam width model of Fig. 6.13 (a). The results of the analyses performed with several effective width coefficients are shown in Fig. 6.14.

For the present test specimen geometry ($l_1=l_2$, $c_2/l_2=0.075$), theoretical effective beam width coefficients for Eq. (6.3) have been determined by past researchers to be approximately 0.65 using Levy, finite difference, and finite element methods [33]. Figure 6.14 shows that 0.65 is an upper bound solution for the initial lateral stiffness of the test specimens. The theoretical methods ignore inelastic behavior such as cracking and bond slip.

A more representative effective beam width coefficient is dependent on the choice of an acceptable drift under working load conditions (Fig. 6.14 (b)). There is currently no consensus on what constitutes an acceptable drift criterion nor whether a criterion should be based on static or dynamic behavior. The static criterion of 1/500 (0.2%) of the structure's height is used in the present study since this value is most often quoted as a limit for wind design in the literature.

Using the 0.2% drift criterion in Fig. 6.14 (b) results in an effective width coefficient of 0.20 that best models the experimental results. At 0.2% drift, the 0.20 width coefficient produces a line that averages the

two secant stiffnesses of the biaxial tests (Test 2 and Test 4). Uniaxial tests (Tests 1 and 3) are not considered when determining the best effective width coefficient since they do not simulate actual conditions in a building that experiences wind loads from many different directions. An average is taken because the actual live load on the flat slab building is unlikely to be zero or near the full design live load but rather in between the extremes. Test 2 (high gravity), with almost the full live load, can be considered to provide a lower bound on stiffness; Test 4 (low gravity), with almost no live load, provides an upper bound condition. A 0.2 effective width coefficient can be considered equivalent to the theoretical coefficient (0.65) modified by a stiffness reduction factor of 0.31.

6.8.2 Equivalent Frame Model

The equivalent frame model or lateral torsional member model was calibrated using the results of comprehensive studies of reinforced concrete floor slabs and has been adopted by the ACI code since 1971 [7]. The model was originally developed from flat slab structures with typical configurations and gravity loads only. The validity of extending the equivalent frame model into lateral load analysis is presently uncertain.

The equivalent frame model is comparable to the effective beam width model in representing a three-dimensional slab system by an elastic two dimensional frame (Fig. 6.13 (b)). It has been devised to provide a better representation of the slab system through the strategy of defining flexural stiffnesses that reflect the torsional rotations possible in the three-dimensional slab system.

The equivalent frame model uses an effective slab moment of inertia, I_{eff} , equal to the gross moment of inertia of the full slab width (I_2); Vanderbilt and Corley [33] have recommended that the value of I_{eff} be modified by the coefficient β to account for cracking and inelastic behavior. In the joint region, the inertia of the slab is magnified by dividing I_{eff} by the quantity $(1-c_2/l_2)^2$ [7].

A lateral torsional member is considered in the equivalent frame model to account for the torsional flexibility of the slab-to-column connection. The lateral torsional member of the test specimen is formed by a slab strip of one column width that extends from the column face to the side of the slab [7]. Stiffness, K_t , of the torsional members is calculated by the following expression [7]:

$$K_t = \sum \frac{9E_{cs} C_t}{l_2 \left(1 - \frac{c_2}{l_2}\right)^3} \quad (6.4)$$

where E_{cs} is the modulus of elasticity of the slab concrete. The constant C_t in Eq. (6.4) is the torsional constant and for the rectangular slab is approximated as follows [7],

$$C_t = \left(1 - 0.63 \frac{h}{c_2}\right) \frac{h^3 c_2}{3} \quad (6.5)$$

The torsional member need not be directly included in the equivalent frame model (Fig. 6.13 (b)). Its torsional stiffness, K_t , is combined with the stiffness of the column, K_c , to form an equivalent column stiffness, K_{cc} . The flexibility of the equivalent column is taken as the sum of the flexibility of the columns and the flexibility of the torsion members. Thus K_{cc} is defined as [7]:

$$K_{cc} = \frac{\sum K_c}{1 + \frac{\sum K_c}{K_t}} \quad (6.6)$$

Knowing the equivalent stiffnesses of the column and slab, the equivalent frame model can be analyzed using any acceptable method of elastic structural analysis such as moment distribution or the direct stiffness method. For the present study, a direct stiffness program (SAP80[34]) was used to analyze the model. The results of the equivalent frame analyses using various values of β are shown in Fig. 6.15. Applying the same 0.2% drift and modelling criteria discussed in the previous section, a β coefficient of 0.33 gives the best stiffness model for the experimental results (Fig. 6.15 (b)). $\beta=0.33$ has also been recommended in previous studies (i.e. Vanderbilt and Corley [33]). This stiffness reduction is similar to that required for the effective beam width model (0.31).

The present study has shown that both the equivalent frame and effective beam width models can provide good estimates of lateral stiffness. For both models, the choice of an appropriate stiffness reduction factor is most essential for accurate modelling of stiffness. The main difference between the two models is the inclusion of a lateral torsional element in the equivalent frame model. The equivalent frame model has an advantage in being applicable for gravity load analysis ($\beta=1.0$), but the effective beam width model is a simpler model that can be readily applied in structural analysis programs commonly used in design practice.

6.9 Ultimate Strength

When substantial lateral forces due to wind or earthquakes are expected, it is important to accurately predict the ultimate shear and unbalanced moment transfer capacities of slab-column connections. This section compares with the experimental results three methods of ultimate strength prediction: the linear stress variation model, the beam analogy by Hawkins, and the Park and Islam model.

6.9.1 Linear Stress Variation Model

Specified by ACI 318-83 [7], the linear stress variation model assumes that shear stresses, v_c , on a critical perimeter vary linearly with distance from the centroidal axis of the perimeter and are induced by the shear force and part of the unbalanced bending moment (Fig. 6.16). The remainder of the unbalanced bending moment is carried by flexure in the slab. The method is semi-empirical and the critical perimeter is assumed at a distance $d/2$ away from the face of the column. The maximum shear stress, v_{\max} , is calculated by Eq. (6.7):

$$v_{\max} = \frac{V_g}{A_c} + \frac{\gamma_v M_t c_c}{J_c} \quad (6.7)$$

where

V_g = the gravity shear force on the connection,

A_c = area of critical section = $2d(c_1 + c_2 + 2d)$,

γ_v = the fraction of transfer moment that is considered transferred by eccentricity of shear
= 0.4 for a square column [7],

M_t = the transfer moment,

c_c = the distance from the centroid of the critical perimeter to the critical section = $(c_1 + d)/2$,

J_c = property of the critical section analogous to the polar moment of inertia given as

$$J_c = \frac{d(c_1 + d)^3}{6} + \frac{(c_1 + d)d^3}{6} + \frac{d(c_2 + d)(c_1 + d)^2}{2} \quad (6.8)$$

For the biaxial tests (Tests 2, 4, and 5), an additional $(\gamma_v M'_t c_c / J_c)$ term is added to Eq. (6.7) to account for moment transfer in two directions (Fig. 6.16 (b)).

According to ACI 318-83, v_{\max} is limited to $4\sqrt{f'_c}$ psi ($0.33\sqrt{f'_c}$ MPa). This limit is conservative compared with the experimental results of Tests 1 to 4 (Fig. 6.17). Maximum shear stresses are computed to be higher for the biaxial tests (Tests 2 and 4) compared with their uniaxial companions (Tests 1 and 3). The model predicts higher maximum shear stresses when the gravity load is reduced (Tests 3 and 4 versus Tests 1 and 2). The repaired specimen (Test 5) fails below the ACI limit.

The linear stress variation model is a simple elastic model that was originally developed from uniaxial test results. The actual distribution of flexural, torsional, and shear stresses around the column is complex. After cracking of the concrete and inelastic deformations have commenced, stress redistribution of internal actions will occur [1]. It is likely that the effect of stress redistribution is more significant under biaxial loading.

Alternatively, a shear-moment interaction relationship can be derived from Eq. (6.7) to assess the ultimate strength of slab-column connections. In Fig. 6.18, the ordinate (V_g/V_o) is the ratio of the gravity shear force to the shear strength from Eq. (6.7) when $M_t=0$. The abscissa ($\gamma_v M_t/\gamma_v M_o$) is the ratio of unbalanced bending moment transferred to column by shear to the moment strength from Eq. (6.7) when $V_g=0$. Three points are plotted for each biaxial test (Tests 2, 4, and 5): (1) EW+NS, considers the combined moment transfer in the east-west and north-south direction; (2) EW only, considers moment transfer in the east-west direction only; and (3) NS only, considers moment transfer in the north-south direction only. Even though the effect of biaxial loading was not included in the original development of the ACI limit, it remains conservative for all three points of each biaxial tests (Fig. 6.18). Only the repair specimen (Test 5) falls below the ACI limit.

Overall, the linear stress variation model provides the designer with a simple and conservative method of estimating the strength of reinforcement concrete flat plate connections. The present study has shown evidence that the method can be conservatively applied for biaxial cases.

6.9.2 Beam Analogy Model by Hawkins

In the beam analogy model, the slab is attached to the column by short beams that frame into each column face (Fig. 6.19). The flexural elements in the front and back of the column have a width equal to

c_2 and length equal to h . The torsional elements at the sides of the columns have a width equal to c_1 and a length equal to $1.5h$. Each short element is assigned trilinear stiffness and hysteretic characteristics based on accepted reinforced concrete theory and experimental data [3]. Bond slip is included in the model as shown in Fig. 6.19. The bond slip stiffness is based on experimental data and is a function of the bar diameter and concrete strength. The connecting bar between the flexural and torsional elements is rigid except for a portion $(h-d/2)$ in length located at the corners. The properties of the corners are related to the cracked stiffnesses of the flexural and torsional elements and were calibrated from experimental analysis [3]. A torsion and shear interaction relationship similar to the ACI relationships is included in the beam analogy model. The cracked torsional stiffness is multiplied by $(h/(h-0.27c_1))$ or 2.0, whichever is less, to account for the stiffening effect of the surrounding slab.

After the strength-deformation characteristics of each connection element are defined, a combined stiffness matrix of the slab-column is formed in accordance with the equations of equilibrium and compatibility. Lateral load is applied incrementally and the load deformation equations are solved by iteration. Stiffness and strength of all the elements are monitored for their cracking, yielding, or ultimate conditions. Hawkins has developed a computer algorithm to implement the beam analogy model. In typical cases, the algorithm is stable and converges rapidly.

For interior connections, the beam analogy model predicts seven stages of behavior (i.e. torsional cracking or back flexural cracking, front or back flexural yielding, etc.). Various rules are included in the model to govern the redistribution of shear stresses between flexural and torsional elements. Failure is assumed when at least three elements framing into the column have reached their collapse condition. Three basic modes of failure are assumed: (1) flexural crushing, (2) torsional crushing, and (3) shear punching.

Since the application of the complete beam analogy method is a relatively complicated and exhaustive process, beyond the scope of the present study, the simplified version of the model proposed by Hawkins [3] is adopted here. The simplified version is based on the same formulation of the complete beam analogy model but does not use an incremental procedure. It assumes a trilinear curve for the slab-column load-displacement relationship. The first break in the curve corresponds to full yielding of the flexural ele-

ments and cracking of the torsional elements. The second break corresponds to crushing of the flexural and torsional elements. Drifts are predicted based on the analytical flexural and torsional stiffnesses of the elements and includes bond slip. Figure 6.20 compares the results of the simplified beam analogy model with the experimental results of Tests 1 to 4. The model closely follows the experimental load-displacement relationship. The present form of the beam analogy method can not consider the effects of biaxial loading.

6.9.3 Park and Islam Model

Park and Islam developed a more easily applied beam analogy model. Their purpose was to provide a model more suitable for design [25]. The general theory of their model contains a number of simplifying assumptions but is conceptually similar to the beam analogy model by Hawkins (Fig. 6.19). They assume that there is sufficient ductility in the connection to enable the full flexural and torsional strengths of the connection to develop. The Park and Islam Model gives the unbalanced bending moment strength of the slab-column connection as

$$M_u = (m_u + m'_u)(c_2 + d) + [4\sqrt{f'_c}(c_2 + d)d - 0.25V_u](c_1 + d) + \frac{2}{3}h^2(c_1 + d)4.8\sqrt{f'_c} \left[1 - \left(\frac{v_u}{4\sqrt{f'_c}} \right)^2 \right]^{1/2} \quad (6.9)$$

where m_u and m'_u are the ultimate negative and positive flexural capacity of the slab per unit width according to standard flexural theory. The model does not predict displacements nor considers the effects of biaxial loading.

The Park and Islam model gives conservative estimates of the ultimate moment transfer capacities as compared with the experimental results of Tests 1 to 4 (Fig. 6.21). The maximum lateral load of Test 1 is 53% greater than the value predicted by the model, Test 3 is 49% greater. These values are consistent with the study made by Park and Islam in which the model very conservatively predicted the results of 19 slab-column tests [25].

Compared with the linear stress variation model, the beam analogy models of Hawkins and Park and Islam appear to be more rational approaches to the problem by considering the individual ultimate flexural and torsional capacities of the slab-column connection. The Park and Islam model is generally conservative and involves solving only one equation (Eq. (6.9)). The beam analogy method proposed by Hawkins is

more complicated but can serve as a valuable research tool. The simplified version provides a good prediction of behavior. In estimating ultimate strength, the main difference between Hawkins and the Park and Islam model lie in the calculation of torsional strength. Park and Islam adopts a simpler elastic theory that assumes a maximum torsional stress of concrete at $4.8\sqrt{f'_c}$ psi. Hawkins uses a more accurate method and considers the slab reinforcement explicitly.

7. DUCTILITY AND DRIFT CAPACITY

7.1 Introduction

In design of buildings to resist earthquake ground motions, the prevailing ductile design philosophy typically requires that elements of the structural system be capable of deforming into the inelastic range. This requirement often, but not always, extends to elements that are not considered in design as part of the lateral load resisting system. For example, a common form of construction in seismic zones in the United States combines flat-plate frames, to carry gravity loads, with shear walls, to resist the earthquake loads. It is unclear in this form of construction whether the flat-plate connection will possess sufficient lateral displacement capacity to survive the lateral deformations that can reasonably be expected during a strong earthquake.

The objective of this chapter is to examine the available data, and therefrom develop an understanding of the major parameters that influence the lateral displacement capacity and ductility of reinforced concrete flat plates. The significant effects of gravity load and biaxial lateral loading are reiterated. Implications of the findings with regard to seismic design and performance are discussed in Chapter 9.

7.2 Review of Experimental Observations

Together with the tests results presented in Chapter 5, experimental data from several research investigations reported in the literature were gathered for this study (Table 7.1). Included are data from Hawkins et. al. [13], Morrison and Sozen [22], Ghali et. al. [10], Islam and Park [16], Hanson and Hanson [11], Zee and Moehle [35], and Symonds, et. al.[30]. Prerequisites for selection of these data were: (1) specimens represented interior connections, (2) specimens contained no slab shear reinforcement, and (3) specimens were loaded to simulate effects of shears and moments due to vertical and lateral loads. Some of the specimens [Spec. No. 1-15, 19-21] were subjected to reversed cyclic lateral loads simulating severe seismic loading. Others [Spec. No. 16-18, 22-23] were subjected to effectively monotonic lateral loading.

Relevant data of these experiments are tabulated in Table 7.1. Brief descriptions of the specimens, test procedures, and principal results follow. More detailed information can be found in the original papers.

7.2.1 Tests Description

All of the test specimens reported herein were similar in that a single interior connection sub-assembly was isolated from an idealized structure and loads were applied to simulate lateral load effects (Fig. 7.1). The column in each test specimen extended above and below the slab to "pinned" connections located at a point equivalent to the column mid-height of an idealized building. In the direction parallel to lateral loading, the slab extended on either side to a point equivalent to midspan of the prototype slab, except for Specimens No. 5-10 which extended 0.3 times the slab span. In the transverse direction, the total slab width ranged between half the longitudinal span and the full longitudinal span.

Slab gravity loads were simulated in some of the tests [Spec. No. 1-2, 5-10, 14-15, 19-21]. The procedure of adding these vertical loads varied; in some cases subsidiary weights were placed on the slab surface [Spec. No. 1-2, 14-15, 19-21], and in other cases vertical actuators applied the load [Spec. No. 5-10].

In some of the tests [Spec. No. 1-4, 11-19] lateral load effects were simulated by attaching the slab edge to "roller" supports and then loading laterally at the top of the column (Fig. 7.1 (a)). In the other tests lateral load effects were simulated by actuators that applied equal and opposite vertical loads to the ends of the slab while the columns were restrained against lateral displacement (Fig. 7.1 (b)). There is no general agreement as to which of these two testing techniques is more representative of actual conditions. Both probably represent situations to which a redundant, nonlinear building system is exposed.

All tests reported previously in the literature have considered only uniaxial lateral loadings. Only the test results of the present study [Spec. No. 1-4] considered both uniaxial and biaxial lateral loadings.

7.2.2 Lateral Load-Displacement Relations

For those specimens that were tested by laterally displacing the upper column [Spec. No. 1-4, 11-19], the lateral load-displacement relation is self-evident from measured lateral loads and displacements at the top of the upper column. For the specimens that were loaded by vertically displacing the slab ends [Spec. No. 5-10, 20-23], the lateral load (reaction at the upper column) was resolved by statics. Lateral displacement of the specimen, D_h , was taken as

$$D_h = D_v(h_c/l_1) \quad (7.1)$$

in which D_h = difference of the vertical displacements at opposite ends of the slab at the point of vertical load application, h_c = total column height, and l_1 = total span of the slab in the direction of lateral loading (Fig. 7.1). For Specimens No. 5-10, effective lateral displacements, D_h , obtained by Eq. (7.1) were further multiplied by a factor 1/0.6 because, as described in references [13] and [30], the slab span of the specimen represents approximately 0.6 times the total span of the slab in the prototype.

Measured lateral load-displacement relations from three of the specimens that were subjected to reversed cyclic lateral loads are plotted in Fig. 7.2. These relations display the broad range of behaviors observed for the connections included in Table 7.1. The data in Fig. 7.2 (a) reveal a relatively stable hysteretic response to lateral drifts well beyond the range of practical interest in building design. The data in Fig. 7.2 (b) also reveal a stable hysteretic response, but to significantly less drift than obtained for the specimen in Fig. 7.2 (a). Failure occurred in a relatively sudden punching shear mode after the slab reinforcement near the column had yielded. Lateral drift at failure in this case can be reasonably expected for a multistory building subjected to a intense earthquake motion [24]. Unless measures are taken to control lateral drift, this connection may not be suitable in a building designed to resist strong earthquakes. Figure 7.2 (c) presents a response history that is even further curtailed by punching shear failure. The low level of lateral drift, and complete lack of apparent ductility, make this type of specimen clearly unsuitable for almost all types of buildings subject to severe earthquake loading.

It is useful to qualitatively classify responses of the specimens in Table 7.1 according to the response types depicted in Fig. 7.2. Column 8 of Table 7.2 lists the assigned classification, either A, B, or C, signifying behavior similar to that plotted in Fig. 7.2 (a), 7.2 (b), or 7.2 (c), respectively.

Two measures are used in this study to quantify the lateral deformation capacities of the specimens. The first measure is the maximum drift which is defined as the lateral drift at failure, D_u , as a percent of specimen height, h_c . Lateral drift at failure is tabulated for each specimen in column 6 of Table 7.2.

The second measure of deformation capacity is the lateral displacement ductility at failure, μ . Lateral displacement ductility cannot be uniquely defined for slab-column connections because the force-displacement relation has no distinct yield point (because yield spreads gradually across the slab transverse width [13]). To overcome the uncertainty in defining the yield displacement, an arbitrary procedure was

applied. The procedure, illustrated in Fig. 7.3, was to first construct the envelope relation between lateral displacement and lateral load. The envelope relation was then idealized by an elasto-plastic relation (Fig. 7.3). The initial slope of the idealized relation is a secant through the measured relation at a load equal to two-thirds of the measured strength. The plastic portion of the idealized relation passes through the maximum load and the maximum deformation at failure. The intersection between these two lines defines an effective yield displacement. Displacement ductility is then calculated as the ratio between the ultimate displacement and yield displacement ($\mu=D_u/D_y$) of the idealized relation (Fig. 7.3). The computed lateral displacement ductilities (μ) for the test specimens are listed in column 5 of Table 7.2.

7.3 The Effect of Gravity Load on Lateral Displacement Ductility

As pointed out in Section 6.2, the level of gravity load carried by the slab is a primary variable affecting the apparent lateral ductility. This phenomenon has also been identified in earlier tests by Kanoh and Yoshizaki [19]. The same trend is apparent in the relations plotted in Fig. 7.2. In that figure, lateral displacement ductility decreases from Fig. 7.2 (a) to 7.2 (c), as gravity load carried by the slab increases (column 7, Table 7.2).

In order to generalize the conclusion that gravity load affects lateral displacement capacity of the connection, lateral displacement ductility, μ (column 5, Table 7.2), was plotted versus the normalized gravity shear ratio, V_g/V_o (column 7, Table 7.2), for each connection. The value V_g is the vertical shear acting at failure on the slab critical section defined at a distance $d/2$ from the column face, in which d = the average slab effective depth. The quantity V_o is the theoretical punching shear strength in the absence of moment transfer, as given for these connections by Eq. (7.2) [1],

$$V_o = 4\sqrt{f'_c} b_o d \quad (7.2)$$

in which V_o is in pounds, f'_c = concrete compressive strength in psi, and b_o = perimeter length of the slab critical section (b_o and d have in. units.)

The relation between lateral displacement ductility, μ , and the gravity shear ratio, V_g/V_o is plotted in Fig. 7.4. Clearly, for values of V_g/V_o exceeding approximately 0.4 there is virtually no lateral displacement ductility ($\mu=1$), that is, the connection fails by punching before any yield in the load-displacement relation is detected. As gravity shear decreases, there is an increase in the available ductility.

The effect of gravity shear on lateral drift at failure is presented in Fig. 7.5. As in Fig. 7.4, there is a reduction in available drift with increasing gravity shear ratio.

The observation that lateral deformation capacity and gravity shear are related is not surprising and has been identified previously [13,19]. According to the ACI Building Code [7], shear strength for square interior columns is defined by Eq. (7.2). This limiting shear strength has been established from test of slab-column connections for which shear failure occurred before widespread yielding of the slab reinforcement [14]. The condition for which this limiting shear stress is defined is consistent with the philosophy of the main body of the ACI Building Code, namely, that design loads are set sufficiently high and inelastic redistribution is sufficiently limited that significant yield at connections will not occur. Under this loading condition, the surrounding slab confines the connection region. This confinement is believed to be the reason why observed nominal shear stresses at failure are larger for slab-column connections than for linear elements such as beams [1]. Some researchers [14] have hypothesized that the confining effect of the slab is diminished when widespread yield of the slab reinforcement occurs in the connection region. Experimental data in support of this hypothesis have been presented previously [14] for connections loaded solely by vertical loads. The data for lateral load tests presented in Fig. 7.4 augment these vertical load data.

The ACI linear stress variation model (Section 6.9.1) provides a simplified explanation of the reduction in deformation capacity due to higher gravity loads. Shear stresses at the slab-column connection are induced by two sources: (1) gravity loads, and (2) lateral loads. Gravity loads induce shear stresses directly on the connection. Lateral loads produce a moment transfer that is resisted by flexure and eccentric shear at the connection. Therefore, with higher gravity loads, less shear capacity is left over in the connection to resist the eccentric shear produced by lateral loading. Consequently, failure in the connection occurs at a lower deformation level.

7.4 The Effect of Biaxial Lateral Loading on Lateral Displacement Ductility

During wind or earthquake loading, the slab-column connection resists lateral loads acting in multiple directions. As pointed out in Section 6.3, biaxially loaded specimens (Specimen No. 2 and 4) failed at an earlier stage of testing in comparison with their companion uniaxially-loaded specimens (Specimen No. 1 and 3). Both stiffness and strength were less for the biaxially-loaded specimens than for the equivalent

uniaxially-loaded specimens. The reduction in drift capacity due to biaxial loading can be seen in Fig. 7.5. The effect of biaxial loading is less significant when gravity loads are high.

The lower resistance and toughness of the biaxially loaded specimens is explained as follows. Under uniaxial loading, resistance is attributable to torsion on faces AB and CD and shear and moment on faces BC and DA [13] (Fig. 7.6). If a uniaxially-loaded connection is subsequently loaded in the transverse direction, faces AB and CD (which had previously been loaded in torsion) begin to develop flexure and shear, while faces BC and DA (which had previously been loaded in moment and shear) begin to develop torsion. The interaction between flexure, shear and torsion [26] are such that the net connection resistance in any given direction is less under biaxial loading than under uniaxial loading. Similarly, more rapid degradation of the concrete occurs under biaxial loading.

Based on the observations of the present experimental study, it is concluded that biaxial lateral loading, as might occur during an earthquake or wind loading, reduces the available strength, stiffness, and overall lateral displacement capacity of slab-column connections. Thus, since most of the data included in Figs. 7.4 and 7.5 were obtained from uniaxial tests, conclusions drawn therefrom may be on the unconservative side if biaxial loading occurs.

7.5 Effects of Other Parameters on Drift Capacity

Other parameters such as the level of reinforcement in the slab and the slab-column geometry (c/l , h/l) are also likely to have some influence on drift capacity. However, no significant trends are apparent from Fig. 7.7. There are a number of probable reasons why the effects of reinforcement and geometry are not readily apparent. Together with gravity load, these and other parameters are complexly inter-related. A multivariate analysis with a larger sample of test data would be required for a trend to become observable. Furthermore, the present data are based on a variety of tests with different types of boundary and lateral loading conditions that are likely to distort the influence of these sensitive parameters.

7.6 Ductility, Drift, and Seismic Performance

The data in Figs. 7.4 and 7.5 indicate that the available lateral displacement ductility of reinforcement concrete flat-plate connections without shear reinforcement is low by comparison with values often

considered marginally acceptable in seismic design [26]. However, the existence of low ductility does not de facto equate with poor performance during a strong earthquake loading. For typical slab-column connections, relatively high flexibility may protect the connection from large displacement ductility demands. For example, Fig. 7.8 presents idealized load-displacement envelopes of a typical slab-column connection [35] and a slender shear wall [15] that might be used to stiffen a flat-plate building. If the wall is sufficiently stiff to restrain lateral interstory drifts to approximately 1.5 percent of story height (a value occasionally quoted as a reasonable upper bound for severe seismic loading [29]), the required displacement ductility of the wall will be approximately six. The required displacement ductility of the slab-column connection will be less than two. It is recommended that interstory drift be used to assess the seismic performance of reinforced concrete flat-plate connections. It has the advantages of providing an absolute index of performance and is relatively simple to calculate.

8. Studies of the Seismic Response of Reinforced Concrete Buildings with Flat Slab Construction

8.1 Introduction

A common form of construction in seismic zones combines a flat slab floor system with shear walls or ductile moment resistant frames. For example, Fig. 8.1 shows a typical multistory flat slab building combined with core walls being built in a seismic active region in California. It is uncertain whether the flat slab, in particular its connection, possesses sufficient lateral displacement capacity to survive the lateral deformations that can be reasonably expected during a strong earthquake.

This chapter presents nonlinear dynamic analysis results of typical building systems with flat slab construction. Drift is used as a criterion to evaluate the performance of the flat slab under seismic conditions. A design recommendation that limits gravity shear stresses on the connection is proposed.

8.2 Description of Buildings

The present study includes three buildings located in a moderate seismic area (UBC Zone No. 2 [32]) and two buildings located in a severe seismic area (UBC Zone No. 4). Typical plans and elevations are shown in Fig. 8.2. The configuration of these generic buildings is similar except for the type of lateral load resisting system used: frame, shear wall, or flat plate. The buildings are ten story high with equal story heights of 10 ft. Three 20-ft bays span each direction. All floors have a slab thickness of 8 in. and the foundation is assumed to be supported on stiff soil. To simplify the design and analysis, columns, beams, and walls keep the same dimensions throughout each building.

8.2.1 Buildings in UBC Zone No. 2

The flat plate system has square columns with dimensions of 24 in. (Fig. 8.2 (a)). The frame system has exterior beams with a width of 16 in. and a depth of 20 in. Columns are square with dimensions of 20 in. The walls of the shear wall system have a thickness of 8 in. and a length of 14 ft. Columns are 18 in. square.

8.2.2 Buildings in UBC Zone No. 4

For the frame system, columns have square dimensions of 24 in. Beams have a width of 18 in. and a depth of 24 in. (Fig. 8.2 (b)). Ductile moment resisting frames are located at the exterior of the building. In the shear wall system, 10-in. thick walls, 18 ft in length, are located at the middle bays of the exterior frames. All columns are square with dimensions of 18 in.

8.3 Design

The design of the buildings follows the provisions of the 1985 Uniform Building Code [32]. All floors are designed for a live load of 50 psf and a superimposed dead load of 20 psf. A basic wind speed of 70 mph is assumed for wind load analysis. The specified material properties are: $f'_c=4000$ psi normal weight concrete, and $f_y=60,000$ psi reinforcement.

According to the 1985 UBC, the seismic design base shear is given by Eq. (8.1),

$$V = ZICSKW \quad (8.1)$$

where V = service level design base shear, Z = numerical coefficient dependent on the seismic zone ($Z=1.0$ for Zone No. 4, $Z=3/8$ for Zone No. 2), I = occupancy importance factor (taken as 1.0), S = numerical coefficient for site-structure resonance (taken as 1.5), K = a numerical coefficient dependent on the framing type ($K=1.0$ for all building systems of the present study), W = total dead load of the building, and C is given by Eq. (8.2),

$$C = \frac{1}{15\sqrt{T}} \quad (8.2)$$

The value of C need not exceed 0.12 and T is the fundamental period of the building.

It is noted that the 1988 UBC provisions differ from those used above. However, the difference is not likely to significantly change the design of the generic buildings. Figure 8.2 (c) compares the base shear coefficients of shear wall buildings computed by the 1985 and 1988 codes.

Following the procedures in the UBC, the base shear is distributed to each floor. Accidental torsion is considered and is equal to the story shear acting with an eccentricity of 5% of the building width. A concentrated force, $F_t = 0.07TV$, is added to the top of the building.

In the shear wall and frame systems, walls and ductile moment resistant frames are designed to resist the total lateral seismic forces. The flat slab is designed to carry gravity loads and is assumed in design not to resist any seismic forces. For the flat-plate building system in Zone No. 2 (Fig. 8.2 (a)), the total seismic forces are resisted by equivalent slab-column frames. An effective slab width of $0.25l_2$ is assumed. The value of $0.25l_2$ is considered to approximate the cracked member stiffness; the elastic effective width ($\approx 0.5l_2$) is halved to account for cracking.

The dimensions and reinforcement levels of the column, beam, and wall element are determined based on UBC provisions and current seismic design practise [7,26,32]. The main design criteria are : (1) lateral drifts are limited to 0.5% for each story, (2) strength requirements are based on factored load combinations, (3) elements are detailed to satisfy requirements of App. A of ACI 318-83. To simplify the nonlinear dynamic modelling, reinforcement quantities for each wall, column, and beam elements change no more than three times over the building height. In computing drifts and periods (Table 8.1) for design, half the gross moment of inertia of columns and beams is assumed. For shear walls, the total gross moment of inertia is taken. Maximum interstory drifts computed ranged from 0.47% to 0.50%. It is noted that the UBC does not strictly specify how element stiffnesses should be computed when computing lateral drifts. Gross section properties could have been assumed for columns and beams, thereby resulting in lower computed drifts.

8.4 Dynamic Analysis

The computer program DRAIN-2D [18] is used for the nonlinear dynamic analysis of the buildings. In this program, the structure is idealized as a two dimensional planar assemblage of discrete elements. Analysis is by the direct stiffness method, with the nodal displacements as unknowns. Each node possesses up to three displacement degrees of freedom. The structural mass is assumed to be lumped at the nodes so that the mass matrix is diagonal. Viscous damping of mass-dependent and/or stiffness-dependent type may be specified. The earthquake excitation is defined by time variation of ground acceleration.

The dynamic response is determined by step-by-step integration, with a constant acceleration assumption within any step. The tangent stiffness of the structure is used for each step, and linear structural behavior is assumed during the step. If an element yields or unloads, information is returned from

the element subroutine. Changes are then made to the tangent stiffness matrix and the triangularization of Gauss elimination is repeated. Any unbalanced loads resulting from errors in the assumed linear behavior within the step are eliminated by applying corrective loads in the subsequent time step.

8.4.1 Modelling

By symmetry, it is necessary to model only half of each building plan shown in Fig. 8.2. These are then subdivided into two planar frames which are connected by rigid links pinned at both ends. The base of the frames are fixed. As an example, the computer model of the shear wall building is shown in Fig. 8.3. The properties and reinforcement percentages of the building systems are tabulated in Table 8.1.

DRAIN-2D uses the simplified bilinear Takeda model [18] with degrading stiffness to model reinforced concrete elements. Beam, column, and wall members are modelled by elastic elements with inelastic hinges at the ends (Fig. 8.4 (a)). The hinges model inelastic action and their hysteretic behavior follow various loading and unloading rules proposed by Takeda [18]. The form of the hinge moment-rotation relationship is a bilinear curve with initial stiffness and subsequent strain hardening (Fig. 8.4 (a)).

The Takeda model is also adapted to model the flat slab of the buildings. Slabs are modelled as beams with effective widths. The load-displacement relationship of these effective slab-beams are interpolated from the experimental results presented in Chapter 5 since similar geometry and loading conditions exist between the buildings and the experimental prototype. The properties of the inelastic hinges are determined such that the load-displacement relation of a slab-column model closely approximates the experimental results. Figure 8.4 (b) compares the computed moment-drift response of a slab-column connection with the experimental results. This slab-column connection is taken from the fifth story of the shear wall system in UBC Zone No. 4. For the flat-plate system in UBC Zone No. 2, the load-displacement relationship of slab elements are derived using the simplified beam analogy model by Hawkins (Section 6.9.2).

Rigid zones are modelled between column and beam elements. Walls have rigid zones with width equal to the wall width and zero height. $P-\Delta$ effects are considered in DRAIN-2D.

8.4.2 Mass and Damping

The mass of the buildings consists of the self-weight, superimposed dead load, and half of the live load. The mass of each floor, including portion of columns and walls, is lumped at nodes corresponding to floor centerlines.

Rayleigh Damping (mass and stiffness proportional) is assumed for the buildings. A critical damping ratio of 4% is assumed and specified for the first and fourth modes of each model.

8.4.3 Ground Motions

To obtain a broad picture of response, each building is analyzed under three ground records (Fig. 8.5): (a) 1985 Mexico City (SCT site, EW component), (b) El Centro, California, 1940 Imperial Valley earthquake (NS component). (c) 1952 Taft, California (S21W component). For the UBC Zone No. 4 buildings, the El Centro and Taft records are normalized to a peak ground acceleration of 0.4g in order to simulate earthquakes of intense magnitudes. For Zone No. 2, they are normalized to 0.2g which approximates the 0.2g EPA index for these regions as suggested in the ATC recommendations [8]. The elastic spectra of the ground records are shown in Fig. 8.6. Vertical ground accelerations are not considered in the present analysis.

8.5 Discussion of Analysis Results

Response of the five generic buildings to the three ground motions at various intensities were computed as described above. Partial computed results are presented in Figs. 8.7 and 8.8. Examples of drift histories are shown in Fig. 8.7. Interstory drifts are computed as the ratio of relative horizontal displacement to interstory height. The total building drift is defined as the ratio of relative horizontal displacement at the roof to the total building height.

Figures 8.7 (a) to (c) show the computed responses of the shear wall system in UBC Zone No. 2 subjected to the Mexico, El Centro, and Taft ground motions. Figures 8.7 (d) to (g) show the responses of the other building systems subjected to the El Centro motion. These figures show that interstory drifts typically vary along the building height. Due to frame behavior, higher interstory drifts occur at the lower stories of frame systems. For shear wall systems, cantilever action causes higher drifts at the upper stories.

It is also apparent from Fig. 8.7 that the fundamental period of the buildings elongates due to yielding of members. For example, consider the total drift history of the shear wall building in Zone No. 4 subjected to El Centro (Fig. 8.7 (g)). The initial period (time between three successive zero crossings) is approximately 1.1 sec. at the beginning of the motion. The period increases to as much as 1.7 sec. later in the response. The original period computed for the building is 1.1 sec. (Table 8.1 (e)).

The effect of higher modes on drifts can be seen from the high frequency content of the ninth and second interstory drift histories shown in Fig. 8.7. The influence of higher modes is less significant under the Mexico record as compared with the El Centro and Taft records. Comparing the response spectra of Fig. 8.6, the Mexico spectrum peaks at a period of approximately 2.0 sec. This sharp peak tends to dominate the overall response.

Maximum interstory drifts are summarized in Figs. 8.8 (a) and (b). The majority of interstory drifts are below 1.5%. Drifts are generally higher for the Mexico record which can again be explained by the sharp peak of its elastic spectrum that occurs near the fundamental period of the buildings (Fig. 8.6). The flexible flat plate system also exhibited higher drifts.

Maximum computed interstory drifts from the DRAIN-2D analyses are compared with the maximum design drifts in Figs. 8.8 (c) and (d). Computed drifts are 2.3 to 5.1 times greater than the design drifts. Maximum design drifts determined by elastic analysis are approximately equal to the UBC limit of 0.5%, but it should be noted that generally conservative assumptions were used in the analysis and design of the buildings.

There are few recorded response of actual flat slab buildings to corroborate the present analytical study. The Holiday Inn building (Orion Street) located in Southern California was equipped with strong motion accelerographs during the 1971 San Fernando Earthquake [31]. The Holiday Inn is a seven-story flat-slab building with edge beams and was built in 1966 (Fig. 8.9). No structural walls are present. During the 1971 earthquake a peak acceleration of 0.251g was recorded at the ground floor. A maximum total building drift of 1.35% was determined from the accelerograph record at the roof level. This value is in the same range of drifts obtained from the the present analysis.

8.6 Design of Flat Slab Connections under Seismic Conditions

The results of the preceding analysis indicate that interstory drift of 1.5%, and in some cases higher, can be expected for buildings with flat slab construction designed based on present code provisions. This value of drift has also been quoted by past researchers for typical reinforced concrete buildings [29]. According to the data presented in Fig. 7.5, a slab-column connection can be expected to possess a drift capacity of at least 1.5% of interstory height, only if the vertical shear on the connection is less than or equal to approximately 40 percent of the direct punching shear strength. Expressed in terms of shear stresses, the nominal shear stress due to vertical loads should be limited to approximately $(0.4)(4\sqrt{f'_c}) \approx 1.5\sqrt{f'_c}$ psi on the slab critical section. Therefore, to ensure the integrity of slab-column connections under severe seismic loading, it is recommended that connections be designed to satisfy Eq. (8.3),

$$V_g \leq 1.5\sqrt{f'_c} b_o d \quad (8.3)$$

The vertical load, V_g , should be taken at least equal to the gravity load shear. Although it is likely that vertical accelerations during earthquakes (frequently of the same magnitude as the lateral ground accelerations) will further increase the total connection shear, there is no evidence at the present time to prove that this effect should be included when computing the vertical connection shear. Likewise, there is no evidence to confute this possibility.

It should be emphasized that the design drift may be much less than the actual drifts a building experiences during a strong earthquake. For the structures considered, computed drifts were as much as five times greater than the design values computed using the UBC (Fig. 8.8 (c) and (d)). Therefore, it is essential that the design recommendation of Eq. 8.3 be followed even in cases where the design drifts are well below the UBC limit of 0.5%.

The performance of the Holiday Inn building is evidence that slab-column connections are capable of sustaining drifts with magnitudes of up to 1.5%. The shear stress, v_c , at the critical section of the connections were estimated to be below $1.3\sqrt{f'_c}$. None of the slab-column connections failed in that building and structural repair was only necessary for a few beam-column joints. About 80 percent of the cost of repair was spent on extensive nonstructural damage of partitions, tiling, and plumbing. From an economic standpoint, to reduce the costs of nonstructural damage, it may be desirable to design flat slab buildings

that have higher lateral stiffness. This can be done by providing shear walls or moment resistant frames of sufficient stiffness.

It must be noted that other factors not considered in the present study, such as vertical accelerations, torsion, soil-structure interaction, and poor construction quality, have the potential to increase drifts significantly. Ground motions with characteristics similar to the Mexican earthquake will also likely push drifts above 1.5%. The uncertainty in predicting seismic performance point to the importance of slab-column detailing to avoid progressive collapse and ensuring life safety. If drifts exceed 1.5% and failure of the slab-column connection occurs, collapse can be prevented by continuous bottom reinforcement placed directly over columns to suspend the slab [14] (Fig. 8.10). The minimum bottom reinforcement, A_{bm} , recommended is [14]

$$A_{bm} = \frac{0.5w_u l_1 l_2}{\phi f_y} \quad (8.4)$$

where w_u = factored ultimate load in psf, but not less than twice the slab dead load, l_1 and l_2 = center-to-center span in each principle direction, f_y = yield stress of steel, and $\phi=0.9$. The experiments reported in the present study demonstrate that this quantity of reinforcement is sufficient to suspend the slab and enable the floor system to sustain the earthquake motions even after initial punching.

9. SUMMARY AND CONCLUSIONS

9.1 Summary

The objective of this study was to investigate the behavior of reinforced concrete flat plates under combined gravity and lateral loads with emphasis on earthquake loading. The scope of this investigation includes : (1) the effects of biaxial lateral loading, (2) the influence of gravity loads on lateral behavior, (3) the post-failure behavior of slab-column connections, (4) the behavior of a repaired connection, (5) an assessment of existing strength and stiffness models, (6) an investigation of the ductility and drift capacity of slab-column connections, and (7) a study on the seismic performance of typical flat-plate buildings.

An experimental program on interior slab-column subassemblages was conducted and was followed by analytical studies. Descriptions of the prototype, test specimens, and testing procedures are in Chapters 2 through 4. The test results are presented in Chapter 5. Discussion of these results and the findings of the analytical studies are included in Chapters 6 through 8.

The prototype structure selected for the experimental study is a typical reinforced concrete flat-plate building with span lengths of 20-ft in both directions. The prototype slab is 8 in. thick and is supported by 18-in. square columns without drop panels, column capitals, or slab shear reinforcement. Four test specimens, modelled after the interior slab-column connection of the prototype structure, were constructed at 60 percent of full scale. All were nominally identical in configuration, reinforcement, and materials. The specimen slab has plan dimensions of 13 ft by 13 ft and a thickness of 4.8 in. A heavily reinforced column extends 3 ft above and below the center of the specimen. Specified material properties are 4,000 psi normal weight concrete and Grade 60 reinforcement. All slab bars are No. 3 with top reinforcement ratios ranging from 0.25% in middle strips to 0.76% near the column. The bottom slab reinforcement ratio is 0.25% and, as is recommended to prevent progressive collapse, continuous bars are placed directly over the column.

During testing, the slab-column specimen was supported at the base of the column and at the slab ends. Lateral loads were applied by hydraulic actuators connected to the top of the column. Vertical loads were simulated by lead blocks placed on the slab and by a vertical jack located below the column. Speci-

mens were instrumented to measure forces, displacements, and strains. A space truss was attached to the west side of slab to restrain the specimen from rigid-body twisting when lateral loads were applied.

Five tests (Tests 1 to 5) were conducted. Specimens were constructed and tested in pairs, one under uniaxial lateral loads followed by the other under biaxial loading. One test (Test 5) was conducted to study the effectiveness of a connection repaired by high-strength grout and epoxy. "High" gravity load conditions ($1.4\sqrt{f'_c}$ connection shear stress due to vertical loads) were simulated in Tests 1 and 2. "Low" gravity load conditions ($0.88\sqrt{f'_c}$) were simulated in Tests 3, 4, and 5. Uniaxial cyclic loading was applied laterally in Tests 1 and 3. The specimens of Tests 2, 4, and 5 were subjected to biaxial loading applied in a "clover leaf" pattern.

A maximum lateral force of 6.62 kips and a maximum drift of 1.54% were reached in Test 1 which had high gravity load and uniaxial loading. With biaxial loading and the same gravity loading, Test 2 resulted in a lower maximum force of 5.24 kips. Maximum drift for Test 2 was similar to that of Test 1, but failure occurred under fewer cycles. Strength and drift capacities increased significantly when gravity load was reduced in Tests 3 and 4. The uniaxial Test 3 reached a force and drift of 10.02 kips and 4.76%, respectively. Its biaxial companion, Test 4, had a maximum force of 9.61 kips and drift of 3.21%. The repaired specimen (Test 5) retained less than half of its original lateral capacity, but experienced no reduction in drift capacity.

To assess the effectiveness of bottom reinforcement detailing, additional cyclic loading and vertical loads were applied to the specimens after punching failure. The details were observed to be sufficient to sustain vertical load in the presence of continued lateral deformation after initial punching occurred.

The experimental investigation was followed by several analytical studies. Three existing strength models for slab-column connections were compared with the test results: (1) the ACI linear stress variation model, (2) the beam analogy model by Hawkins, and (3) the beam analogy proposed by Park and Islam. Lateral stiffness of the slab-column specimens was compared with computed stiffnesses using the effective beam width model and the equivalent frame model. Data from past research were collected to investigate the ductility and drift capacity of slab-column connections. Studies were conducted on the seismic response of buildings with flat-slab construction. Typical building systems in UBC Seismic Zone No. 4 and No. 2

were designed and analyzed. Nonlinear dynamic analyses were performed assuming the El Centro, Taft, and Mexico City earthquakes.

9.2 Conclusions

Based on the results of the study, and within the limitations of that study, the following conclusions are made:

(1) *Biaxial Loading*

Biaxial lateral loading reduces the lateral stiffness, strength, and available drift capacity of reinforced concrete slab-column connections. It is concluded that the effects of biaxial loading should be considered in order to obtain an accurate analysis and proper design of flat-plate structures. Further testing and research in this area is recommended. Parameters such as reinforcement ratios and slab geometry should be varied in order to study their effects on biaxial behavior.

(2) *Gravity Load*

The magnitude of the gravity load shear carried by the slab is a primary variable affecting the lateral behavior of reinforced concrete flat plates. Significant increases in strength, stiffness, and displacement capacities were observed in the test specimens when gravity shear stress on the slab critical section was reduced from $1.4\sqrt{f'_c}$ to $0.88\sqrt{f'_c}$.

(3) *Seismic Design*

The magnitudes of gravity loads and lateral inter-story drifts should be controlled to ensure that the integrity of slab-column connections is maintained under seismic loading. Lateral interstory drifts under an extreme earthquake loading should not exceed 1.5 percent of interstory height. At this level of deformation, the available data indicate that the flat-plate connection will perform adequately if the gravity level shear stress acting on the slab critical section does not exceed $1.5\sqrt{f'_c}$. At higher drift or higher shear, available data indicate that connection failures are possible.

(4) *Detailing*

Continuous bottom slab reinforcement should be placed directly over the columns of flat plates to prevent progressive collapse in the event of a connection shear failure. Bottom bars effectively suspend the

slab after punching failure and enable the slab-column connection to sustain gravity and lateral loads. The recommendation should be applied to all connections of flat plate buildings.

(5) Repaired Connections

The results of the repaired slab-column test suggest that repaired connections retain their original drift capacities and are not likely to fail prematurely under a subsequent strong earthquake. However, repaired slab-column frames should not be considered effective for resisting lateral forces. To make up for the loss of strength and stiffness in the structure, retrofitting with bracings or shear walls is recommended. Further study on repair and retrofit is recommended to substantiate these conclusions. Other methods of repair should also be investigated.

(6) Stiffness Models

The effective beam width model and the equivalent frame model can provide a reasonably close estimate of lateral stiffness for slab-column connections. For both models, the choice of an appropriate stiffness reduction factor is essential to obtain reasonable results. Based on a 0.2% drift criterion, an effective beam width coefficient equal to one-third of the elastic value gave a close estimate of stiffness for the test specimens. For the equivalent frame model, a good estimate of lateral stiffness was obtained when a stiffness reduction factor of one-third was applied to the slab.

(7) Strength Models

For evaluating the the moment transfer strength of slab-column connections, the ACI linear stress variation method is conservative for both uniaxial and biaxial cases. The beam analogy models by Hawkins and by Park and Islam provide a reasonably good estimate of moment transfer strength.

REFERENCES

- [1] ASCE-ACI Committee 426, "The Shear Strength of Reinforced Concrete Members - Slabs," *Journal of the Structural Division*, ASCE, Vol. 100, No. ST8, August 1974, pp. 1543-1591.
- [2] Aalami, Bijan, "Moment Rotation Relationship Between Column and Slab," *ACI Journal*, Proceedings Vol. 69, No. 5, May 1972, pp. 262-269.
- [3] Akiyama, H., and Hawkins, N. M., "Response of Flat-Plate Concrete Structures to Seismic and Wind Forces," Structures and Mechanics Report SM 84-1, University of Washington, Seattle, July 1984, 267 pp.
- [4] Algermissen, S. T., *An Introduction to the Seismicity of the United States*, Earthquake Engineering Research Institute, Berkeley, California, August 1983, 148 pp.
- [5] Allen, F. H., "Lateral Load Characteristics of Flat Plate Structures," MSc. thesis, Monash University, Melbourne, June 1976.
- [6] Allen, F., and Darvall, P. L., "Lateral Load Equivalent Frame," *ACI Journal*, Proceedings V. 74, No. 7, July 1977, pp. 294-299.
- [7] American Concrete Institute Committee 318, "Building Code Requirements for Reinforced Concrete," ACI 318-83, Detroit, Michigan, 1983, 102 pp.
- [8] Applied Technology Council, "Tentative Provisions for the Development of Seismic Regulations for Buildings," ATC 3-06, prepared by a Joint Committee of the Building Seismic Safety Council and the National Bureau of Standards, Palo Alto, CA., 1984, 599 pp.
- [9] Elias, Z. M., "Sidesway Analysis of Flat Plate Structures," *ACI Journal*, Proceedings V. 76, No. 3, Mar. 1979, p. 421-442.
- [10] Ghali, A., Elmasri, M. Z., and Dilger, W., "Punching of Flat Plates Under Static and Dynamic Horizontal Forces," *ACI Journal*, Title No. 73-47, October, 1976, pp. 566-572.
- [11] Hanson, N. W., and Hanson, J. M., "Shear and Moment Transfer Between Concrete Slabs and Columns," *Journal of the Portland Cement Association*, Research and Development Laboratories, Vol.

- 10, No. 1, Jan., 1968, pp 2-16.
- [12] Hawkins, N. M., "Shear Strength of Slabs with Moments Transferred to Columns," *Shear in Reinforced Concrete*, SP-42, American Concrete Institute, Detroit, 1973, pp. 817-846.
- [13] Hawkins, N. M., Mitchell D., and Sheu M. S., "Cyclic Behavior of Six Reinforced Concrete Slab-Column Specimens Transferring Moment and Shear," Progress Report 1973-74 on NSF Project GI-38717, Section II, Dept. of Civil Engineering, University of Washington, Seattle, WA, 1974.
- [14] Hawkins, N. M., and Mitchell, D., "Progressive collapse of Flat Plate Structures," *ACI Journal*, Vol. 76, No. 7, July 1979, pp. 775-808.
- [15] Hiraishi, H., Nakata, S., and Kaminosono, T., "Static Tests on Shear Walls and Beam-Column Assemblies and Study on Correlation between Shaking Table Tests and Pseudo-Dynamic Tests," *Earthquake Effects on Reinforced Concrete Structures*, US-Japan Research, James K. Wight, Editor, American Concrete Institute, SP-84, Detroit, 1985.
- [16] Islam, S., and Park, R., "Tests on Slab-Column Connections with Shear and Unbalanced Flexure," *Journal of the Structural Division*, ASCE, Vol.102, No. ST3, March, 1976, pp. 549-568.
- [17] Kaba, S. A., and Mahin, S. A., "Interactive Computer Analysis Methods for Predicting the Inelastic cyclic Behavior of Structural Sections," Earthquake Engineering Research Center, Report No. UCB/EERC-83118, University of California at Berkeley, July, 1983.
- [18] Kannan, A. E., and Powell, G. H., "DRAIN-2D: A General Purpose Computer Program for Dynamic Analysis of Inelastic Plane Structures," National Information Service for Earthquake Engineering/Computer Applications, Earthquake Engineering Research Center, Report No. EERC 73-6 and EERC 73-22, April 1973, Revised Sept. 1973 and Aug. 1975.
- [19] Kanoh, Y., and Yoshizaki, S., "Experiments on Slab-Column and Slab-Wall Connections of Flat Plate Structures," *Concrete Journal*, Japan Concrete Institute, Vol. 13, June, 1975, pp. 7-19.
- [20] Mehrain, M., and Aalami, B., "Rotational Stiffness of Concrete Slabs," *ACI Journal*, Proceedings V. 71, No. 9, Sept. 1974, pp. 429-435.
- [21] Moehle, J. P., and Diebold, J., "Experimental Study of the Seismic Response of a Two Story Flat

- Plate Structure," Earthquake Engineering Research Center, Report No. UCB/EERC-84/08, August 1984, University of California at Berkeley, 206 pp.
- [22] Morrison, D. G., Sozen, M. A., "Response of Reinforce Concrete Plate-Column Connections to Dynamic and Static Horizontal Loads," Civil Engineering Studies, Structural Research Series No. 490, University of Illinois at Urbana-Champaign, Urbana, Illinois, April, 1981, 560 pp.
- [23] Mulcahy, J. F., and Rotter, J. M., "Moment Rotation Characteristics of Flat Plate and Column Systems," *ACI Journal*, Vol. 80, No. 2, March-April, 1983, pp. 85-92.
- [24] Newmark, N. M., and Hall, W. J., "Earthquake Spectra and Design," *Engineering Monographs on Earthquake Criteria: Structural Design and Strong Motion*, Earthquake Engineering Engineering Research Institute, 1982, 103 pp.
- [25] Park, R., and Islam, S., "Strength of Slab-Column Connections with Shear and Unbalanced Flexure," *Journal of the Structural Division*, ASCE, Vol. 102, No. ST9, September, 1976, pp. 1879-1901.
- [26] Park, R., and Pauley, T., *Reinforced Concrete Structures*, John Wiley & Son, 1975, 769 p.
- [27] Pecknold, David A., "Slab Effective Width for Equivalent Frame Analysis," *ACI Journal*, Proceedings V. 72, No. 4, April 1975, pp. 135-137.
- [28] Sheu, M. S., and Hawkins, N. M., "Grid Model for Predicting the Monotonic and Hysteretic Behavior of Slab-Column Connections Transferring Moments," *Reinforced Concrete Structures Subjected to Wind and Earthquake Forces*, SP-63, American Concrete Institute, Detroit, 1980, pp. 79-111.
- [29] Sozen, M. A., "Review of Earthquake Response of Reinforced Concrete Buildings with a View to Drift Control," *State-of-the Art in Earthquake Engineering*, Seventh World Conference on Earthquake Engineering, Istanbul, 1980, pp.119-174.
- [30] Symonds, D. W., Mitchell, D., and Hawkins, N. M., "Slab-Column Connections Subjected to High Intensity Shears and Transferring Reversed Moments" Progress Report on NSF Project GI-38717, Dept. of Civil Engineering, University of Washington, Seattle, WA, August, 1976.
- [31] USGS Report, "San Fernando Earthquake of 1971," John A. Blume and Associates, Engineers, San Francisco, California, May 1972.

- [32] *Uniform Building Code*, International Conference of Building Officials, Whittier, California, 1985, 780 pp.
- [33] Vanderbilt, M. D., and Corley, W. G., "Frame Analysis of Concrete Buildings," *Concrete International*, American Concrete Institute, Dec., 1983, pp. 33-43.
- [34] Wilson,, E. L., and Habibullah, A., *SAP80 Structural Analysis Programs: A Series of Computer Programs for the Static and Dynamic Finite Element Analysis of Structures*, Computers & Structures Inc., Berkeley, California, August, 1984, 193 pp.
- [35] Zee, H. L., and Moehle, J. P., "Behavior of Interior and Exterior Flat Plate Connections Subjected to Inelastic Load Reversals," Earthquake Engineering Research Center, Report No. UCB/EERC-84/07, August, 1984, University of California, Berkeley, 130 pp.

Materials	Percent Used	Cubic Feet Absolute Vol.	Specific Gravity	Saturated Surface Dry Wts./Cu. Yd.
Cement		2.630	3.15	517
Water: 34 gal.		4.535	1.00	283
Radum 1" x #4 Gravel	52.0	10.314	2.68	1725
Radum Top Sand	36.0	7.141	2.68	1194
Blend Sand	12.0	2.380	2.60	386
Totals	100.0	27.000		4105

Mix #K557-115: 5.5 sk., 1" max., 4" slp., 4000 psi in 28 days, Zeecon R40 @6 oz./cwt.

Table 3.1 - Concrete Mix Design

Test Specimens 1 and 2			Test Specimens 3 and 4		
Mat. Prop.	Mean	Std. Dev.	Mat. Prop.	Mean	Std. Dev.
f'c (psi)	4825	303	f'c (psi)	4550	364
ft (psi)	570	26	ft (psi)	540	22
Et (ksi)	3958	120	Et (ksi)	3689	147
E45 (ksi)	3762	145	E45 (ksi)	3505	132

Note: Six cylinders tested for each set.

Table 3.2 - Concrete Properties

Mat. Property	Mean	Std. Dev.
Yield Stress (psi)	68440	1234
Tensile Stress (psi)	106430	4509
Elastic Modulus (ksi)	29500	1870
Ultimate Strain (in./in.)	0.104	0.008

Table 3.3 - Slab Reinforcement Properties

TEST NO.	1	2	3	4	5
SPECIMEN NO.	1	2	3	4	R*
LATERAL LOAD	Uniaxial	Biaxial	Uniaxial	Biaxial	Biaxial
GRAVITY LOAD (psi)	$1.4\sqrt{f'_c}$	$1.4\sqrt{f'_c}$	$0.88\sqrt{f'_c}$	$0.88\sqrt{f'_c}$	$0.88\sqrt{f'_c}$

* Repaired Specimen No. 4

Table 4.1 - Test Program

Test	Direction	Gravity Load (kips)	Maximum Lateral Force (kips)	Maximum Drift (%)
1	EW	25	6.62	1.54
2	EW	25	5.24	1.51
2	NS	25	4.21	1.04
3	EW	11	10.02	4.76
4	EW	11	9.61	3.21
4	NS	11	7.91	1.54
5	EW	11	3.92	3.22
5	NS	11	2.36	3.24

Table 6.1 - Summary of Test Results

Specimen Number	Label *	Researchers	c1 (in.)	c2 (in.)	h (in.)	davg (in.)	l1 (in.)	l2 (in.)	hc (in.)	ptc+3h **	psc+3h ***	fy (psi)	f'c (psi)
1	Test 1		10.8	10.8	4.84	4.07	144	144	72	0.0076	0.0029	68440	4825
2	Test 2	Present	10.8	10.8	4.84	4.07	144	144	72	0.0076	0.0029	68440	4825
3	Test 3	Study	10.8	10.8	4.84	4.07	144	144	72	0.0076	0.0029	68440	4550
4	Test 4		10.8	10.8	4.84	4.07	144	144	72	0.0076	0.0029	68440	4550
5	S1		12	12	6	4.6	144	84	102	0.012	0.0059	66600	5050
6	S2	Hawkins	12	12	6	4.6	144	84	102	0.0084	0.0049	67100	3400
7	S3	et al	12	12	6	4.6	144	84	102	0.0055	0.004	66000	3200
8	S4		12	12	6	4.6	144	84	102	0.012	0.0059	66600	4690
9	S6	Symonds et	12	12	6	4.6	144	84	102	0.0181	0.0091	66600	3360
10	S7	al	12	12	6	4.6	144	84	102	0.0084	0.0049	67100	3840
11	S1		12	12	3	2.36	72	72	44	0.0065	0.0065	46800	6640
12	S2	Morison	12	12	3	2.36	72	72	44	0.0098	0.0098	47900	5090
13	S3	and	12	12	3	2.36	72	72	44	0.0131	0.0131	48600	4920
14	S4	Sozen	12	12	3	2.36	72	72	44	0.0098	0.0098	46000	5060
15	S5		12	12	3	2.36	72	72	44	0.0098	0.0098	49300	5110
16	SM 0.5	Ghali	12	12	6	4.75	72	72	46	0.005	0.00167	69000	5329
17	SM 1.0	et	12	12	6	4.75	72	72	46	0.01	0.00333	69000	4835
18	SM 1.5	al	12	12	6	4.75	72	72	46	0.015	0.005	69000	5794
19	INT	Zee	5.4	5.4	2.4	1.99	72	72	36	0.008	0.006	63100	5400
20	IP2	Islam &	9	9	3.5	2.75	108	90	60	0.0106	0.00534	54200	4630
21	IP3C	Park	9	9	3.5	2.75	108	90	60	0.0106	0.00534	45800	4310
22	B7	Hanson &	12	6	3	2.25	72	48	63	0.015	0.015	51400	4780
23	C8	Hanson	6	12	3	2.25	72	48	63	0.015	0.015	59600	4760

* Designation used by original researchers.

** Top steel ratio within 3h strip over column.

*** Bottom steel ratio within 3h strip over column.

Note : 1 in. = 25.4 mm 1 psi = 6895 Pa

Table 7.1 - Data of Experimental Specimens

Specimen Number	Label	Researchers	Vg (kips)	Ductility Ratio	Maximum Drift	Vg/Vo	Classification
1	Test 1		23.32	1.7	1.54%	0.353	B
2	Test 2	Present Study	23.32	1.87	1.51%	0.353	B
3	Test 3		14.12	2.32	4.76%	0.223	B
4	Test 4		14.12	2.11	3.21%	0.223	B
5	S1		28.8	1.58	3.75%	0.332	A
6	S2	Hawkins et al	32	1	2.00%	0.449	C
7	S3		31.2	1	2.00%	0.451	C
8	S4		33.7	1.9	2.60%	0.403	B
9	S6		61	1	1.10%	0.861	C
10	S7	Symonds et al	61	1	1.00%	0.806	C
11	S1		1.35	5.2	4.70%	0.031	A
12	S2	Morison and Sozen	1.35	2.9	2.80%	0.035	B
13	S3		1.35	3.9	4.20%	0.035	A
14	S4		3	4.2	4.50%	0.078	A
15	S5		6.42	4	4.80%	0.166	A
16	SM 0.5		29	3.5	6.00%	0.312	A
17	SM 1.0	Ghali et al	29	1.4	2.70%	0.328	B
18	SM 1.5		29	1.8	2.70%	0.299	B
19	INT		3.6	3.2	3.30%	0.208	B
20	IP2	Islam & Park	6.42	3.2	5.00%	0.182	A
21	IP3C		7.64	4	4.00%	0.225	B
22	B7	Hanson & Hanson	1.1	3.4	3.80%	0.039	B
23	C8		1.26	2.8	5.80%	0.045	A

Note : 1 Kip = 4.448 KN

Table 7.2 - Summary of Analysis Results

$$W = 5384 \text{ Kips}$$

$$T = 2.1 \text{ seconds} *$$

$$V = 152 \text{ Kips}$$

Reinforcement Percentage

Size	Column 20"X20"		Beam 16"X20"	
	Ext.	Int.	Ext.	Int.
10	1.34	2.21	1.12	1.12
9	1.34	2.21	1.12	1.12
8	1.34	2.21	1.12	1.12
7	1.34	2.21	1.12	1.12
6	1.85	2.88	1.44	1.44
5	1.85	2.88	1.44	1.44
4	1.85	2.88	1.44	1.44
3	3.36	4.20	1.75	1.75
2	3.36	4.20	1.75	1.75
1	3.36	4.20	1.75	1.75

* Stiffness According to Section 8.3

Table 8.1 (a) - Properties of Frame System in UBC Zone No. 2

$$W = 5016 \text{ Kips}$$

$$T = 1.6 \text{ seconds}$$

$$V = 148 \text{ Kips}$$

Reinforcement Percentage

Story	Ext. Column 18"X18"	Slab Col. Strip t=8"	Shear Wall 8"X168"
10	0.74	0.57	0.51
9	0.74	0.57	0.51
8	0.74	0.57	0.51
7	0.74	0.57	0.51
6	0.94	0.57	0.88
5	0.94	0.57	0.88
4	0.94	0.57	0.88
3	1.86	0.57	1.45
2	1.86	0.57	1.45
1	1.86	0.57	1.45

Table 8.1 (b) - Properties of Shear Wall System in UBC Zone No. 2

$$W = 5280 \text{ Kips}$$

$$T = 2.3 \text{ seconds}$$

$$V = 164 \text{ Kips}$$

Reinforcement Percentage

Size	Slab Col. Strip t=8"		Column 24"X24"	
Story	Ext.	Int.	Ext.	Int.
10	0.62	0.59	0.81	1.25
9	0.62	0.59	0.81	1.25
8	0.62	0.59	0.81	1.25
7	0.62	0.59	0.81	1.25
6	0.82	0.78	0.81	1.56
5	0.82	0.78	0.81	1.56
4	0.82	0.78	0.81	1.56
3	0.82	0.78	2.51	2.76
2	0.82	0.78	2.51	2.76
1	0.82	0.78	2.51	2.76

Table 8.1 (c) - Properties of Flat Plate System in UBC Zone No. 2

$$W = 5594 \text{ Kips}$$

$$T = 1.7 \text{ seconds}$$

$$V = 437 \text{ Kips}$$

Reinforcement Percentage

Size	Column 24"X24"		Beam 18"X24"	
	Ext.	Int.	Ext.	Int.
10	1.60	2.89	1.34	1.34
9	1.60	2.89	1.34	1.34
8	1.60	2.89	1.34	1.34
7	1.60	3.69	1.34	1.34
6	1.94	3.69	1.83	1.83
5	1.94	3.69	1.83	1.83
4	1.94	3.69	1.83	1.83
3	4.24	4.86	2.34	2.34
2	4.24	4.86	2.34	2.34
1	4.24	4.86	2.34	2.34

Table 8.1 (d) - Properties of Frame System in UBC Zone No. 4

$$W = 5178 \text{ Kips}$$

$$T = 1.1 \text{ seconds}$$

$$V = 482 \text{ Kips}$$

Reinforcement Percentage

Story	Ext. Column 18"X18"	Slab Col. Strip t=8"	Shear Wall 10"X216"
10	0.92	0.57	0.73
9	0.92	0.57	0.73
8	0.92	0.57	0.73
7	0.92	0.57	0.73
6	1.15	0.57	1.22
5	1.15	0.57	1.22
4	1.15	0.57	1.22
3	2.32	0.57	1.81
2	2.32	0.57	1.81
1	2.32	0.57	1.81

Table 8.1 (e) - Properties of Shear Wall System in UBC Zone No. 4

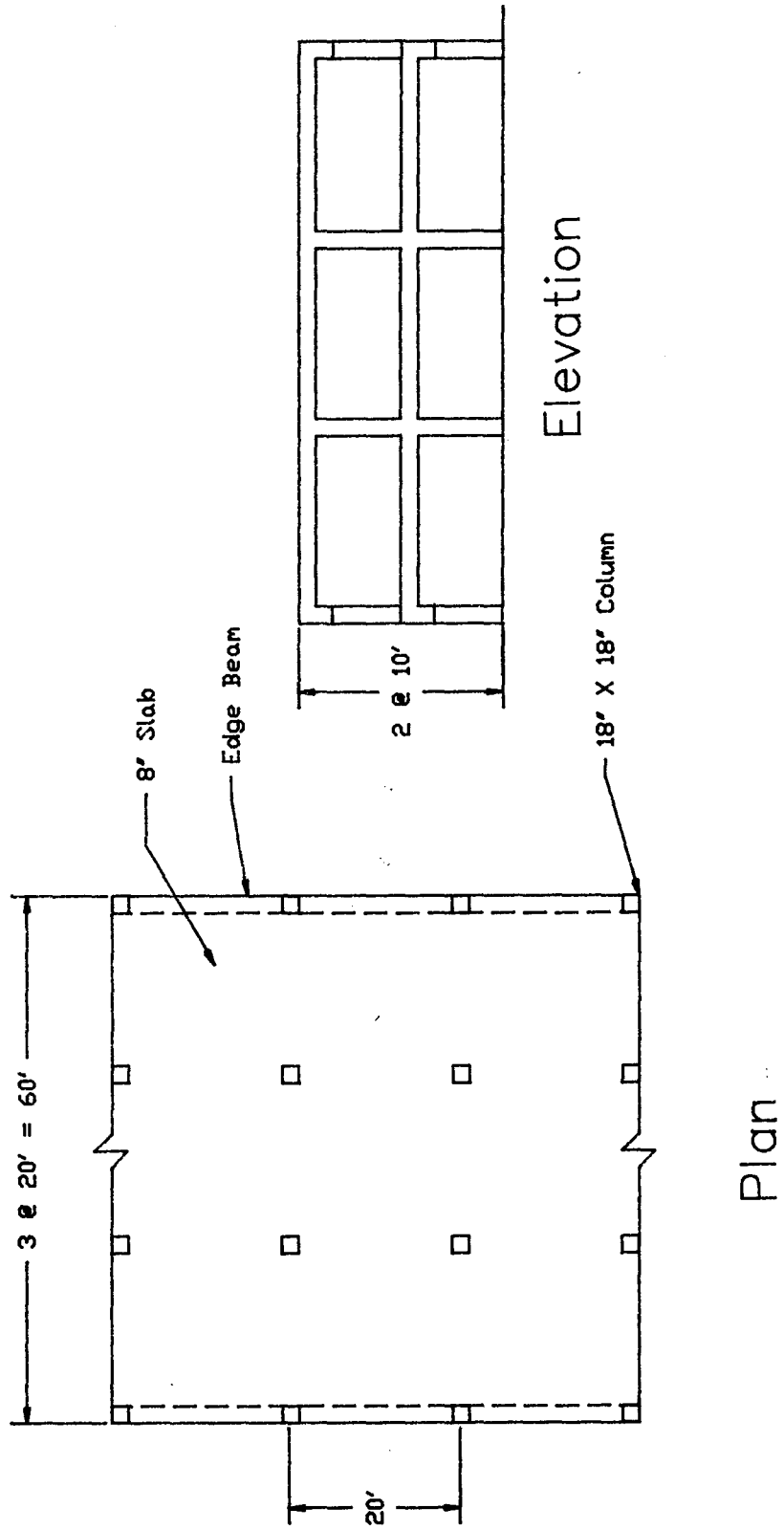


Fig. 2.1 Plan and Elevation of Prototype

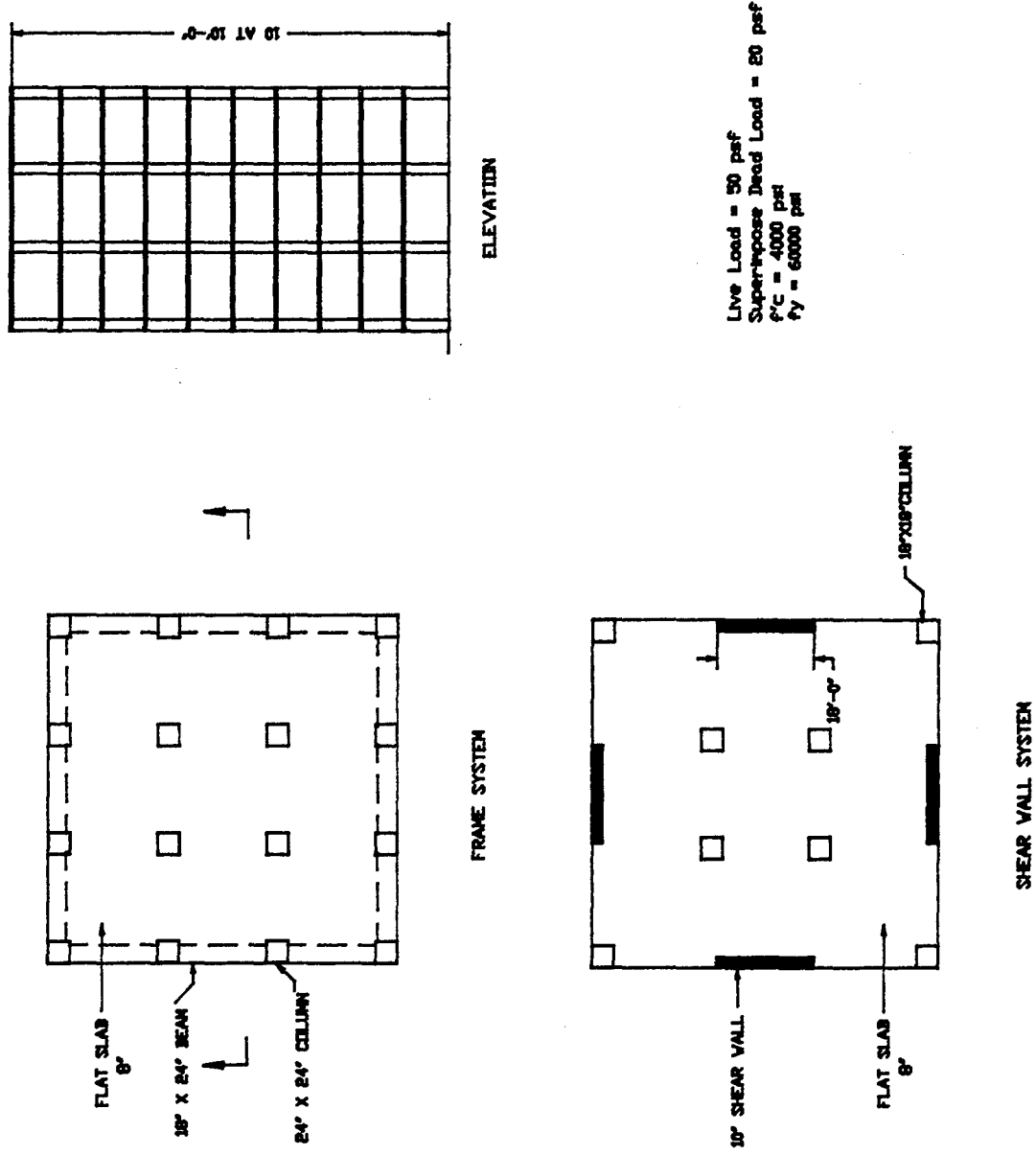
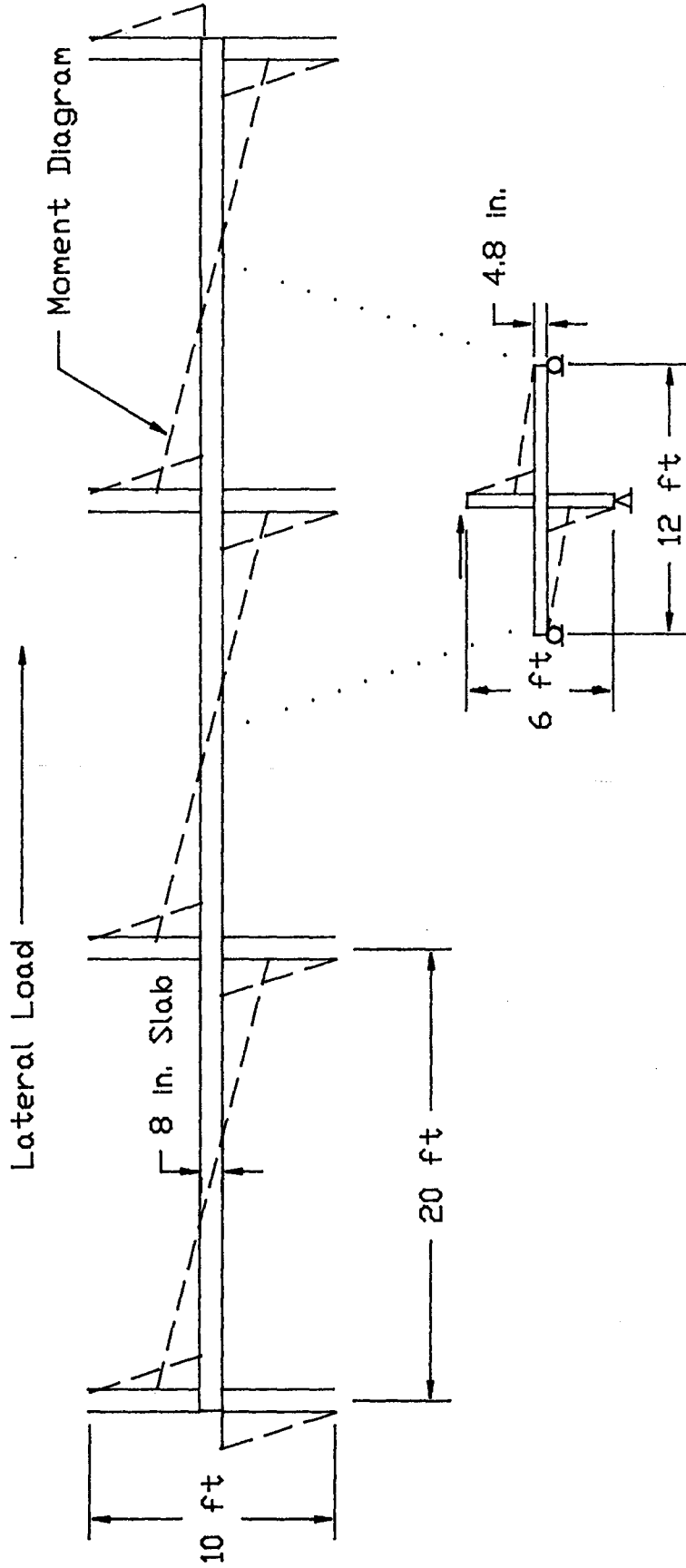


Fig. 2.2 Alternative Prototype Structures

Full-Scale Prototype



Test Specimen

Fig. 3.1 Relation of Test Specimen to Prototype

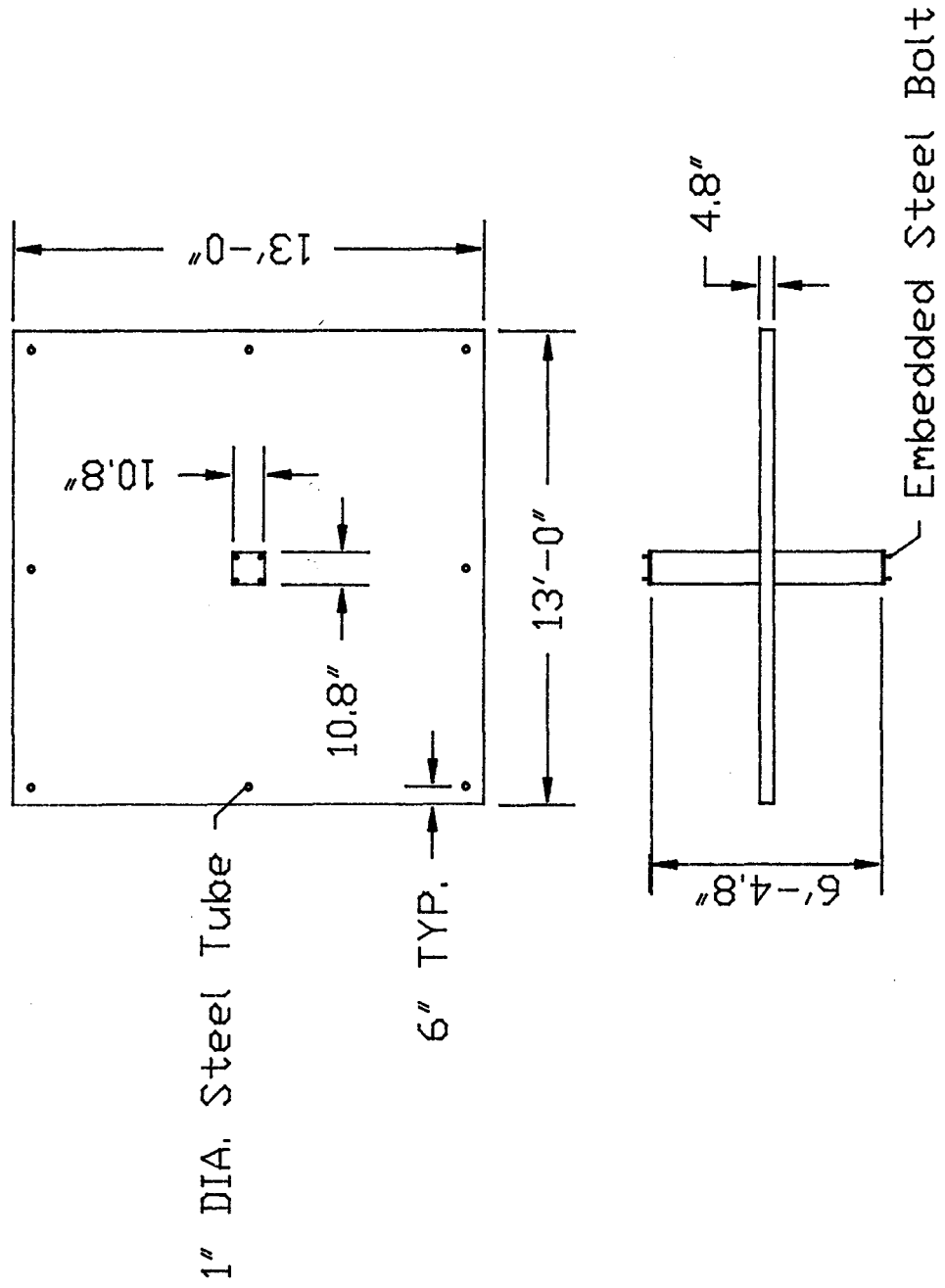


Fig. 3.2 Test Specimen

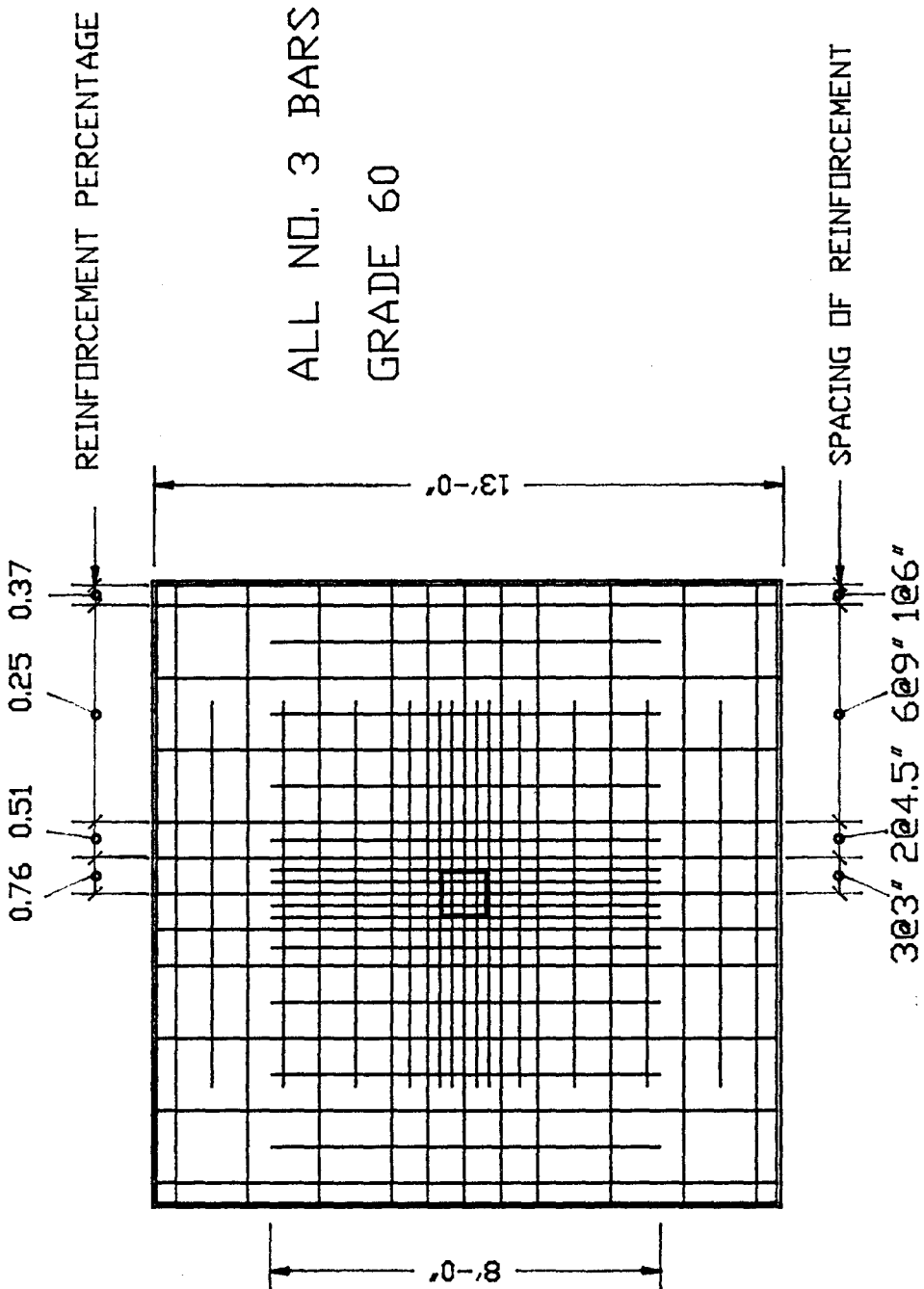


Fig. 3.3 Top Slab Reinforcement

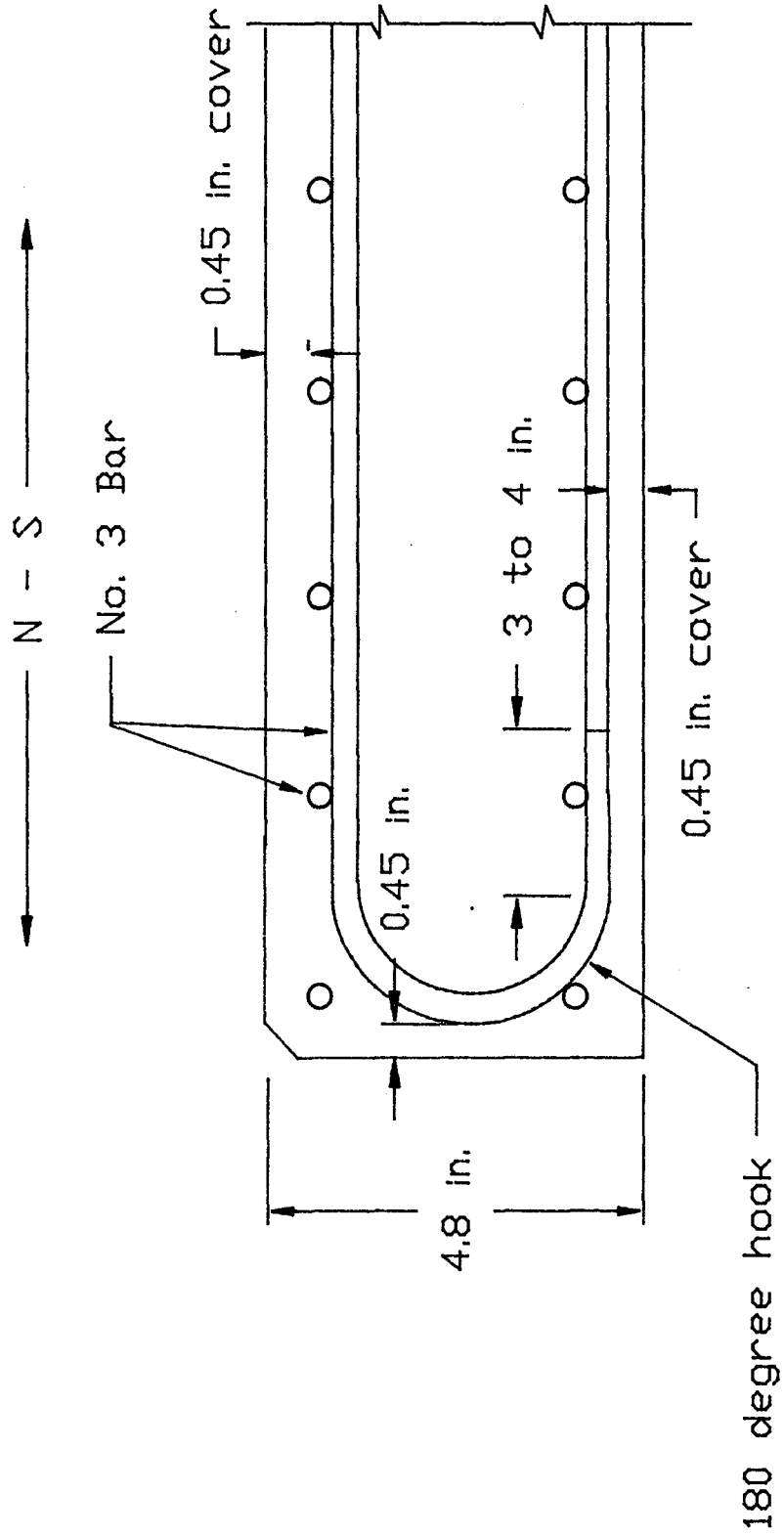


Fig. 3.4 Slab Reinforcement Detail

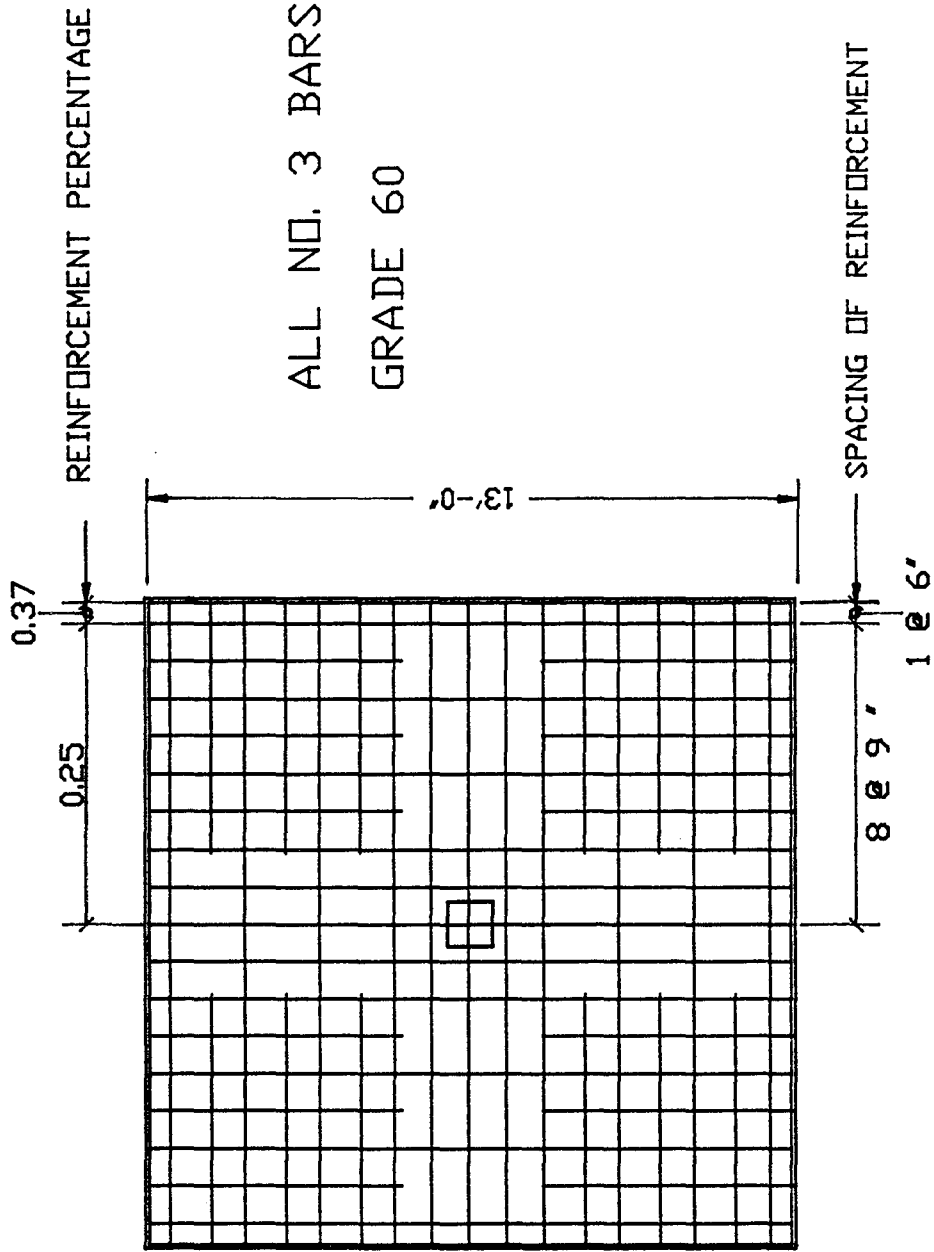


Fig. 3.5 Bottom Slab Reinforcement

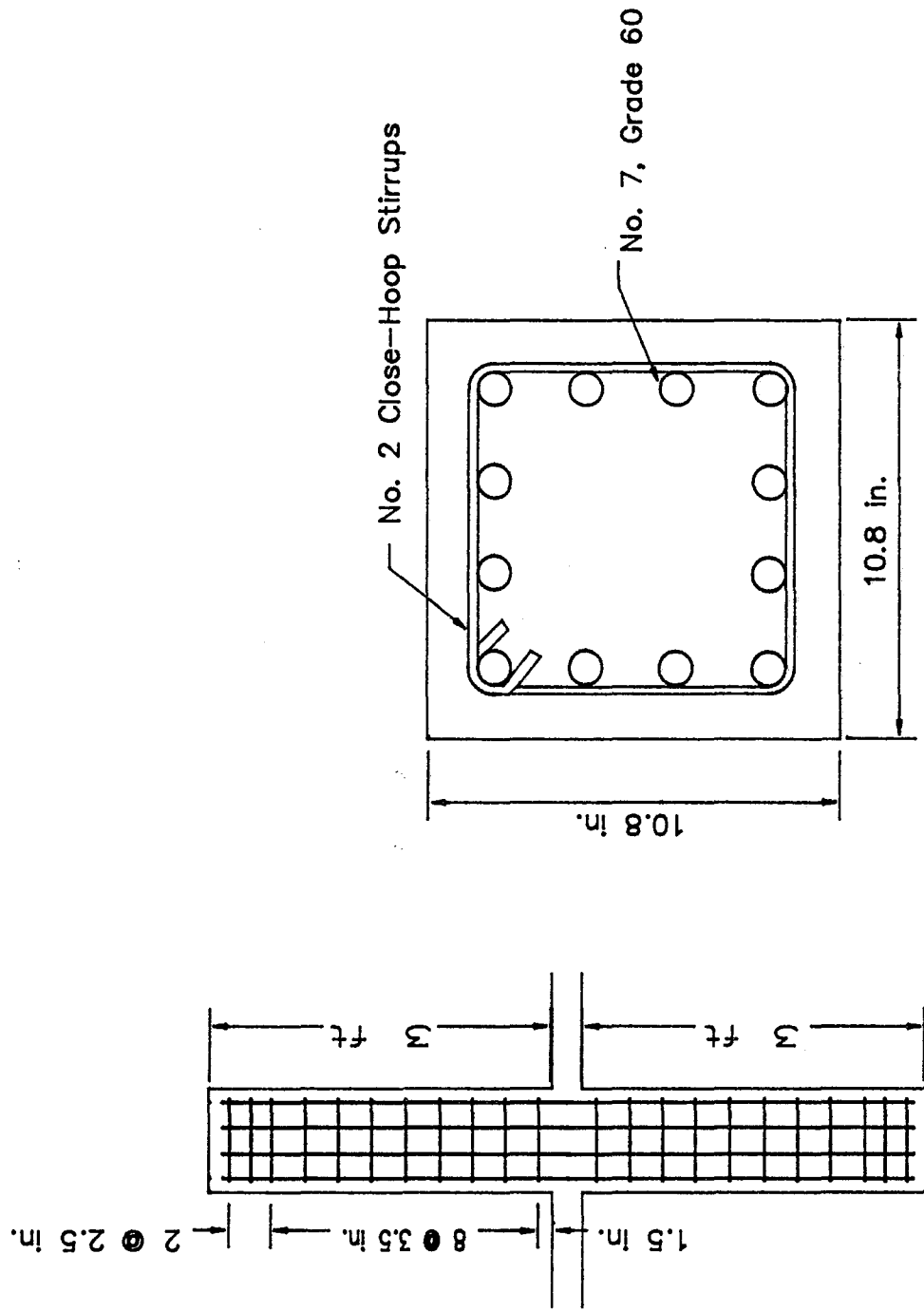


Fig. 3.6 Column Reinforcement



Fig. 3.7 Photo of Test Specimens



Fig. 3.8 Honeycombs in Column of Specimen 3

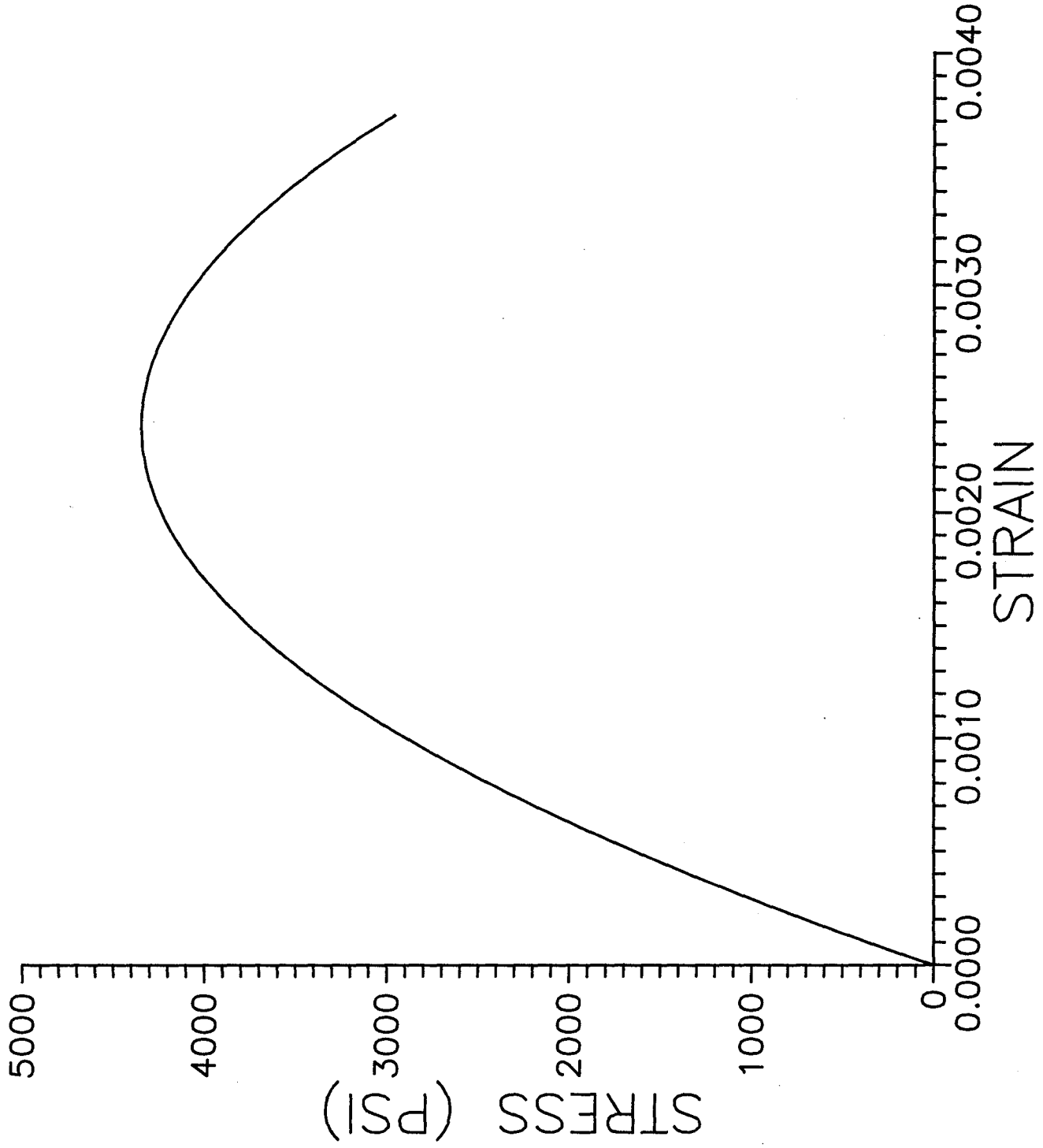


Fig. 3.9 Measured Concrete Stress-Strain for Specimens 3 and 4 (Cylinder B)

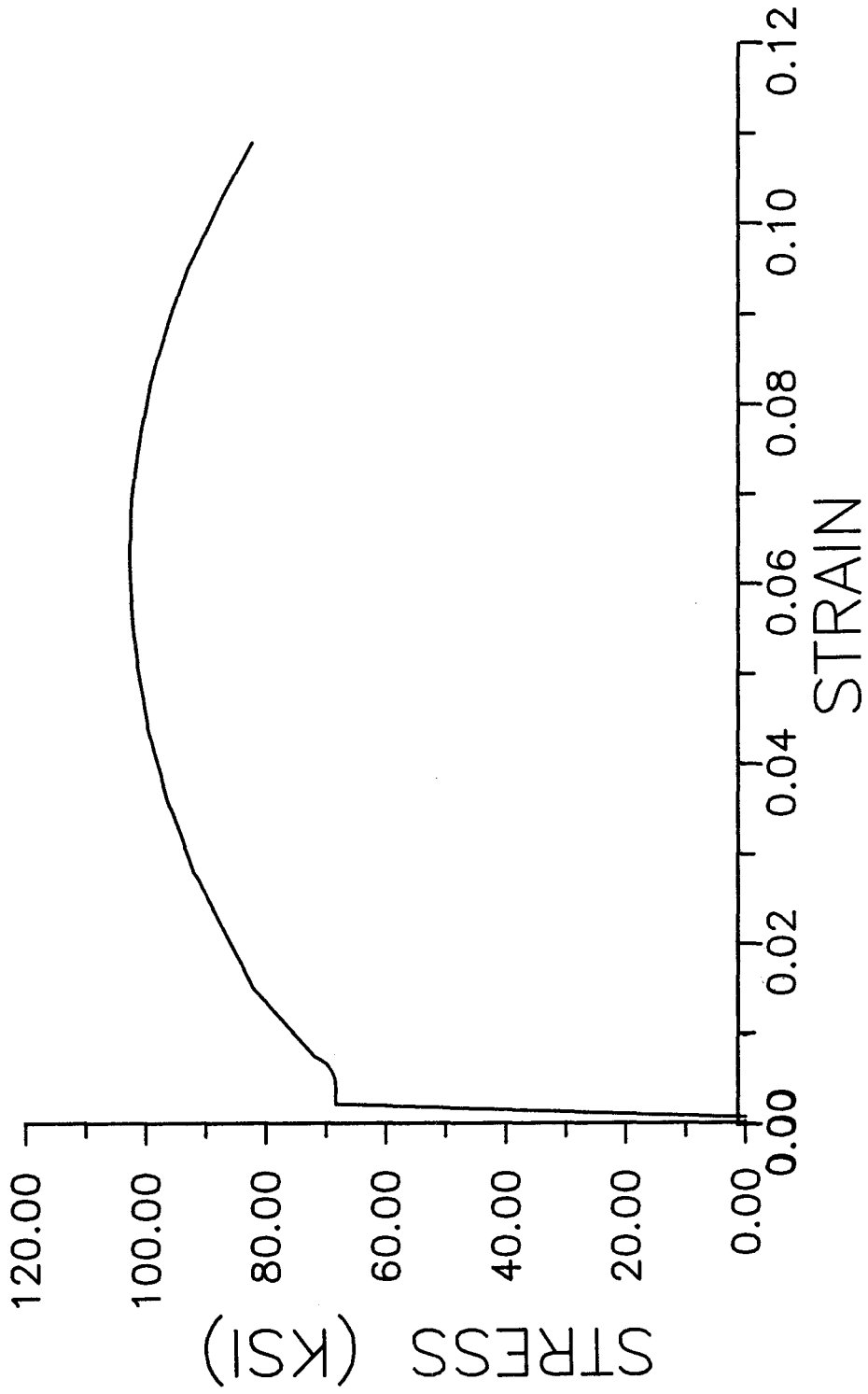


Fig. 3.10 Measured Stress-Strain of Slab Reinforcement - No. 3, Grade 60

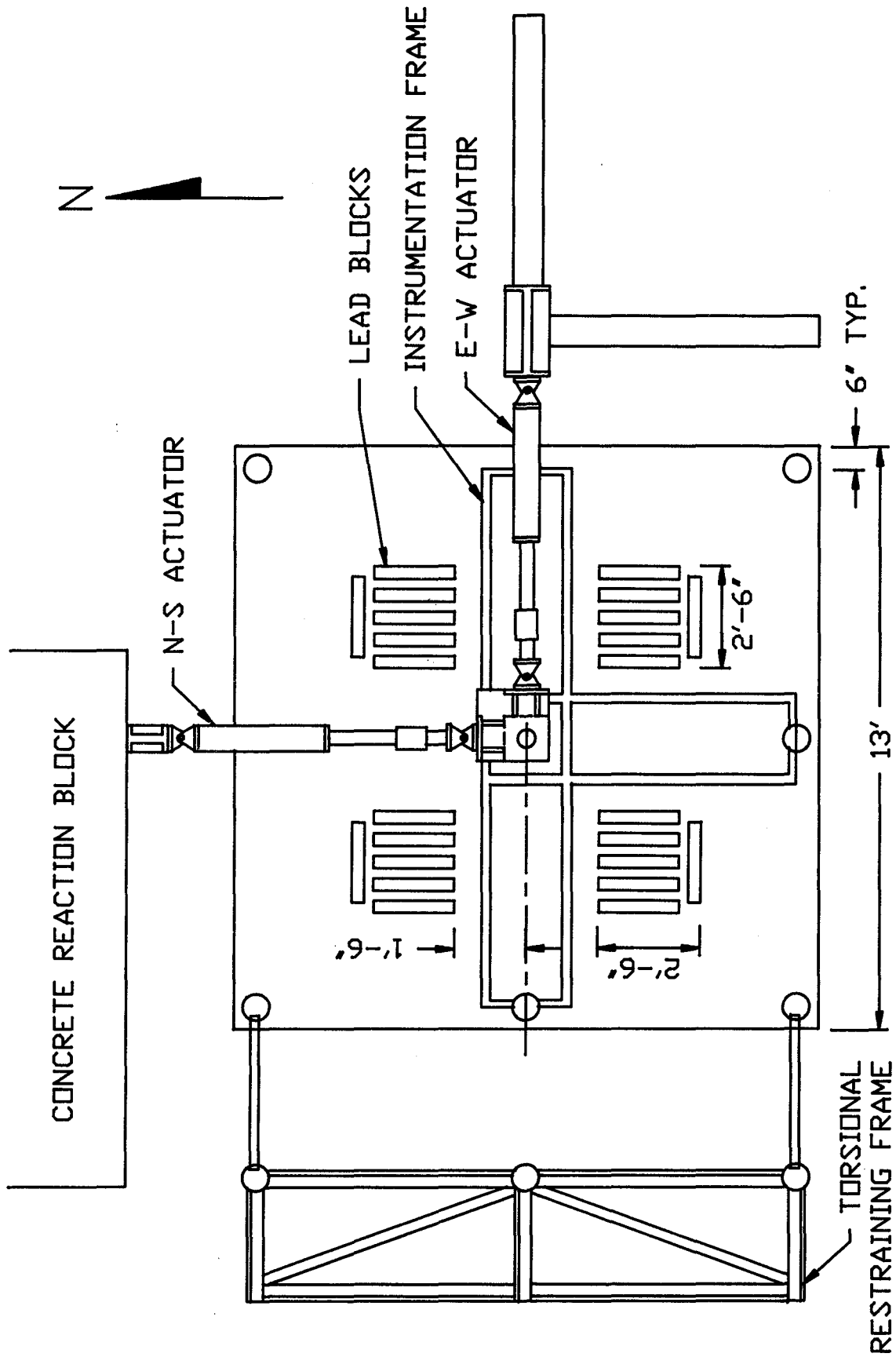


Fig. 4.1 (a) Test Setup - Plan

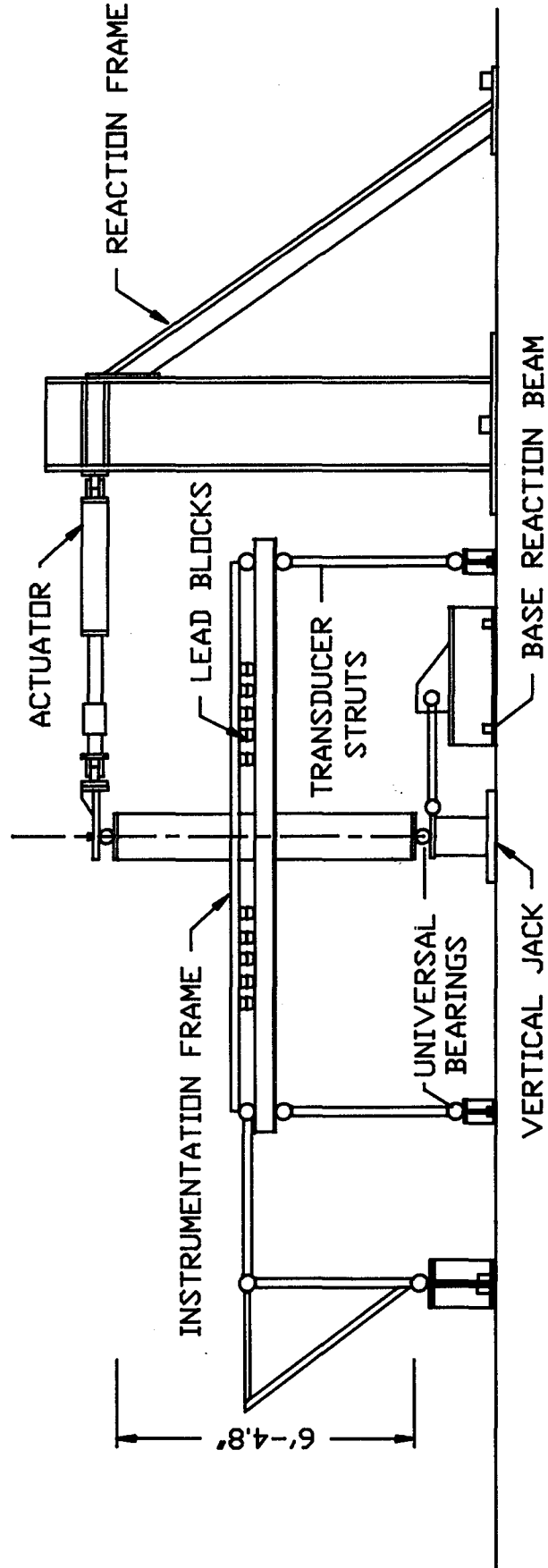


Fig. 4.1 (b) Test Setup - Elevation

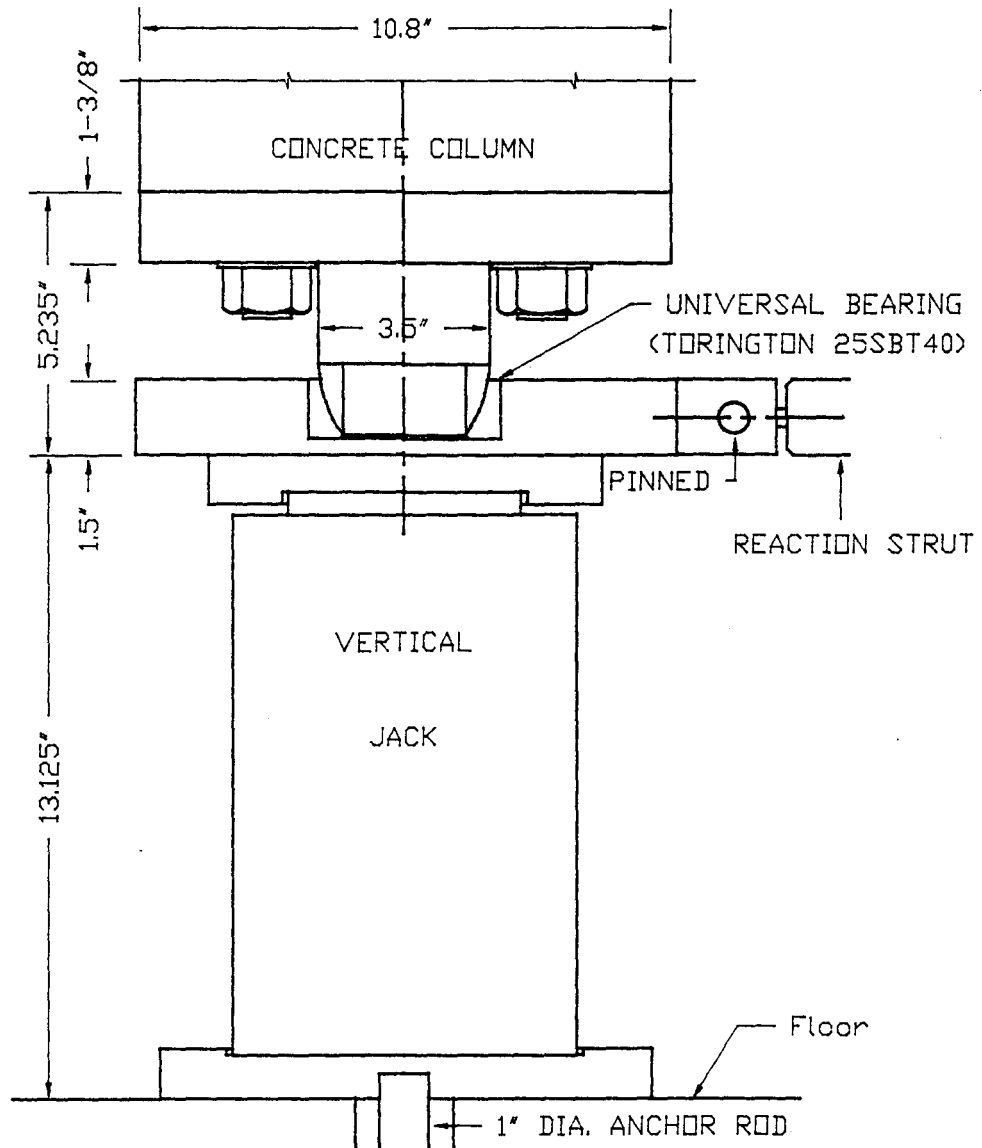


Fig. 4.2 Detail of Column Base

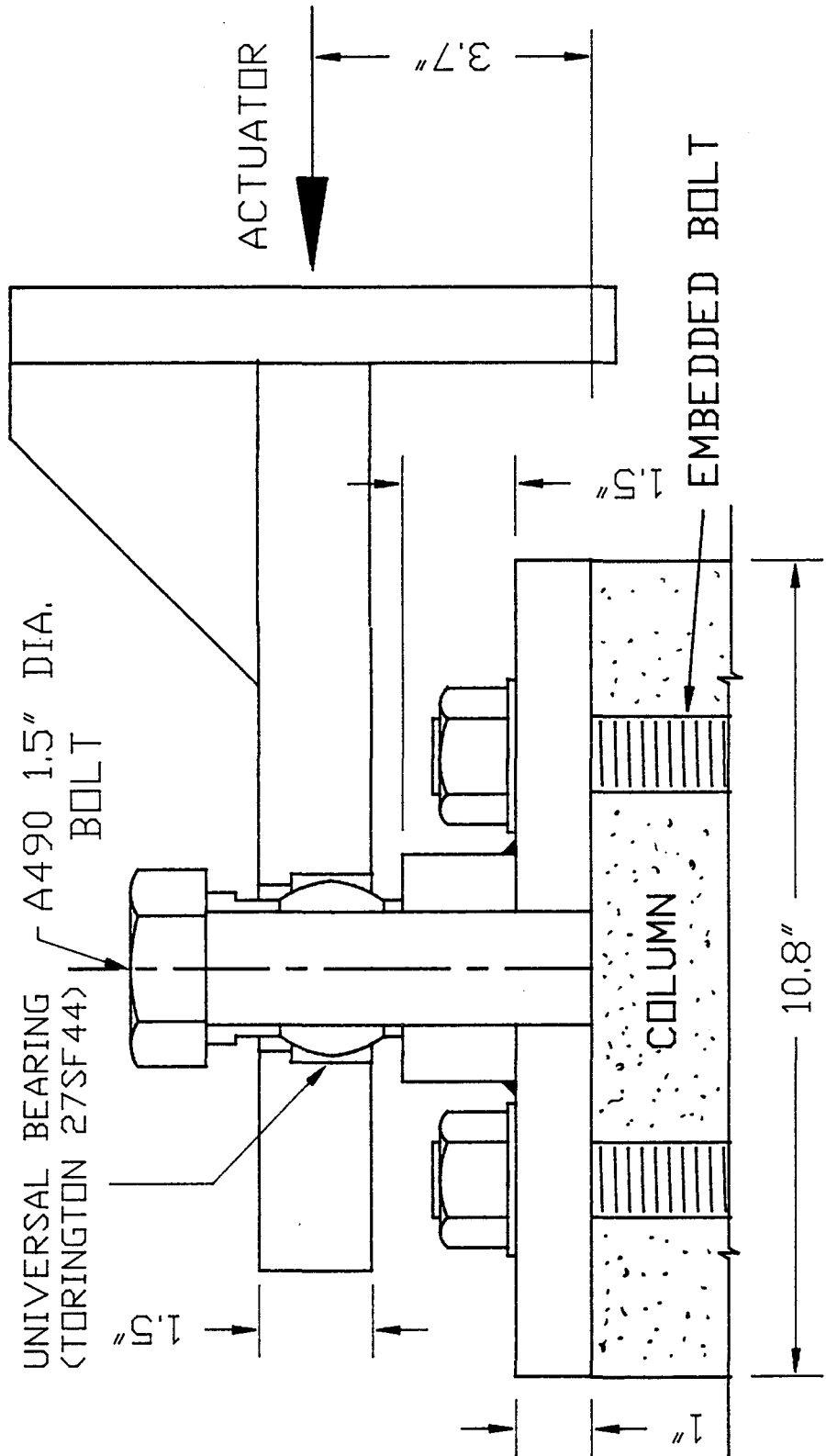


Fig. 4.3 Detail of Column Top

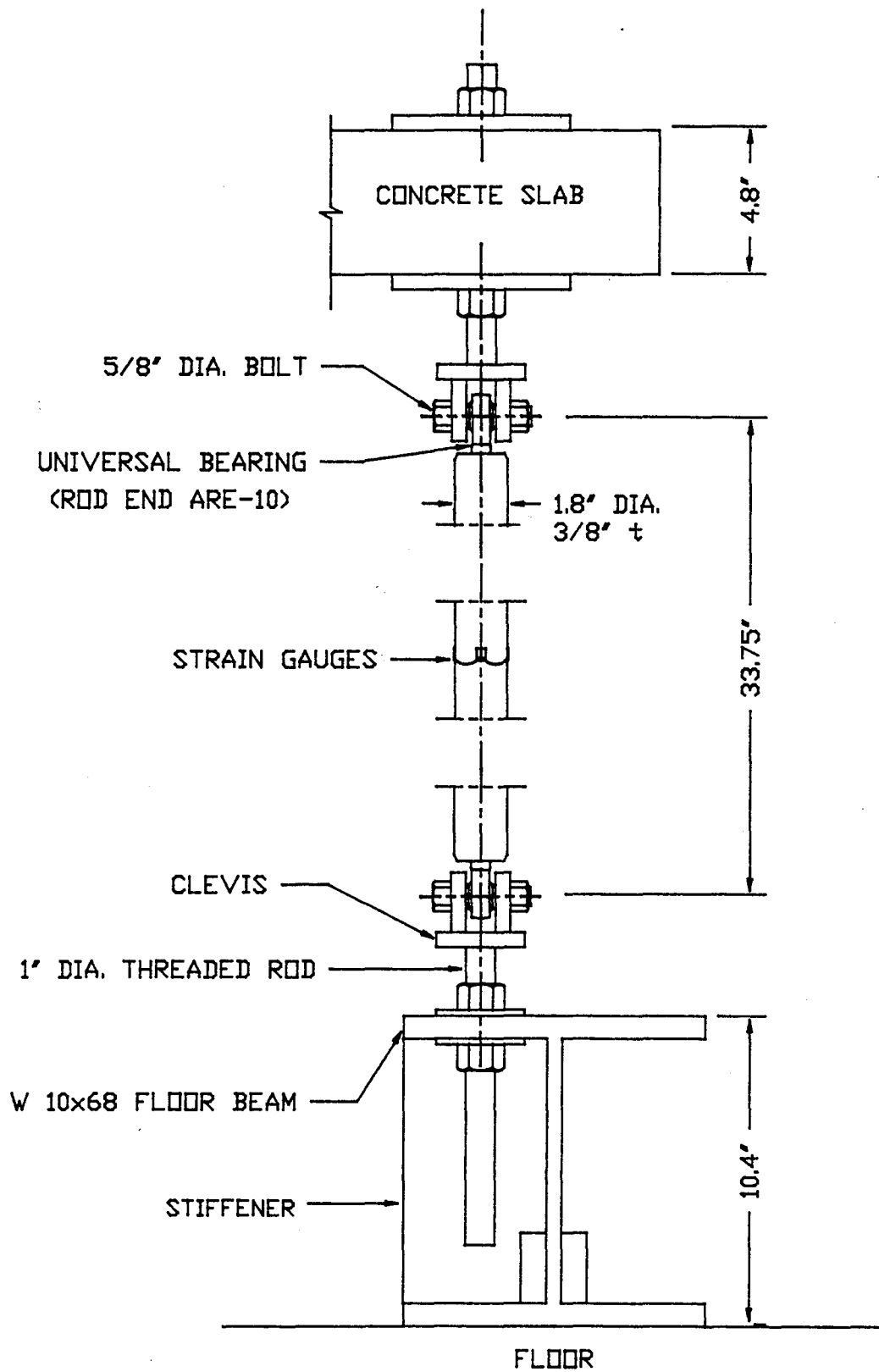


Fig. 4.4 Transducer Strut

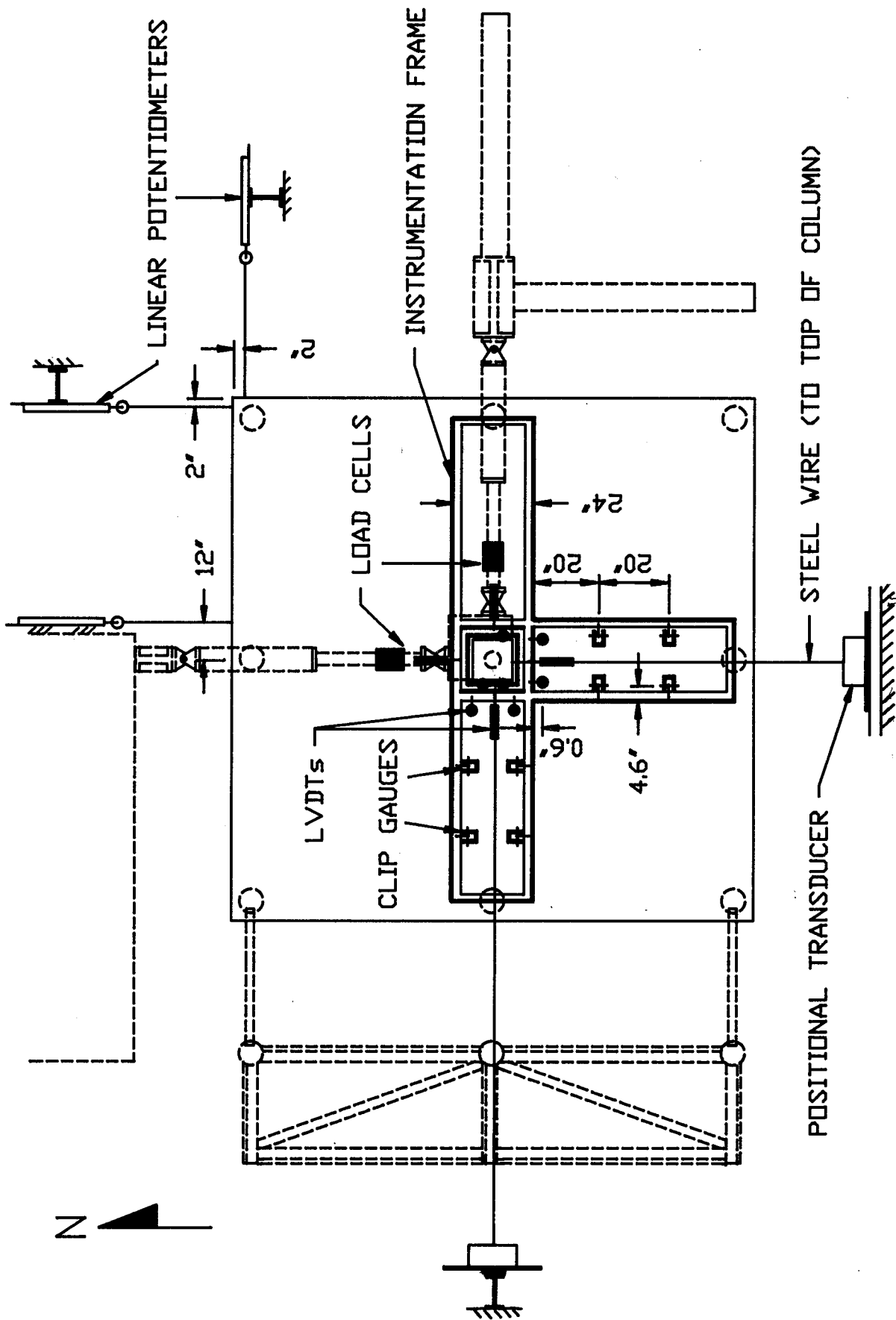


Fig. 4.5 (a) Instrumentation - Plan

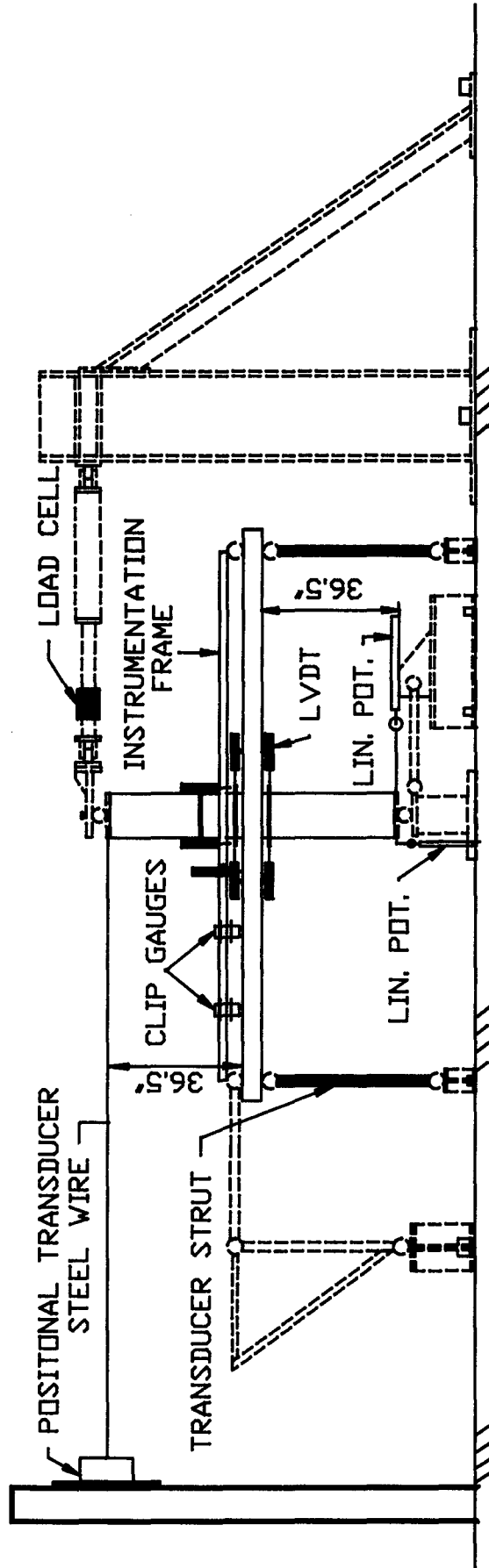


Fig. 4.5 (b) Instrumentation - Elevation

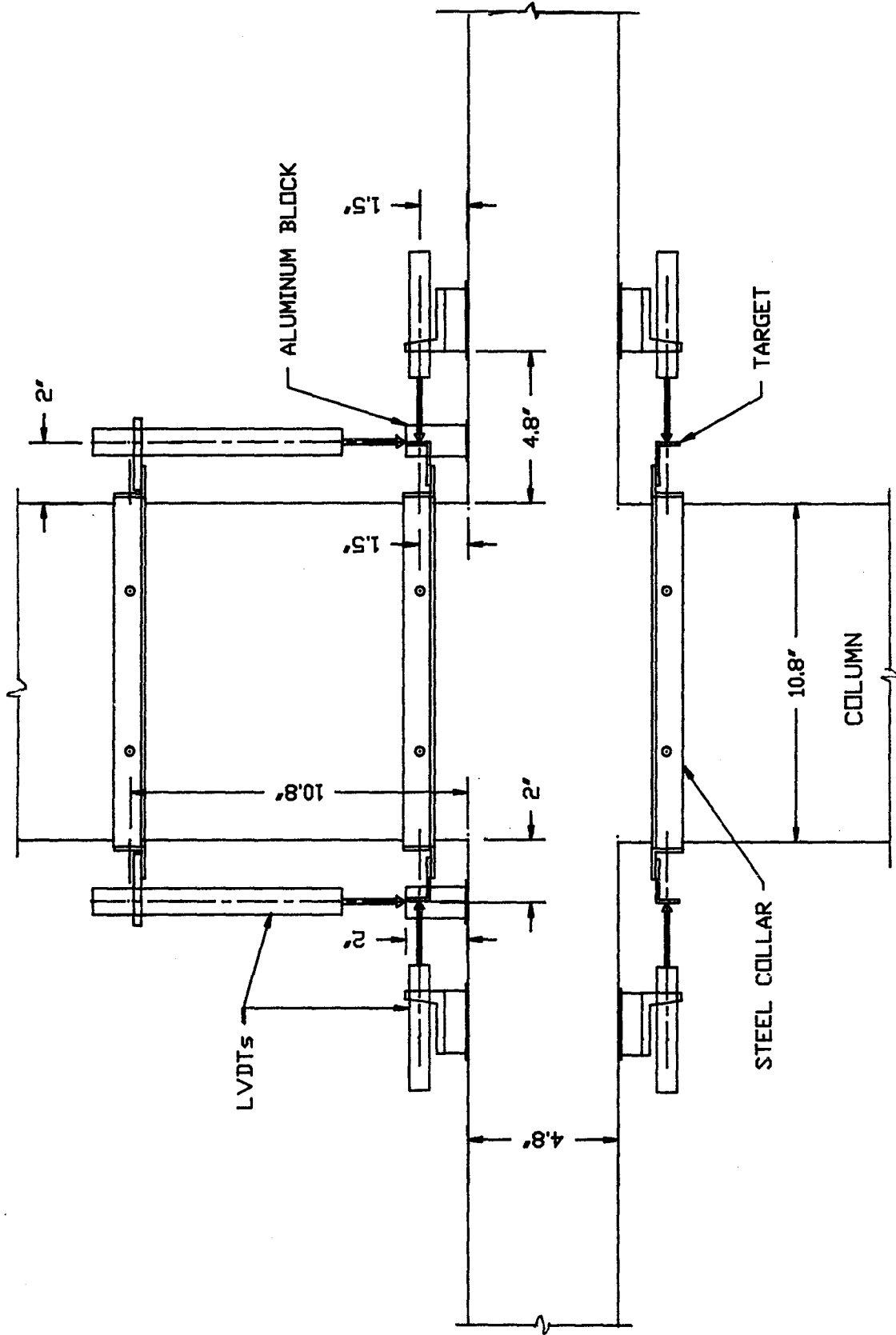


Fig. 4.6 Slab-Column Instrumentation

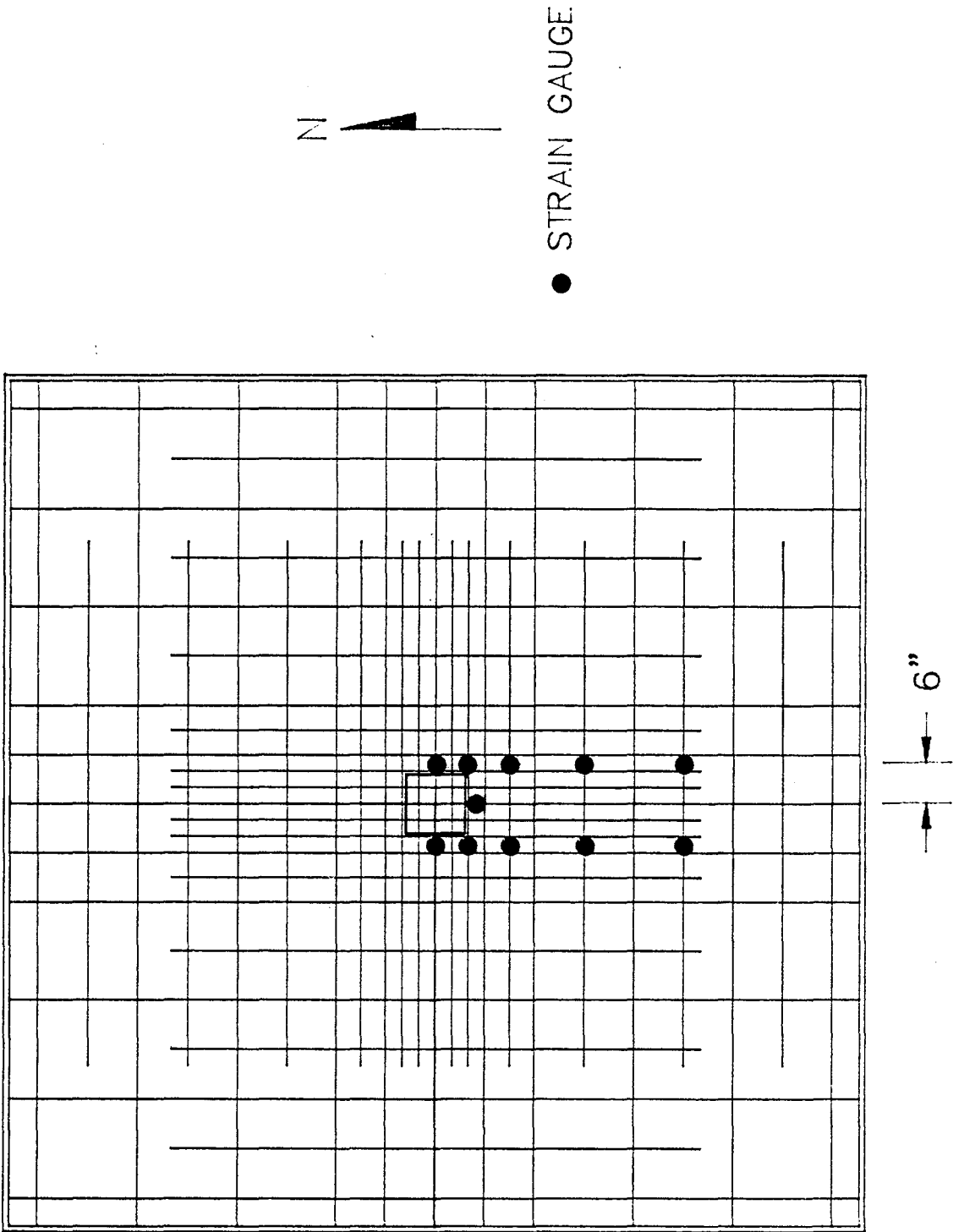


Fig. 4.7 Top Strain Gauge Locations - Uniaxial Tests

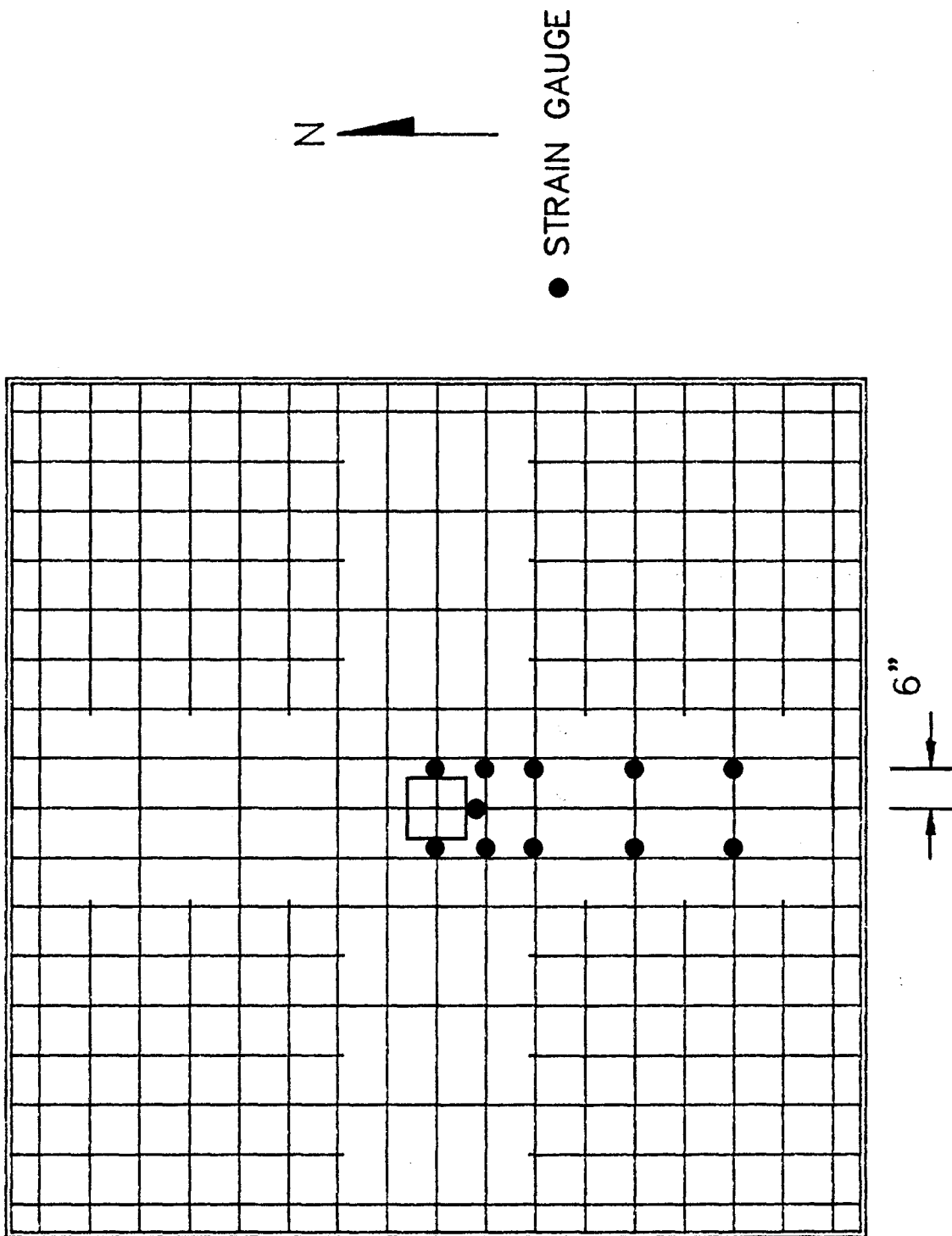


Fig. 4.8 Bottom Strain Gauge Locations - Uniaxial Tests

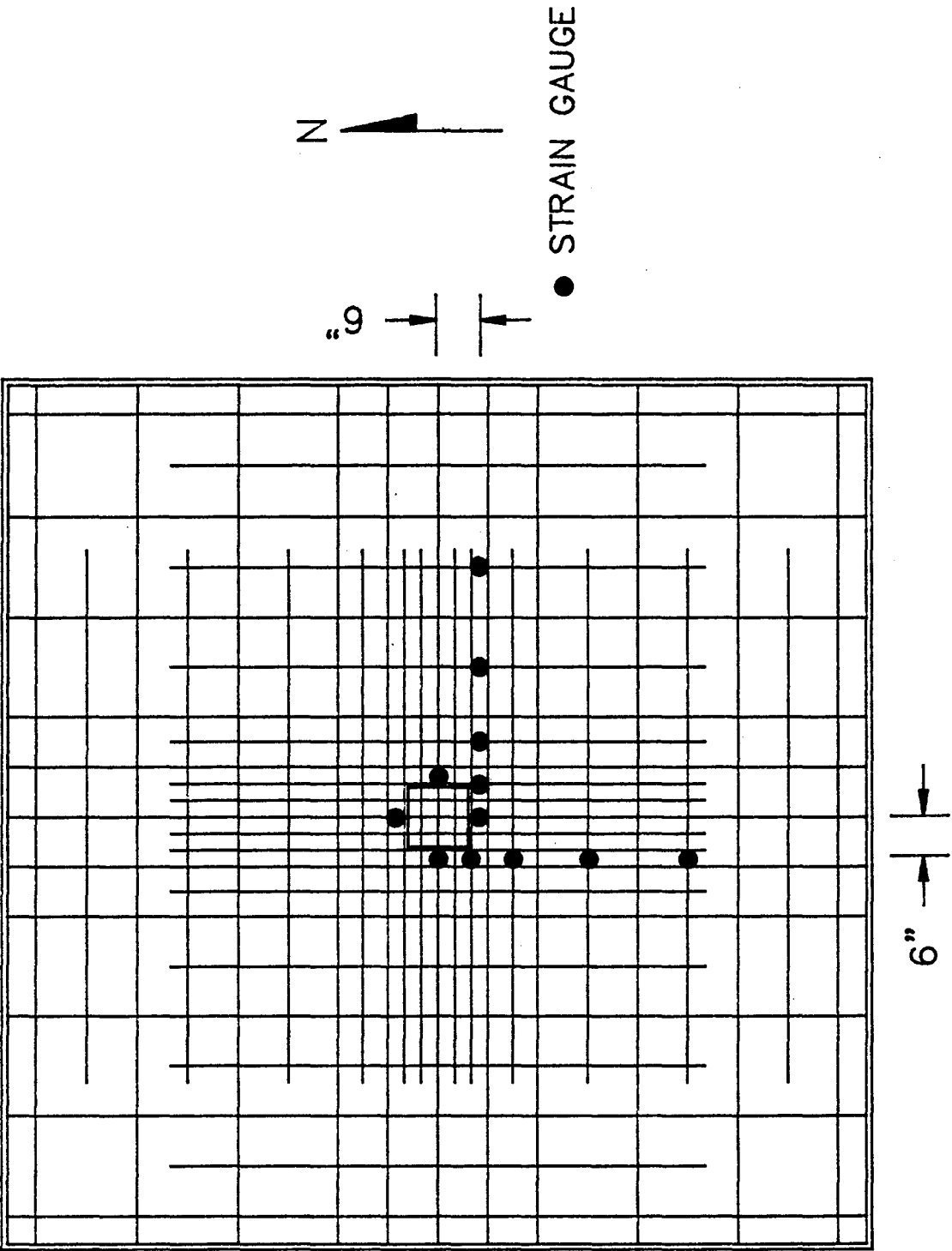


Fig. 4.9 Top Strain Gauge Locations - Biaxial Tests

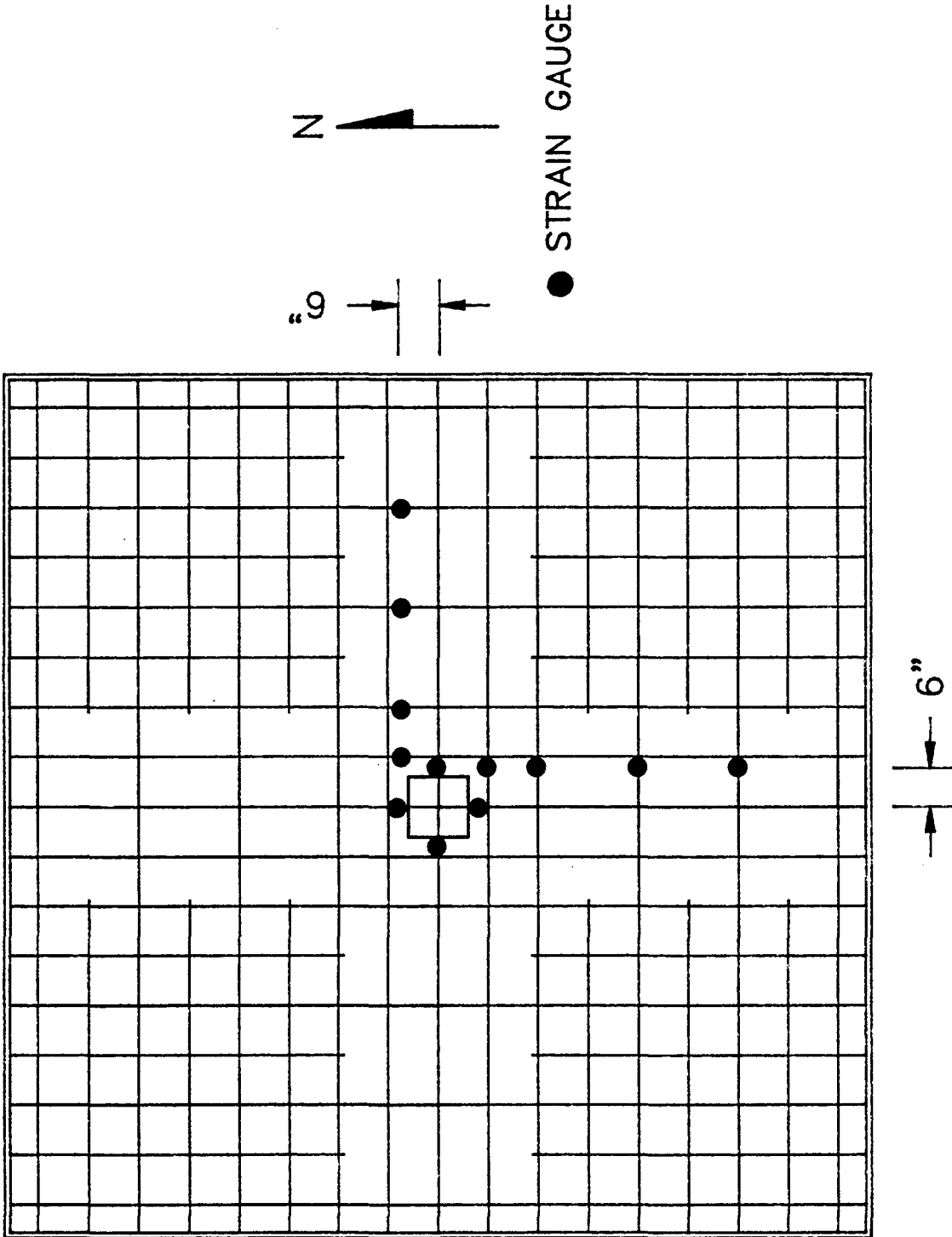
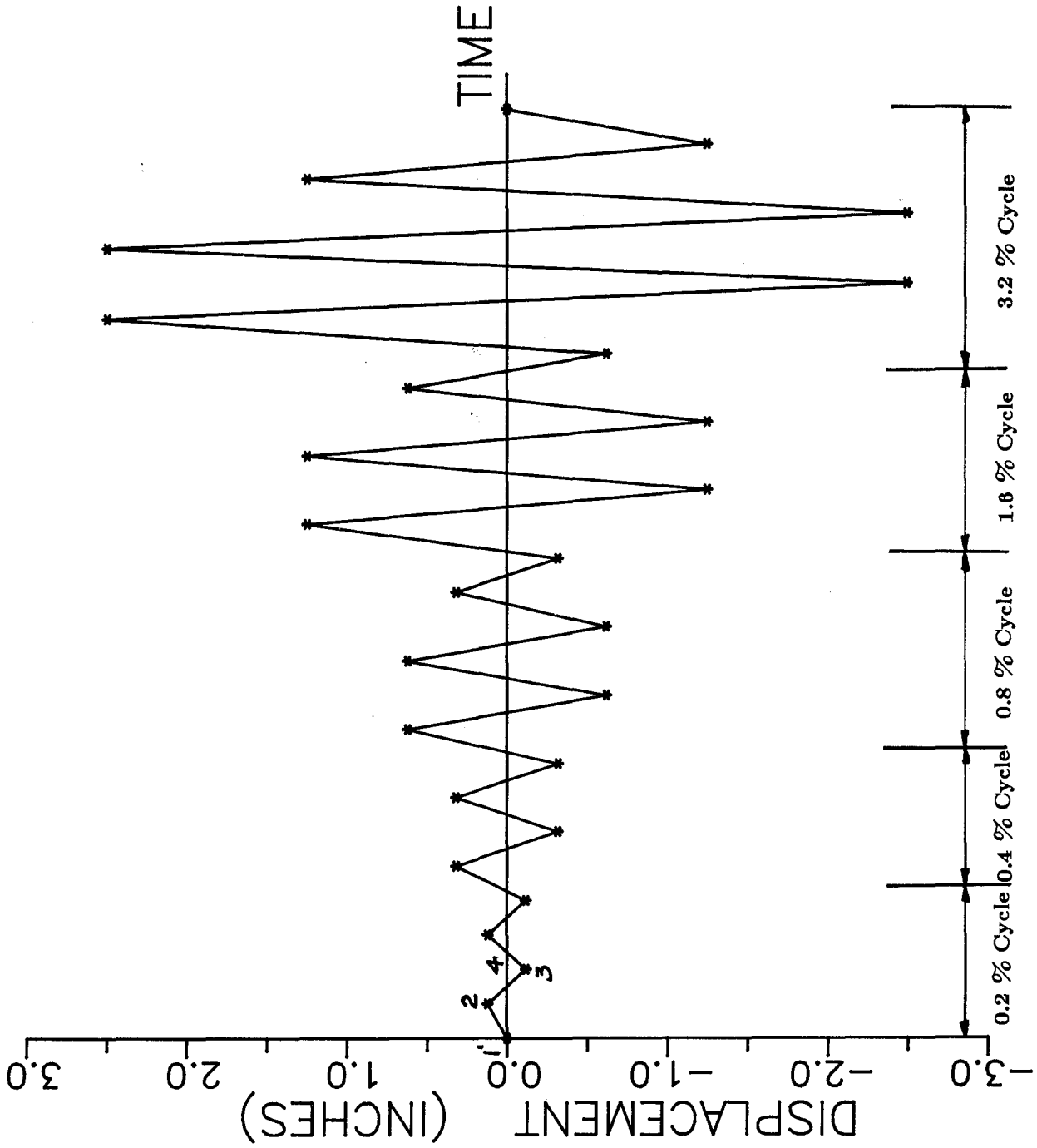
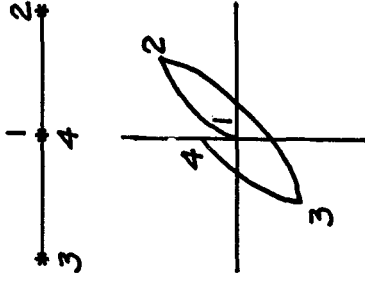


Fig. 4.10 Bottom Strain Gauge Locations - Biaxial Tests



UNI-DIRECTIONAL



101

BI-DIRECTIONAL

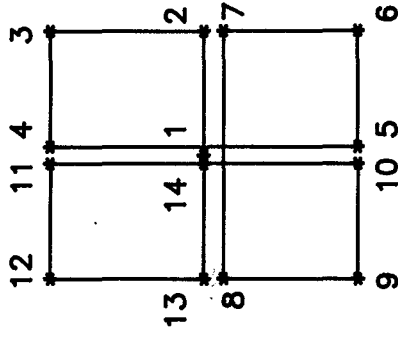


Fig. 4.1.1 Lateral Displacement History and Loading Patterns

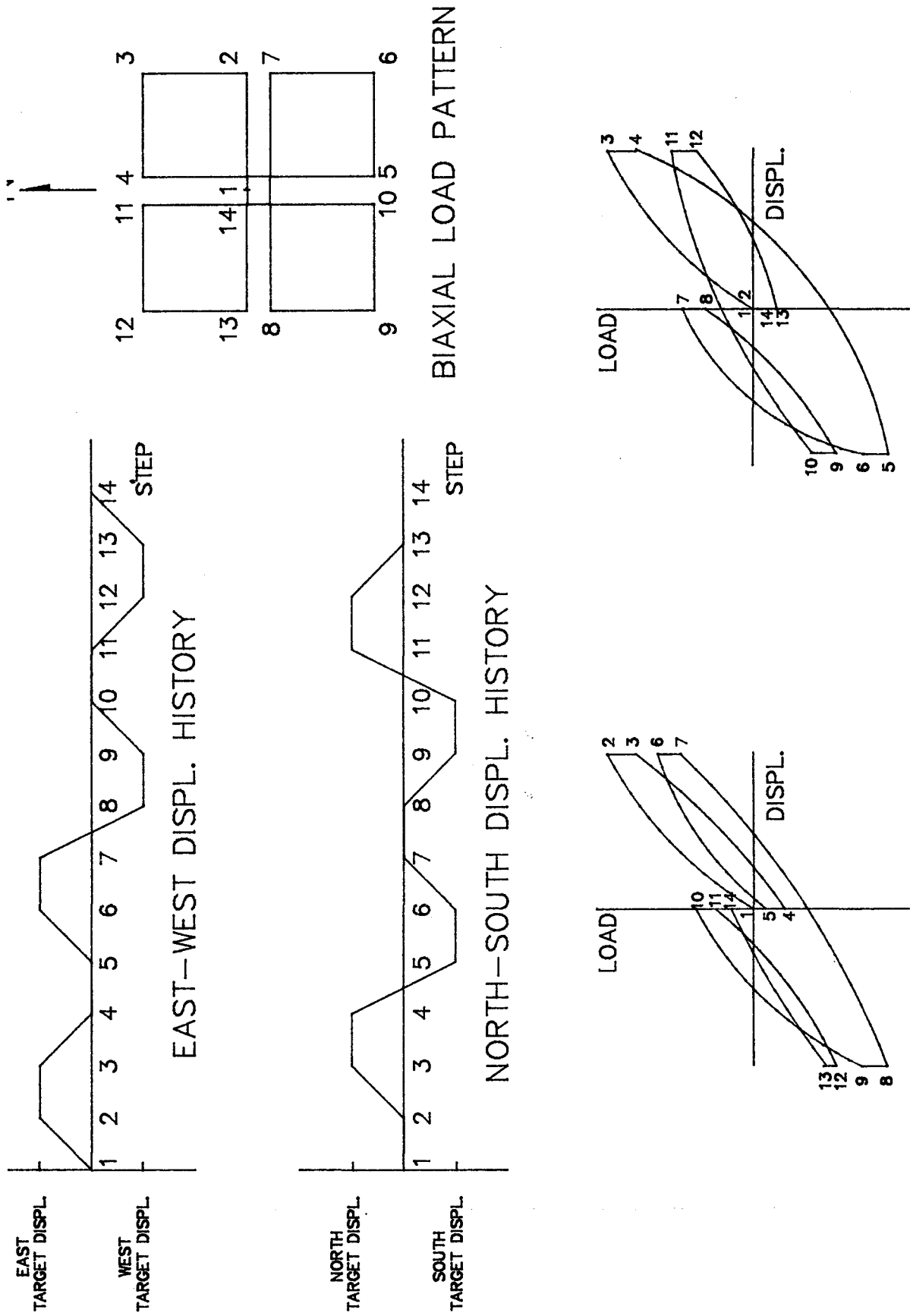


Fig. 4.12 Biaxial Loading

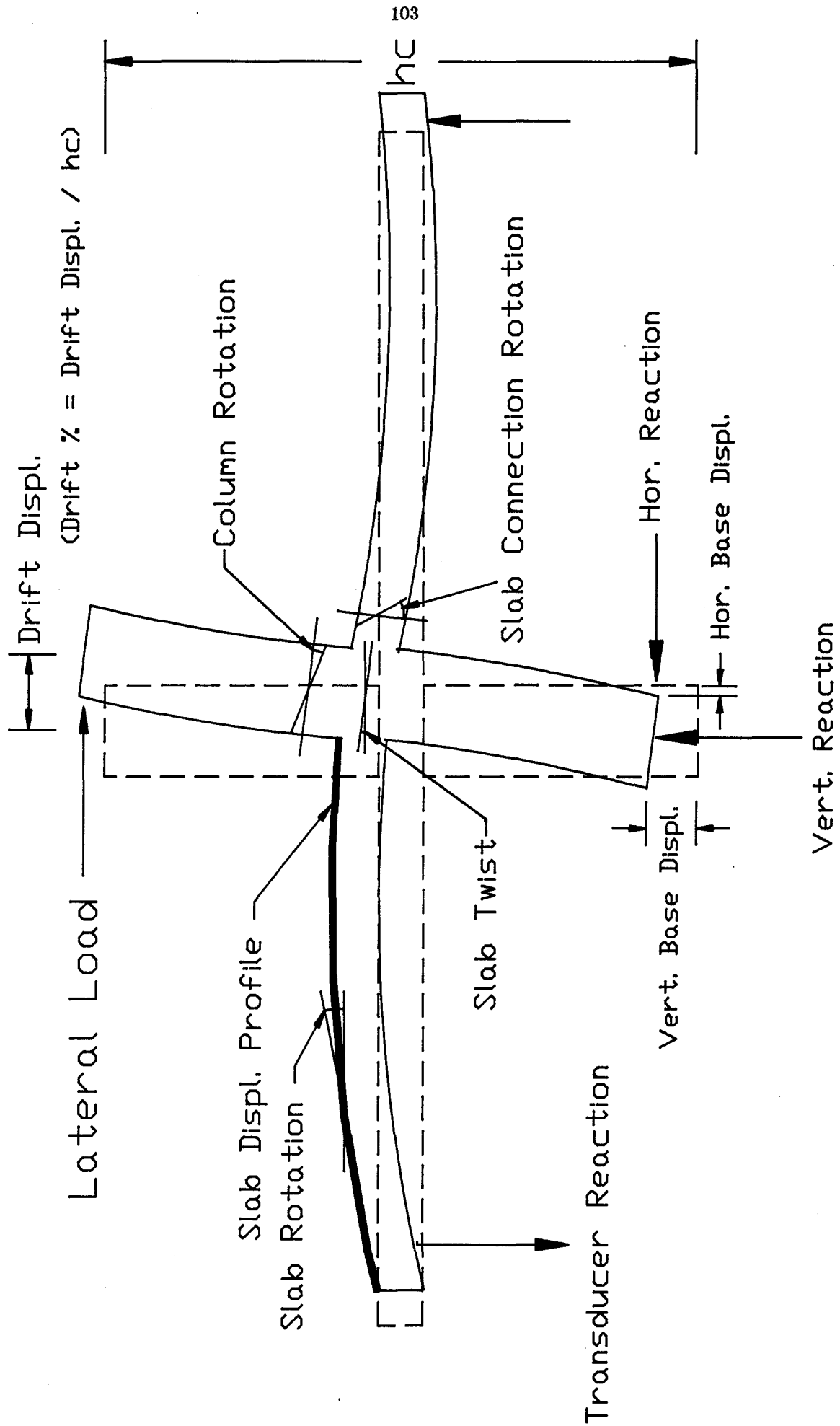


Fig. 5.1 Schematic Drawing of Test

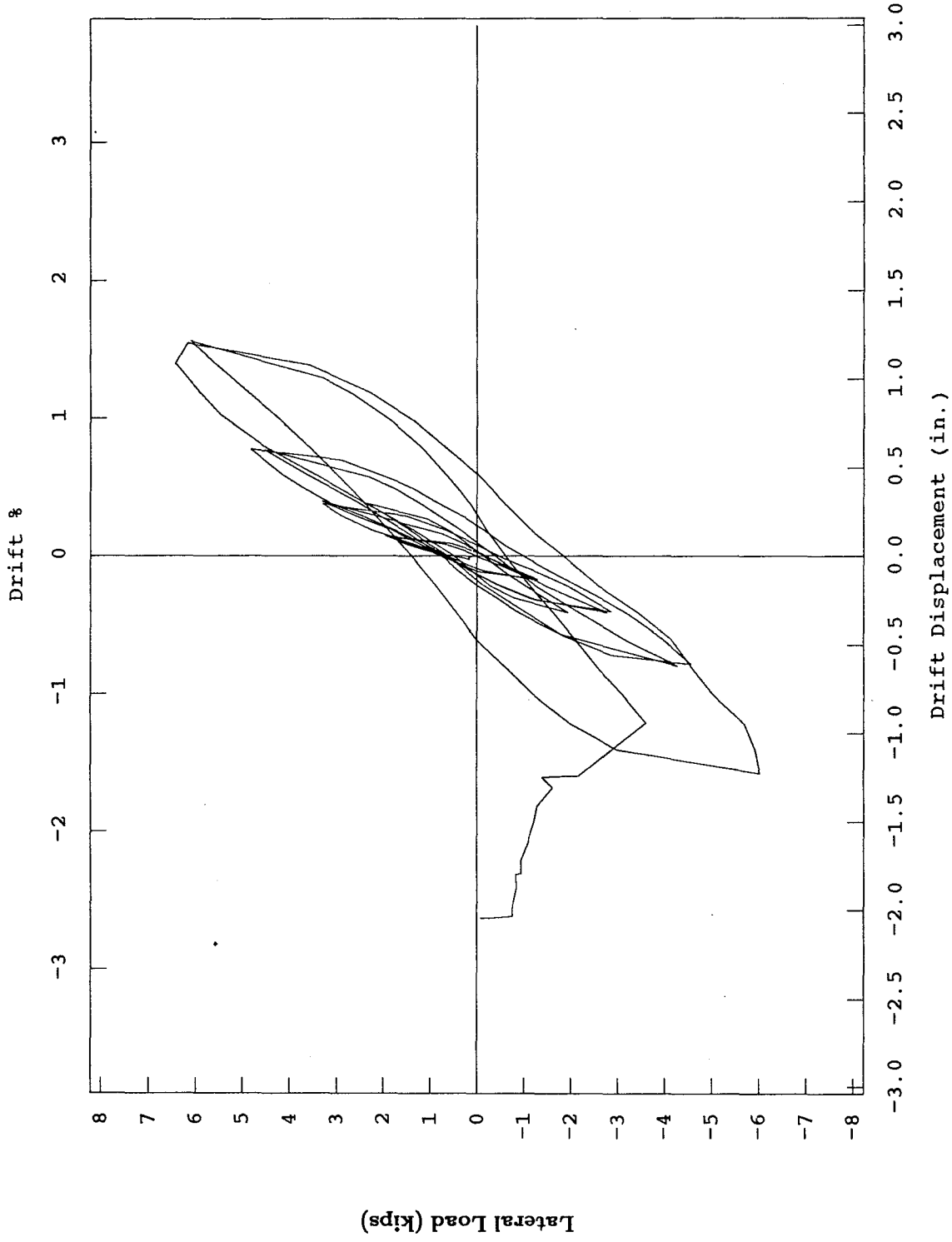


Fig. 5.2 EW Lateral Load vs Displacement - Test 1

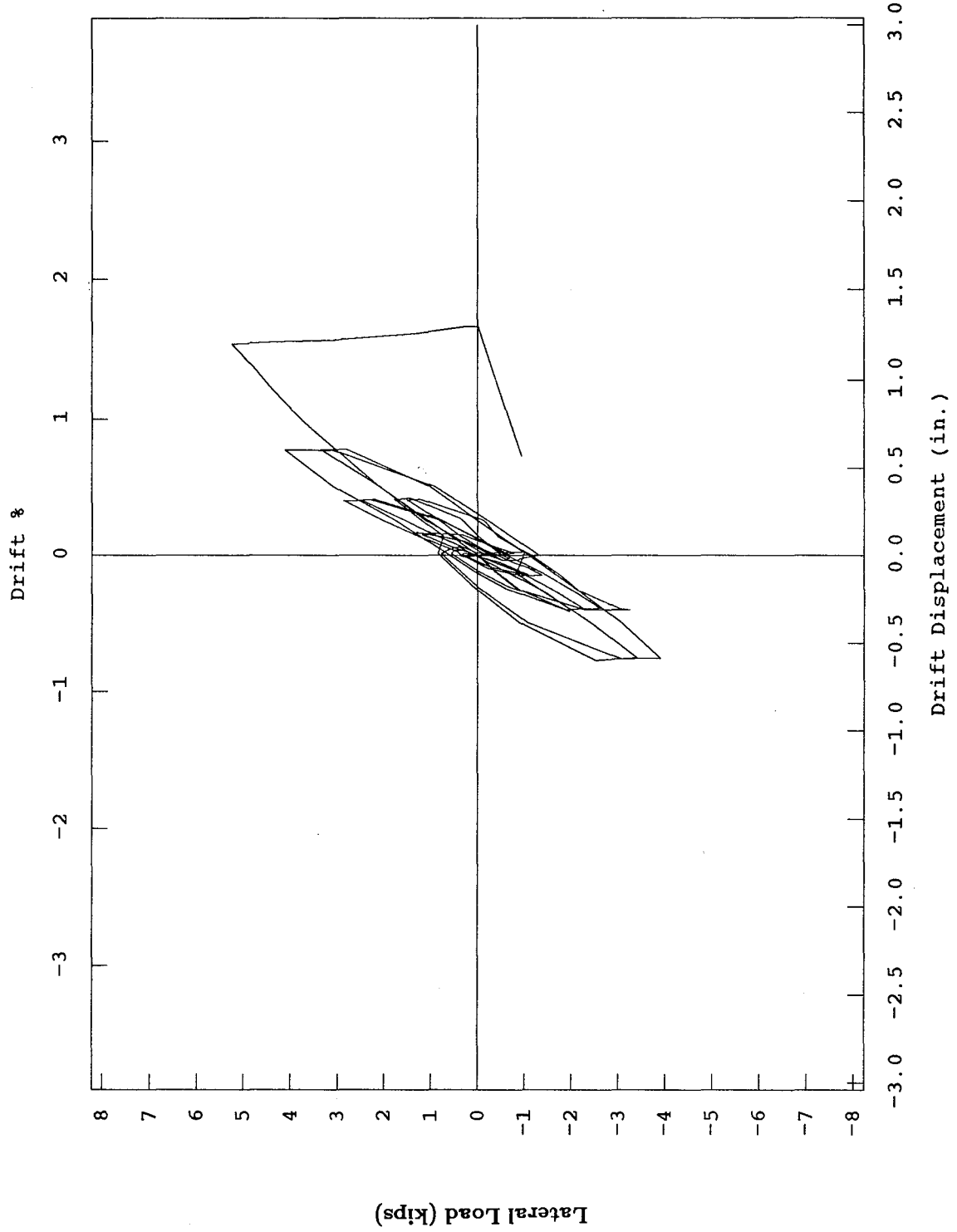


Fig. 5.3 (a) EW Lateral Load vs Displacement - Test 2

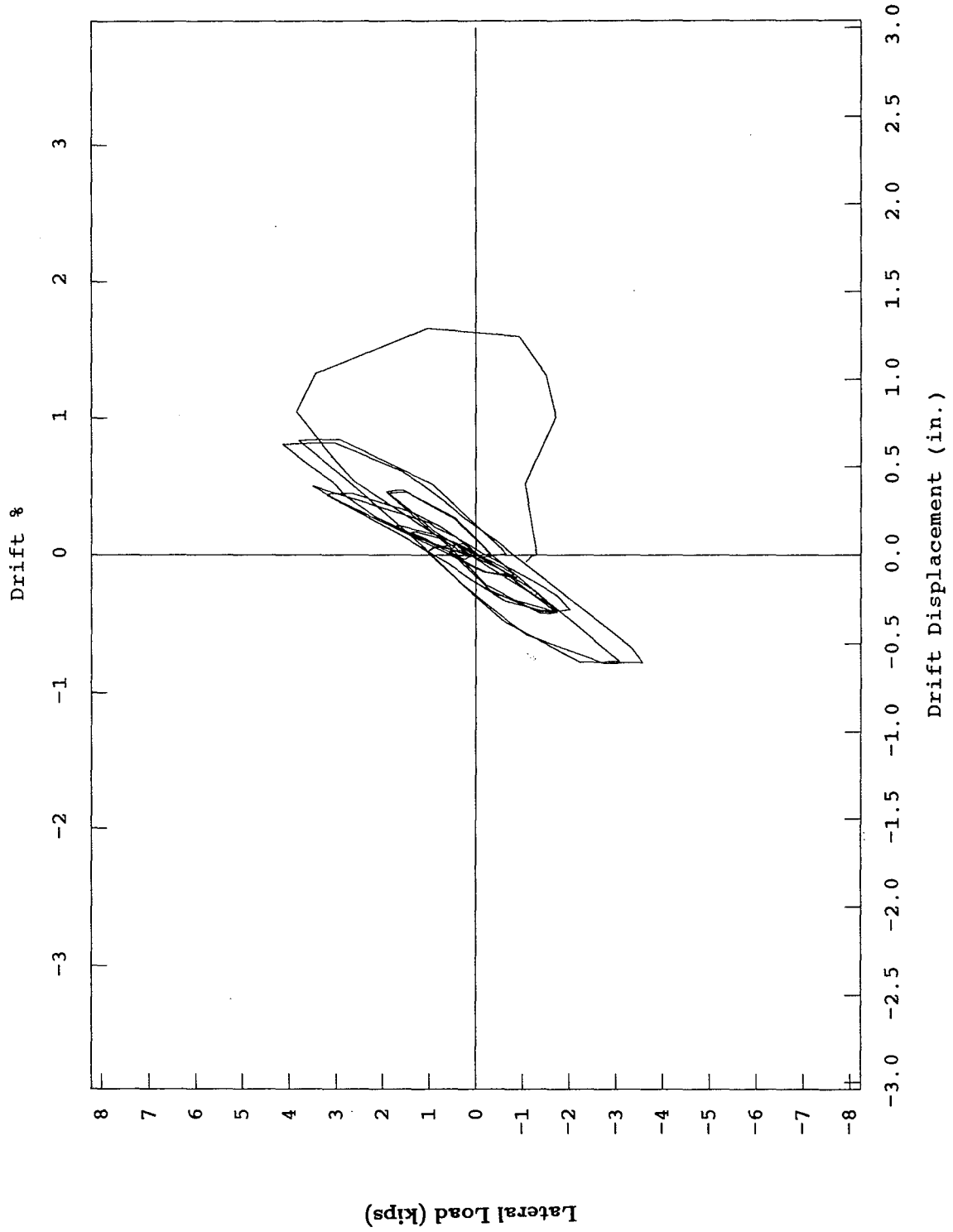


Fig. 5.3 (b) NS Lateral Load vs Displacement - Test 2

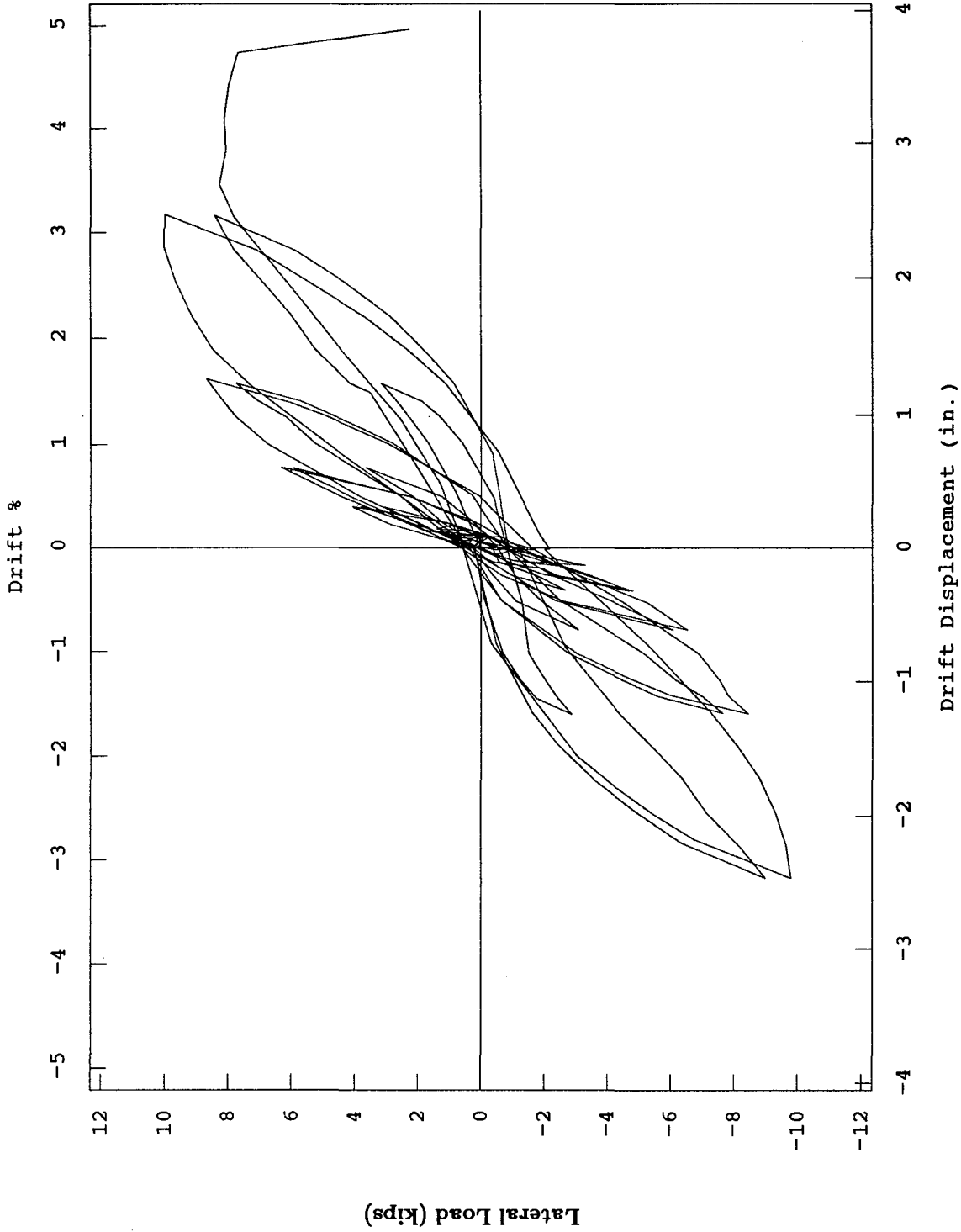


Fig. 5.4 EW Lateral Load vs Displacement - Test 3

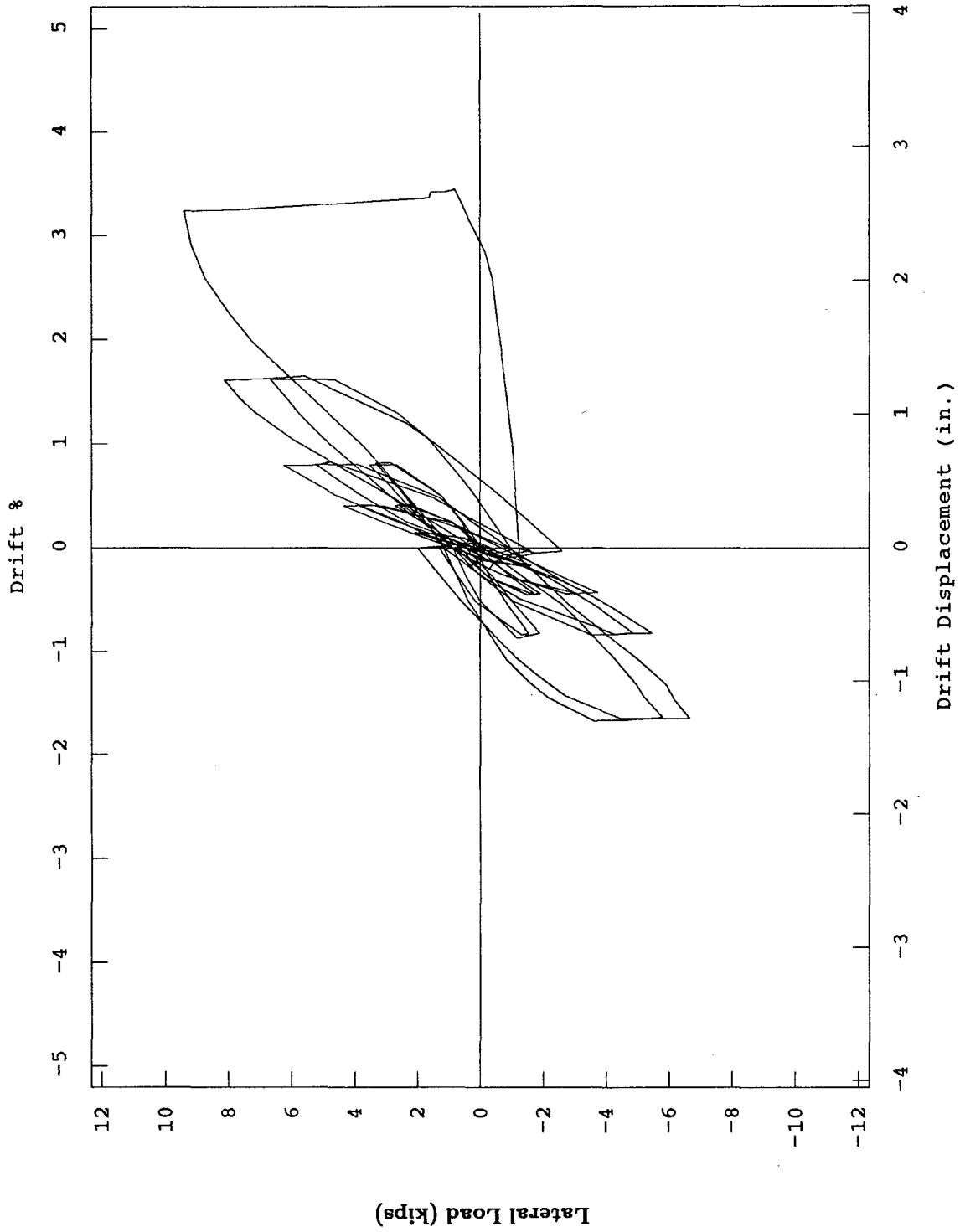


Fig. 5.5 (a) EW Lateral Load vs Displacement - Test 4

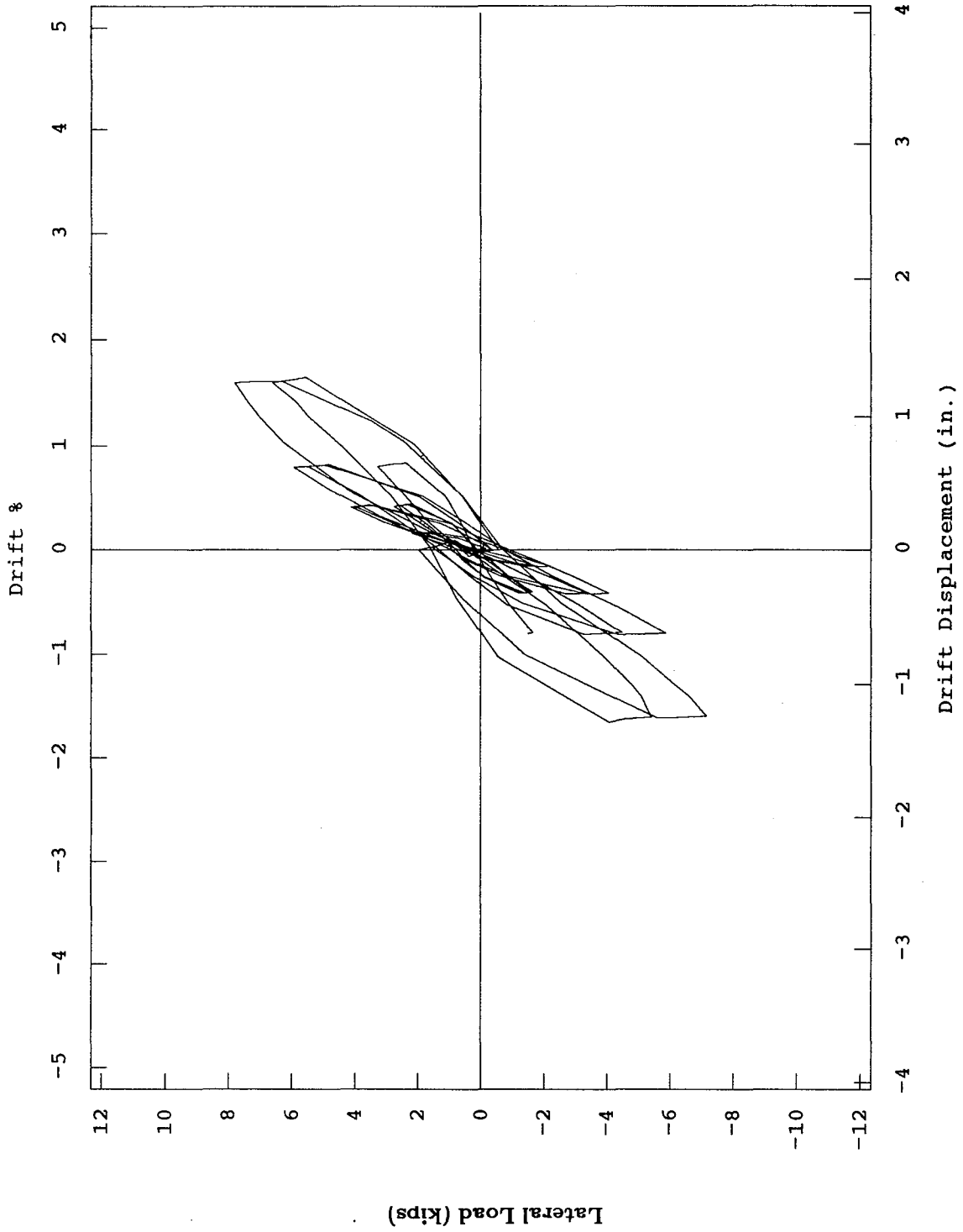


Fig. 5.5 (b) NS Lateral Load vs Displacement - Test 4

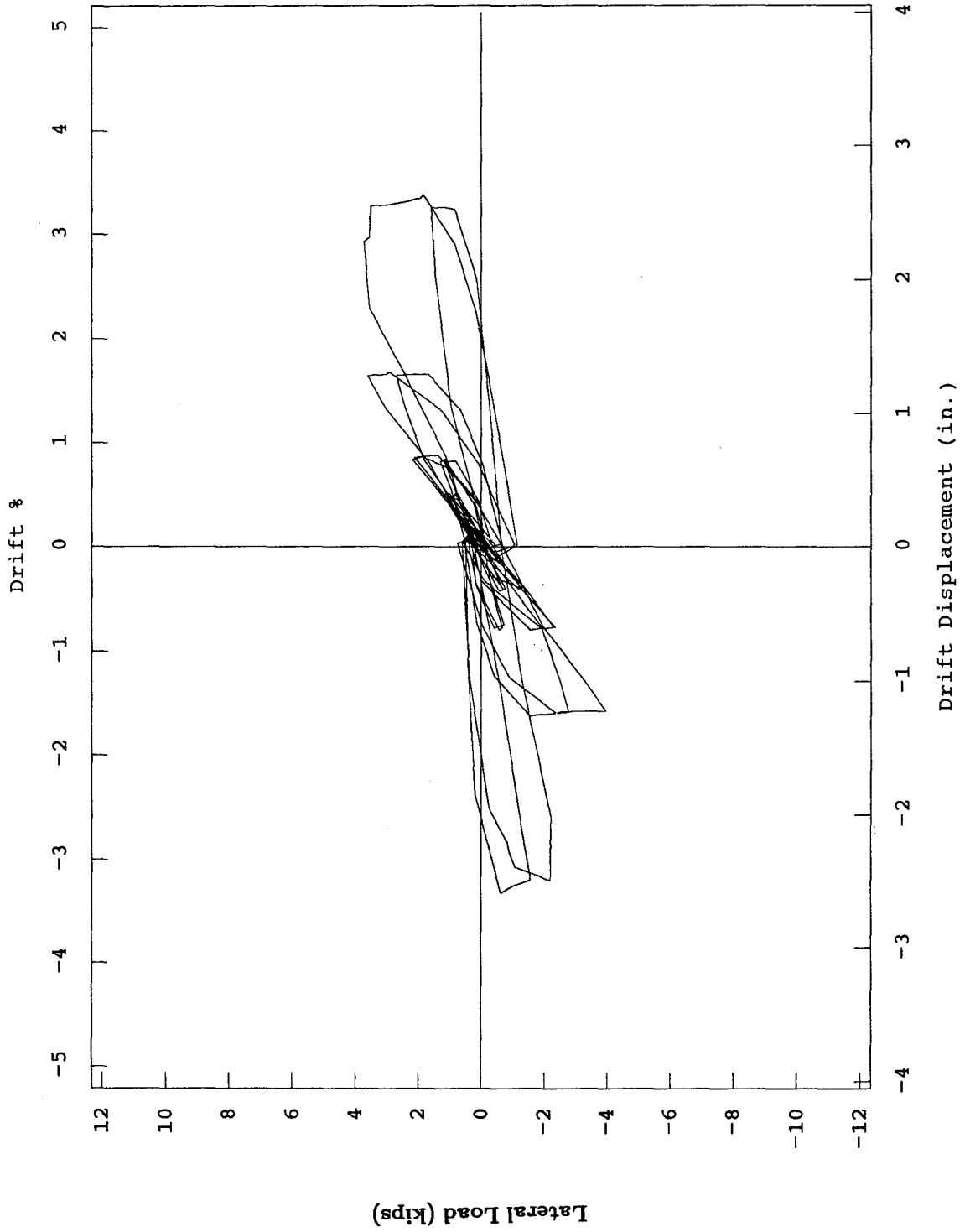


Fig. 5.6 (a) EW Lateral Load vs Displacement - Test 5

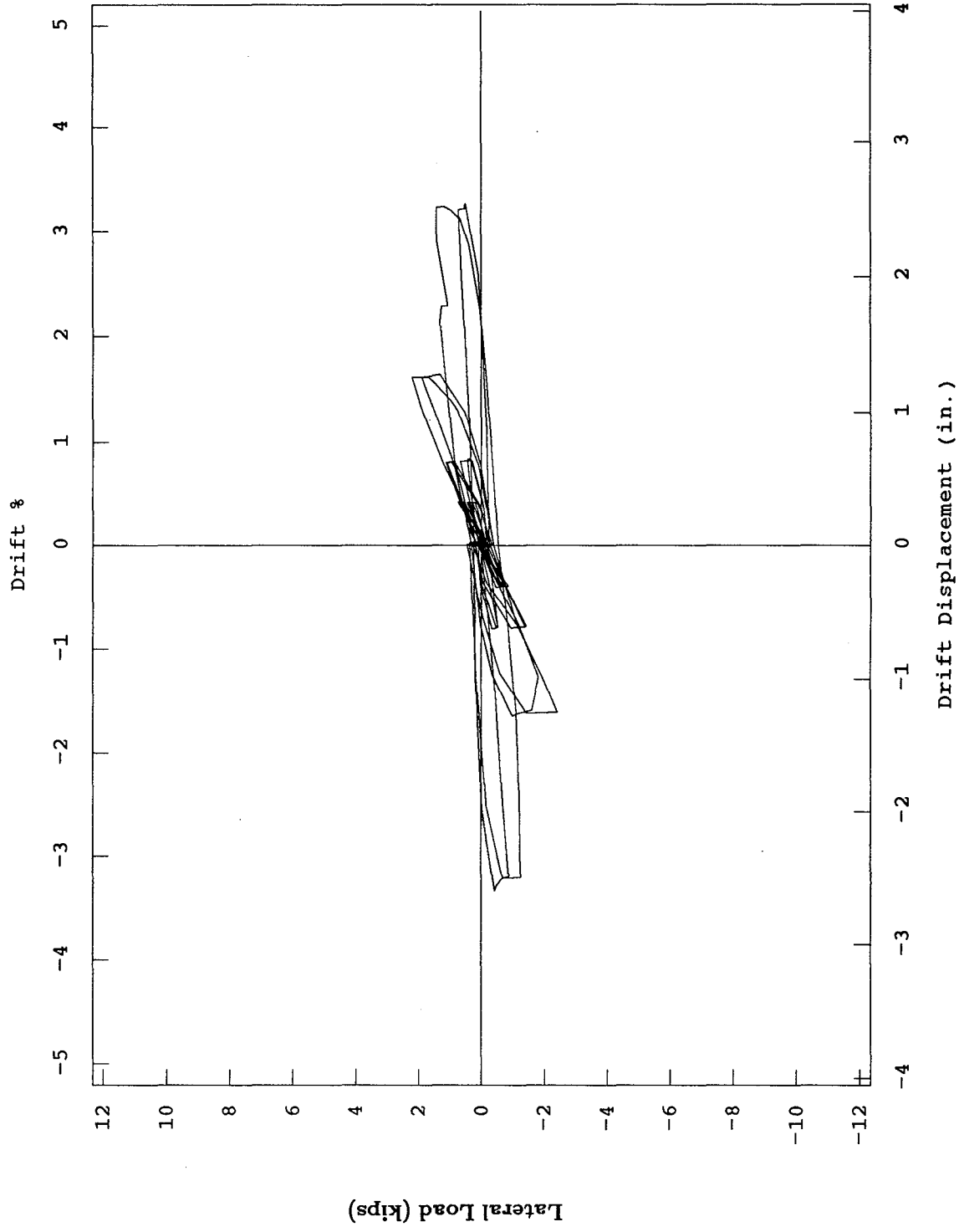


Fig. 5.6 (b) NS Lateral Load vs Displacement - Test 5

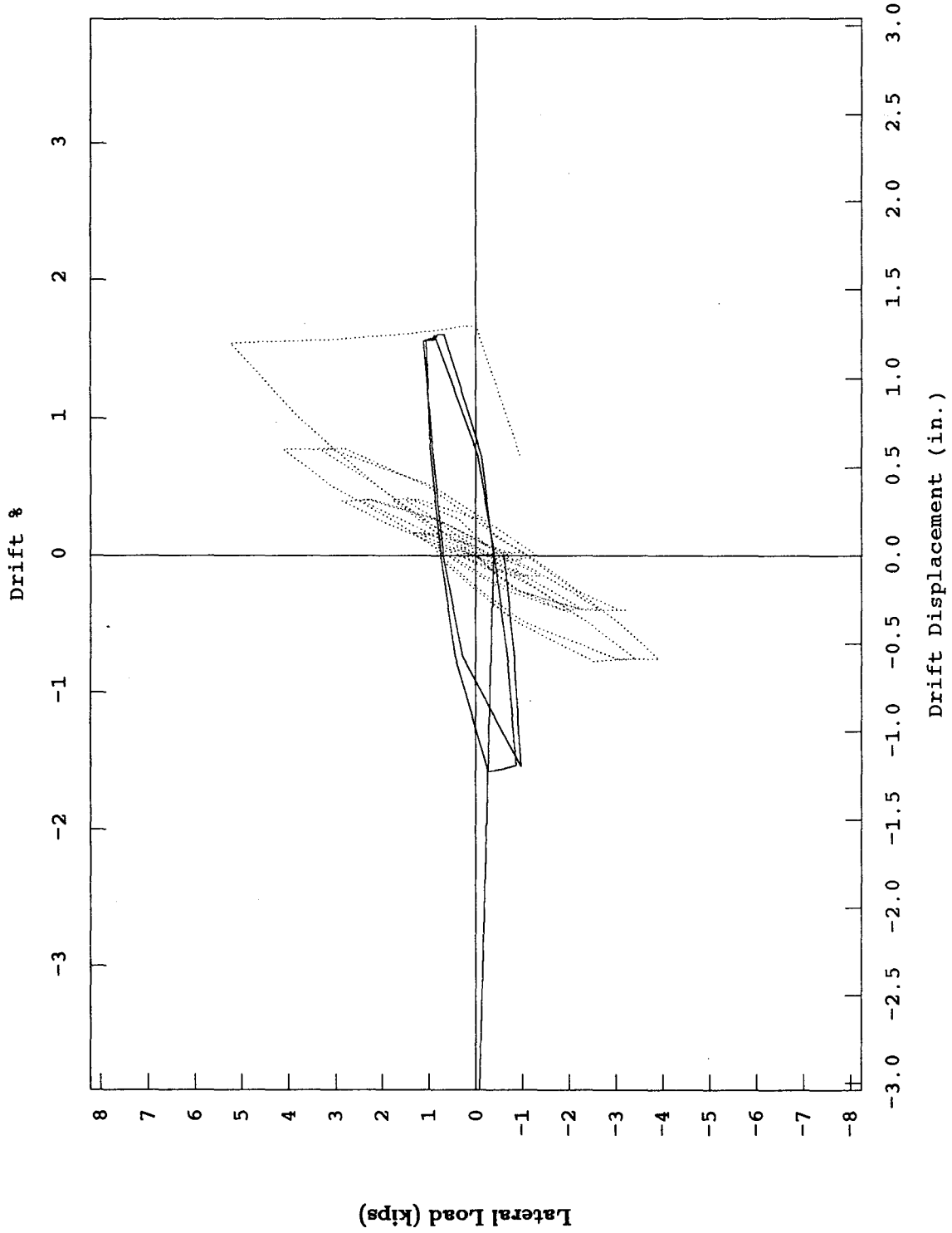


Fig. 5.7 (a) Post-Failure Lateral Load vs Displacement (EW - Test 2)

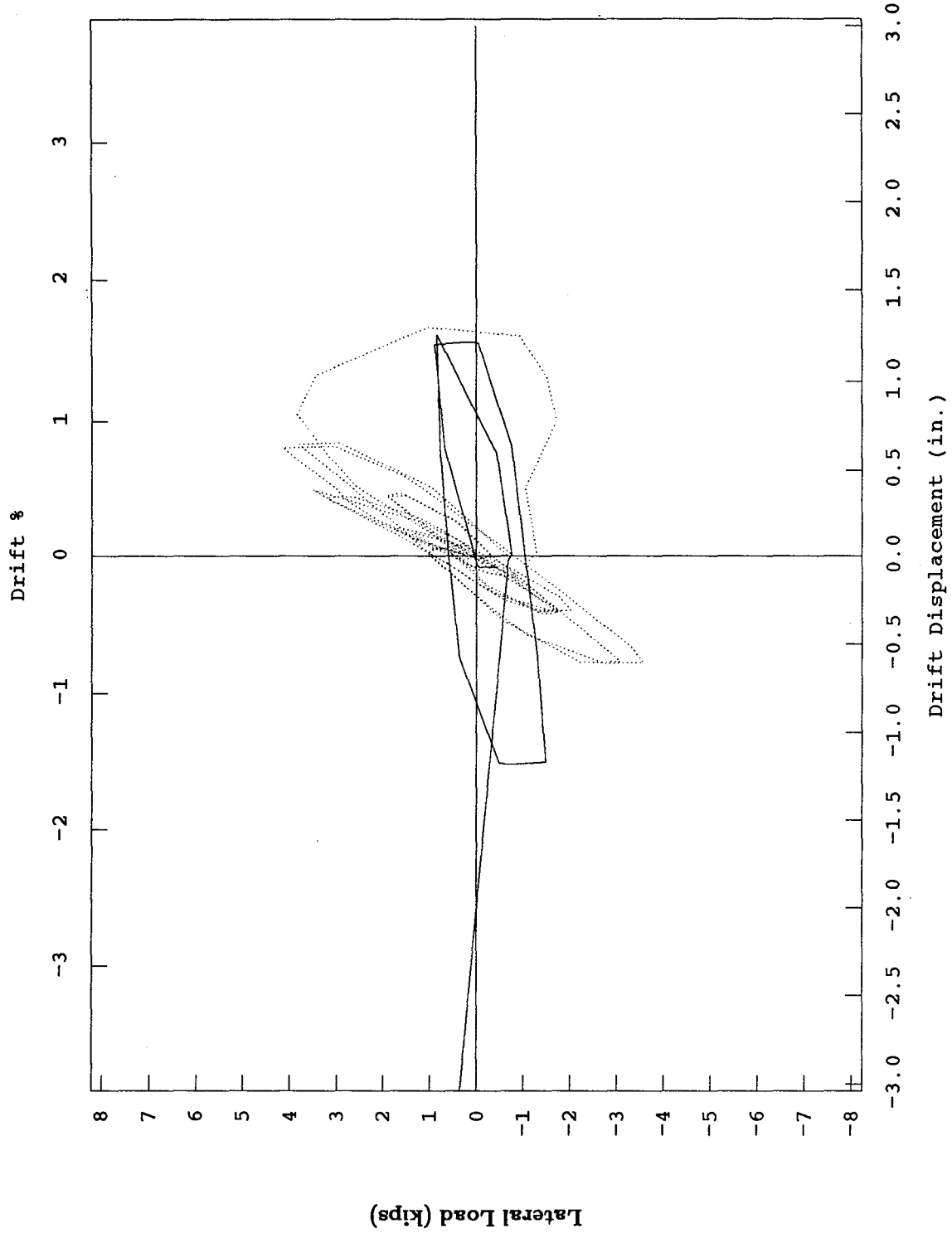


Fig. 5.7 (b) Post-Failure Lateral Load vs Displacement (NS - Test 2)

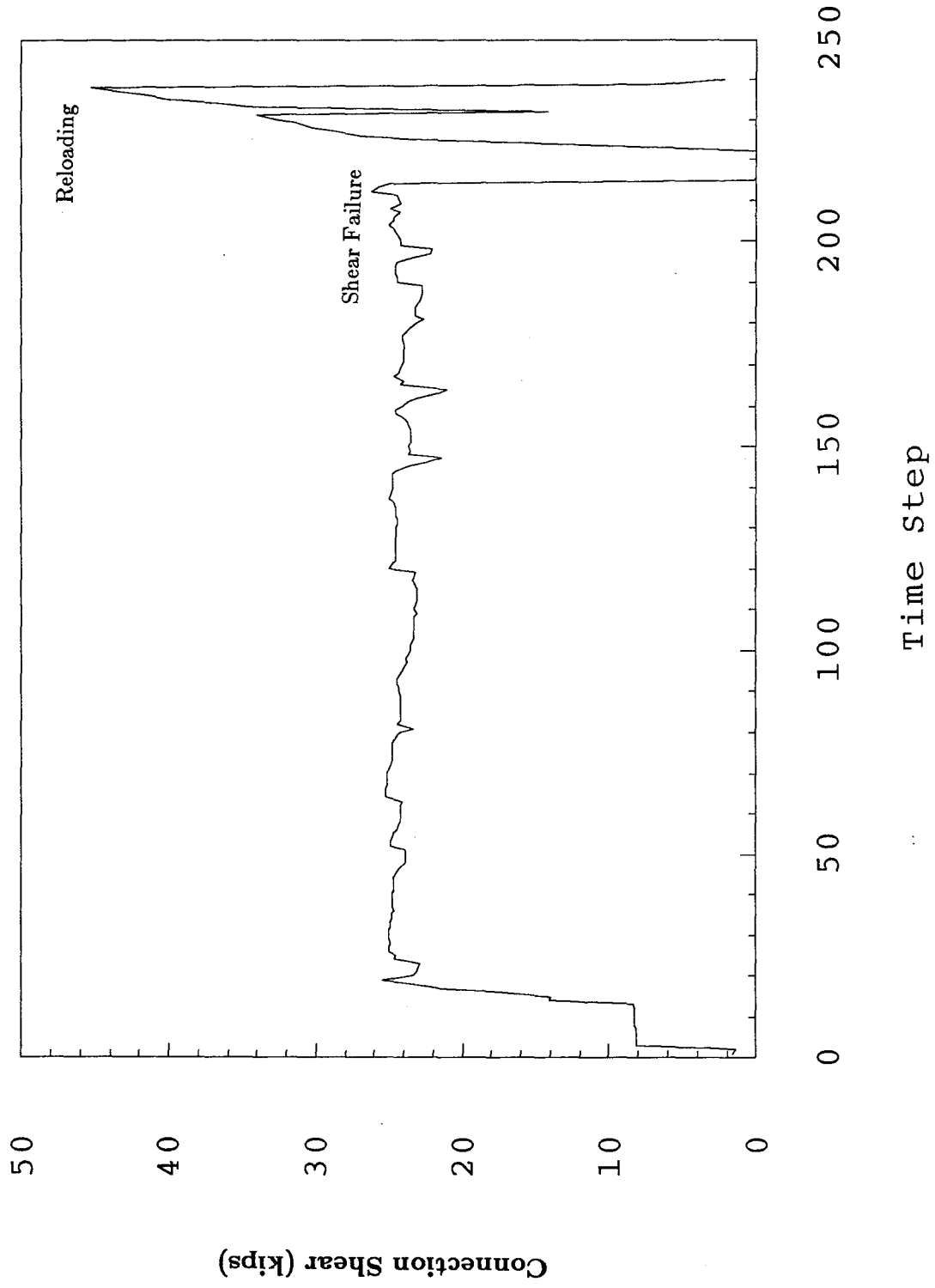


Fig. 5.8 Connection Shear History - Test 1

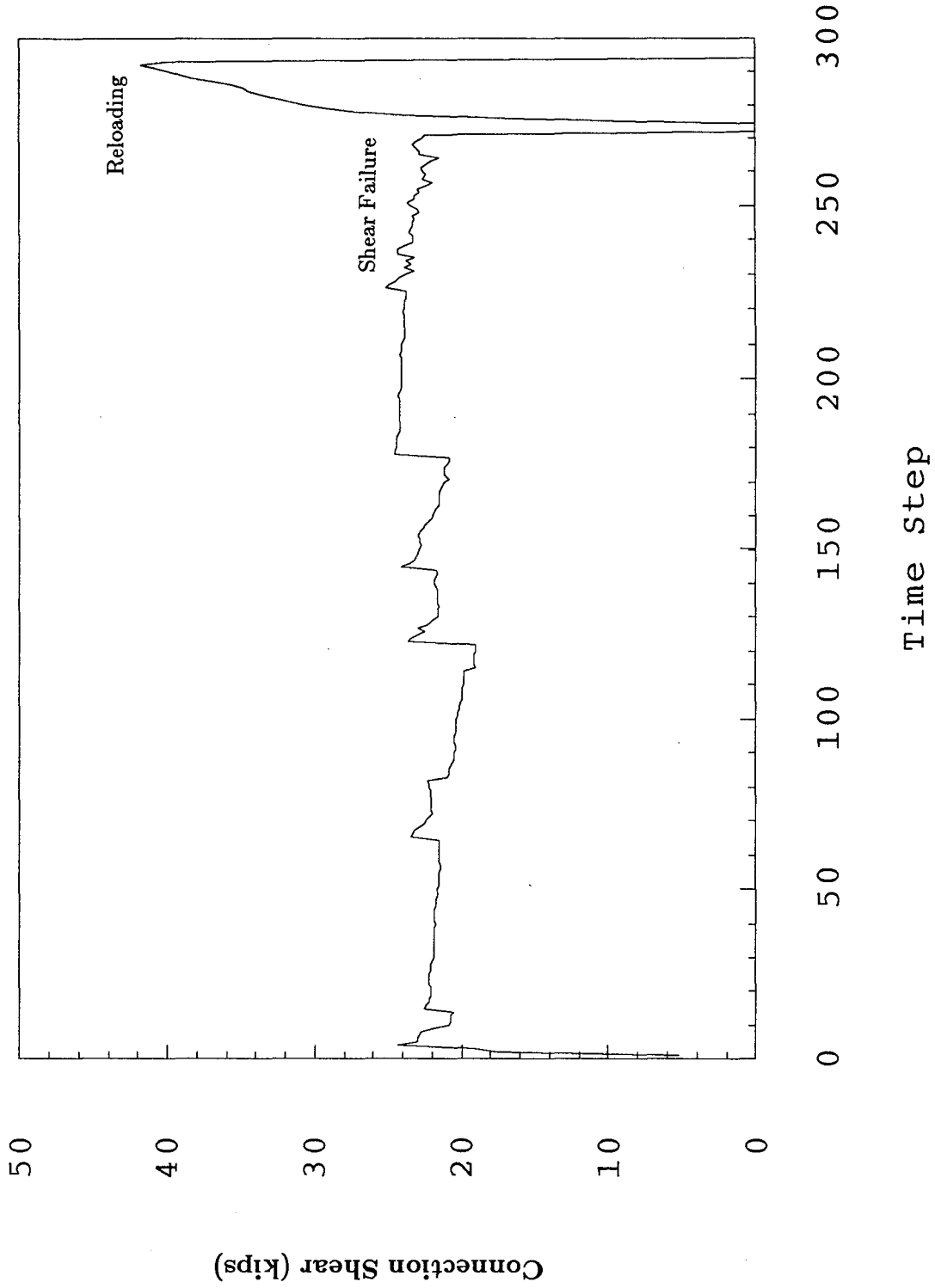


Fig. 5.9 Connection Shear History - Test 2

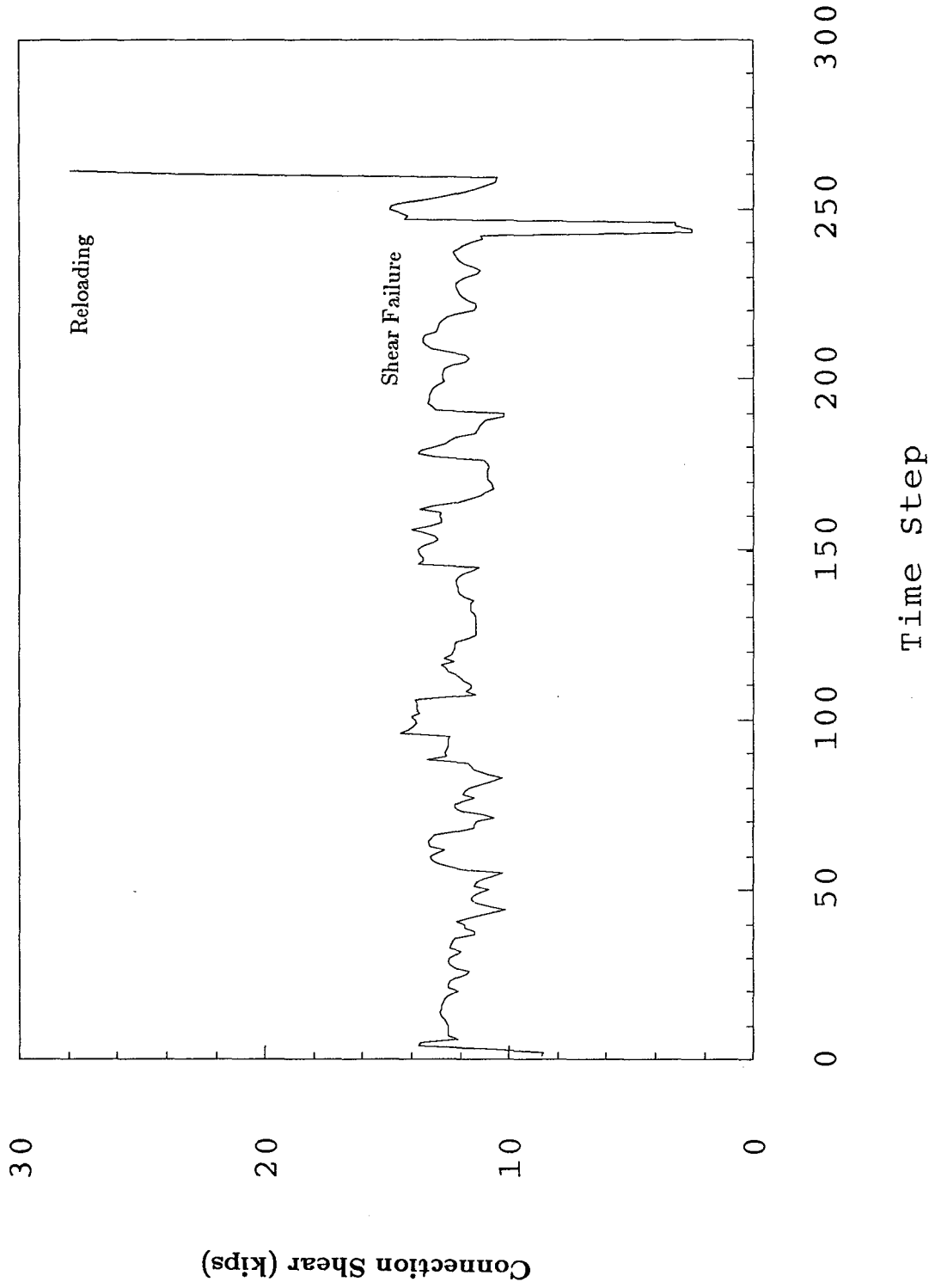


Fig. 5.10 Connection Shear History - Test 3

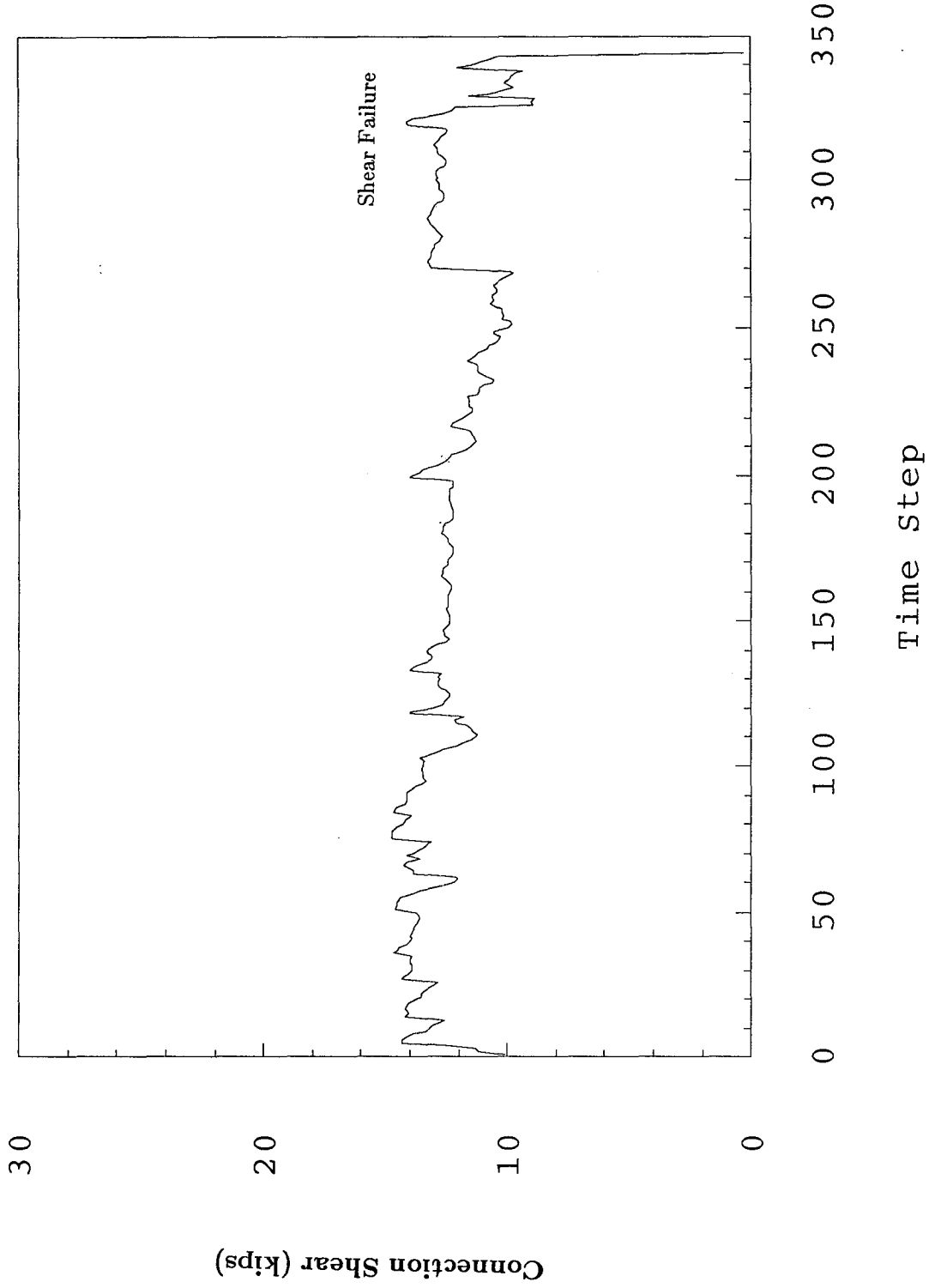


Fig. 5.11 Connection Shear History - Test 4

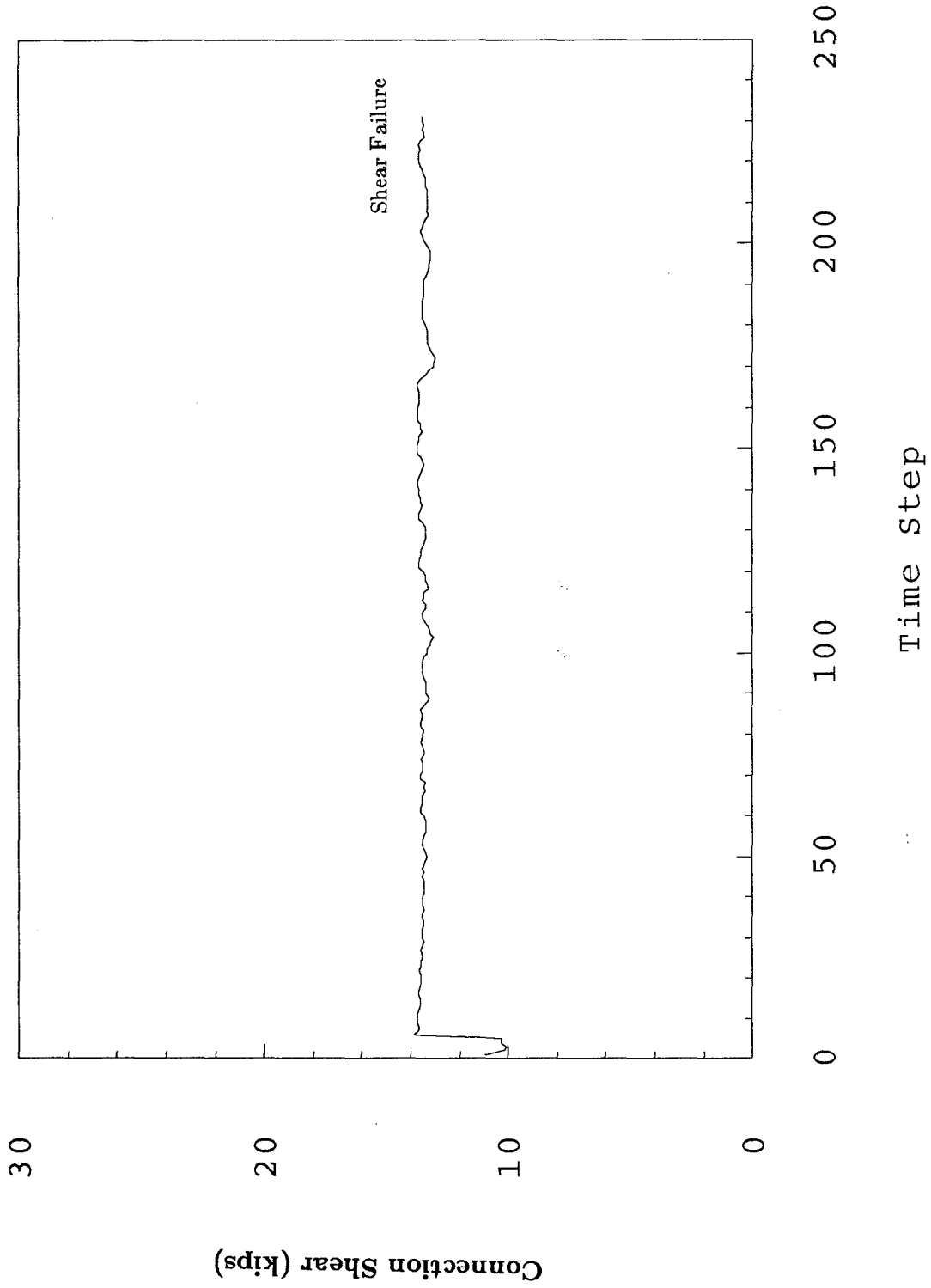


Fig. 5.12 Connection Shear History - Test 5

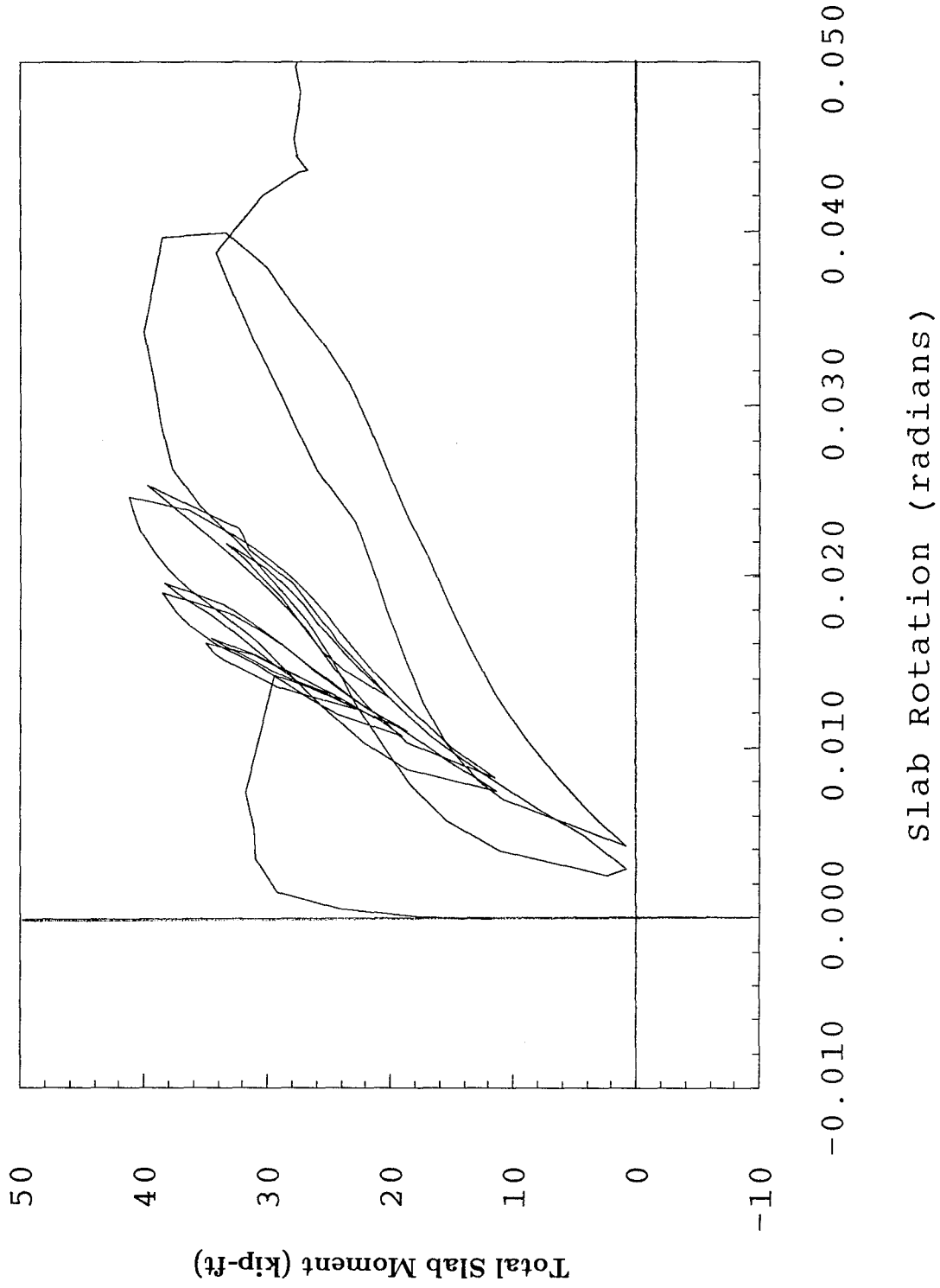


Fig. 5.13 (a) Slab Moment vs Rotation (East Side) - Test I

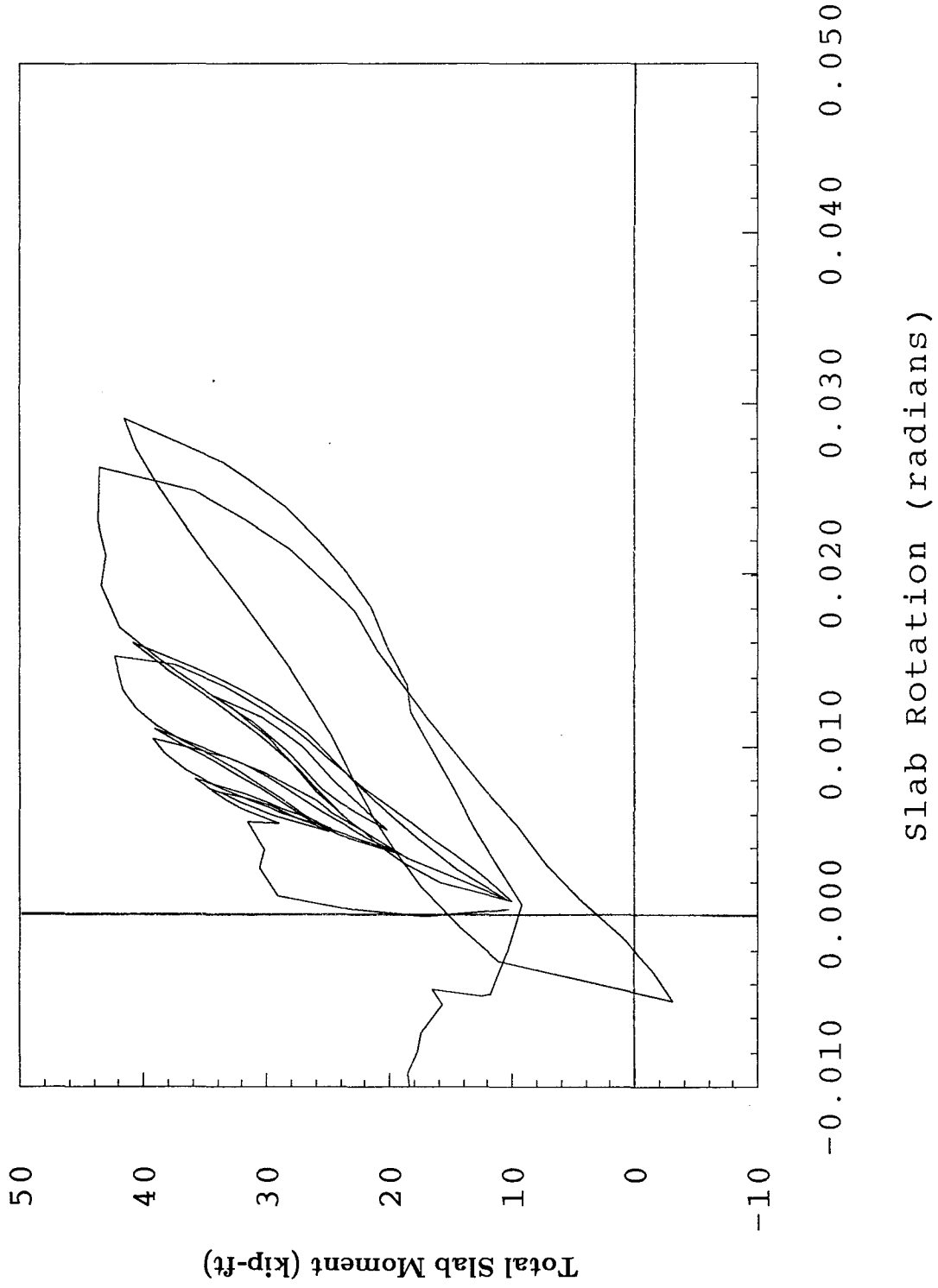


Fig. 5.13 (b) Slab Moment vs Rotation (West Side) - Test I

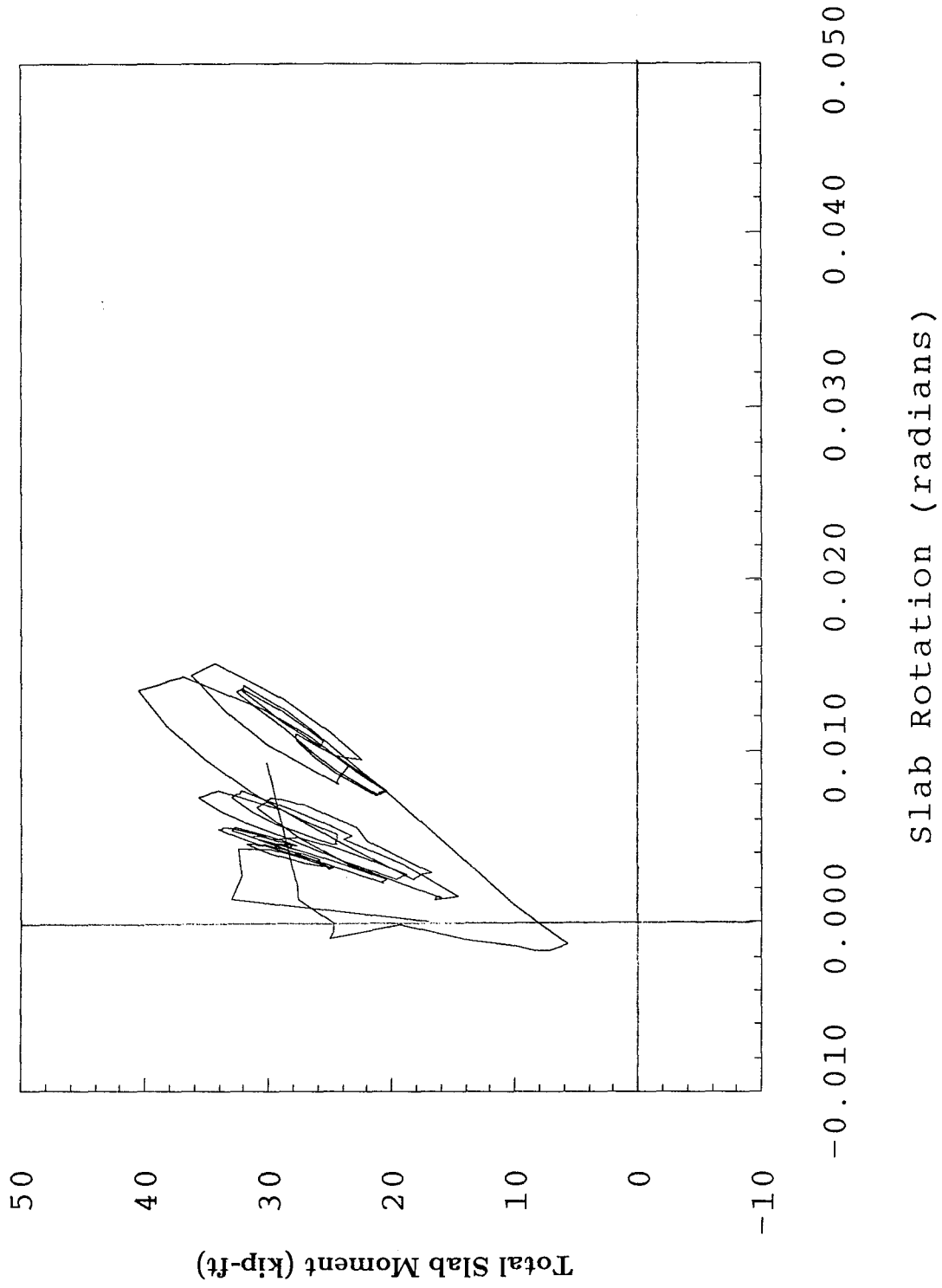


Fig. 5.14 (a) Slab Moment vs Rotation (East Side) - Test 2

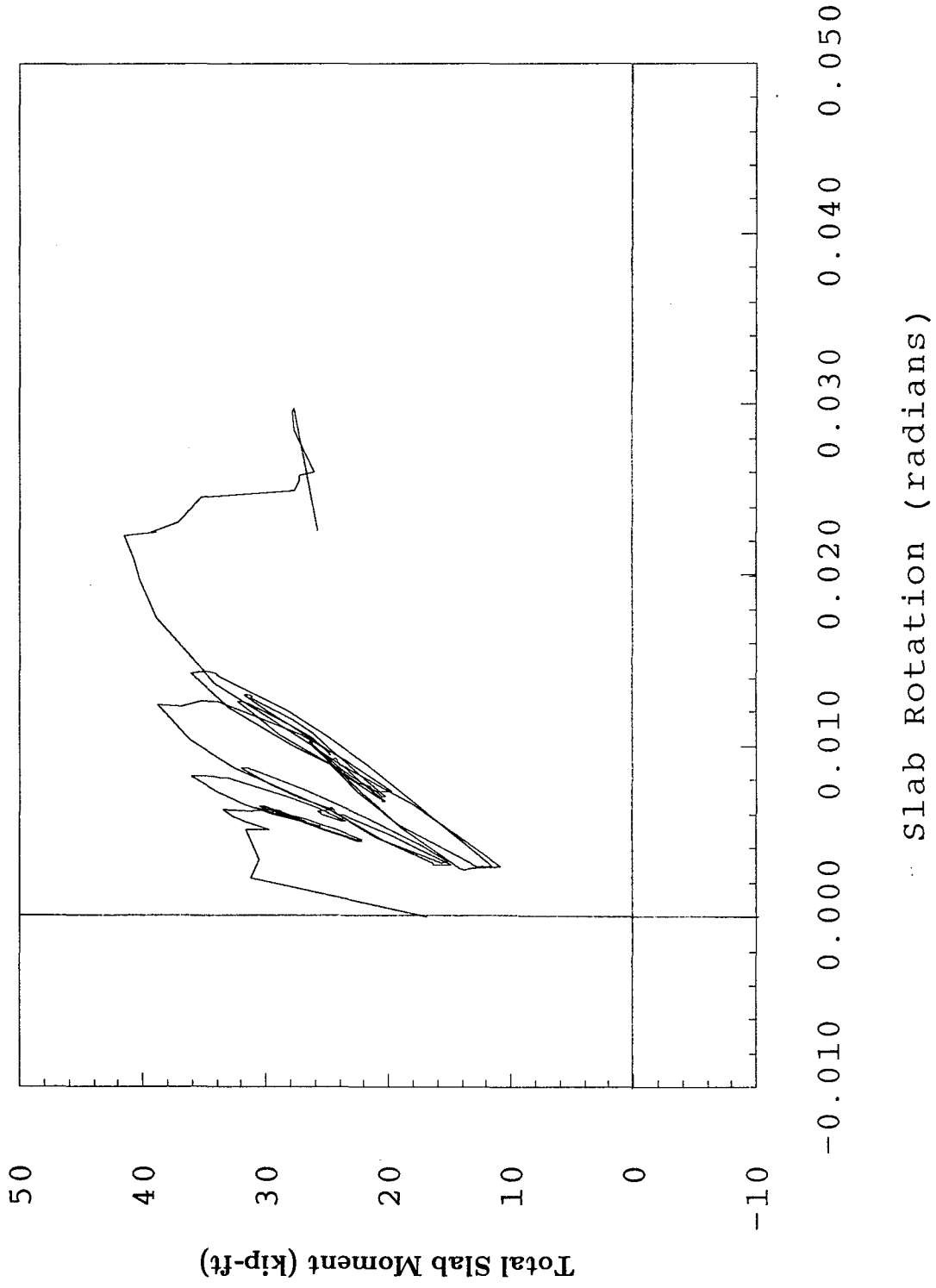


Fig. 5.14 (b) Slab Moment vs Rotation (West Side) - Test 2

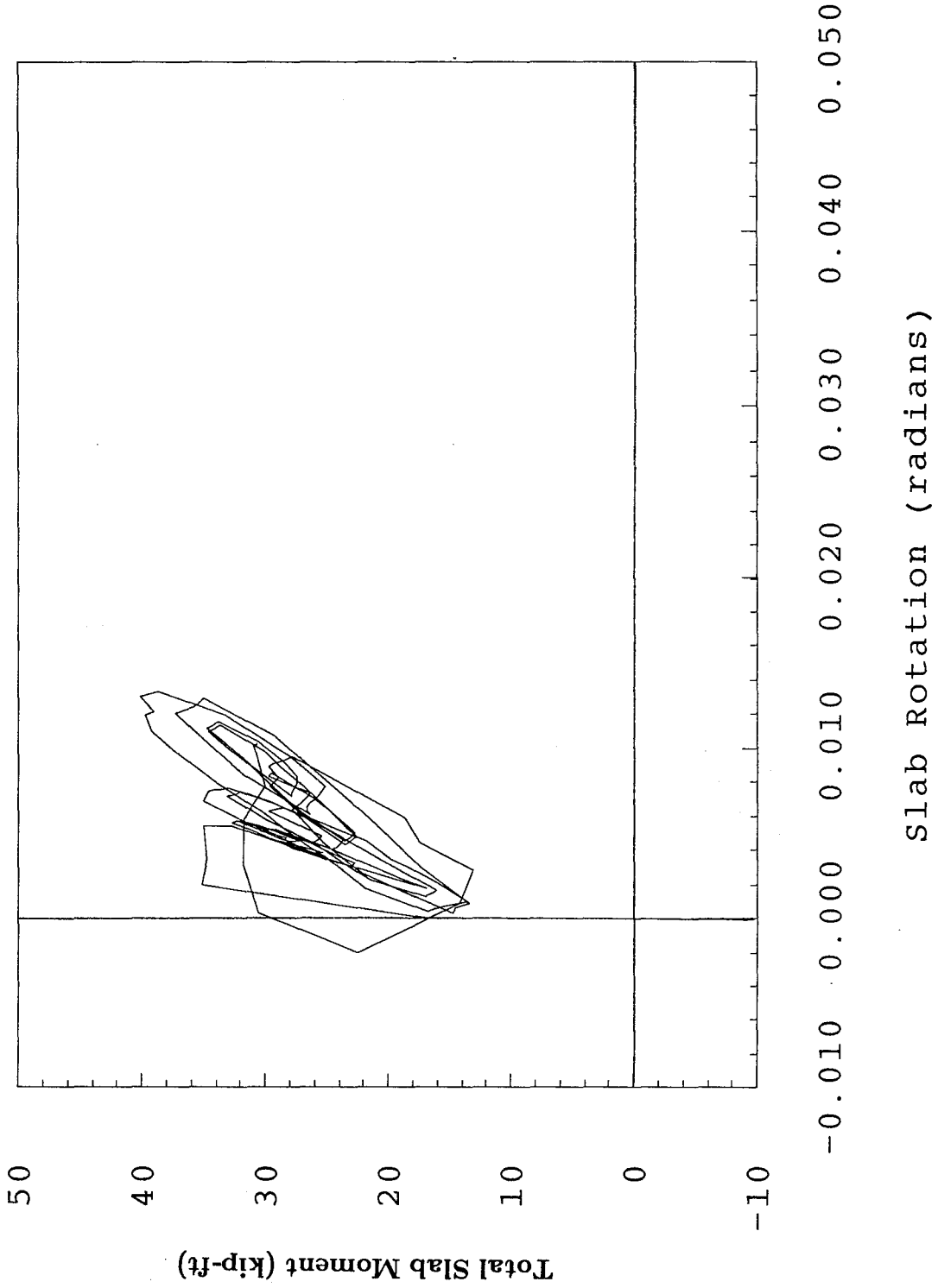


Fig. 5.14 (c) Slab Moment vs Rotation (North Side) - Test 2

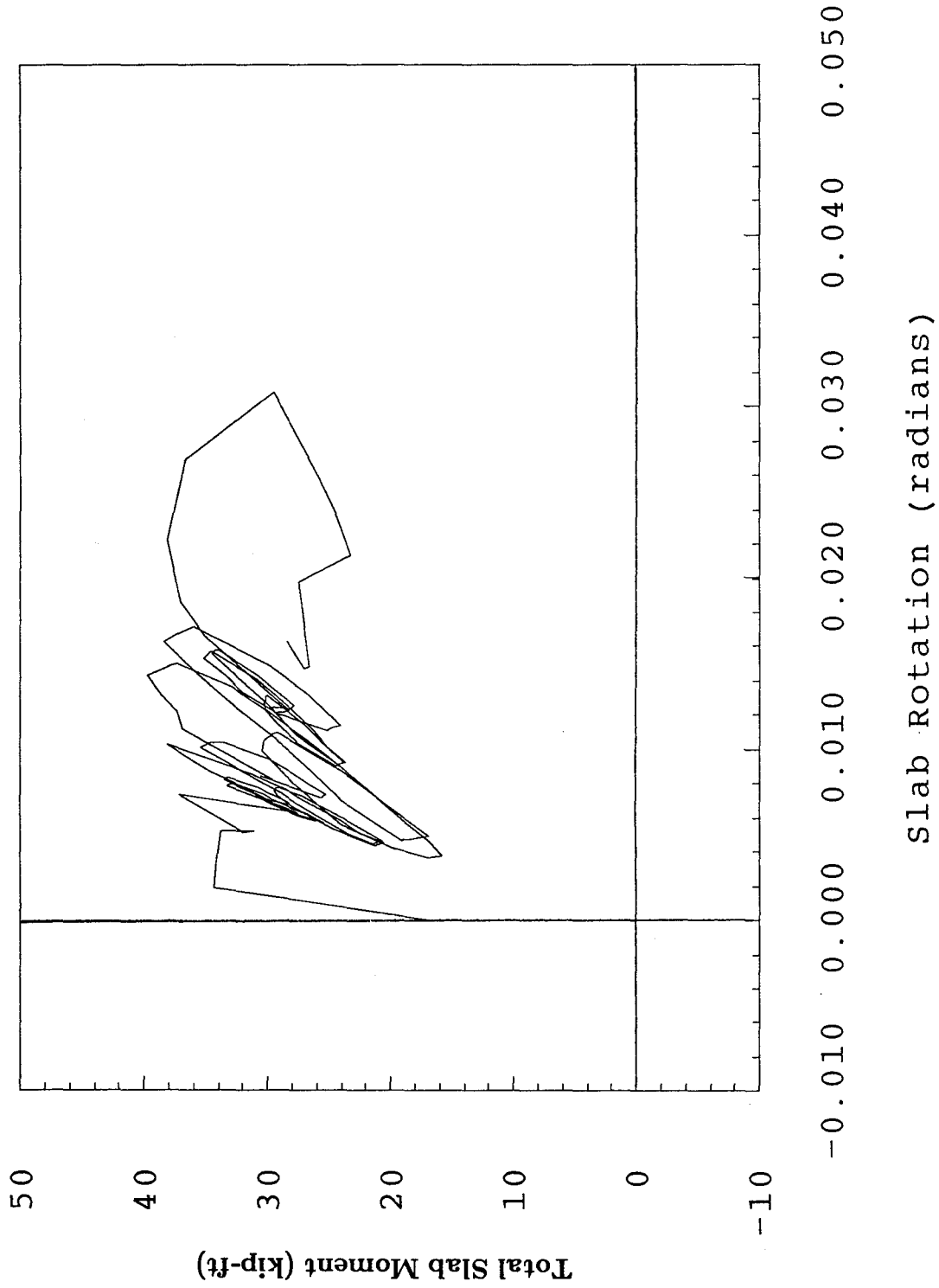


Fig. 5.14 (d) Slab Moment vs Rotation (South Side) - Test 2

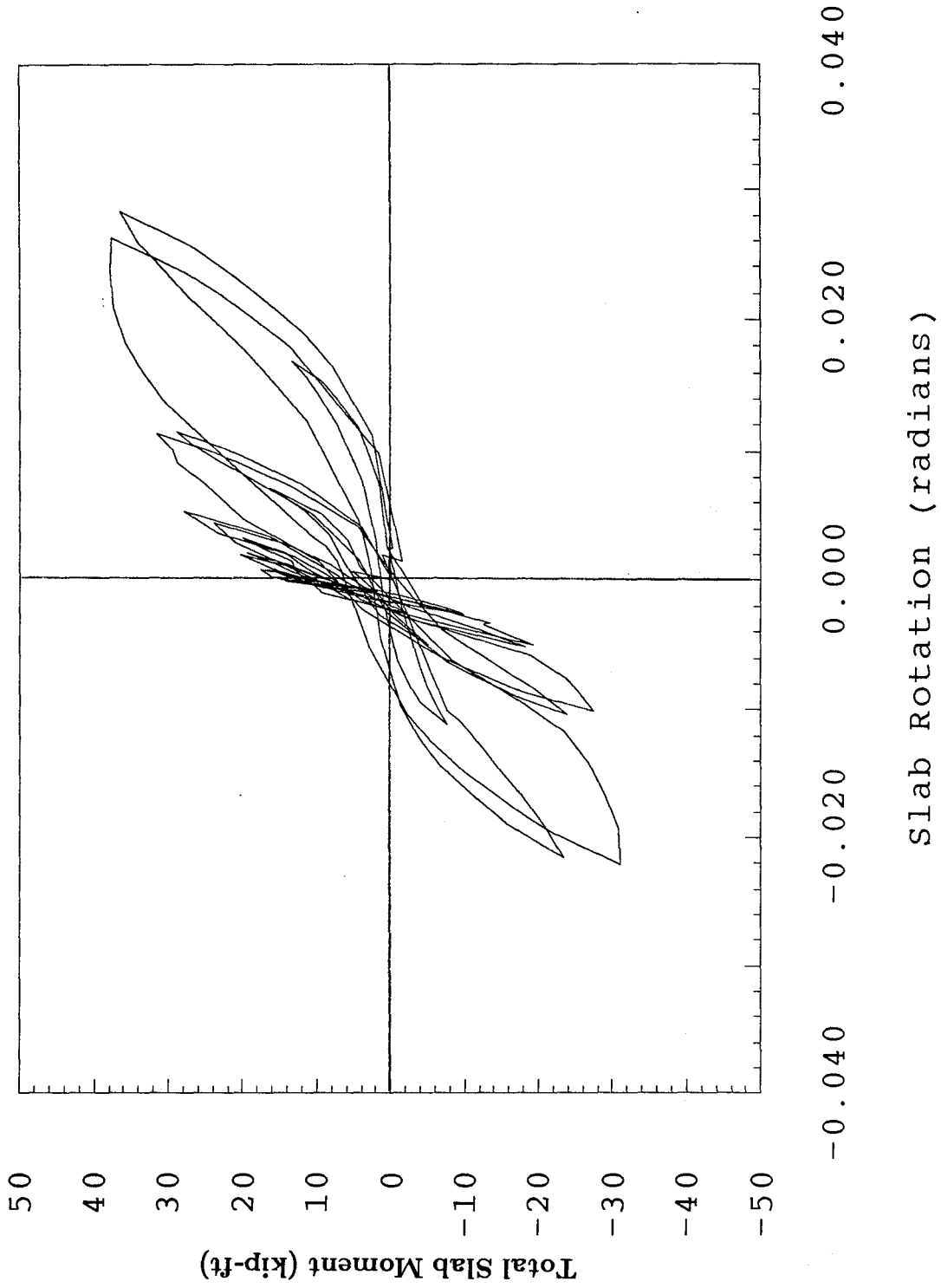


Fig. 5.15 (a) Slab Moment vs Rotation (East Side) - Test 3

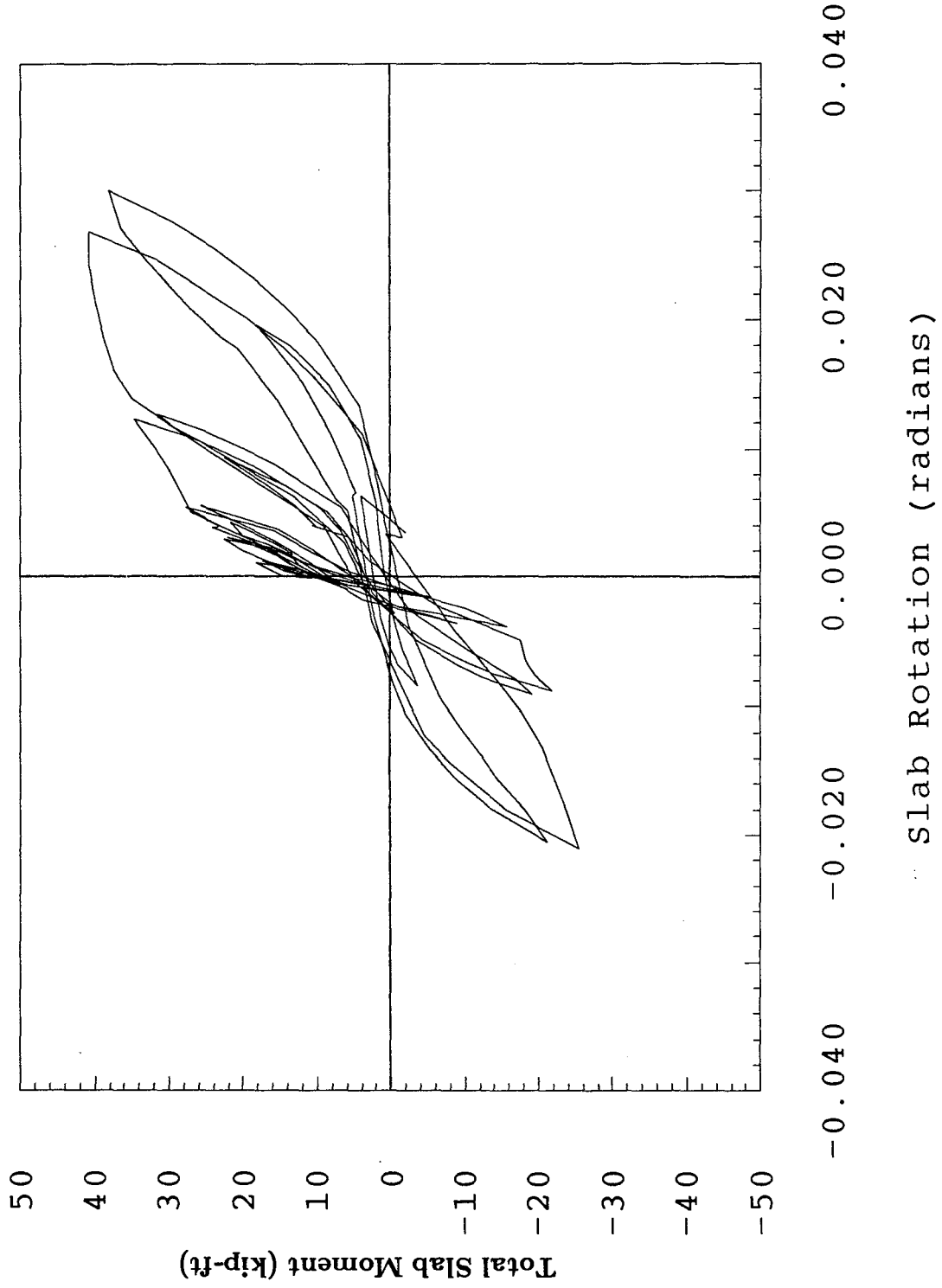


Fig. 5.15 (b) Slab Moment vs Rotation (West Side) - Test 3

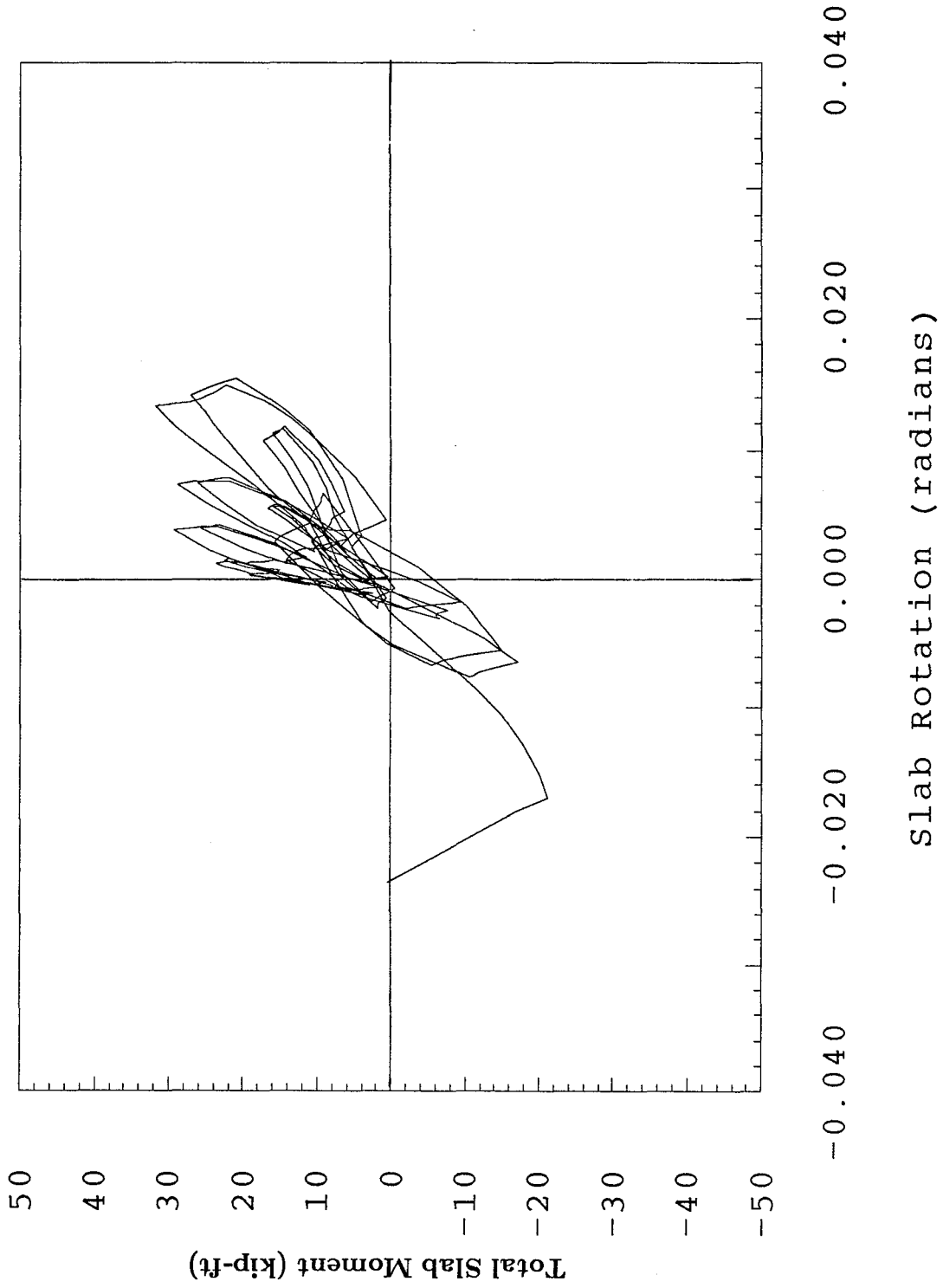


Fig. 5.16 (a) Slab Moment vs Rotation (East Side) - Test 4

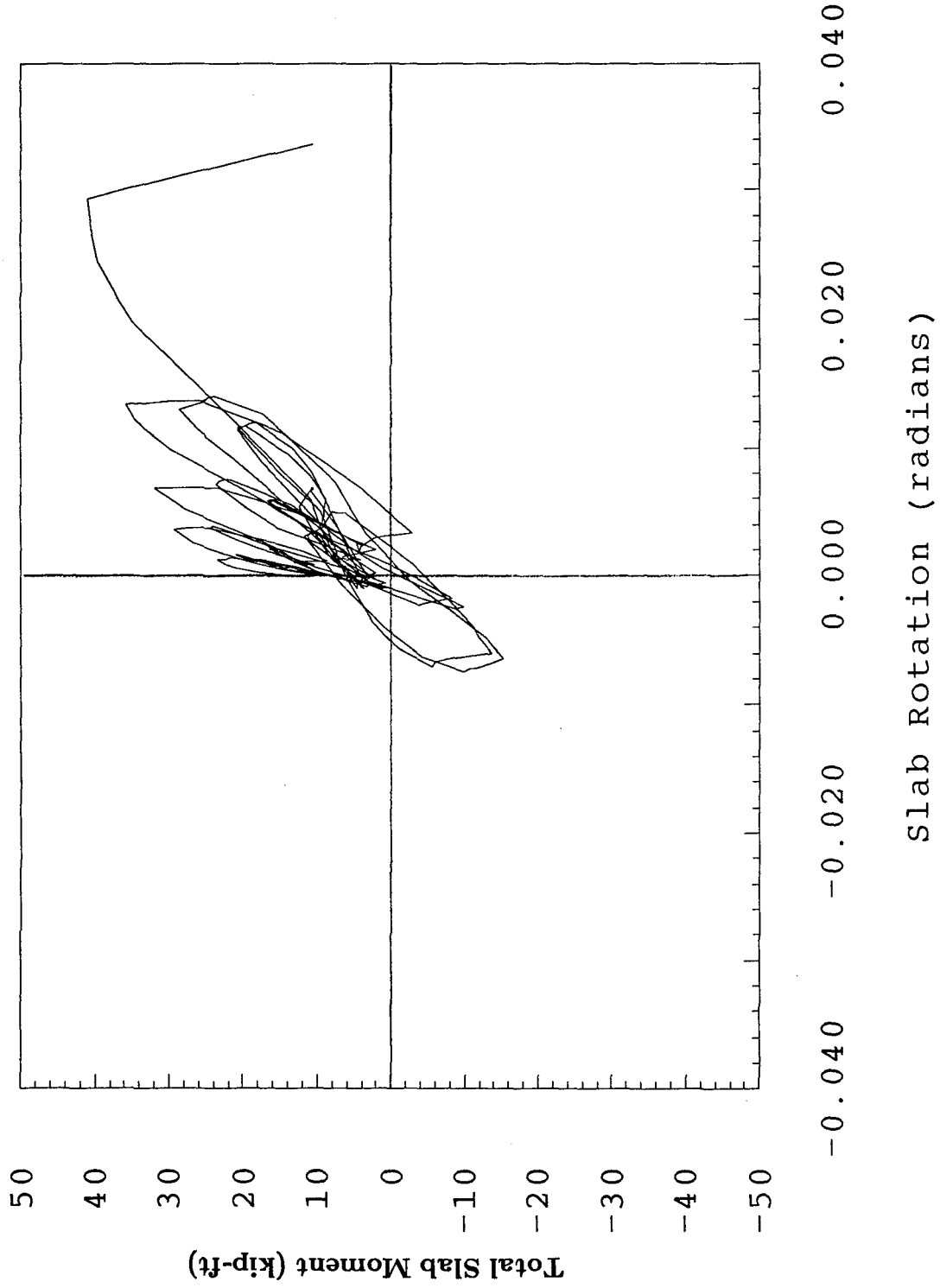


Fig. 5.16 (b) Slab Moment vs Rotation (West Side) - Test 4

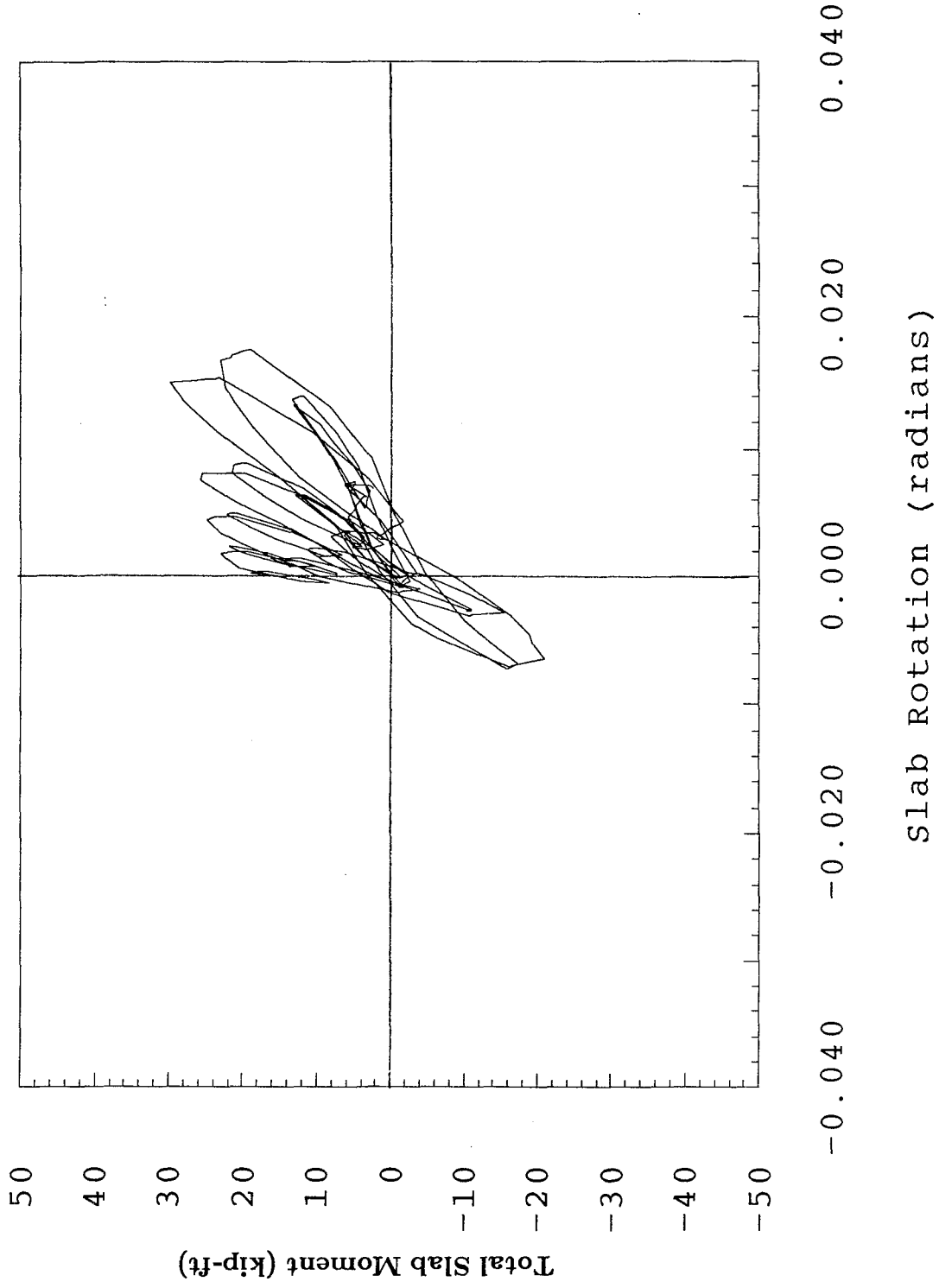


Fig. 5.16 (c) Slab Moment vs Rotation (North Side) - Test 4

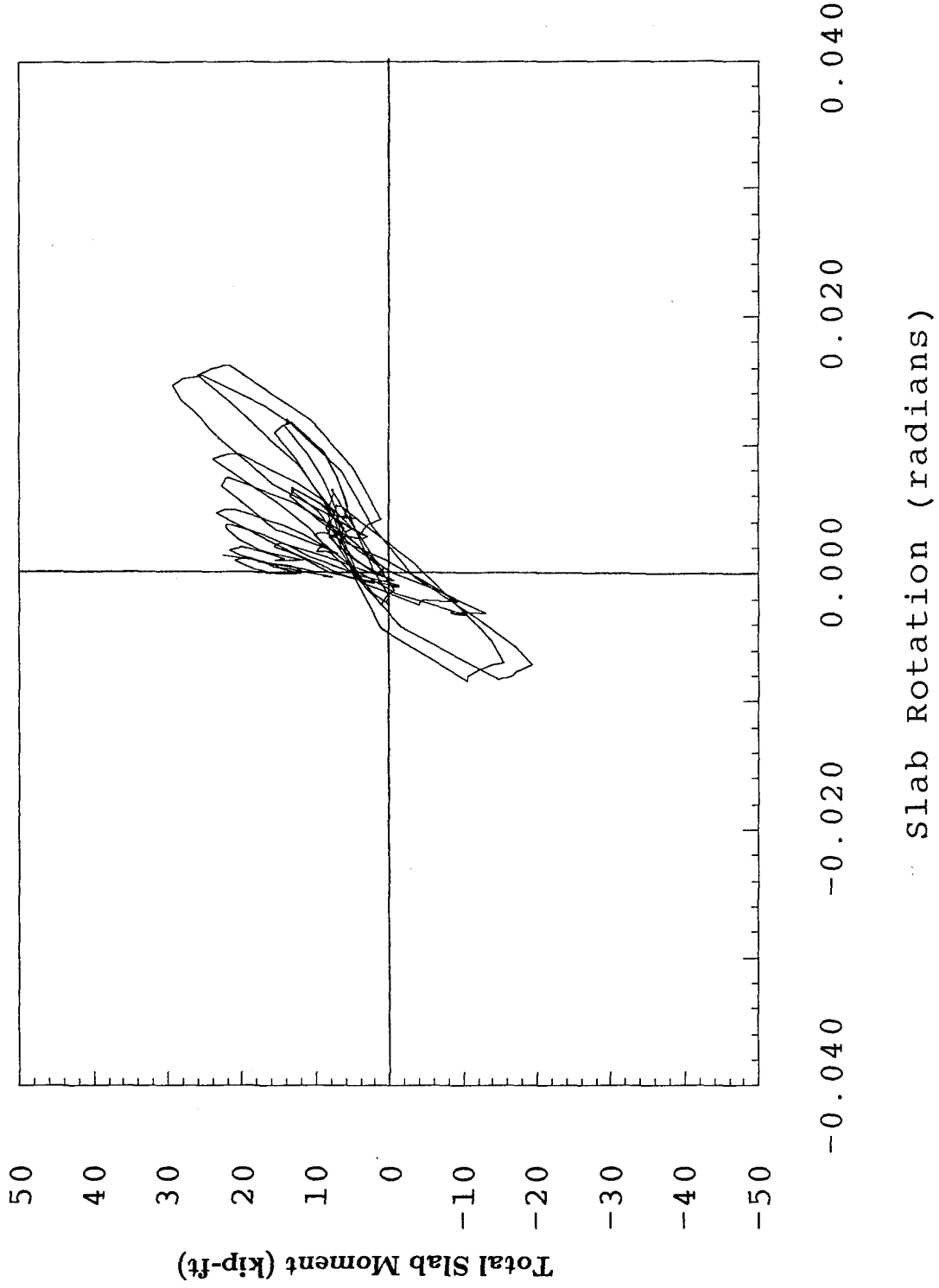


Fig. 5.16 (d) Slab Moment vs Rotation (South Side) - Test 4

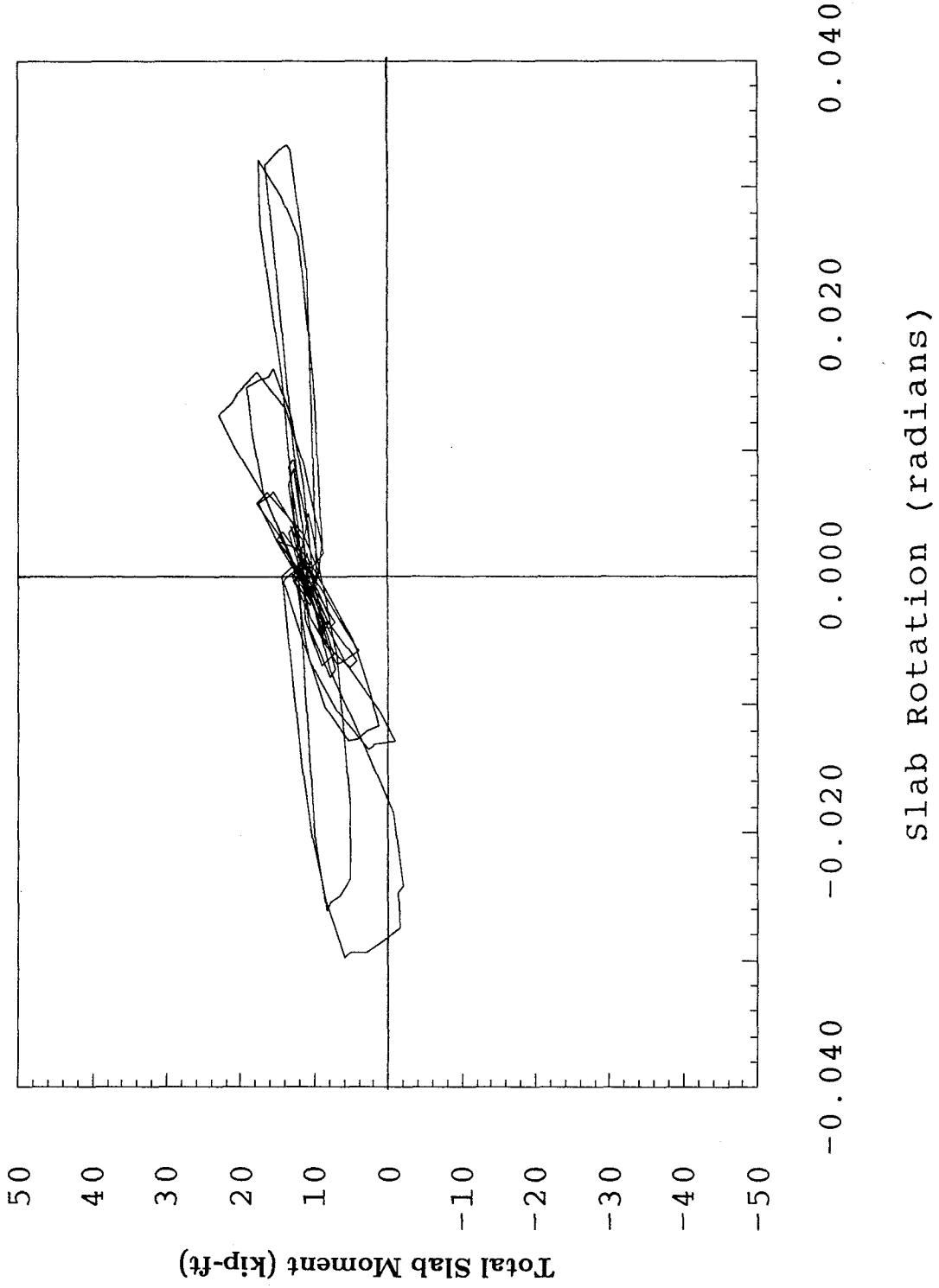


Fig. 5.17 (a) Slab Moment vs Rotation (East Side) - Test 5

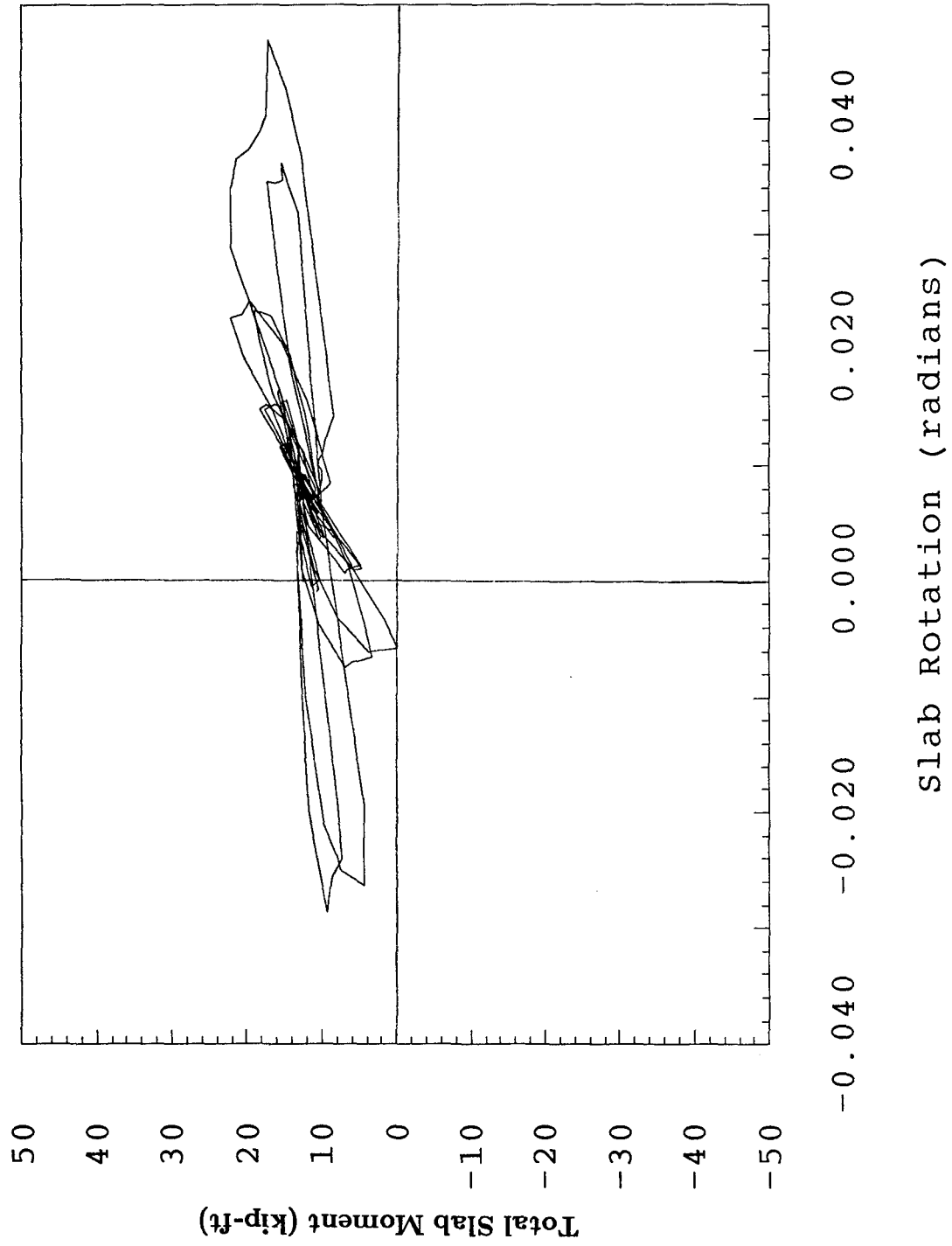


Fig. 5.17 (b) Slab Moment vs Rotation (West Side) - Test 5

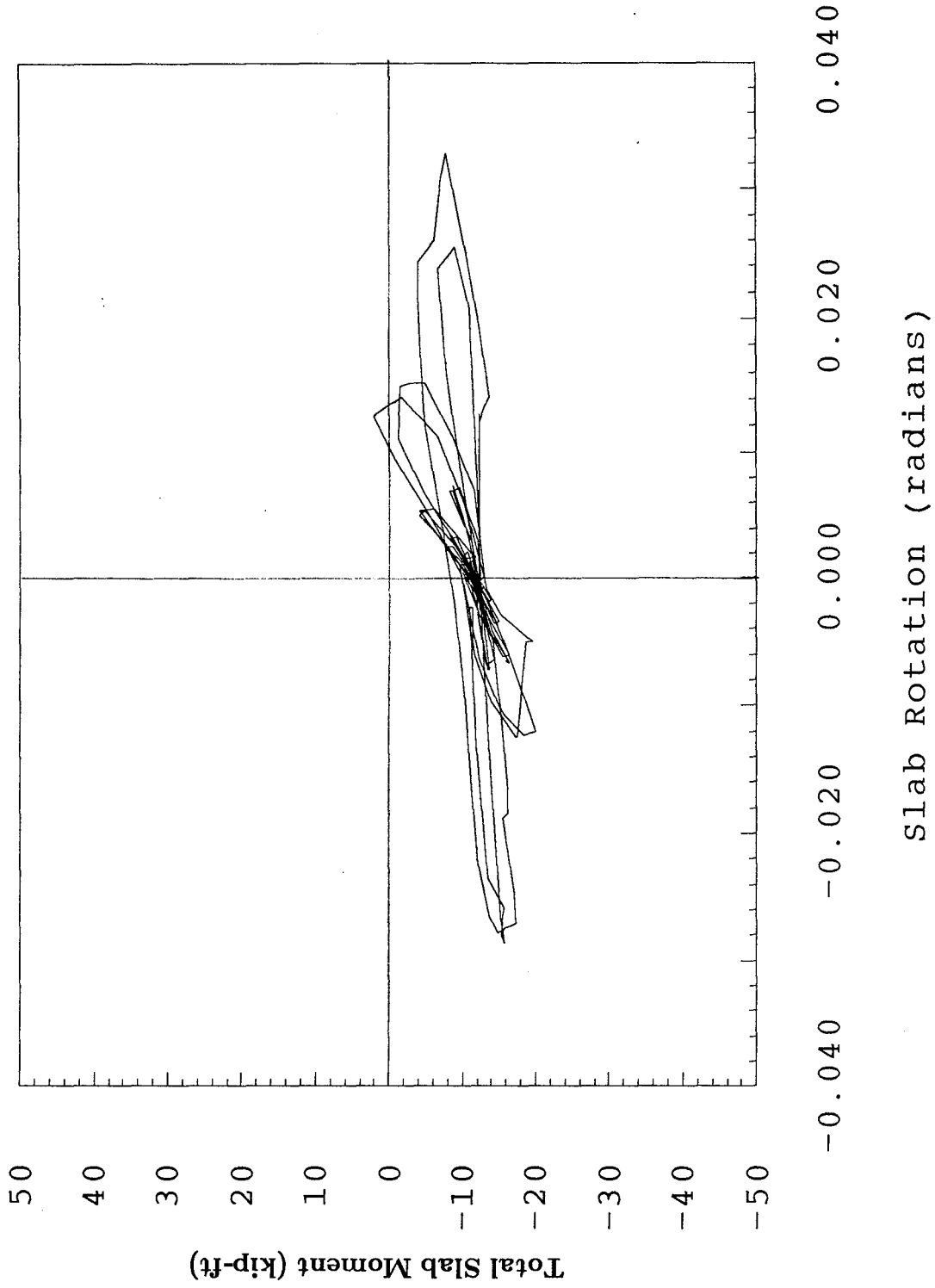


Fig. 5.17 (c) Slab Moment vs Rotation (North Side) - Test 5

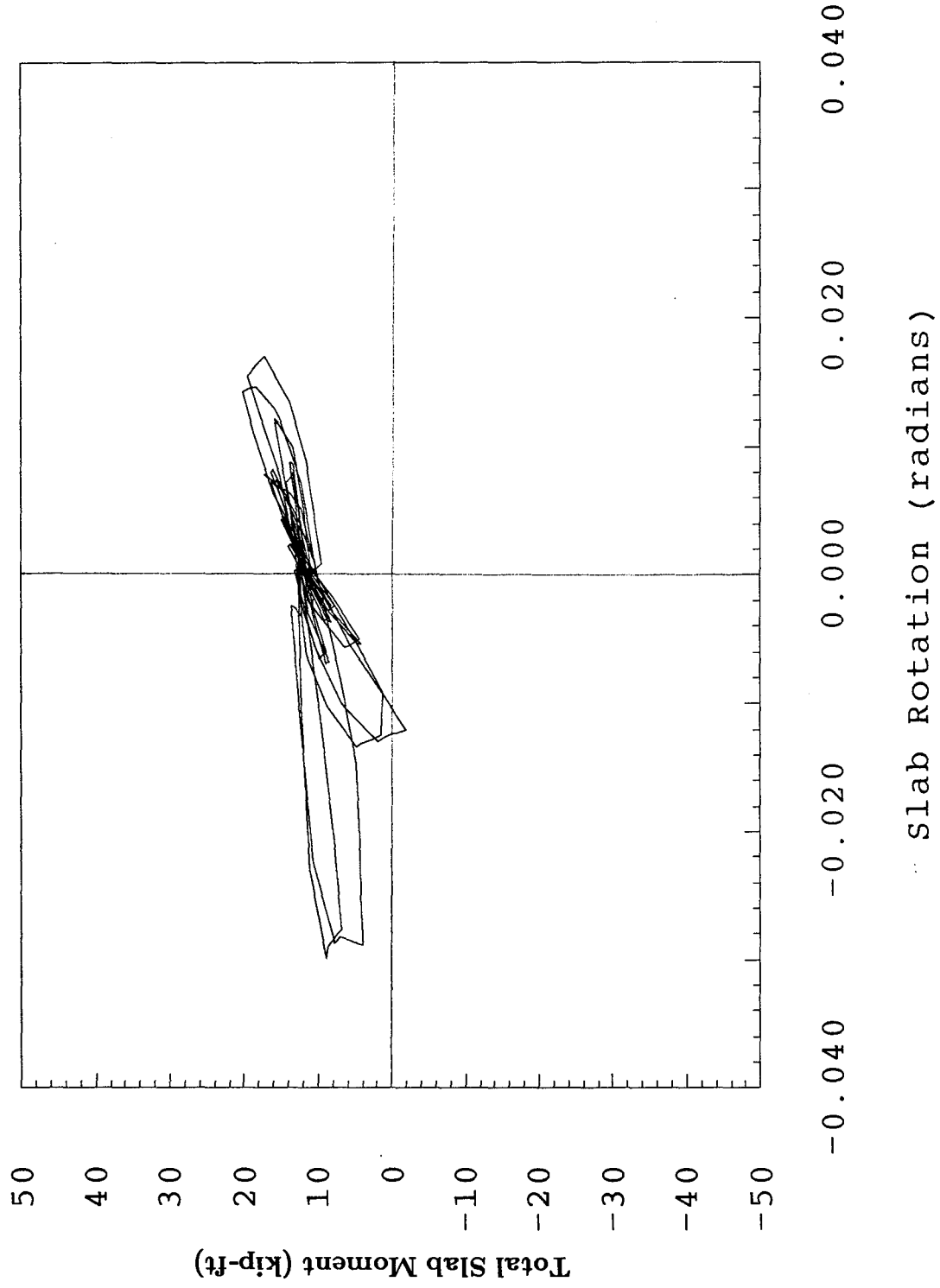


Fig. 5.17 (d) Slab Moment vs Rotation (South Side) - Test 5

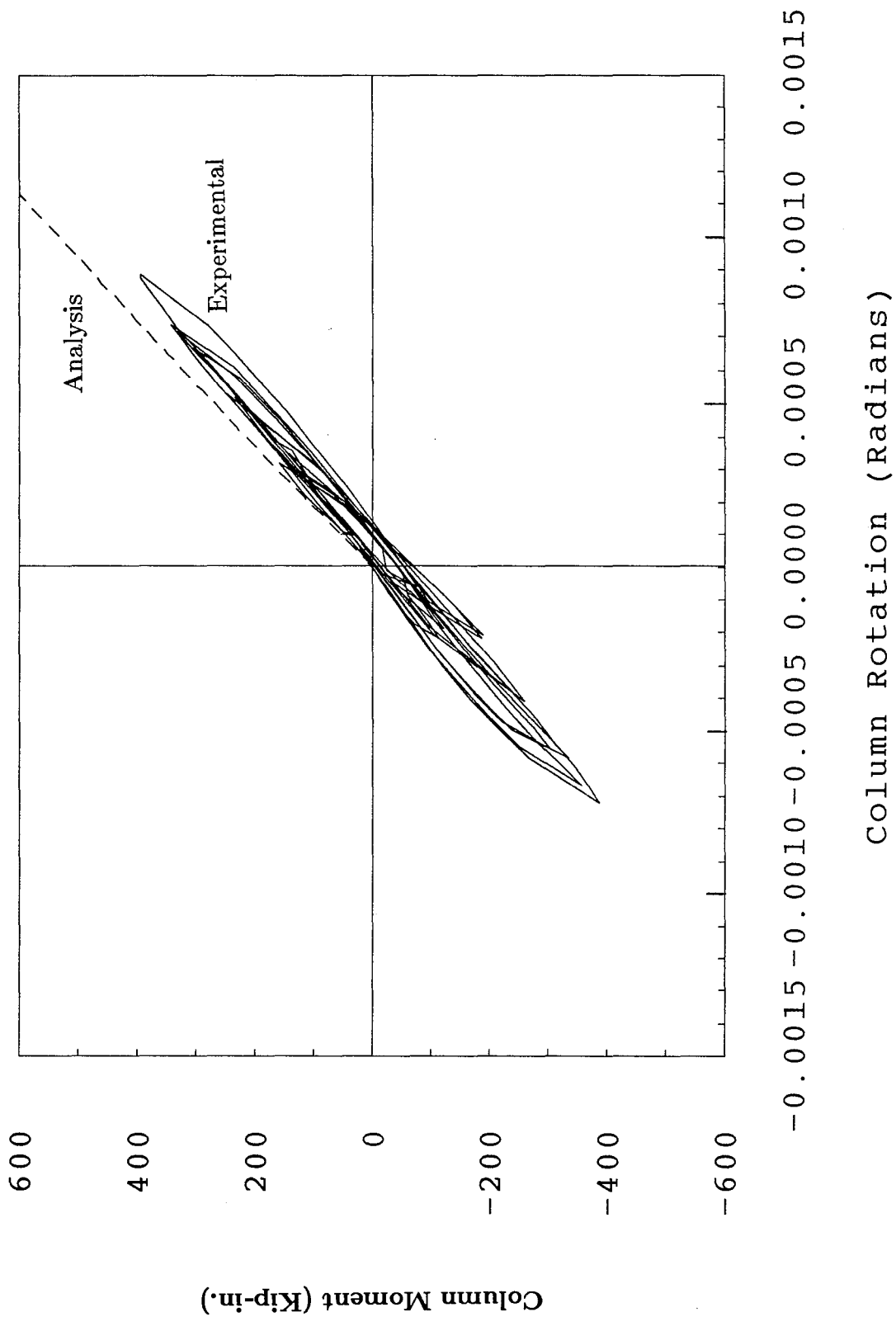


Fig. 5.18 Column Moment vs Rotation (Test 3)

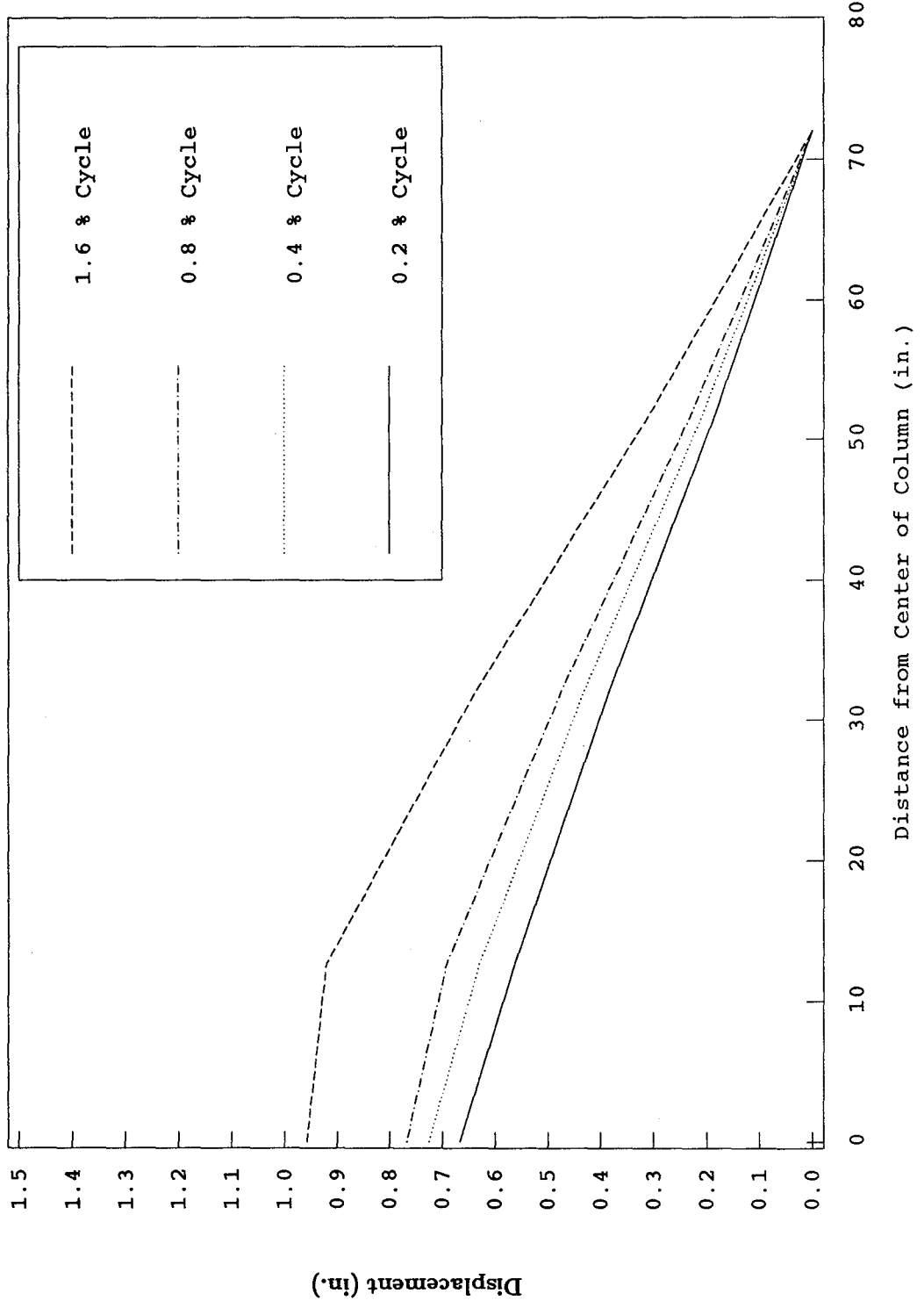


Fig. 5.19 (a) Slab Displacement Profiles (West Side) - Test 1

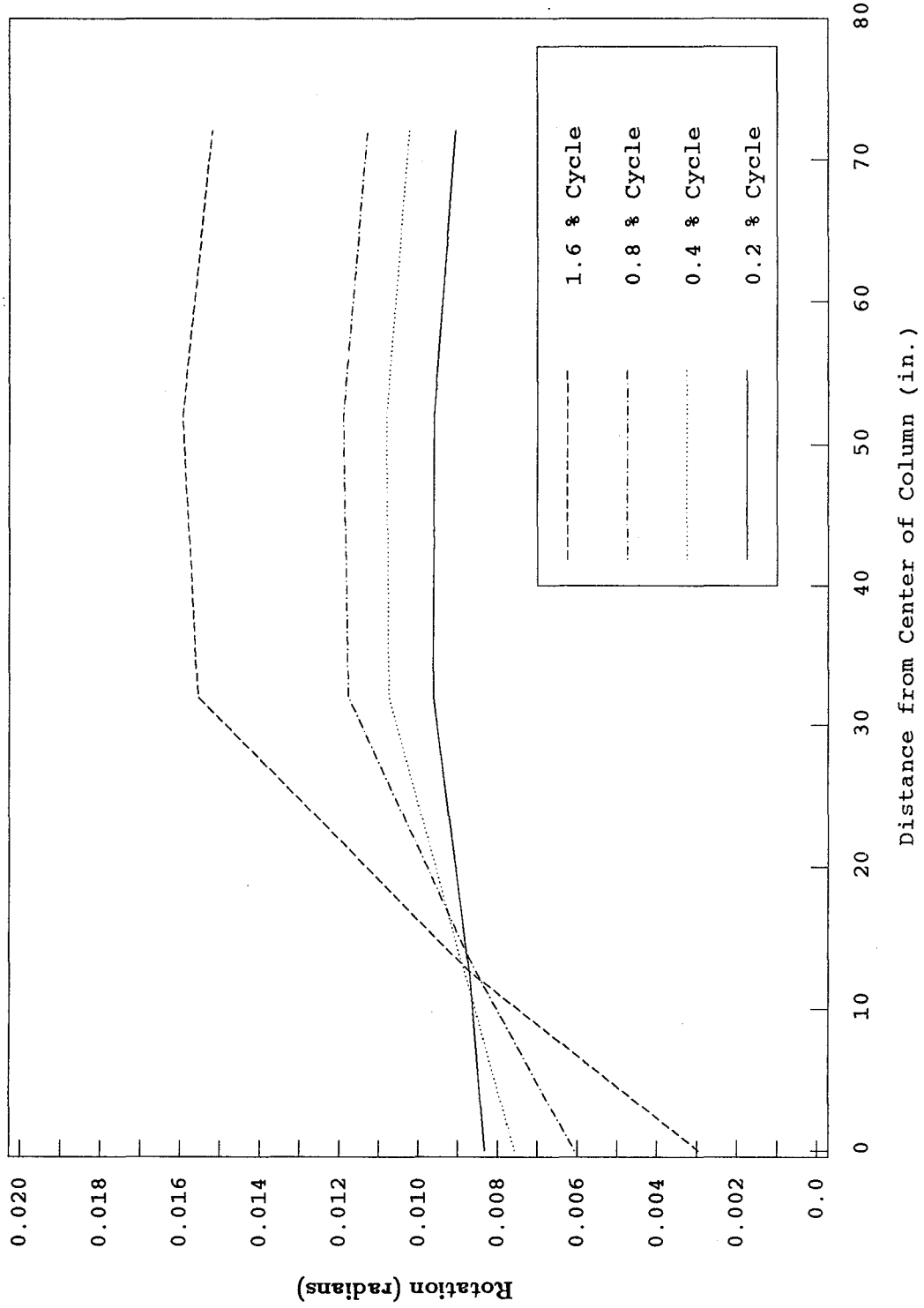


Fig. 5.19 (b) Slab Rotation Profiles (West Side) - Test 1

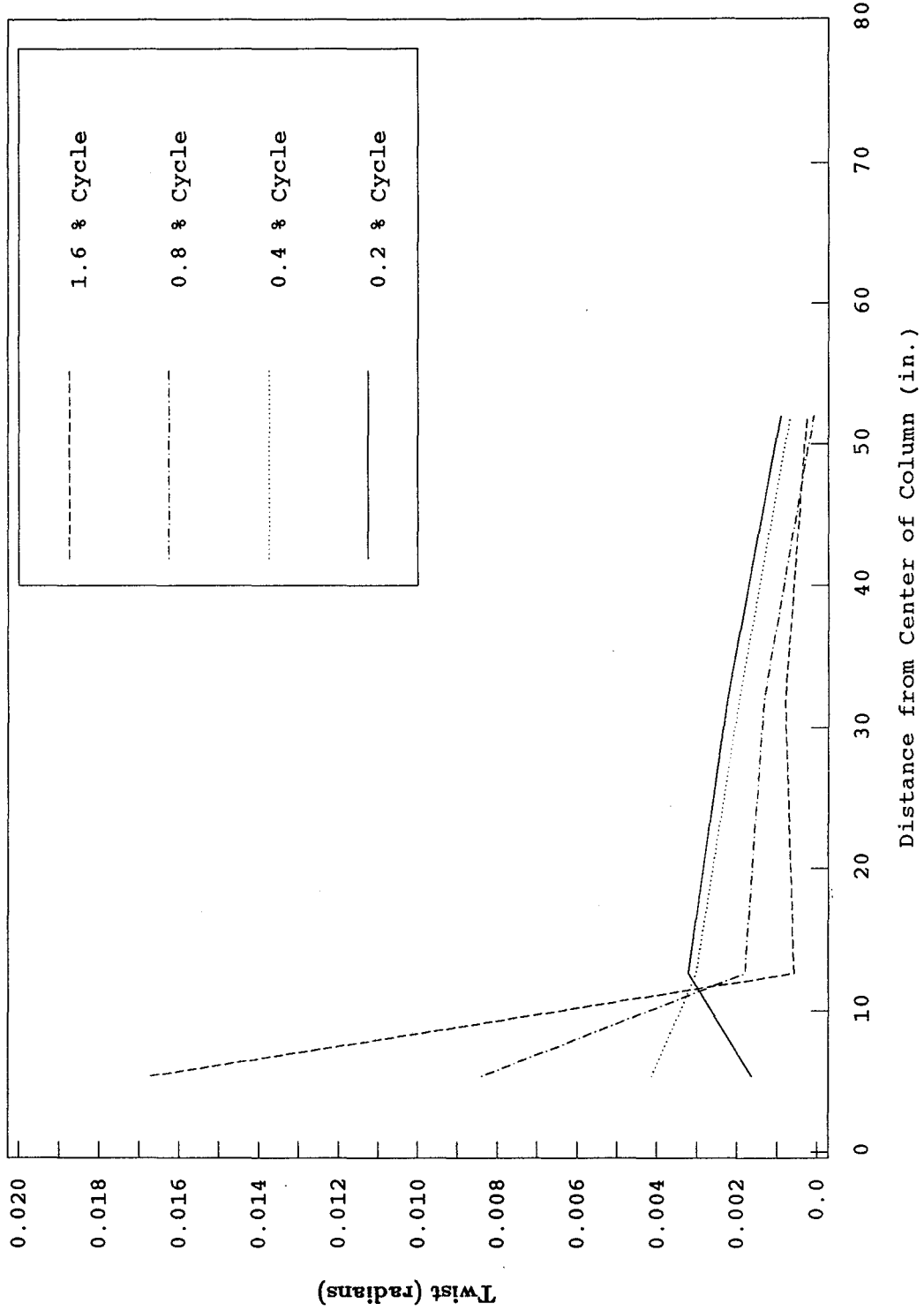


Fig. 5.19 (c) Slab Twist Profiles (South Side) - Test 1

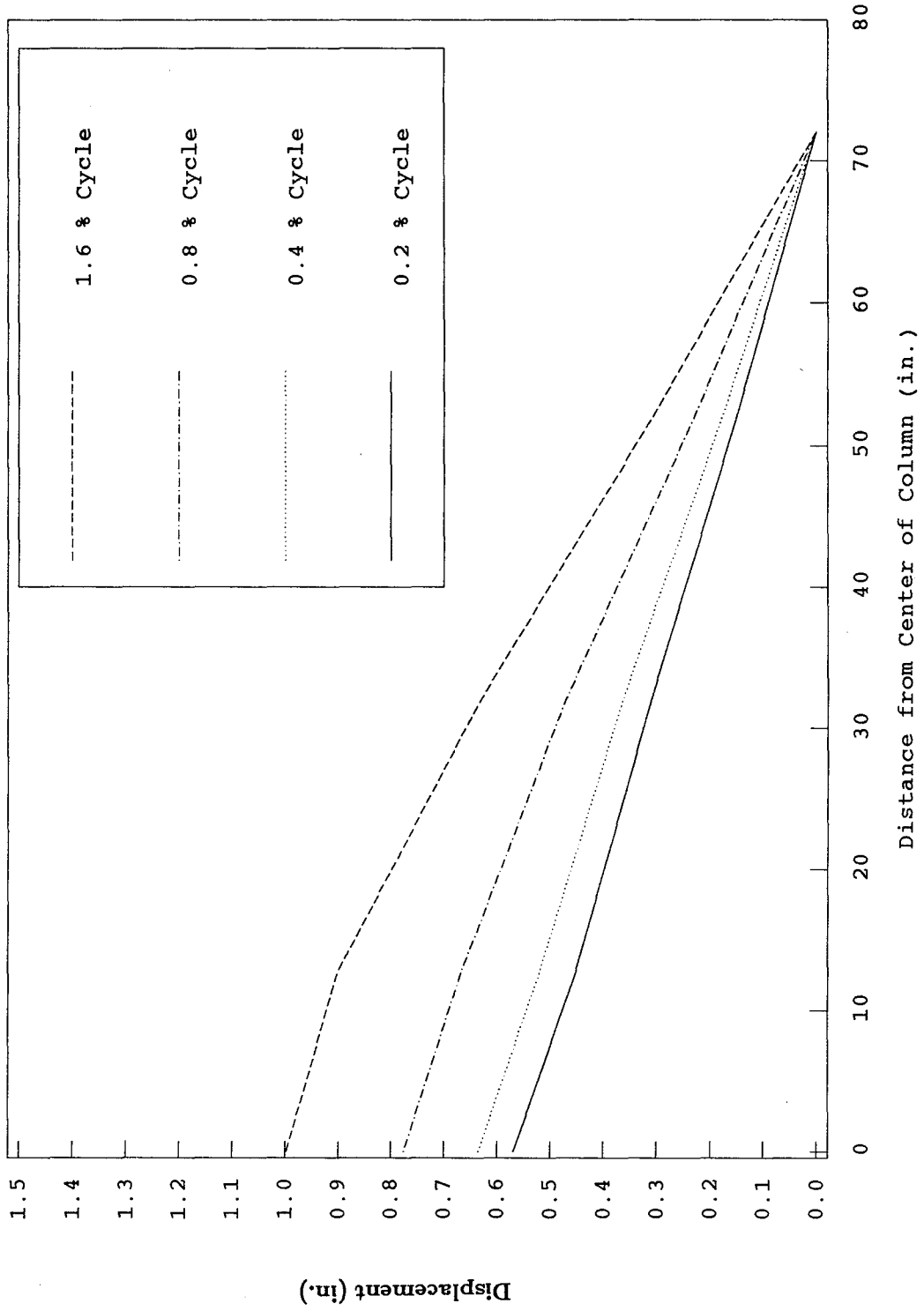


Fig. 5.20 (a) Slab Displacement Profiles (West Side) - Test 2

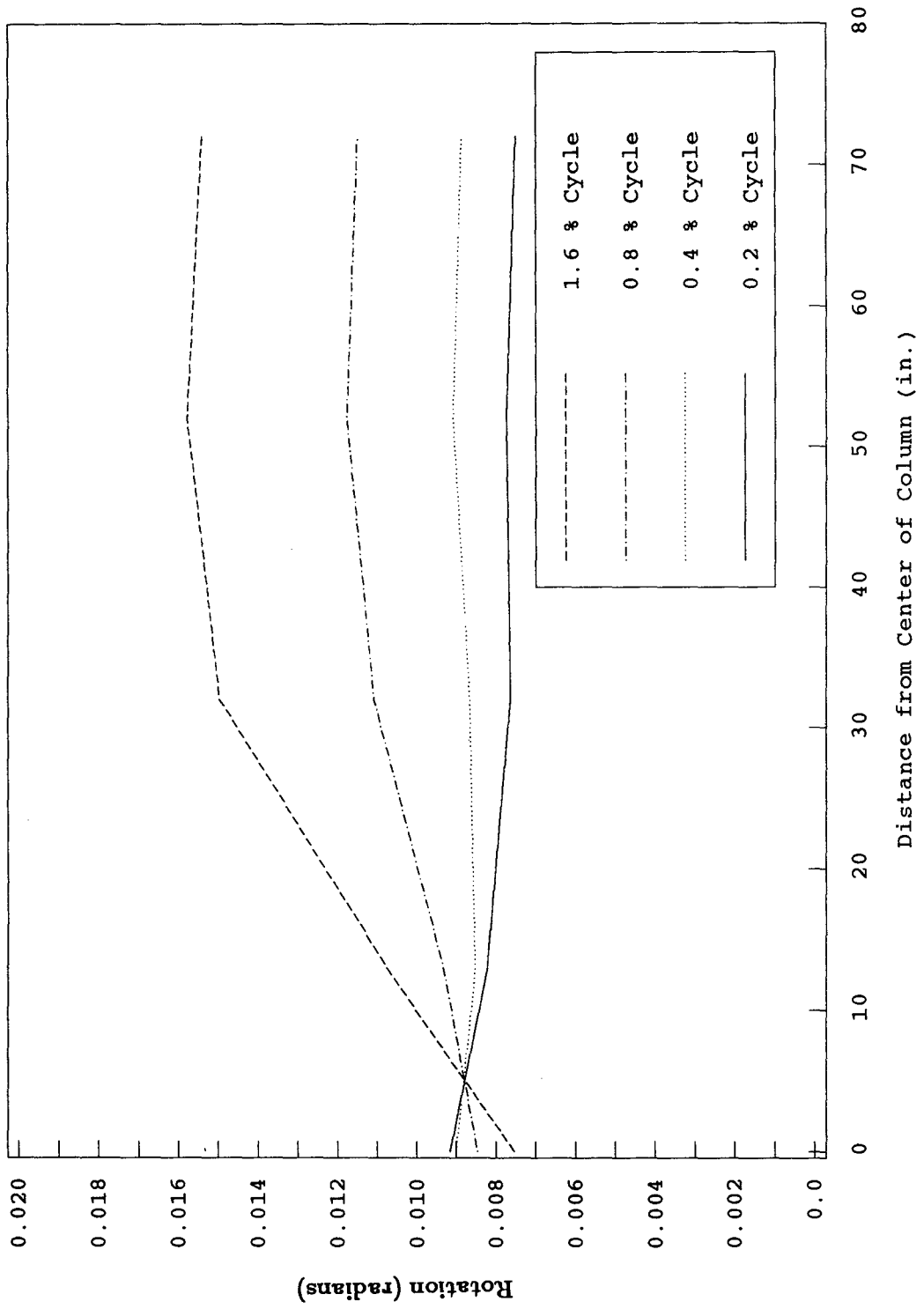


Fig. 5.20 (b) Slab Rotation Profiles (West Side) - Test 2

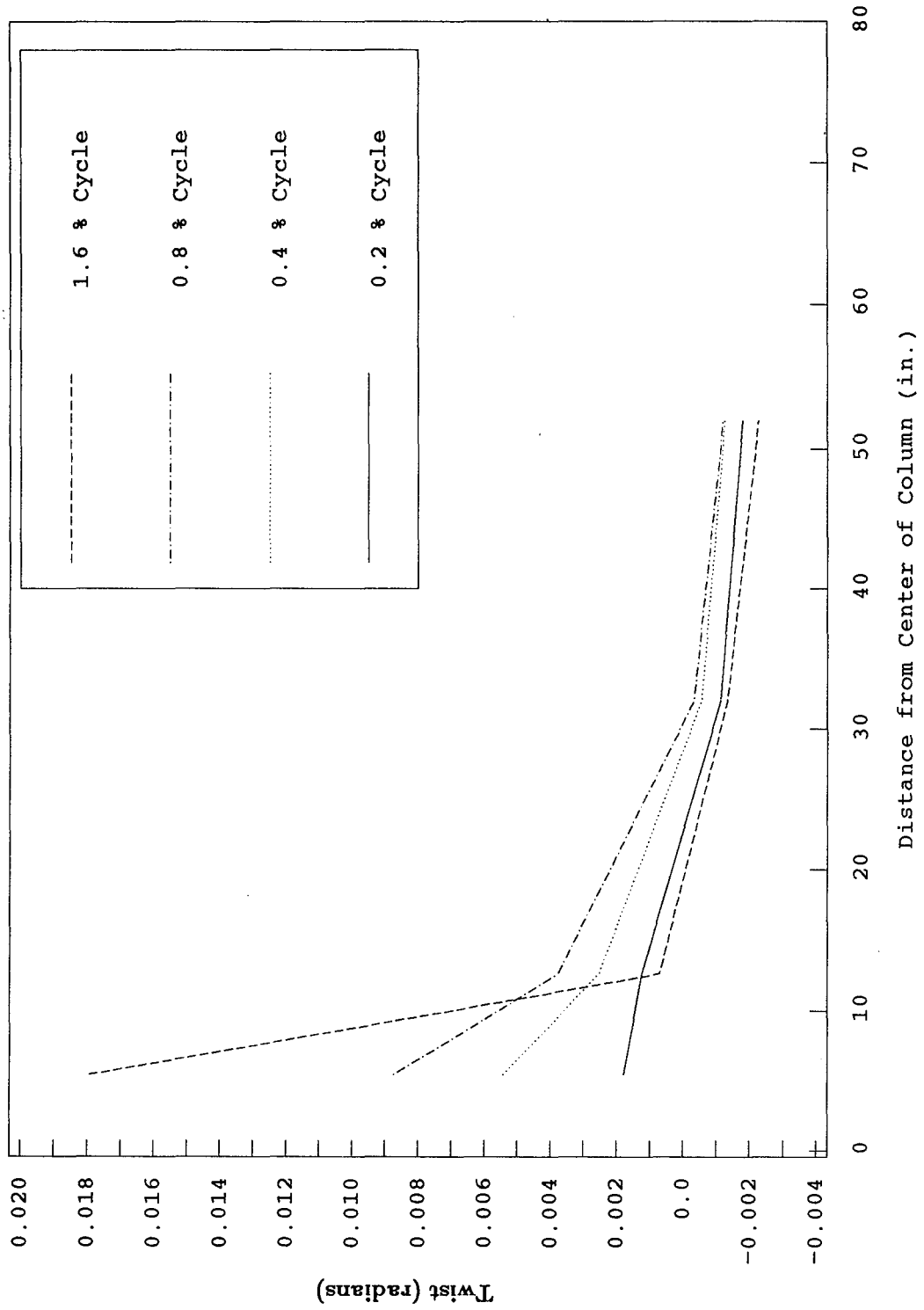


Fig. 5.20 (c) Slab Twist Profiles (West Side) - Test 2

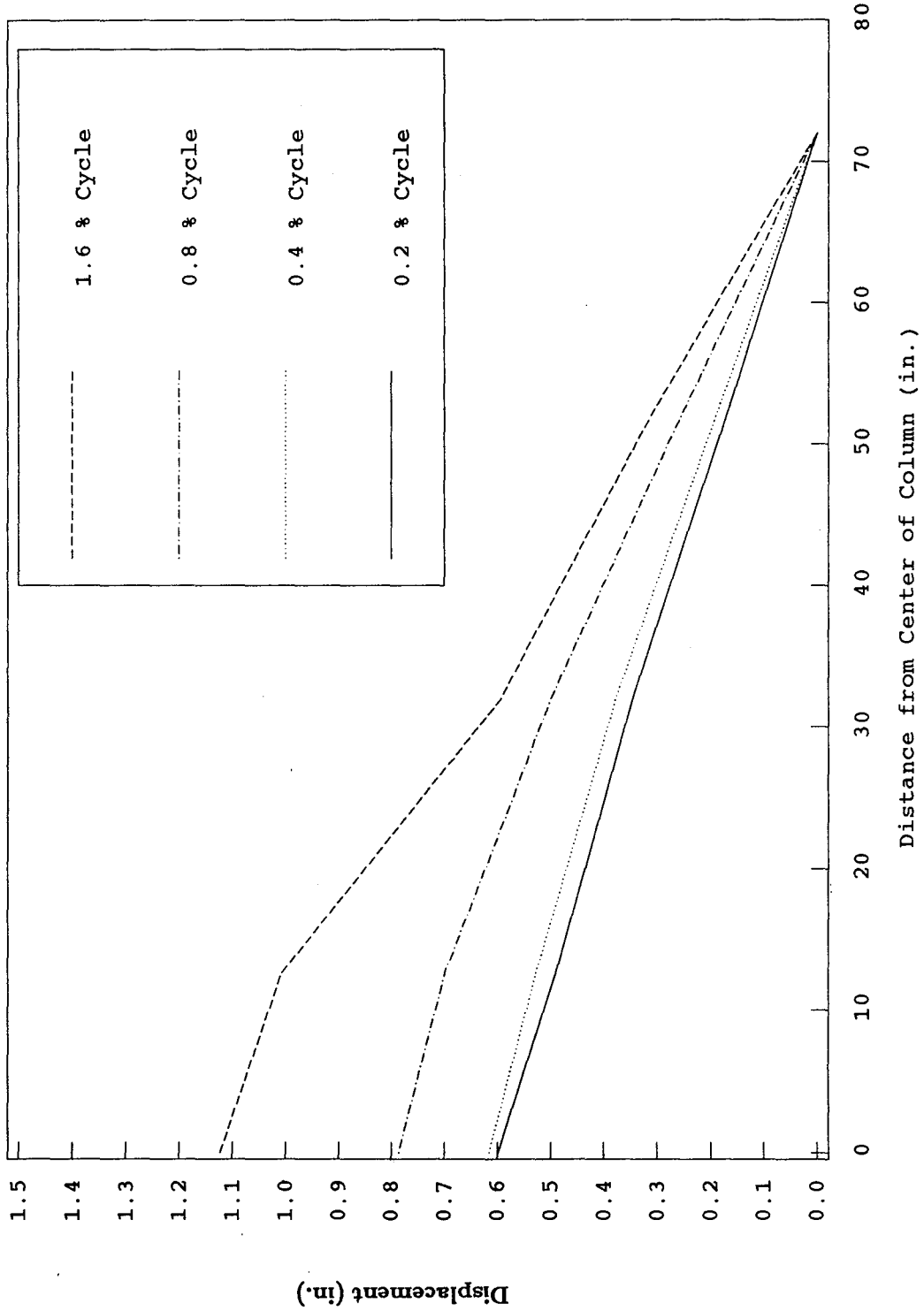


Fig. 5.20 (d) Slab Displacement Profiles (South Side) - Test 2

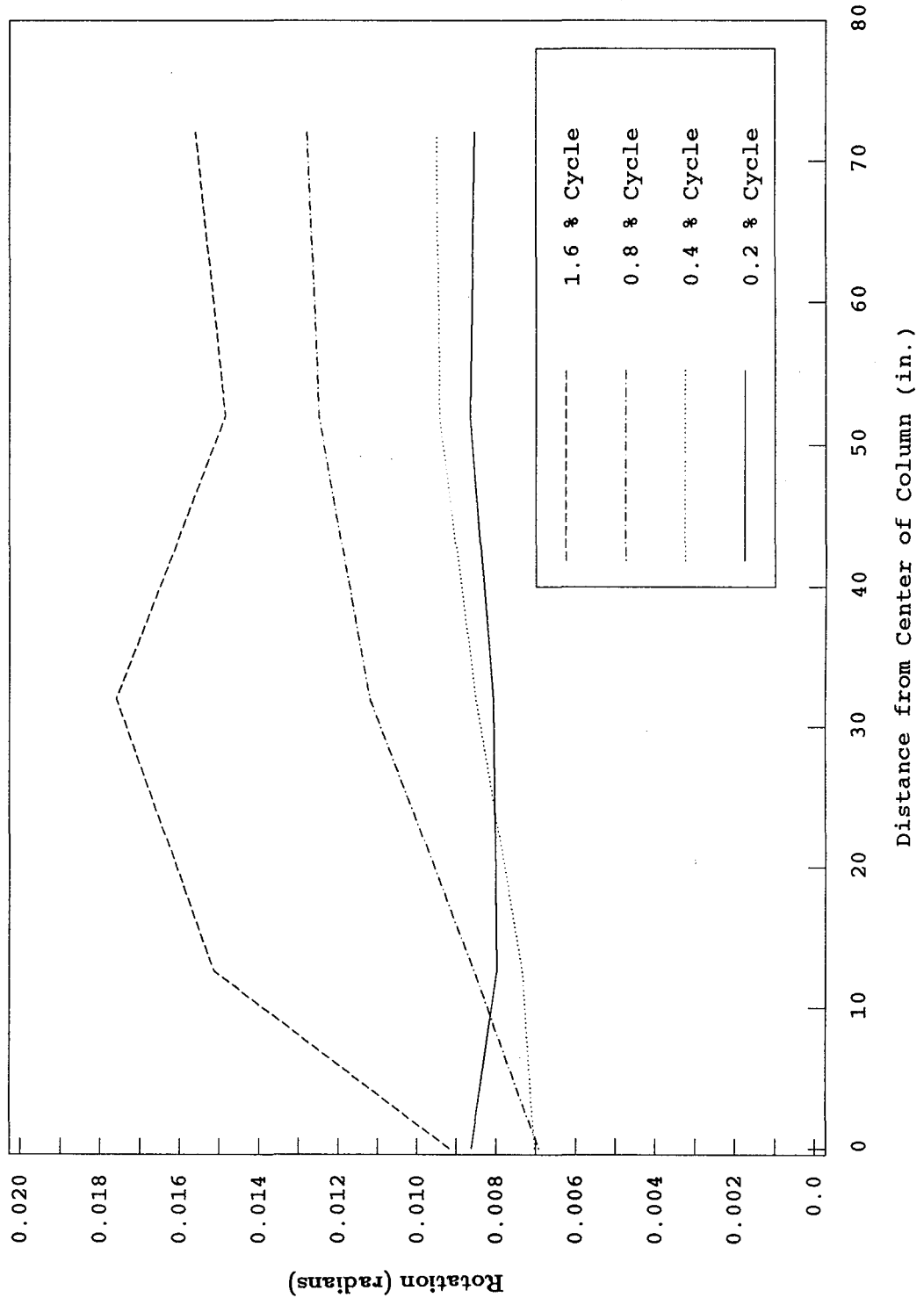


Fig. 5.20 (e) Slab Rotation Profiles (South Side) - Test 2

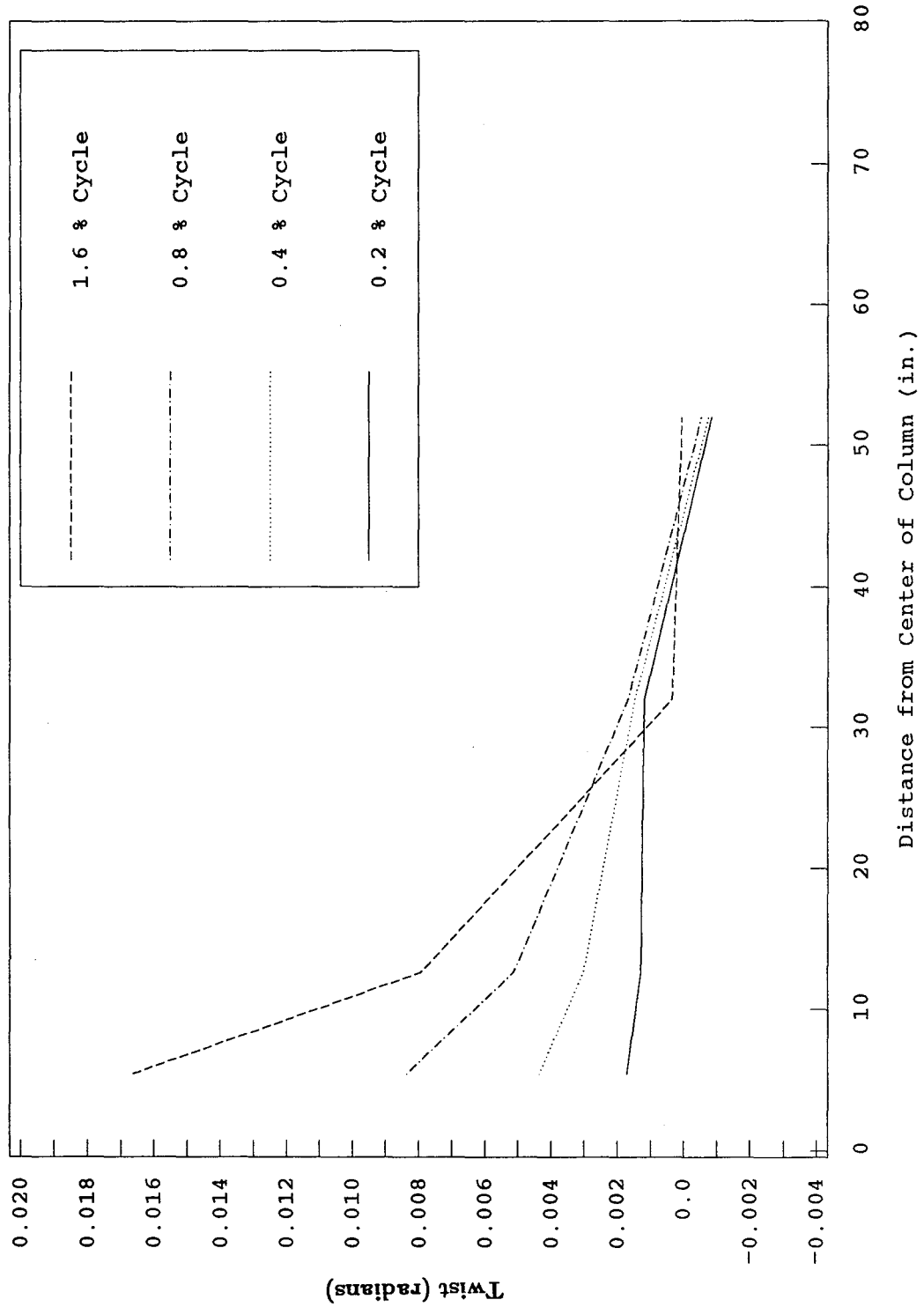


Fig. 5.20 (f) Slab Twist Profiles (South Side) - Test 2

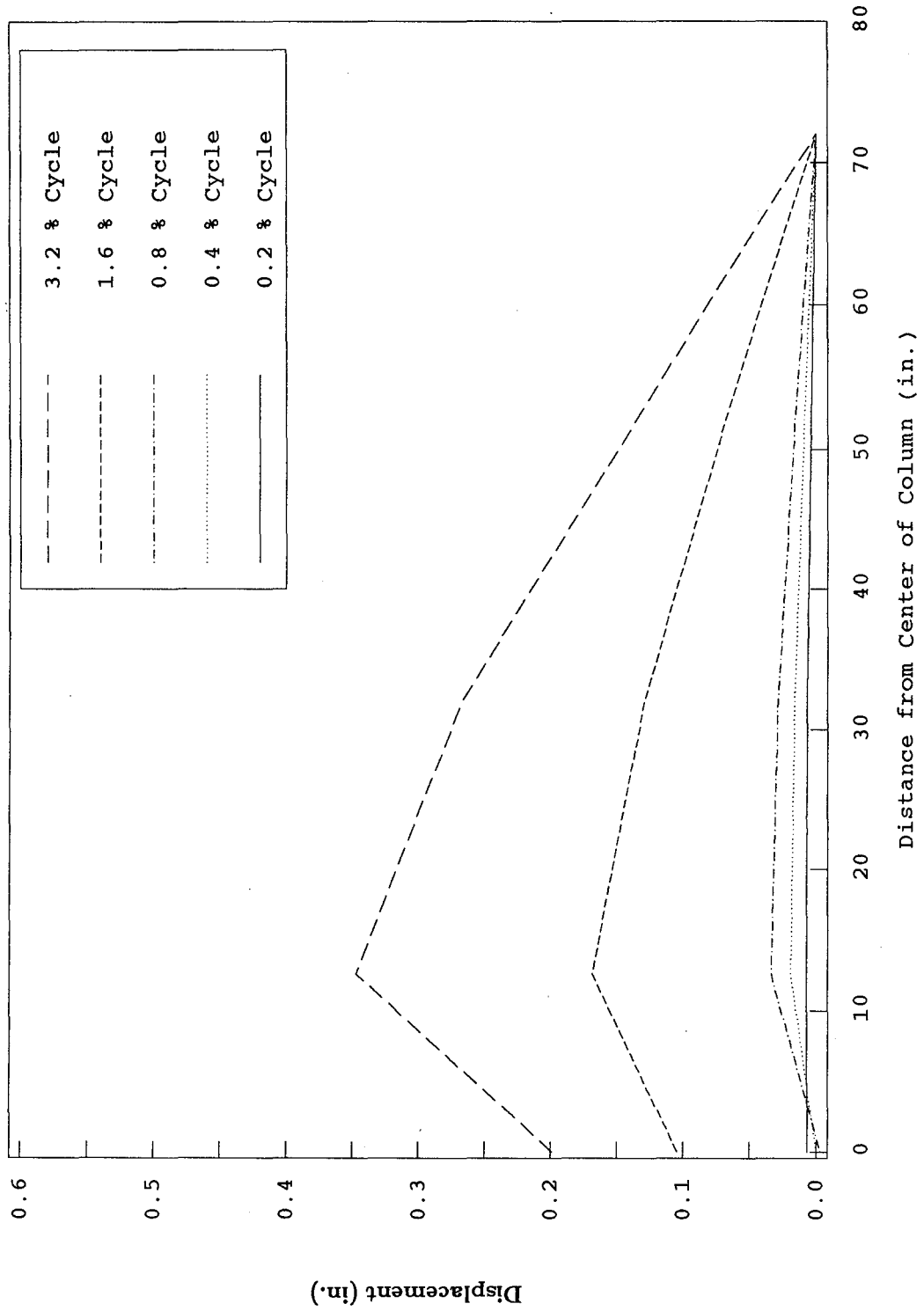


Fig. 5.21 (a) Slab Displacement Profiles (West Side) - Test 3

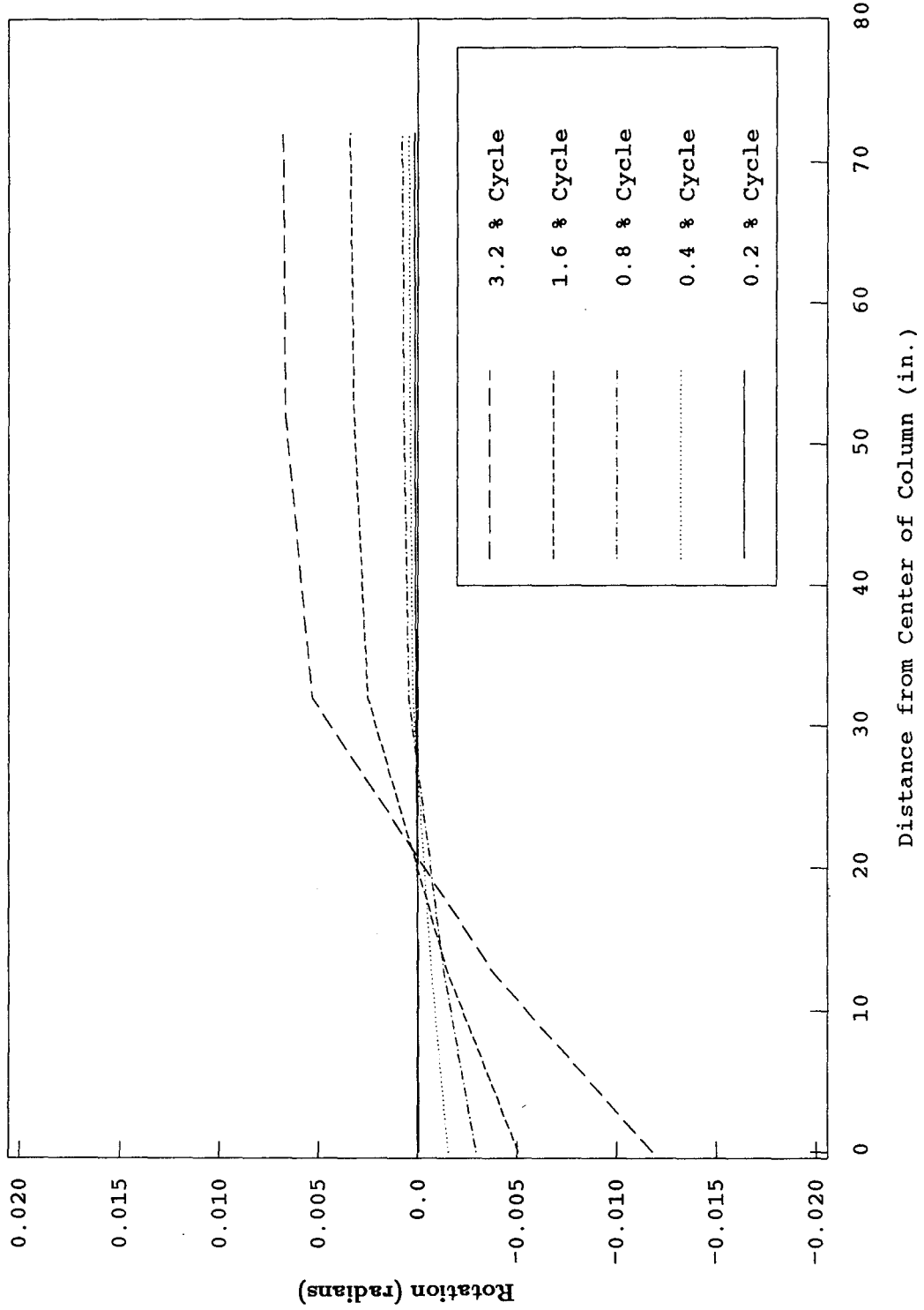


Fig. 5.21 (b) Slab Rotation Profiles (West Side) - Test 3

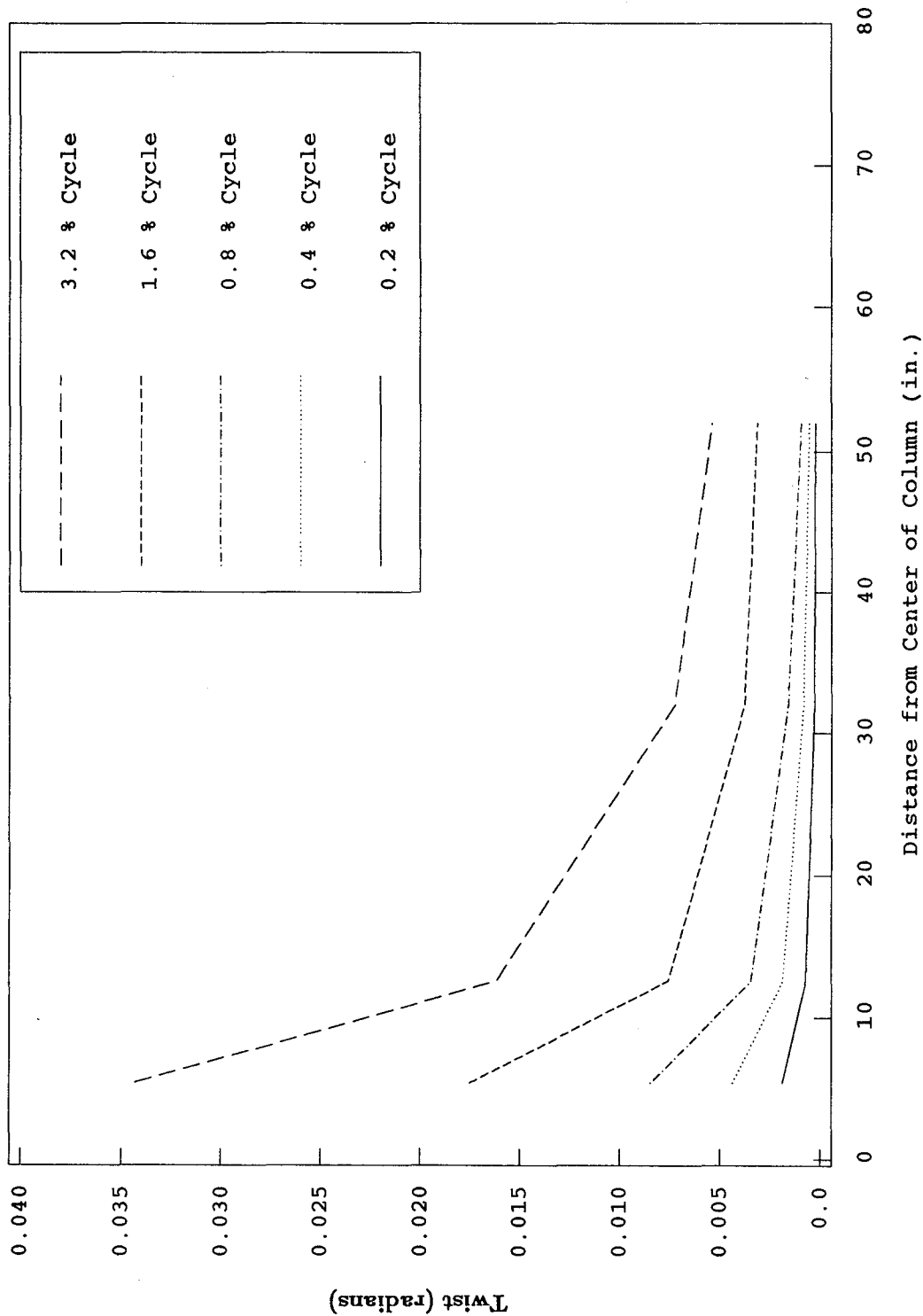


Fig. 5.21 (c) Slab Twist Profiles (South Side) - Test 3

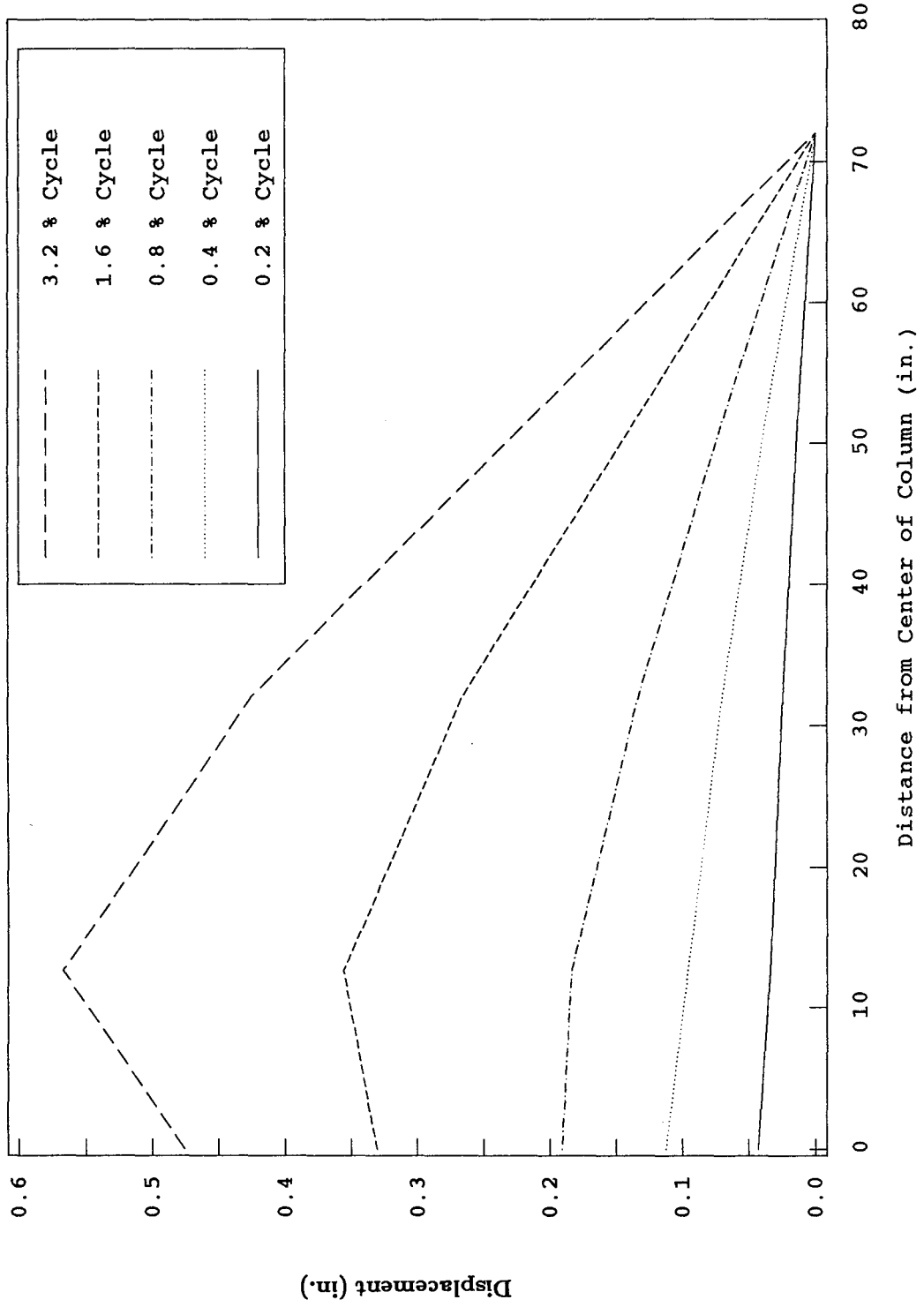


Fig. 5.22 (a) Slab Displacement Profiles (West Side) - Test 4

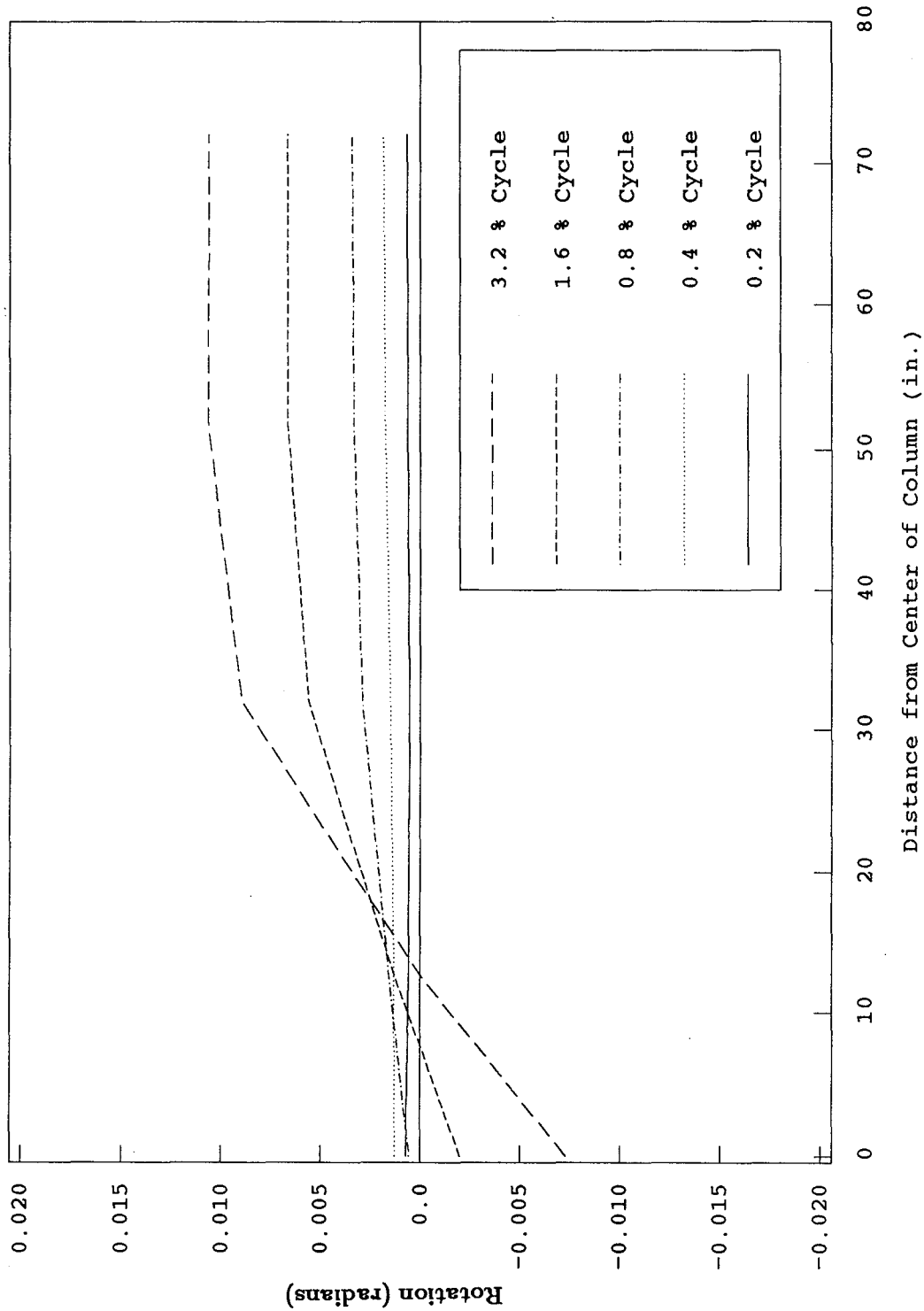


Fig. 5.22 (b) Slab Rotation Profiles (West Side) - Test 4

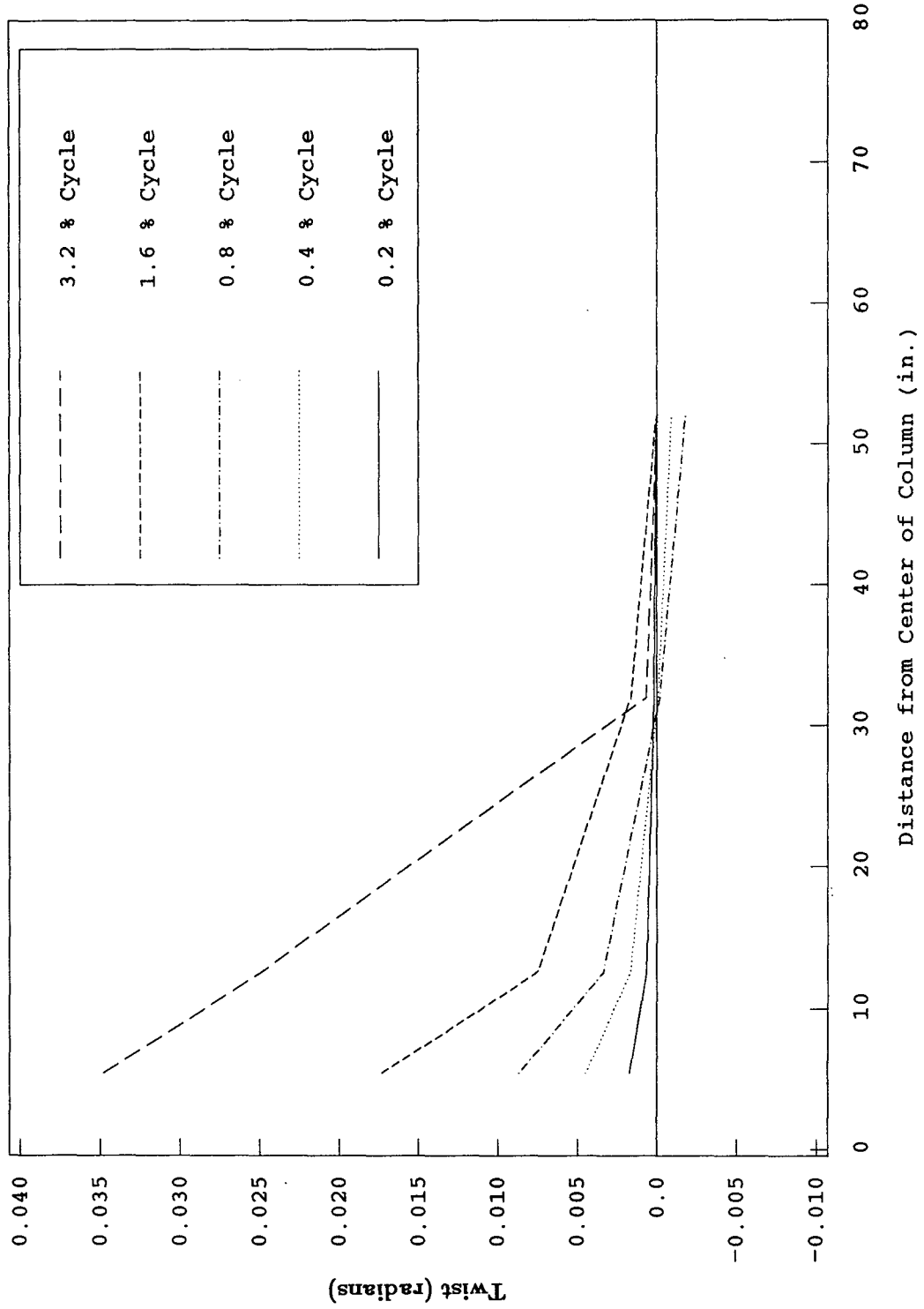


Fig. 5.22 (c) Slab Twist Profiles (West Side) - Test 4

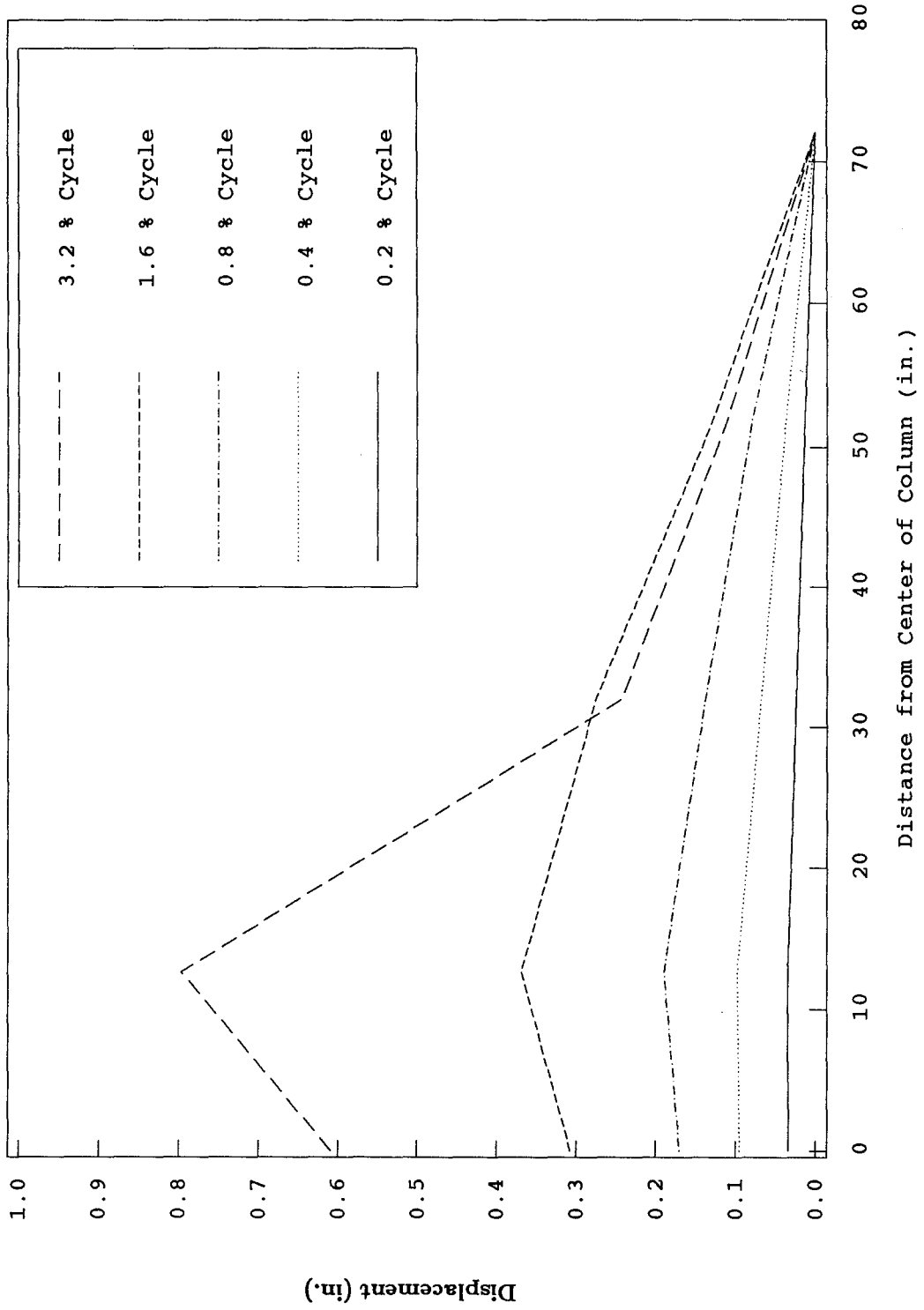


Fig. 5.22 (d) Slab Displacement Profiles (South Side) - Test 4

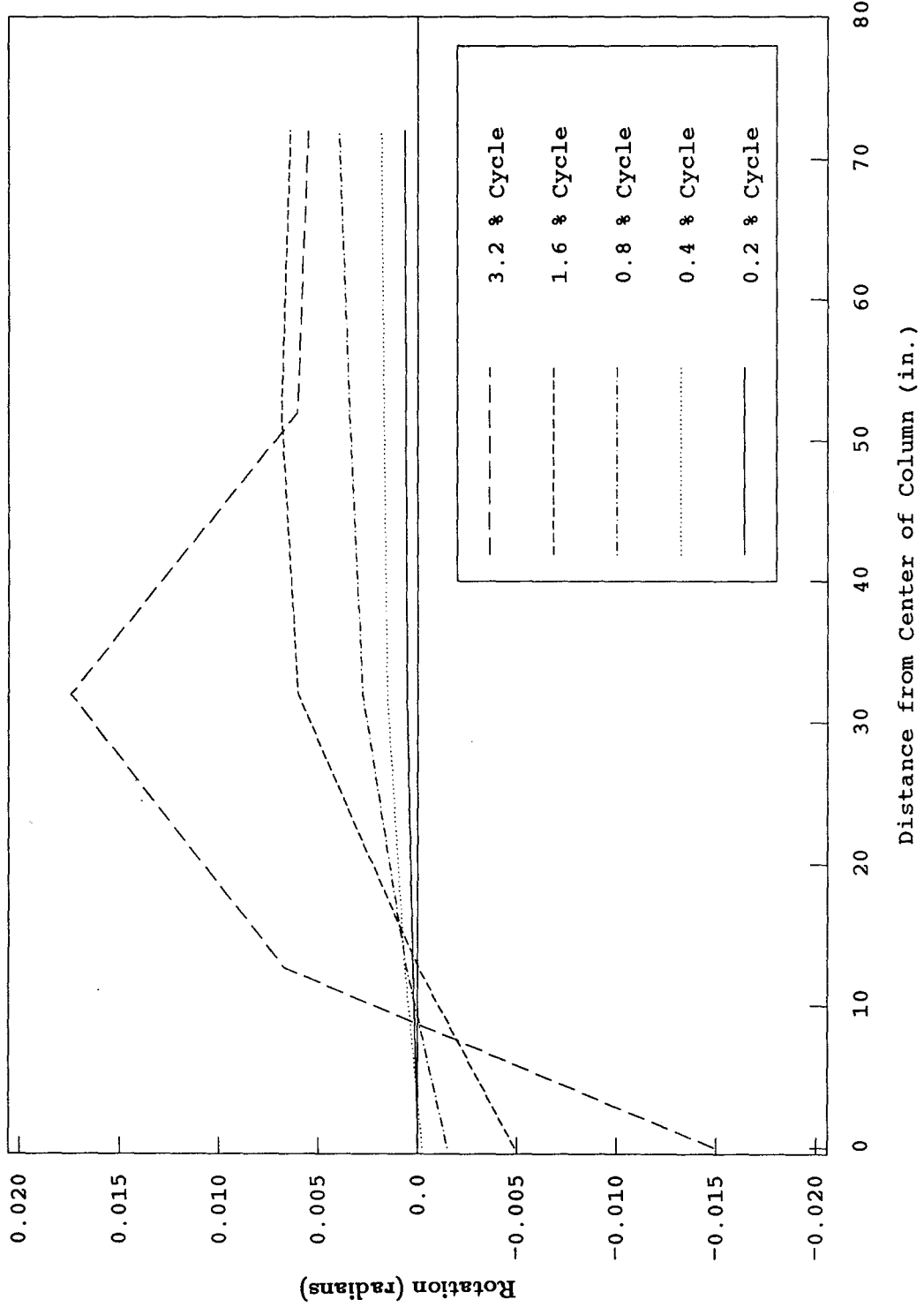


Fig. 5.22 (e) Slab Rotation Profiles (South Side) - Test 4

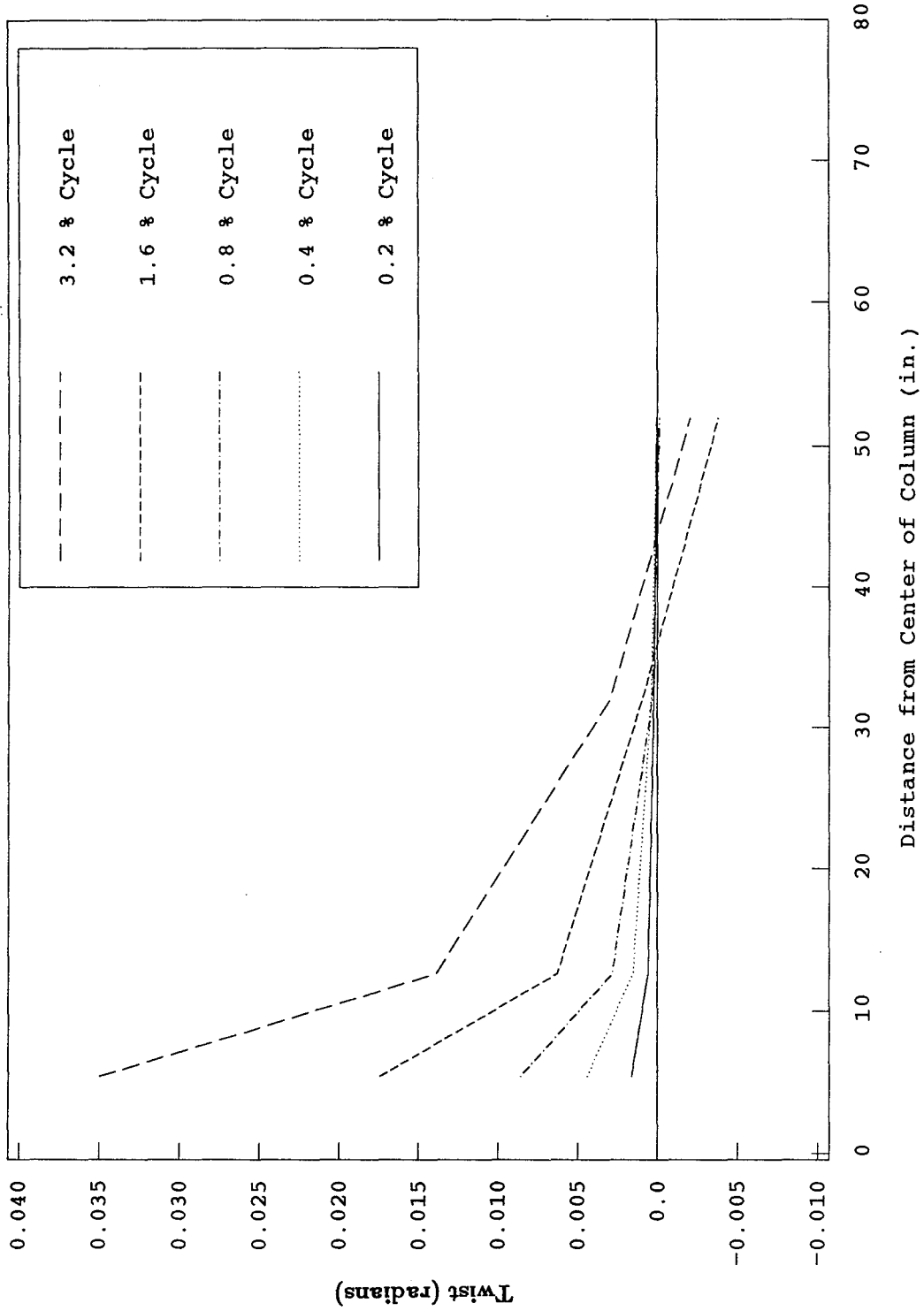


Fig. 5.22 (f) Slab Twist Profiles (South Side) - Test 4

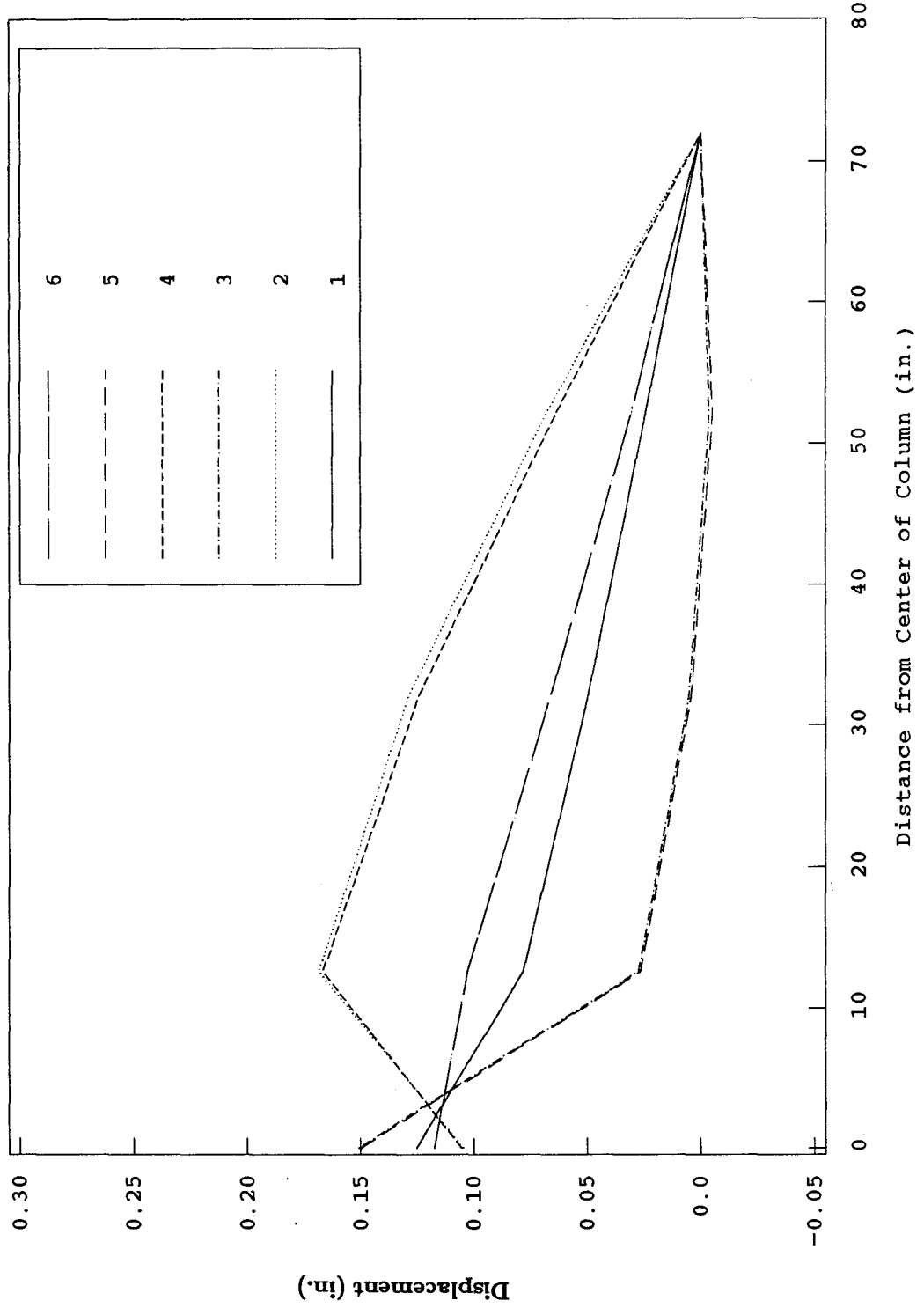


Fig. 5.23 (a) Slab Displacement Profile History (West Side - Test 3)

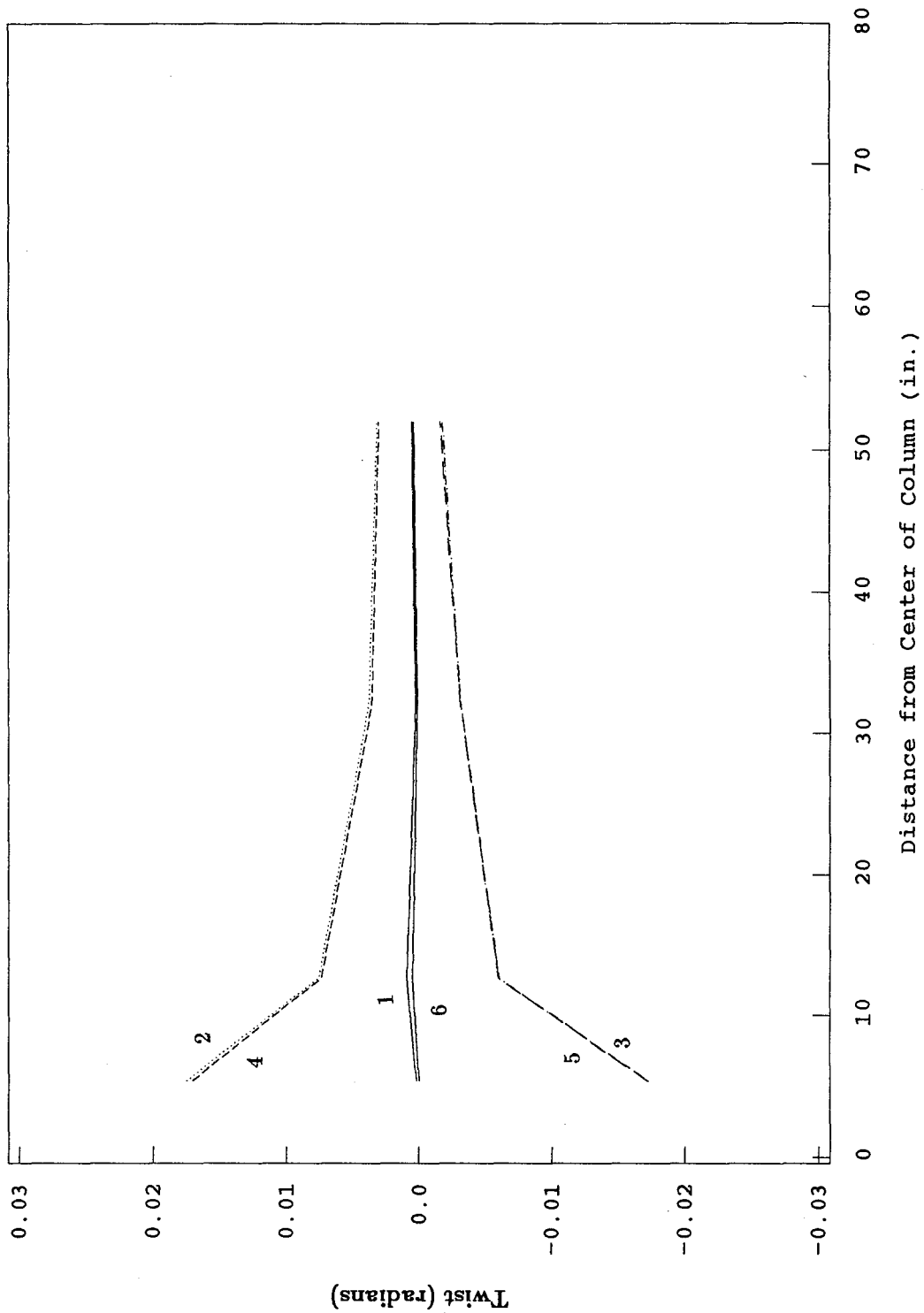


Fig. 5.23 (b) Slab Twist Profile History (South Side - Test 3)

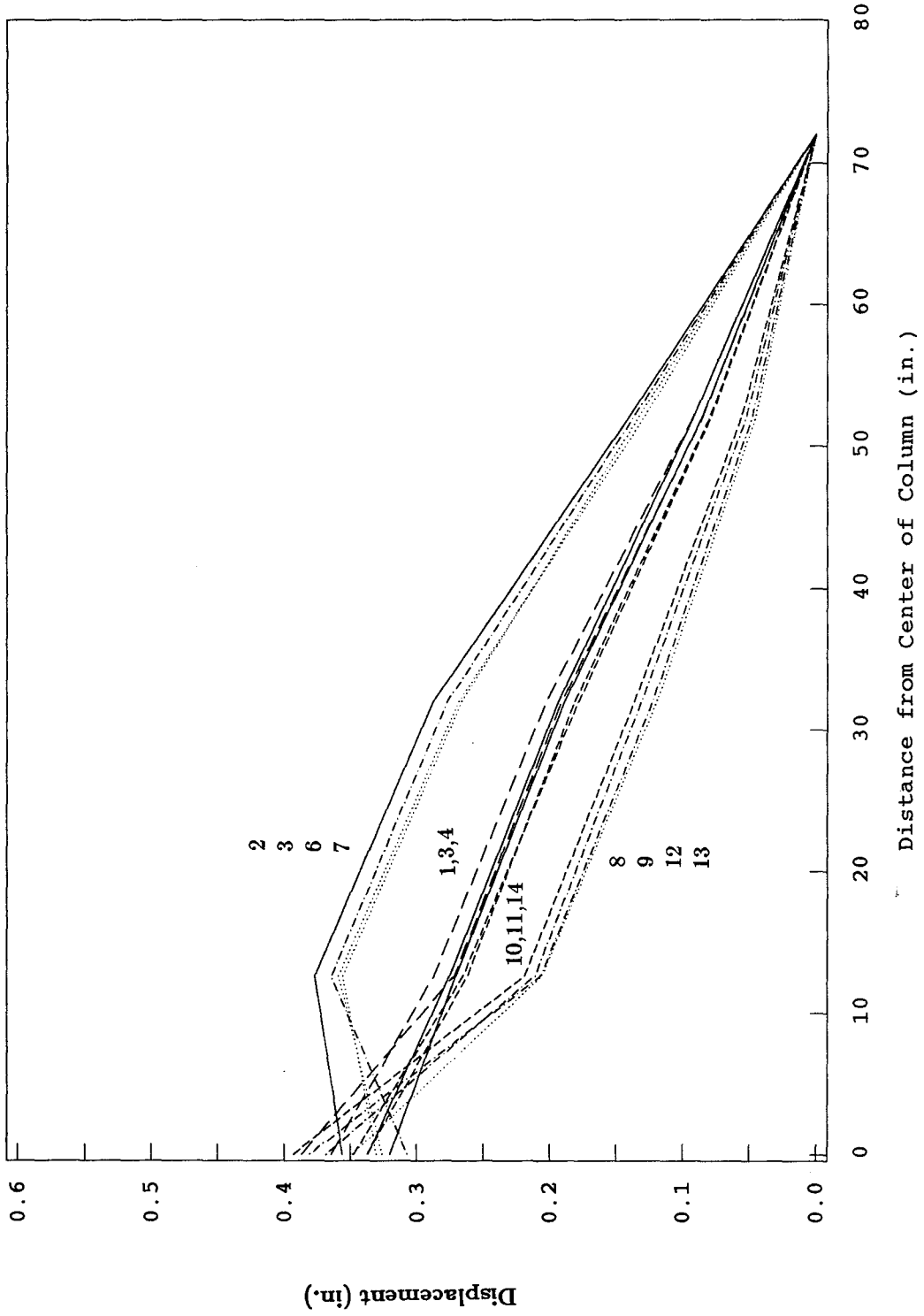


Fig. 5.24 (a) Slab Displacement Profile History (West Side - Test 4)

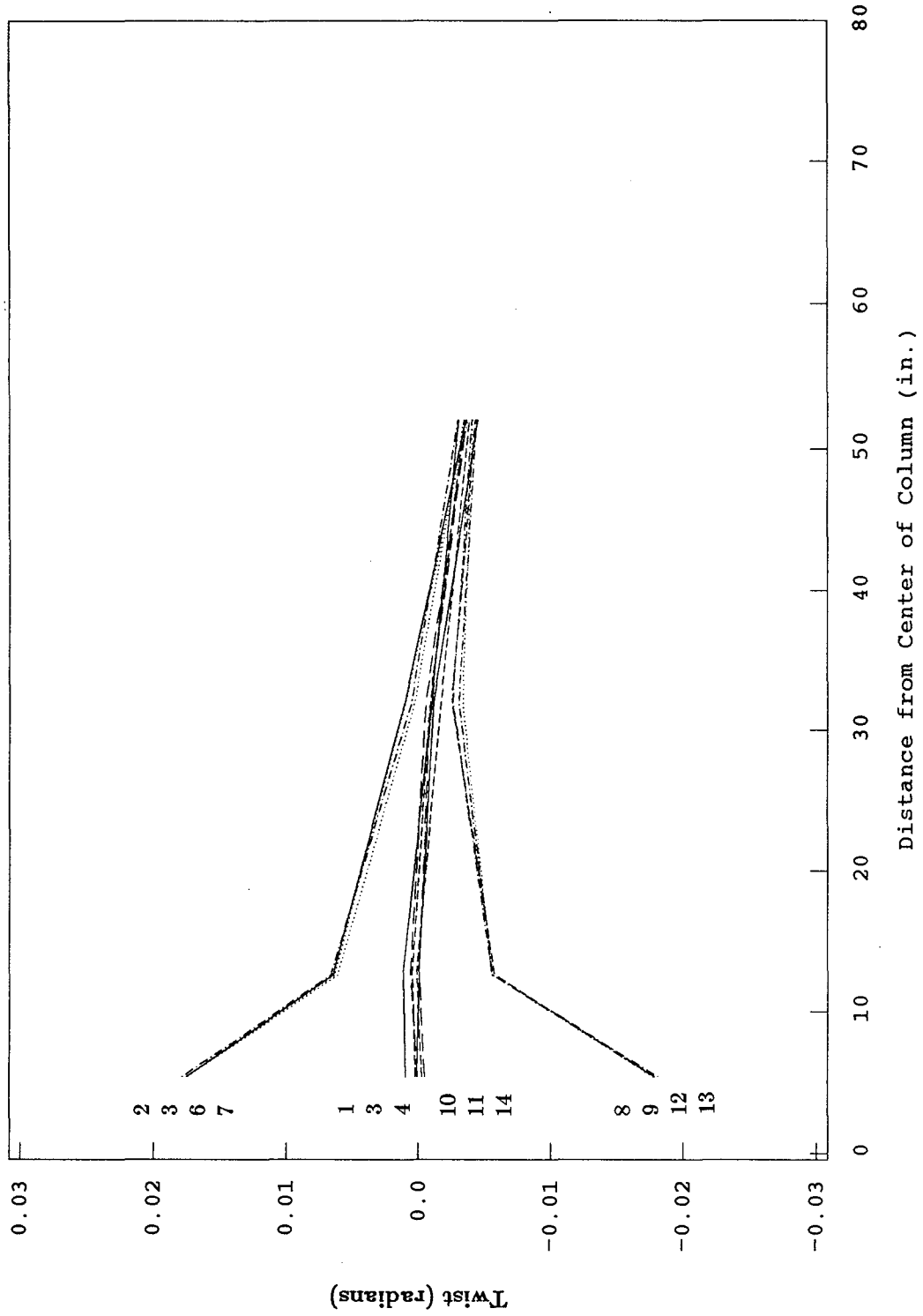
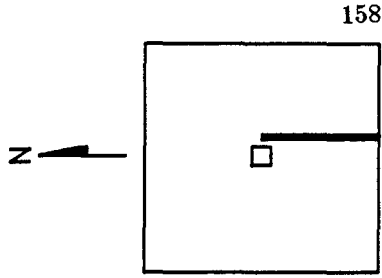
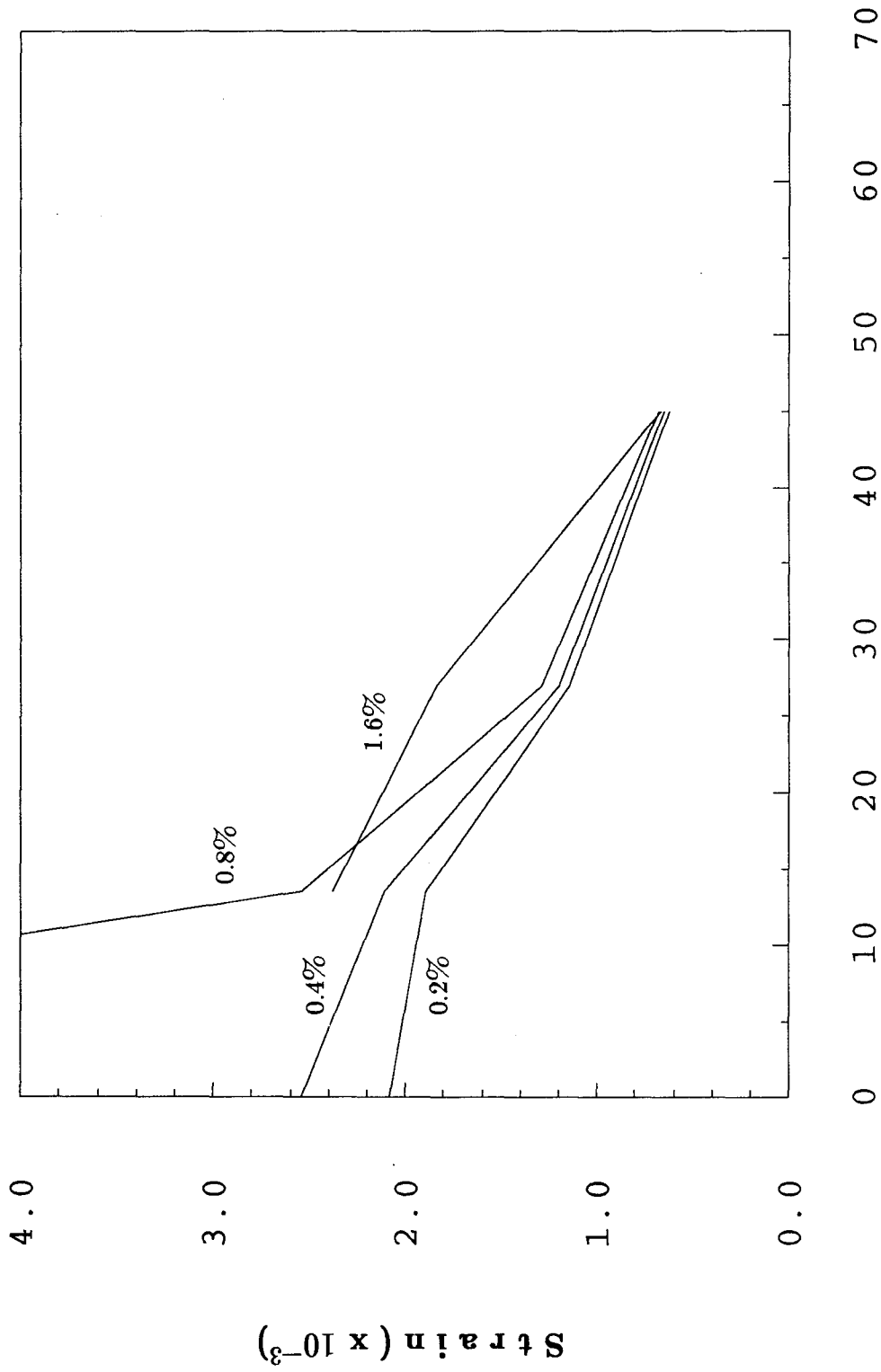


Fig. 5.24 (b) Slab Twist Profile History (South Side - Test 4)



Distance from Center of Column (in.)

Fig. 5.25 (a) Top Reinforcement Strain Profiles (East Side) - Test 1

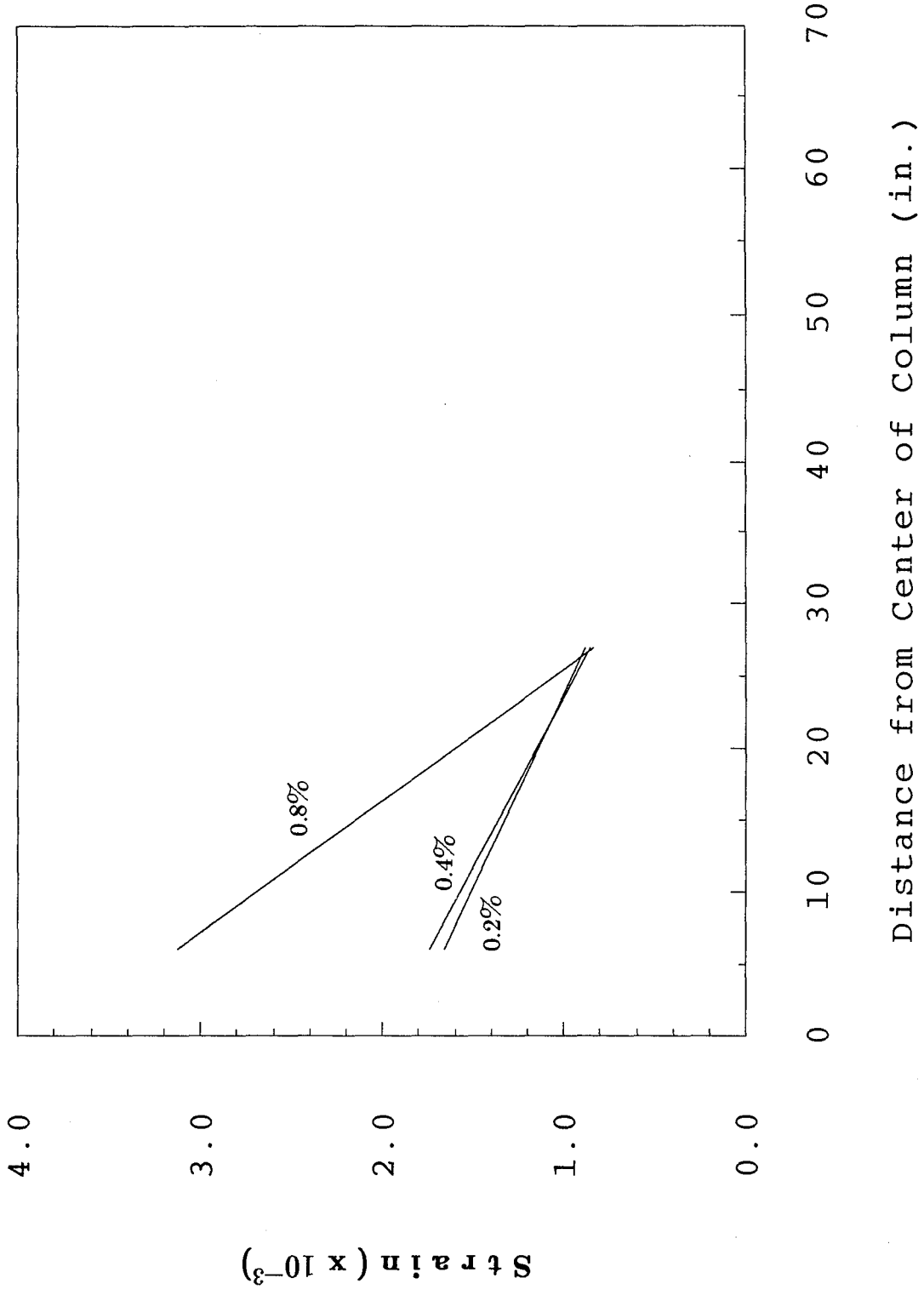
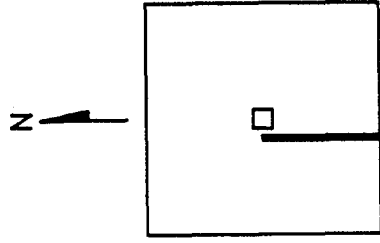
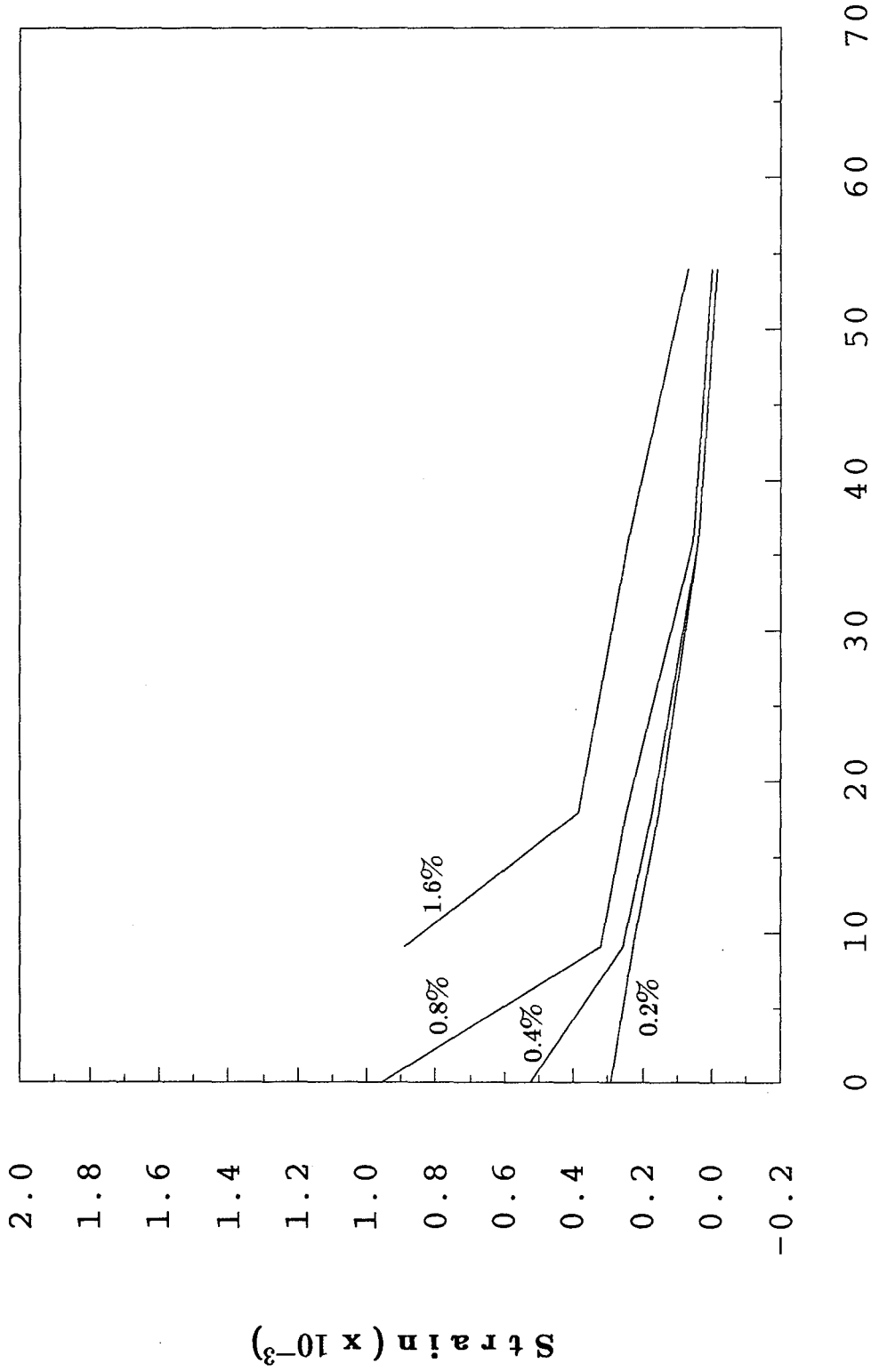


Fig. 5.25 (b) Top Reinforcement Strain Profiles (West Side) - Test 1



Distance from Center of Column (in.)

Fig. 5.25 (c) Bottom Reinforcement Strain Profiles (East Side) - Test 1

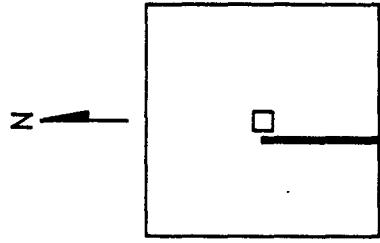
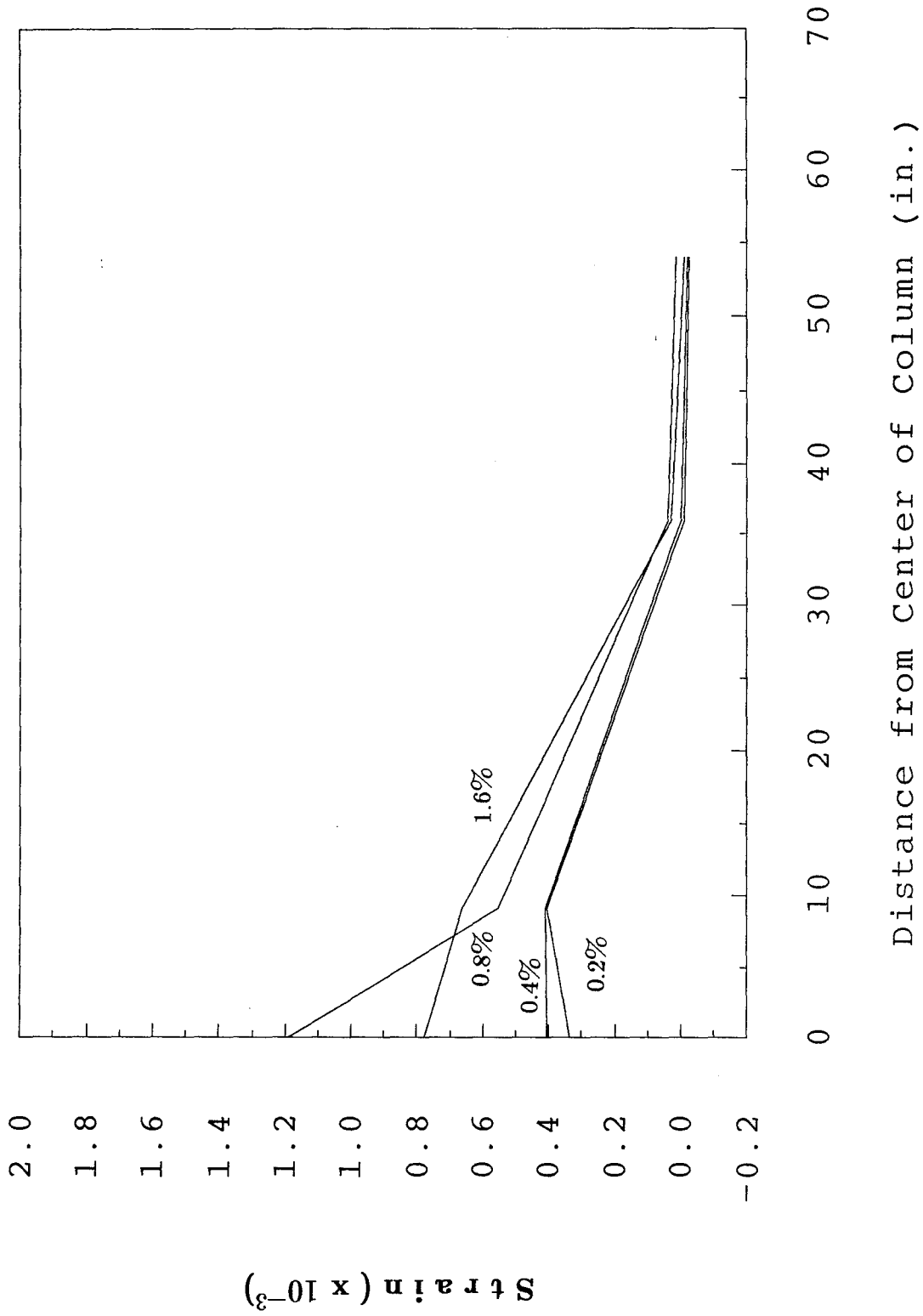


Fig. 5.25 (d) Bottom Reinforcement Strain Profiles (West Side) - Test 1

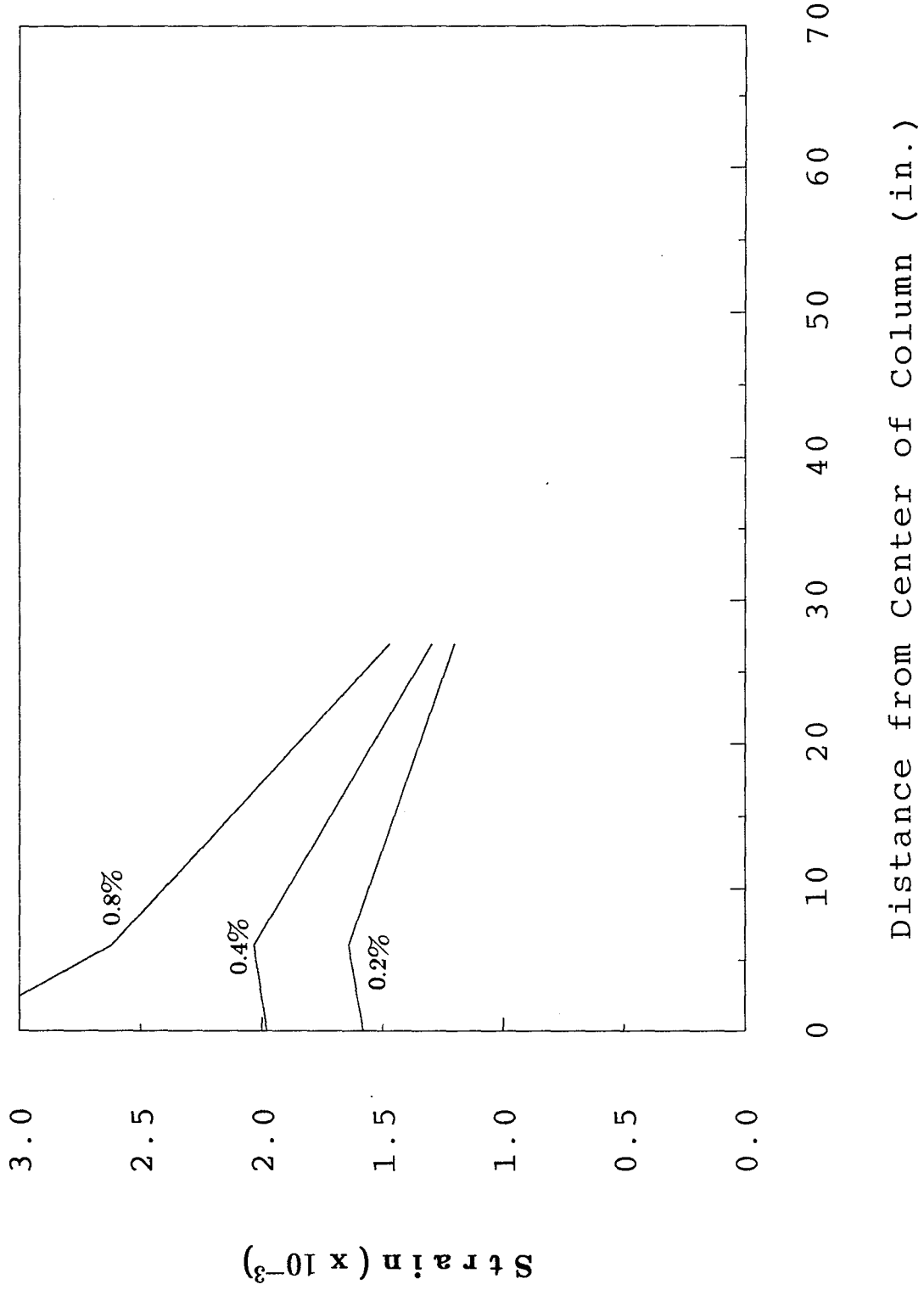
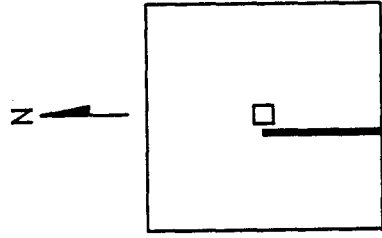
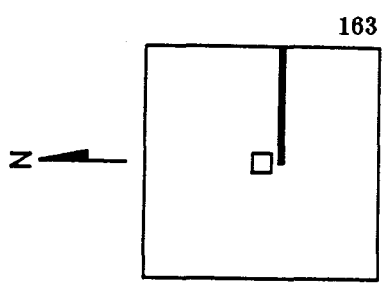
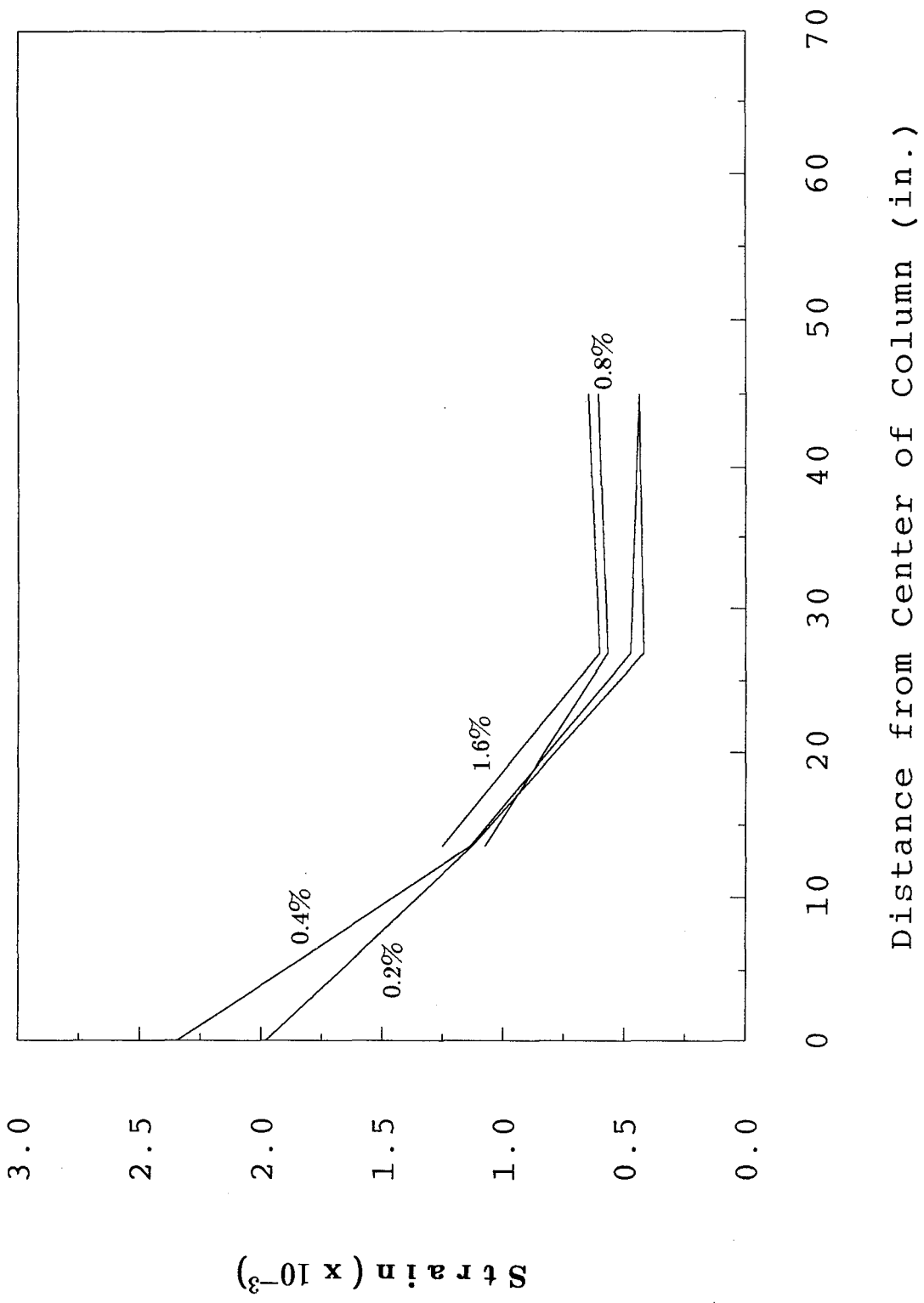


Fig. 5.26 (a) Top Reinforcement Strain Profiles (West Side) - Test 2



Distance from Center of Column (in.)

Fig. 5.26 (b) Top Reinforcement Strain Profiles (South Side) - Test 2

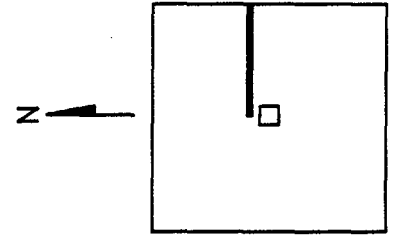
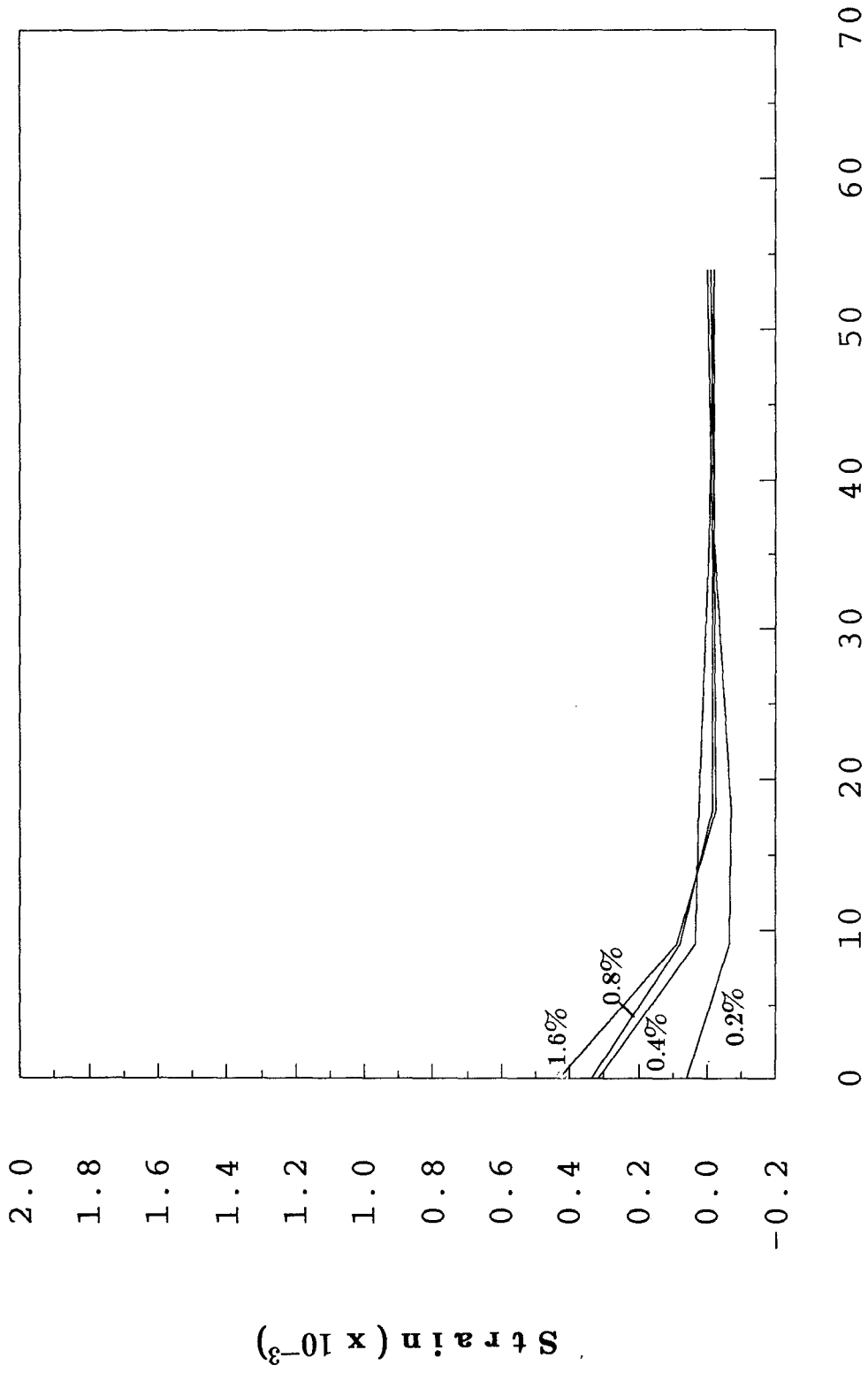


Fig. 5.26 (c) Bottom Reinforcement Strain Profiles (North Side) - Test 2

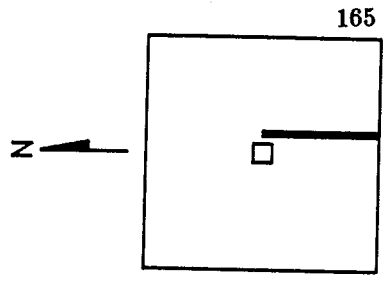
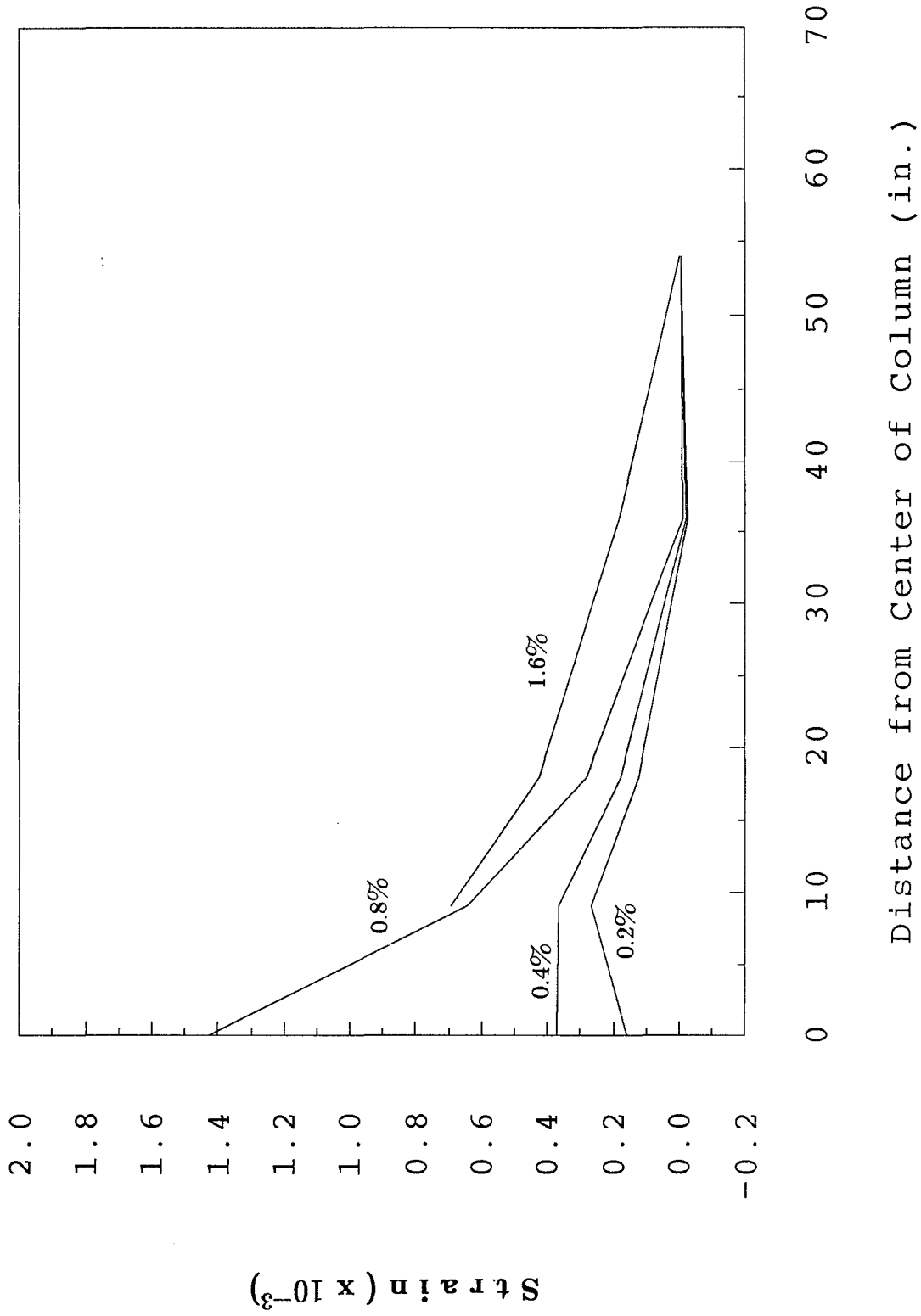


Fig. 5.26 (d) Bottom Reinforcement Strain Profiles (East Side) - Test 2

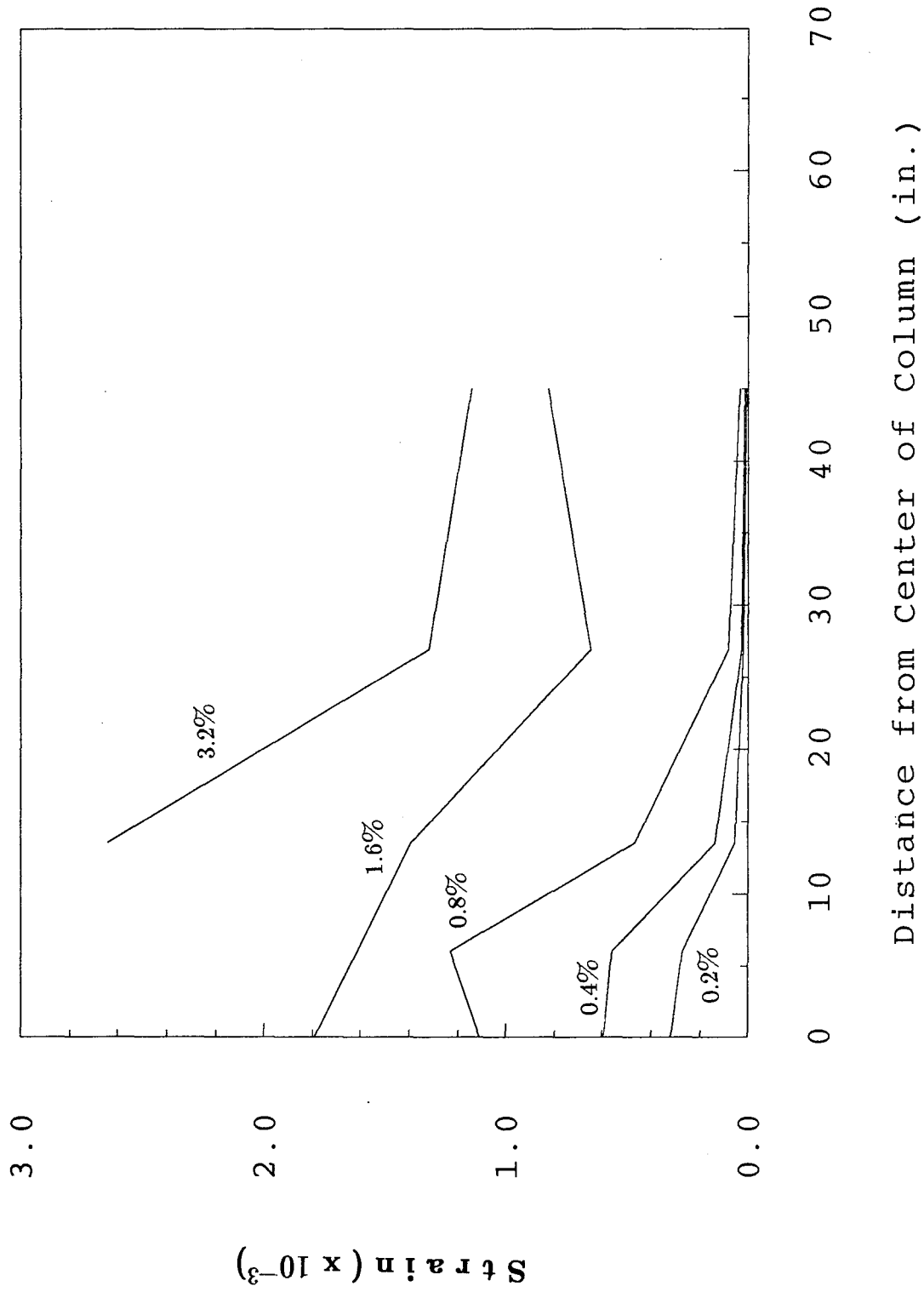


Fig. 5.27 (a) Top Reinforcement Strain Profiles (East Side) - Test 3

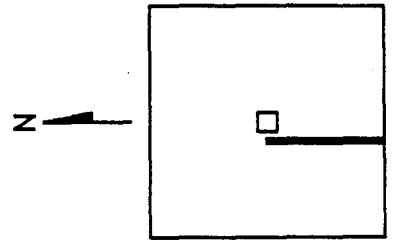
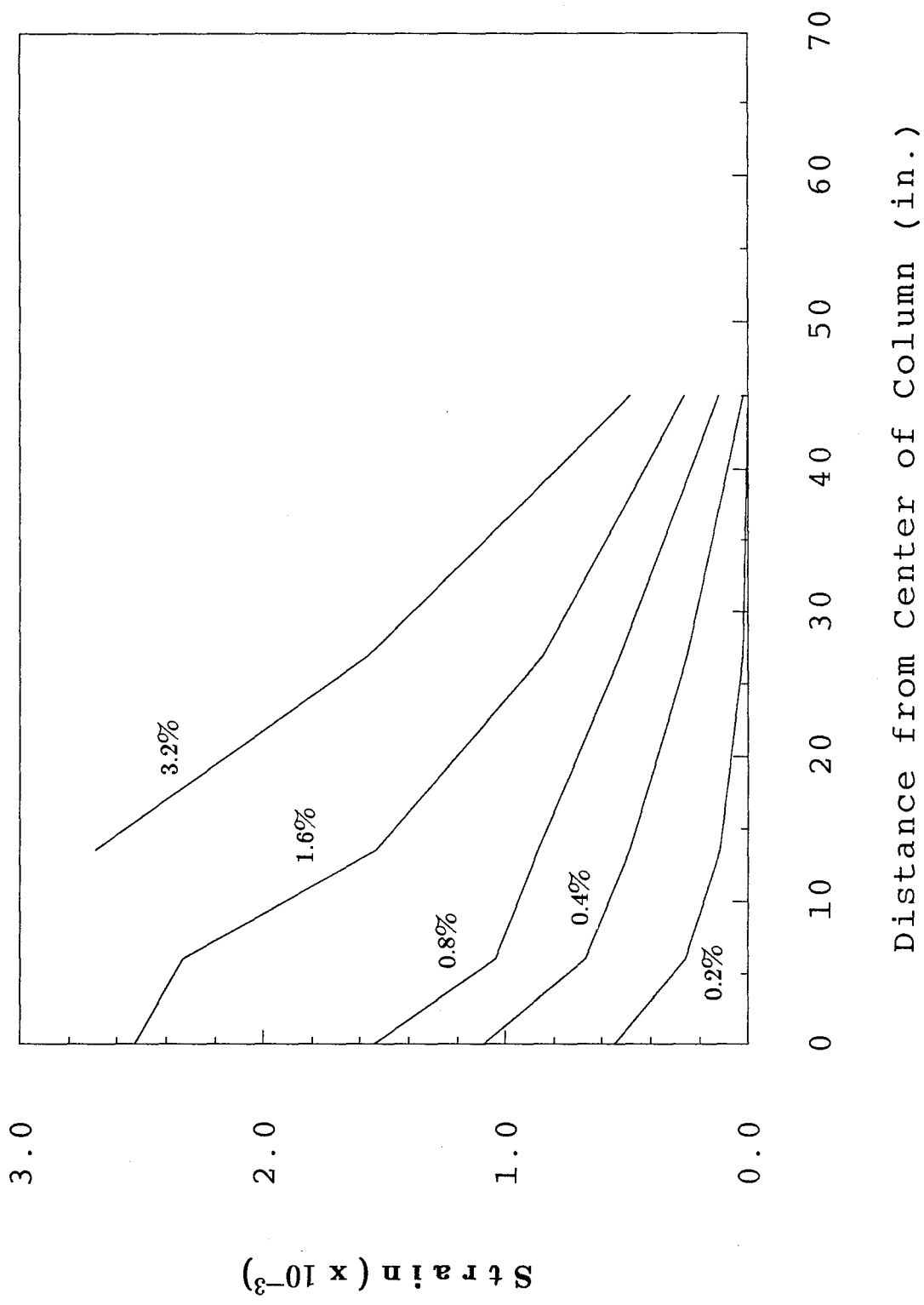


Fig. 5.27 (b) Top Reinforcement Strain Profiles (West Side) - Test 3

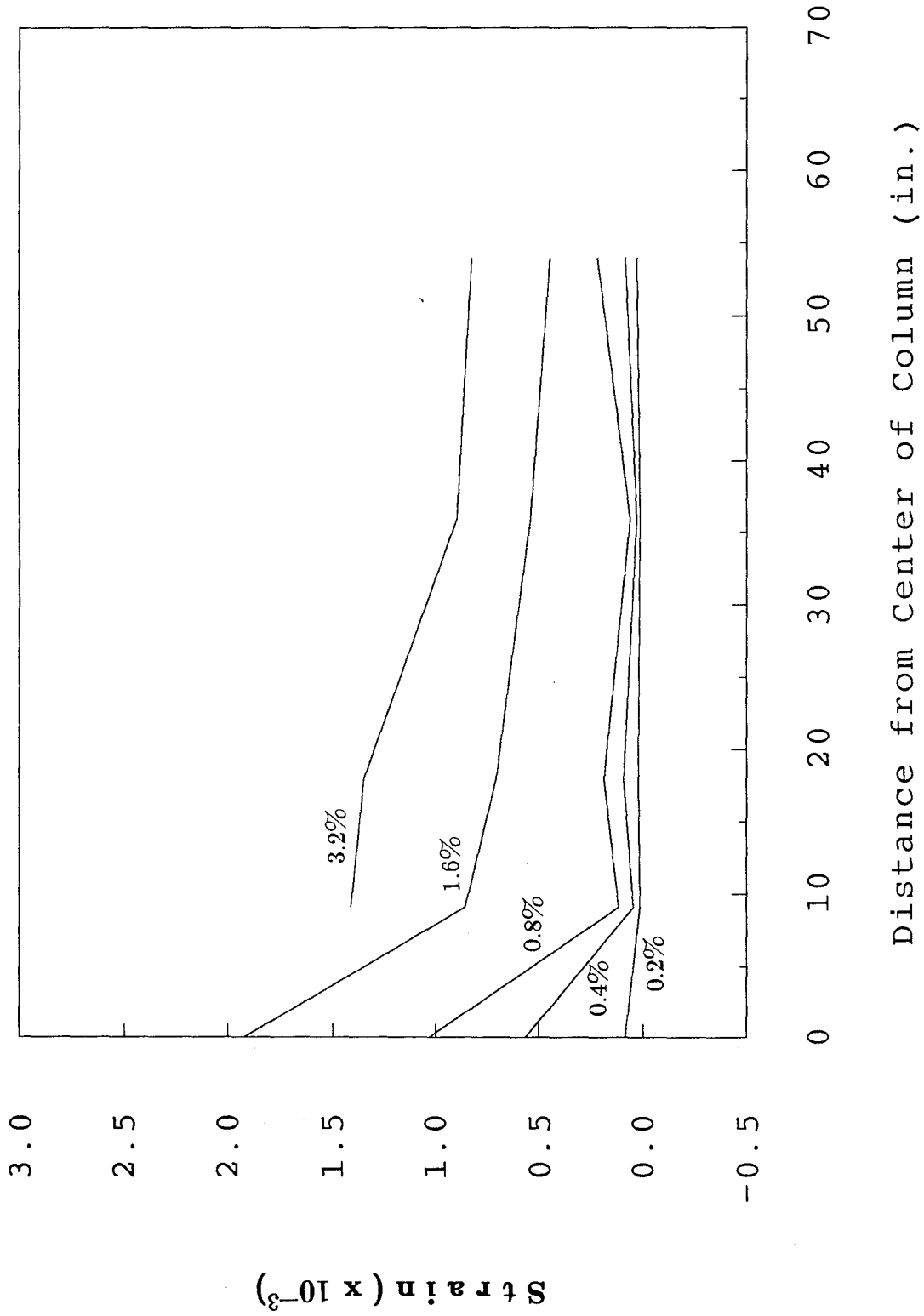


Fig. 5.27 (c) Bottom Reinforcement Strain Profiles (East Side) - Test 3

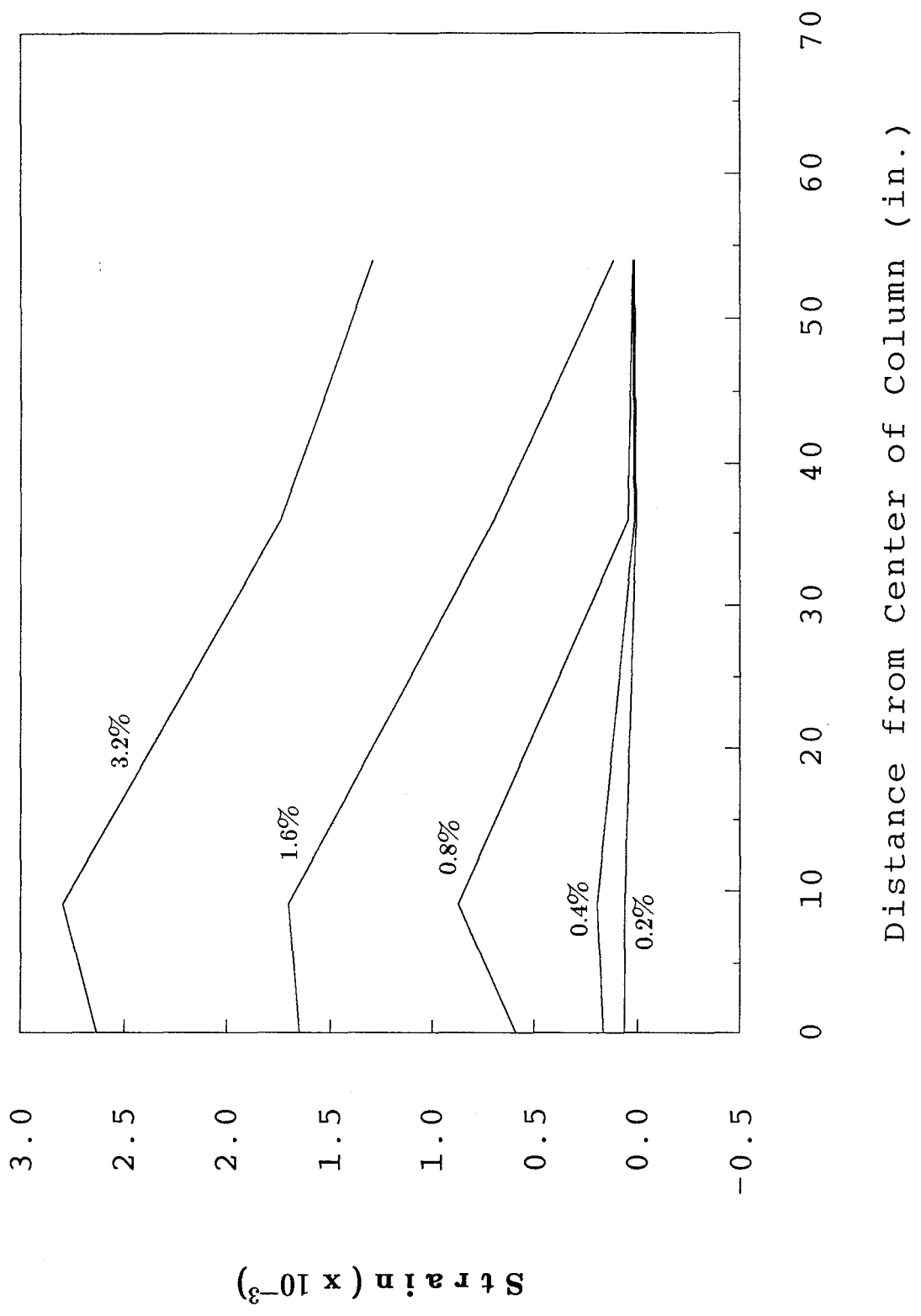
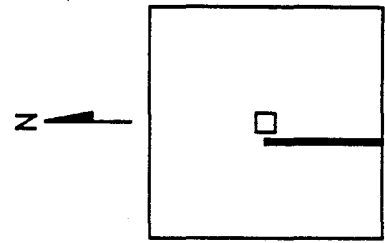


Fig. 5.27 (d) Bottom Reinforcement Strain Profiles (West Side) - Test 3

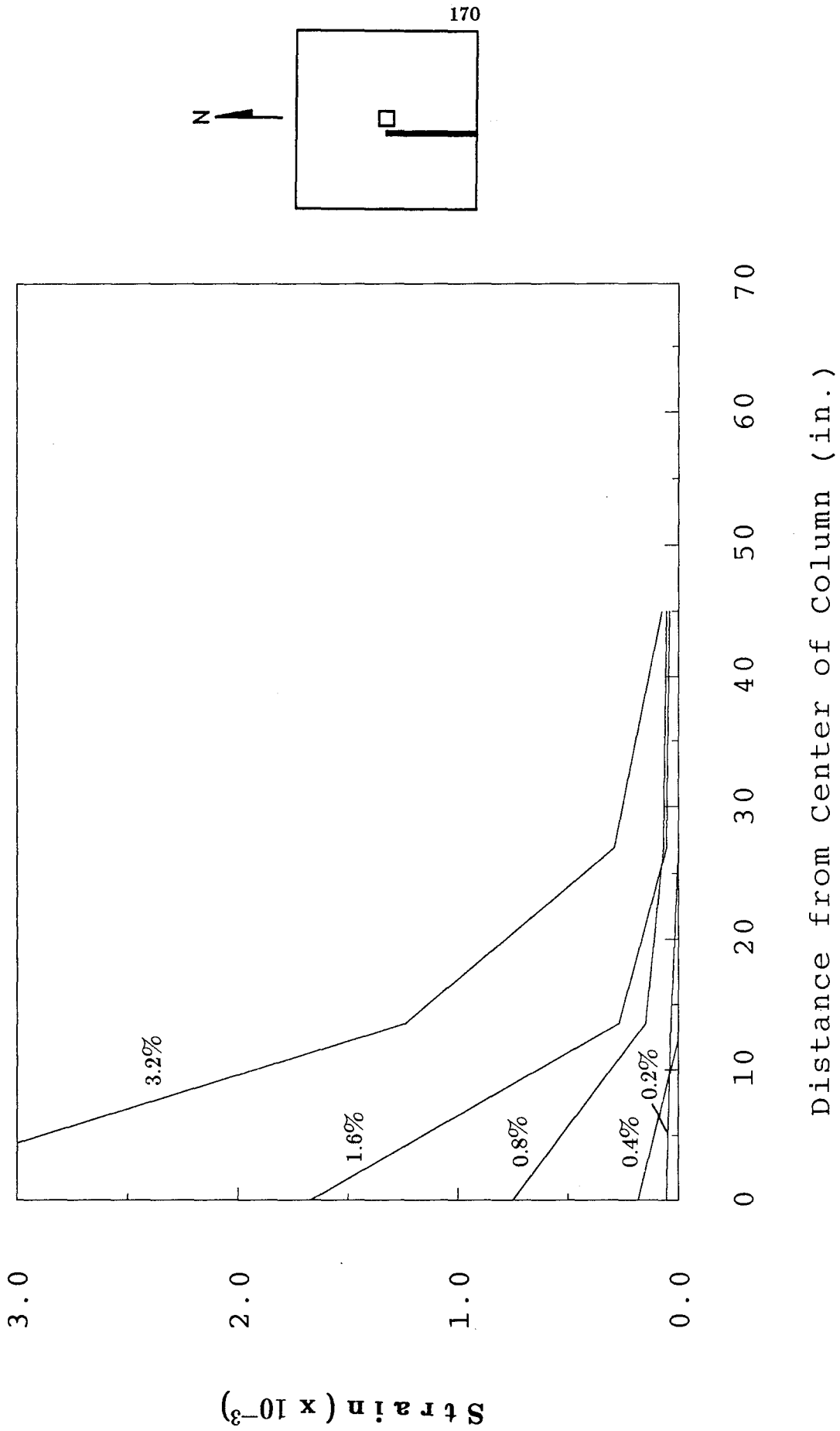


Fig. 5.28 (a) Top Reinforcement Strain Profiles (West Side) - Test 4

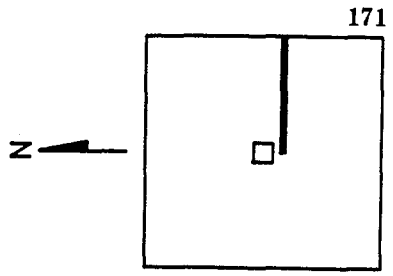
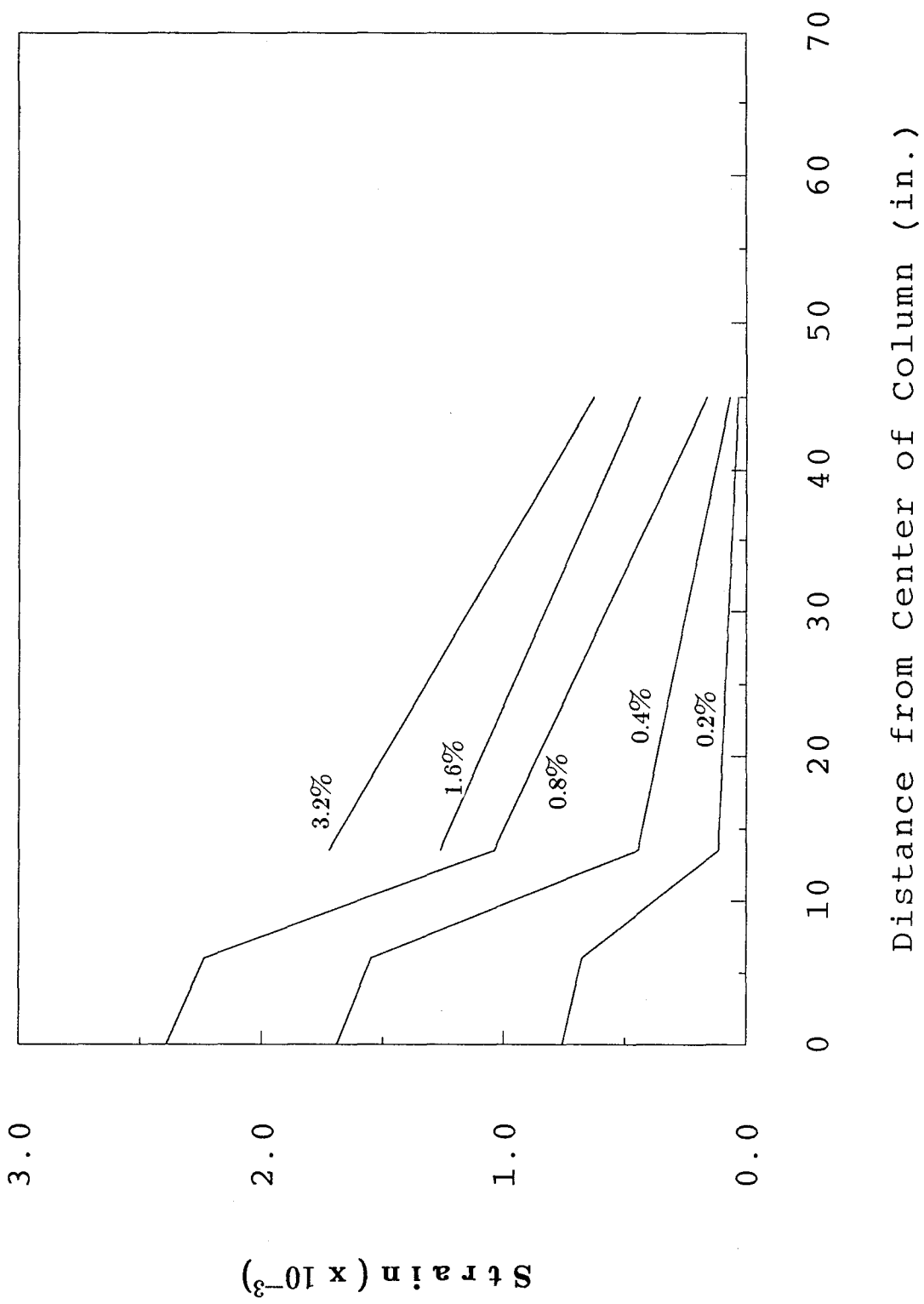


Fig. 5.28 (b) Top Reinforcement Strain Profiles (South Side) - Test 4

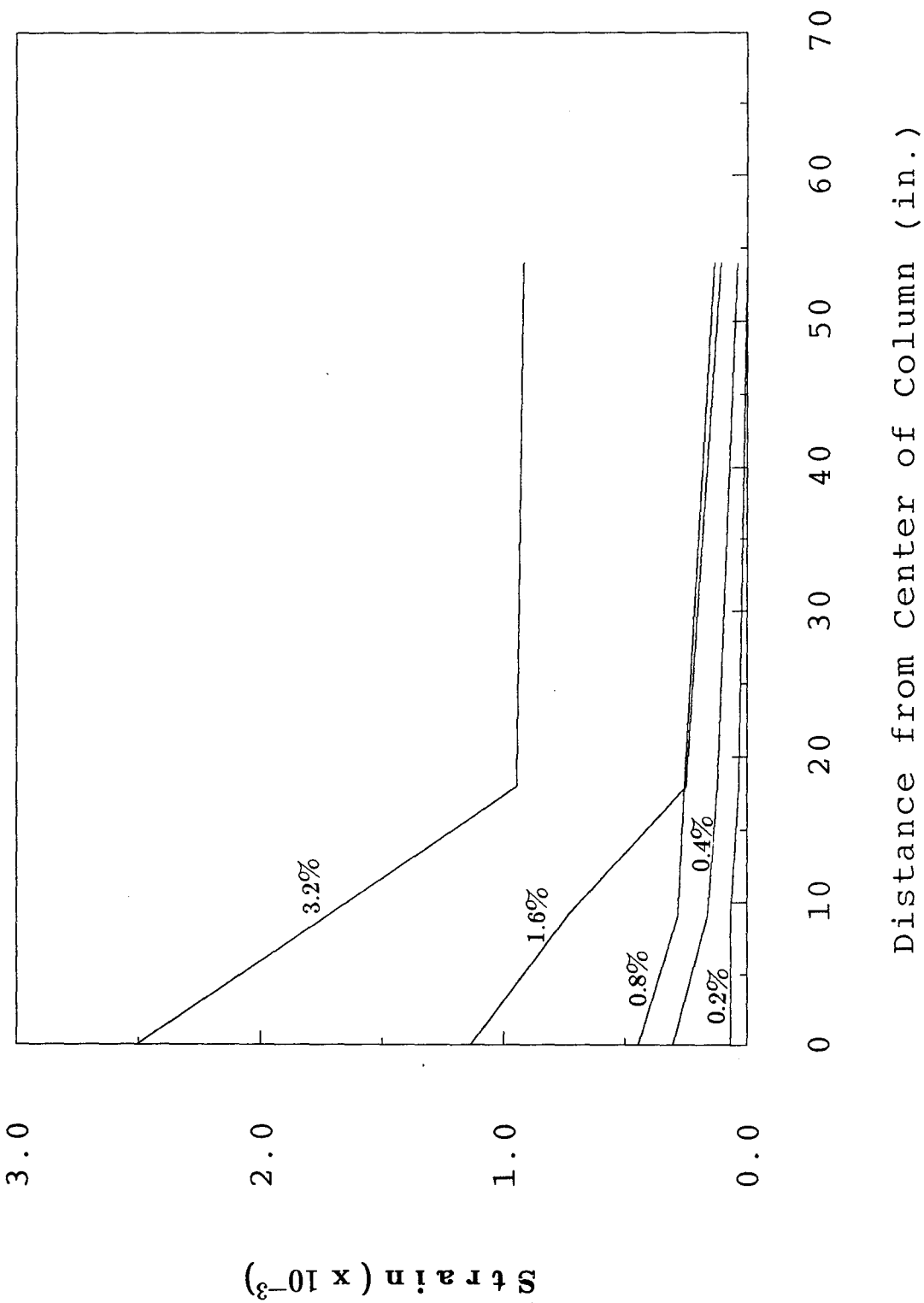
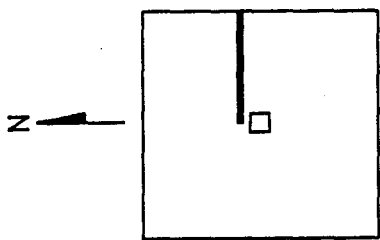


Fig. 5.28 (c) Bottom Reinforcement Strain Profiles (North Side) - Test 4

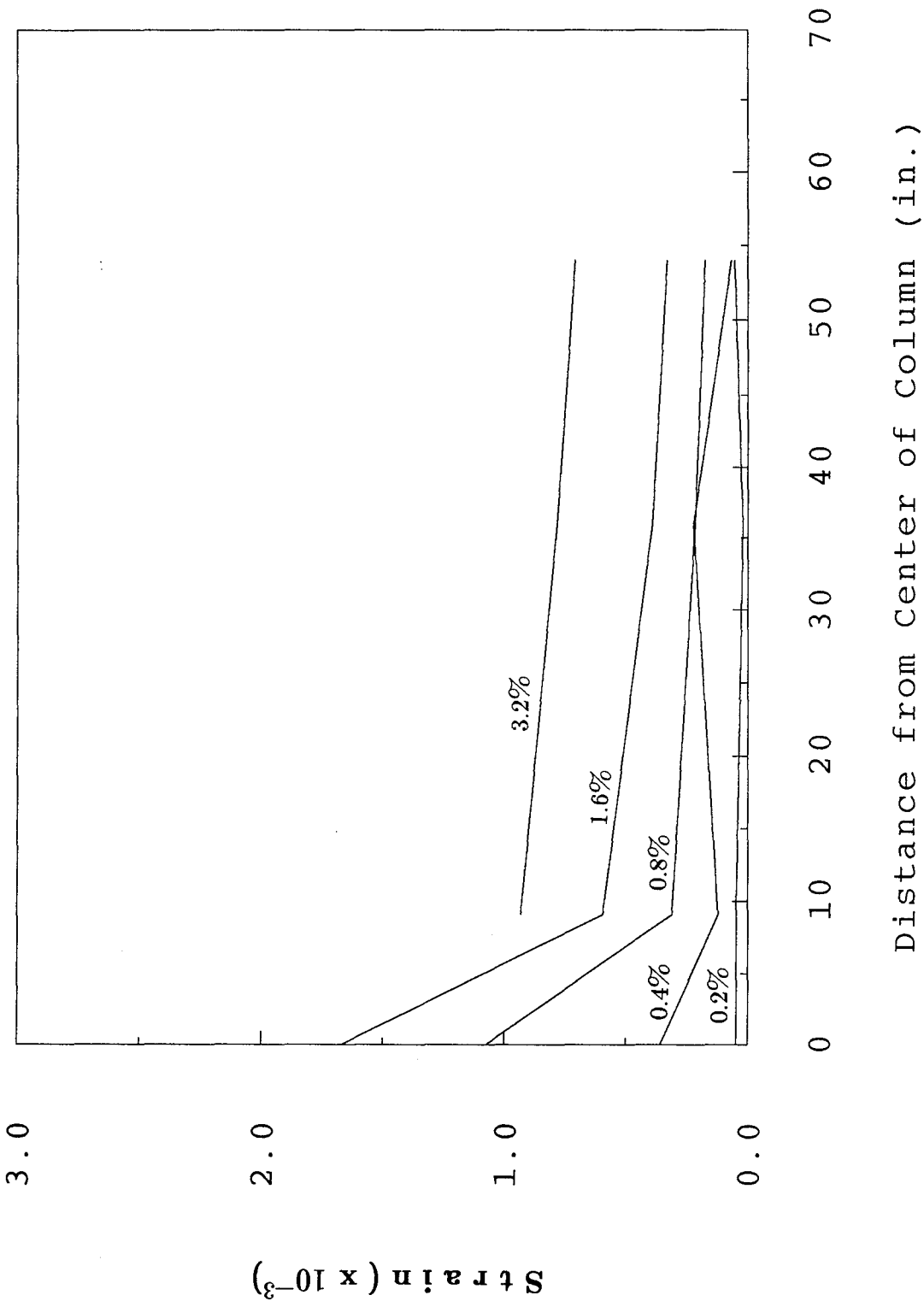
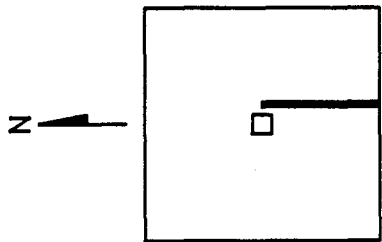


Fig. 5.28 (d) Bottom Reinforcement Strain Profiles (East Side) - Test 4

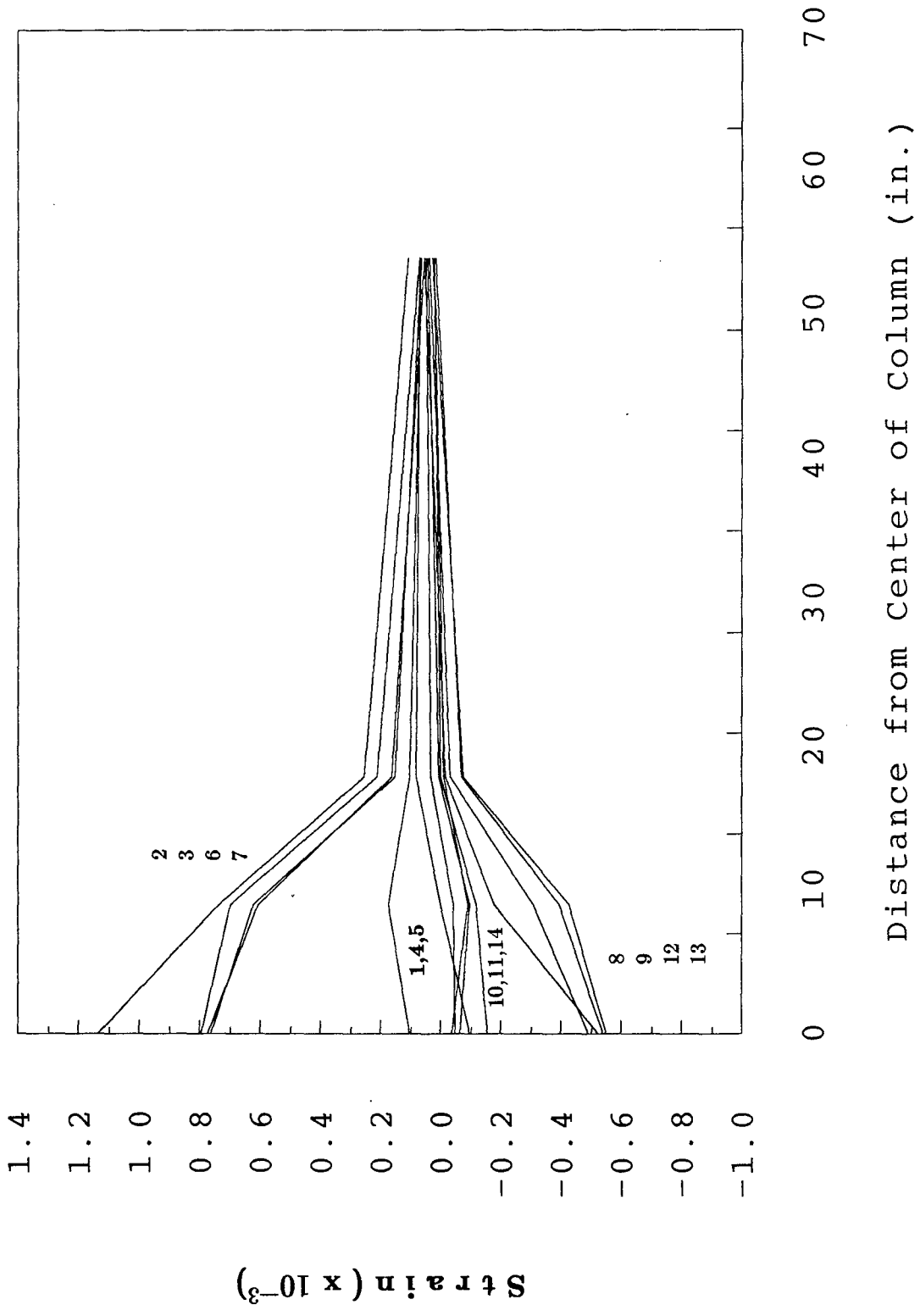


Fig. 5.29 Reinforcement Strain Profile History (Top West Side - Test 3)

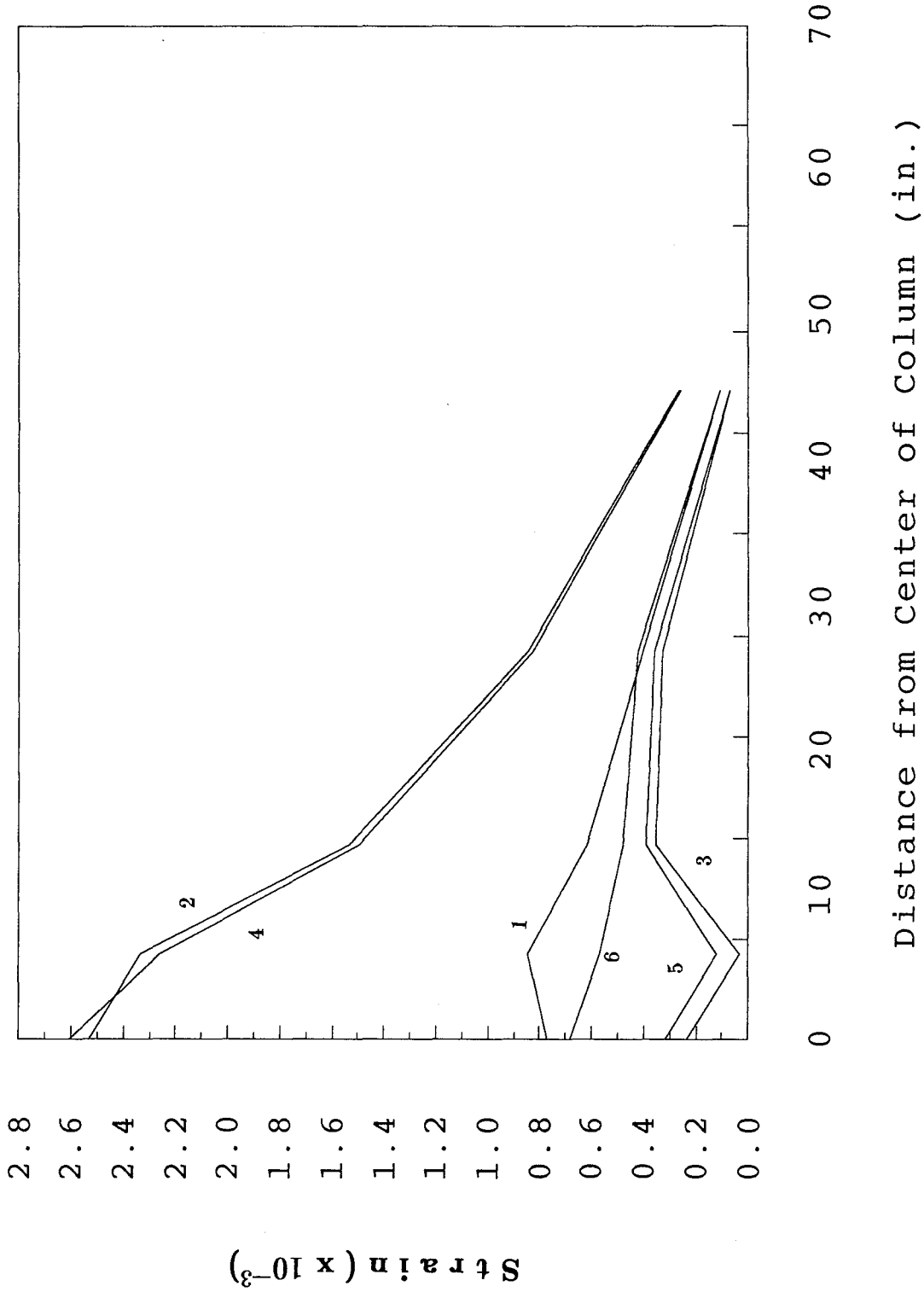


Fig. 5.30 Reinforcement Strain Profile History (Bottom North Side - Test 4)

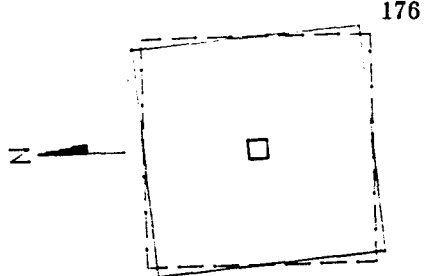
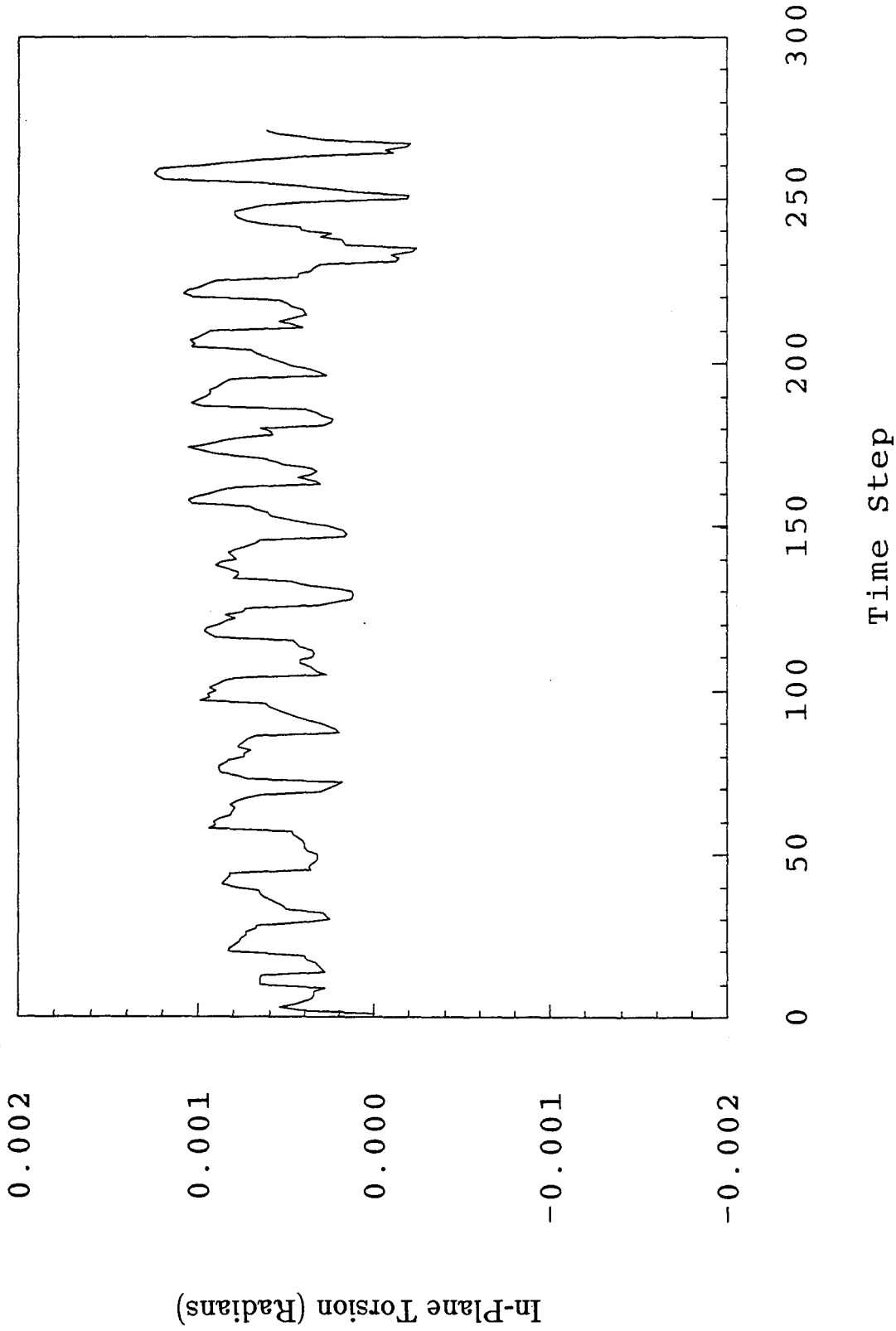


Fig. 5.31 In-Plane Torsion History (Test 2)

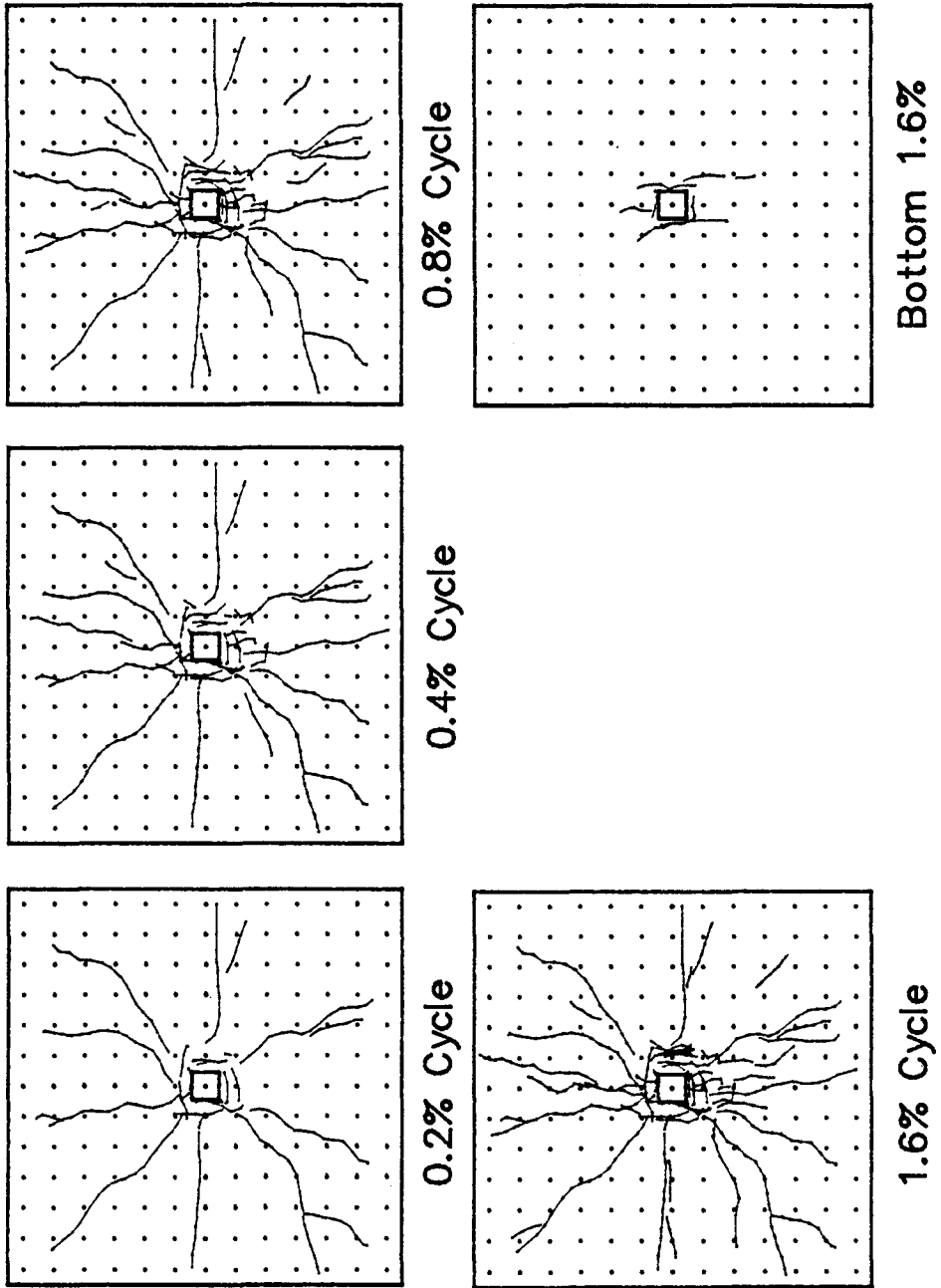


Fig. 5.32 Crack Patterns - Test 1

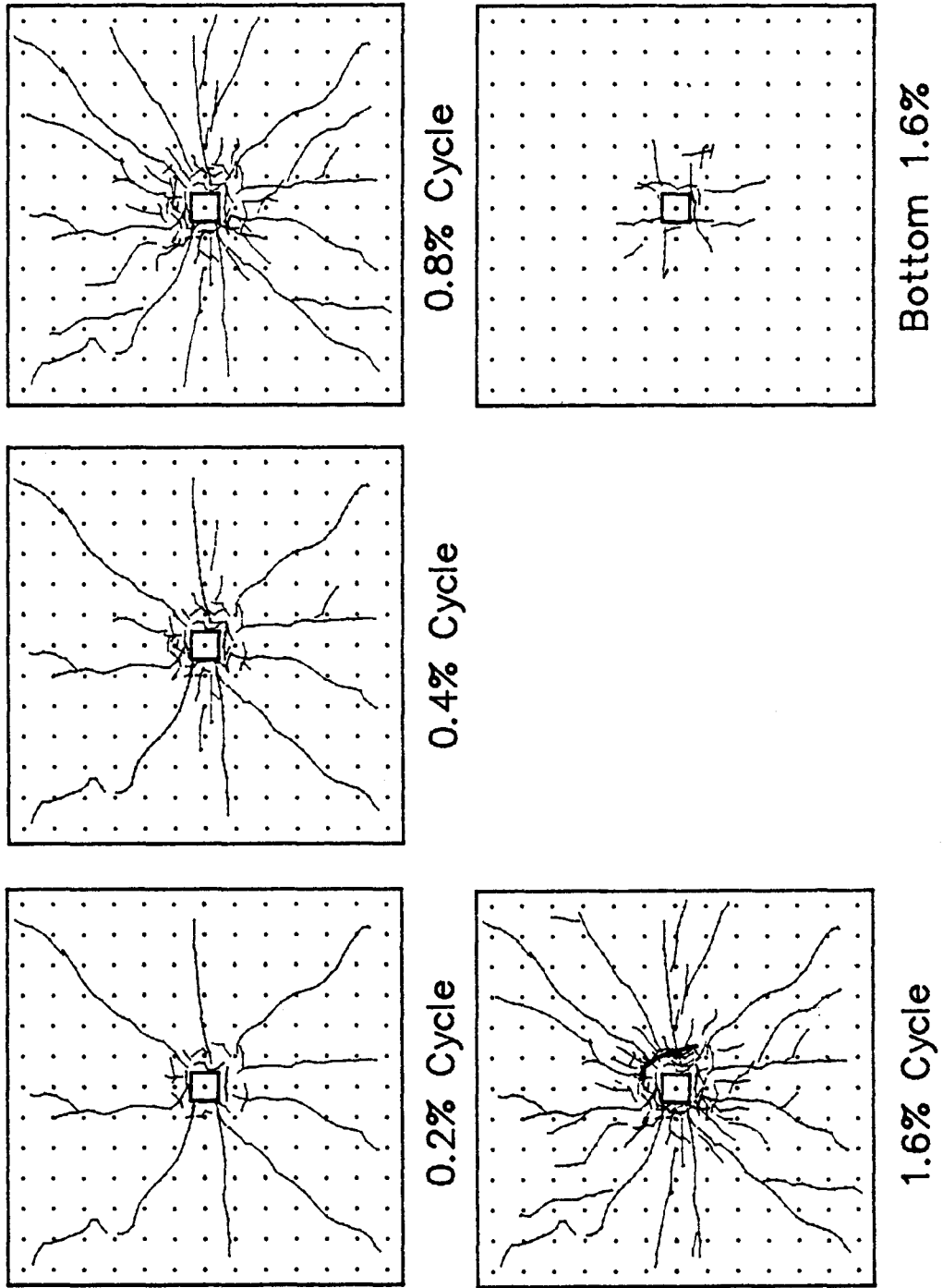


Fig. 5.33 Crack Patterns - Test 2

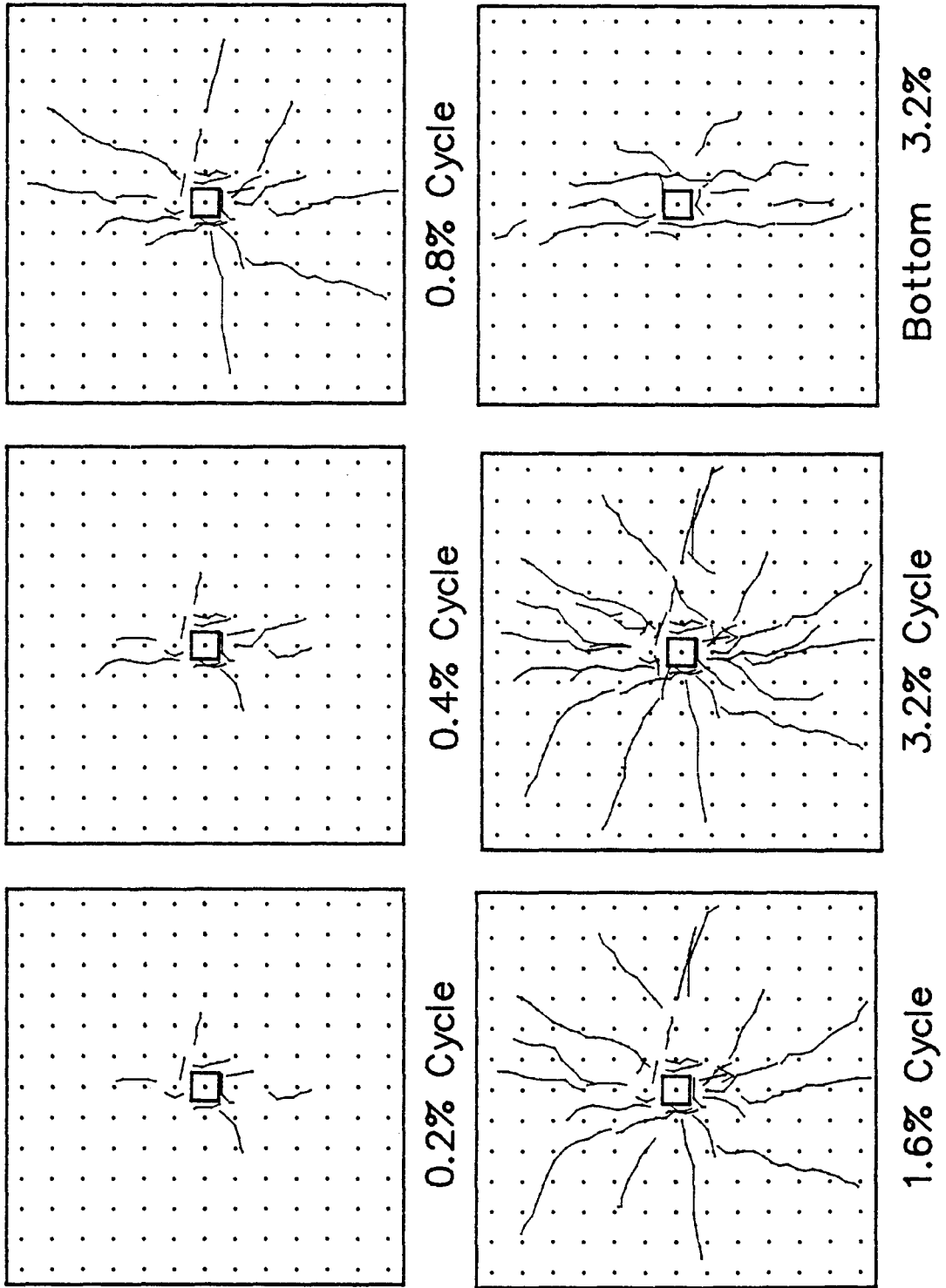


Fig. 5.34 Crack Patterns - Test 3

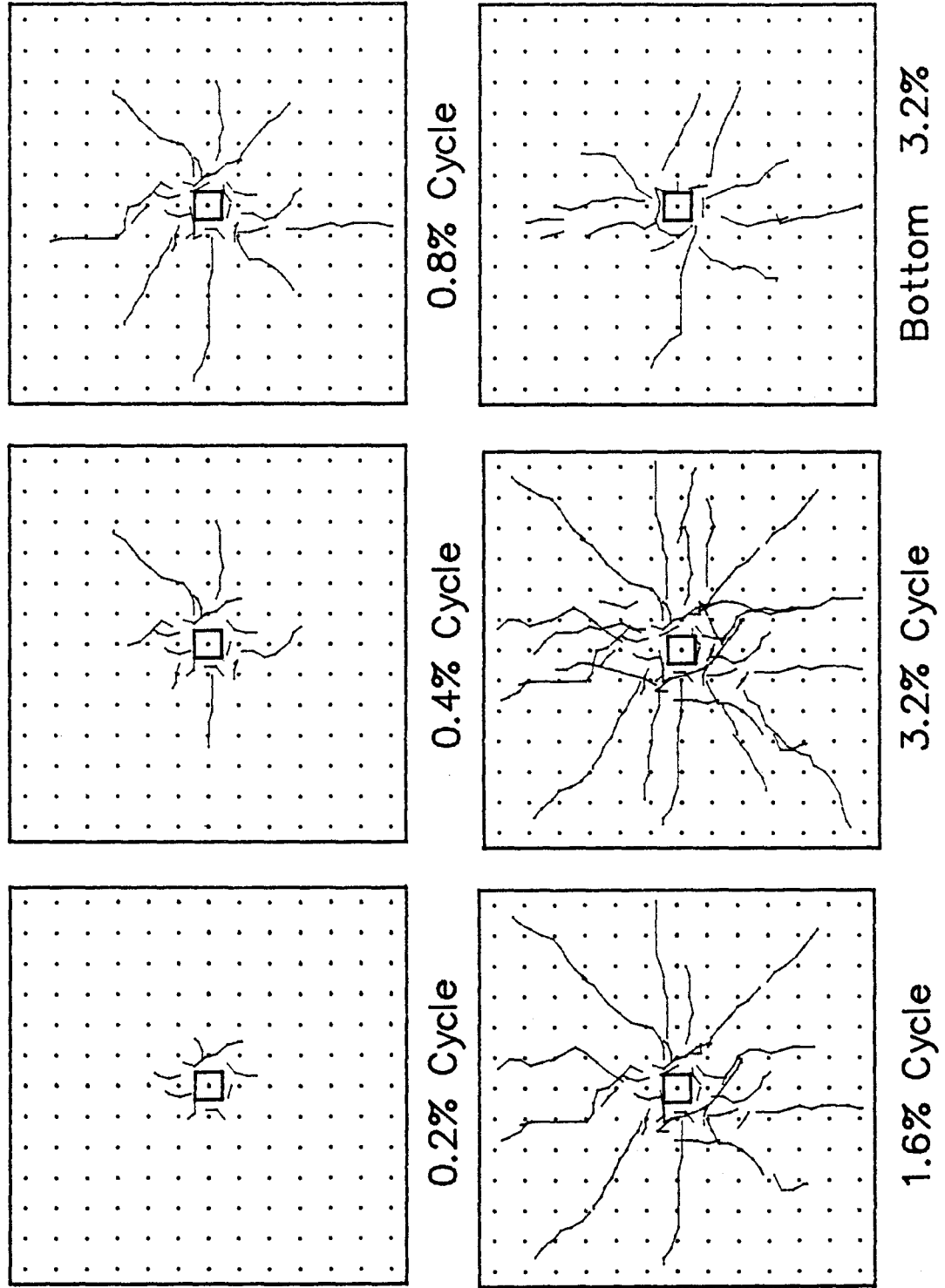


Fig. 5.35 Crack Patterns - Test 4

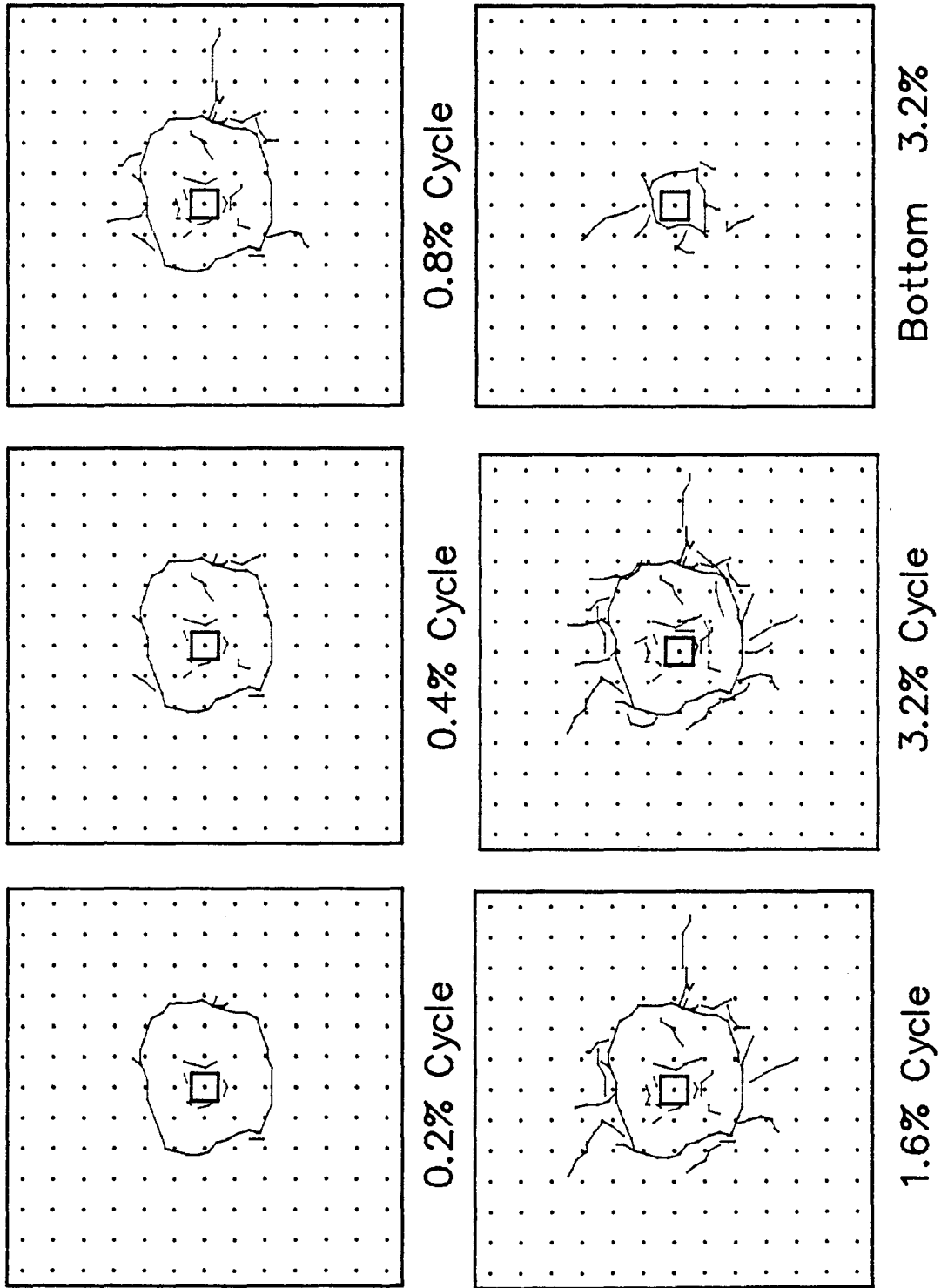


Fig. 5.36 Crack Patterns - Test 5

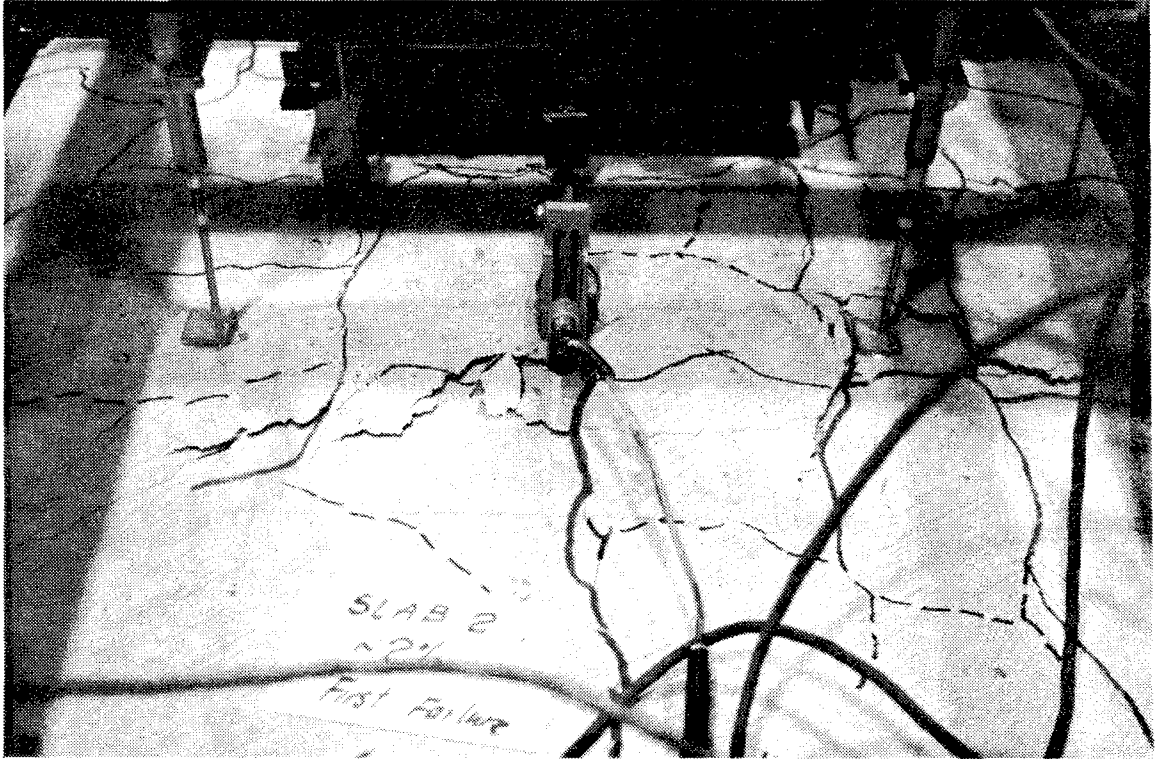


Fig. 5.37 (a) Initial Failure - Test 2

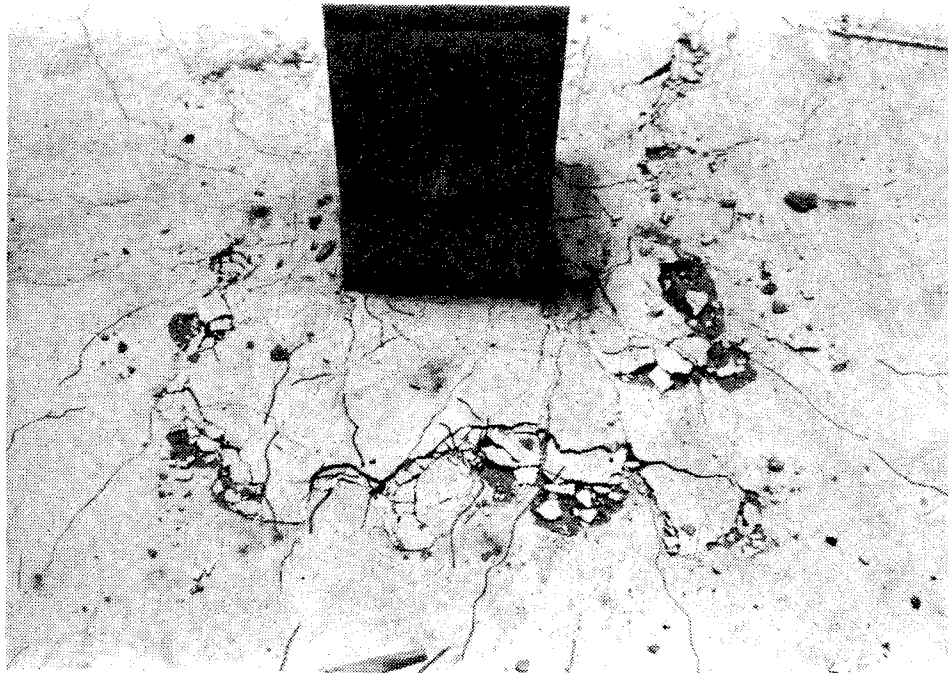


Fig. 5.37 (b) Connection After Experiment - Test 3

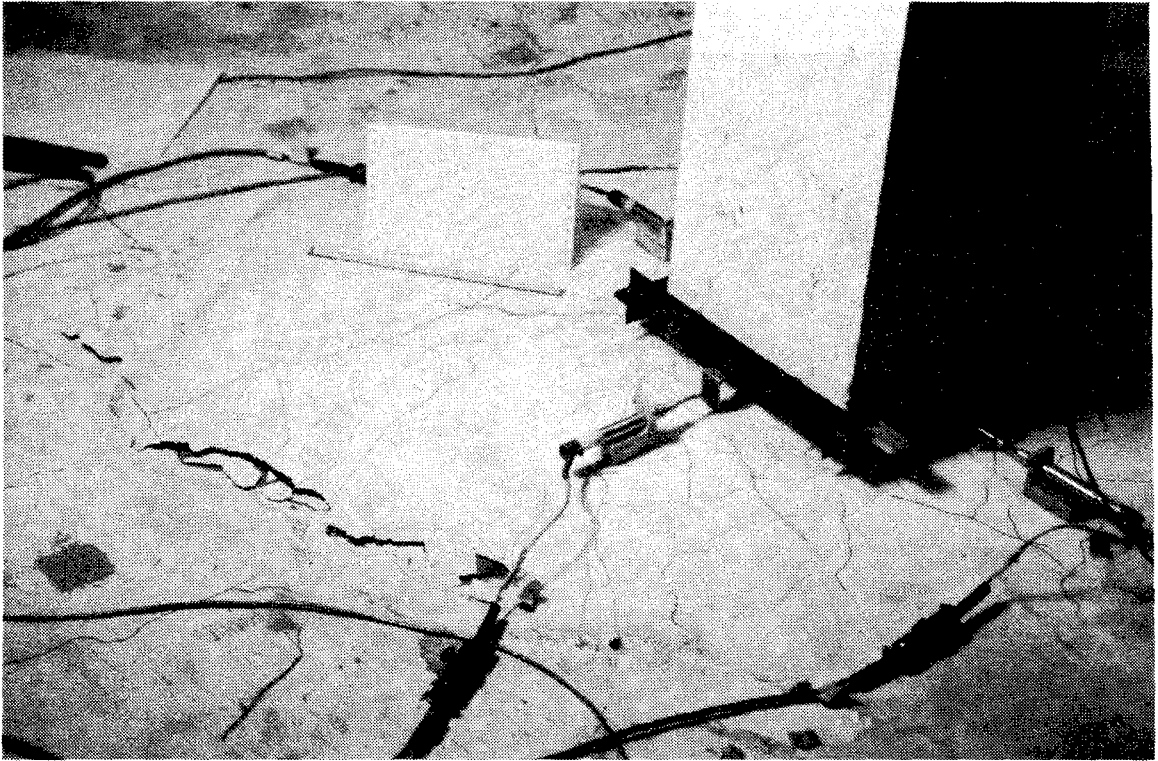


Fig. 5.37 (c) Initial Failure of Repaired Specimen - Test 5

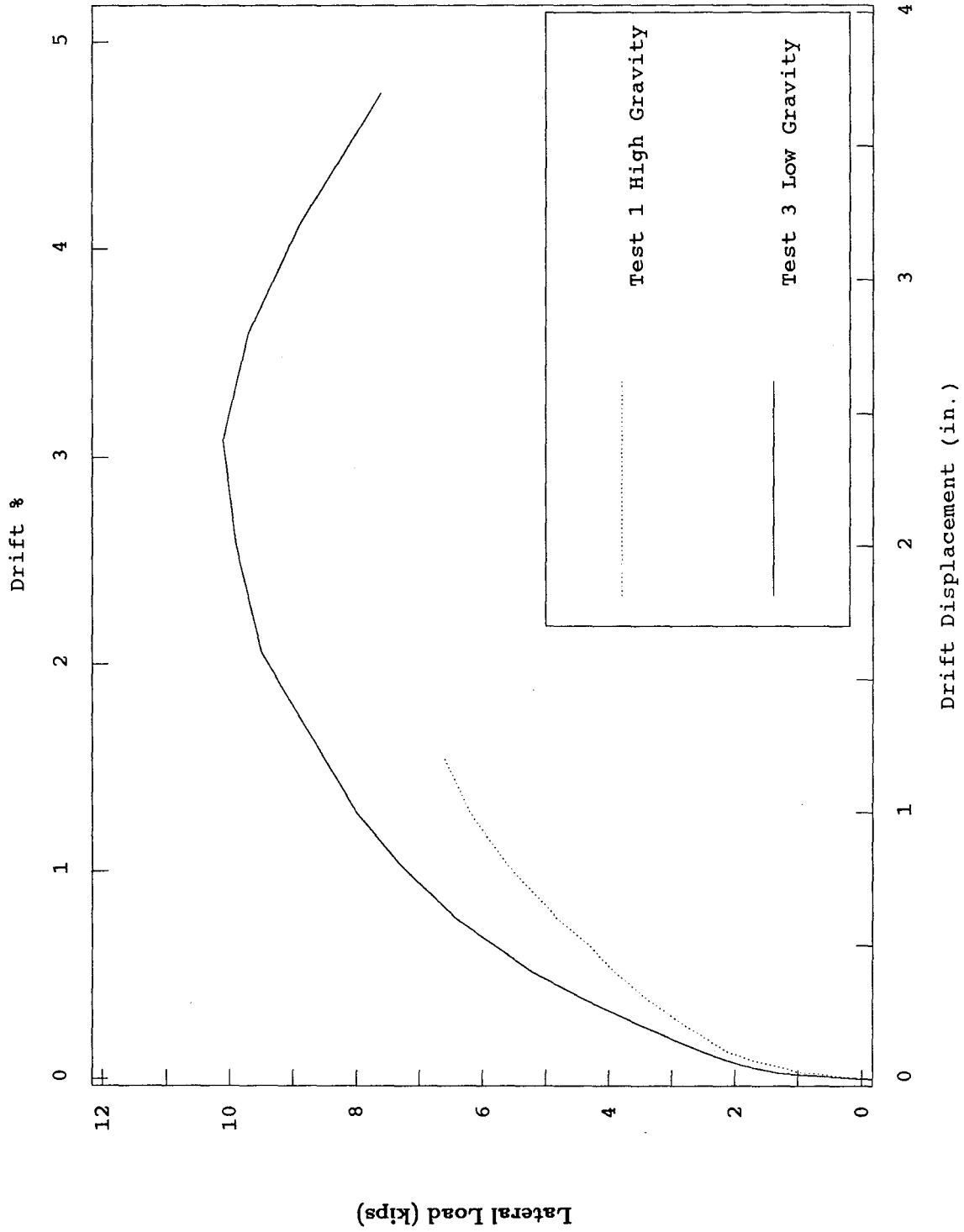


Fig. 6.1 (a) Effect of Gravity Loads - Uniaxial Tests

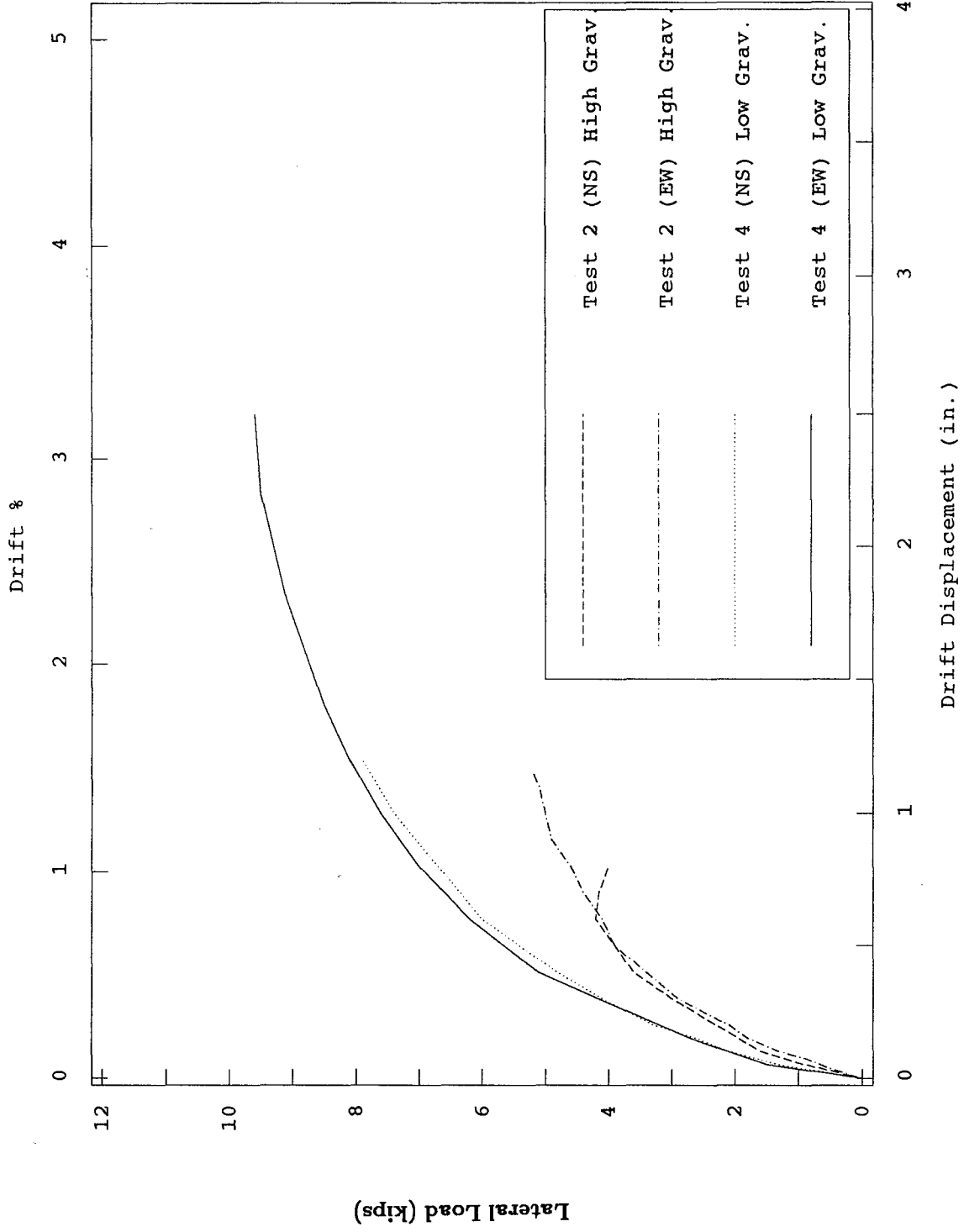


Fig. 6.1 (b) Effect of Gravity Loads - Biaxial Tests

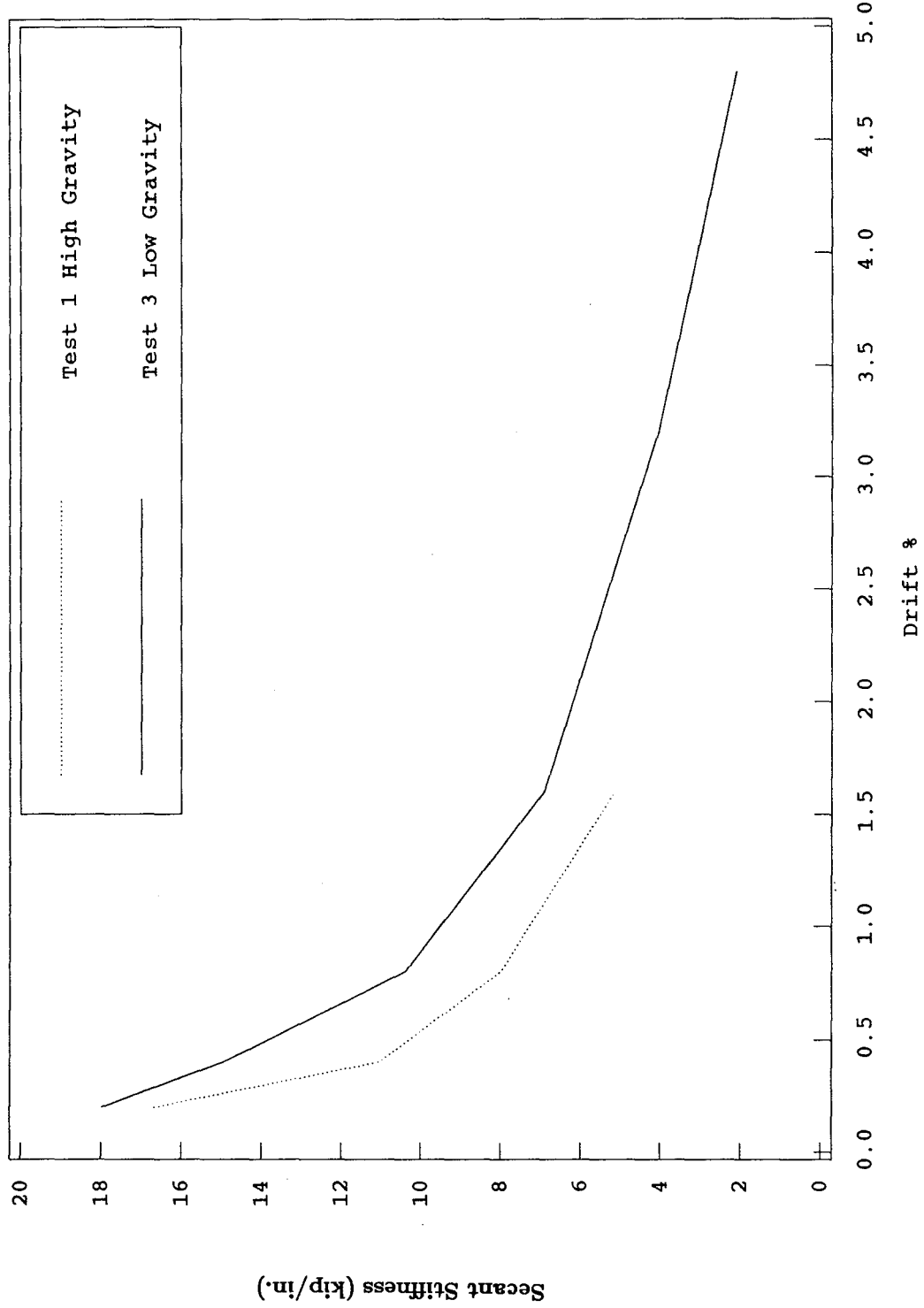


Fig. 6.2 (a) Effect of Gravity Loads on Stiffness - Uniaxial Tests

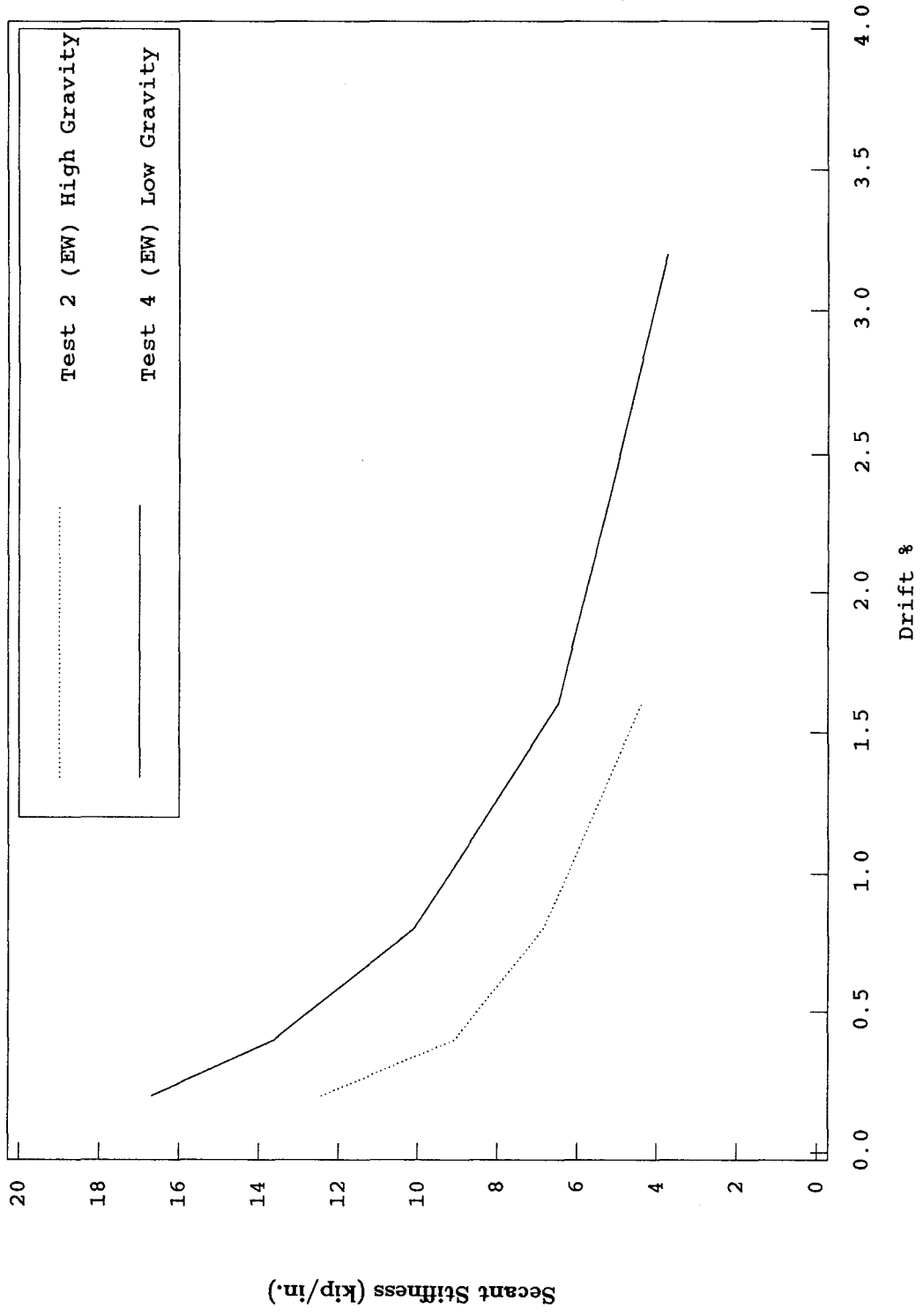


Fig. 6.2 (b) Effect of Gravity Loads on Stiffness - Biaxial Tests

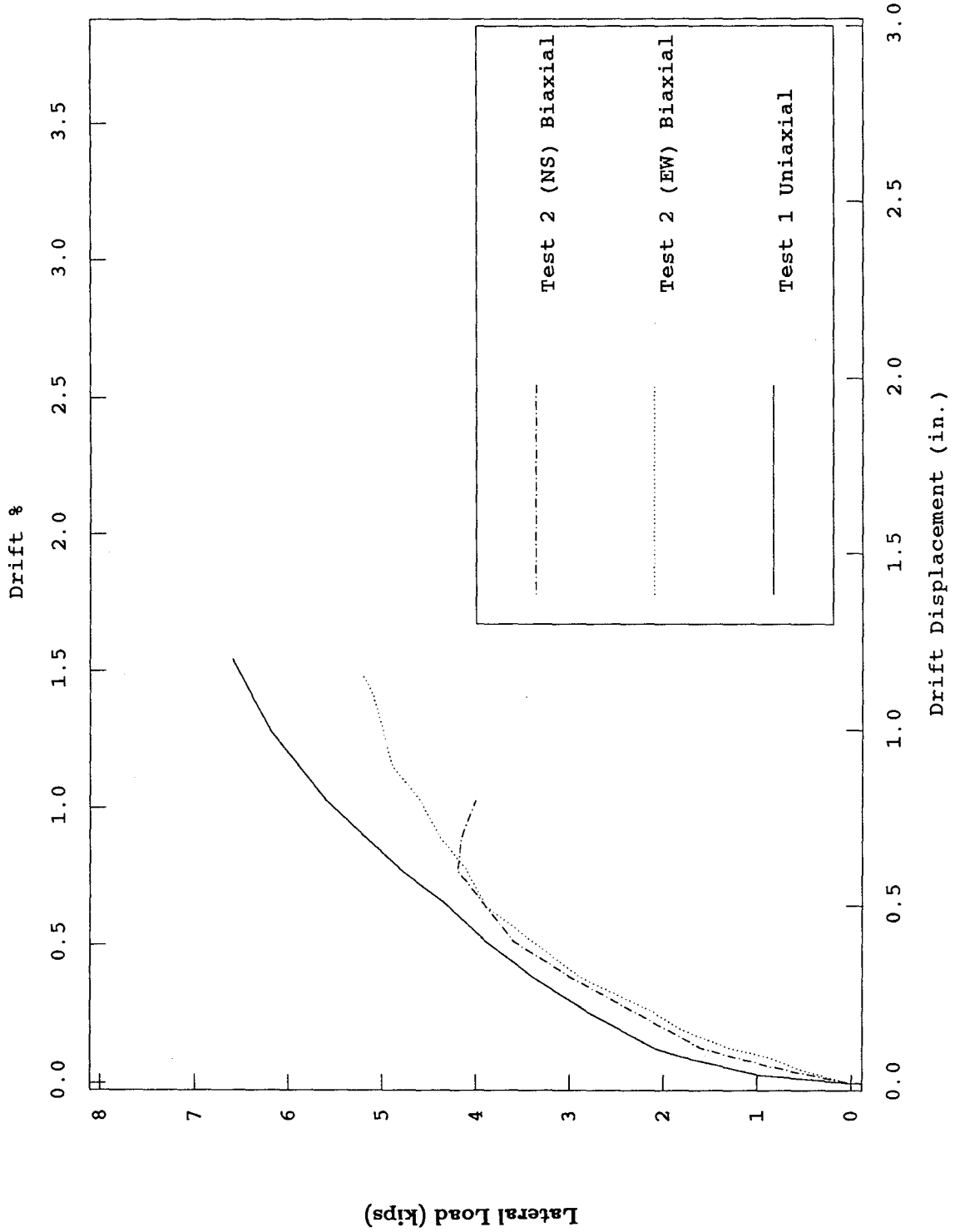


Fig. 6.3 (a) Effect of Biaxial Loading - Tests with High Gravity Loads

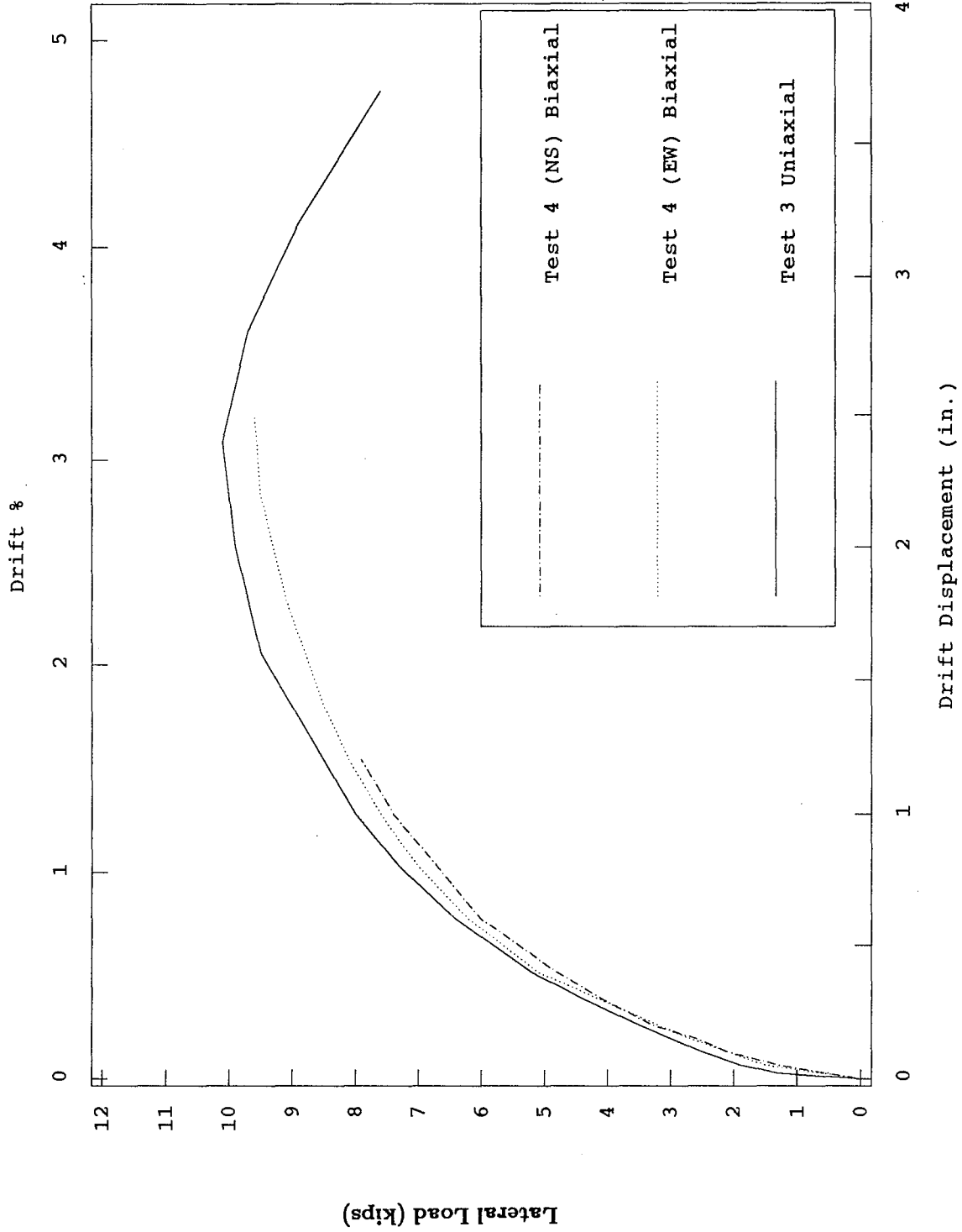


Fig. 6.3 (b) Effect of Biaxial Loading - Tests with Low Gravity Loads

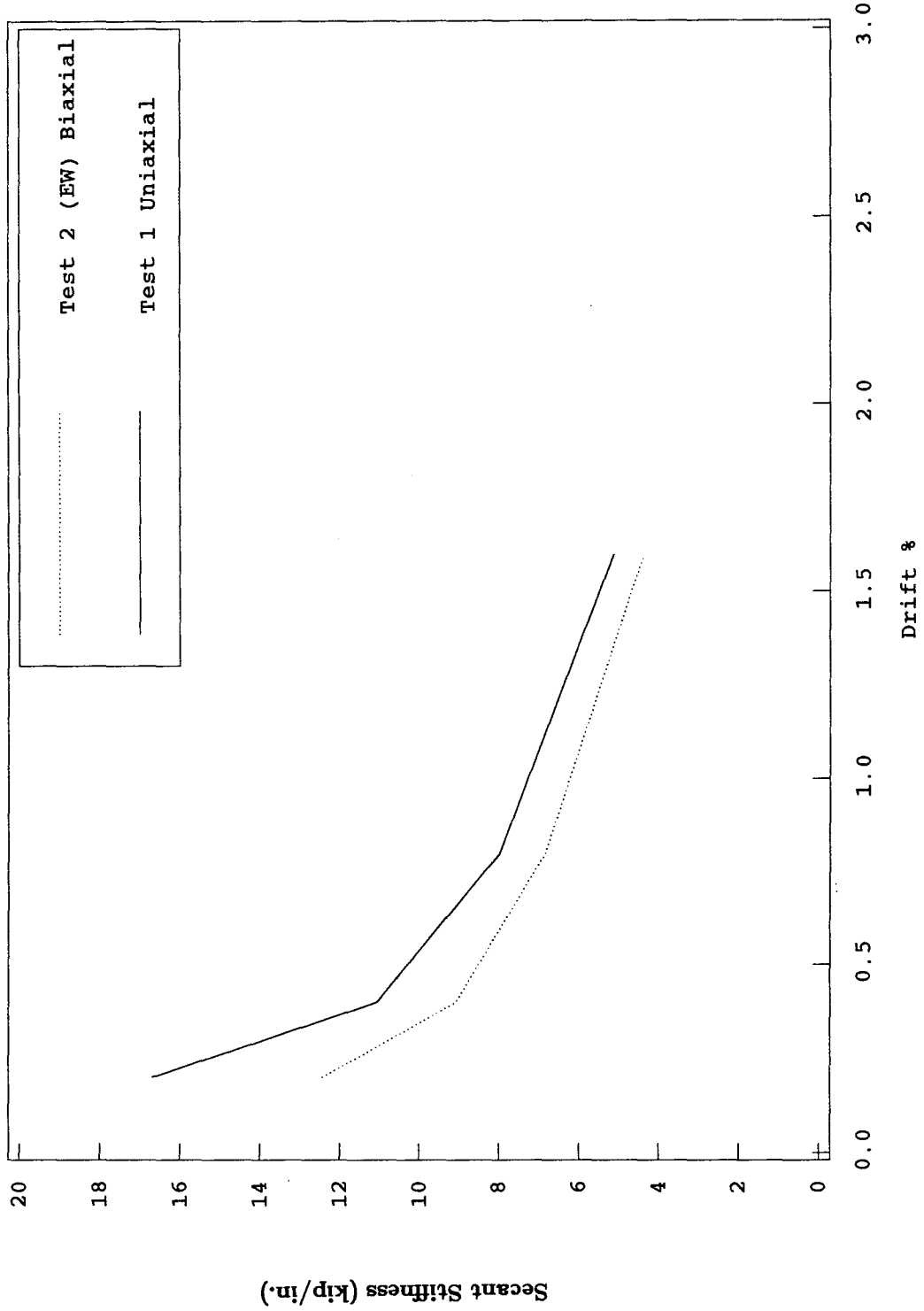


Fig. 6.4 (a) Effect of Biaxial Loading on Stiffness - Tests with High Gravity Loads

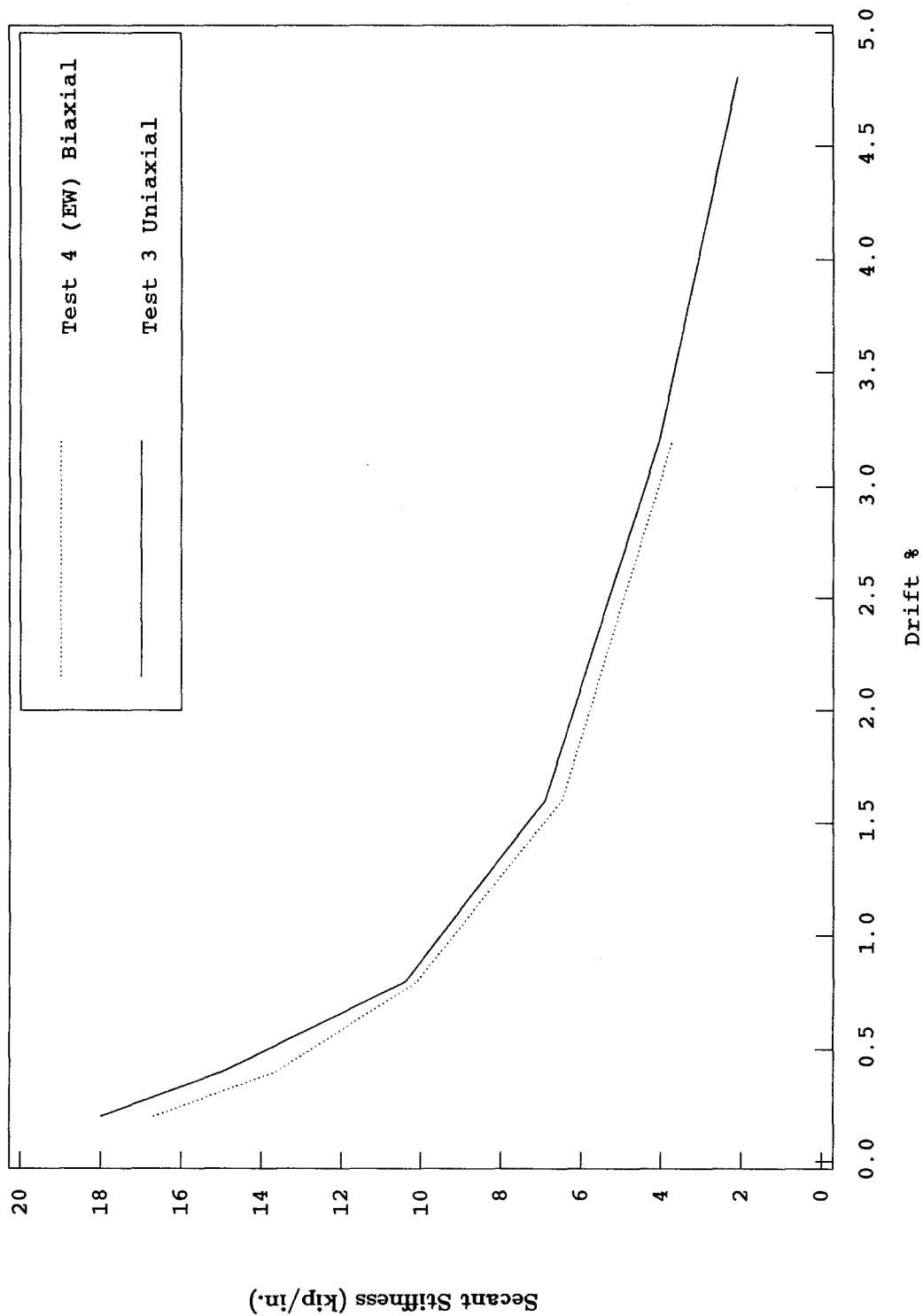


Fig. 6.4 (b) Effect of Biaxial Loading on Stiffness - Tests with Low Gravity Loads

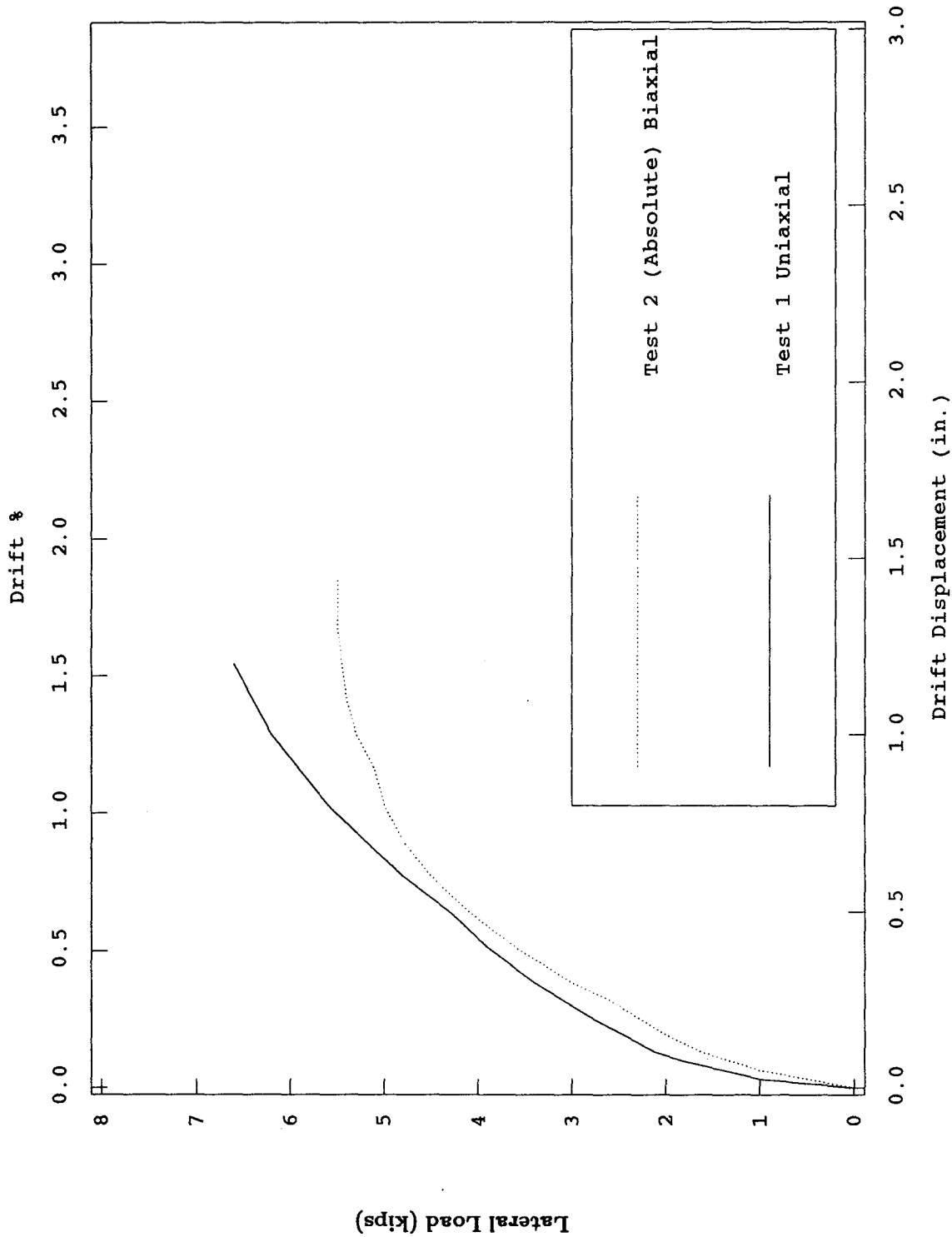


Fig. 6.5 (a) Comparison of Absolute Load-Displacement Envelopes (High Gravity Loads)

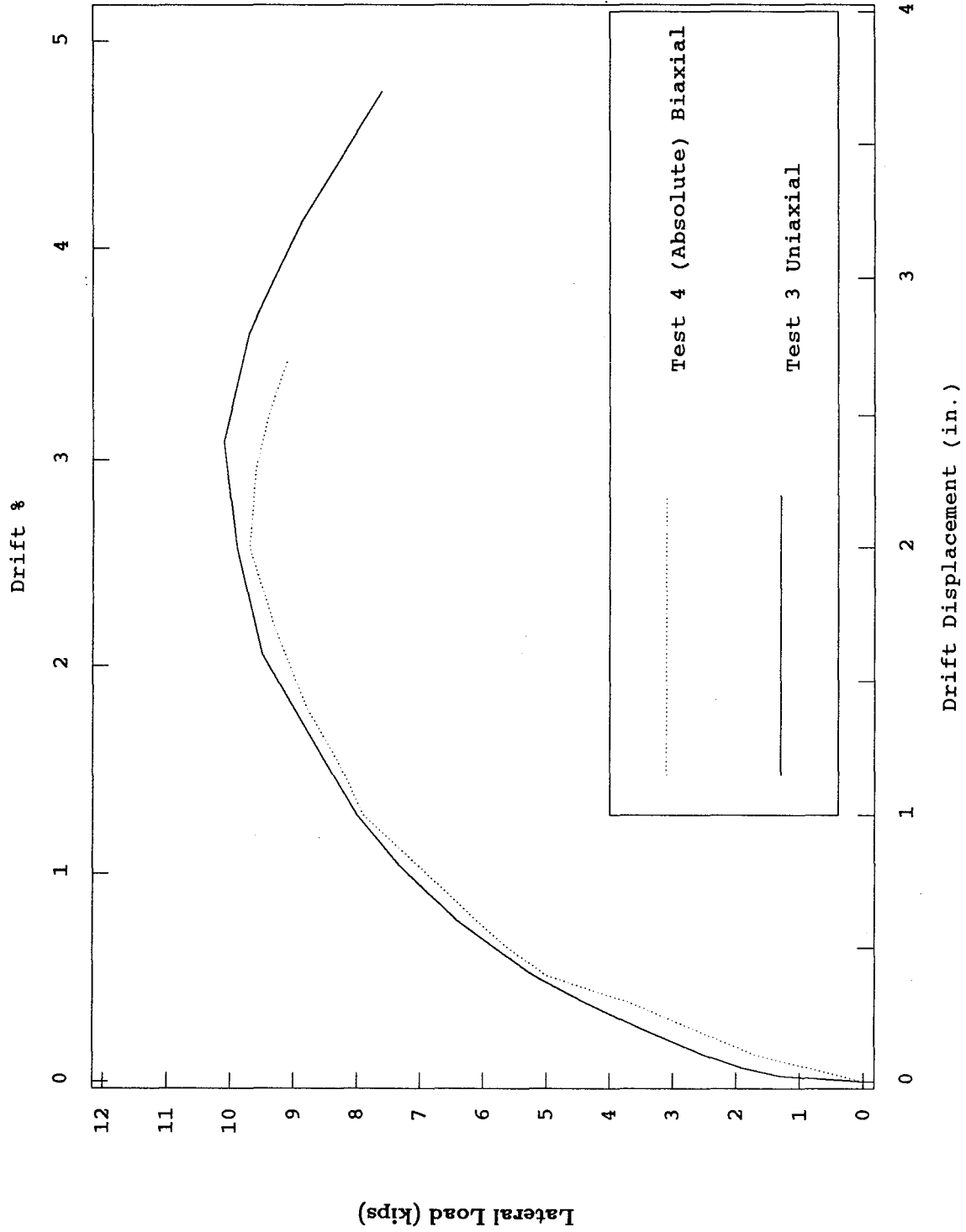


Fig. 6.5 (b) Comparison of Absolute Load-Displacement Envelopes (Low Gravity Loads)

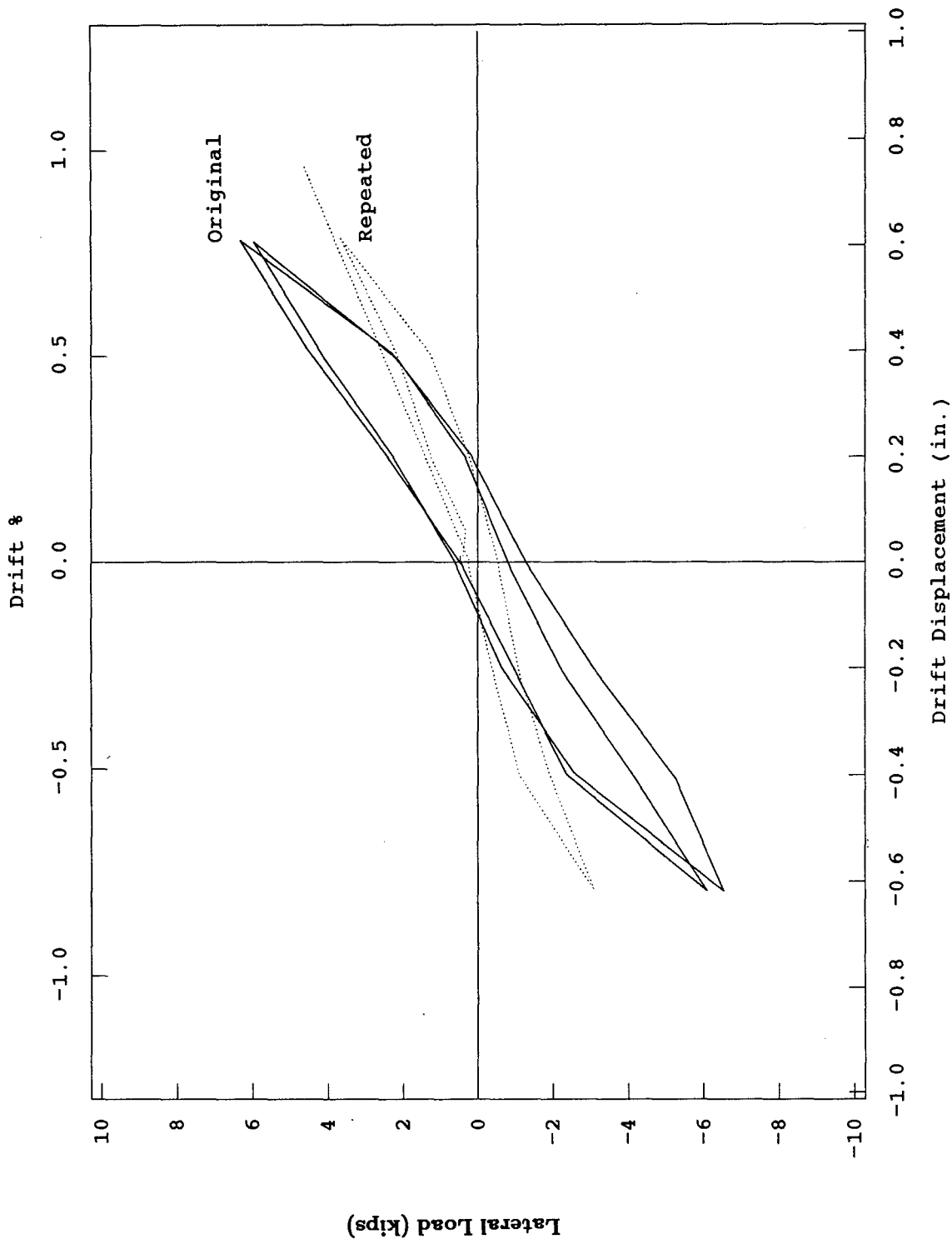


Fig. 6.6 (a) Repeated Load Cycles (0.8 % Drift Cycle - Test 3)

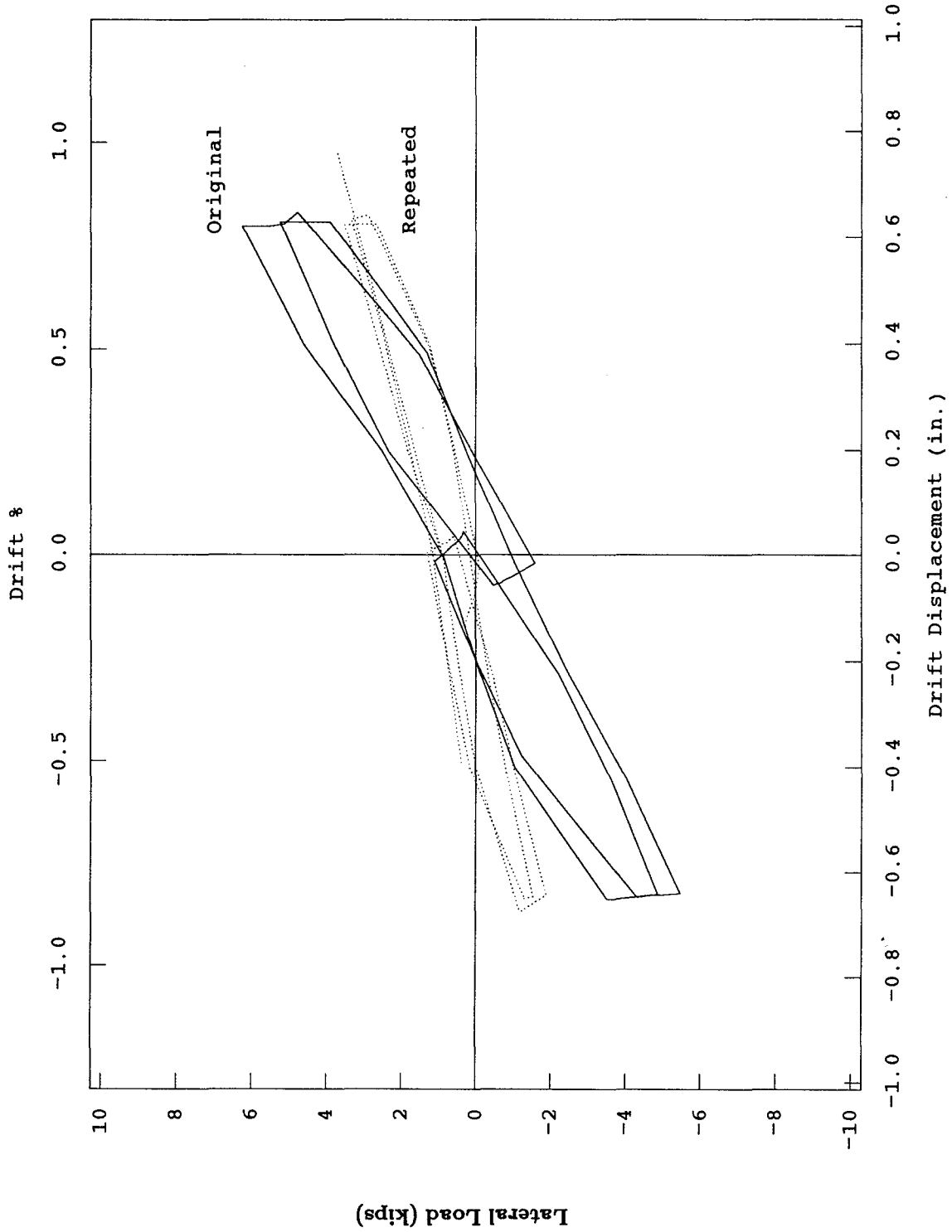


Fig. 6.6 (b) Repeated Load Cycles (0.8 % Drift Cycle - Test 4 (EW))

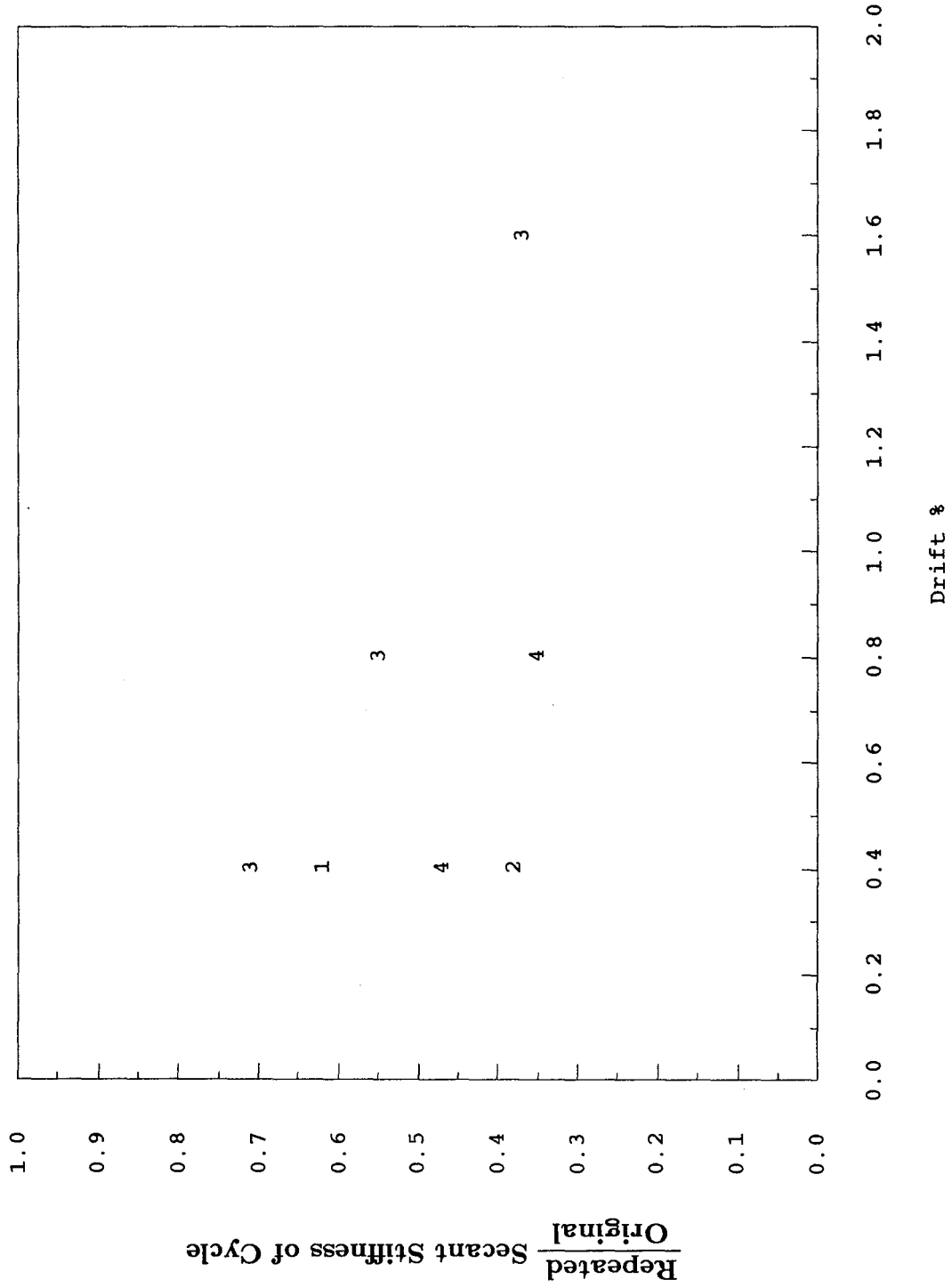


Fig. 6.7 Stiffness Degradation

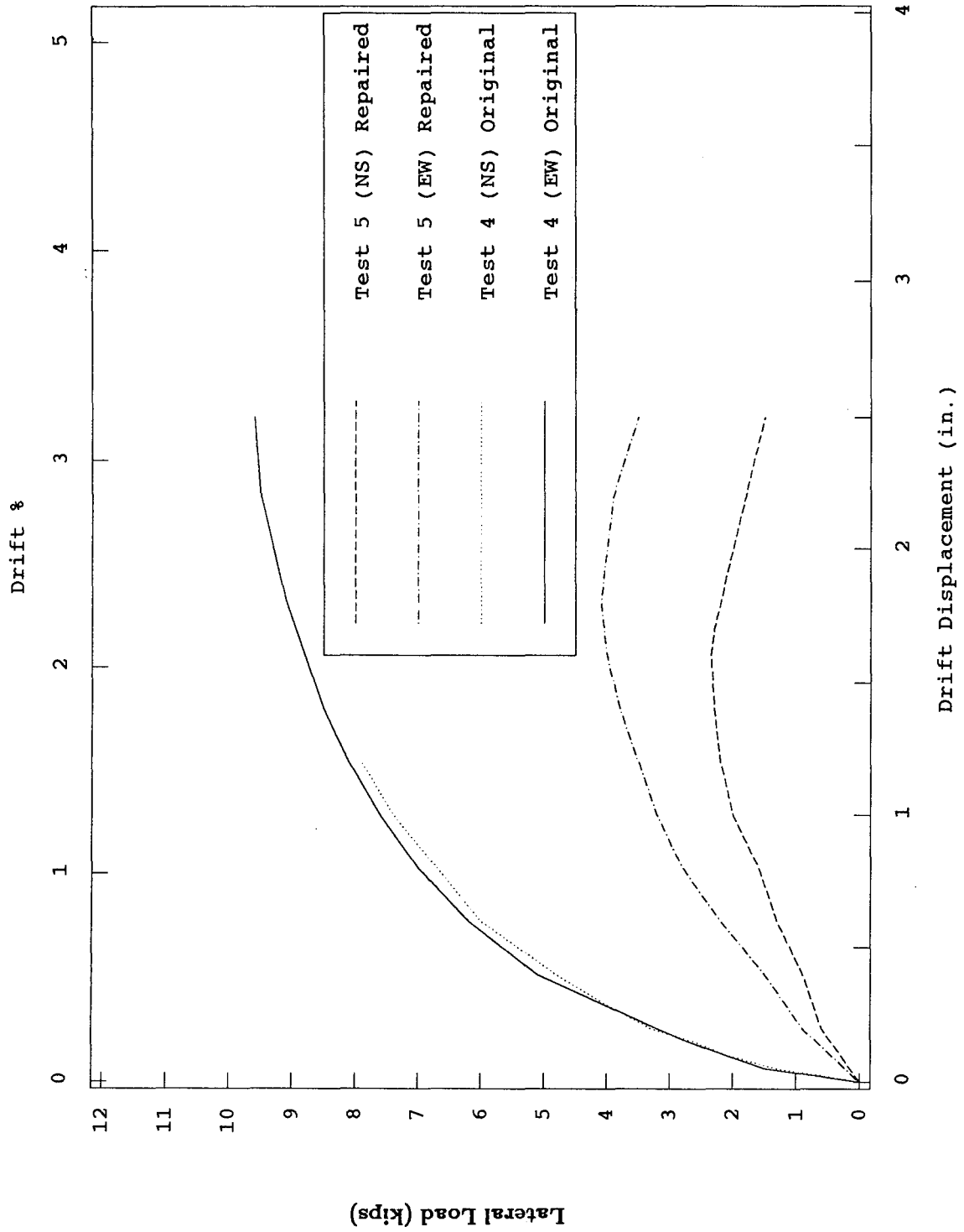


Fig. 6.8 Load-Displacement Envelopes of Repaired and Original Specimens

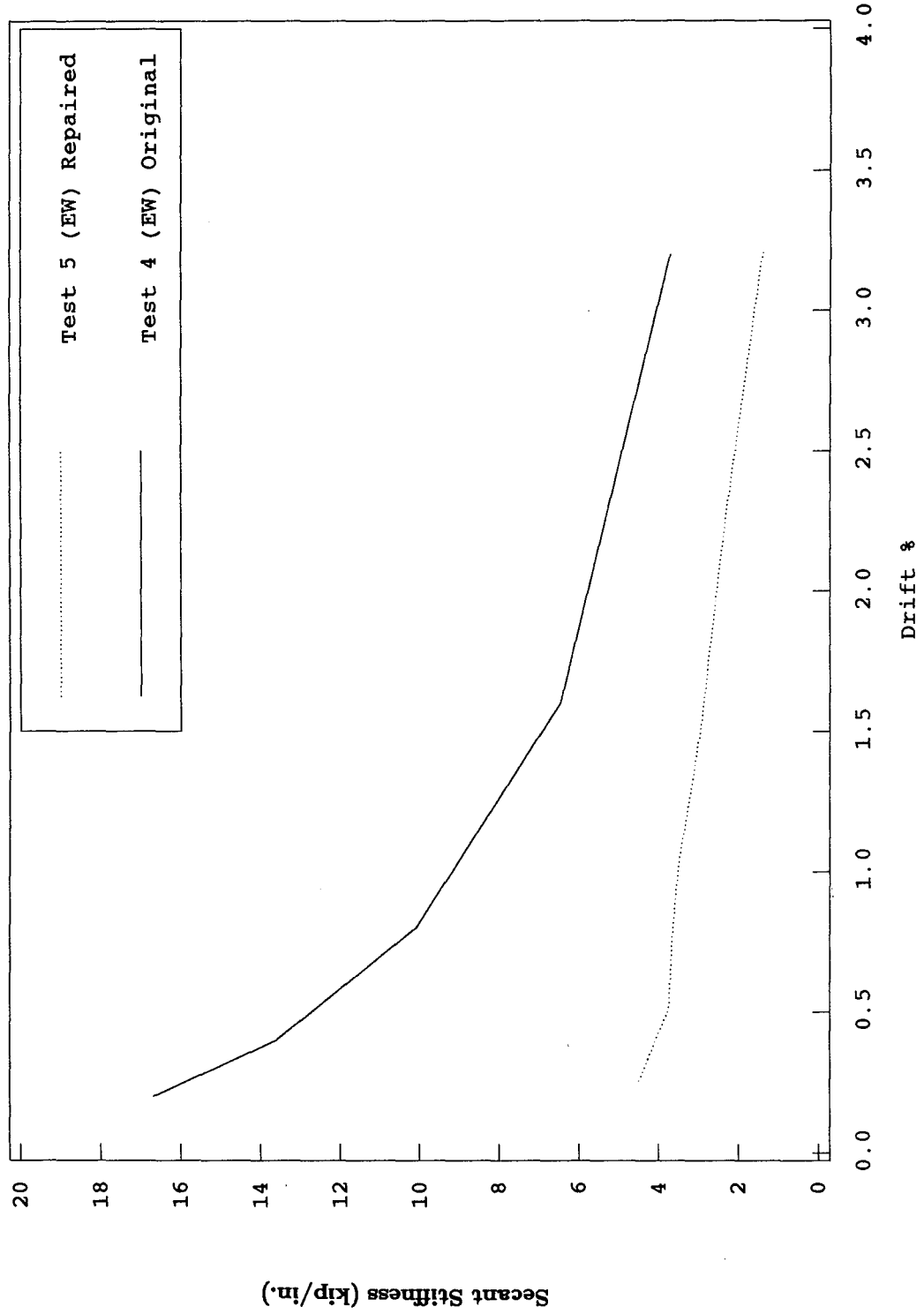


Fig. 6.9 Comparison of Stiffness Between Repaired and Original Specimens

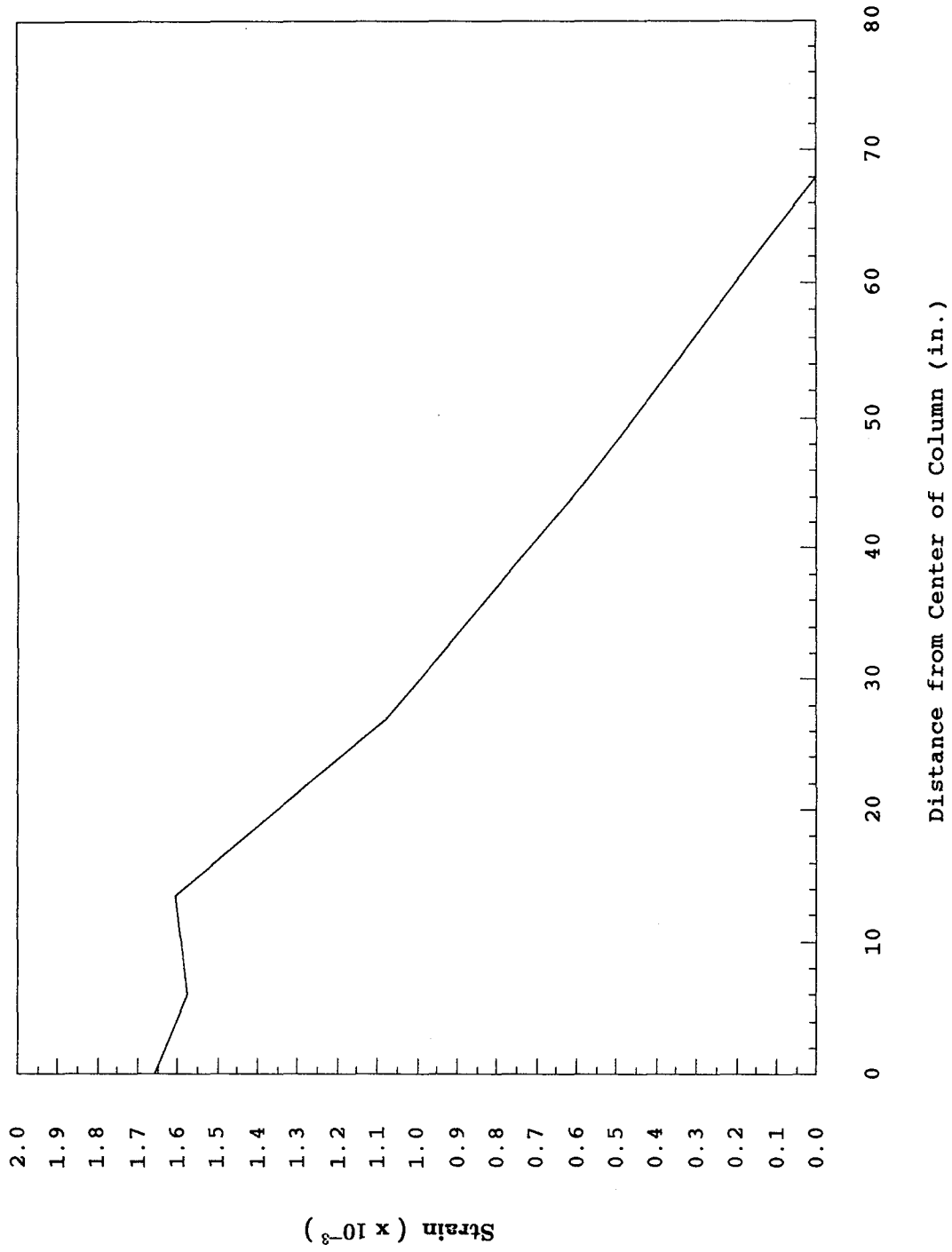


Fig. 6.10 Measured Top Reinforcement Strain Profile Due to Gravity Loads
(East Side - Test 1)

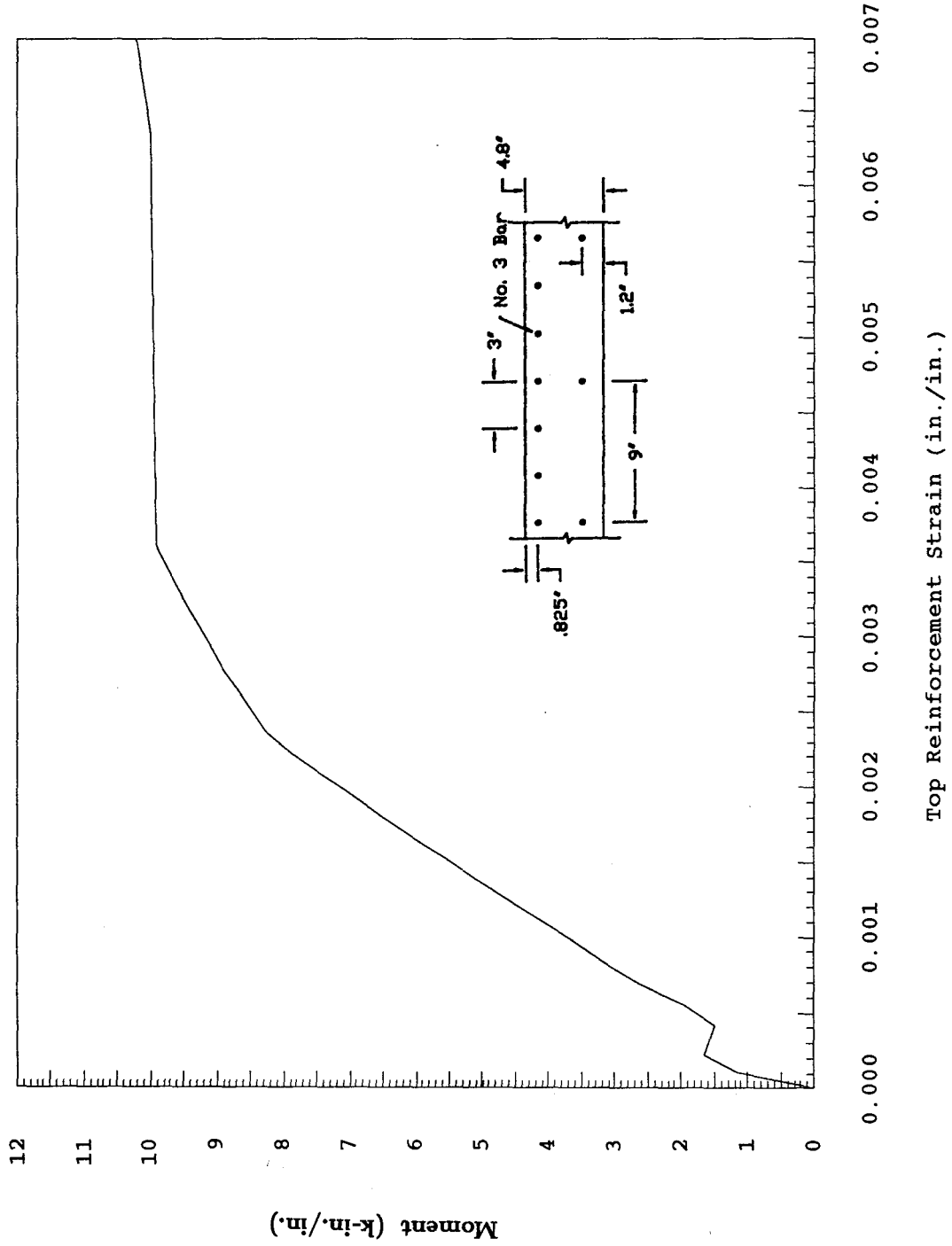


Fig. 6.11 Moment-Strain Relationship of Slab Section (3 in. Top Reinforcement Spacing)

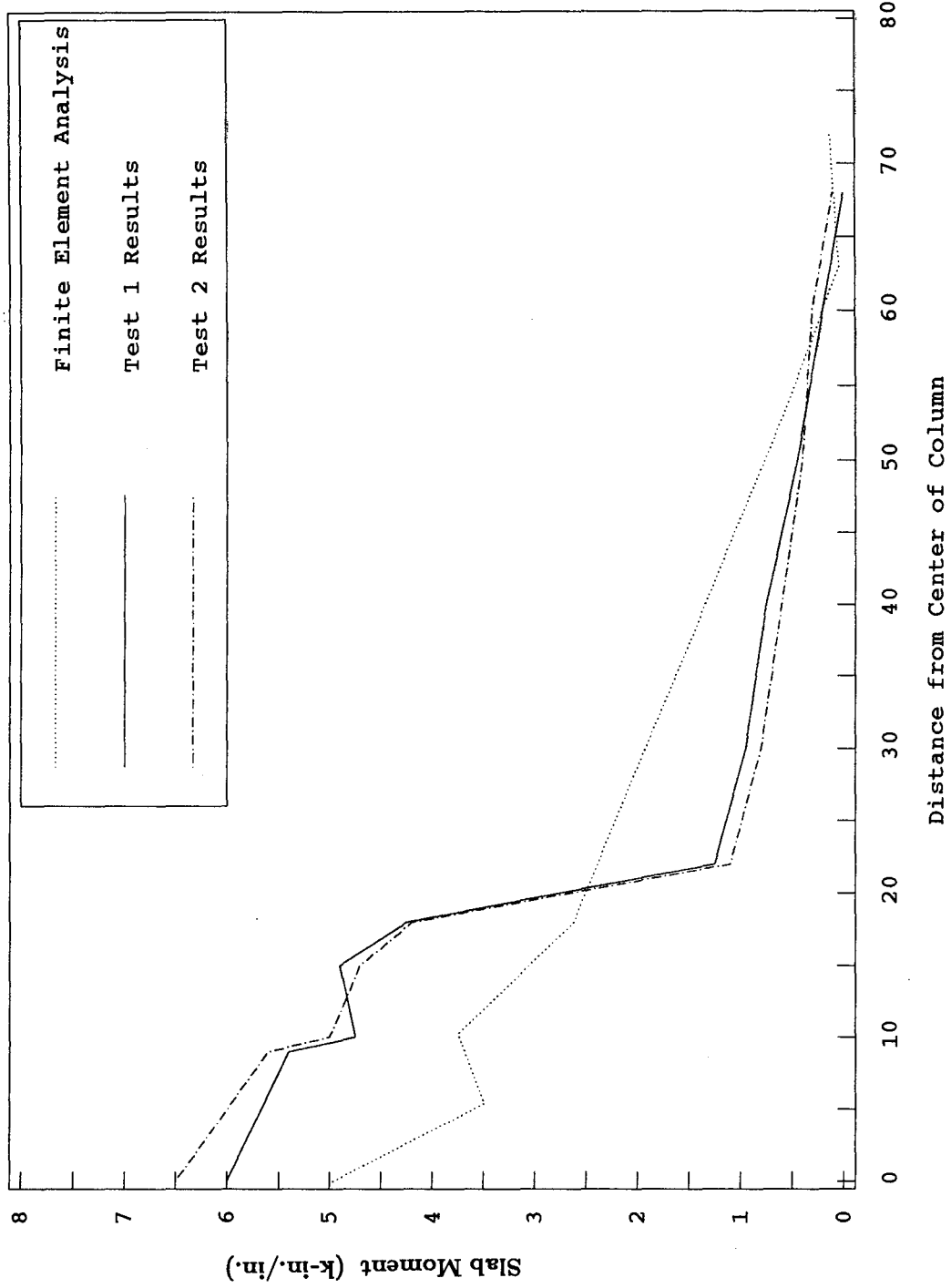


Fig. 6.12 (a) Experimental and Finite Element Gravity Moment Profiles - High Gravity Load Tests

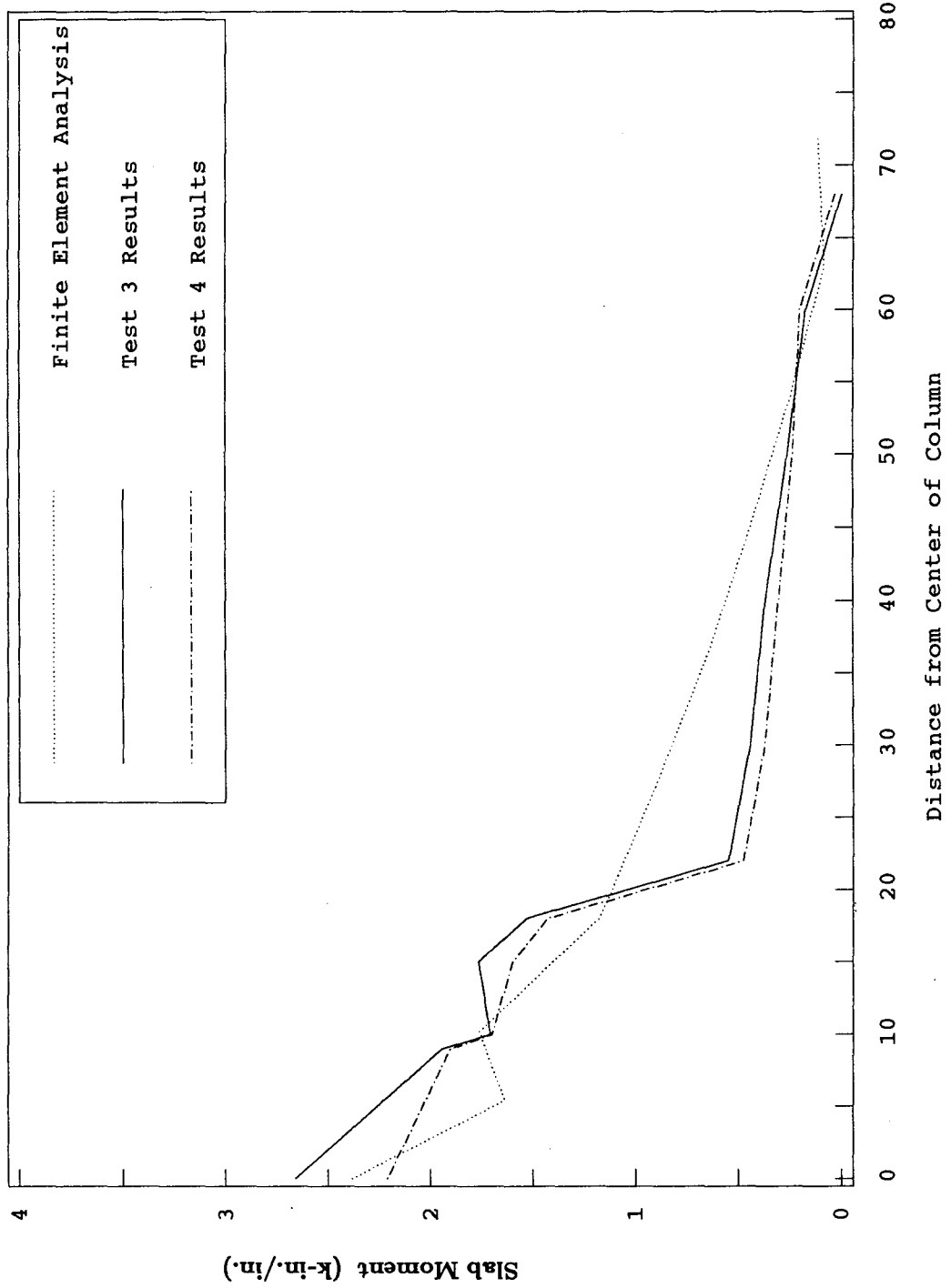


Fig. 6.12 (b) Experimental and Finite Element Gravity Moment Profiles - Low Gravity Load Tests

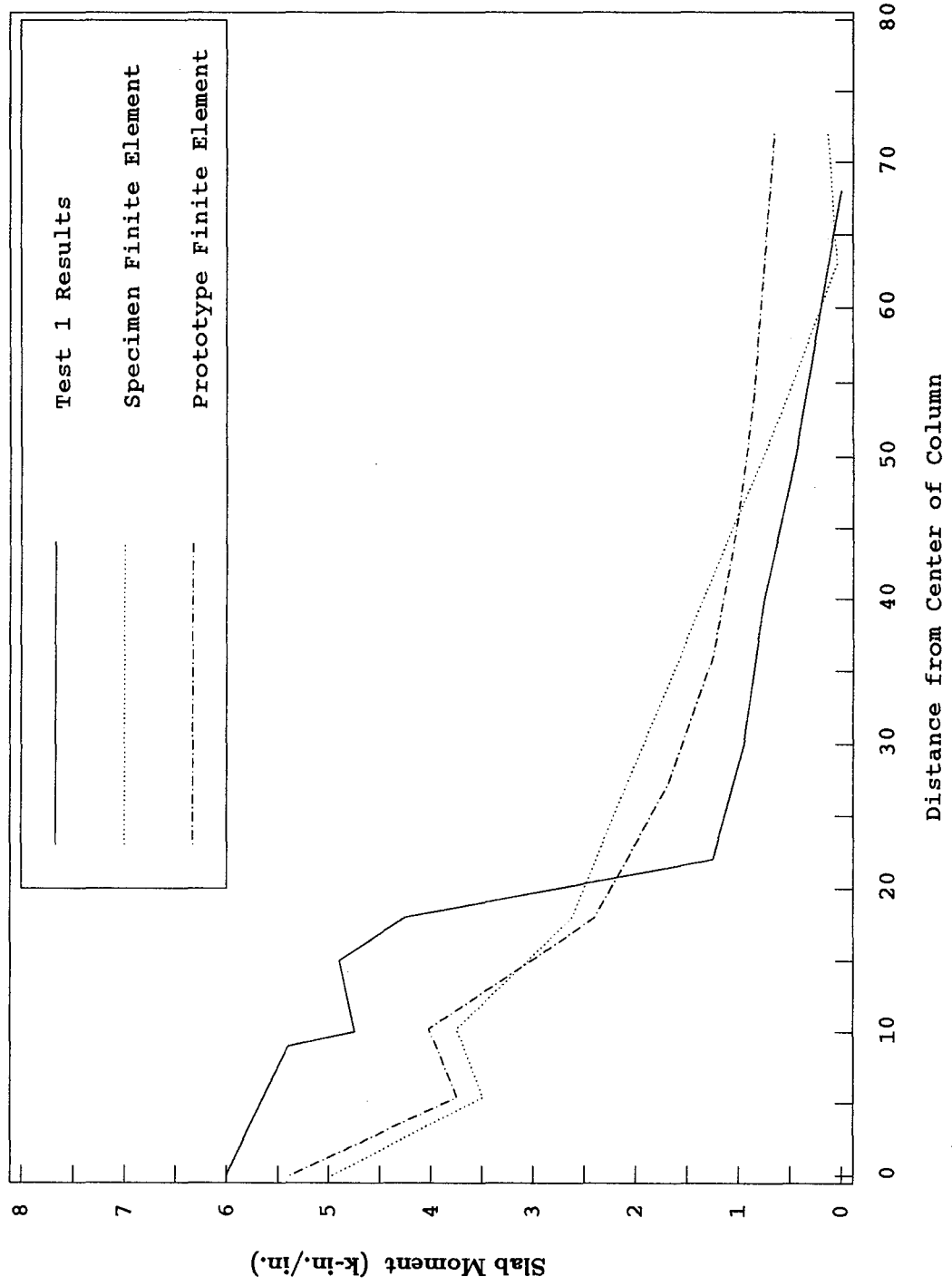
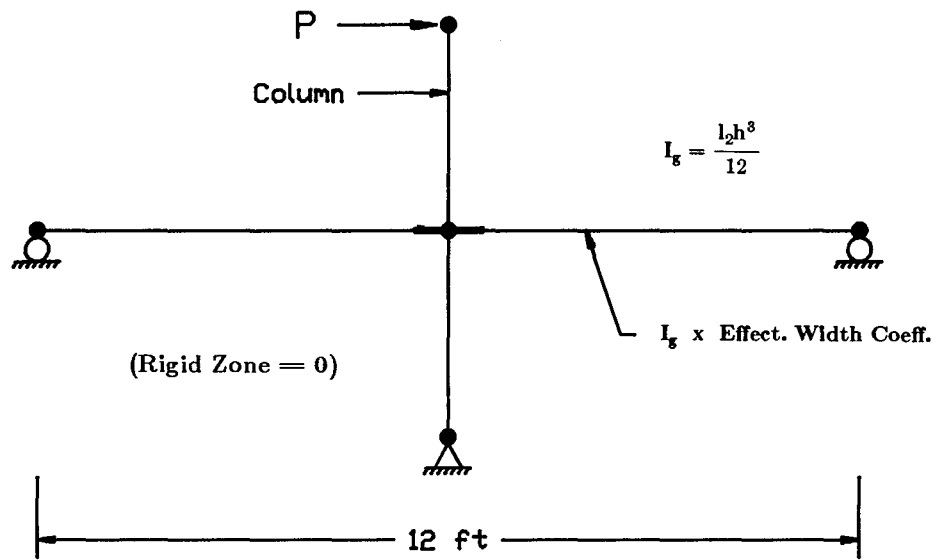
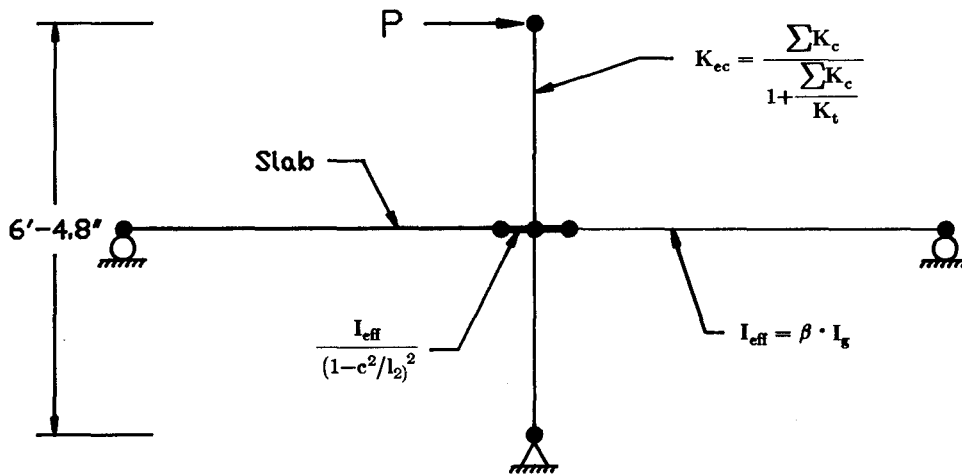


Fig. 6.12 (c) Comparison of Gravity Moment Profiles (Test 1)



(a) Effective Beam Width Model



(b) Equivalent Frame Model

Fig. 6.13 Lateral Stiffness Models

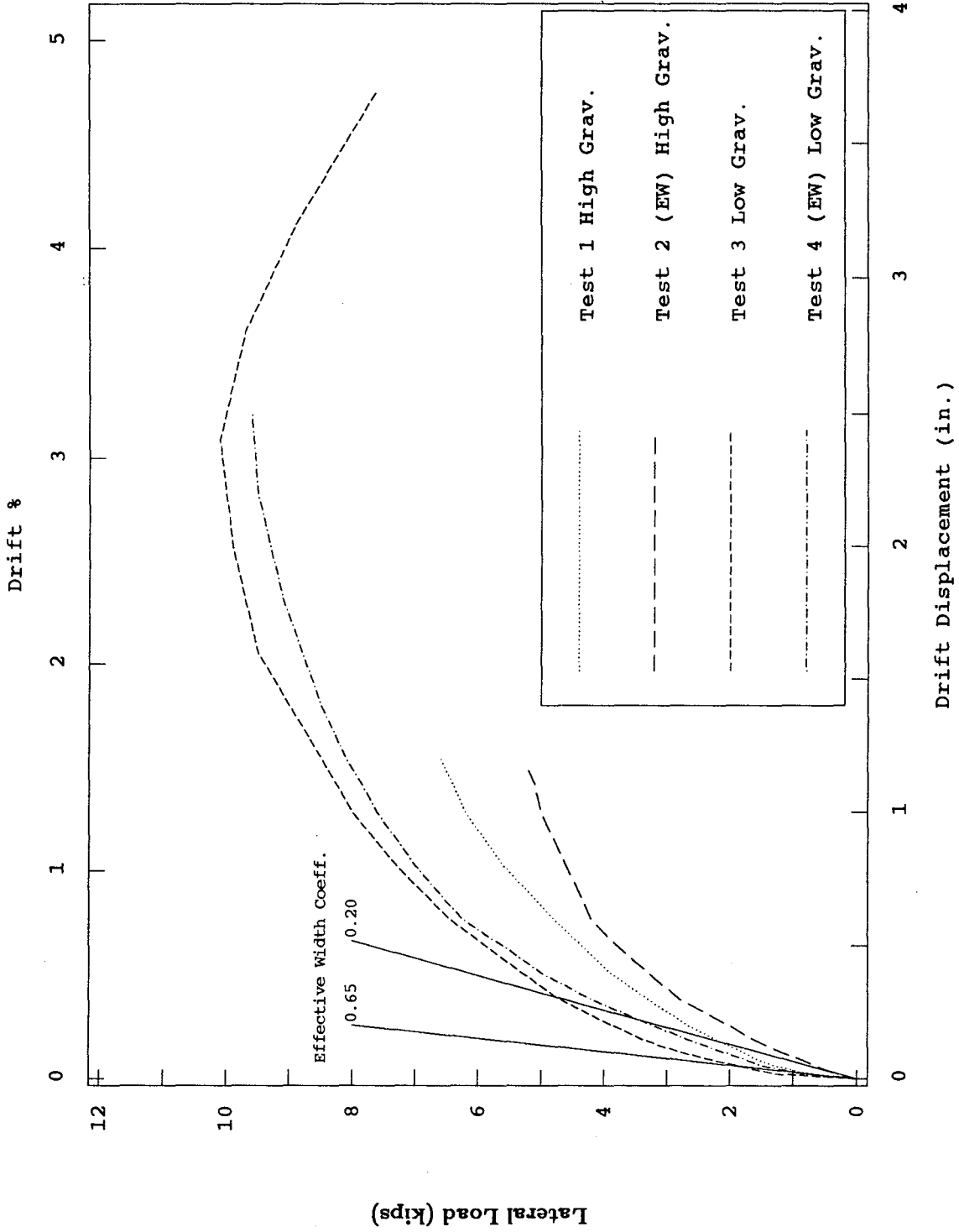


Fig. 6.14 (a) Comparison Between Effective Beam Width Model and Experimental Envelopes

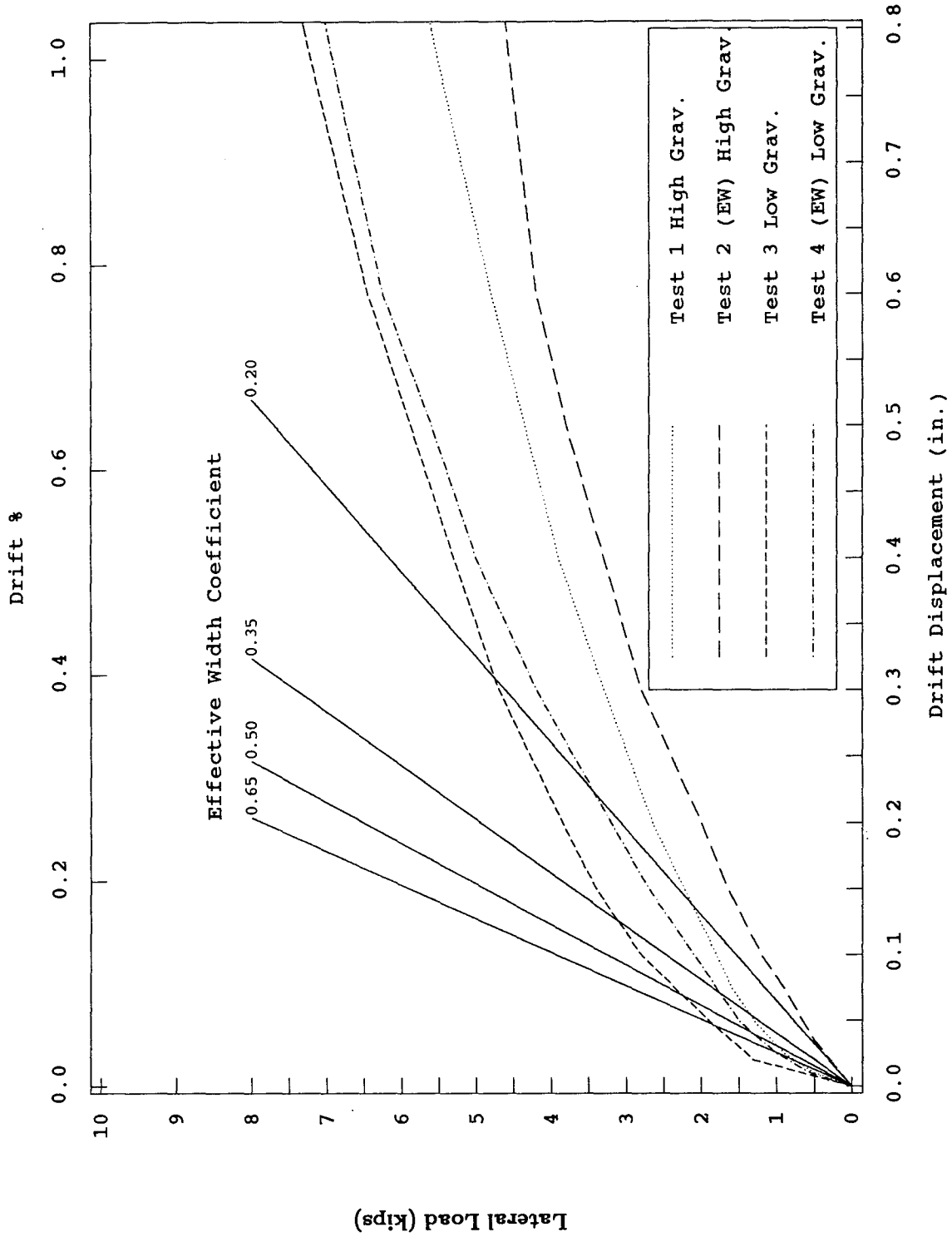


Fig. 6.14 (b) Comparison Between Effective Beam Width Model and Experimental Envelopes

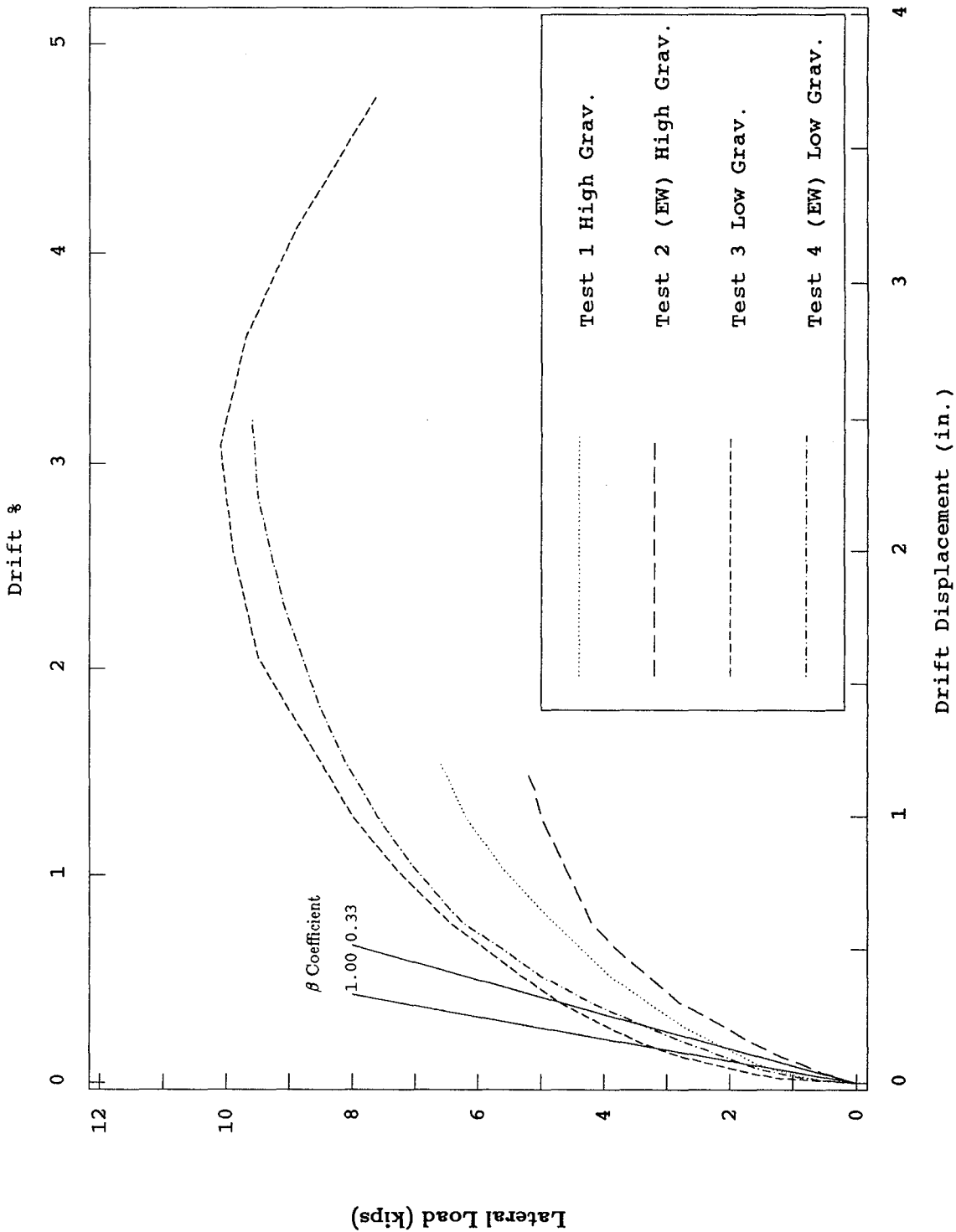


Fig. 6.15 (a) Comparison Between Equivalent Frame Model and Experimental Envelopes

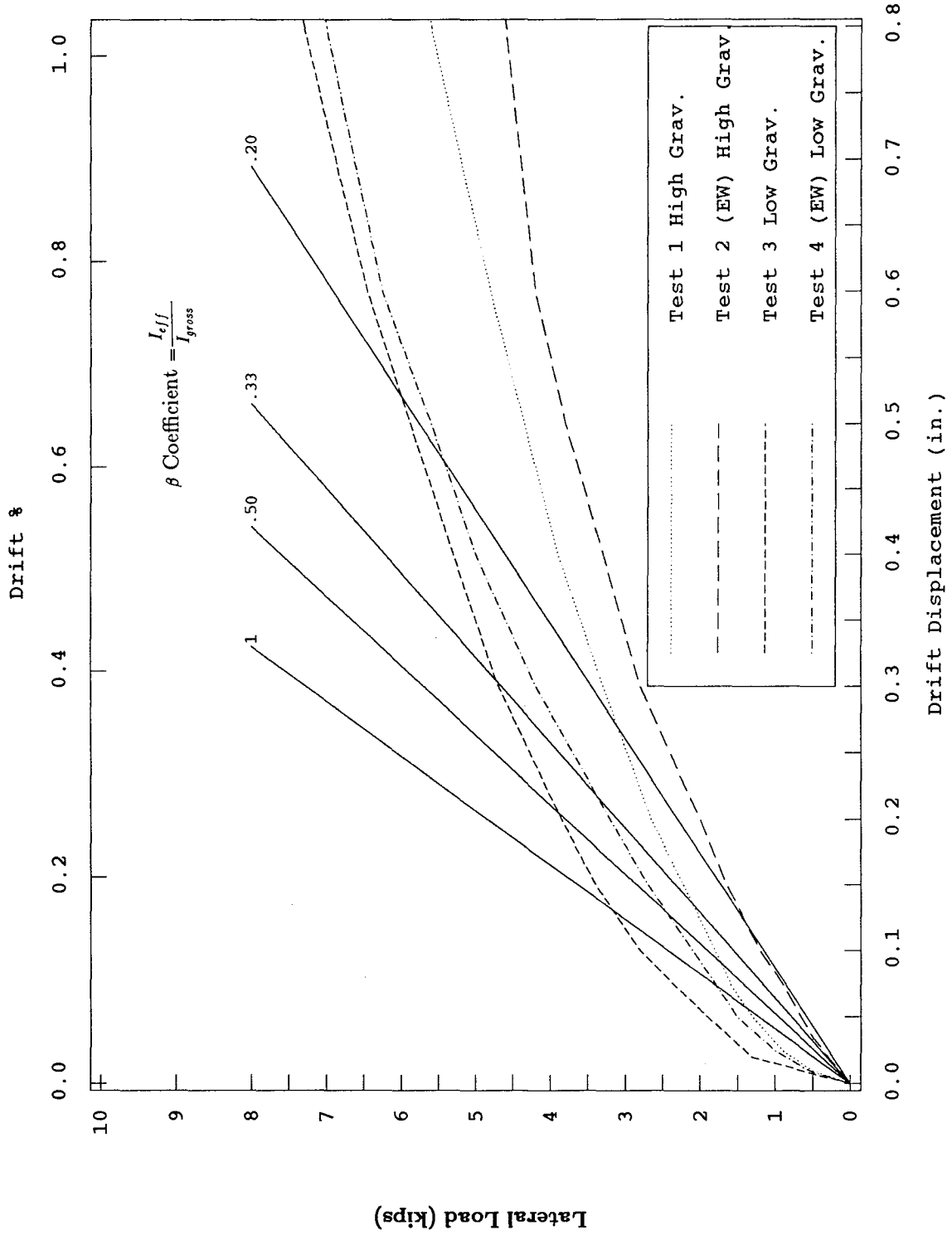
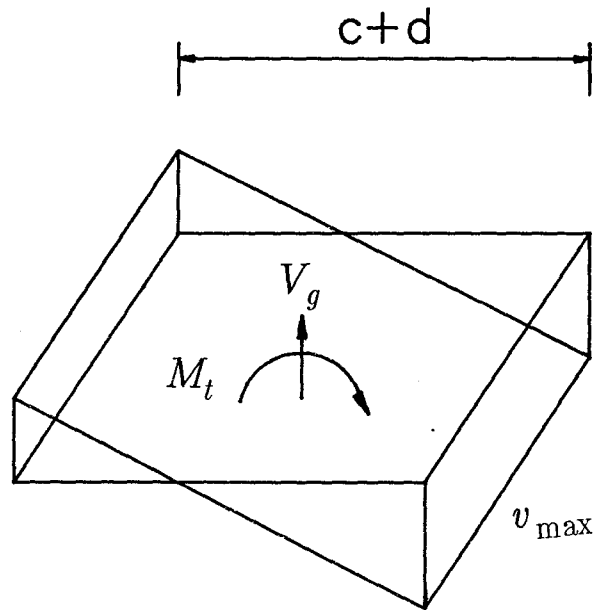
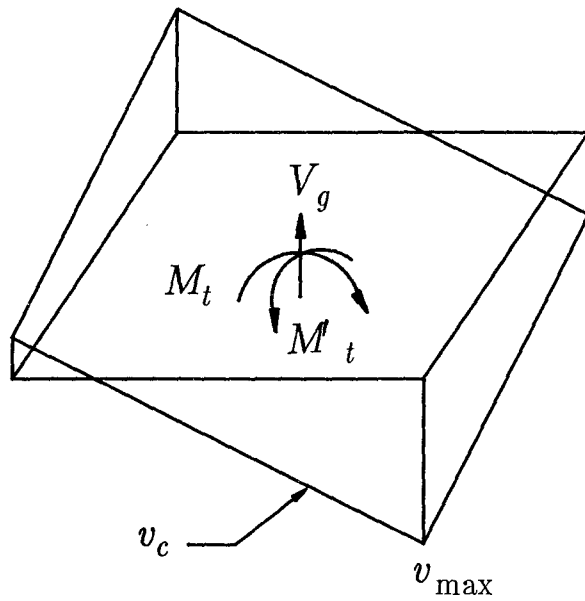


Fig. 6.15 (b) Comparison Between Equivalent Frame Model and Experimental Envelopes



(a) Uniaxial



(b) Biaxial

Fig. 6.16 Linear Stress Variation Model

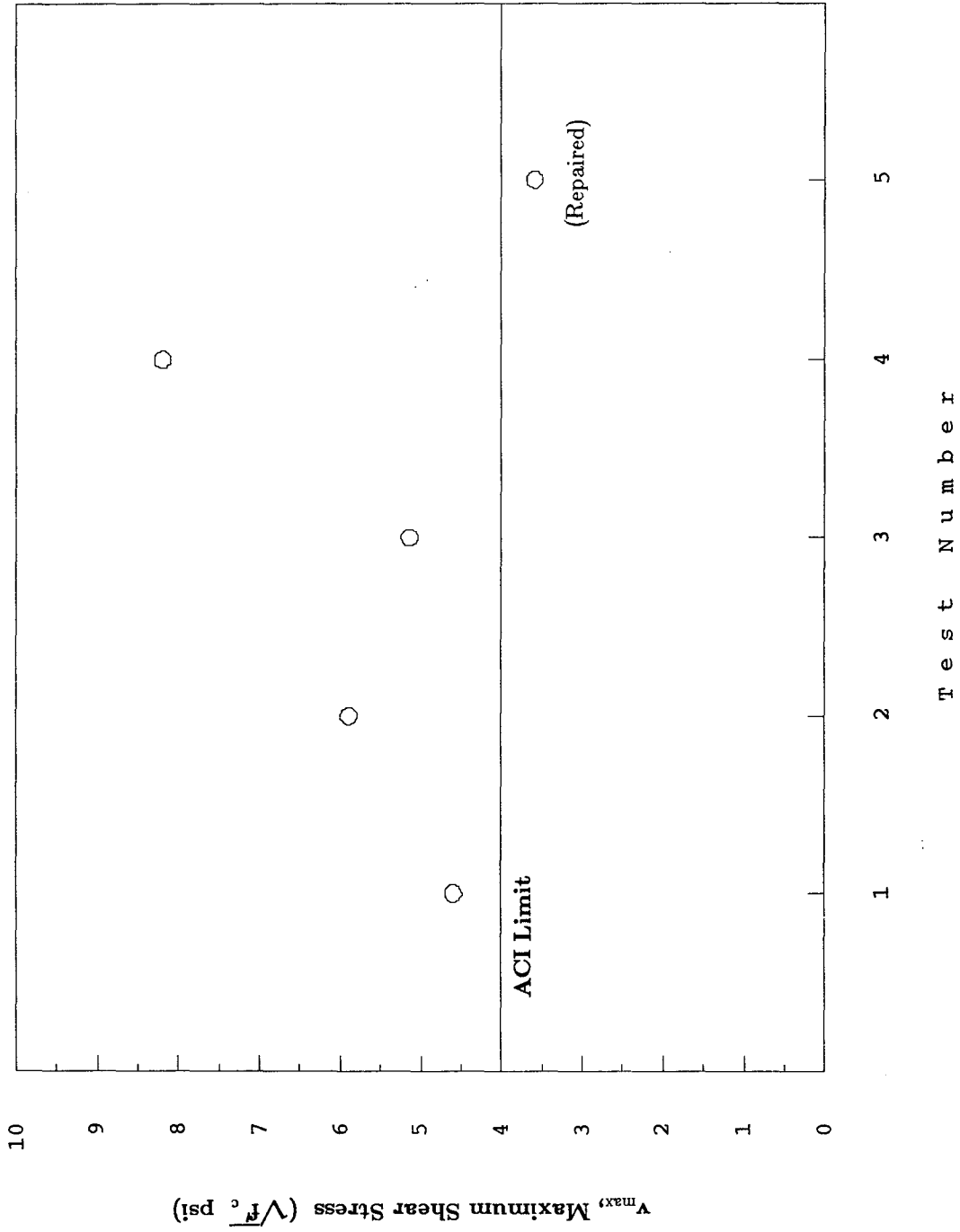


Fig. 6.17 Maximum Shear Stress by the Linear Stress Variation Model

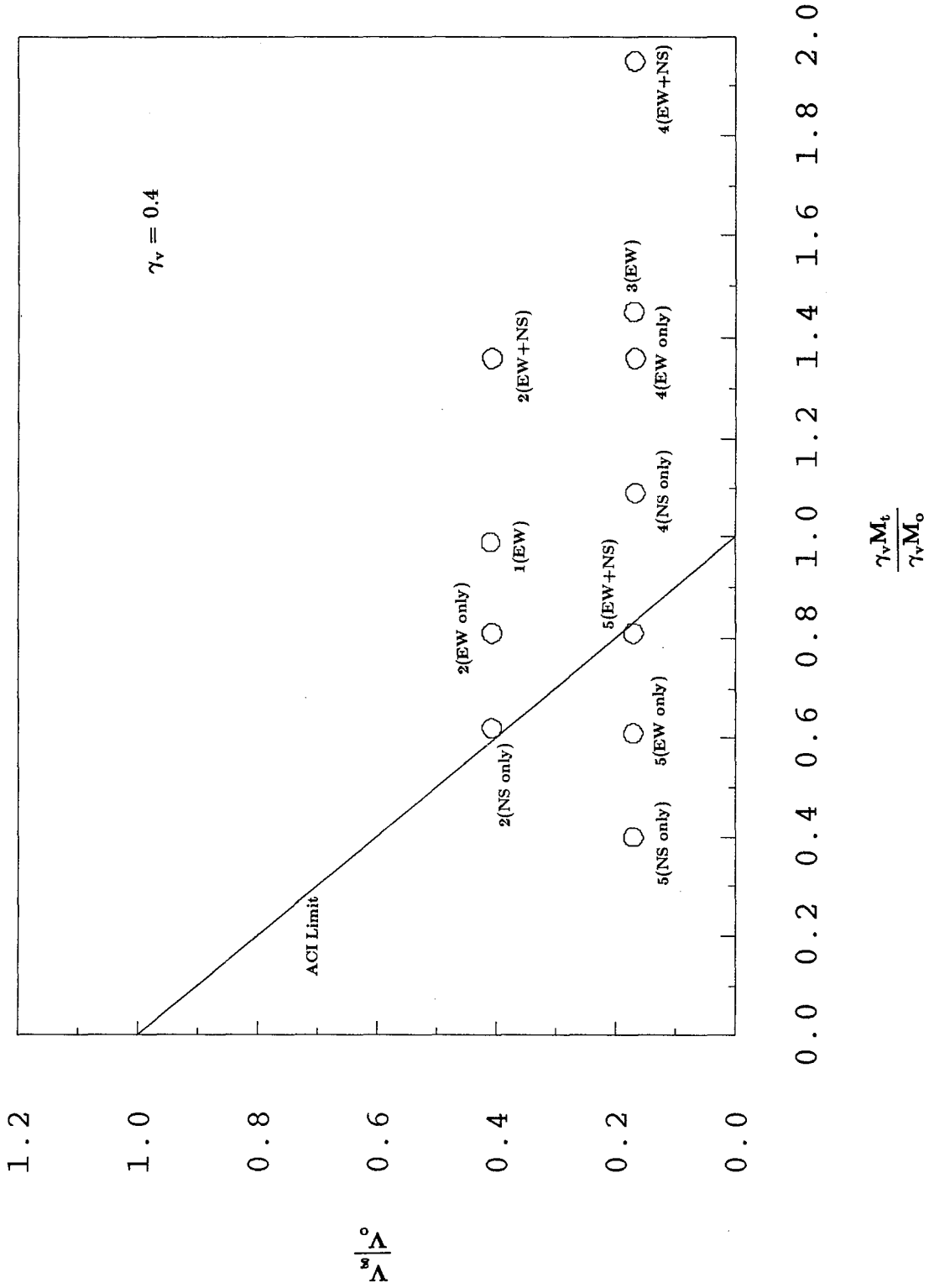


Fig. 6.18 Test Results on Shear-Moment Interaction Diagram

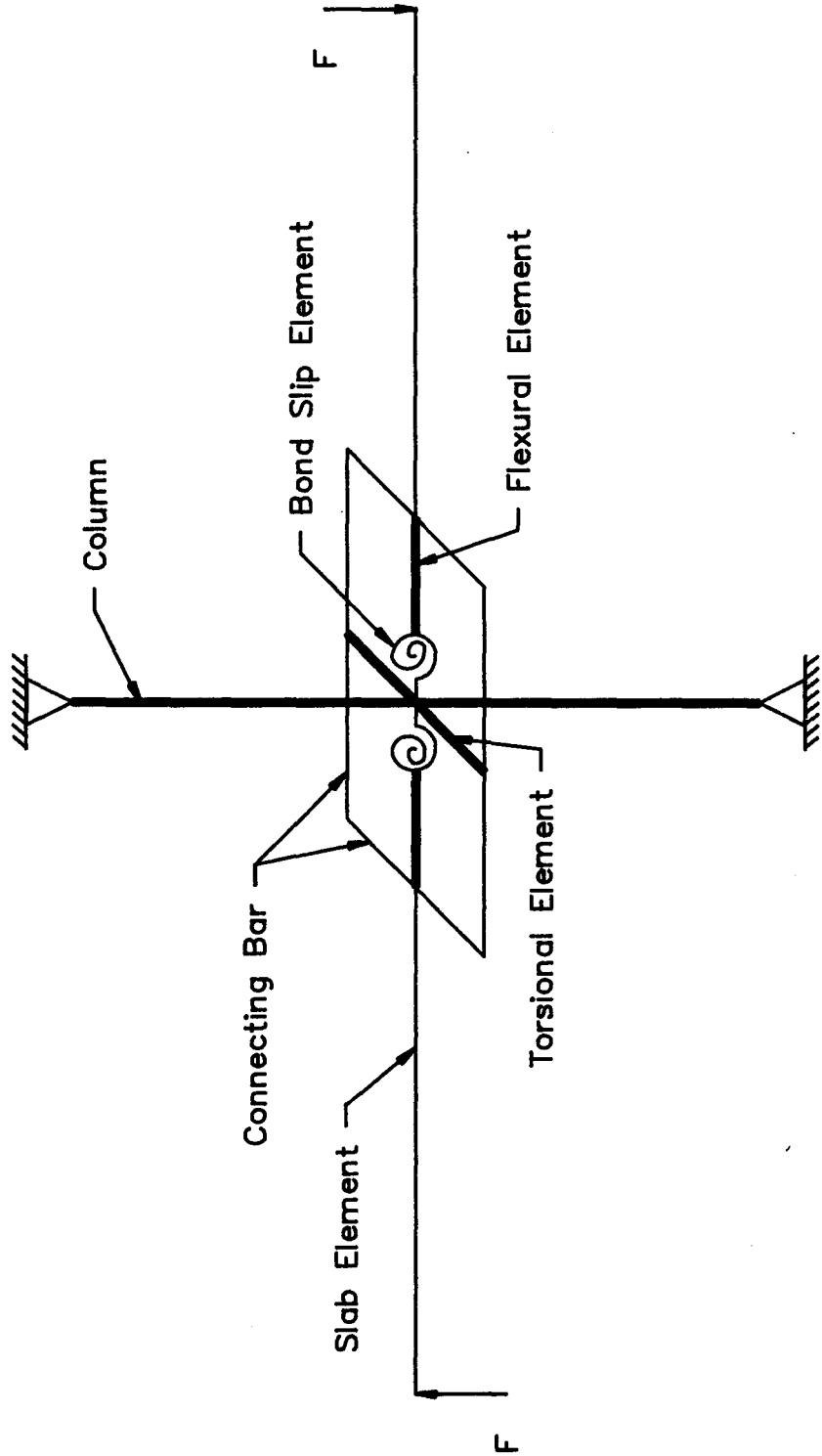


Fig. 6.19 Beam Analogy Model

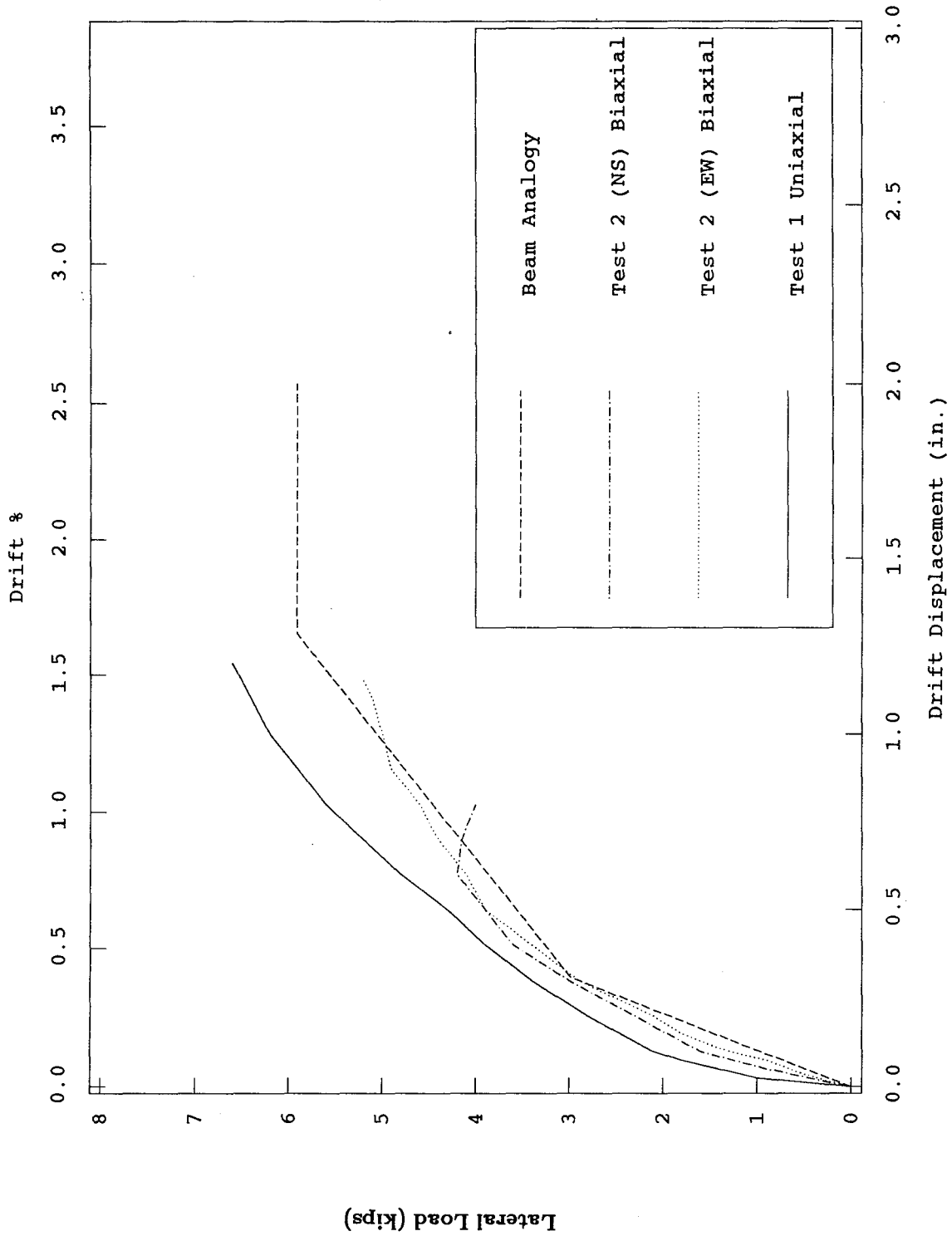


Fig. 6.20 (a) Comparison Between Beam Analogy Model and Experimental Envelopes
 - High Gravity Load Tests

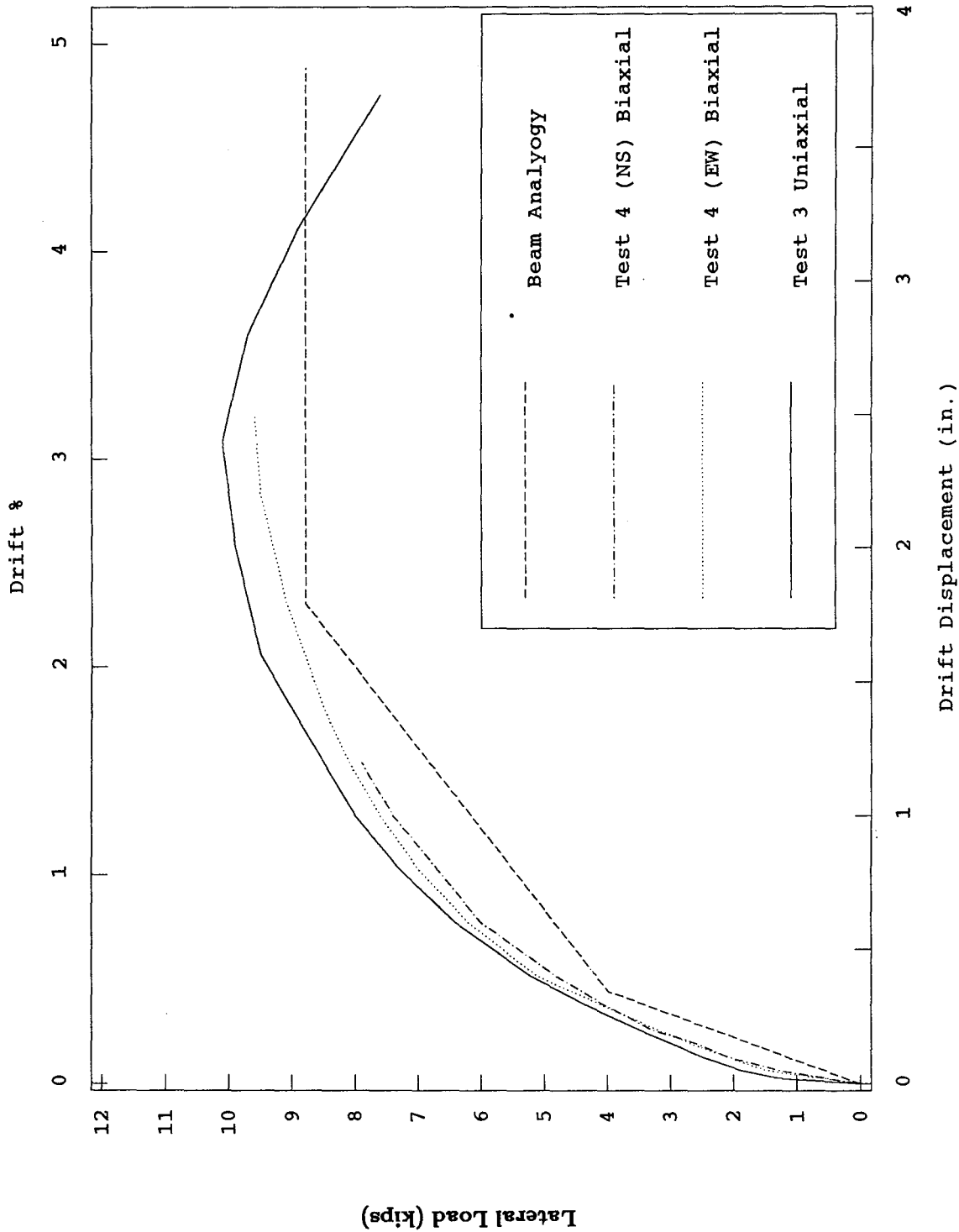


Fig. 6.20 (b) Comparison Between Beam Analyogy Model and Experimental Envelopes - Low Gravity Load Tests

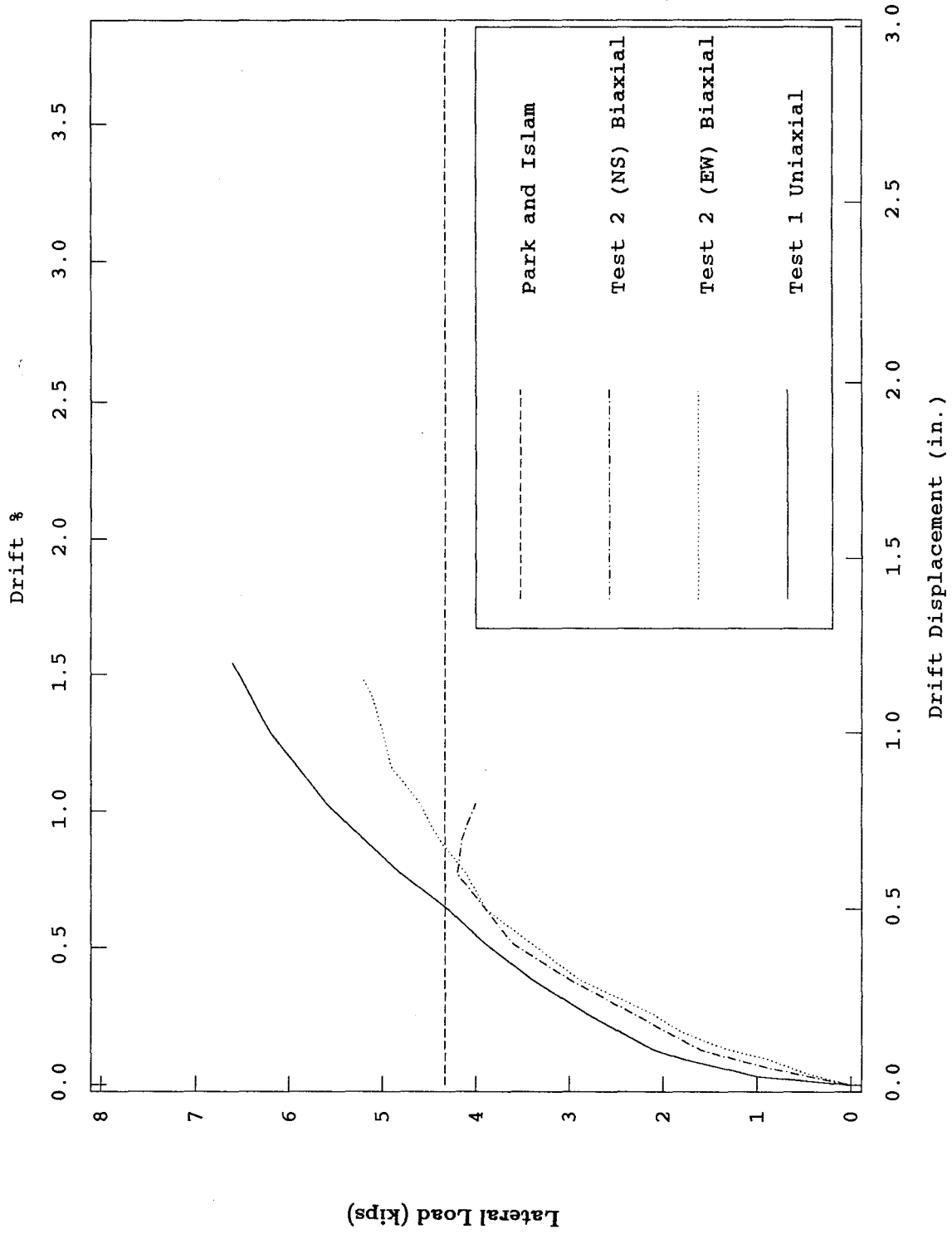


Fig. 6.21 (a) Comparison Between Park and Islam Model and Experimental Envelopes
 - High Gravity Load Tests

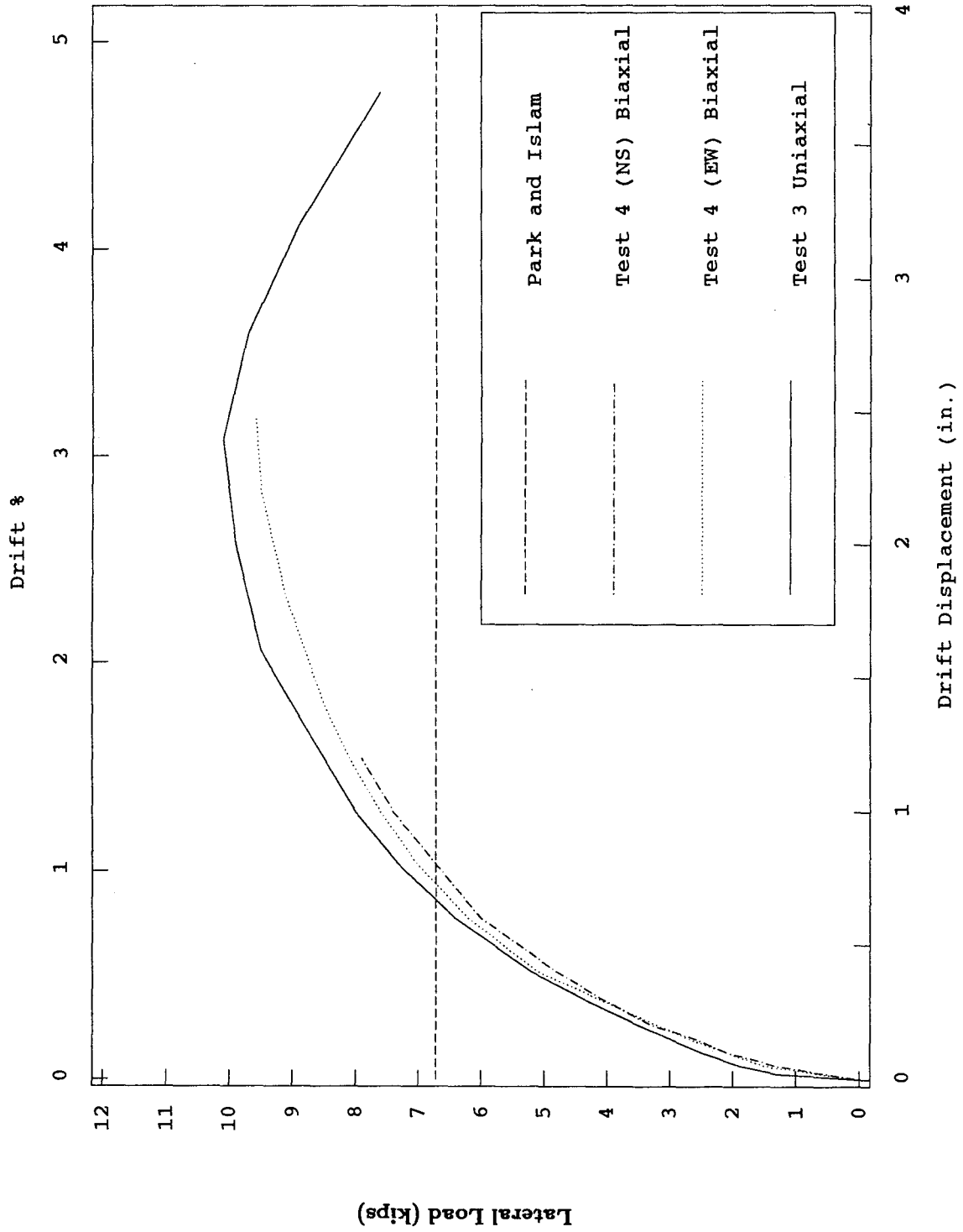
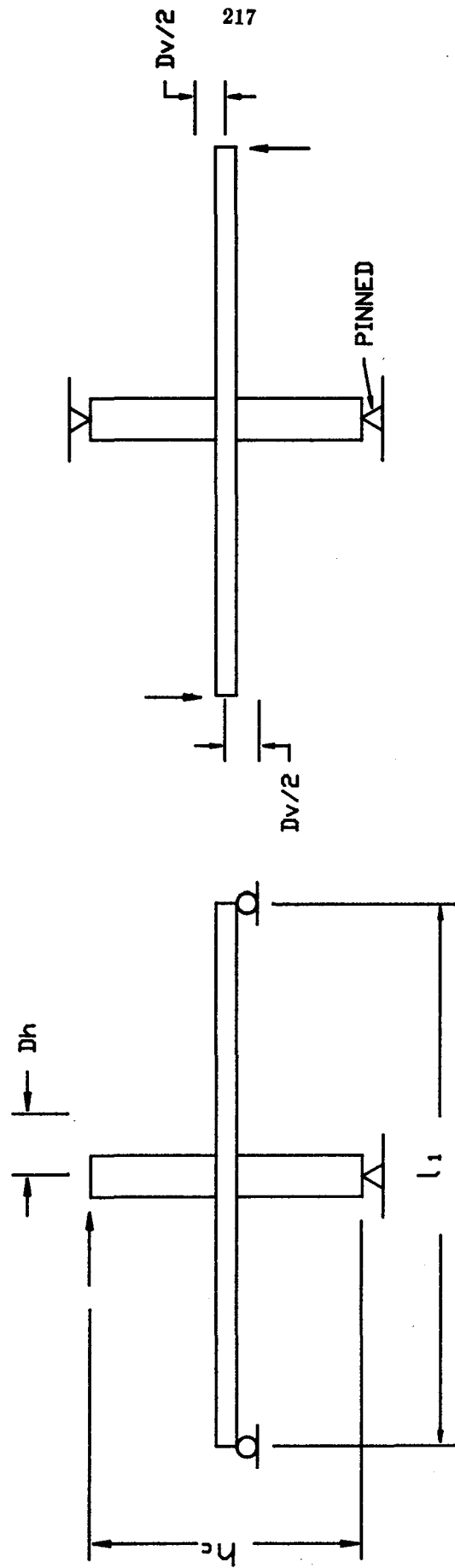


Fig. 6.21 (b) Comparison Between Park and Islam Model and Experimental Envelopes - Low Gravity Load Tests



(a) Lateral Load at Column (b) Vertical Load at Slab Ends

Fig. 7.1 Lateral Load Simulation

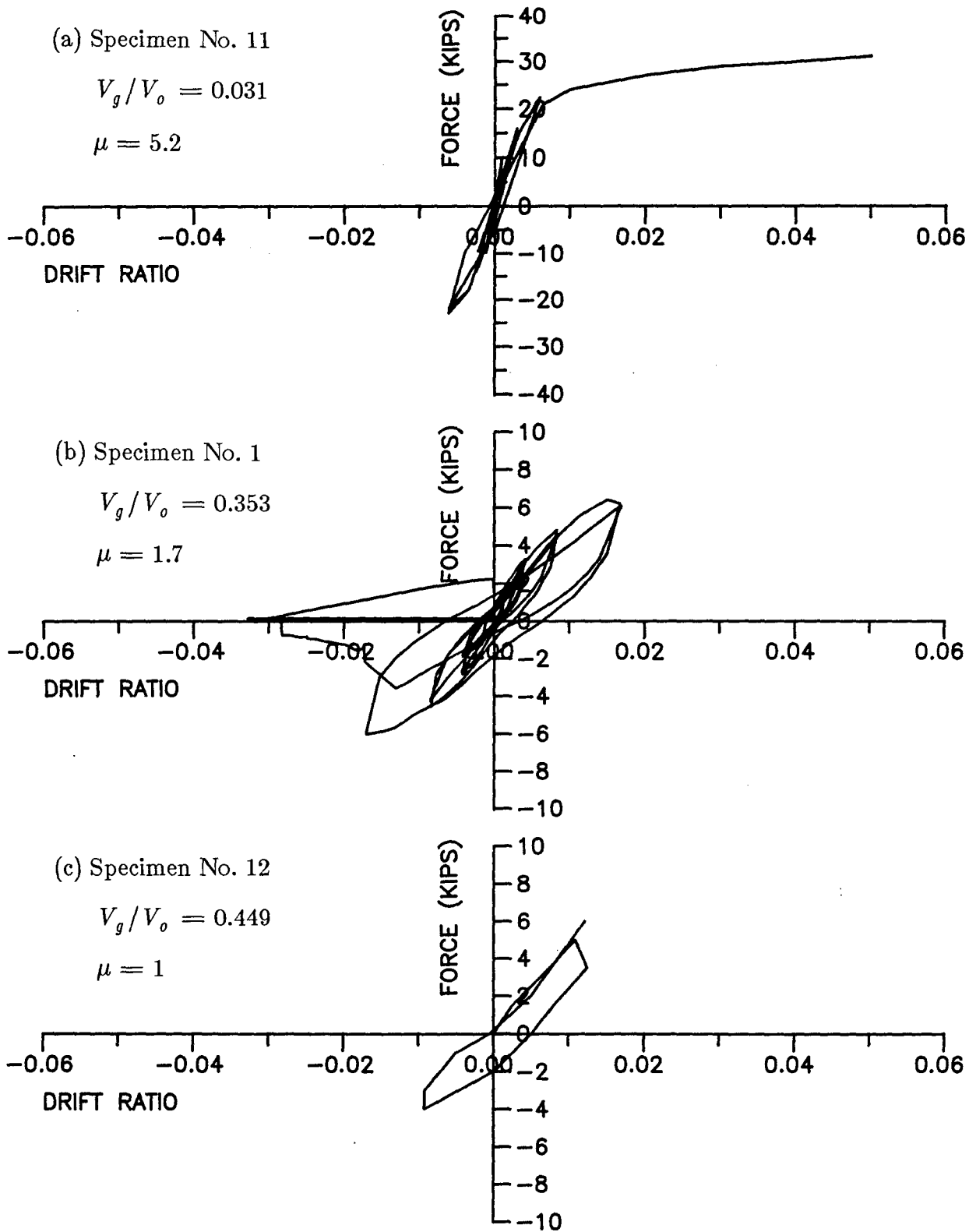


Fig. 7.2 Classification of Specimen Response

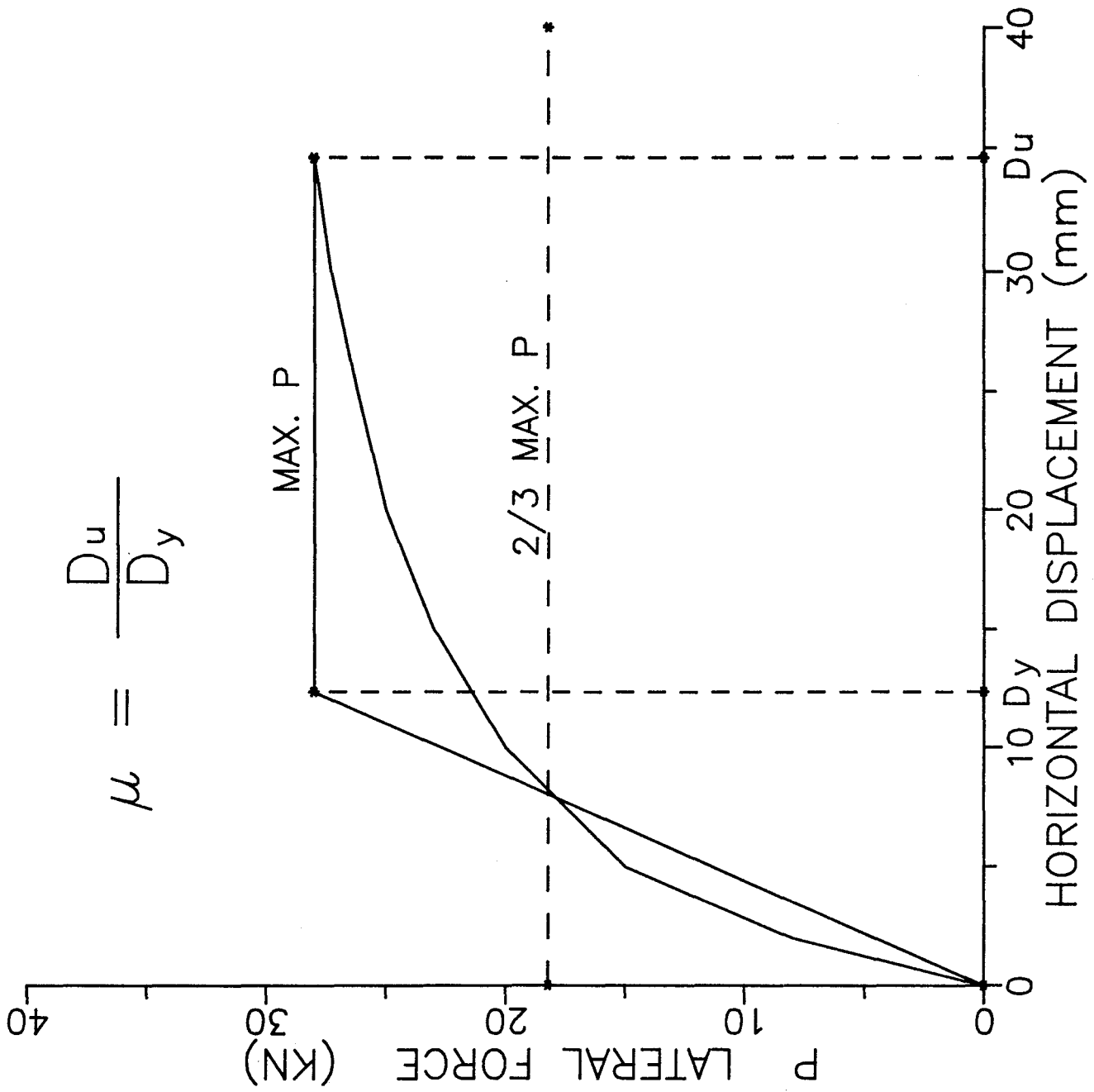


Fig. 7.3 Definition of Displacement Ductility

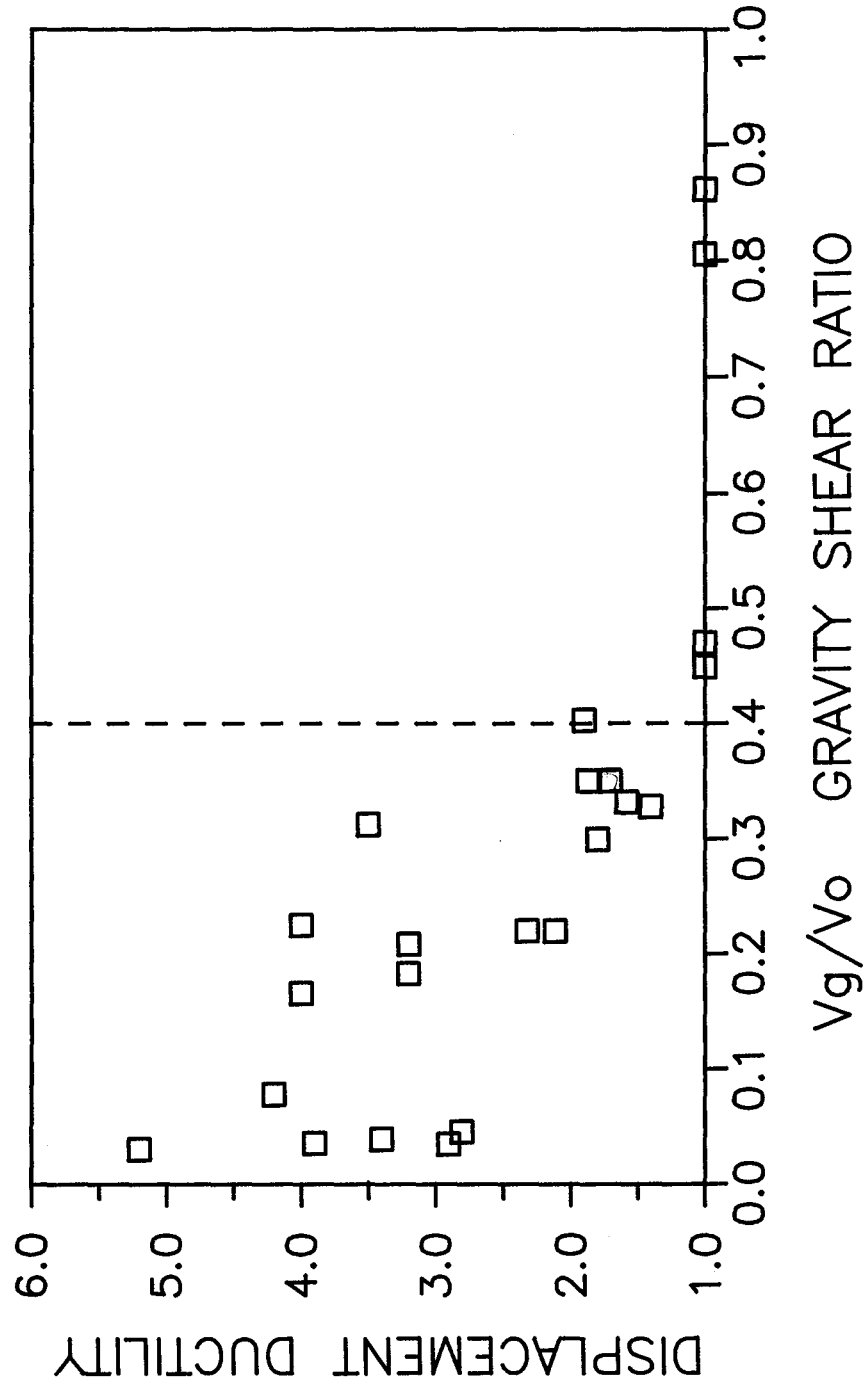


Fig. 7.4 Effect of Gravity Load on Ductility

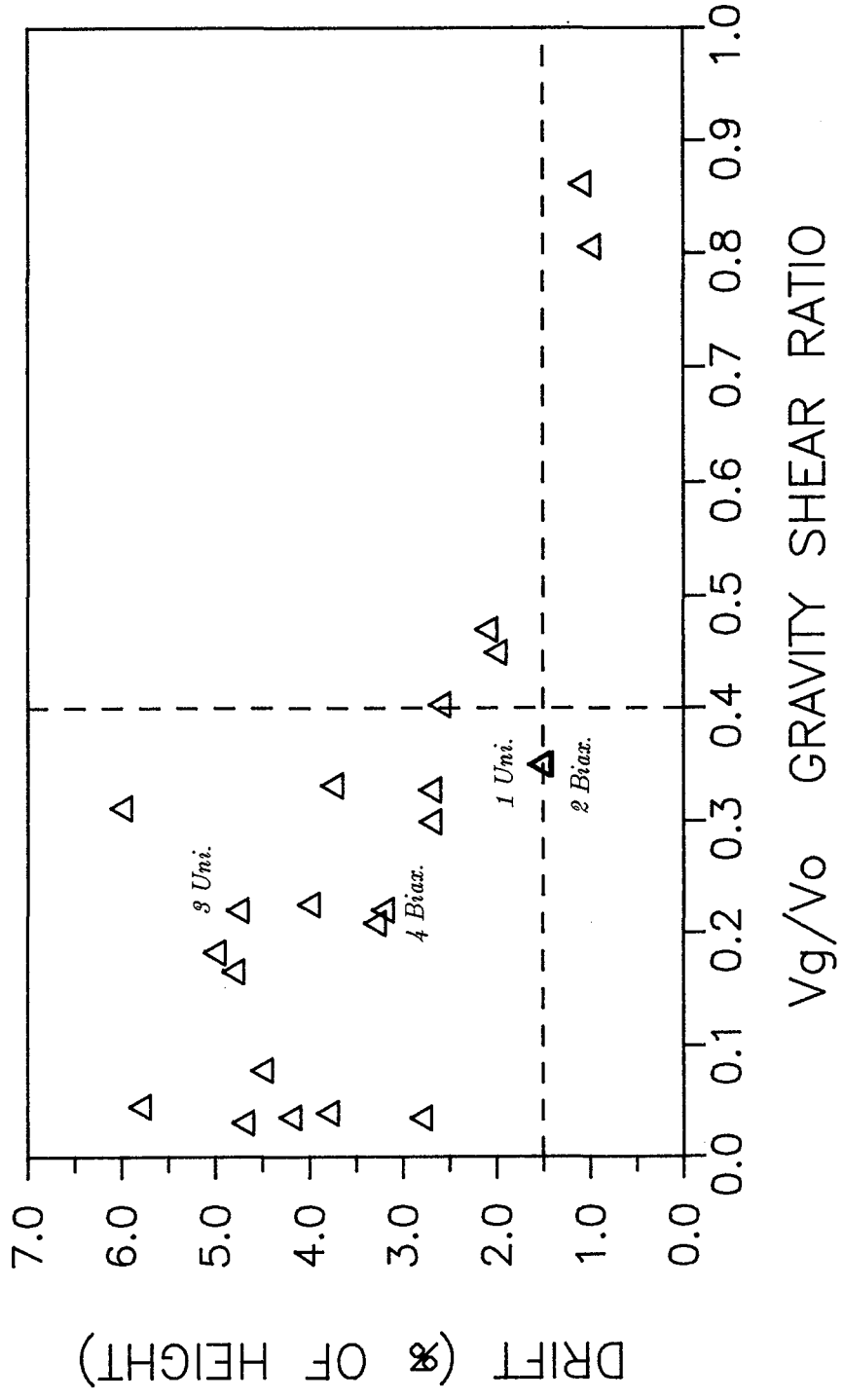


Fig. 7.5 Effect of Gravity Load on Drift

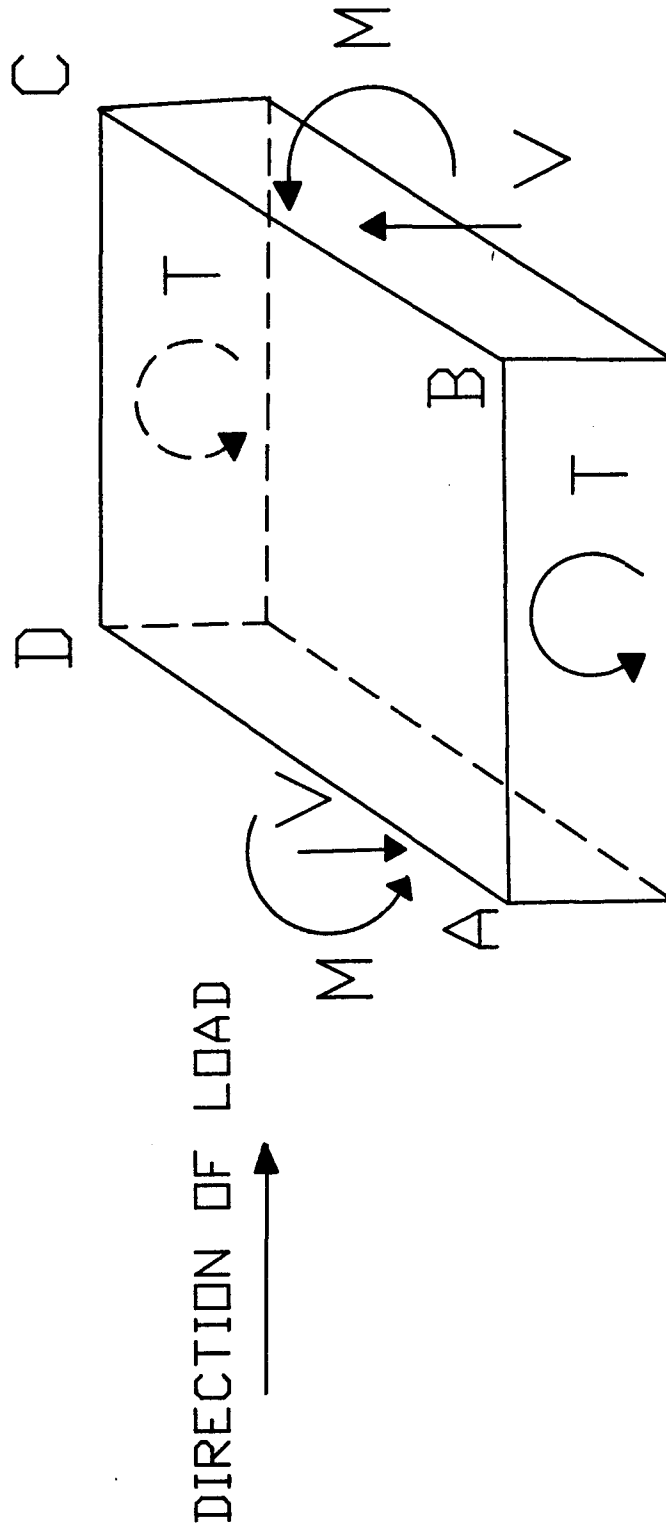


Fig. 7.6 Forces on Connection under Uniaxial Loading

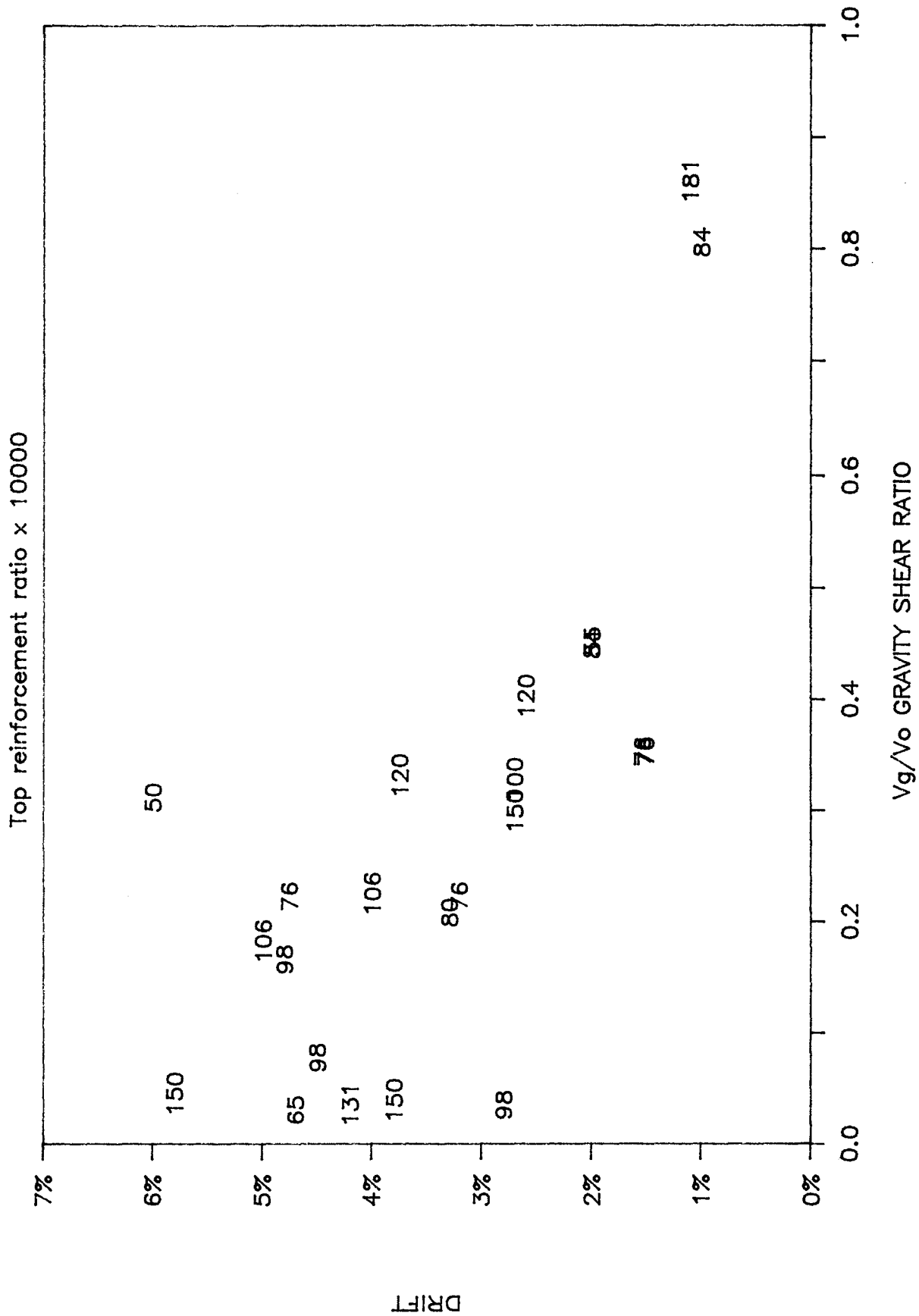


Fig. 7.7 (a) Effect of Top Reinforcement Ratio on Drift

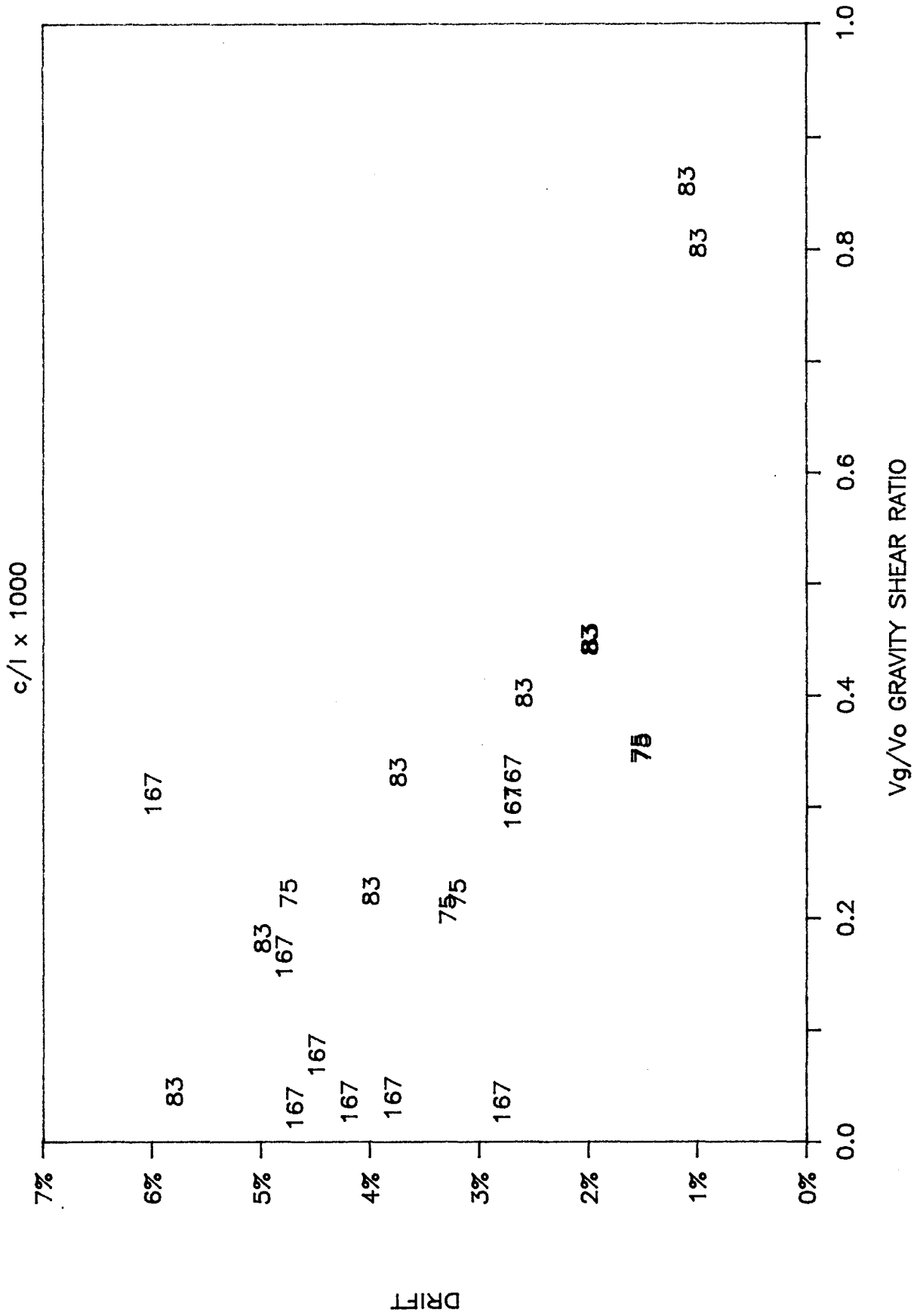


Fig. 7.7 (b) Effect of Column Size to Span Length Ratio on Drift

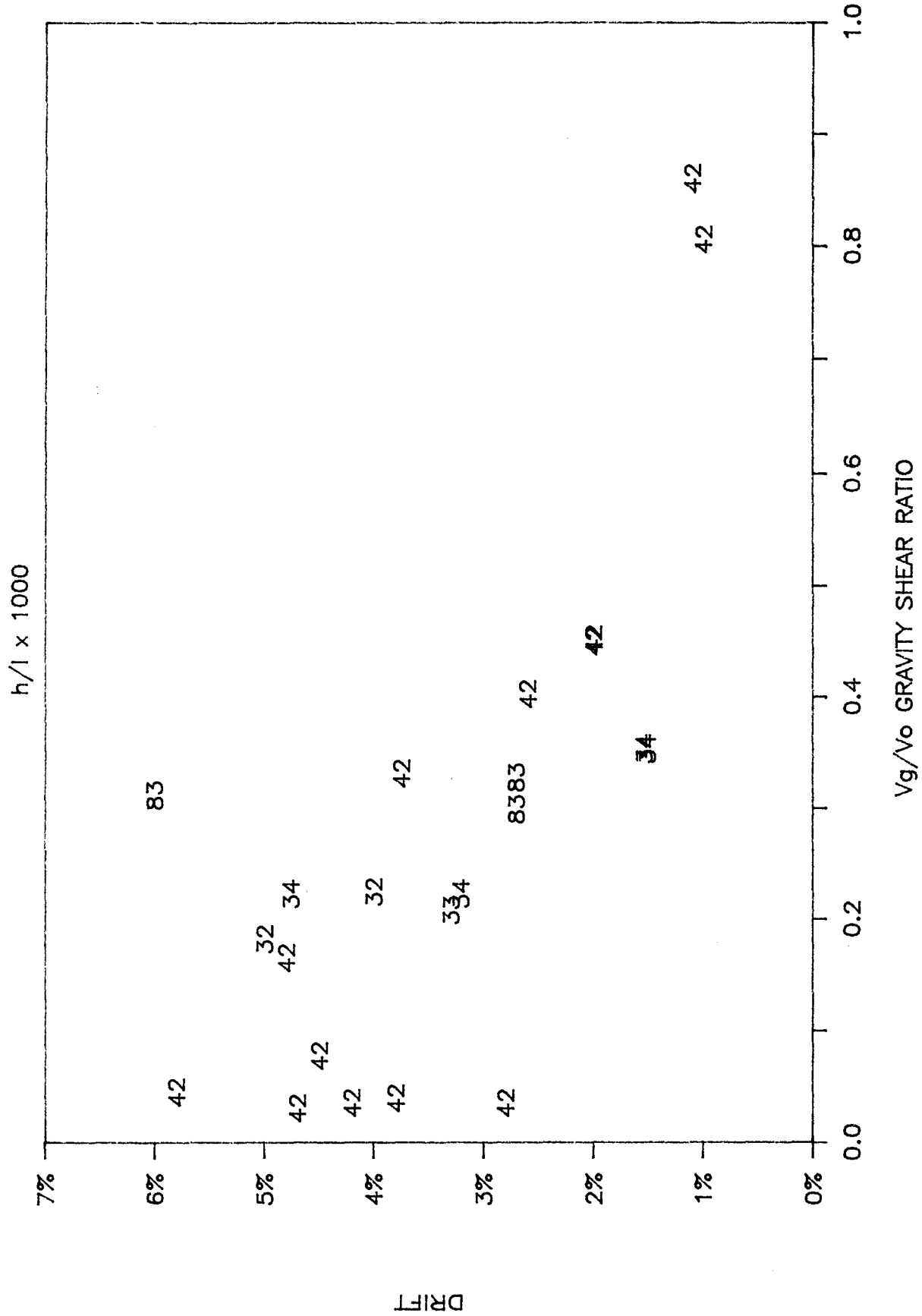


Fig. 7.7 (c) Effect of Slab Thickness to Span Length Ratio on Drift

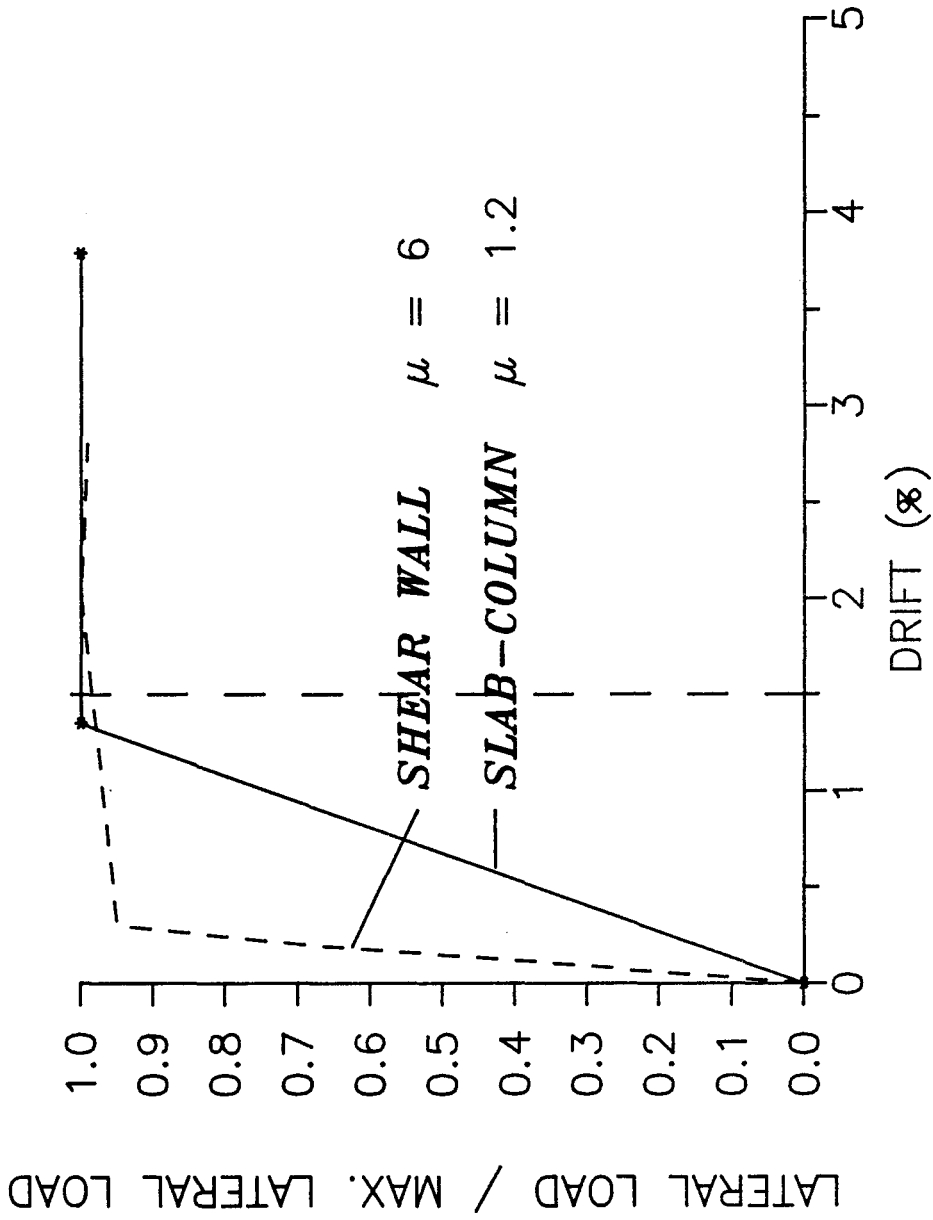


Fig. 7.8 Comparison of Ductility Requirements at 1.5 Percent Drift



Fig. 8.1 A Multistory Building With Flat-Slab Construction

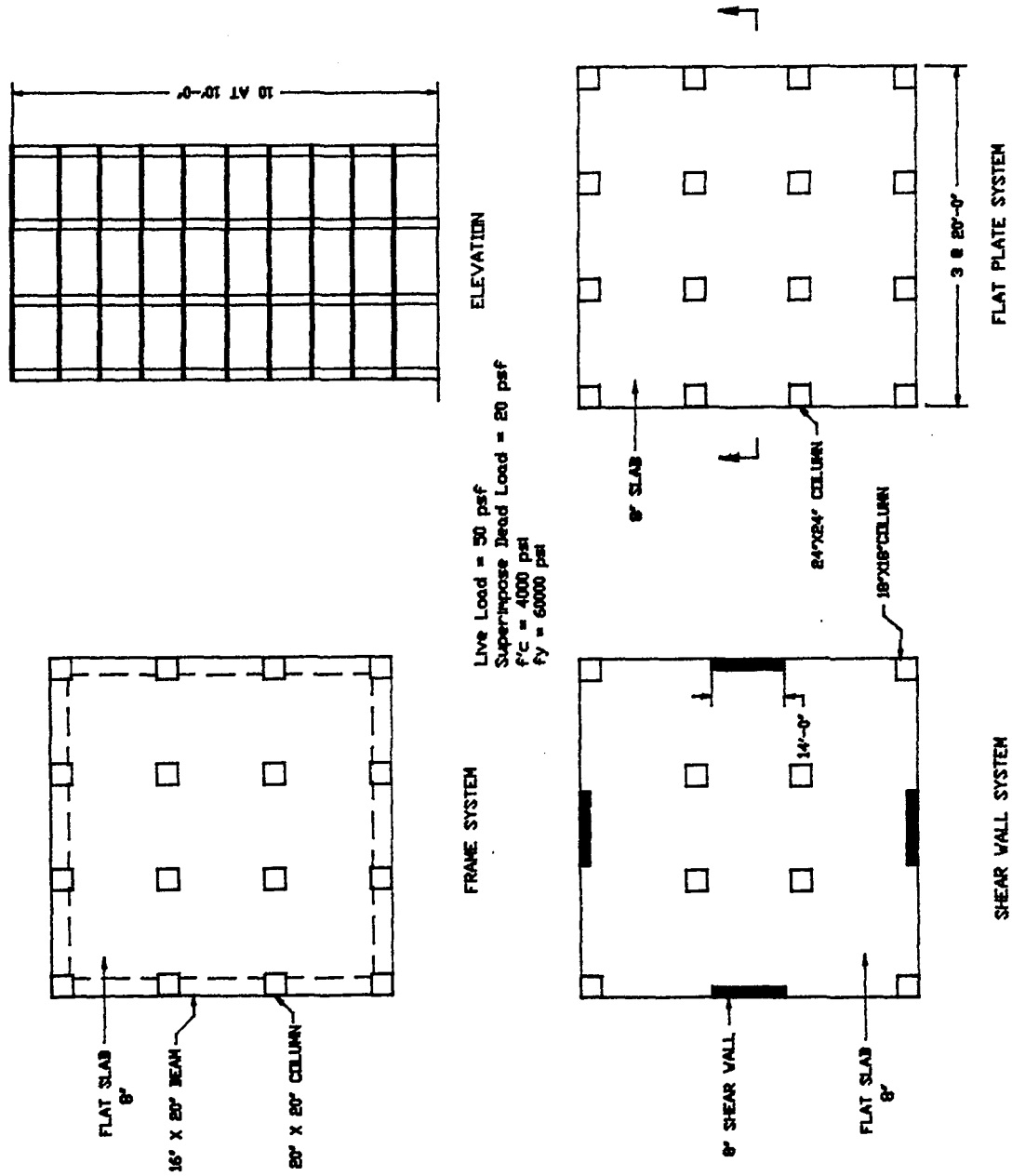
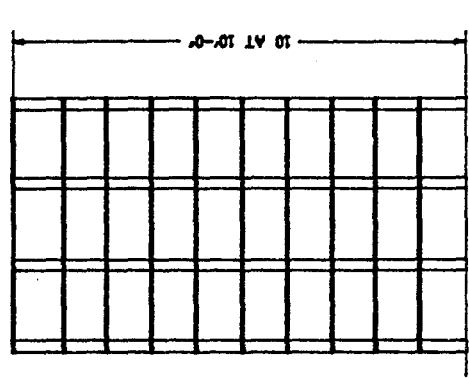
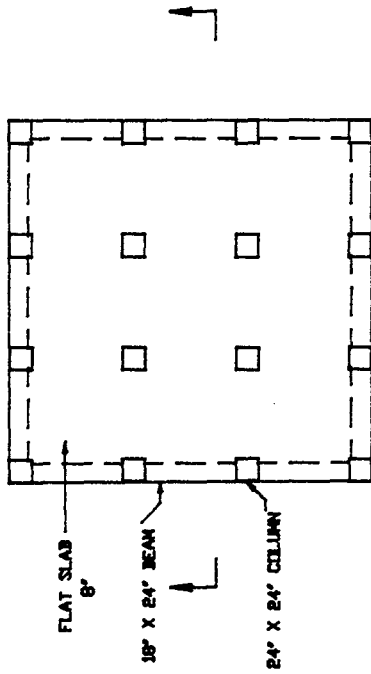


Fig. 8.2 (a) Generic Buildings in UBC Zone No. 2

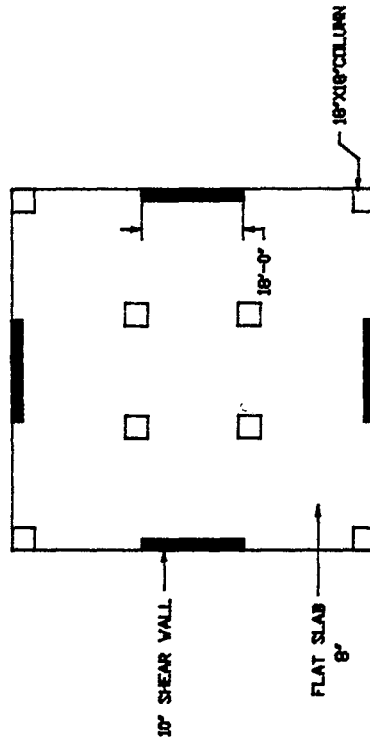


ELEVATION

Live Load = 50 psf
Superimpose Dead Load = 20 psf
f'c = 4000 psi
fy = 60000 psi

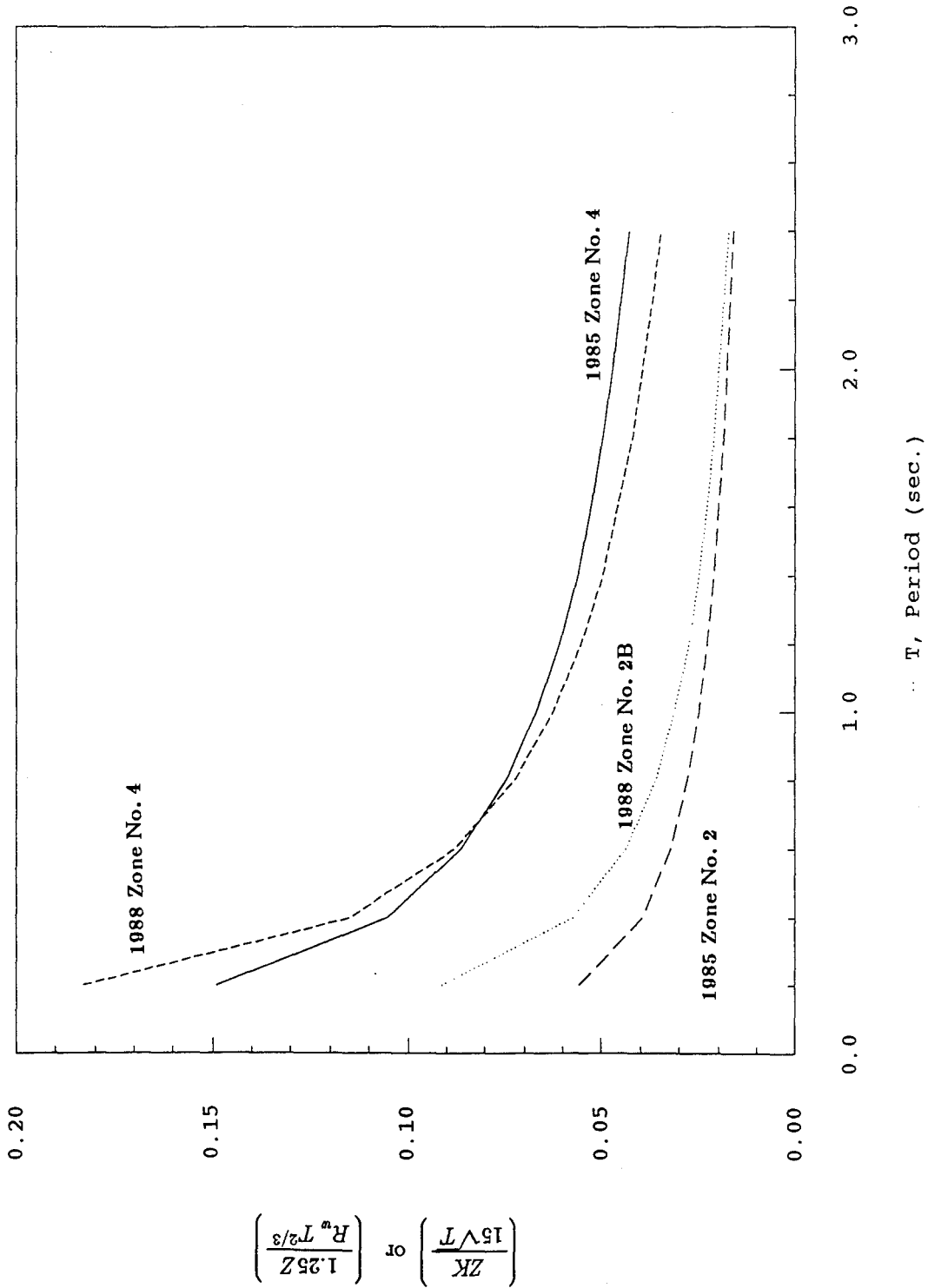


FRAME SYSTEM



SHEAR WALL SYSTEM

Fig. 8.2 (b) Generic Buildings in UBC Zone No. 4



1985 Code:

$$V = ZIKCSW = \left(\frac{ZK}{15\sqrt{T}} \right) ISW$$

$K=1.0$

$Z=1.0$ for Zone No. 4;

$Z=3/8$ for Zone No. 2

1988 Code :

$$V = \frac{ZIC}{R_w} W = \left(\frac{1.25Z}{R_w T^{2/3}} \right) ISW$$

$R_w=8$

$Z=0.4$ for Zone No. 4;

$Z=0.2$ for Zone No. 2B

Fig. 8.2 (c) Comparison Between 1985 and 1988 UBC Seismic Provisions

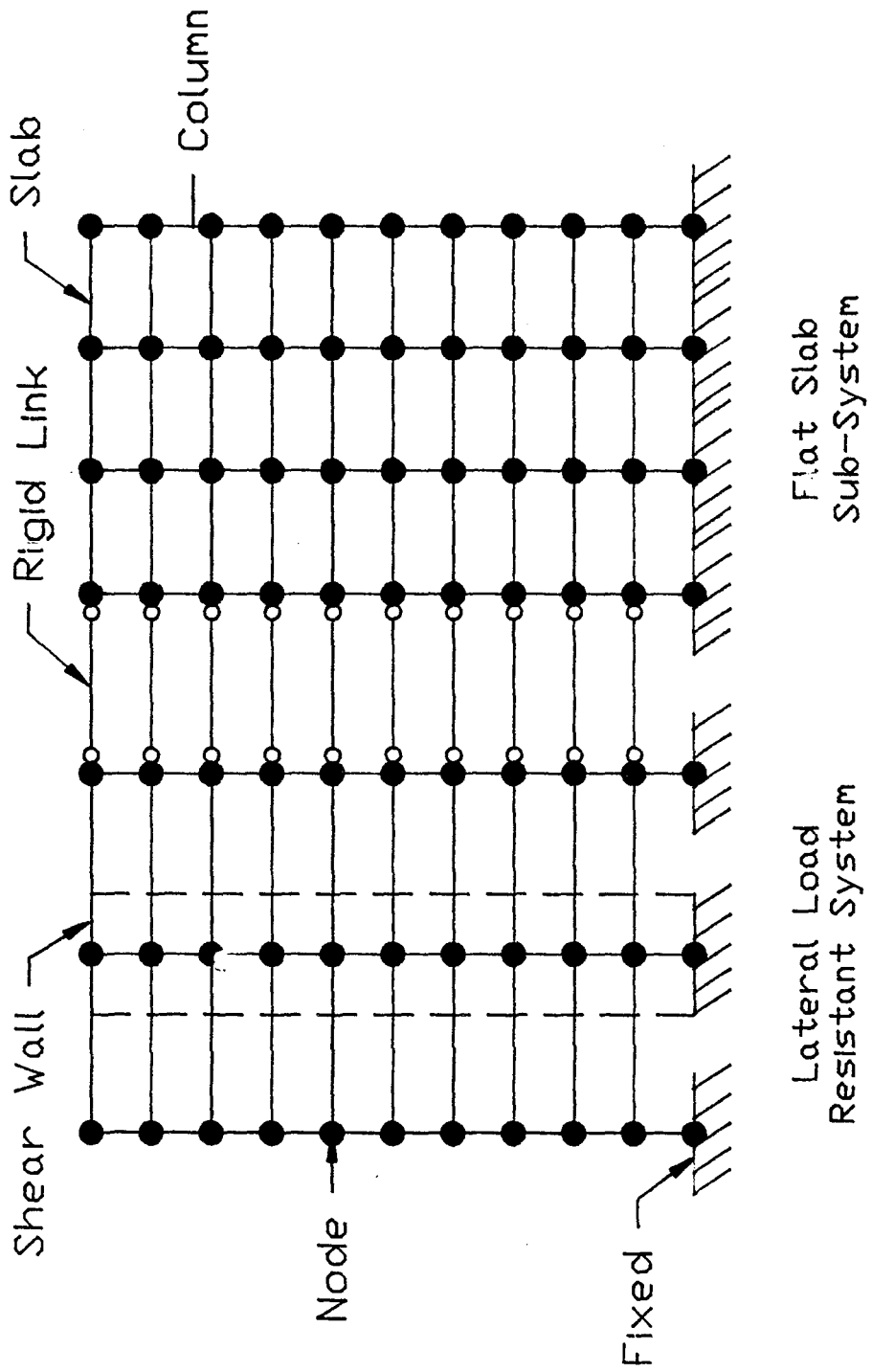
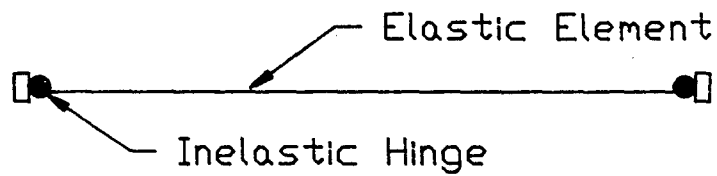
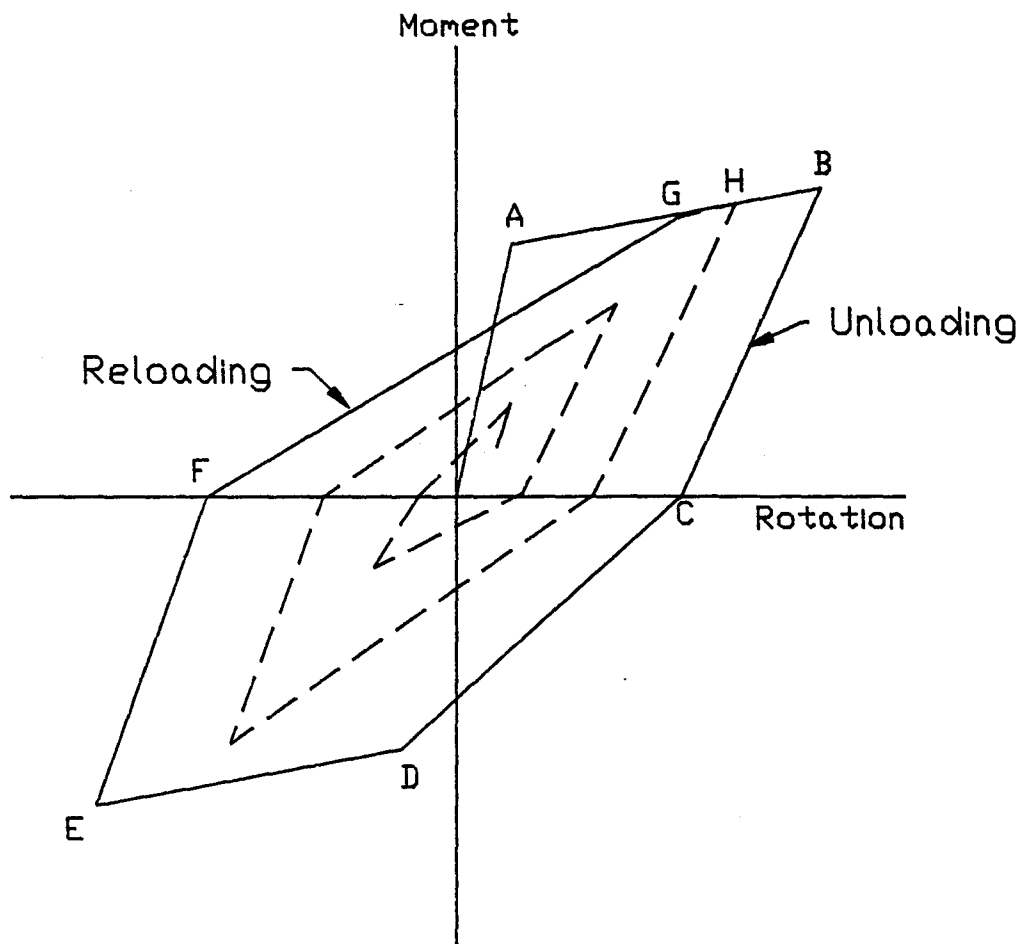


Fig. 8.3 Computer Model of Shear Wall Building



Element Idealization



Hinge Moment-Rotation Relationship

Fig. 8.4 (a) Simplified Takeda Model with Degrading Stiffness

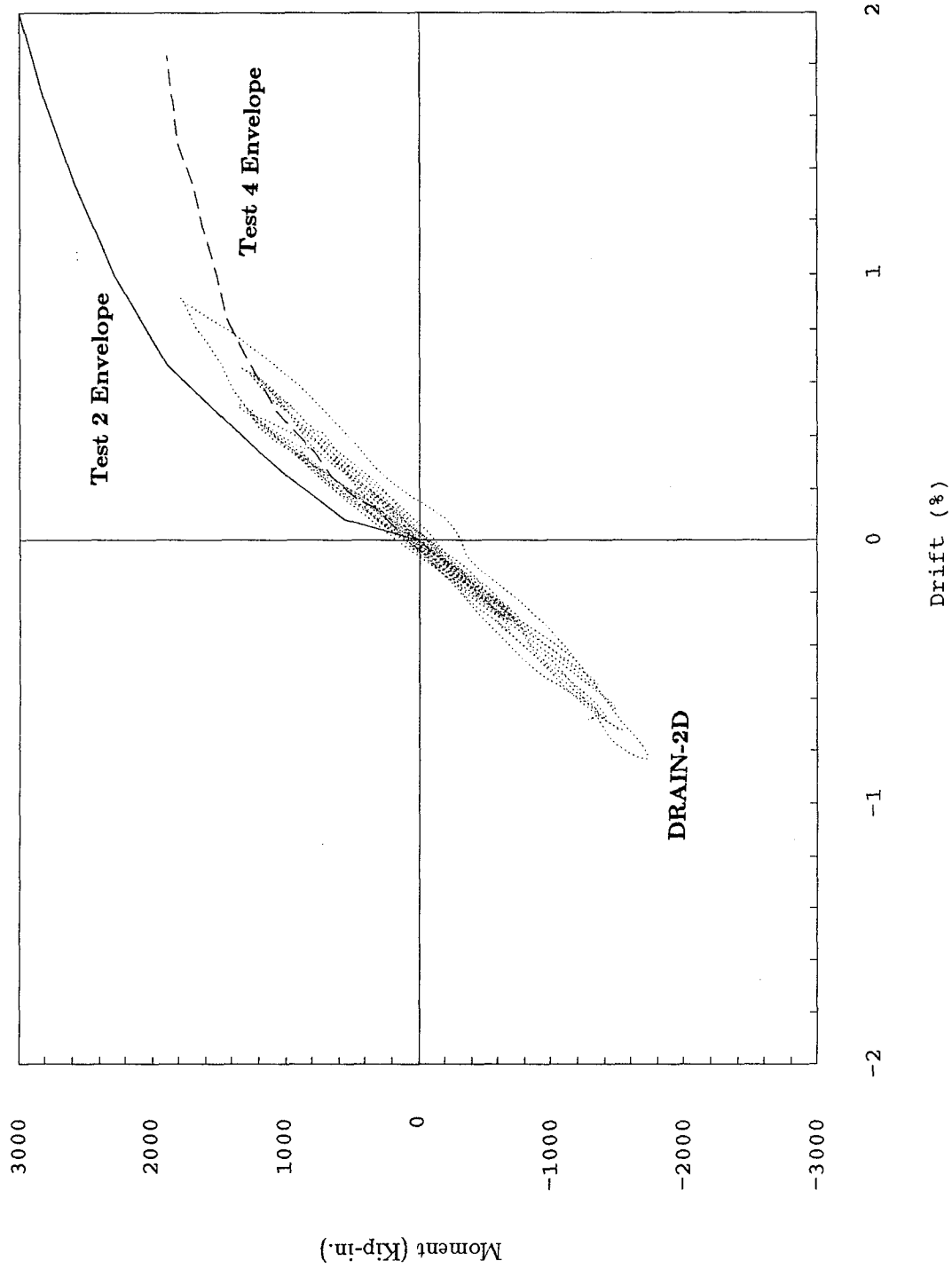
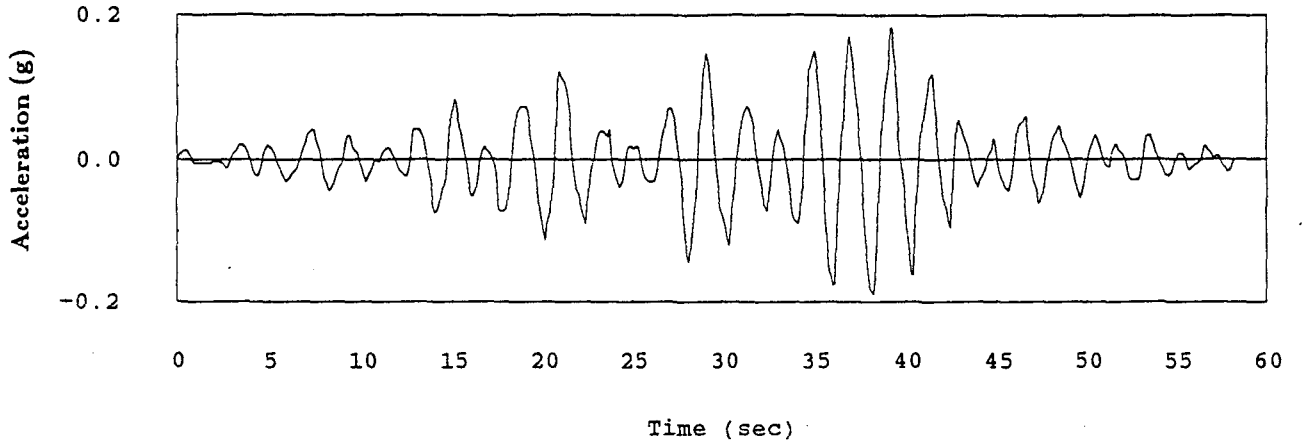
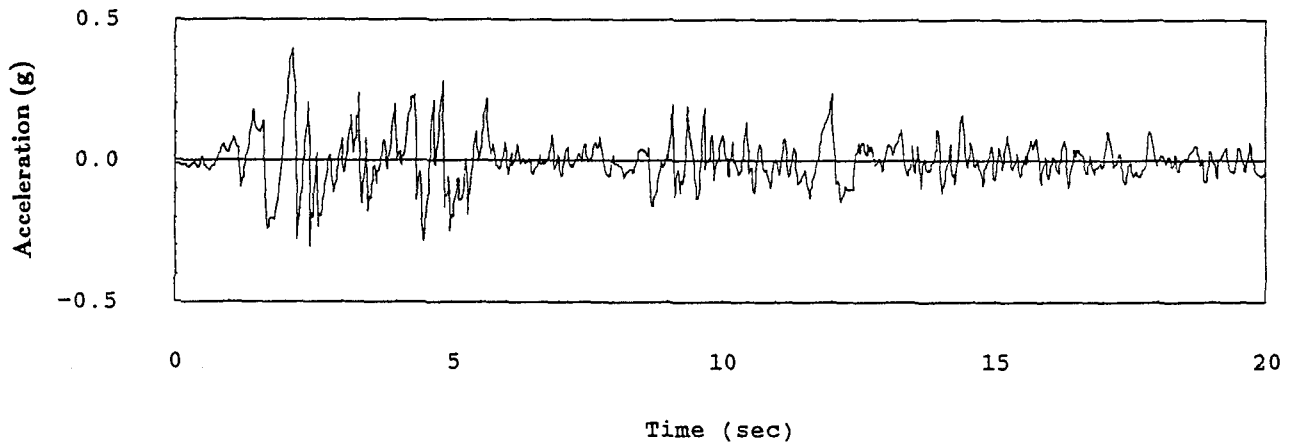


Fig. 8.4 (b) Total Slab Connection Moment vs Interstory Drift - El Centro
(Fifth Story (Interior), Shear Wall Building - UBC Zone No. 4)

Mexico Ground Acceleration History



El Centro (0.4g) Ground Acceleration History



Taft (0.4g) Ground Acceleration History

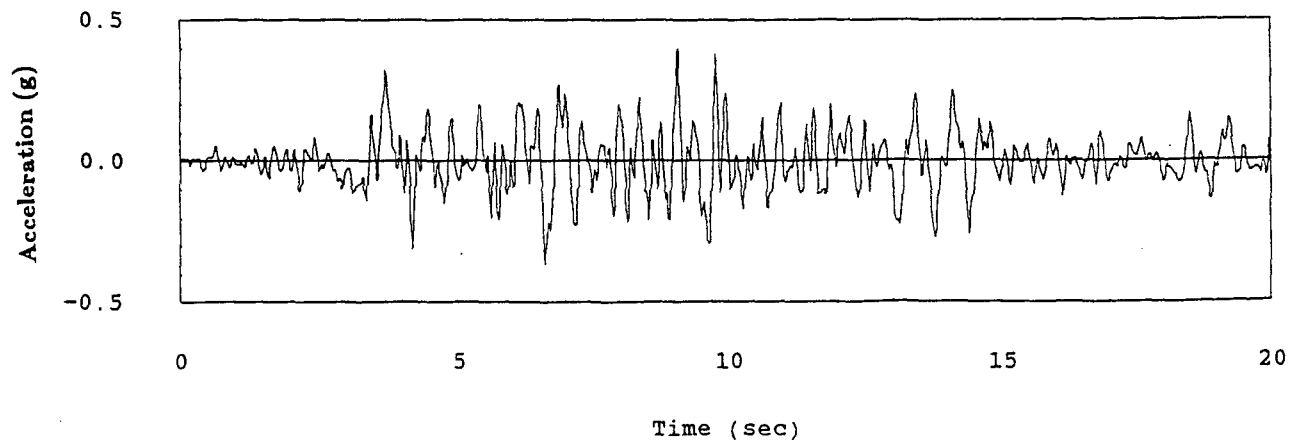


Fig. 8.5 Records of Ground Motion

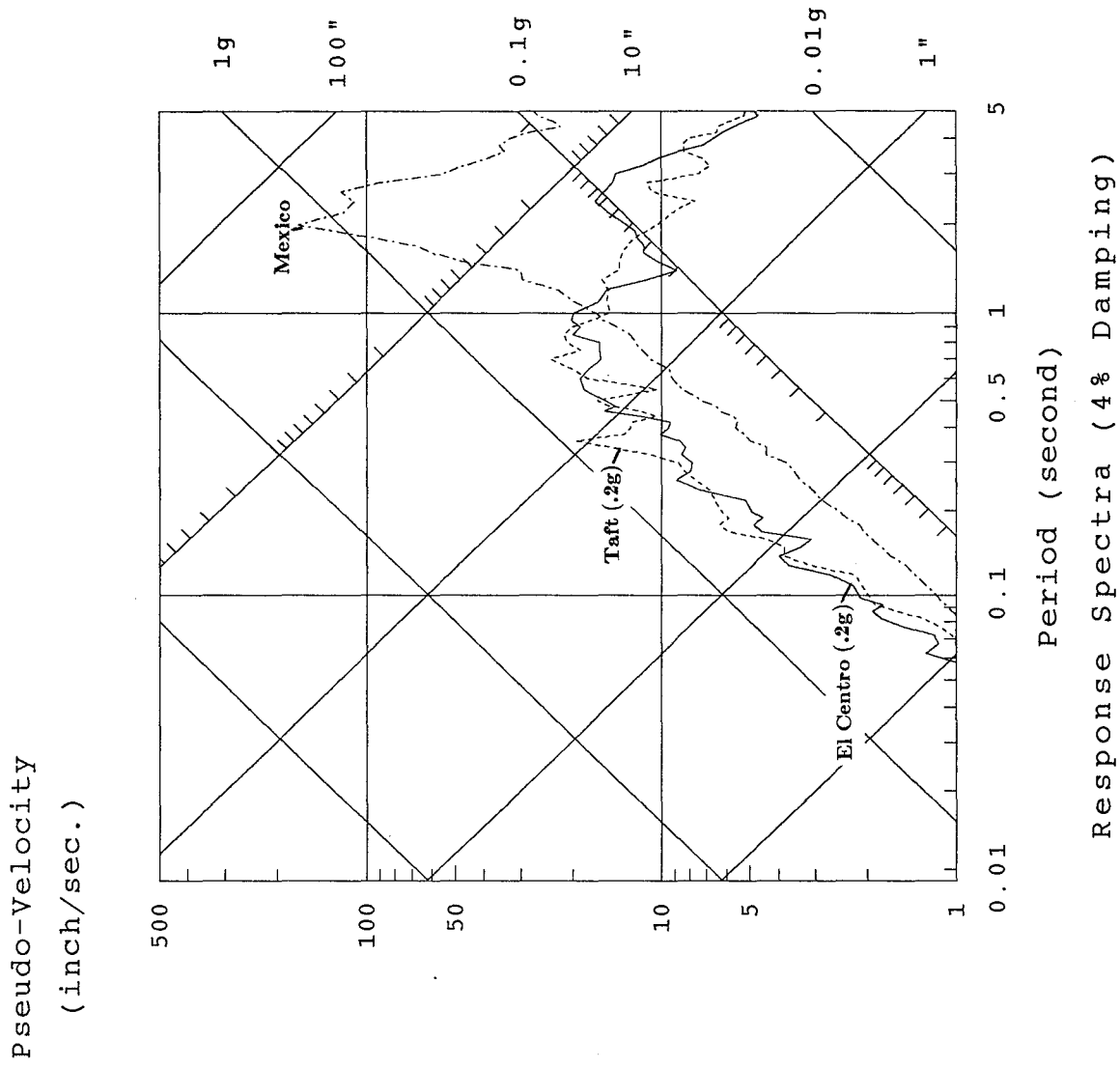


Fig. 8.6 (a) Elastic Response Spectra (UBC Zone No. 2)

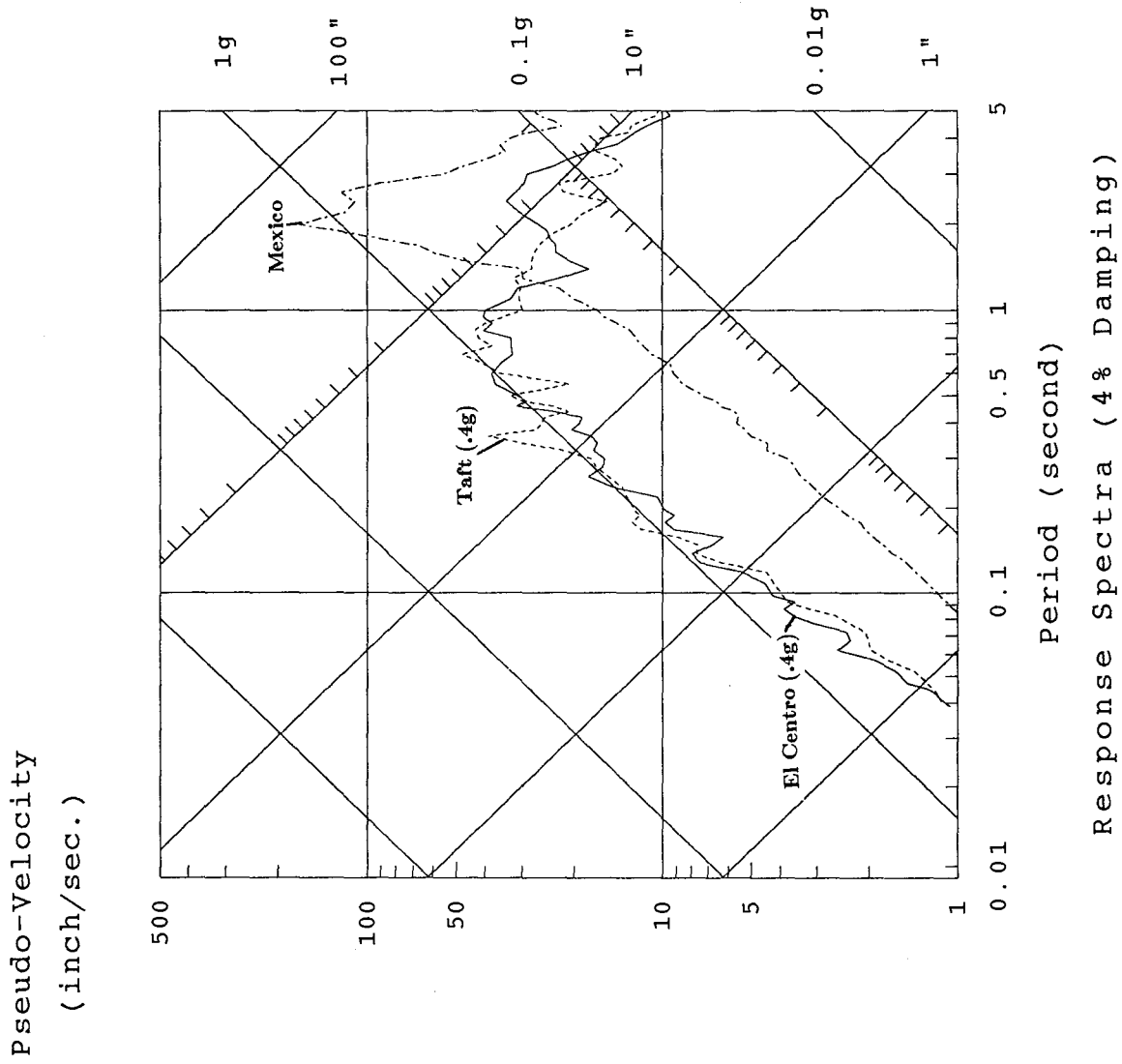
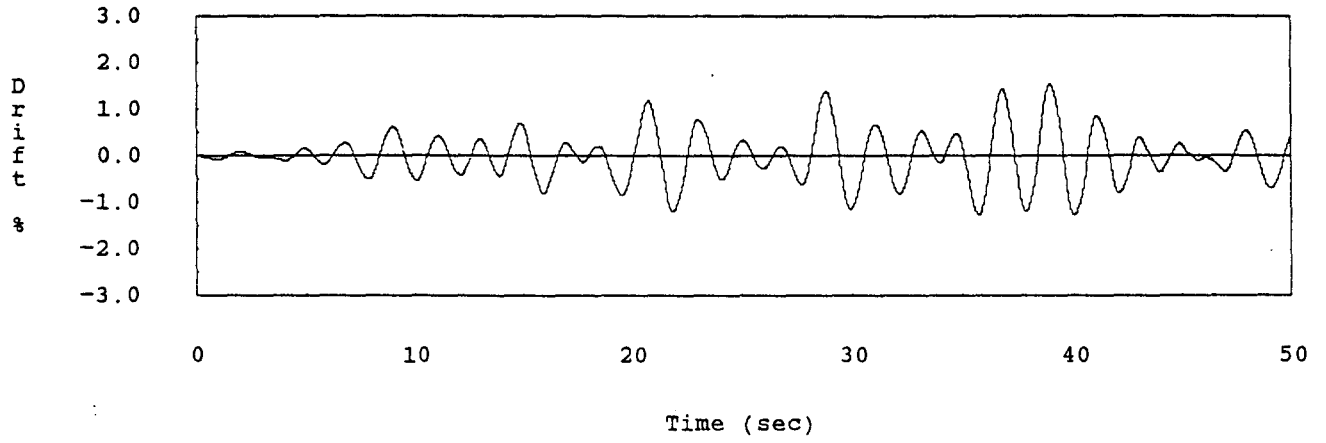
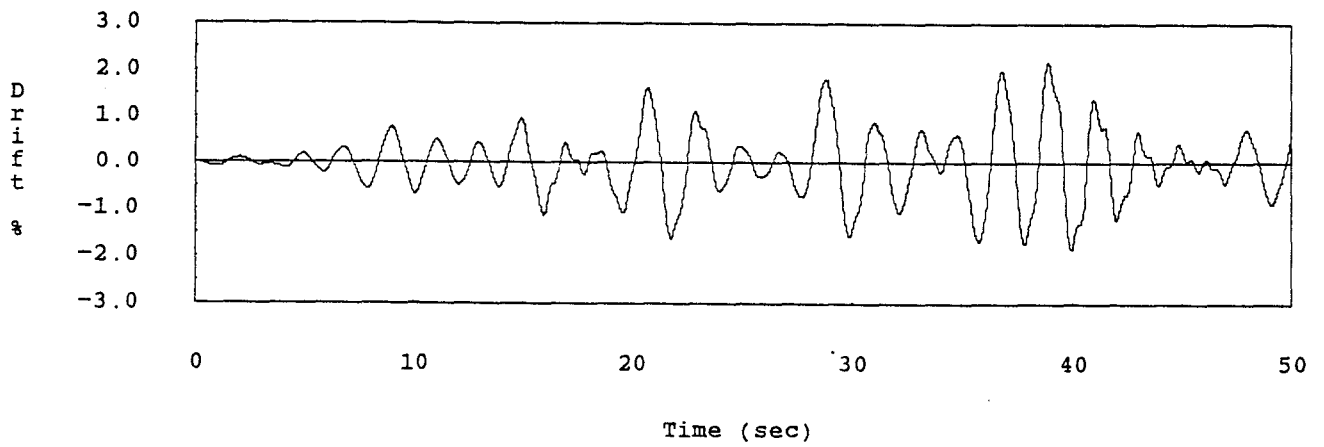


Fig. 8.6 (b) Elastic Response Spectra (UBC Zone No. 4)

(a) Total Building Drift History



(b) Ninth Interstory Drift History



(c) Second Interstory Drift History

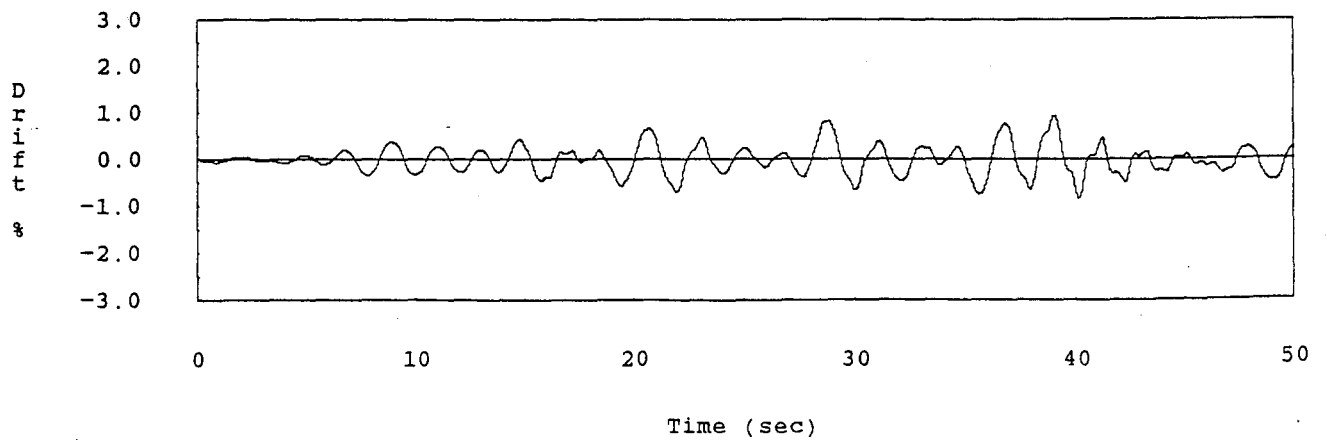
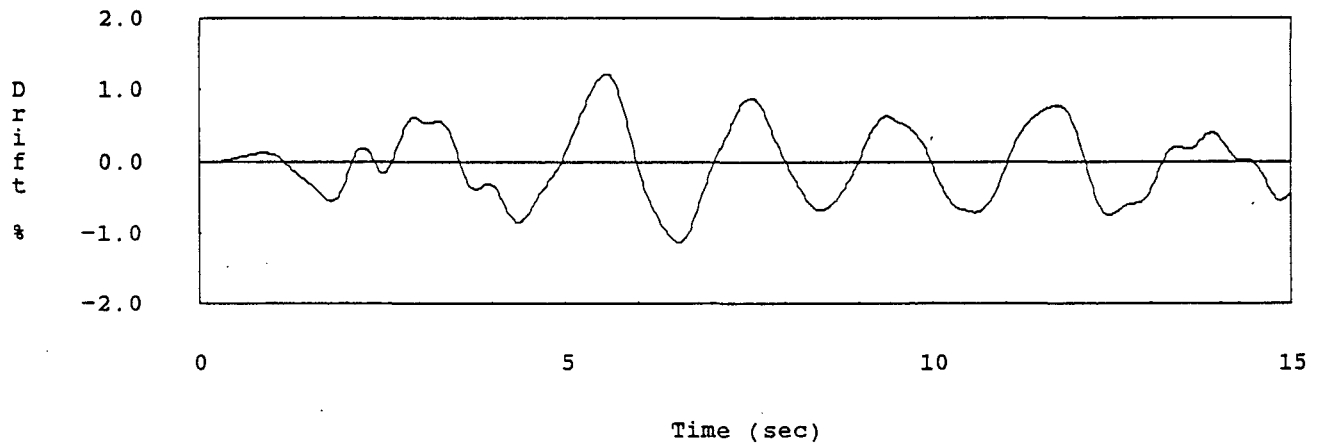
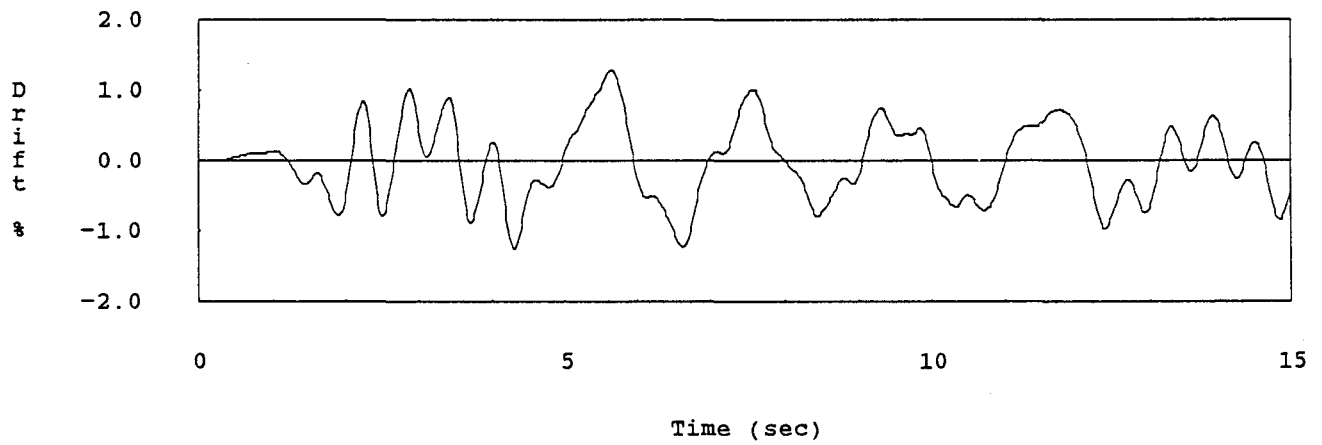


Fig. 8.7 (a) Response of Shear Wall Building (UBC Zone No. 2) - Mexico City Record

(a) Total Building Drift History



(b) Ninth Interstory Drift History



(c) Second Interstory Drift History

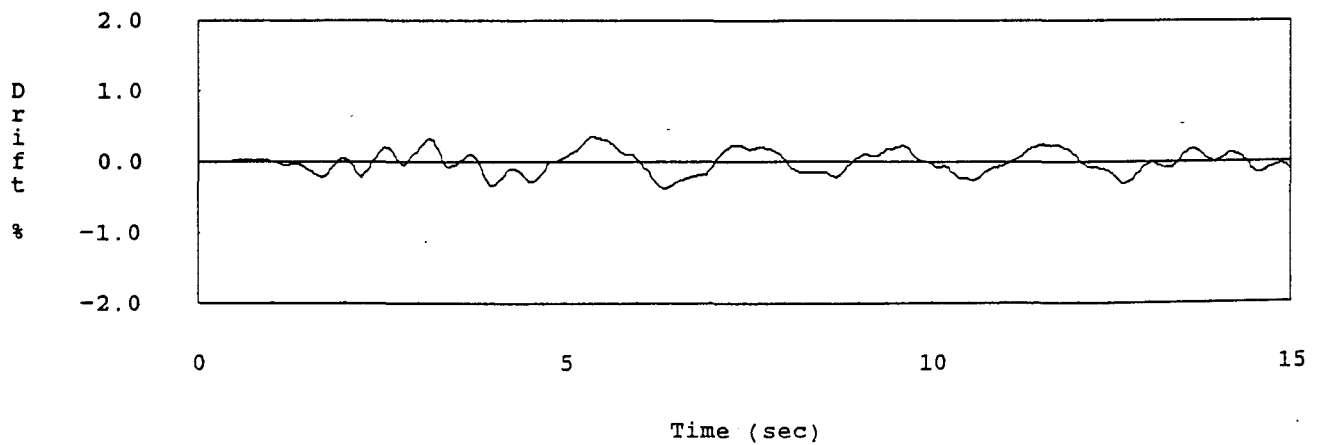
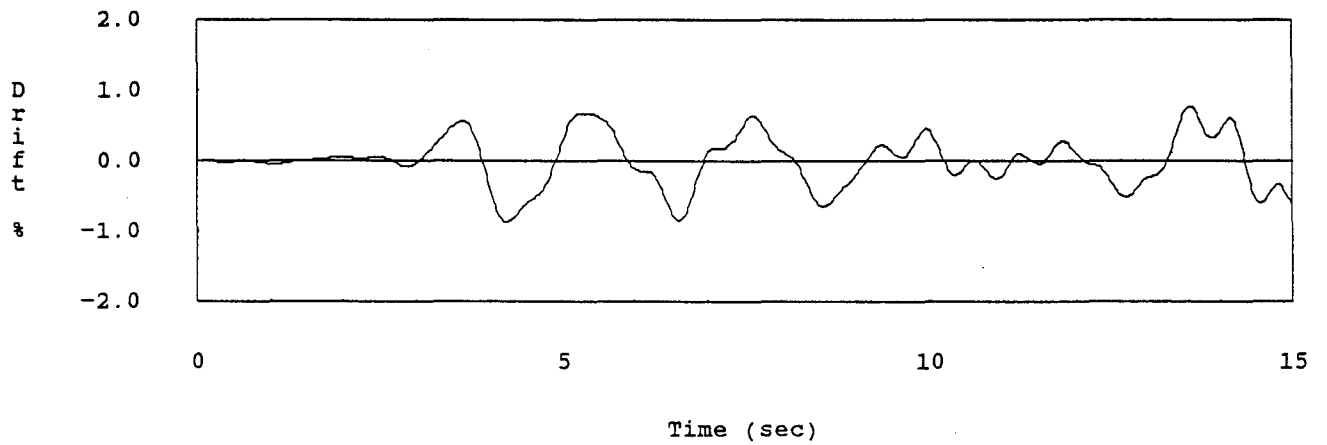
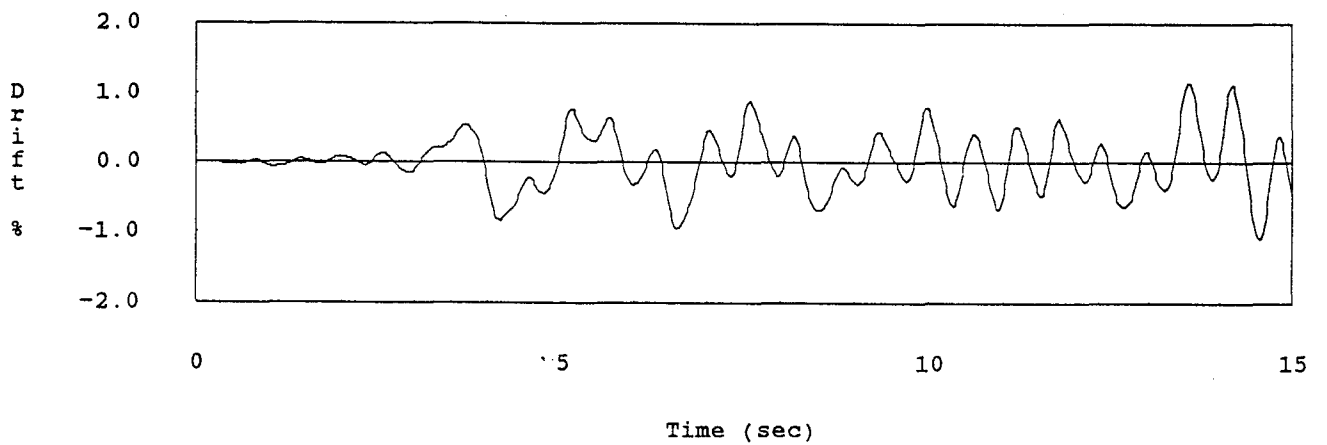


Fig. 8.7 (b) Response of Shear Wall Building (UBC Zone No. 2) - 0.2g El Centro Record

(a) Total Building Drift History



(b) Ninth Interstory Drift History



(c) Second Interstory Drift History

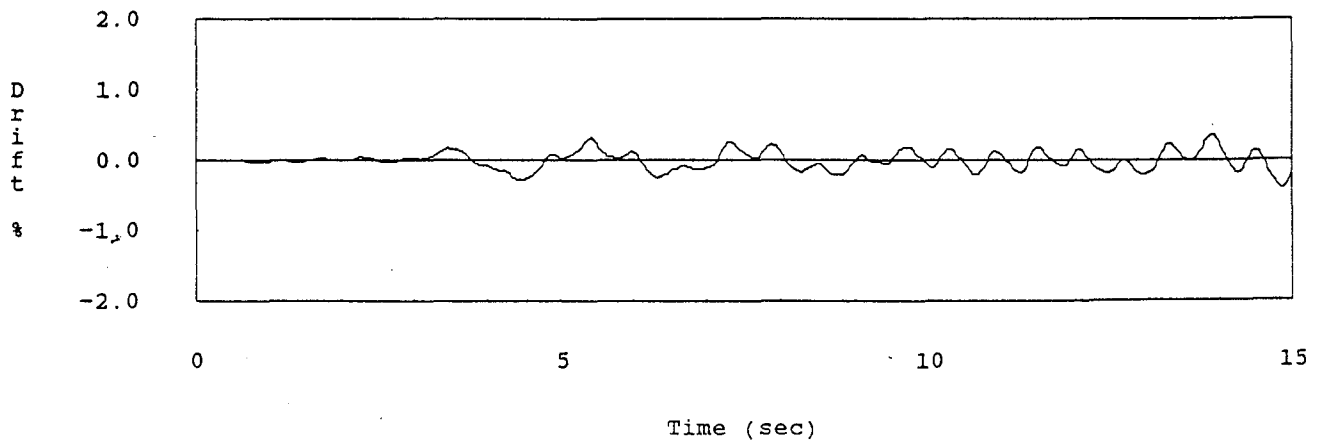
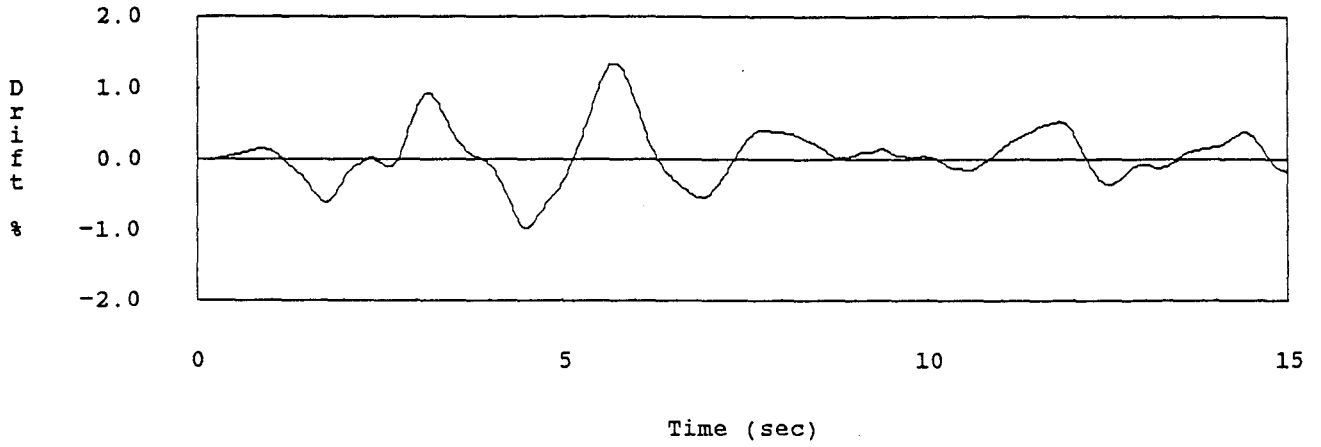
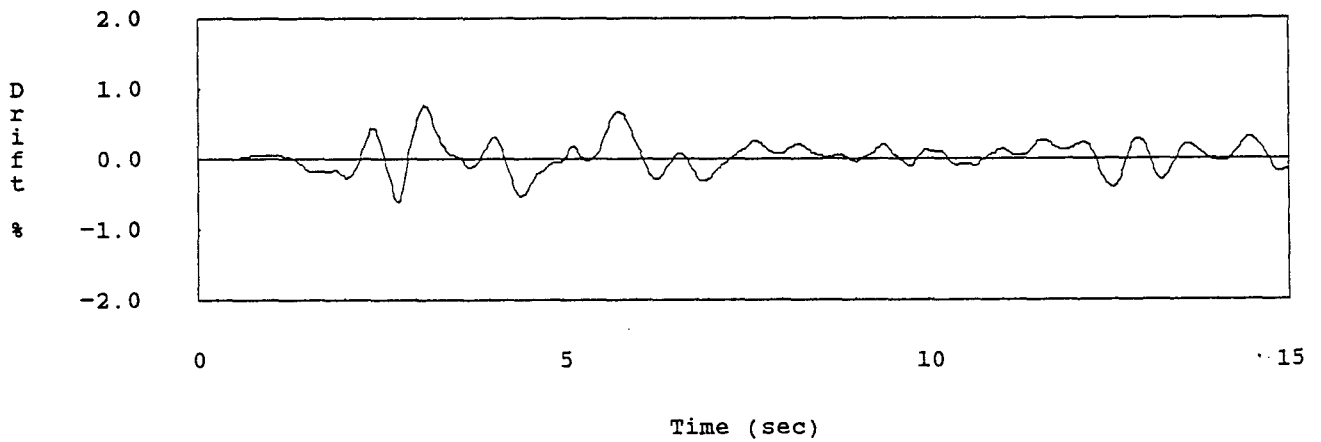


Fig. 8.7 (c) Response of Shear Wall Building (UBC Zone No. 2) - 0.2g Taft Record

(a) Total Building Drift History



(b) Ninth Interstory Drift History



(c) Second Interstory Drift History

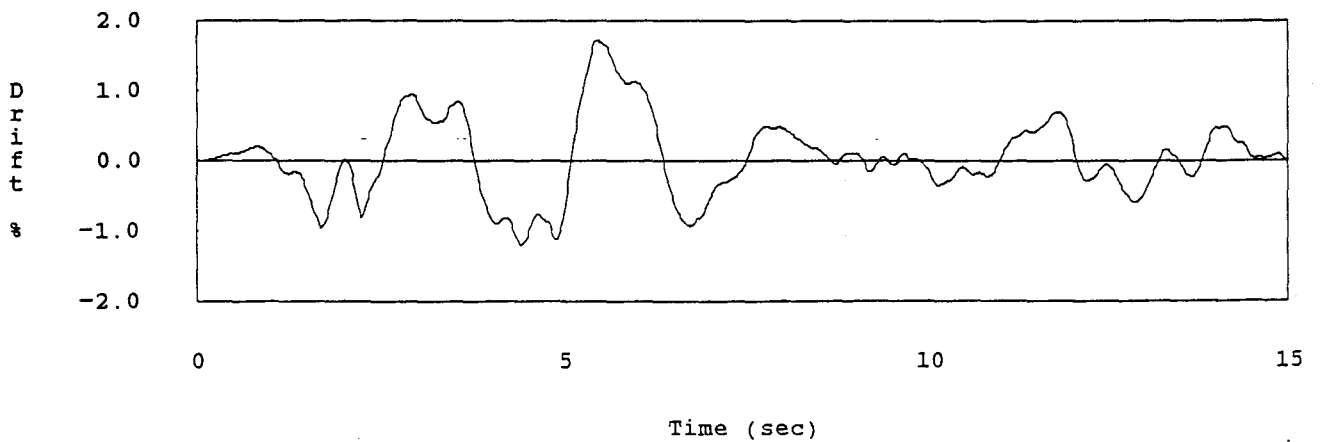
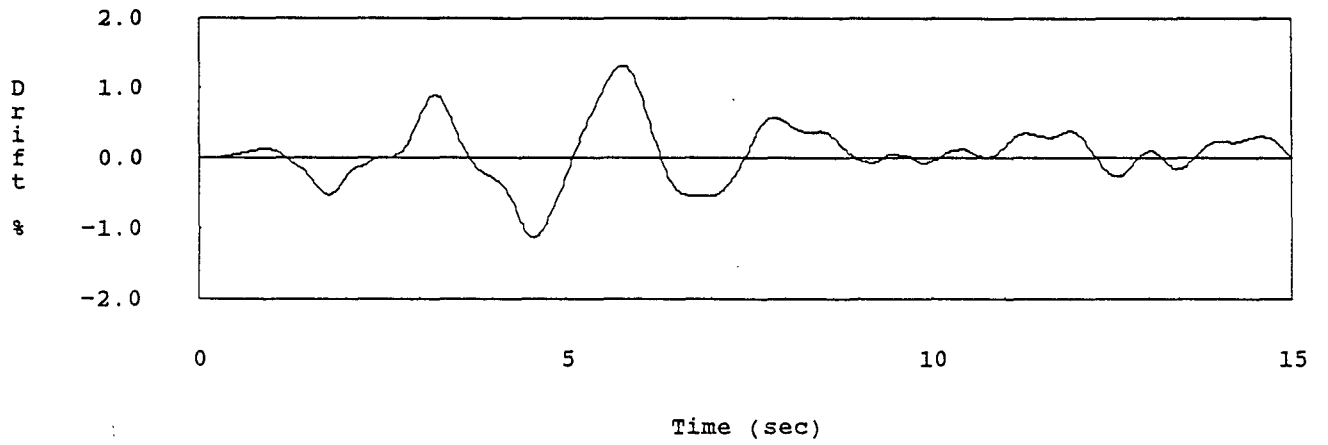
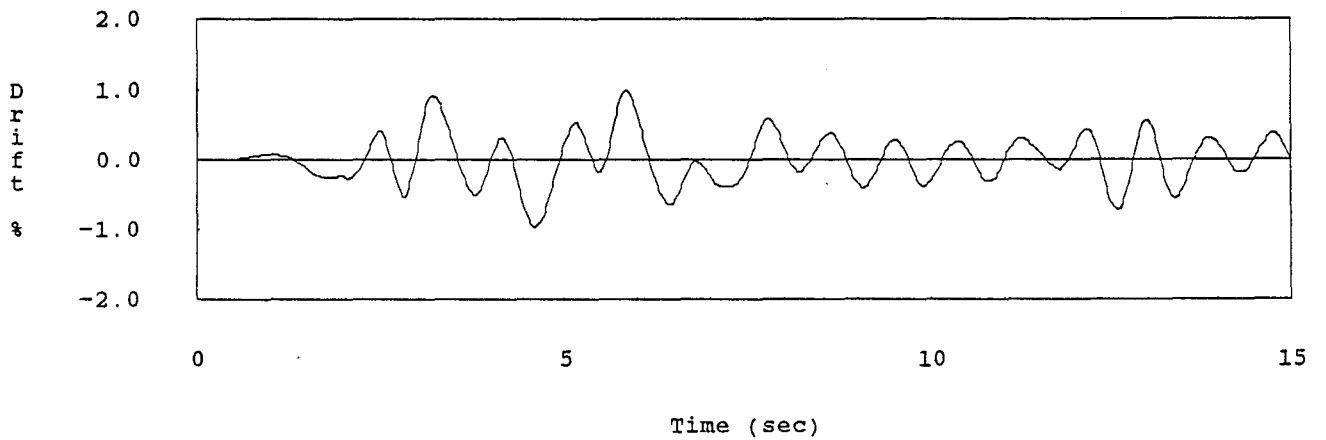


Fig. 8.7 (d) Response of Frame Building (UBC Zone No. 2) - 0.2g El Centro Record

(a) Total Building Drift History



(b) Ninth Interstory Drift History



(c) Second Interstory Drift History

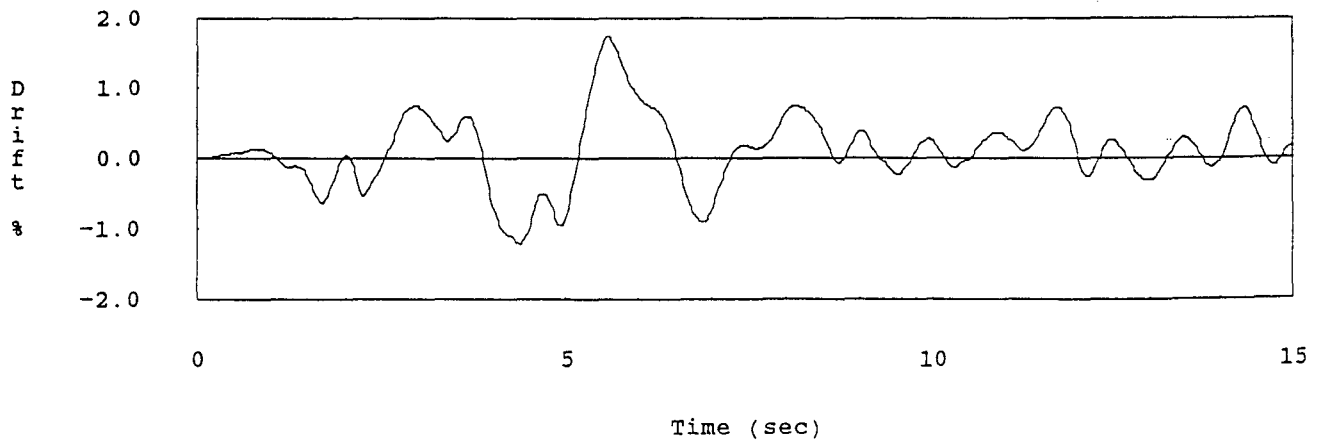
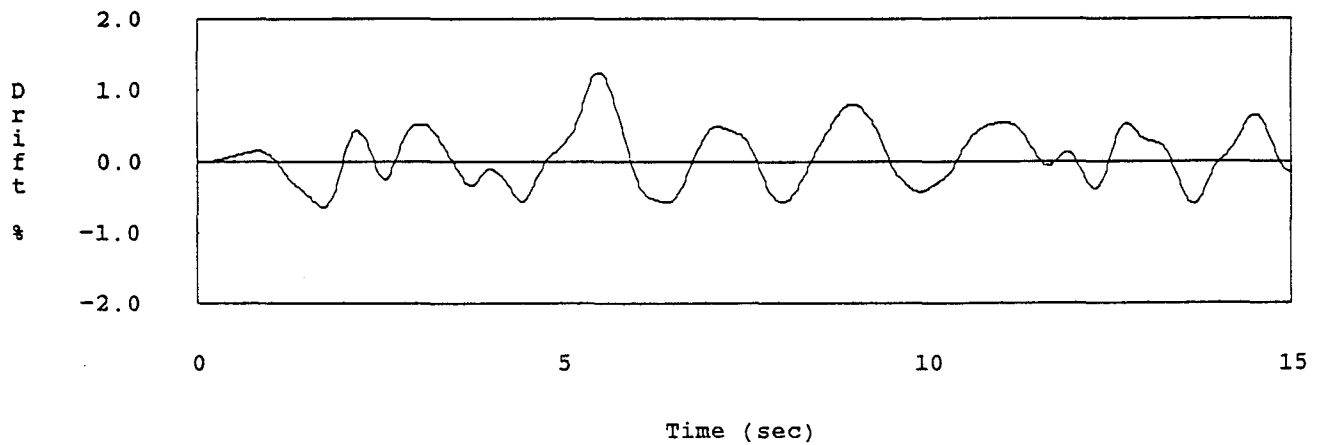
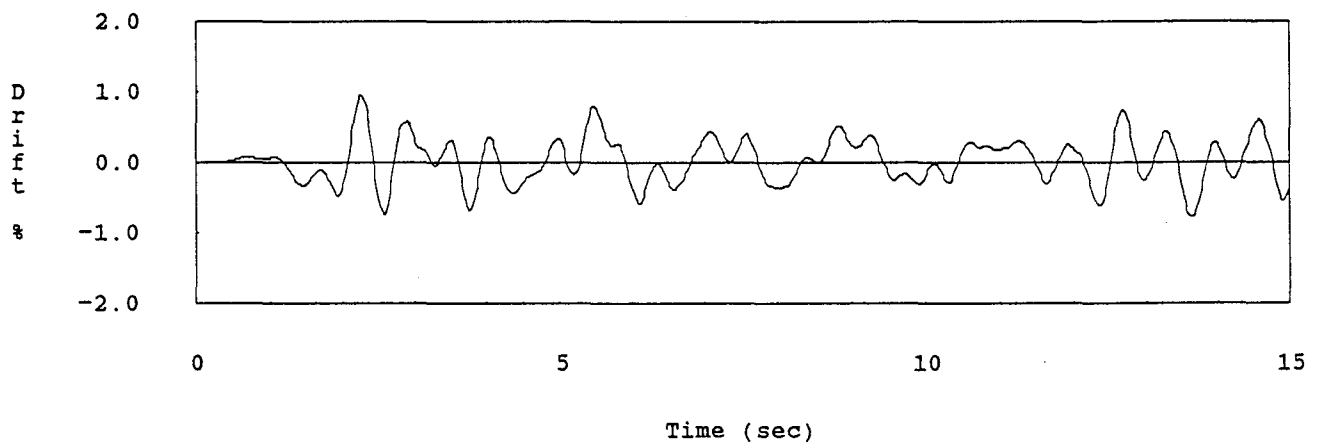


Fig. 8.7 (e) Response of Flat-Plate Building (UBC Zone No. 2) - 0.2g El Centro Record

(a) Total Building Drift History



(b) Ninth Interstory Drift History



(c) Second Interstory Drift History

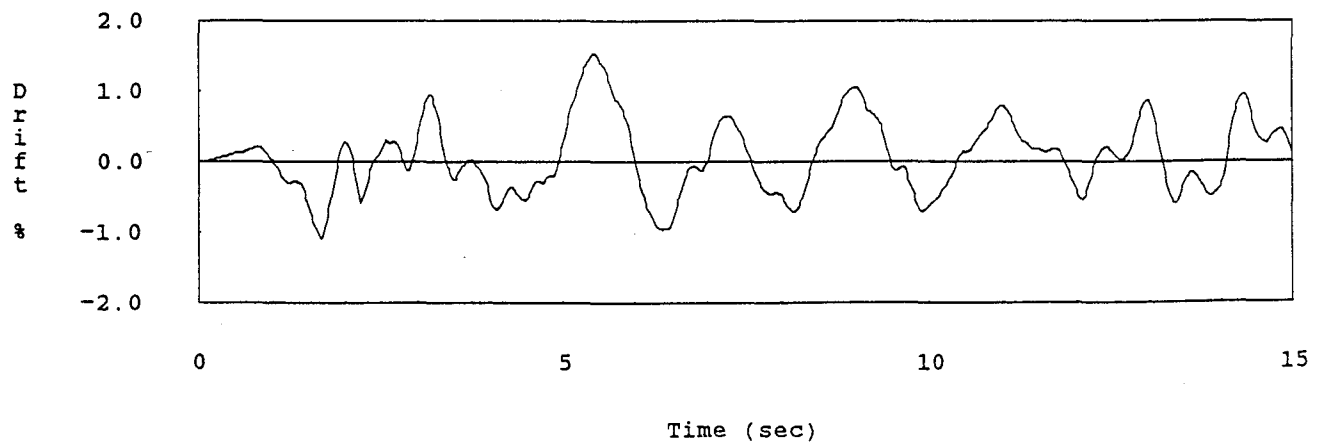
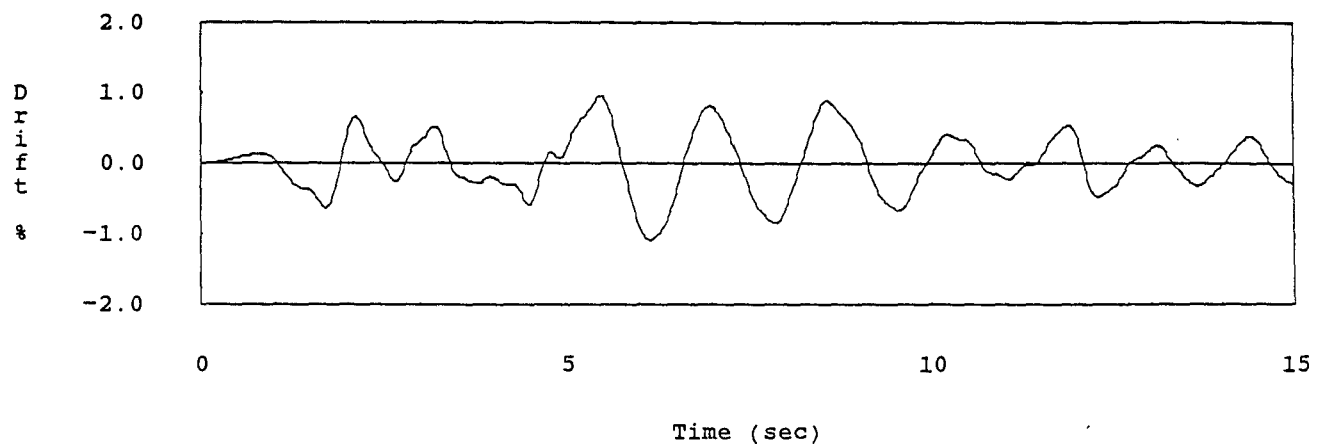
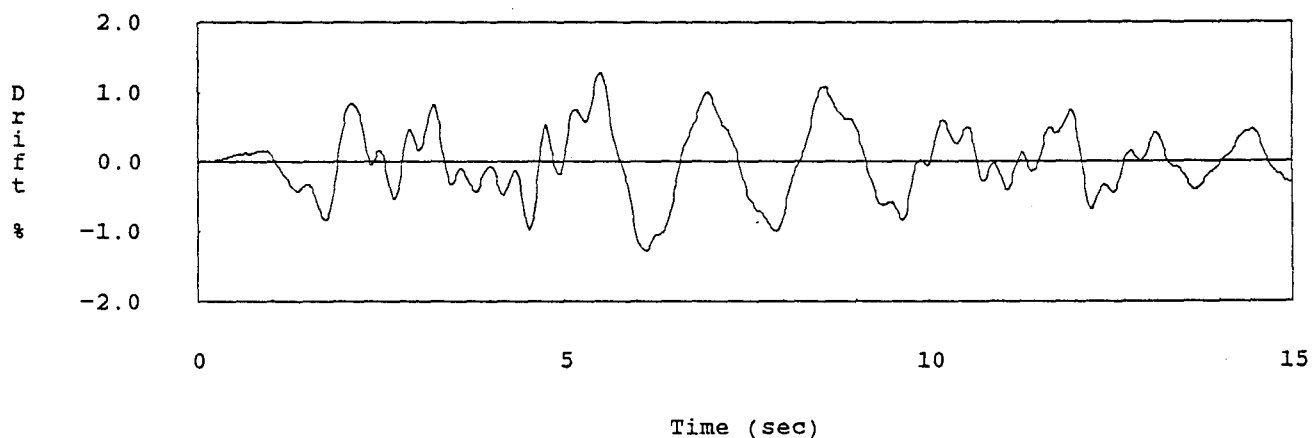


Fig. 8.7 (f) Response of Frame Building (UBC Zone No. 4) - 0.4g El Centro Record

(a) Total Building Drift History



(b) Ninth Interstory Drift History



(c) Second Interstory Drift History

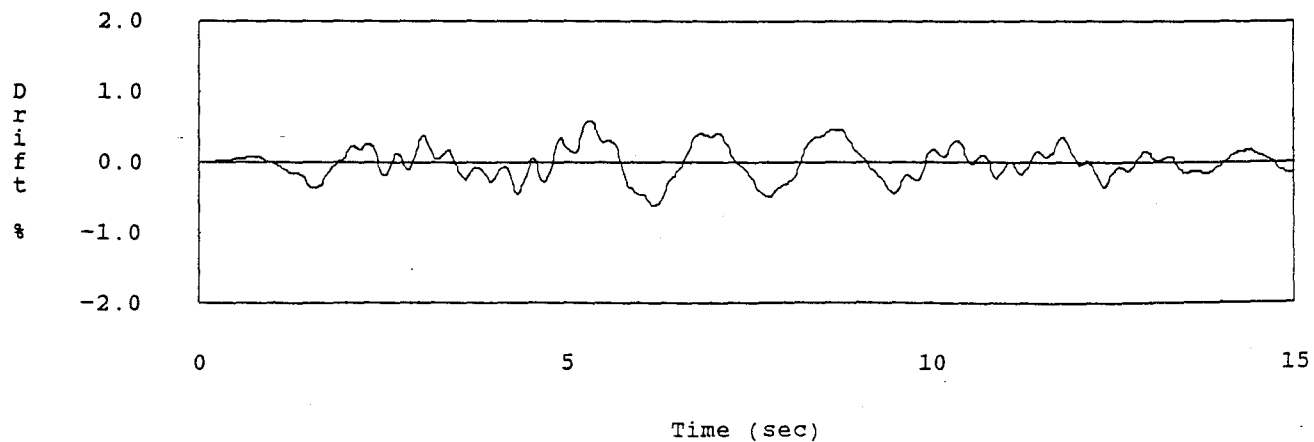


Fig. 8.7 (g) Response of Shear Wall Building (UBC Zone No. 4) - 0.4g El Centro Record

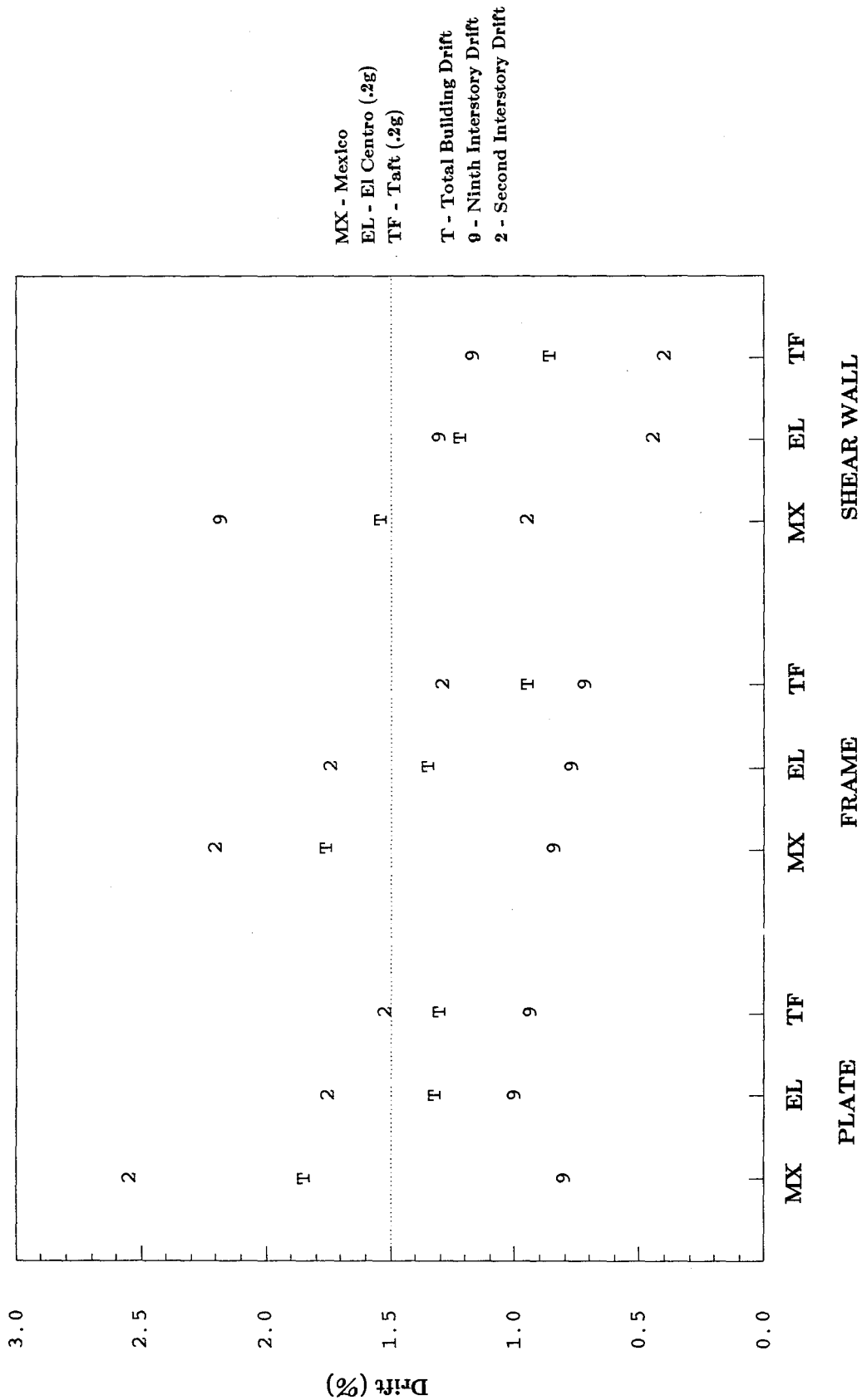
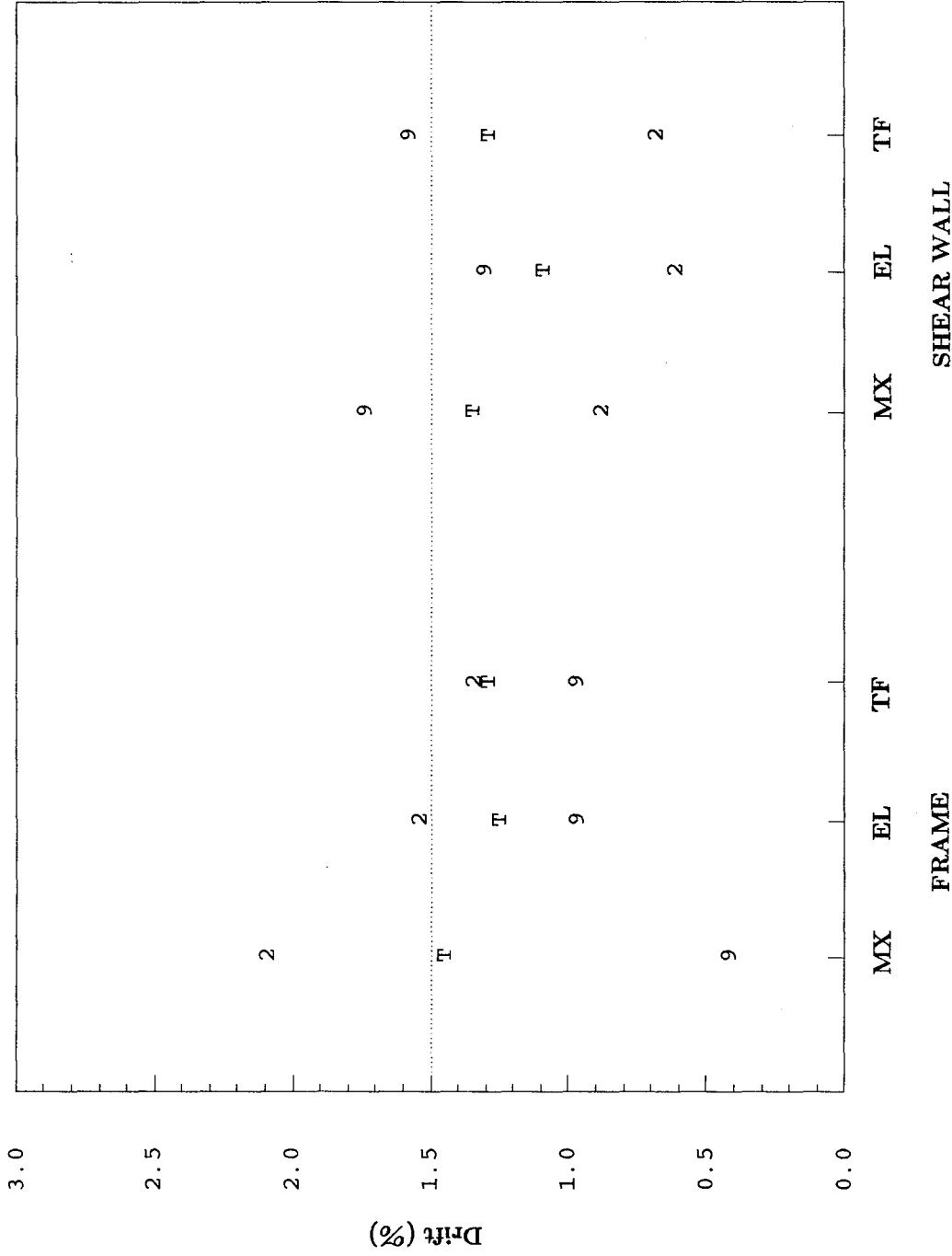


Fig. 8.8 (a) Summary of Maximum Drifts - UBC Zone No. 2 Buildings



MX - Mexico
 EL - El Centro (.4g)
 TF - Taft (.4g)

T - Total Building Drift
 9 - Ninth Interstory Drift
 2 - Second Interstory Drift

Fig. 8.8 (b) Summary of Maximum Drifts - UBC Zone No. 4 Buildings

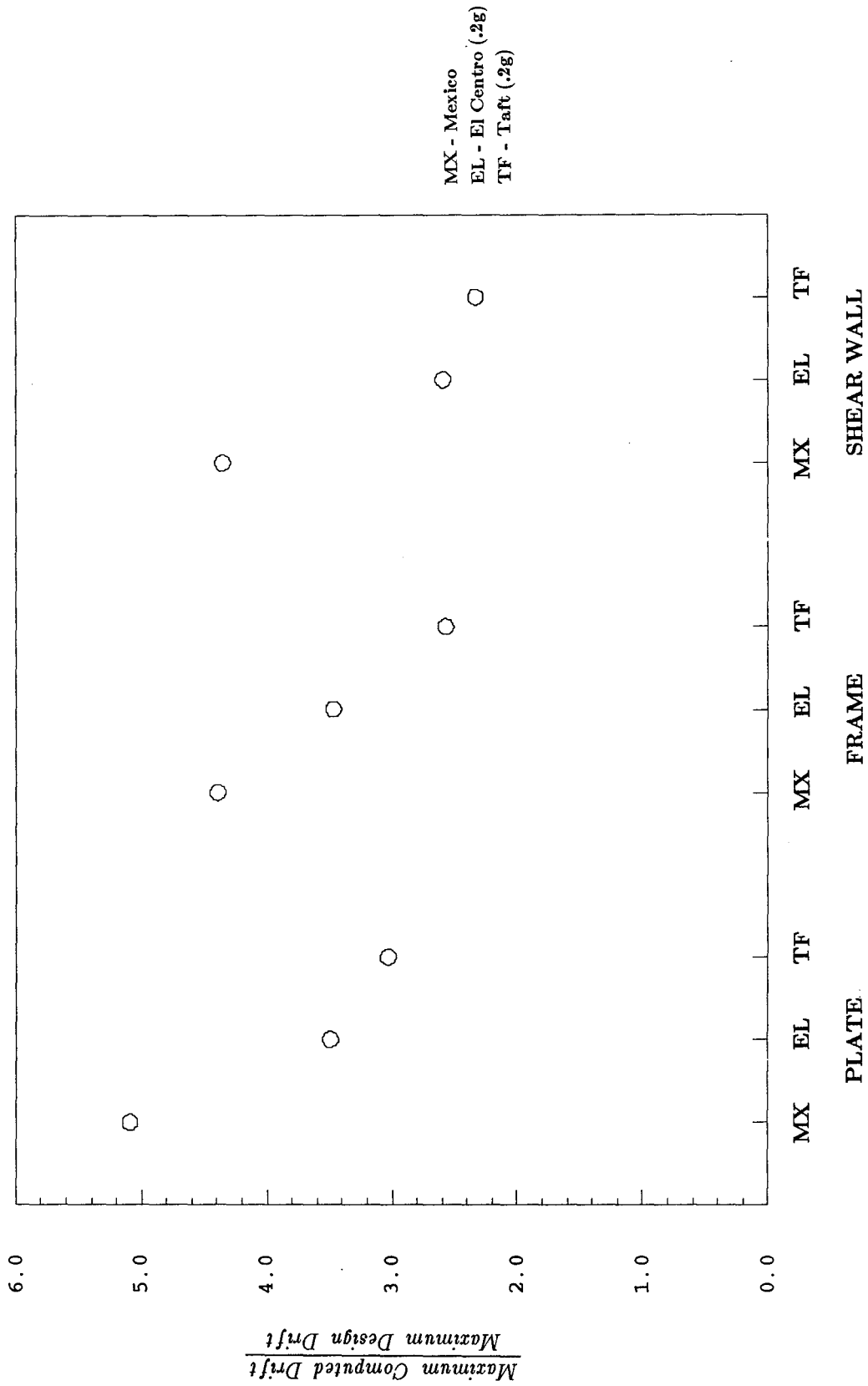


Fig. 8.8 (c) Comparison of Computed Drifts to Design Drifts - UBC Zone No. 2 Buildings

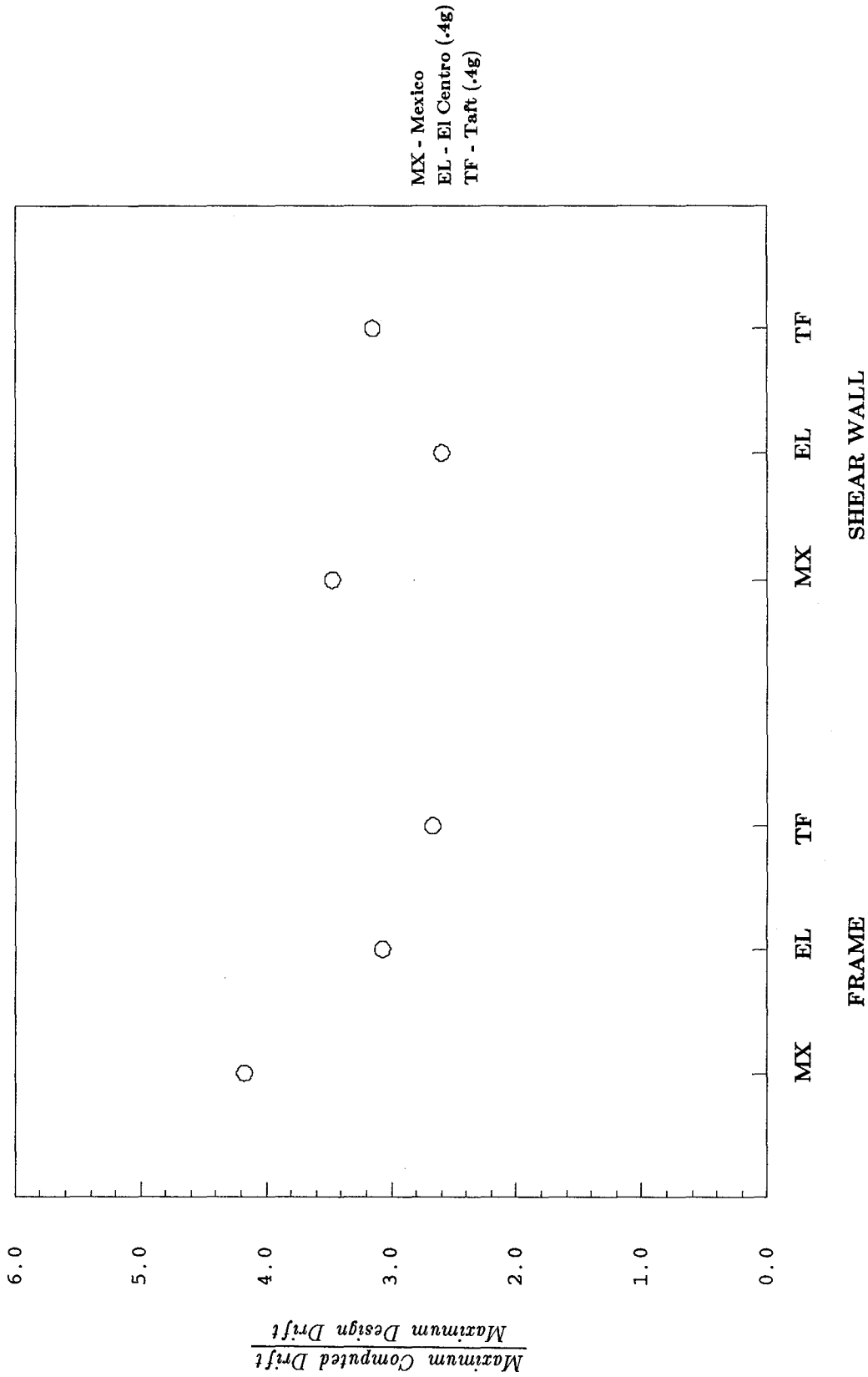


Fig. 8.8 (d) Comparison of Computed Drifts to Design Drifts - UBC Zone No. 4 Buildings

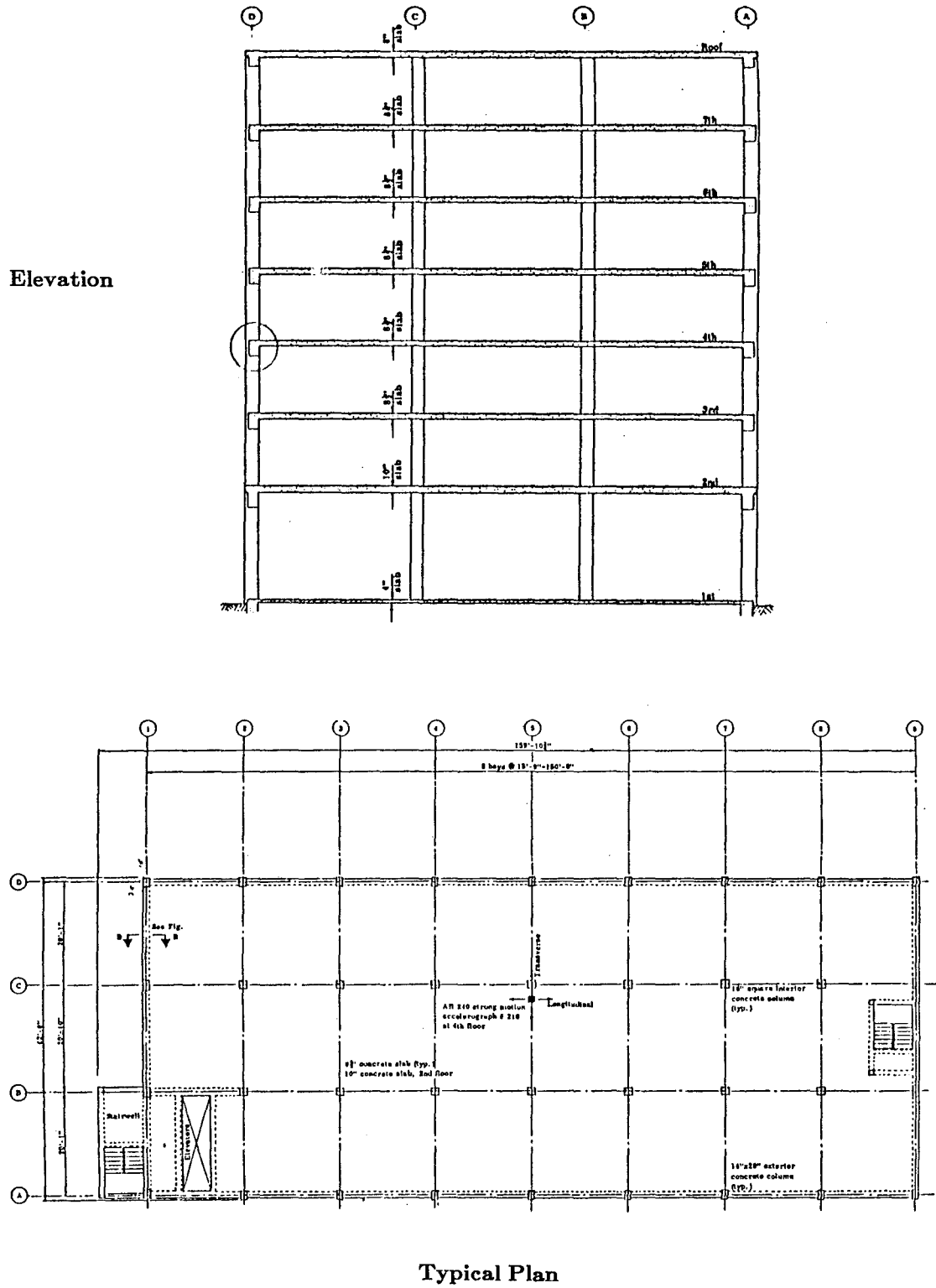


Fig. 8.9 Holiday Inn Building (Orion Avenue)

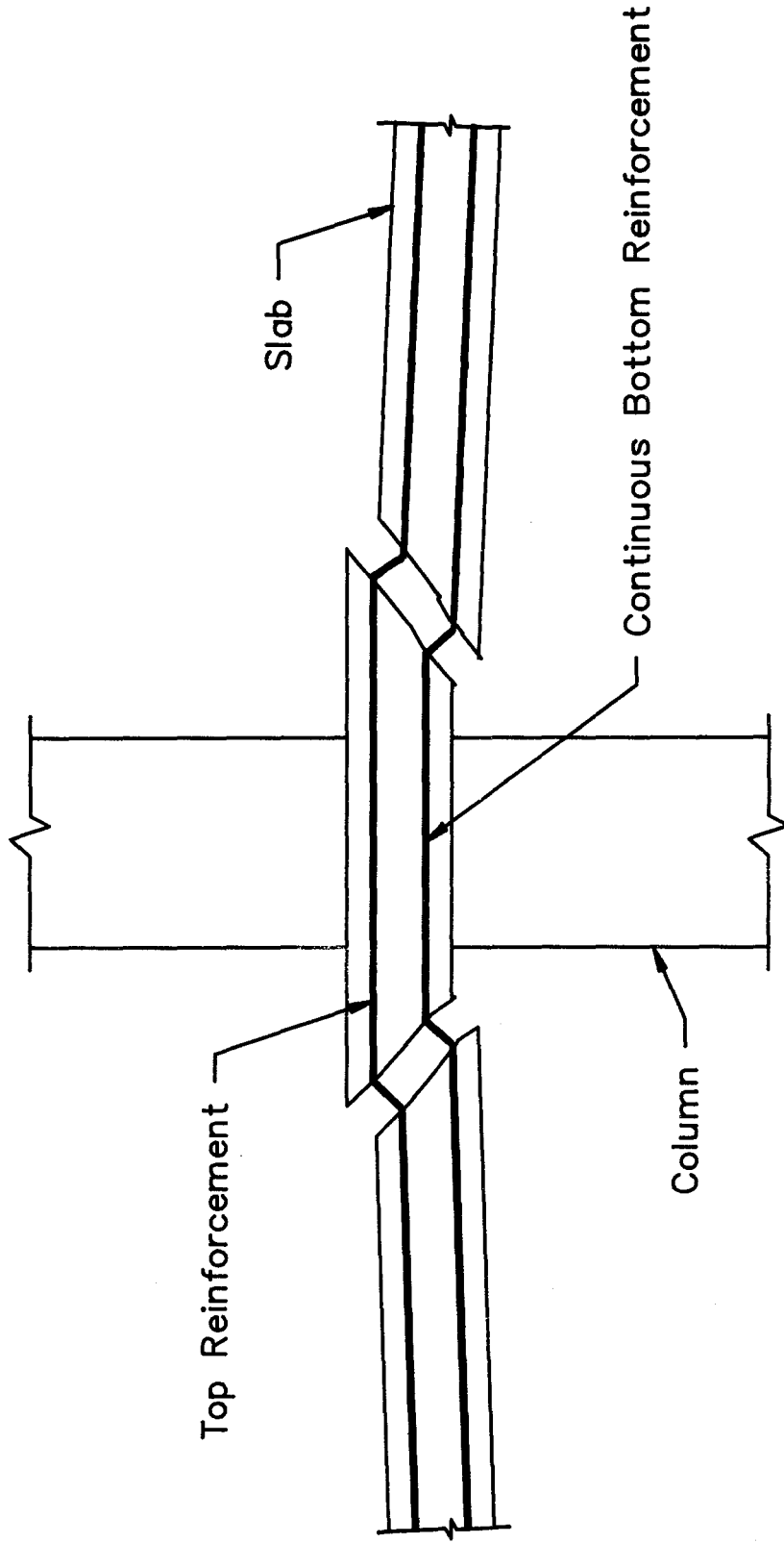


Fig. 8.10 Detailing of Flat Plate Connections to Prevent Progressive Collapse

APPENDIX A: INSTRUMENTATION CHANNEL NUMBERS

All experimental data were recorded on a Data General Nova computer and stored on magnetic tapes. Data from Tests 1 through 5 are stored in filenames labelled as: slab1, slab2, slab3, slab4, and slabr, respectively. Refer to Section 4.3 for a discussion on instrumentation and data recording.

Channel No.	Type	Units	Location
1	LVDT	in.	Slab connection - north side
3	LVDT	in.	Slab connection - south side
4	LVDT	in.	Slab connection - west side
5	LVDT	in.	Slab connection - west side
6	LVDT	in.	Slab connection - north side
8	LVDT	in.	Slab connection - west side
9	LVDT	in.	Column - SE corner
11	LVDT	in.	Column - NE corner
12	LVDT	in.	Instrumentation frame - west side
13	LVDT	in.	Instrumentation frame - west side
14	LVDT	in.	Slab connection - east side
15	LVDT	in.	Column - NW corner
18	LVDT	in.	Instrumentation frame - south side
19	LVDT	in.	Instrumentation frame - south side
20	LVDT	in.	Slab connection - south side
24	Lin. Pot.	in.	Slab edge - north side
25	Lin. Pot.	in.	Slab edge - NE corner
26	Lin. Pot.	in.	Slab edge - NE corner
27	Lin. Pot.	in.	Column base
28	Trans. Strut.	kip	NE corner
29	Trans. Strut.	kip	East side
30	Trans. Strut.	kip	SE corner
32	Trans. Strut.	kip	South side
33	Trans. Strut.	kip	NW corner
35	Trans. Strut.	kip	SW corner
36	Pos. Trans.	in.	South side
37	Pos. Trans.	in.	West side
38	Load Cell	kip	East side
39	Load Cell	kip	North side
41	Trans. Strut.	kip	North side
44	Trans. Strut.	kip	East side
48	Clip Gauge	in.	Instrumentation frame - south side
49	Clip Gauge	in.	Instrumentation frame - south side
50	Clip Gauge	in.	Instrumentation frame - south side
52	Clip Gauge	in.	Instrumentation frame - south side
53	Clip Gauge	in.	Instrumentation frame - west side
54	Clip Gauge	in.	Instrumentation frame - west side
55	Clip Gauge	in.	Instrumentation frame - west side
56	Clip Gauge	in.	Instrumentation frame - west side
57	Lin. Pot.	in.	Column base
58	Lin. Pot.	in.	Column base
64-89	Strain Gauge	mil. strain	See Figs. A.2 and A.3

Note: see also Figure A.1.

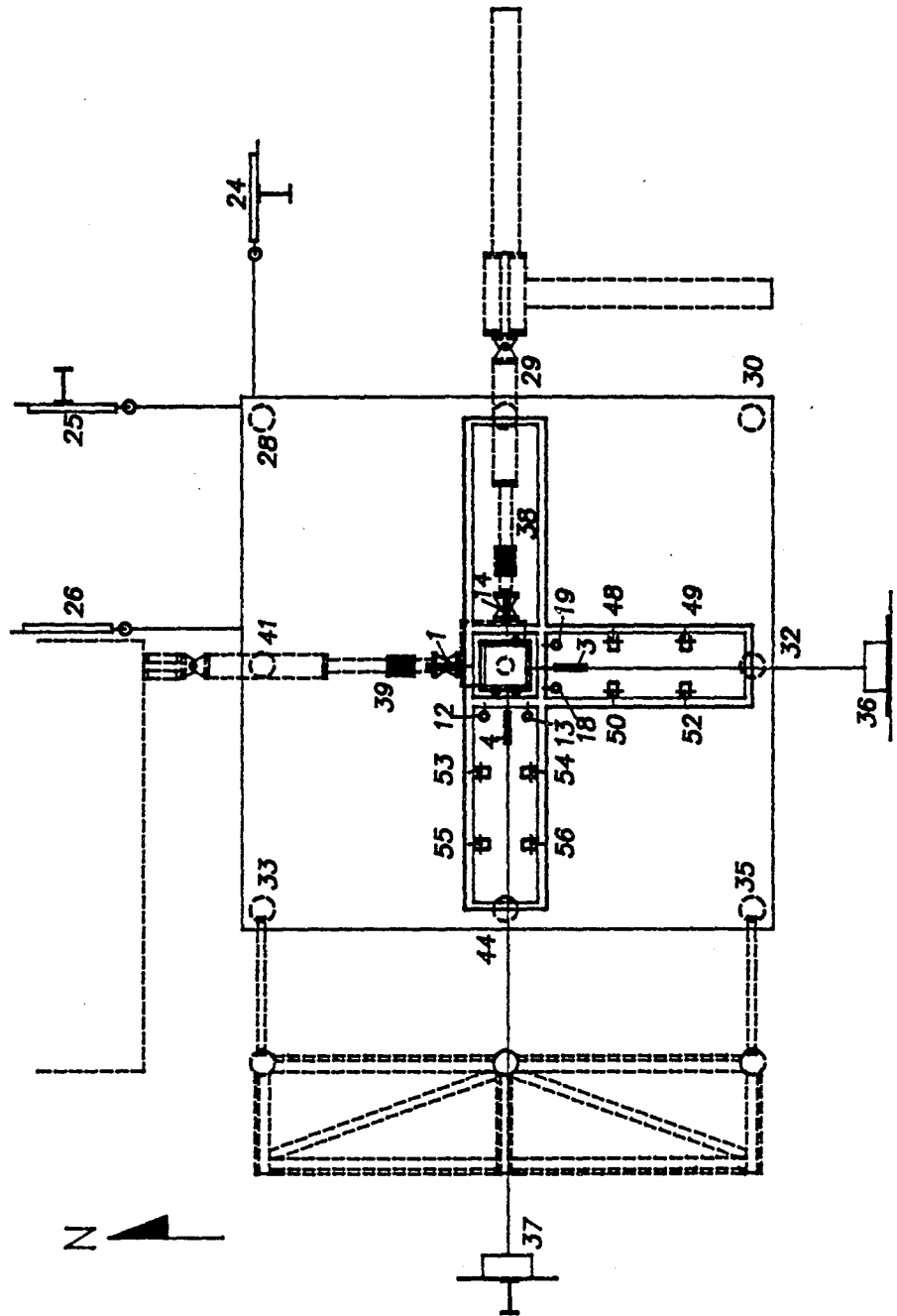


Fig. A.1 (a) Instrumentation Channel Numbers - Plan

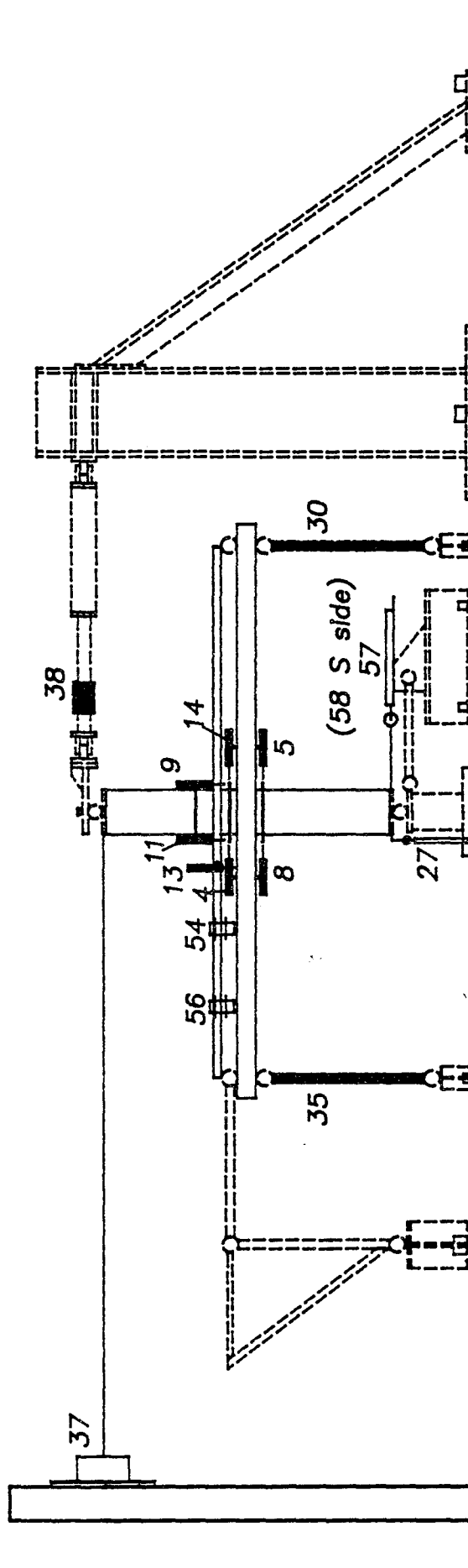


Fig. A.1 (b) Instrumentation Channel Numbers - Elevation

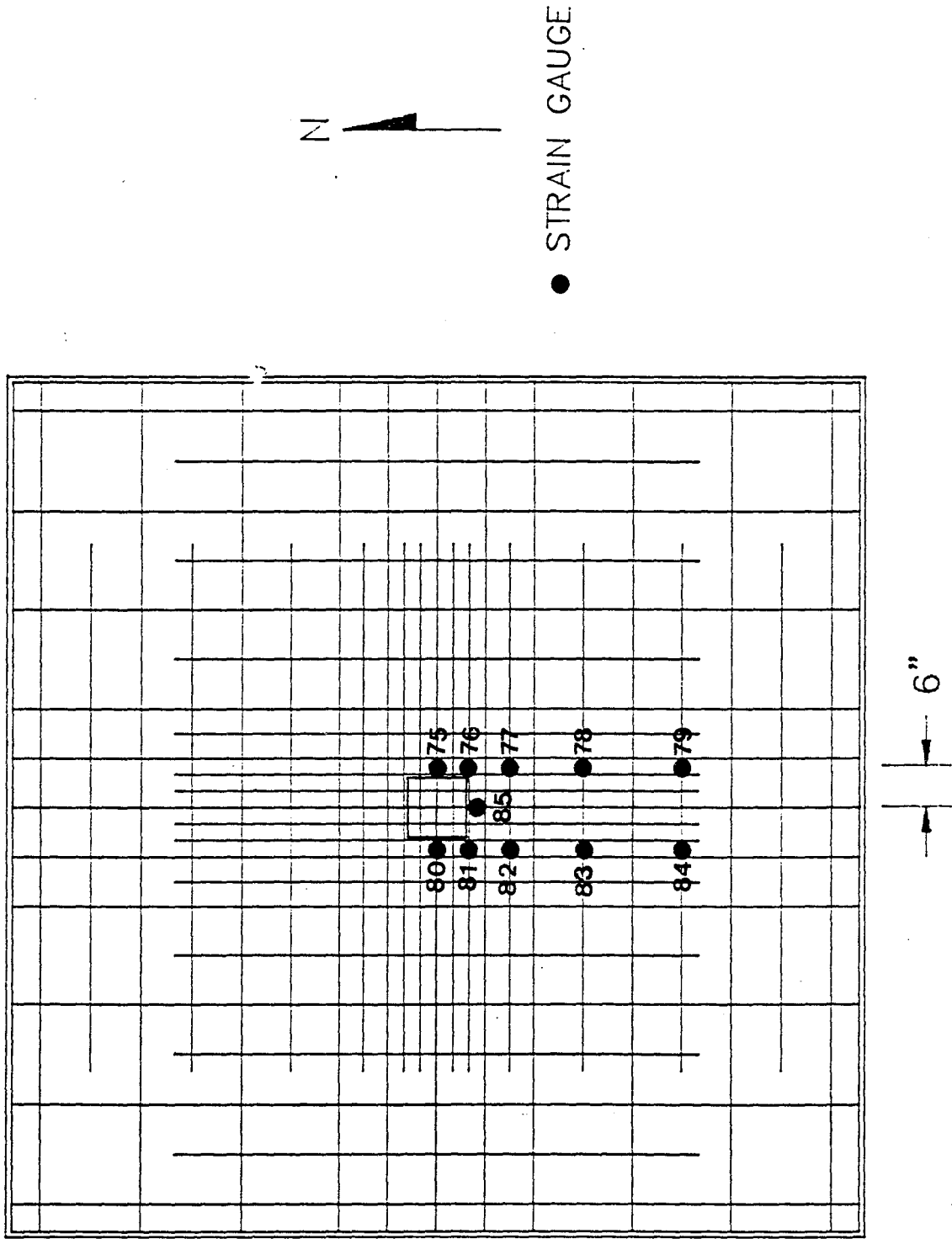


Fig. A.2 (a) Top Strain Gauge Numbers - Tests 1 and 3

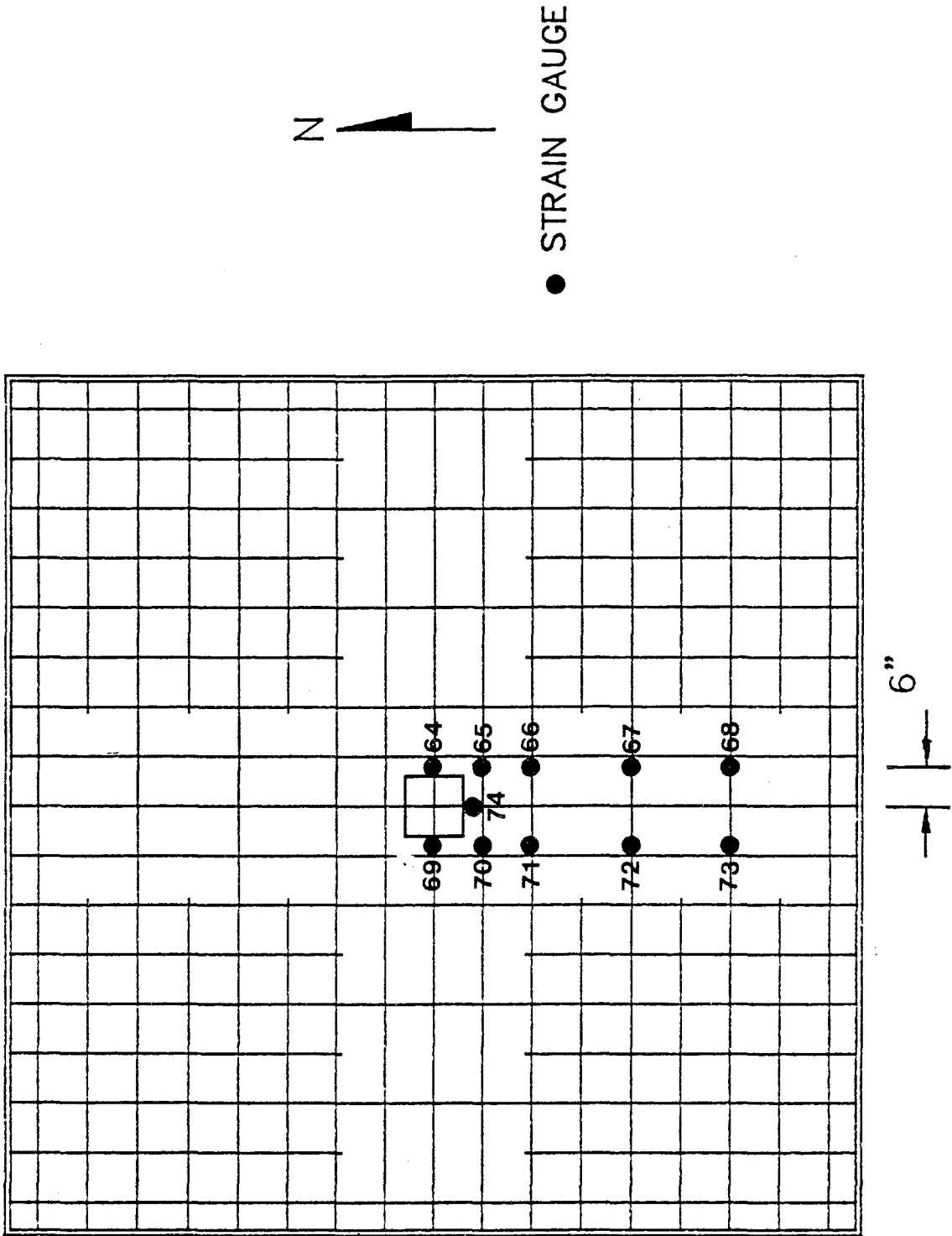


Fig. A.2 (b) Bottom Strain Gauge Numbers - Tests 1 and 3

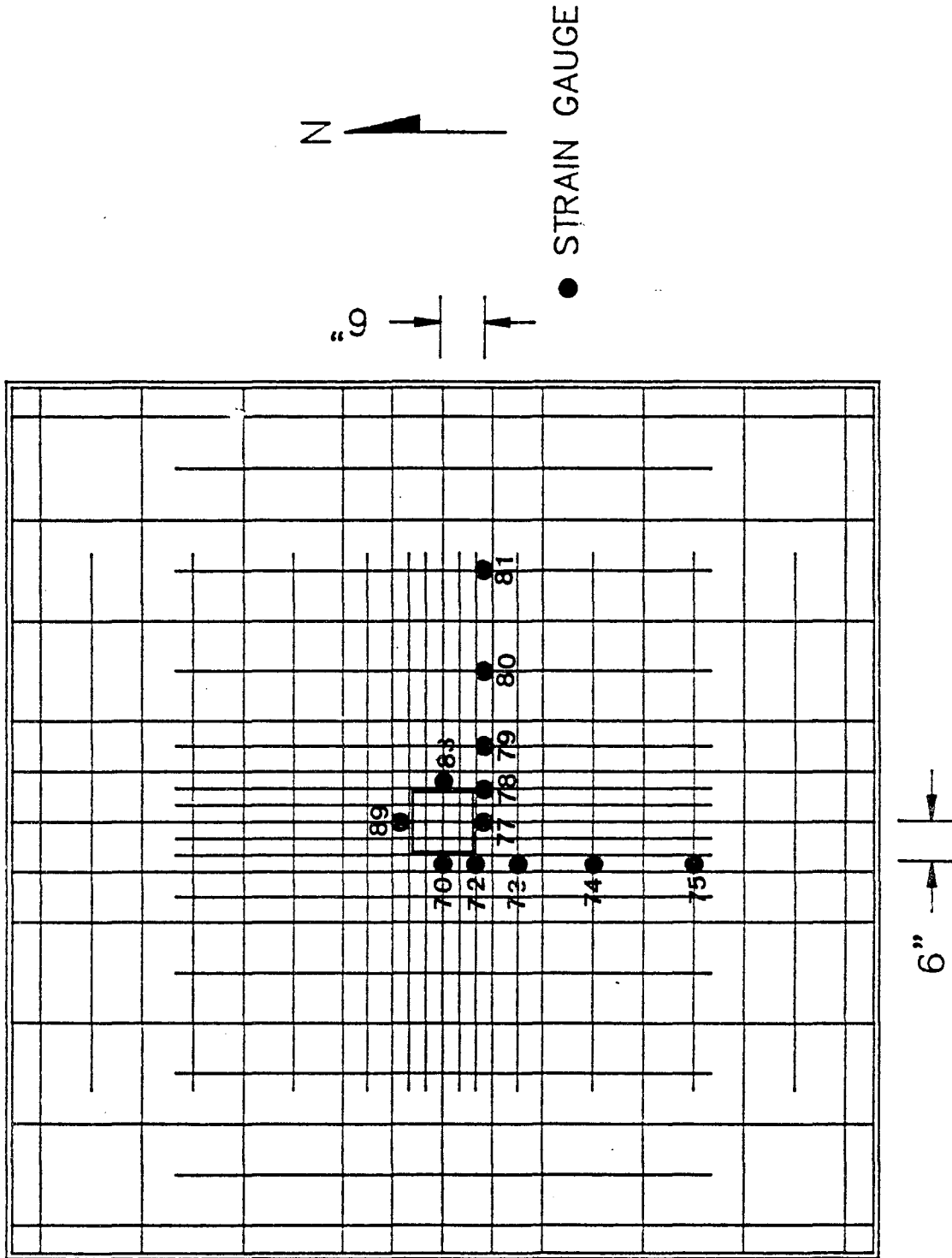


Fig. A.3 (a) Top Strain Gauge Numbers - Tests 2 and 4

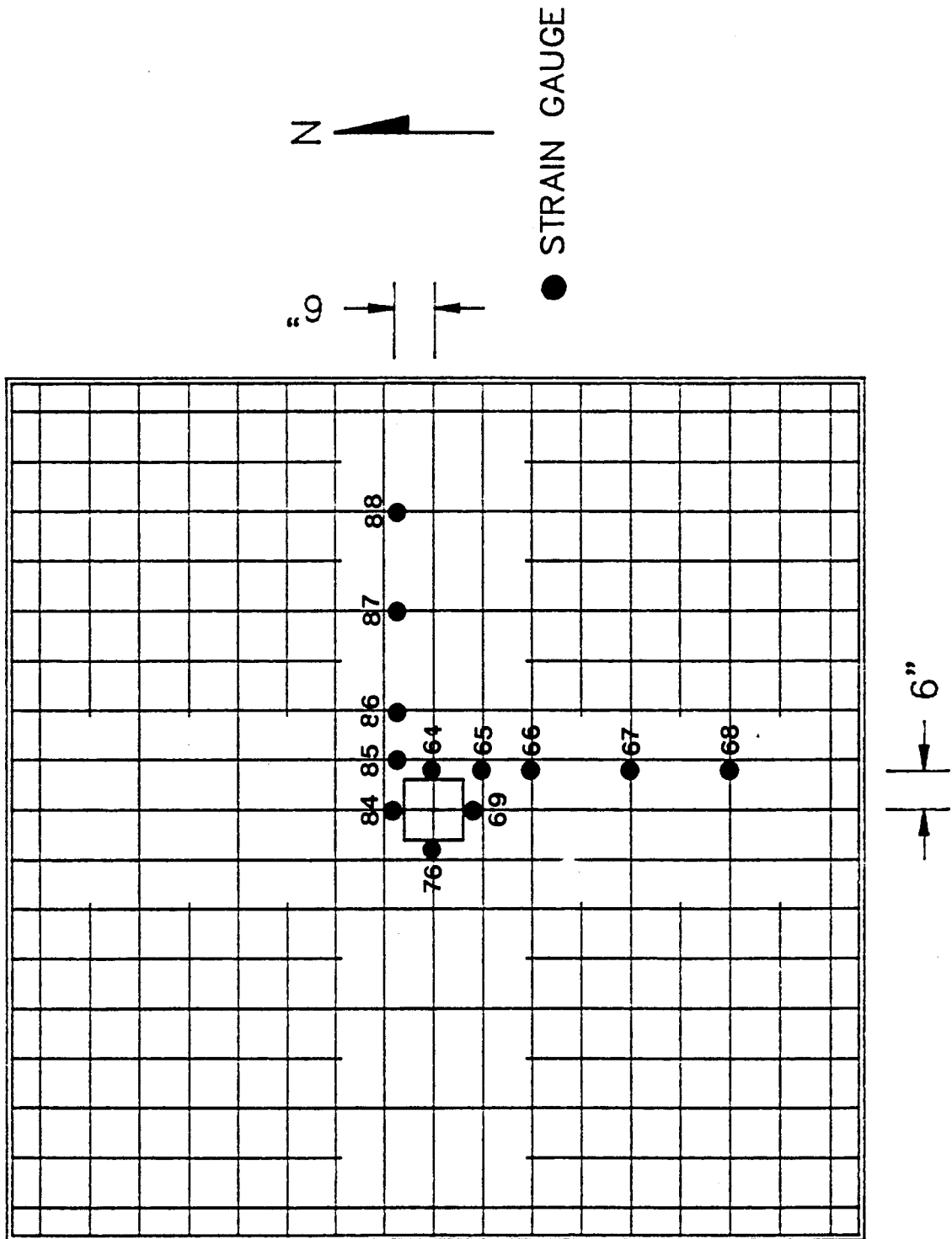


Fig. A.3 (b) Bottom Strain Gauge Numbers - Tests 2 and 4

EARTHQUAKE ENGINEERING RESEARCH CENTER REPORT SERIES

EERC reports are available from the National Information Service for Earthquake Engineering (NISEE) and from the National Technical Information Service (NTIS). Numbers in parentheses are Accession Numbers assigned by the National Technical Information Service; these are followed by a price code. Contact NTIS, 5285 Port Royal Road, Springfield Virginia, 22161 for more information. Reports without Accession Numbers were not available from NTIS at the time of printing. For a current complete list of EERC reports (from EERC 67-1) and availability information, please contact University of California, EERC, NISEE, 1301 South 46th Street, Richmond, California 94804.

- UCB/EERC-80/01 "Earthquake Response of Concrete Gravity Dams Including Hydrodynamic and Foundation Interaction Effects," by Chopra, A.K., Chakrabarti, P. and Gupta, S., January 1980, (AD-A087297)A10.
- UCB/EERC-80/02 "Rocking Response of Rigid Blocks to Earthquakes," by Yim, C.S., Chopra, A.K. and Penzien, J., January 1980, (PB80 166 002)A04.
- UCB/EERC-80/03 "Optimum Inelastic Design of Seismic-Resistant Reinforced Concrete Frame Structures," by Zagajski, S.W. and Bertero, V.V., January 1980, (PB80 164 635)A06.
- UCB/EERC-80/04 "Effects of Amount and Arrangement of Wall-Panel Reinforcement on Hysteretic Behavior of Reinforced Concrete Walls," by Iliya, R. and Bertero, V.V., February 1980, (PB81 122 525)A09.
- UCB/EERC-80/05 "Shaking Table Research on Concrete Dam Models," by Niwa, A. and Clough, R.W., September 1980, (PB81 122 368)A06.
- UCB/EERC-80/06 "The Design of Steel Energy-Absorbing Restrainers and their Incorporation into Nuclear Power Plants for Enhanced Safety (Vol 1a): Piping with Energy Absorbing Restrainers: Parameter Study on Small Systems," by Powell, G.H., Oughourlian, C. and Simons, J., June 1980.
- UCB/EERC-80/07 "Inelastic Torsional Response of Structures Subjected to Earthquake Ground Motions," by Yamazaki, Y., April 1980, (PB81 122 327)A08.
- UCB/EERC-80/08 "Study of X-Braced Steel Frame Structures under Earthquake Simulation," by Ghanaat, Y., April 1980, (PB81 122 335)A11.
- UCB/EERC-80/09 "Hybrid Modelling of Soil-Structure Interaction," by Gupta, S., Lin, T.W. and Penzien, J., May 1980, (PB81 122 319)A07.
- UCB/EERC-80/10 "General Applicability of a Nonlinear Model of a One Story Steel Frame," by Sveinsson, B.I. and McNiven, H.D., May 1980, (PB81 124 877)A06.
- UCB/EERC-80/11 "A Green-Function Method for Wave Interaction with a Submerged Body," by Kioka, W., April 1980, (PB81 122 269)A07.
- UCB/EERC-80/12 "Hydrodynamic Pressure and Added Mass for Axisymmetric Bodies," by Nilrat, F., May 1980, (PB81 122 343)A08.
- UCB/EERC-80/13 "Treatment of Non-Linear Drag Forces Acting on Offshore Platforms," by Dao, B.V. and Penzien, J., May 1980, (PB81 153 413)A07.
- UCB/EERC-80/14 "2D Plane/Axisymmetric Solid Element (Type 3-Elastic or Elastic-Perfectly Plastic) for the ANSR-II Program," by Mondkar, D.P. and Powell, G.H., July 1980, (PB81 122 350)A03.
- UCB/EERC-80/15 "A Response Spectrum Method for Random Vibrations," by Der Kiureghian, A., June 1981, (PB81 122 301)A03.
- UCB/EERC-80/16 "Cyclic Inelastic Buckling of Tubular Steel Braces," by Zayas, V.A., Popov, E.P. and Mahin, S.A., June 1981, (PB81 124 885)A10.
- UCB/EERC-80/17 "Dynamic Response of Simple Arch Dams Including Hydrodynamic Interaction," by Porter, C.S. and Chopra, A.K., July 1981, (PB81 124 000)A13.
- UCB/EERC-80/18 "Experimental Testing of a Friction Damped Aseismic Base Isolation System with Fail-Safe Characteristics," by Kelly, J.M., Beucke, K.E. and Skinner, M.S., July 1980, (PB81 148 595)A04.
- UCB/EERC-80/19 "The Design of Steel Energy-Absorbing Restrainers and their Incorporation into Nuclear Power Plants for Enhanced Safety (Vol.1B): Stochastic Seismic Analyses of Nuclear Power Plant Structures and Piping Systems Subjected to Multiple Supported Excitations," by Lee, M.C. and Penzien, J., June 1980, (PB82 201 872)A08.
- UCB/EERC-80/20 "The Design of Steel Energy-Absorbing Restrainers and their Incorporation into Nuclear Power Plants for Enhanced Safety (Vol 1C): Numerical Method for Dynamic Substructure Analysis," by Dickens, J.M. and Wilson, E.L., June 1980.
- UCB/EERC-80/21 "The Design of Steel Energy-Absorbing Restrainers and their Incorporation into Nuclear Power Plants for Enhanced Safety (Vol 2): Development and Testing of Restraints for Nuclear Piping Systems," by Kelly, J.M. and Skinner, M.S., June 1980.
- UCB/EERC-80/22 "3D Solid Element (Type 4-Elastic or Elastic-Perfectly-Plastic) for the ANSR-II Program," by Mondkar, D.P. and Powell, G.H., July 1980, (PB81 123 242)A03.
- UCB/EERC-80/23 "Gap-Friction Element (Type 5) for the Ansr-II Program," by Mondkar, D.P. and Powell, G.H., July 1980, (PB81 122 285)A03.
- UCB/EERC-80/24 "U-Bar Restraint Element (Type 11) for the ANSR-II Program," by Oughourlian, C. and Powell, G.H., July 1980, (PB81 122 293)A03.
- UCB/EERC-80/25 "Testing of a Natural Rubber Base Isolation System by an Explosively Simulated Earthquake," by Kelly, J.M., August 1980, (PB81 201 360)A04.
- UCB/EERC-80/26 "Input Identification from Structural Vibrational Response," by Hu, Y., August 1980, (PB81 152 308)A05.
- UCB/EERC-80/27 "Cyclic Inelastic Behavior of Steel Offshore Structures," by Zayas, V.A., Mahin, S.A. and Popov, E.P., August 1980, (PB81 196 180)A15.
- UCB/EERC-80/28 "Shaking Table Testing of a Reinforced Concrete Frame with Biaxial Response," by Oliva, M.G., October 1980, (PB81 154 304)A10.
- UCB/EERC-80/29 "Dynamic Properties of a Twelve-Story Prefabricated Panel Building," by Bouwkamp, J.G., Kollegger, J.P. and Stephen, R.M., October 1980, (PB82 138 777)A07.
- UCB/EERC-80/30 "Dynamic Properties of an Eight-Story Prefabricated Panel Building," by Bouwkamp, J.G., Kollegger, J.P. and Stephen, R.M., October 1980, (PB81 200 313)A05.
- UCB/EERC-80/31 "Predictive Dynamic Response of Panel Type Structures under Earthquakes," by Kollegger, J.P. and Bouwkamp, J.G., October 1980, (PB81 152 316)A04.
- UCB/EERC-80/32 "The Design of Steel Energy-Absorbing Restrainers and their Incorporation into Nuclear Power Plants for Enhanced Safety (Vol 3): Testing of Commercial Steels in Low-Cycle Torsional Fatigue," by Spanner, P., Parker, E.R., Jongewaard, E. and Dory, M., 1980.

- UCB/EERC-80/33 "The Design of Steel Energy-Absorbing Restrainers and their Incorporation into Nuclear Power Plants for Enhanced Safety (Vol 4): Shaking Table Tests of Piping Systems with Energy-Absorbing Restrainers," by Stiemer, S.F. and Godden, W.G., September 1980, (PB82 201 880)A05.
- UCB/EERC-80/34 "The Design of Steel Energy-Absorbing Restrainers and their Incorporation into Nuclear Power Plants for Enhanced Safety (Vol 5): Summary Report," by Spencer, P., 1980.
- UCB/EERC-80/35 "Experimental Testing of an Energy-Absorbing Base Isolation System," by Kelly, J.M., Skinner, M.S. and Beucke, K.E., October 1980, (PB81 154 072)A04.
- UCB/EERC-80/36 "Simulating and Analyzing Artificial Non-Stationary Earth Ground Motions," by Nau, R.F., Oliver, R.M. and Pister, K.S., October 1980, (PB81 153 397)A04.
- UCB/EERC-80/37 "Earthquake Engineering at Berkeley - 1980," by , September 1980, (PB81 205 674)A09.
- UCB/EERC-80/38 "Inelastic Seismic Analysis of Large Panel Buildings," by Schricker, V. and Powell, G.H., September 1980, (PB81 154 338)A13.
- UCB/EERC-80/39 "Dynamic Response of Embankment, Concrete-Gavity and Arch Dams Including Hydrodynamic Interaction," by Hall, J.F. and Chopra, A.K., October 1980, (PB81 152 324)A11.
- UCB/EERC-80/40 "Inelastic Buckling of Steel Struts under Cyclic Load Reversal.," by Black, R.G., Wenger, W.A. and Popov, E.P., October 1980, (PB81 154 312)A08.
- UCB/EERC-80/41 "Influence of Site Characteristics on Buildings Damage during the October 3,1974 Lima Earthquake," by Repetto, P., Arango, I. and Seed, H.B., September 1980, (PB81 161 739)A05.
- UCB/EERC-80/42 "Evaluation of a Shaking Table Test Program on Response Behavior of a Two Story Reinforced Concrete Frame," by Blondet, J.M., Clough, R.W. and Mahin, S.A., December 1980, (PB82 196 544)A11.
- UCB/EERC-80/43 "Modelling of Soil-Structure Interaction by Finite and Infinite Elements," by Medina, F., December 1980, (PB81 229 270)A04.
- UCB/EERC-81/01 "Control of Seismic Response of Piping Systems and Other Structures by Base Isolation," by Kelly, J.M., January 1981, (PB81 200 735)A05.
- UCB/EERC-81/02 "OPTNSR- An Interactive Software System for Optimal Design of Statically and Dynamically Loaded Structures with Nonlinear Response," by Bhatti, M.A., Ciampi, V. and Pister, K.S., January 1981, (PB81 218 851)A09.
- UCB/EERC-81/03 "Analysis of Local Variations in Free Field Seismic Ground Motions," by Chen, J.-C., Lysmer, J. and Seed, H.B., January 1981, (AD-A099508)A13.
- UCB/EERC-81/04 "Inelastic Structural Modeling of Braced Offshore Platforms for Seismic Loading," by Zayas, V.A., Shing, P.-S.B., Mahin, S.A. and Popov, E.P., January 1981, (PB82 138 777)A07.
- UCB/EERC-81/05 "Dynamic Response of Light Equipment in Structures," by Der Kiureghian, A., Sackman, J.L. and Nour-Omid, B., April 1981, (PB81 218 497)A04.
- UCB/EERC-81/06 "Preliminary Experimental Investigation of a Broad Base Liquid Storage Tank," by Bouwkamp, J.G., Kollegger, J.P. and Stephen, R.M., May 1981, (PB82 140 385)A03.
- UCB/EERC-81/07 "The Seismic Resistant Design of Reinforced Concrete Coupled Structural Walls," by Aktan, A.E. and Bertero, V.V., June 1981, (PB82 113 358)A11.
- UCB/EERC-81/08 "Unassigned," by Unassigned, 1981.
- UCB/EERC-81/09 "Experimental Behavior of a Spatial Piping System with Steel Energy Absorbers Subjected to a Simulated Differential Seismic Input," by Stiemer, S.F., Godden, W.G. and Kelly, J.M., July 1981, (PB82 201 898)A04.
- UCB/EERC-81/10 "Evaluation of Seismic Design Provisions for Masonry in the United States," by Sveinsson, B.I., Mayes, R.L. and McNiven, H.D., August 1981, (PB82 166 075)A08.
- UCB/EERC-81/11 "Two-Dimensional Hybrid Modelling of Soil-Structure Interaction," by Tzong, T.-J., Gupta, S. and Penzien, J., August 1981, (PB82 142 118)A04.
- UCB/EERC-81/12 "Studies on Effects of Infills in Seismic Resistant R/C Construction," by Brokken, S. and Bertero, V.V., October 1981, (PB82 166 190)A09.
- UCB/EERC-81/13 "Linear Models to Predict the Nonlinear Seismic Behavior of a One-Story Steel Frame," by Valdimarsson, H., Shah, A.H. and McNiven, H.D., September 1981, (PB82 138 793)A07.
- UCB/EERC-81/14 "TLUSH: A Computer Program for the Three-Dimensional Dynamic Analysis of Earth Dams," by Kagawa, T., Mejia, L.H., Seed, H.B. and Lysmer, J., September 1981, (PB82 139 940)A06.
- UCB/EERC-81/15 "Three Dimensional Dynamic Response Analysis of Earth Dams," by Mejia, L.H. and Seed, H.B., September 1981, (PB82 137 274)A12.
- UCB/EERC-81/16 "Experimental Study of Lead and Elastomeric Dampers for Base Isolation Systems," by Kelly, J.M. and Hodder, S.B., October 1981, (PB82 166 182)A05.
- UCB/EERC-81/17 "The Influence of Base Isolation on the Seismic Response of Light Secondary Equipment," by Kelly, J.M., April 1981, (PB82 255 266)A04.
- UCB/EERC-81/18 "Studies on Evaluation of Shaking Table Response Analysis Procedures," by Blondet, J. M., November 1981, (PB82 197 278)A10.
- UCB/EERC-81/19 "DELIGHT.STRUCT: A Computer-Aided Design Environment for Structural Engineering," by Balling, R.J., Pister, K.S. and Polak, E., December 1981, (PB82 218 496)A07.
- UCB/EERC-81/20 "Optimal Design of Seismic-Resistant Planar Steel Frames," by Balling, R.J., Ciampi, V. and Pister, K.S., December 1981, (PB82 220 179)A07.
- UCB/EERC-82/01 "Dynamic Behavior of Ground for Seismic Analysis of Lifeline Systems," by Sato, T. and Der Kiureghian, A., January 1982, (PB82 218 926)A05.
- UCB/EERC-82/02 "Shaking Table Tests of a Tubular Steel Frame Model," by Ghanaat, Y. and Clough, R.W., January 1982, (PB82 220 161)A07.

- UCB/EERC-82/03 "Behavior of a Piping System under Seismic Excitation: Experimental Investigations of a Spatial Piping System supported by Mechanical Shock Arrestors," by Schneider, S., Lee, H.-M. and Godden, W. G., May 1982, (PB83 172 544)A09.
- UCB/EERC-82/04 "New Approaches for the Dynamic Analysis of Large Structural Systems," by Wilson, E.L., June 1982, (PB83 148 080)A05.
- UCB/EERC-82/05 "Model Study of Effects of Damage on the Vibration Properties of Steel Offshore Platforms," by Shahriyar, F. and Bouwkamp, J.G., June 1982, (PB83 148 742)A10.
- UCB/EERC-82/06 "States of the Art and Practice in the Optimum Seismic Design and Analytical Response Prediction of R/C Frame Wall Structures," by Aktan, A.E. and Bertero, V.V., July 1982, (PB83 147 736)A05.
- UCB/EERC-82/07 "Further Study of the Earthquake Response of a Broad Cylindrical Liquid-Storage Tank Model," by Manos, G.C. and Clough, R.W., July 1982, (PB83 147 744)A11.
- UCB/EERC-82/08 "An Evaluation of the Design and Analytical Seismic Response of a Seven Story Reinforced Concrete Frame," by Charney, F.A. and Bertero, V.V., July 1982, (PB83 157 628)A09.
- UCB/EERC-82/09 "Fluid-Structure Interactions: Added Mass Computations for Incompressible Fluid," by Kuo, J.S.-H., August 1982, (PB83 156 281)A07.
- UCB/EERC-82/10 "Joint-Opening Nonlinear Mechanism: Interface Smeared Crack Model," by Kuo, J.S.-H., August 1982, (PB83 149 195)A05.
- UCB/EERC-82/11 "Dynamic Response Analysis of Techi Dam," by Clough, R.W., Stephen, R.M. and Kuo, J.S.-H., August 1982, (PB83 147 496)A06.
- UCB/EERC-82/12 "Prediction of the Seismic Response of R/C Frame-Coupled Wall Structures," by Aktan, A.E., Bertero, V.V. and Piazza, M., August 1982, (PB83 149 203)A09.
- UCB/EERC-82/13 "Preliminary Report on the Smart 1 Strong Motion Array in Taiwan," by Bolt, B.A., Loh, C.H., Penzien, J. and Tsai, Y.B., August 1982, (PB83 159 400)A10.
- UCB/EERC-82/14 "Shaking-Table Studies of an Eccentrically X-Braced Steel Structure," by Yang, M.S., September 1982, (PB83 260 778)A12.
- UCB/EERC-82/15 "The Performance of Stairways in Earthquakes," by Roha, C., Axley, J.W. and Bertero, V.V., September 1982, (PB83 157 693)A07.
- UCB/EERC-82/16 "The Behavior of Submerged Multiple Bodies in Earthquakes," by Liao, W.-G., September 1982, (PB83 158 709)A07.
- UCB/EERC-82/17 "Effects of Concrete Types and Loading Conditions on Local Bond-Slip Relationships," by Cowell, A.D., Popov, E.P. and Bertero, V.V., September 1982, (PB83 153 577)A04.
- UCB/EERC-82/18 "Mechanical Behavior of Shear Wall Vertical Boundary Members: An Experimental Investigation," by Wagner, M.T. and Bertero, V.V., October 1982, (PB83 159 764)A05.
- UCB/EERC-82/19 "Experimental Studies of Multi-support Seismic Loading on Piping Systems," by Kelly, J.M. and Cowell, A.D., November 1982.
- UCB/EERC-82/20 "Generalized Plastic Hinge Concepts for 3D Beam-Column Elements," by Chen, P. F.-S. and Powell, G.H., November 1982, (PB83 247 981)A13.
- UCB/EERC-82/21 "ANSR-II: General Computer Program for Nonlinear Structural Analysis," by Oughourlian, C.V. and Powell, G.H., November 1982, (PB83 251 330)A12.
- UCB/EERC-82/22 "Solution Strategies for Statically Loaded Nonlinear Structures," by Simons, J.W. and Powell, G.H., November 1982, (PB83 197 970)A06.
- UCB/EERC-82/23 "Analytical Model of Deformed Bar Anchorages under Generalized Excitations," by Ciampi, V., Eligehausen, R., Bertero, V.V. and Popov, E.P., November 1982, (PB83 169 532)A06.
- UCB/EERC-82/24 "A Mathematical Model for the Response of Masonry Walls to Dynamic Excitations," by Sucuoglu, H., Mengi, Y. and McNiven, H.D., November 1982, (PB83 169 011)A07.
- UCB/EERC-82/25 "Earthquake Response Considerations of Broad Liquid Storage Tanks," by Cambra, F.J., November 1982, (PB83 251 215)A09.
- UCB/EERC-82/26 "Computational Models for Cyclic Plasticity, Rate Dependence and Creep," by Mosaddad, B. and Powell, G.H., November 1982, (PB83 245 829)A08.
- UCB/EERC-82/27 "Inelastic Analysis of Piping and Tubular Structures," by Mahasuverachai, M. and Powell, G.H., November 1982, (PB83 249 987)A07.
- UCB/EERC-83/01 "The Economic Feasibility of Seismic Rehabilitation of Buildings by Base Isolation," by Kelly, J.M., January 1983, (PB83 197 988)A05.
- UCB/EERC-83/02 "Seismic Moment Connections for Moment-Resisting Steel Frames," by Popov, E.P., January 1983, (PB83 195 412)A04.
- UCB/EERC-83/03 "Design of Links and Beam-to-Column Connections for Eccentrically Braced Steel Frames," by Popov, E.P. and Malley, J.O., January 1983, (PB83 194 811)A04.
- UCB/EERC-83/04 "Numerical Techniques for the Evaluation of Soil-Structure Interaction Effects in the Time Domain," by Bayo, E. and Wilson, E.L., February 1983, (PB83 245 605)A09.
- UCB/EERC-83/05 "A Transducer for Measuring the Internal Forces in the Columns of a Frame-Wall Reinforced Concrete Structure," by Sause, R. and Bertero, V.V., May 1983, (PB84 119 494)A06.
- UCB/EERC-83/06 "Dynamic Interactions Between Floating Ice and Offshore Structures," by Croteau, P., May 1983, (PB84 119 486)A16.
- UCB/EERC-83/07 "Dynamic Analysis of Multiply Tuned and Arbitrarily Supported Secondary Systems," by Igusa, T. and Der Kiureghian, A., July 1983, (PB84 118 272)A11.
- UCB/EERC-83/08 "A Laboratory Study of Submerged Multi-body Systems in Earthquakes," by Ansari, G.R., June 1983, (PB83 261 842)A17.
- UCB/EERC-83/09 "Effects of Transient Foundation Uplift on Earthquake Response of Structures," by Yim, C.-S. and Chopra, A.K., June 1983, (PB83 261 396)A07.
- UCB/EERC-83/10 "Optimal Design of Friction-Braced Frames under Seismic Loading," by Austin, M.A. and Pister, K.S., June 1983, (PB84 119 288)A06.
- UCB/EERC-83/11 "Shaking Table Study of Single-Story Masonry Houses: Dynamic Performance under Three Component Seismic Input and Recommendations," by Manos, G.C., Clough, R.W. and Mayes, R.L., July 1983, (UCB/EERC-83/11)A08.
- UCB/EERC-83/12 "Experimental Error Propagation in Pseudodynamic Testing," by Shiing, P.B. and Mahin, S.A., June 1983, (PB84 119 270)A09.
- UCB/EERC-83/13 "Experimental and Analytical Predictions of the Mechanical Characteristics of a 1/5-scale Model of a 7-story R/C Frame-Wall Building Structure," by Aktan, A.E., Bertero, V.V., Chowdhury, A.A. and Nagashima, T., June 1983, (PB84 119 213)A07.

- UCB/EERC-83/14 "Shaking Table Tests of Large-Panel Precast Concrete Building System Assemblages," by Oliva, M.G. and Clough, R.W., June 1983, (PB86 110 210/AS)A11.
- UCB/EERC-83/15 "Seismic Behavior of Active Beam Links in Eccentrically Braced Frames," by Hjelmstad, K.D. and Popov, E.P., July 1983, (PB84 119 676)A09.
- UCB/EERC-83/16 "System Identification of Structures with Joint Rotation," by Dimsdale, J.S., July 1983, (PB84 192 210)A06.
- UCB/EERC-83/17 "Construction of Inelastic Response Spectra for Single-Degree-of-Freedom Systems," by Mahin, S. and Lin, J., June 1983, (PB84 208 834)A05.
- UCB/EERC-83/18 "Interactive Computer Analysis Methods for Predicting the Inelastic Cyclic Behaviour of Structural Sections," by Kaba, S. and Mahin, S., July 1983, (PB84 192 012)A06.
- UCB/EERC-83/19 "Effects of Bond Deterioration on Hysteretic Behavior of Reinforced Concrete Joints," by Filippou, F.C., Popov, E.P. and Bertero, V.V., August 1983, (PB84 192 020)A10.
- UCB/EERC-83/20 "Analytical and Experimental Correlation of Large-Panel Precast Building System Performance," by Oliva, M.G., Clough, R.W., Velkov, M. and Gavrilovic, P., November 1983.
- UCB/EERC-83/21 "Mechanical Characteristics of Materials Used in a 1/5 Scale Model of a 7-Story Reinforced Concrete Test Structure," by Bertero, V.V., Aktan, A.E., Harris, H.G. and Chowdhury, A.A., October 1983, (PB84 193 697)A05.
- UCB/EERC-83/22 "Hybrid Modelling of Soil-Structure Interaction in Layered Media," by Tzong, T.-J. and Penzien, J., October 1983, (PB84 192 178)A08.
- UCB/EERC-83/23 "Local Bond Stress-Slip Relationships of Deformed Bars under Generalized Excitations," by Eligehausen, R., Popov, E.P. and Bertero, V.V., October 1983, (PB84 192 848)A09.
- UCB/EERC-83/24 "Design Considerations for Shear Links in Eccentrically Braced Frames," by Malley, J.O. and Popov, E.P., November 1983, (PB84 192 186)A07.
- UCB/EERC-84/01 "Pseudodynamic Test Method for Seismic Performance Evaluation: Theory and Implementation," by Shing, P.-S.B. and Mahin, S.A., January 1984, (PB84 190 644)A08.
- UCB/EERC-84/02 "Dynamic Response Behavior of Kiang Hong Dian Dam," by Clough, R.W., Chang, K.-T., Chen, H.-Q. and Stephen, R.M., April 1984, (PB84 209 402)A08.
- UCB/EERC-84/03 "Refined Modelling of Reinforced Concrete Columns for Seismic Analysis," by Kaba, S.A. and Mahin, S.A., April 1984, (PB84 234 384)A06.
- UCB/EERC-84/04 "A New Floor Response Spectrum Method for Seismic Analysis of Multiply Supported Secondary Systems," by Asfura, A. and Der Kiureghian, A., June 1984, (PB84 239 417)A06.
- UCB/EERC-84/05 "Earthquake Simulation Tests and Associated Studies of a 1/5th-scale Model of a 7-Story R/C Frame-Wall Test Structure," by Bertero, V.V., Aktan, A.E., Charney, F.A. and Sause, R., June 1984, (PB84 239 409)A09.
- UCB/EERC-84/06 "R/C Structural Walls: Seismic Design for Shear," by Aktan, A.E. and Bertero, V.V., 1984.
- UCB/EERC-84/07 "Behavior of Interior and Exterior Flat-Plate Connections subjected to Inelastic Load Reversals," by Zee, H.L. and Moehle, J.P., August 1984, (PB86 117 629/AS)A07.
- UCB/EERC-84/08 "Experimental Study of the Seismic Behavior of a Two-Story Flat-Plate Structure," by Moehle, J.P. and Diebold, J.W., August 1984, (PB86 122 553/AS)A12.
- UCB/EERC-84/09 "Phenomenological Modeling of Steel Braces under Cyclic Loading," by Ikeda, K., Mahin, S.A. and Dermitzakis, S.N., May 1984, (PB86 132 198/AS)A08.
- UCB/EERC-84/10 "Earthquake Analysis and Response of Concrete Gravity Dams," by Fenves, G. and Chopra, A.K., August 1984, (PB85 193 902/AS)A11.
- UCB/EERC-84/11 "EAGD-84: A Computer Program for Earthquake Analysis of Concrete Gravity Dams," by Fenves, G. and Chopra, A.K., August 1984, (PB85 193 613/AS)A05.
- UCB/EERC-84/12 "A Refined Physical Theory Model for Predicting the Seismic Behavior of Braced Steel Frames," by Ikeda, K. and Mahin, S.A., July 1984, (PB85 191 450/AS)A09.
- UCB/EERC-84/13 "Earthquake Engineering Research at Berkeley - 1984," by , August 1984, (PB85 197 341/AS)A10.
- UCB/EERC-84/14 "Moduli and Damping Factors for Dynamic Analyses of Cohesionless Soils," by Seed, H.B., Wong, R.T., Idriss, I.M. and Tokimatsu, K., September 1984, (PB85 191 468/AS)A04.
- UCB/EERC-84/15 "The Influence of SPT Procedures in Soil Liquefaction Resistance Evaluations," by Seed, H.B., Tokimatsu, K., Harder, L.F. and Chung, R.M., October 1984, (PB85 191 732/AS)A04.
- UCB/EERC-84/16 "Simplified Procedures for the Evaluation of Settlements in Sands Due to Earthquake Shaking," by Tokimatsu, K. and Seed, H.B., October 1984, (PB85 197 887/AS)A03.
- UCB/EERC-84/17 "Evaluation of Energy Absorption Characteristics of Bridges under Seismic Conditions," by Imbsen, R.A. and Penzien, J., November 1984.
- UCB/EERC-84/18 "Structure-Foundation Interactions under Dynamic Loads," by Liu, W.D. and Penzien, J., November 1984, (PB87 124 889/AS)A11.
- UCB/EERC-84/19 "Seismic Modelling of Deep Foundations," by Chen, C.-H. and Penzien, J., November 1984, (PB87 124 798/AS)A07.
- UCB/EERC-84/20 "Dynamic Response Behavior of Quan Shui Dam," by Clough, R.W., Chang, K.-T., Chen, H.-Q., Stephen, R.M., Ghanaat, Y. and Qi, J.-H., November 1984, (PB86 115177/AS)A07.
- UCB/EERC-85/01 "Simplified Methods of Analysis for Earthquake Resistant Design of Buildings," by Cruz, E.F. and Chopra, A.K., February 1985, (PB86 112299/AS)A12.
- UCB/EERC-85/02 "Estimation of Seismic Wave Coherency and Rupture Velocity using the SMART 1 Strong-Motion Array Recordings," by Abrahamson, N.A., March 1985, (PB86 214 343)A07.

- UCB/EERC-85/03 "Dynamic Properties of a Thirty Story Condominium Tower Building," by Stephen, R.M., Wilson, E.L. and Stander, N., April 1985, (PB86 118965/AS)A06.
- UCB/EERC-85/04 "Development of Substructuring Techniques for On-Line Computer Controlled Seismic Performance Testing," by Dermitzakis, S. and Mahin, S., February 1985, (PB86 132941/AS)A08.
- UCB/EERC-85/05 "A Simple Model for Reinforcing Bar Anchorages under Cyclic Excitations," by Filippou, F.C., March 1985, (PB86 112 919/AS)A05.
- UCB/EERC-85/06 "Racking Behavior of Wood-framed Gypsum Panels under Dynamic Load," by Oliva, M.G., June 1985.
- UCB/EERC-85/07 "Earthquake Analysis and Response of Concrete Arch Dams," by Fok, K.-L. and Chopra, A.K., June 1985, (PB86 139672/AS)A10.
- UCB/EERC-85/08 "Effect of Inelastic Behavior on the Analysis and Design of Earthquake Resistant Structures," by Lin, J.P. and Mahin, S.A., June 1985, (PB86 135340/AS)A08.
- UCB/EERC-85/09 "Earthquake Simulator Testing of a Base-Isolated Bridge Deck," by Kelly, J.M., Buckle, I.G. and Tsai, H.-C., January 1986, (PB87 124 152/AS)A06.
- UCB/EERC-85/10 "Simplified Analysis for Earthquake Resistant Design of Concrete Gravity Dams," by Fenves, G. and Chopra, A.K., June 1986, (PB87 124 160/AS)A08.
- UCB/EERC-85/11 "Dynamic Interaction Effects in Arch Dams," by Clough, R.W., Chang, K.-T., Chen, H.-Q. and Ghanaat, Y., October 1985, (PB86 135027/AS)A05.
- UCB/EERC-85/12 "Dynamic Response of Long Valley Dam in the Mammoth Lake Earthquake Series of May 25-27, 1980," by Lai, S. and Seed, H.B., November 1985, (PB86 142304/AS)A05.
- UCB/EERC-85/13 "A Methodology for Computer-Aided Design of Earthquake-Resistant Steel Structures," by Austin, M.A., Pister, K.S. and Mahin, S.A., December 1985, (PB86 159480/AS)A10.
- UCB/EERC-85/14 "Response of Tension-Leg Platforms to Vertical Seismic Excitations," by Liou, G.-S., Penzien, J. and Yeung, R.W., December 1985, (PB87 124 871/AS)A08.
- UCB/EERC-85/15 "Cyclic Loading Tests of Masonry Single Piers: Volume 4 - Additional Tests with Height to Width Ratio of 1," by Sveinsson, B., McNiven, H.D. and Sucuoglu, H., December 1985.
- UCB/EERC-85/16 "An Experimental Program for Studying the Dynamic Response of a Steel Frame with a Variety of Infill Partitions," by Yanev, B. and McNiven, H.D., December 1985.
- UCB/EERC-86/01 "A Study of Seismically Resistant Eccentrically Braced Steel Frame Systems," by Kasai, K. and Popov, E.P., January 1986, (PB87 124 178/AS)A14.
- UCB/EERC-86/02 "Design Problems in Soil Liquefaction," by Seed, H.B., February 1986, (PB87 124 186/AS)A03.
- UCB/EERC-86/03 "Implications of Recent Earthquakes and Research on Earthquake-Resistant Design and Construction of Buildings," by Bertero, V.V., March 1986, (PB87 124 194/AS)A05.
- UCB/EERC-86/04 "The Use of Load Dependent Vectors for Dynamic and Earthquake Analyses," by Leger, P., Wilson, E.L. and Clough, R.W., March 1986, (PB87 124 202/AS)A12.
- UCB/EERC-86/05 "Two Beam-To-Column Web Connections," by Tsai, K.-C. and Popov, E.P., April 1986, (PB87 124 301/AS)A04.
- UCB/EERC-86/06 "Determination of Penetration Resistance for Coarse-Grained Soils using the Becker Hammer Drill," by Harder, L.F. and Seed, H.B., May 1986, (PB87 124 210/AS)A07.
- UCB/EERC-86/07 "A Mathematical Model for Predicting the Nonlinear Response of Unreinforced Masonry Walls to In-Plane Earthquake Excitations," by Mengi, Y. and McNiven, H.D., May 1986, (PB87 124 780/AS)A06.
- UCB/EERC-86/08 "The 19 September 1985 Mexico Earthquake: Building Behavior," by Bertero, V.V., July 1986.
- UCB/EERC-86/09 "EACD-3D: A Computer Program for Three-Dimensional Earthquake Analysis of Concrete Dams," by Fok, K.-L., Hall, J.F. and Chopra, A.K., July 1986, (PB87 124 228/AS)A08.
- UCB/EERC-86/10 "Earthquake Simulation Tests and Associated Studies of a 0.3-Scale Model of a Six-Story Concentrically Braced Steel Structure," by Uang, C.-M. and Bertero, V.V., December 1986, (PB87 163 564/AS)A17.
- UCB/EERC-86/11 "Mechanical Characteristics of Base Isolation Bearings for a Bridge Deck Model Test," by Kelly, J.M., Buckle, I.G. and Koh, C.-G., 1987.
- UCB/EERC-86/12 "Effects of Axial Load on Elastomeric Isolation Bearings," by Koh, C.-G. and Kelly, J.M., November 1987.
- UCB/EERC-87/01 "The FPS Earthquake Resisting System: Experimental Report," by Zayas, V.A., Low, S.S. and Mahin, S.A., June 1987.
- UCB/EERC-87/02 "Earthquake Simulator Tests and Associated Studies of a 0.3-Scale Model of a Six-Story Eccentrically Braced Steel Structure," by Whitaker, A., Uang, C.-M. and Bertero, V.V., July 1987.
- UCB/EERC-87/03 "A Displacement Control and Uplift Restraint Device for Base-Isolated Structures," by Kelly, J.M., Griffith, M.C. and Aiken, I.D., April 1987.
- UCB/EERC-87/04 "Earthquake Simulator Testing of a Combined Sliding Bearing and Rubber Bearing Isolation System," by Kelly, J.M. and Chalhoub, M.S., 1987.
- UCB/EERC-87/05 "Three-Dimensional Inelastic Analysis of Reinforced Concrete Frame-Wall Structures," by Moazzami, S. and Bertero, V.V., May 1987.
- UCB/EERC-87/06 "Experiments on Eccentrically Braced Frames with Composite Floors," by Ricles, J. and Popov, E., June 1987.
- UCB/EERC-87/07 "Dynamic Analysis of Seismically Resistant Eccentrically Braced Frames," by Ricles, J. and Popov, E., June 1987.
- UCB/EERC-87/08 "Undrained Cyclic Triaxial Testing of Gravels-The Effect of Membrane Compliance," by Evans, M.D. and Seed, H.B., July 1987.
- UCB/EERC-87/09 "Hybrid Solution Techniques for Generalized Pseudo-Dynamic Testing," by Thewalt, C. and Mahin, S.A., July 1987.
- UCB/EERC-87/10 "Ultimate Behavior of Butt Welded Splices in Heavy Rolled Steel Sections," by Bruneau, M., Mahin, S.A. and Popov, E.P., July 1987.
- UCB/EERC-87/11 "Residual Strength of Sand from Dam Failures in the Chilean Earthquake of March 3, 1985," by De Alba, P., Seed, H.B., Retamal, E. and Seed, R.B., September 1987.

- UCB/EERC-87/12 "Inelastic Seismic Response of Structures with Mass or Stiffness Eccentricities in Plan," by Bruneau, M. and Mahin, S.A., September 1987.
- UCB/EERC-87/13 "CSTRUCT: An Interactive Computer Environment for the Design and Analysis of Earthquake Resistant Steel Structures," by Austin, M.A., Mahin, S.A. and Pister, K.S., September 1987.
- UCB/EERC-87/14 "Experimental Study of Reinforced Concrete Columns Subjected to Multi-Axial Loading," by Low, S.S. and Moehle, J.P., September 1987.
- UCB/EERC-87/15 "Relationships between Soil Conditions and Earthquake Ground Motions in Mexico City in the Earthquake of Sept. 19, 1985," by Seed, H.B., Romo, M.P., Sun, J., Jaime, A. and Lysmer, J., October 1987.
- UCB/EERC-87/16 "Experimental Study of Seismic Response of R. C. Setback Buildings," by Shahrooz, B.M. and Moehle, J.P., October 1987.
- UCB/EERC-87/17 "The Effect of Slabs on the Flexural Behavior of Beams," by Pantazopoulou, S.J. and Moehle, J.P., October 1987.
- UCB/EERC-87/18 "Design Procedure for R-FBI Bearings," by Mostaghel, N. and Kelly, J.M., November 1987.
- UCB/EERC-87/19 "Analytical Models for Predicting the Lateral Response of R C Shear Walls: Evaluation of their Reliability," by Vulcano, A. and Bertero, V.V., November 1987.
- UCB/EERC-87/20 "Earthquake Response of Torsionally-Coupled Buildings," by Hejal, R. and Chopra, A.K., December 1987.
- UCB/EERC-87/21 "Dynamic Reservoir Interaction with Monticello Dam," by Clough, R.W., Ghanaat, Y. and Qiu, X-F., December 1987.
- UCB/EERC-87/22 "Strength Evaluation of Coarse-Grained Soils," by Siddiqi, F.H., Seed, R.B., Chan, C.K., Seed, H.B. and Pyke, R.M., December 1987.
- UCB/EERC-88/01 "Seismic Behavior of Concentrically Braced Steel Frames," by Khatib, I., Mahin, S.A. and Pister, K.S., January 1988.
- UCB/EERC-88/02 "Experimental Evaluation of Seismic Isolation of Medium-Rise Structures Subject to Uplift," by Griffith, M.C., Kelly, J.M., Coveney, V.A. and Koh, C.G., January 1988.
- UCB/EERC-88/03 "Cyclic Behavior of Steel Double Angle Connections," by Astaneh-Asl, A. and Nader, M.N., January 1988.
- UCB/EERC-88/04 "Re-evaluation of the Slide in the Lower San Fernando Dam in the Earthquake of Feb. 9, 1971," by Seed, H.B., Seed, R.B., Harder, L.F. and Jong, H.-L., April 1988.
- UCB/EERC-88/05 "Experimental Evaluation of Seismic Isolation of a Nine-Story Braced Steel Frame Subject to Uplift," by Griffith, M.C., Kelly, J.M. and Aiken, I.D., May 1988.
- UCB/EERC-88/06 "DRAIN-2DX User Guide," by Allahabadi, R. and Powell, G.H., March 1988.
- UCB/EERC-88/07 "Cylindrical Fluid Containers in Base-Isolated Structures," by Chalhoub, M.S. and Kelly, J.M., April 1988.
- UCB/EERC-88/08 "Analysis of Near-Source Waves: Separation of Wave Types using Strong Motion Array Recordings," by Darragh, R.B., June 1988.
- UCB/EERC-88/09 "Alternatives to Standard Mode Superposition for Analysis of Non-Classically Damped Systems," by Kusainov, A.A. and Clough, R.W., June 1988.
- UCB/EERC-88/10 "The Landslide at the Port of Nice on October 16, 1979," by Seed, H.B., Seed, R.B., Schlosser, F., Blondeau, F. and Juran, I., June 1988.
- UCB/EERC-88/11 "Liquefaction Potential of Sand Deposits Under Low Levels of Excitation," by Carter, D.P. and Seed, H.B., August 1988.
- UCB/EERC-88/12 "Nonlinear Analysis of Reinforced Concrete Frames Under Cyclic Load Reversals," by Filippou, F.C. and Issa, A., September 1988.
- UCB/EERC-88/13 "Earthquake-Resistant Design of Building Structures: An Energy Approach," by Uang, C.-M. and Bertero, V.V., September 1988.
- UCB/EERC-88/14 "An Experimental Study of the Behavior of Dual Steel Systems," by Whittaker, A.S., Uang, C.-M. and Bertero, V.V., September 1988.
- UCB/EERC-88/15 "Dynamic Moduli and Damping Ratios for Cohesive Soils," by Sun, J.I., Golesorkhi, R. and Seed, H.B., August 1988.
- UCB/EERC-88/16 "Reinforced Concrete Flat Plates Under Lateral Load: An Experimental Study Including Biaxial Effects," by Pan, A. and Moehle, J., November 1988.

REPORT DOCUMENTATION PAGE	1. REPORT NO. NSF/ENG-88052	2.	3. Recipient's Accession No. PB91-210856
4. Title and Subtitle "Reinforced Concrete Flat Plates under Lateral Loading: An Experimental Study Including Biaxial Effects."			5. Report Date October 1988
7. Author(s) Austin A. Pan, Jack P. Moehle			6.
9. Performing Organization Name and Address Earthquake Engineering Research Center University of California 1301 South 46th Street			8. Performing Organization Rept. No. UCB/EERC-88/16
12. Sponsoring Organization Name and Address National Science Foundation 1800 G. Street, NW Washington D.C. 20550			10. Project/Task/Work Unit No.
			11. Contract(C) or Grant(G) No. (C) (G) ECE-8410738
			13. Type of Report & Period Covered
			14.

15. Supplementary Notes**16. Abstract (Limit 200 words)**

"Slab-column subassemblages, modelled after a reinforced concrete flat plate building, are tested under combined gravity and lateral loads. The test include different levels of gravity loads and compare biaxial lateral loading with uniaxial loading. To study the behavior of a repaired connection, one test is repeated after the slab-column specimen is repaired with epoxy and grout. The post-failure behavior of slab-column connections is investigated and the adequacy of bottom slab reinforcement detailing to prevent progressive collapse is assessed. Existing strength and lateral stiffness models are compared with the experimental results. Data from past research are collected to investigate the ductility and drift capacity of slab-column connections. Studies are conducted on the seismic response of reinforced concrete buildings with flat slab construction. Nonlinear dynamic analyses are performed on five typical building systems. A simple seismic design recommendation is proposed for slab-column connections that limits the level of gravity shear to ensure minimal drift capacity.

17. Document Analysis a. Descriptors**b. Identifiers/Open-Ended Terms****c. COSATI Field/Group****18. Availability Statement:**

Release Unlimited

19. Security Class (This Report)

Release Unlimited

20. Security Class (This Page)**21. No. of Pages**

283

22. Price

